

AD735006

Reproduced by  
**NATIONAL TECHNICAL  
INFORMATION SERVICE**  
Springfield, Va. 22151

**BEST  
AVAILABLE COPY**

**UNCLASSIFIED**

Security Classification

**DOCUMENT CONTROL DATA - R & D**

(Security classification of title, body of abstract and indexing annotation must be entered when the overall report is classified)

1. ORIGINATING ACTIVITY (Corporate author) <b>INSTITUTE FOR DEFENSE ANALYSES 400 Army-Navy Drive Arlington, Virginia 22202</b>		2a. REPORT SECURITY CLASSIFICATION <b>UNCLASSIFIED</b>	
		2b. GROUP <b>--</b>	
3. REPORT TITLE <b>Low-Light-Level Devices: A Designers' Manual</b>			
4. DESCRIPTIVE NOTES (Type of report and inclusive dates) <b>Report R-169, August 1971</b>			
5. AUTHOR(S) (First name, middle initial, last name) <b>Lucien M. Biberman, Frederick A. Rosell, Otto H. Schade, Sr., Alvin D. Schnitzler, Harry L. Snyder</b>			
6. REPORT DATE <b>August 1971</b>		7a. TOTAL NO. OF PAGES <b>522</b>	7b. NO. OF REFS <b>109</b>
8a. CONTRACT OR GRANT NO. <b>DAHC15 67 C 0011</b>		8b. ORIGINATOR'S REPORT NUMBER(S) <b>R-169</b>	
8c. PROJECT NO. <b>Task T-36</b>		8d. OTHER REPORT NO(S) (Any other numbers that may be assigned this report) <b>None</b>	
10. DISTRIBUTION STATEMENT			
11. SUPPLEMENTARY NOTES <b>NA</b>		12. SPONSORING MILITARY ACTIVITY <b>Advanced Research Projects Agency Arlington, Virginia 22209</b>	
13. ABSTRACT <p>Excellent correlation exists between the quality of aerial photographs as measured by the modulation transfer function area (MTFA) and as measured by observer performance. The MTFA and the signal-to-noise ratio at the display (<math>SNR_D</math>), derived in this report, are closely related, and the <math>SNR_D</math> is adopted here as the main criterion of equipment quality.</p> <p>Present commercially specified parameters are unsatisfactory means for predicting equipment performance. This report considers the parameters that are directly related to observer performance as the truly meaningful ones and flags them out as such.</p> <p>In the design of both remote-view television and direct-view image-intensifier systems, it is important to present the output image to the eye at luminance and angular size sufficient that the required modulation is determined not by the optical properties of the eye and the neurological organization of the retina but rather by the fundamental effects of output luminous fluctuations on the decision process.</p> <p>Also, we point out that reduction of display luminance below the usual working level has a dramatic effect on the required modulation as a function of frequency.</p> <p>Using the criterion of <math>SNR_D</math>, one can rank present-day low-light-level camera tubes. This report does so in detail in Section V-A-4. However, it is clearly difficult to specify a "best" tube without a rather complete understanding of the relative importance to system performance of sensitivity versus light levels, detail rendition, and lag. A small change in the relative importance of these factors can seriously affect choice of the "best" tube.</p> <p>For years the image orthicon was the preferred tube. Beginning about 1963-64, the secondary electron conduction (SEC) camera tube replaced it in favor, since the low lag of the SEC tube outweighed the need for very low-light-level performance in many aircraft systems. More recently, both the improved image isocon and the silicon-electron-bombardment induced-response (SEBIR) camera tube have emerged. They will probably replace the SEC tube.</p>			

**DD FORM 1473**  
1 NOV 66**UNCLASSIFIED**  
Security Classification

**UNCLASSIFIED**

Security Classification

14

## KEY WORDS

## LINK A

## LINK B

## LINK C

ROLE

WT

ROLE

WT

ROLE

WT

aliasing  
display signal-to-noise ratio  
image intensifiers  
image quality  
low-light-level devices  
low-light-level television  
raster effects  
real-time sensors  
sensors  
television camera tubes  
television displays  
vision  
visual systems

**UNCLASSIFIED**

Security Classification



REPORT R-169

## LOW-LIGHT-LEVEL DEVICES: A DESIGNERS' MANUAL

Lucien M. Biberman  
Institute for Defense Analyses

Frederick A. Rosell  
Westinghouse Defense and Space Center

Alvin D. Schnitzler  
Institute for Defense Analyses

*with contributions by:*

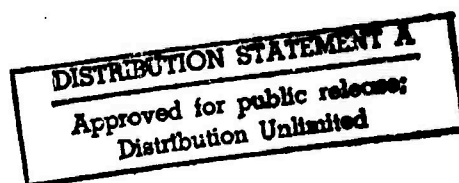
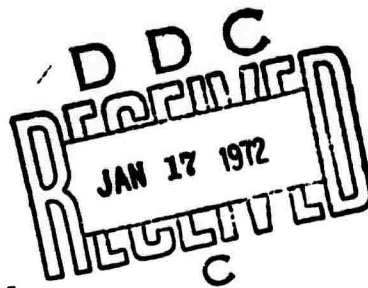
Otto H. Schade, Sr.,  
Consultant

Harry L. Snyder  
Virginia Polytechnic Institute and State University

August 1971



INSTITUTE FOR DEFENSE ANALYSES  
SCIENCE AND TECHNOLOGY DIVISION  
400 Army-Navy Drive, Arlington, Virginia 22202



Compiled by the Institute for Defense Analyses as IDA Report R-169 for the Director, Defense Research and Engineering, Department of Defense, and published by direction of the Advanced Research Projects Agency Contract DAHC15 67 C 0011.

Publication of this IDA Report does not indicate endorsement by the Department of Defense, nor should the contents be construed as reflecting the official position of that agency.

Approved for public release; distribution unlimited.



## FOREWORD

The performance of night vision devices has reached a level where the limitations can often be found to reside in the chosen size or quality of the display rather than in the quality of the sensor. A lack of general understanding of visual requirements often results in display specifications that produce an image too small, too dim, or too fuzzy to present the picture to the eye as well as the sensor has recorded it.

Buyers tend to accept night vision devices that will measure up to the standards of the commercial home entertainment television to which they are accustomed, not realizing that such equipment will be inadequate to meet the exacting demands of military viewing. But buyers are not completely at fault. Manufacturers--especially tube manufacturers--have refrained from publishing the very characteristics of their products that govern the quality of the television picture displayed.

The Night Vision Laboratories, recognizing the problem, have established a specification and procurement framework for direct-viewing (intensifier) devices but have not yet extended this sufficiently for raster-producing imaging devices.

About three years ago, at the request of the Air Force Systems Command, the Office of the Director of Defense Research and Engineering (ODDR&E) asked the Institute for Defense Analyses (IDA) to furnish guidelines to bring order into what was indeed chaotic procurement of night vision devices. In response, IDA has presented a series of lectures and has published papers in the open and classified literature to encourage the use of real and effective criteria in the design, specification, testing, and acceptance of photoelectronic image forming

devices. The IDA effort has culminated in the publication of a two-volume treatise, Photoelectronic Image Forming Devices, edited by Biberman and Nudelman and released in January 1971 by Plenum Press, New York.

Portions of that treatise (basically Chapters 4, 11, and 19 of Vol. I and Chapter 22 of Vol. II) are extended in this paper at a level of detail not feasible in a commercial publication.

This work has been supported as a continuing task for ODPD&E under the general direction of E.N. Myers.

## ACKNOWLEDGMENT

This report is the result of much work by many over a period of years. Although it represents considerable effort at IDA, it also includes contributions from many of our colleagues in industrial and government laboratories. An important contribution, Part V, is the work of Frederick A. Rosell and his associates at the Westinghouse Defense and Space Center, Baltimore. Much of the experimental psychophysical work described in Part V was carried out by Robert H. Willson. Part II includes a summary of work in image evaluation by Harry L. Snyder and his former colleagues at the Boeing Company, Seattle. We are indeed indebted to Westinghouse and Boeing for making possible the cooperation of their staffs in the preparation of this document. Part II also includes a summary of raster effects on image reproduction, so kindly written by Otto H. Schade, Sr., to fill an obvious gap in this report.

Part IV was compiled from information supplied by the Army Night Vision Laboratories and some of the principal developers and producers of image intensifiers. The latter include: Aerojet Delft; the International Telephone and Telegraph Company; the Radio Corporation of America; the Machlett Laboratories Division of Raytheon; Varian Associates; Varo, Incorporated; the Westinghouse Electric Corporation; and the Rauland Division of the Zenith Radio Corporation. We acknowledge with sincere thanks the contributions of these organizations.

After Part V was written, the material was forwarded to the manufacturers of the tubes for which data are shown. The manufacturers were asked to verify or authenticate the data, if possible, or, if they did not wish to go to that amount of trouble, to indicate that they had no substantive technical disagreement with our reporting of the characteristics of their products.

We would like to acknowledge the cooperation of RCA on data on the vidicon, orthicon, and isocor tubes. Similarly, we want to thank the Amperex Corporation for reviewing the data and calculations on the Plumbicon, and the Westinghouse Electric Corporation for reviewing the data on the SEC camera tube and the silicon-diode-array equivalent of the SEC. We also wish to thank RCA for their data on this latter tube.

The information on burn resistance of the newer tubes was extracted from data made available by Martin Green and Peter R. Collings of the Westinghouse Electronic Tube Division, Elmira, N.Y. The information on "blooming" was extracted from data made available by Stephen B. Campana of the Naval Air Development Center, Johnsville, Pa.

We have depended heavily upon the discerning criticism of our reviewers, Otto H. Schade, Sr., James A. Hall of the University of Rhode Island, Kenneth J. Ando of the Jet Propulsion Laboratory, and R.W. Redington of the General Electric Company, whose assistance, suggestions, and encouragement we acknowledge with heartfelt thanks.

Finally, we wish to acknowledge the critical editing of B.F. Roberts and the careful, intelligent copy preparation of Evelyn L. McBride.

## ABSTRACT

Excellent correlation exists between the quality of aerial photographs as measured by the modulation transfer function area (MTFA) and as measured by observer performance. The MTFA and the signal-to-noise ratio at the display ( $SNR_D$ ), derived in this report, are closely related, and the  $SNR_D$  is adopted here as the main criterion of equipment quality.

Present commercially specified parameters are unsatisfactory means for predicting equipment performance. This report considers the parameters that are directly related to observer performance as the truly meaningful ones and flags them out as such.

In the design of both remote-view television and direct-view image-intensifier systems, it is important to present the output image to the eye at luminance and angular size sufficient that the required modulation is determined not by the optical properties of the eye and the neurological organization of the retina but rather by the fundamental effects of output luminous fluctuations on the decision process.

Also, we point out that reduction of display luminance below the usual working level has a dramatic effect on the required modulation as a function of frequency.

Using the criterion of  $SNR_D$ , one can rank present-day low-light-level camera tubes. This report does so in detail in Section V-A-4. However, it is clearly difficult to specify a best tube without a rather complete understanding of the relative importance to system performance of sensitivity versus light levels, detail rendition, and lag. A small change in the relative importance of these factors can seriously affect choice of the "best" tube.

For years the image orthicon was the preferred tube. Beginning about 1963-64, the secondary electron conduction (SEC) camera tube replaced it in favor, since the low lag of the SEC tube outweighed the need for very low-light-level performance in many aircraft systems. More recently, both the improved image isocon and the silicon-electron-bombardment induced-response (SEBIR) camera tube have emerged. They will probably replace the SEC tube.



## CONTENTS

SUMMARY by Lucien M. Biberman	1
A. Historical Background	1
B. Effects of Image Quality on Operator Performance	5
C. Low-Light-Level Performance of Visual Systems	9
D. Image-Intensifier Tube Structures	19
E. Television Camera Tube Performance and Data	23
F. Comparison of Low-Light-Level Camera Tubes	26
Bibliography	33
I. INTRODUCTION by Lucien M. Biberman	35
A. Purpose	37
B. Organization	38
C. Early History of the Development of Low-Light-Level Television	40
D. Criteria for System Quality	48
References	55
II. IMAGE QUALITY	59
PHOTOGRAPHIC IMAGE QUALITY AND OPERATOR PERFORMANCE by Harry L. Snyder	63
A. Introduction	63
B. Modulation Transfer Function Area (MTFA)	64
C. Evaluation of the MTFA	69
D. Conclusions and Cautions	76
References	81
IMAGE REPRODUCTION BY A LINE RASTER PROCESS by Otto H. Schade, Sr.	83
A. The Sampling Process of a Line Raster	83
B. Raster Line Frequencies and MTF Combinations for Low Spurious Response	88
C. System Design	91
References	95

III.	LOW-LIGHT-LEVEL PERFORMANCE OF VISUAL SYSTEMS by Alvin D. Schnitzler	97
	Symbols	99
	A. Low-Light-Level Performance of the Eye	101
	B. Low-Light-Level Performance of Binoculars	109
	C. Basic Parameters and Theory of Performance of Photoelectronic Imaging Systems	111
	References	135
IV.	IMAGE-INTENSIFIER TUBE STRUCTURES by Alvin D. Schnitzler	137
	A. Basic Single-Stage Structure	139
	B. Cascade Image Intensifiers	144
	C. Second-Generation Image Intensifiers	158
	References	173
V.	TELEVISION CAMERA TUBE PERFORMANCE AND DATA by Frederick A. Rosell	175
	Symbols	177
	A. Introduction	185
	B. Image Converters and Image Intensifiers	245
	C. Vidicon Camera Tubes	257
	D. The Secondary Electron Conduction Camera Tube and its Intensified Version	316
	E. The Image Orthicon and the Image Isocon	371
	F. The Silicon Electron Bombardment Induced Response Camera Tube and its Intensified Version	437
	G. Correlation between MTF and $SNR_D$	457
	References	463
VI.	A COMPARISON OF TELEVISION CAMERA TUBES by Lucien M. Biberman	465
	A. Introduction	467
	B. Damage to Electron Charge Storage Targets	471
	C. The Blooming Problem: Low-Light-Level Imaging in the Presence of High-Intensity Point Sources	486
	D. Various Spread Effects in SEIR Tubes	496
	References	501
VII.	SOME BRIEF COMMENTS ON IMPORTANT TUBE PARAMETERS AND THEIR SPECIFICATION by Lucien M. Biberman	503
	A. Signal-to-Noise Dependence on Spectral Composition	505
	B. Signal-to-Noise versus Limiting Resolution	505
	C. Spectral Response	505
	D. Sensitivity and Resolution	507
	E. Lag Effects	508
	F. Other Factors	514
	References	515
	APPENDIX--Derivation of Detection Probability Curve	517

## SUMMARY

by Lucien M. Biberman

### A. HISTORICAL BACKGROUND

Low-light-level devices originated, conceptually at least, in the 1920s, when it was realized that some of the various means of focusing electrons and forming beams also amplified the energy of the electrons being focused and thus provided, in principle, a mechanism for light amplification. Unfortunately, the technology of that period was so rudimentary compared to that we know now that efforts to achieve light amplification by those means were frustrated by the very poor efficiencies of coupling and of converting light into electrons and electrons back into light.

Later, as cathode and phosphor efficiencies improved to the extent that an image amplifier or intensifier could produce more light at its output than it received at its input, it became obvious that such devices could be cascaded to increase gain exponentially. The first patent on such a concept was issued in France in 1936, but the first working device was not demonstrated until 1952 and then in the United States.

In the early phases of American development of low-light-level devices the emphasis was on light amplification. It was only rather late in the program, in the mid-sixties, that serious attention was paid to the companion problem of image quality. It is interesting to note that the Dutch and English philosophy, pretty well driven by the arguments of Peter Schagen of Mullard, concentrated on simple one-stage devices of good image quality but quite low picture brightness. American tubes were being pressed toward quite high gain, i.e., output images about 50,000 times as bright photometrically as the input to the tube. The Dutch and British tubes were more apt to provide gains of a few hundred.

Both routes of development suffered from fixation of the established concepts and points of view.

It is easy to point out in retrospect that when the scene was very dark the low-gain, high-resolution devices of the Dutch and British were of precious little use--the image quality might very well have been excellent but the image was so very dim that often a human eye could not see it or required too much time to see it. On the other hand, the high-gain American devices did penetrate the darkness well enough for viewing rather large objects not too far away. As the light level increased, the performance of the American devices increased only until they became limited by a variety of image quality limitations. Thus, we had good image quality from the English and Dutch devices and good gain from the American devices.

Brightness gain is not the only important standard by which the performance of low-light-level devices must be specified. This fact has only recently found acceptance among members of the R&D community and, unfortunately, its acceptance outside that community has been even slower. The importance of proper specifications must be impressed upon operations, procurement, and maintenance personnel in the Services if U.S. forces are to achieve an image quality in night vision that is comparable to the image quality in day vision.

During the early development of low-light-level devices, prospective users would ask, "How dark is it when you can just see a specified object, and how much farther can you see with your device than I can see with my unaided eyes or looking through binoculars?" Darkness was measured by instruments that corresponded to the eye. The night-vision aids, however, were in reality near-infrared devices. This was apparently too complicated to explain, and thus the eye-related units of brightness--the lumen, the lambert, and the foot-candle--became the standards by which one measured light and darkness and specified the performance of night-vision devices.

As time progressed, low-light-level devices improved in several ways. A principal improvement was extension of the response of the

sensing layer (or cathode) to longer wavelengths to capture more of the available radiation--light in both the visual and infrared portions of the spectrum. Most of this increased response was in the infrared.

These improvements were important for several reasons. First, the "light" (invisible radiation) from photochemical reactions in the night sky increases dramatically as one looks deeper into the near infrared. Second, the contrast of most scenes is greater at wavelengths above about 600 nanometers--the deep red part of the visual spectrum extending into the near infrared.

As these improvements progressed they laid the groundwork for much confusion and semantic difficulty. Those engaged in development and procurement had learned a lingo that never was correct but had not previously caused difficulty. Now they specified light levels as seen or measured by eye while looking with a device that saw in a region of the spectrum unseen by the eye. Thus, it was possible for things to be bright to a night-vision device and dark to the eye and vice versa. This very property was exploited fully in various traveling exhibitions and demonstrations that showed military scenes on or in some staged setting of scale models nicely illuminated by "invisible light" from a bank of special electric lamps tucked away out of sight. The "invisible light" was invisible to the naked eye but not to the devices used to demonstrate night-vision progress.

One must recognize that night-vision devices have a color sensitivity different from the eye and that they see wavelengths the eye cannot. Specifications written in terms of standards based on the sensitivity of the eye cannot help but lead to confusion or disappointment or both.

It is actually much more meaningful to specify the performance of a device under conditions of full moonlight, which is about  $2 \times 10^{-2}$  footcandles, then it is to specify  $2 \times 10^{-2}$  footcandles alone. Full moonlight has a color spectrum that is real, known, and reproducible. The  $2 \times 10^{-2}$  footcandles could apply to any kind of light of any color that the eye could see. Later in this report we show

typical but erroneous nomographs, once in general use, that indicate performance measured under illumination from a tungsten lamp. These nomographs imply that performance will be equally good when light sources providing illumination equal to that of the tungsten lamp (2854° Kelvin) but of different spectral distribution are used. NOT SO!

Many other methods of specification hang on from the days in which television was aborning. One of the most common of these is the method of measuring device performance by noting those objects that the observer knows are there but that he can no longer see fifty percent of the time. According to this practice, the limiting resolution is the smallest, or narrowest, set of objects that still remains liminally visible (visible 50 percent of the time) on the television display. Often this is shown in a plot of the frequency of the fine lines liminally visible as the light on the scene is increased. This is alleged to represent the quality of the television device. This method of specification has been used so long that many people accept it and some actually believe it.

The entire topic of the utility of low-light-level devices is a complex one, and the task of writing specifications for such a device that will truly improve its user's information-gathering and decision-making performance has heretofore been easier to avoid than to face. But good specifications can be written, as will be shown below.

To date, only in the case of the B-57G aircraft have specifications for electrooptical sensors been written to address the man-machine perception problem. The low-light-level system for the B-57G has proved to be at least an order of magnitude better than any other flying, judged on its ability to do its mission. Its design addressed those factors that enable the user to detect and recognize; those factors were, in fact, the primary elements driving the design. As a result, this low-light-level television (LLLTV) system gives the viewer better vision at night than he has by day.

Thus, in a period of half a century (1920-1970) an idea emerged and grew to give man the ability to see more clearly at night than he had previously seen with his unaided eyes in bright daylight.

In that half century it has been only recently that serious attention has been given to the needs and requirements of human observers. These are still largely overlooked, but in at least one system the problem has been faced and the results are exemplary.

#### B. EFFECTS OF IMAGE QUALITY ON OPERATOR PERFORMANCE

Image intensifiers, television cameras, and optical devices can be measured and tested in a manner somewhat similar to the one used to test a high-fidelity sound system amplifier or a radar receiver. As the frequency of a sine-wave signal of known amplitude is varied at the input, the amplitude is measured at the output. The ratio of output to input amplitudes, sometimes called the gain, is plotted against frequency to give what is called the frequency response of the amplifier.

In optical devices one provides a test pattern of square waves and sine waves as black and white bars, or a series of black bars that fade through grey to white and back to black, sinusoidally, in a given linear dimension that becomes smaller for each of several sets of test patterns. One measures the brightness of various reproduced patterns and computes the ratio of signal out to signal in. Most commonly the quantity "modulation" is used as the output and input parameters, and thus the modulation transfer function (MTF) is often used as a criterion of optical element quality.

Not only do optical devices have MTF characteristics, but also the eye has demands which are contrary to the MTFs of most such devices.

Telescopes, television cameras, and almost all other optical devices work quite well in producing a nearly 100 percent output modulation for a 100 percent input modulation whenever the source is large or, in other words, a low-frequency signal. As the source size decreases and its reciprocal spatial frequency increases, the MTF falls

off until for some source size (or frequency) it has effectively approached zero and has reached a nonuseful level. On the other hand, the eye requires very little contrast or modulation to see large objects but needs high contrast and bright light to see very small objects. Thus, as the viewed object becomes small, a television system does not produce much modulation, while the eye needs large modulation values to see a small object of high spatial frequency.

For large objects (low frequencies) the television produces much modulation and the eye needs little, and the combined performance is good; for small objects (high frequencies) the television produces little modulation and the eye needs much, and the combined performance is very bad.

Recent experiments have shown that the area (sometimes called MTFA or MTF area) between the MTF plot and eye-demand plot (Fig. 1)

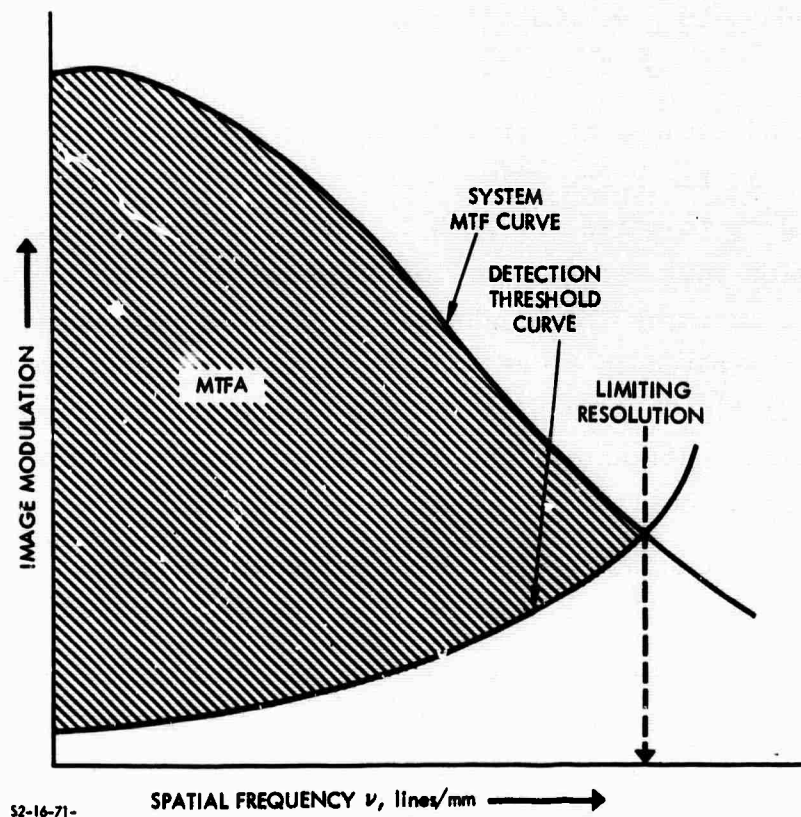


FIGURE 1. Modulation Transfer Function Area (MTFA)



correlates very well with success and failure in the accomplishment of visual tasks. Among other experiments, one series has shown that pilots and other trained observers made few errors when the MTFA (of the imagery they studied) was large, and made many errors when the MTFA was small. The relationship between MTFA and errors was almost a textbook example of correlation (Fig. 2).

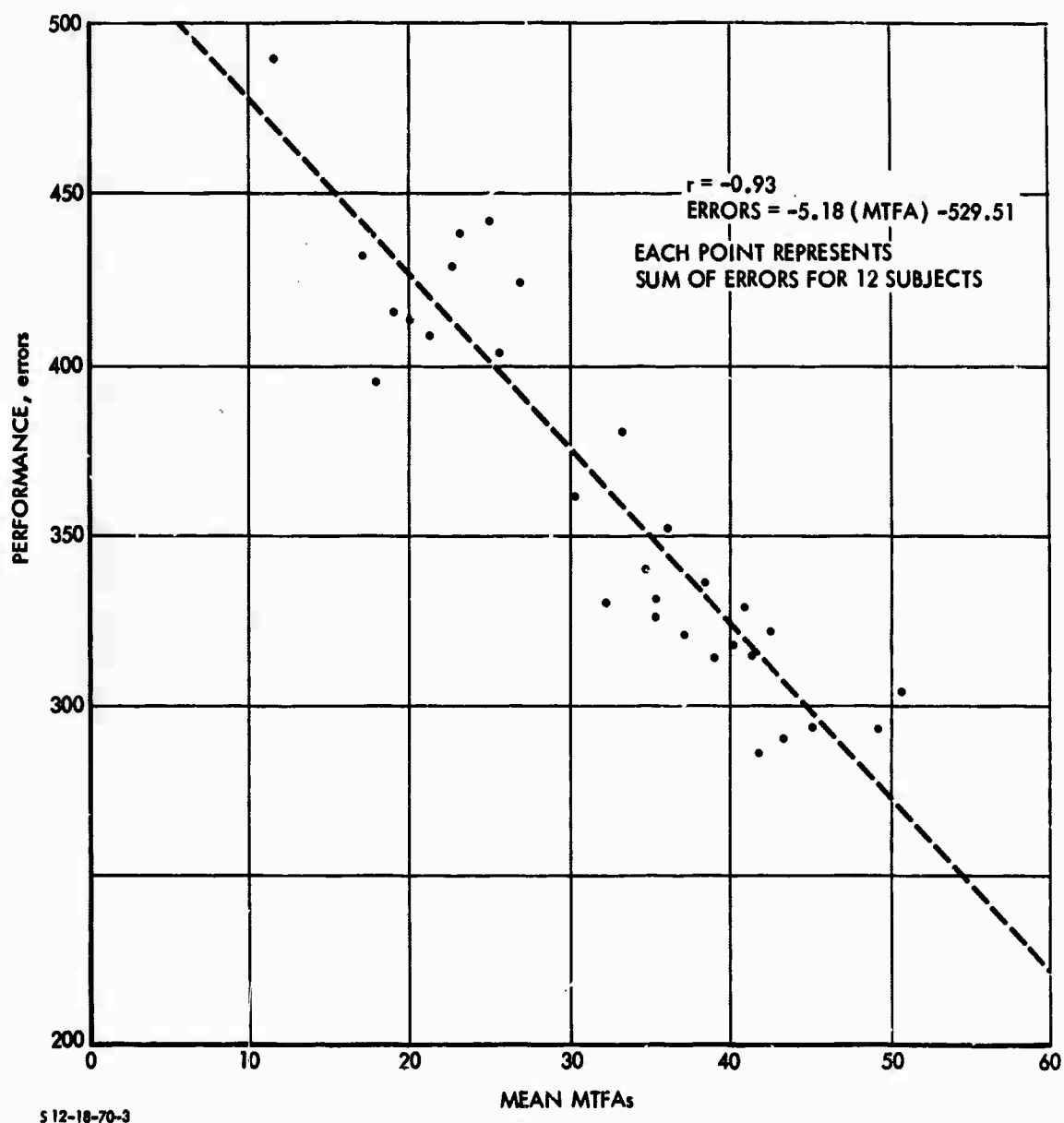


FIGURE 2. Scattergram of Information Extraction Performance Versus MTFA

From an understanding of the MTFA work reported later in Part II and the analysis of component performance in Part V it has been possible to show that the same criteria apply broadly to low-light-level systems, but there are important, if not obvious, differences.

Let it be emphasized, however, that television imagery differs distinctly from photographic imagery in two ways, both of which must be considered with care. First, both photographs and television displays have noise, but not the same kind. Photographs have a "frozen noise" called "grain," whereas television displays have a "dynamic noise" called "snow." Second, most common television displays have a line structure, made up of "raster lines," clearly and sharply evident. Photographs lack such line structure.

Raster lines interfere with viewing in the same manner and from the same approximate cause that the 10-kHz interference whistle in a superheterodyne receiver can interfere with hearing weak signals. Optically, this form of heterodyning is undesirable. It is permitted only because most people do not realize its degrading effect on image quality or because they actually believe sharp raster lines indicate a sharply tuned or focused receiver. This popular belief is very wrong. At normal picture brightness and viewing distance, the line structure of a good television display should be invisible to the eye, or nearly so.

The technology of achieving line rasters without prominent lines has been understood since at least 1934, when Mertz and Gray published their first analysis of the problem. In 1953, Otto Schade quantitatively described the degradation, the acceptable levels of interference, and the means to reduce the raster interference. A review of these raster problems and their effects on image quality appears in the second article in Part II.

### C. LOW-LIGHT-LEVEL PERFORMANCE OF VISUAL SYSTEMS

Any analysis or performance estimate of electrooptical imaging systems is incomplete without an analysis of the sensor performance and a corresponding analysis of the output of that sensor convolved with the input properties of the observer's eye.

The eye is probably the most versatile of all sensors. It functions well when the ambient illumination is as high as  $10^4$  footcandles or as low as  $10^{-2}$  footcandles, and it continues to function, but more slowly and not as well, as the light level is further lowered by more than two orders of magnitude. The eye-brain receptor system adapts to a reduction in light level by one or more of the following mechanisms: enlarging the pupil; integrating the light signal over larger areas (decreasing resolution to permit increased sensitivity); increasing sensitivity by switching from high-resolution, color-sensitive sensors (the cones) to high-sensitivity, lower-resolution sensors (the rods); and increasing the integration time.

At the lower light levels, the ability of the eye to see small, dim objects can be improved if the objects are magnified at the equivalent low brightness. Though this seems sophomoric philosophy, it is quite realistic and is accomplished by using binoculars (night glasses). Typically, a 7 x 50 binocular magnifies the image on the retina by a factor of 7 and thus increases the image area by a factor of 49. At the same time, the diameter of the binocular entrance pupils is 50 mm and that of the dark-adapted eye is about 7 mm. The  $(50/7)^2 \approx 49$  increase in collecting aperture just offsets the increase of 49 in image area. Thus, a sevenfold magnification at equal brightness occurs and makes visible an object that was previously invisible because of its smallness and dimness. Increase in image size at no increase in brightness makes the object visible. Actually, the magnified image is slightly less bright than the unmagnified object seen directly. This decrease in brightness is quite small and is due to the small losses in the lenses and prisms of the binoculars.

The use of binoculars trades magnification for field of view. As magnifications get larger, the corresponding fields of view get smaller. The field of view of 7 x 50 binoculars is typically about 7 deg. Greater magnification would linearly reduce the field; less magnification would increase it. The utility of binoculars as a night-vision aid is tied tightly to magnification and therefore to field of view.

Some electrooptical devices, such as image intensifiers, are light amplifiers. One can design image-intensifier optical devices with a degree of freedom over and above the binocular concept of aids to night vision. One can now choose a field of view and a brightness gain independently within rather broad limits. Further, because of their capacity to amplify light greatly, image intensifiers (or low-light-level television camera tubes) make night vision possible under conditions of much lower flux and much greater distance than binoculars.

The incorporation of image-intensifying devices in visual systems permits the manipulation of design parameters with far greater flexibility than binoculars allow. Image-intensifier night-vision systems incorporate (1) an objective for collecting and focusing the radiant flux emanating from the scene onto a fiber-optic faceplate (the first surface of an image intensifier tube), (2) an image-intensifier tube (at the present time usually containing three stages of intensification), and (3) an eyepiece presenting an enlarged virtual image of the intensifier display. Low-light-level television systems incorporate the following: an objective; a cascaded intensifier and camera tube combination comprising one or more intensifier modules, a camera tube and fiber-optic couplers; a video signal amplifier, and a monitor containing a kinescope for displaying a real image for viewing. The incorporation of image-intensifier devices in visual systems has the effect of decoupling the input and output radiant fluxes, removing some of the optical constraints encountered in binocular systems, and permits: (1) the utilization of radiant flux outside the visible spectrum and generally the use of more efficient image sensors than the eye, (2) independent adjustments of subjective magnification and flux collection

power, (3) the use of integration times longer than that of the eye, (4) independence of the time required for dark adaptation (dark adaptation is not required) and (5) the independent choice of optimum image brightness for high visual acuity and freedom from eyestrain. In addition, such systems may provide greater flexibility of viewing by incorporating remotely placed television displays.

In image-intensifier systems the quantum efficiency of the cathodes is now perhaps 10 percent, so that of every ten arriving photons only one liberates a photoelectron to undergo the amplification process. The amplification takes place in one of two ways:

1. The photoelectron is accelerated through perhaps a 10-kv field and focused upon a phosphor that is covered by a thin aluminum film. Transit through the aluminum film reduces the electron energy by nearly half, leaving about 5000 electron volts to be transferred to a phosphor grain. This transfer of energy results in a large number of 0.5-ev photons. Of these 10,000 potentially liberated photons, perhaps half are trapped within the phosphor layer and end up as heat rather than light.

Of the 5000 photons that are generated, perhaps twenty percent are liberated in a direction in which an optical system can collect and focus them. Thus, about 1000 useful photons are formed for each photoelectron liberated by the photocathode. A gain of about 1000 per photoelectron thus occurs after the photocathode, but the photocathode has only about 10 percent efficiency, and so the overall gain of such a device is perhaps 100 per stage of intensification.

2. The second form of intensification results from a photocathode converting photons into electrons and achieving gain by accelerating the photoelectrons a small amount, causing them to collide with a secondary-electron emitter. This process, repeated many times, multiplies the number of

electrons rather than the energy of the electrons, giving a high exponential gain. The electrons are finally focused onto a phosphor for reconversion to light.

Both of the processes described above start by reducing the number of photons comprising the image. This sampling process is followed by a high-gain process which now creates a bright spot or scintillation for each photoelectron generated at the cathode.

Let us look at an extreme case; an image with  $10^6$  distributed photons focused on a cathode with  $10^{-6}$  quantum efficiency, followed by  $10^6$  gain. There will be  $10^6$  photons in and  $10^6$  photons out. But, the output photons will all be in one bright scintillation and all phase information (that is, the information about the original distribution of photons that made up the light and shadow of the image) is lost.

Figure 3 shows a series of photographs made by George Morton to show image quality as a function of the number of photons comprising the image.

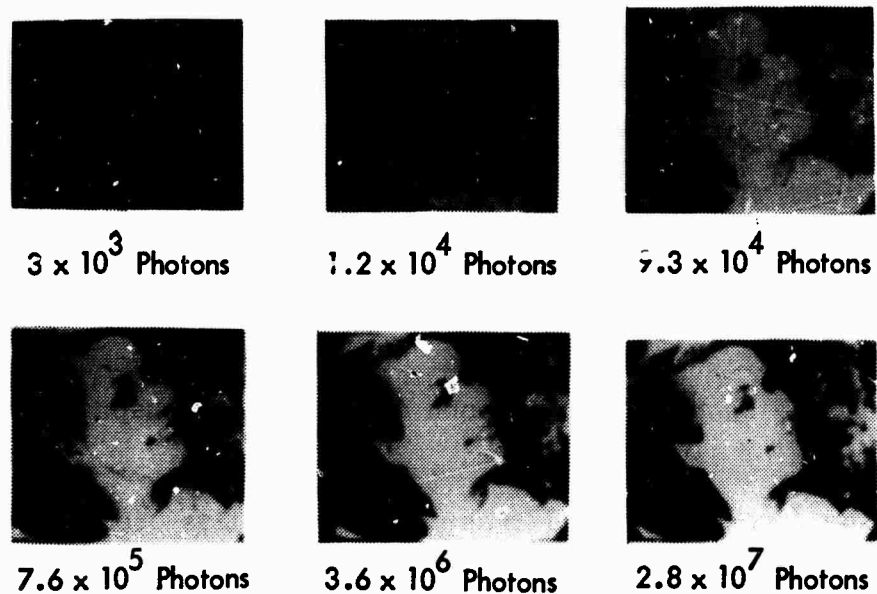


**FIGURE 3. Images Formed by Scintillations. Series of Photographs Showing the Quality of Pictures Obtained with various Numbers of Photons (or Photoelectrons when the Quantum Efficiency is Less than Unity)**

If one uses an image intensifier on the very dim images, i.e., the ones with few photons, one merely gets an image in which the individual scintillations are brighter. Since the sampling of the scene is not significantly improved, the quality (salt and pepper effect) remains the same.

To improve quality one must improve the sampling by increasing the collection of photons by the optical system (larger lenses or mirrors), by increasing the photon collection rate or the efficiency of conversion, or, if the rate cannot be improved, increasing the time. In any case, more input photoelectrons--not more gain--are needed for an image that can be intensified successfully.

It can be seen that gain alone is a poor criterion for performance of image intensifiers.\*

In image-intensifier systems, if sufficient gain is provided, the appearance of a scintillation on the display will educe a visual sensation in the retina. Hence, the quantum efficiency of a visual system incorporating an image intensifier is characteristic of the quantum efficiency of the image-sensing surface of the intensifier.

If the duration of a scintillation produced on the display of an image intensifier is considerably longer than the integration time of the eye, the effective integration time of the complete visual system is characteristic of the integration time of the intensifier. Generally, however, image intensifiers are designed with integration times comparable to that of the eye to avoid loss of visual perception for moving targets.

If the luminance gain of an image intensifier is high enough, the eye will exhibit the high visual acuity and speed of response characteristic of foveal vision even though the scene luminance (as

---

\* It is therefore very important that the more significant factors in low-light-level technology be emphasized in the detail writing of specifications and in procurement negotiations. The present overwhelming fascination with gain should not continue.

seen by the unaided eye) may be as low as  $10^{-5}$  cd/m<sup>2</sup>, corresponding to terrain illuminated by an overcast night. However, it must be emphasized that the structure of an image formed on the retina by an image-intensifier system directed at a dimly illuminated nighttime scene will generally be quite different (coarser grained and scintillating) than the structure of an image of the same luminance produced by a binocular system or the unaided eye. In the case of the intensified image, visual acuity will be limited by fluctuations in the generation of the scintillations forming the image rather than by the properties of the eye.

Remote-view television systems for low-light-level applications offer some additional degrees of design flexibility not available to direct-view image-intensifier systems. Besides the possibility of separating the position of the image sensor from the image display, there is the possibility of enhancing contrast and modifying the image in other ways by means of associated video processing.

These additional degrees of design flexibility in remote-view television systems result from the incorporation of an additional conversion of the two-dimensional electron image generated at the primary photocathode into a video signal current by means of sequential readout of the image elements of the electron image on the camera-tube charge storage target. The conversion of the electron image into a video signal may introduce a limit on sensitivity not associated with the parameters of the eye. The noise generated in the first stage of the video preamplifier will determine the minimum detectable signal current unless there is sufficient electron multiplication of photoelectrons generated at the primary photocathode before video signal injection into the video amplifier. In practice, it has been found that an electron multiplication of about  $10^4$  is required. Electron multiplication may be achieved with image-intensifier modules and/or internal electron multiplication by means of electron bombardment of the storage target.



The gain provided before storage of charge at the "charge storage target" occurs as a low-frequency gain between cathode and target with a relatively narrow bandwidth corresponding roughly to the frame of time of the system.

Video preamplifiers, on the other hand, operate at frequencies corresponding to the comparatively wide band and high frequency of the readout beam--5-50 MHz. Thus, the most useful gain is that associated with the low-noise amplification processes before readout. These are low-noise processes due in no small part to their narrow-band, low-frequency character.

If sufficient electron multiplication is provided, the video current will consist of a coarse-grained signal current of large pulses and a fine-grained noise current. The luminous image formed on the display by conversion of the video current will consist of bright scintillations forming the image and a dim background randomly generated by the video noise current. Under these conditions the quantum efficiency of the total visual system comprising the remote-view television system and the operator will be characteristic of the primary photocathode. As in direct-view image-intensifier systems, threshold sensitivity and integration time will be, to a reasonable extent, at the disposal of the designer, subject to whatever restrictions are imposed by operational requirements, size, weight, and cost.

The same flexibility in design of subjective magnification and radiant-flux collection power exists in remote-view television systems as in direct-view image-intensifier systems. The subjective magnification is not so rigidly specified, however. The difference lies in the fact that the magnification between the display and the observer's retina depends on the viewing distance, which may not be rigidly controlled.

In the process of detecting the input image, converting it to electrons, focusing it onto the phosphor, and recreating a visible image, contrast is lost at each step for the reason that aberrations cause an overlapping of the radiance pattern on the display produced

by the input-image irradiance pattern. In the limit of small image-element sizes, as contrast falls below a few percent, detection probability approaches zero.

Rather than reproduction of contrast on the display as a function of image-element size, it is customary to consider the reproduction of the modulation amplitude of a sinusoidal, spatially modulated, radiant test pattern as a function of spatial frequency. The relation between contrast and modulation amplitude is described below. The modulation transfer function (MTF) or sine-wave response of a photoelectronic imaging (PEI) system is defined as the ratio of the modulation amplitude of the display image to the modulation amplitude of the input image on the photocathode as a function of spatial frequency--normalized to unity as the frequency approaches zero. The sine-wave response can be measured by projecting a sine-wave pattern with 100 percent modulation onto the photocathode. First a sine-wave pattern of low spatial frequency is employed and the peak-to-peak output amplitude is noted. With this amplitude as a reference, the pattern spatial frequency is increased in discrete steps. At each step the new peak-to-peak amplitude is measured, and the ratio of this amplitude to that measured at the low spatial frequency is formed. The plot of these amplitude ratios as a function of pattern spatial frequency constitutes the sine-wave response.

The case of a zoom intensifier merits special attention. If the zoom-intensifier sine-wave response were unity at all spatial frequencies, resolution would be unlimited in both wide-angle and narrow-angle modes. Since the wide-angle mode also covers more view-field as well, there would be little point to zoom. As a practical matter, the intensifier's sine-wave response is limited by aberrations in the electron optics and the phosphor particle sizes. As the view-field is decreased, or zoomed, going from the wide- to the narrow-angle modes, image magnification increases in the same ratio. Consequently, the spatial frequency scale of the sine-wave response curve is compressed by that ratio. Specifically, for an 80/25 mm zoom tube, the

magnification increases from approximately  $1/3$  to unity as the view-field is decreased and the spatial frequency of the wide-angle mode is reduced in the narrow-field mode by approximately three, and the higher amplitude response associated with lower frequencies pertains. Thus, some of the higher sine-wave response at a given target spatial frequency in the narrow-angle mode is sacrificed in the wide-angle mode for the sake of wider viewfield. On the other hand, greater brightness gain is realized in the wide-field mode, and if sufficient brightness gain is not otherwise provided, the wide-field mode may provide some improvement in performance.

For evaluation of the overall performance of a complete visual system comprising both the operator and the PEI system, it is necessary to consider the spatial frequency response of the eye and the magnification between the PEI display and the retina.

The modulation required by the eye to detect a sine-wave-modulated luminance pattern depends on both the optical parameters of the eye and the organization of the neurological centers of the retina. Both are functions of the luminance level on the display. The required modulation will also depend on fluctuations in the luminance of the display.

If the required modulation is plotted as a function of spatial frequency on the display, the frequency scale will depend on the distance from the eye to the display of a television monitor or the subjective magnification of an eyepiece.

The required modulation as a function of frequency in cycles per inch, calculated from retinal modulation sensitivity curves published by A. van Meeteren, reveals that low values of display luminance have a dramatic effect on the required modulation function.

It is important in the design of both remote-view television and direct-view image-intensifier systems to present the output image to the eye at sufficient luminance and angular size so that required modulation is not determined by the optical properties of the eye and the neurological organization of the retina but rather by the fundamental effects of output luminous fluctuations on the decision process.

It has been determined empirically (first article in Part II) that excellent correlation exists between the subjective quality of aerial photographs and the area (MTFA) bounded by the ordinate axis, the modulation of the photographic image, and the required modulation function of the eye. The rationale for the choice of the MTFA as an overall measure of picture quality and observer performance is based on the observation that easy detection of a particular spatial frequency requires that the modulation should be as high (conspicuous) above that required by the eye as possible. In aerial photographs, generally all spatial frequencies are of interest. Hence, the MTFA was proposed as an overall measure of observer performance and picture quality. In visual observation of photographs, the modulation required by the eye at low spatial frequencies depends on the properties of the visual system. At higher spatial frequencies, fluctuations in grain size set the requirement and cause the required modulation to rise.

In the case of low image input irradiances to low-light-level electrooptical systems, a rise in required modulation with increasing frequency is observed, which is due to fluctuations in the output luminance produced by scintillations on the display.

The probability of correctly identifying a known signal in the presence of noise is a function of the signal-to-noise ratio.

For a given input-image element size and sampling time, the signal-to-noise ratio of the output image is determined by four properties of the system:

1. The size of the entrance pupil of the objective.
2. The quantum efficiency of the photocathode.
3. The internal generation of noise such as shot noise in thermionic current, Johnson noise in the input resistor of the video amplifier, and fluctuations in electron multiplication processes.

4. The degree to which the input image can be reproduced on the display without overlap of the luminance of adjacent image elements, i.e., the frequency or sine-wave response.

In image-intensifier tubes, thermionic current and fluctuations in electron multiplication are generally negligible compared to the shot noise of the photocathode current. In low-light-level television systems, if high intensifier gain is provided, the video amplifier output current consists of a coarse-grained current of large pulses and a fine-grained noise current.

If it is anticipated that a system will be used for detection of images of all sizes on the display, then the overall performance of a system and an observer will depend on the signal-to-noise ratio at the display at all frequencies weighted equally.

Besides the combined system and observer performance, it is useful to specify a measure of performance of the system without reference to the eye. Such a measure is the signal-to-noise ratio of the image on the display. The definition of detection efficiency for infrared point detectors can be logically extended to imaging systems by utilizing the image signal-to-noise ratio.

#### D. IMAGE-INTENSIFIER TUBE STRUCTURES

Night-vision systems incorporate a variety of image-intensifier devices, often in combinations, designed to meet various operational conditions and military requirements. The physical electronic functions performed in image intensifiers include (1) conversion of the radiant image formed on the image sensor surface into an electron image, (2) intensification of the electron image, and (3) conversion of the intensified electron image formed on the display surface into a visual image.

In addition to brightness gain, image intensifiers can be used to provide viewfield zoom by simple electronic means. They are also simply coupled to television pickup tubes to increase the sensitivity of low-light-level television systems.

The most common intensifier module sizes are 16/16, 18/18, 25/25, 40/18, 40/25, 40/40, 80/25, and 80/40 mm, where the first number refers to the photocathode diameter and the last refers to the phosphor diameter. The approximate dimensions are given in the table below. These sizes vary considerably from manufacturer to manufacturer but may be thought of as representative.

TYPICAL INTENSIFIER DIMENSIONS

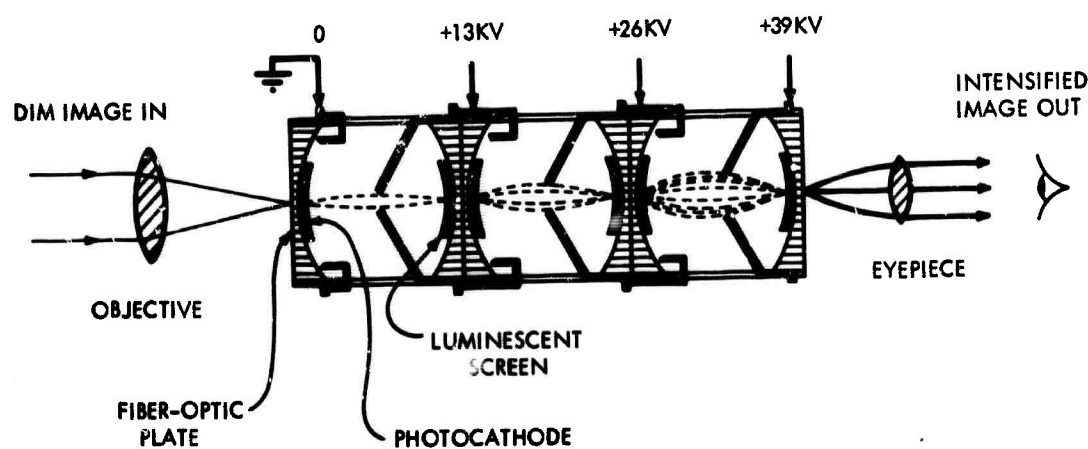
<u>Photocathode/Phosphor Diameter, mm</u>	<u>Zoom Range</u>	<u>Length, in.</u>	<u>Diameter,* in.</u>
16/16	1:1	1.65	1.16
18/18	1:1	2.0	1.35
25/25	1:1	2.4	2.0
40/25	1:1	5.4	4.0
40/40	1:1	3.7	3.0
60/18	3:1	6.0	3.7
80/25	3:1	8.0	6.0
80/40	3:1	8.0	6.0

\*Exclusive of high-voltage insulation

A typical three-stage, modular cascade image-intensifier tube is shown in Fig. 4. The three modules are mechanically and optically coupled together and completely encapsulated with the voltage-multiplier sections of the high-voltage power supply. Electrostatic focusing with approximately unity magnification is employed in each module. Image inversion, occurring in each of the electrostatically focused modules, is canceled by image inversion in the objective of complete visual systems. Cascade image-intensifier tubes are generally made in three standard sizes: one with an 18-mm cathode, one with a 25-mm cathode, and one with a 40-mm cathode.

Development of microchannel-plate secondary-electron-multiplier arrays, capable of producing images of moderate resolution, aroused interest in the possibility of a simple, single-stage, high-gain

image-intensifier tube replacement of the three-stage, modular, cascade image intensifier. It was anticipated that the microchannel intensifiers would offer the advantages not only of smaller size, lighter weight, and lower cost but also better performance (i.e., higher target detection probability due to better spatial frequency response). However, performance to date generally has been considerably less than initially anticipated due to a number of problems peculiar to these devices that have arisen during their development.



53-17-71-11

**FIGURE 4. Schematic Diagram of Modular Cascade Image Intensifier**

The microchannel-plate image-intensifier tube multiplies the number rather than the energy of photoelectrons. It consists of a fiberoptic faceplate, on the back side of which is formed a photocathode, a microchannel-plate secondary-electron multiplier, and a second fiberoptic faceplate, on the front side of which is formed a phosphor screen with the usual aluminum film required to prevent light feedback to the photocathode.

Outgassing by the microchannel plate has the adverse effect of reducing the lifetimes of both the photocathode emission and secondary electron multiplication and yields high ion noise.

The failure of the spatial frequency response function of microchannel-plate image intensifiers to live up to earlier expectations is due to a number of factors, including the use of proximity focusing between the microchannel and phosphor screen, the relatively high applied potential between the microchannel plate and phosphor screen required for efficient electron-to-luminant-image conversion in the phosphor, and the relatively high transverse energies of the secondary electrons emerging from the channels of the microchannel plate.

A more fundamental limitation on frequency response stems from the mosaic structure of the microchannel plate. This limitation depends on the relative spatial phase of the regular array of channels and the periodic test pattern used to measure the frequency response.

Image signal-to-noise ratio reduction occurs in microchannel-plate image intensifiers due to a number of factors in addition to those common to all intensifier systems. First, some of the photoelectric current generated by the input irradiance on the photocathode is lost at the input to the microchannel plate. Second, the secondary-electron multiplication process in the channels introduces fluctuations in the number of output secondary electrons in the output pulses. Fluctuations in the output pulse heights are due to fluctuations in the secondary emission yield, fluctuation in secondary electron escape energy, and fluctuations in escape direction.

Other sources of noise are local variations in the emission properties of channel walls, ionic feedback due to outgassing from the glass surfaces, and electrons either reflected or emitted from the front electrode of the microchannel plate.

The magnitude of the signal-to-noise ratio reduction in microchannel-plate image intensifiers due to each of the above factors is difficult to measure. Wide variations are observed from one tube to another. Efforts to determine the fluctuations in the electron multiplication process often have been masked by the overwhelming effects of ionic feedback noise. Typical values of signal-to-noise ratio reduction are not yet available.



Manufacturers' performance data for representative single-stage and three-stage cascade image-intensifier tubes are presented in this report (Part IV, Tables IV-2 through IV-10). In our report, and in those we recommend, performance data, depending on input radiation, are reported in radiometric units. The use of photometric units based on the lumen, which by definition implicitly depends on the spectral responsivity of the eye, as a measure of input radiation to a physical detector is to be discouraged. Further, Tables IV-2 through IV-10 show:

1. Photocathode responsivity specified in milliamperes per watt of input radiation from a  $2854^{\circ}\text{K}$  tungsten source.
2. Gain specified as the ratio of output luminance in foot-lamberts to input irradiation in watts per square meter from a  $2854^{\circ}\text{K}$  source.
3. Equivalent background input defined as the irradiance of the input face required from a  $2854^{\circ}\text{K}$  source to produce an additional output luminance equal to the mean background luminance existing when the primary photocathode is masked.
4. The modulation transfer function, synonymous with spatial frequency response or sine-wave response measured with a sine-wave test pattern. In some cases the available data are for response to a bar-pattern or square-wave modulated test pattern.

#### E. TELEVISION CAMERA TUBE PERFORMANCE AND DATA

New and different types of television camera tubes are becoming available at an ever increasing rate. While these new sensors must inevitably lead to improved imaging systems, the process of sensor selection becomes more demanding and, should the traditional methods of comparative laboratory evaluation be followed, costs will become prohibitive to all but the largest laboratories. To evaluate a single new developmental sensor can often require an investment of tens of

thousands of dollars and many months of time, and there is no assurance that the results of measurements of a single sample will be representative.

In many cases, however, the need for competitive evaluation can be greatly reduced by use of analytical performance prediction methods. These methods have been developed recently to the point where the computed performance of a sensor such as a television camera tube is found to be in good, if not perfect, agreement with measured capability. Indeed, in most cases, the difference between computed and measured performance is less than the expected error in measurement. Significant differences, where they exist, are being rapidly resolved, but the results now being obtained are quite usable in their present form. This is particularly true in making sensor comparisons because, as far as is known, the calculations do not significantly favor one type of sensor over any other. The principal shortcomings of the analyses are: (1) they apply mainly to laboratory test charts or patterns which are one-dimensional in character; (2) the methods of describing image lag are quite primitive; and (3) other defects such as picture uniformity, graininess and blemishes, which are sometimes lumped into an elusive term called "picture quality," are largely undefined. Thus, while we can greatly narrow tube selection for any application analytically, laboratory evaluations cannot be eliminated completely.

The most useful concepts for judging camera-tube quality are the signal-to-noise ratio at the input to a display,  $SNR_D$ , and the lag. Both quantities are dependent upon signal level.  $SNR_D$  is not only dependent upon the level of the input signal but is also very much dependent upon the contrast and the size (spatial frequency) of the image at the system input.

Thus, one may very well choose a high-gain stack of many intensifiers followed by a garden variety of vidicon if one is looking for a large, high-contrast object and is not interested in surrounding detail or shape. On the other hand, if the light level and contrast

are moderate, an intensifier isocon will show great detail that the intensifier stack coupled to a vidicon should never be expected to show.

Performance of camera tubes can be measured. Actually, computations are probably much faster, more representative, and cheaper than one set of measurements on, say, a \$25,000 low-light-level camera tube assembly, and there is always the possibility that one tube may not be representative.

One should compute the performance over the range of light levels and over the range of image sizes for which a camera is desired. Computations for performance in moving scenes are less reliable but can be approximated.

Basically, the  $SNR_D$  criterion is a composite function that includes sensitivity to light level (the light transfer function) and sensitivity to target size (the aperture function or the modulation transfer function).

If one has to choose one of several camera tubes and wishes to make a spot choice, one should choose some object size or size range and determine whether that corresponds to 100 television lines per picture height, or 10, or 500. For the frequency of interest, say, 400 lines, one should determine the aperture response. This may be given as typically 15 percent or 50 percent of the low-frequency response (usually assumed 100 percent). One should then find the light transfer function for the light level of interest in nanoamperes. The product of the signal current and the aperture function for the light level and target size chosen is the best quick approximation to tube evaluation we know. To that evaluation should be added the lag data that must be determined from the signal current. The choice of the weighting factors to be applied to good lag versus good sensitivity is difficult and must ultimately be made on the basis of human factors. Fortunately, the best tubes tend to be best in both respects.

For more critical work, the computation of  $SNR_D$  is given in Part V of this report. Results are given over the entire span of useful

signal currents (and light levels) and over a wide range of object sizes (spatial frequencies).

This compilation is probably the most complete that is generally available.

#### F. COMPARISON OF LOW-LIGHT-LEVEL TELEVISION CAMERA TUBES

This report, and especially the material in Part V, deals with the better tubes but deals with the SEC tubes at greater length. By far the greatest number and the best in performance of current low-light-level television systems use SEC camera tubes.

It must be recognized that the better low light-level camera tubes available today are compromises. The SEC tube, with their low-capacity, high-gain targets, achieve a moderately good aperture function and a moderately good sensitivity at low light levels. The physical limitations imposed by the low capacitance of the SEC target and the broadness of the reading beam prevent SEC tube performance from increasing dramatically with increasing light levels.

The silicon-electron-bombardment induced-response (SEBIR)\* tubes are generally limited by beam width, beam impedance, and lateral charge diffusion in the target at localized high light levels for bright, small objects in an otherwise dark scene.

At low signal levels the remarkably high gain of an intensifier coupled to a silicon target tube yields the best resolution together with acceptable lag properties at low light levels, and fairly good resolution but increasing lag as the light levels decrease further.

At these very low levels there may be applications where only very low resolution is required. For such applications gain is the principal parameter, and the modulation transfer function, which falls

---

\* Or SiEBIR. Also variously known as the silicon diode array storage tube, the silicon intensifier tube (SIT) (RCA), the electron-bombarded silicon (EBS) tube (Westinghouse), and the intensified diode array camera (IDAC) tube (Army Electronics Command).

but very little at low spatial frequencies, is of little concern. A cheap, effective, but laggy camera for such very-low-level, very-low-resolution television could employ a standard vidicon with three intensifiers as preamplifiers.

At the extreme low light levels, one can decrease lag by the use of an additional intensifier. This further reduces resolution but can result in tolerable levels of lag. The principal disadvantage is the need for very high voltages to permit the application of about 20 kv per intensifier, i.e., about 60 kv for the preamplifier string!

As the light levels increase, little improvement occurs in the imagery of the multiple-intensifier vidicon camera. Though there is more than adequate signal, the cascading of the component MTFs is the primary limitation, resulting in very low image quality.

There is a trend in cheap cameras toward the use of channel-plate light amplifiers coupled to vidicons. Unfortunately, some designers believe that such cameras will yield better performance than the stack of three cascaded intensifiers and a vidicon. The use of a channel plate does make for much smaller size, and the overall lag of channel plate plus vidicon is similar to or slightly better than that of three cascaded intensifiers plus vidicon, but the cost is appreciably higher and the image quality is about the same.

No serious new designs for low-light-level image orthicon cameras have materialized in the past few years. The previous "Queen of the Studio" has been replaced by the Plumbicon<sup>®</sup> PbO vidicon in commercial broadcasting and by the SEC in airborne low-light-level television.

The offshoot of the image orthicon, the image isocon, has recently been simplified so that its improvements over the orthicon can be achieved with rather simple camera circuitry. Unfortunately, the timing of the isocon development was just too late for the commercial studio market and too late for the rush of camera designs for airborne low-light-level applications. Actually, at all but the lowest end of the light scale, the image isocon, with one additional stage of intensification for adequate gain, is about the best of the present

camera tubes. Its excellent electron optics make possible the best aperture function of any low-light-level tubes for light levels of, say, quarter moonlight or more. At lower light levels its performance decreases rather rapidly, but at more modest levels the tube can produce excellent imagery.

All television camera tubes can be permanently damaged if exposed to a sufficiently intense source of illumination for a long enough period of time. The problem is particularly severe for sensitive low-light-level television camera tubes. The very bright sources of illumination to which the tubes can be exposed in the real world represent even more of an extreme stress for them than for the less sensitive conventional pickup tubes.

Recent experiments, to be discussed below, have explored the threshold of permanent burn for a variety of low-light-level television camera tubes. The results of these experiments lead to the following conclusions:

- Despite the choice of the most unfavorable operating conditions (i.e., the use of a fixed photocathode voltage supplied by a low-impedance source), permanent burn did not occur until illuminations of  $10^4$  and  $10^{10}$  times higher than the normal operating ranges were reached.
- The cause of permanent burn in the SEBIR tube appears to be X rays produced by the impact of the photoelectrons on the silicon target.
- For illumination levels up to  $5 \times 10^3$  watts/m<sup>2</sup>, the recently developed burn-resistant SEC camera tube shows a permanent white burn threshold similar to that of the image orthicon and the SEBIR tube. The mesh-supported SEC target is 10 to 30 times more burn resistant than its predecessor.

In most camera-tube applications, the extreme conditions discussed here will not be encountered.

Image devices designed to operate under low-light-level conditions are not, in general, capable of imaging points of high intensity within a low-light-level scene without severe spreading of the point-source image into adjacent areas of the scene. This effect is often called blooming. Low-light-level television systems in use today are often of little use in night surveillance of objects in close proximity to bright man-made illumination sources. These point sources--ground fires, flares, and shipboard, aircraft, vehicle, or runway lights--often contribute a larger integrated flux level at the sensor than that contributed by the entire remainder of the scene while providing little appreciable illumination to the objects under surveillance. The flux emitted by such sources is diffused or spread by the atmosphere and the optics. The resulting photocurrent is, in turn, further spread by the electron optics and is scattered and spread at target material of the camera tubes. The result is a large signal spread over an area many times larger than the point source, obliterating detail over a significant portion of the picture.

These effects must be considered when tube specifications are written. Specifications that define the ratio of acceptable image growth for a given set of point-source-intensity conditions do not adequately reflect the physical characteristics of the SEBIR camera tube. The image diameter for at least three signal levels should be specified for a given input-image size and intensity several orders of magnitude above the saturation point.

The above type of specification may not be welcomed by all tube manufacturers. Depending on his application, a buyer may wish to relax the specification in some respects. However, this kind of specification\* takes into consideration all of the SEBIR characteristics and leaves no room for surprises upon receipt of the tubes. A specification of this kind must be flexible and must be tightened to reflect improvements in silicon diode array technology as they are made.

---

\* See Part VI for details.

## G. IMPORTANT TUBE PARAMETERS AND THEIR SPECIFICATION

Military applications of low-light-level television cameras are quite different from the commercial applications of studio television cameras in bright white light.

A meaningful specification must state the performance of a camera tube on the basis of signal-to-noise ratio at the display versus spatial frequency when the scene is flooded by irradiance of a known spectral composition, preferably similar to that in the environment in which the camera will be used. It makes no sense to calibrate a camera under visible light of some given spectral distribution and to expect the same performance under light of some other distribution, i.e., invisible (covert) irradiance.

Furthermore, we have shown that probability of detection is related to the signal-to-noise ratio as a function of spatial frequency at the display and is in general not determined by "limiting resolution."

If broadband spectral sensitivity is desired, and it is often useful for quality control or rough comparative calculations, one should specify the performance in terms of a source of known distribution and bandwidth, e.g., a 2854°K source between 0.6 and 0.95 microns. Such a specification permits comparison of tubes in a specific region of special interest.

The usual figures of microamperes per lumen used in commercial broadcast television specifications do not offer much help or guidance in evaluating tubes to operate under natural levels and distributions of light from the night sky.

"Sensitivity" and "resolution" must not be quoted as two independent parameters. Rather, one must specify SNR (preferably  $SNR_D$ ) as a function of resolution. As a lesser alternative, one could specify some other function such as resolution versus irradiation at a specified SNR. The actual data required are data of the form of Fig. 5.

Lag in some tubes for special purposes is an asset, but usually it is the chief demerit.



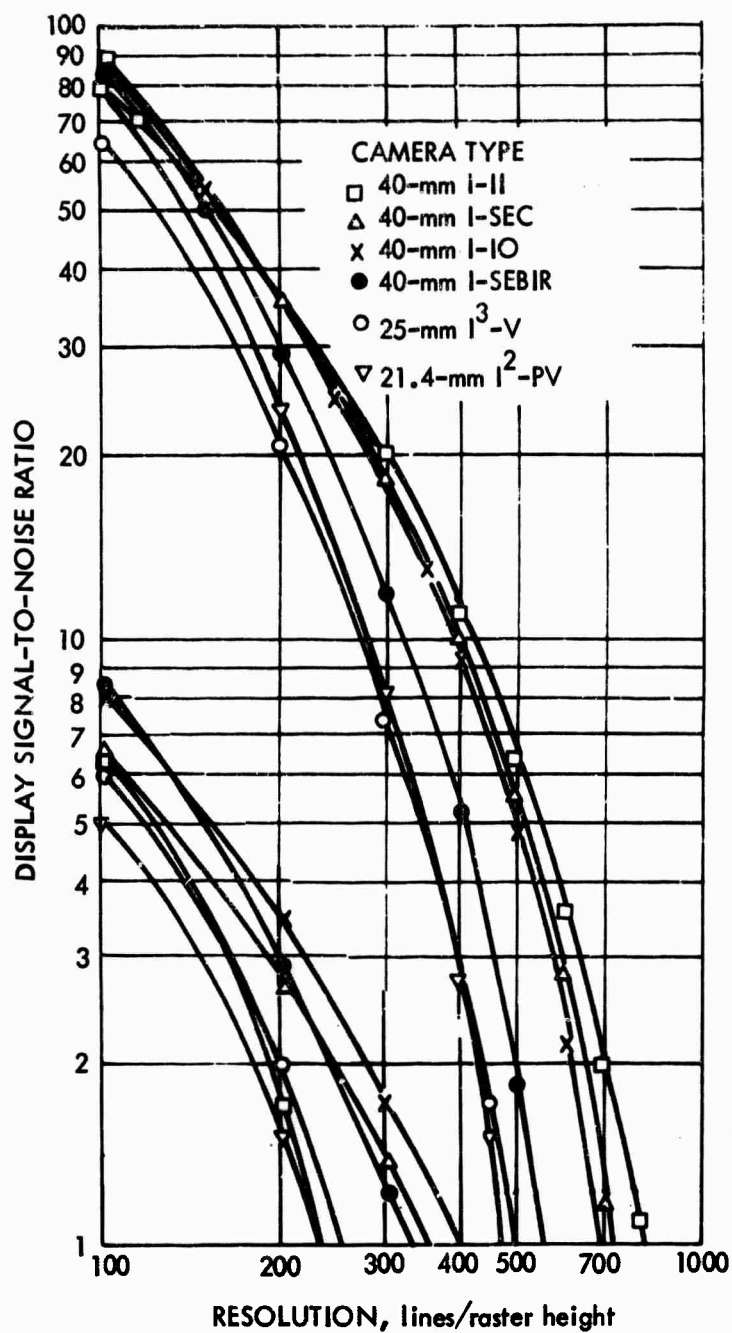


FIGURE 5. Comparison of  $SNR_D$  Versus Resolution for Various Low-Light-Level Cameras at Input Photocathode Currents of  $10^{-12}$  Amp (Curves at Left) and  $10^{-10}$  Amp (Curves at Right)

In addition to the performance of the sensor, one must treat with equal care most of the same topics discussed previously plus all the additional factors of a display that can seriously degrade image quality or perception.

Thus, we must specify for the display an adequate size, brightness, distortion, dynamic range, and freedom from banding, line jitter, crawl, and twinning.

In the recent past, procurement pressures have forced the bypassing of sound engineering specification and test. Demonstration prototypes are seen and liked, and production units are ordered, often as "Chinese copies." In a recent example, the prototype was assembled from 10 percent and 20 percent tolerance components--but these were selected and matched by the best technicians and engineers of the company in their model shop.

The production units were made to the same drawings but without notation about the selection and matching of components. Among other things, the bandwidth of the production units fell by a factor of 3 below that of the demonstration prototype. The manufacturer claimed truthfully that a specification for the selection and matching of components was not part of his contract, but he offered to include it for a substantial fee and to correct the production units to prototype performance. Once again, procurement failed for lack of the important parameters.

In haste for procurement, people have often written specifications that they could easily understand rather than the specifications that would govern the performance of the man-machine combination. The resulting equipment almost always met the specifications agreed to but performed poorly in operations.

## BIBLIOGRAPHY

- Aerospace Group, Hughes Aircraft Company, Airborne Sensor Display Requirements and Approaches, TM-888, G.K. Slocum, September 1967.
- Aerospace Group, Hughes Aircraft Company, The Design of Real Time Displays for Airborne Image Forming Sensors, G.K. Slocum, August 1970.
- Biberman, L.M., and Nudelman, S., eds., Photoelectronic Imaging Devices, Vol. I, Physical Processes and Methods of Analyses, Vol. II, Devices and Their Evaluation, Plenum Press, New York, 1971.
- Campbell, C.E., "The Optimization of Photographic Systems," Photogrammetric Engineering, pp. 446-455, July 1962.
- Coltman, J.W., "Scintillation Limitations to Resolving Power in Imaging Devices," J. Opt. Soc. Am., Vol. 44, No. 3, pp. 234-237, March 1954.
- Coltman, J.W., and Anderson, A.E., "Noise Limitations to Resolving Power in Electronic Imaging," Proc. IRE, Vol. 48, pp. 858-865, May 1960.
- Higgins, G.C., Lamberts, R.L., and Wolfe, R.N., "Validation of Sine-Wave Analysis for Photographic Systems," Optica Acta, Vol. 6, p. 271, 1959.
- Kazan, B., and Knoll, M., Electronic Image Storage, Academic Press, New York, 1968.
- McGee, J.D., et al., eds., Proceedings of the---Symposium on Photo-Electronic Image Devices, in Advances in Electronics and Electron Physics, Vols. XII (First, 1960), XVI (Second, 1962), 22A and 22B (Third, 1965), and 28A and 28B (Fourth, 1969), Academic Press, New York.
- Rose, A., "The Sensitivity Performance of the Human Eye on an Absolute Scale," J. Opt. Soc. Am., Vol. 38, No. 2, pp. 196-208, February 1948.

Schade, O.H., "Electro-Optical Characteristics of Television Systems,"  
RCA Review, Vol. 9, 1948:

- Part I. "Characteristics of Vision and Visual Systems,"  
p. 5, March.
- Part II. "Electro-Optical Specifications for Television  
Systems," p. 245, June.
- Part III. "Electro-Optical Characteristics of Camera Sys-  
tems," p. 490, September.
- Part IV. "Correlation and Evaluation of Electro-Optical  
Characteristics of Imaging Systems," p. 653.

Schade, O.H., Sr., "Image Gradation, Graininess and Sharpness in  
Television and Motion Picture Systems," J. Soc. Motion Picture  
Television Engrs:

- Part I. "Image Structure and Transfer Characteristics,"  
pp. 137-171, February 1951.
- Part II. "The Grain Structure of Motion Picture Images--  
An Analysis of Deviations and Fluctuations of  
the Sample Number," pp. 181-222, March 1952.
- Part III. "The Grain Structure of Television Images," pp.  
97-164, August 1953.
- Part IV, A&B. "Image Analysis in Photographic and Television  
Systems (Definition and Sharpness)," pp.  
593-617, November 1955.

Schade, O.H., Sr., "A New System of Measuring and Specifying Image  
Definition," National Bureau of Standards Circular 526, April  
29, 1954.

Schade, O.H., Sr., "Optical and Photoelectric Analog of the Eye,"  
J. Opt. Soc. Am., Vol. 46, No. 9, pp. 721-739, September 1956.

Schade, O.H., Sr., "An Evaluation of Photographic Image Quality and  
Resolving Power," J. Soc. Motion Picture Television Engrs., Vol.  
73, No. 2, pp. 81-119, February 1954.

Zworykin, V.K., and Morton, G.A., Television, 2nd edition, John Wiley  
and Sons, New York, 1954.

## I. INTRODUCTION

by Lucien M. Biberman

### A. PURPOSE

The purpose of this report is to present in orderly fashion the key factors in the design, analysis, and characterization of low-light-level devices. The parameters of interest are those that have the greatest effect on the transfer of information from the scene before the lens of the television camera to the human looking at the picture tube.

That a good picture is better than a bad picture is clear. What has not been so clear, even to the designers of most television systems, is how to decide whether the picture on the television screen is good or bad.

Designers of optical lenses and airborne cameras have given much thought to the question of how to predict whether their equipment designs will permit their clients to capture and see specified graphic detail. The need to meet contractual specifications for camera and lens performance has promoted a sharper understanding of the lens quality required to produce recognizable pictures of terrain from aircraft or earth satellites. Although questions of image quality, signal, and noise are still argued, the parameters are now so well known that a definite range of performance can be expected from photointerpreters working with imagery produced by lenses and cameras built to a given set of hard physical parameters.

Such predictability can not yet be ascribed to television or other low-light-level systems. It is time that such systems be measured quantitatively in terms of the performance they can yield to human viewers. In his review of this report, Otto Schade points out

quite correctly that the developers of lenses and films have accepted and used the sine-wave response from television systems engineering, whereas the developers of television have been slow to consider their images as two dimensional, like photographs.

This report expounds the principles that, the authors believe, govern low-light-level system performance. The authors hope that designers will adopt these principles and abandon the loose and useless ideas underlying the data that have so long been listed as performance parameters in manufacturers' literature and cataloging.

This is a report for designers who care.

## B. ORGANIZATION

In itemizing and discussing the principles and parameters that govern the operation of low-light-level devices for night vision, one must consider not only the adequacy of sensor parameters but also the visual task, the observer's platform (including its speed and distance from the target), and the a priori information that the observer brings with him to his task. Such task-related factors are in addition to the factors of contrast, motion, clutter, terrain obscuration, shadowing, and the level and quality of irradiance flooding the scene.

Two main sets of factors thus govern the performance of man and his low-light-level viewing aids. The first set is well understood and includes the physics of light, optics, solid state materials, and engineering approaches to the design of photoelectronic devices. The second set, relating the human observer to his task, is less well understood. It includes subjective matters as they are affected by the visual task, image quality, and time.

This report is not a treatise on the psychophysics of vision, but it does attempt to separate the visual processes and the performance of the human eye from the physics of image intensification and television.

After summarizing the early development of low-light-level devices, this Introduction (Part I) briefly reviews some of the subjective factors in visual performance that are of particular interest to designers of devices to aid man in detection, recognition, and identification. Part I concludes by examining specifications for low-light-level devices.

Part II discusses criteria for image quality.

Part III examines the human visual process and optical aids to that process under conditions of low illumination.

Part IV discusses the image intensifier as a device to aid vision at low light levels and lists the parameters of a variety of available image intensifiers.

Part V introduces television camera tubes and develops the concepts leading to  $SNR_D$ , Rosell's signal-to-noise ratio at the display. It is  $SNR_D$ , the authors believe, that is the most powerful means of evaluating "resolution," a term usually used loosely and incorrectly. In  $SNR_D$  one has a meaningful parameter by which to judge television camera tube performance. This is substantiated by a series of psychophysical experiments reported herein. For each tube type, Part V develops the equations to compute  $SNR_D$  and then graphically presents data for many useful parameters, including  $SNR_D$  and the specialized "limiting resolution" case of  $SNR_D$ .

Part VI compares camera tubes on the basis of lag and  $SNR_D$  and discusses adverse factors such as "burning" and "blooming."

Finally, Part VII sums up with some brief comments on important tube parameters and their specification.

### C. EARLY HISTORY OF THE DEVELOPMENT OF LOW-LIGHT-LEVEL TECHNOLOGY

Low-light-level technology had its beginning in the 1930's with the early concepts of image intensification, which were not basically different from those we hold today. Unfortunately, the early devices suffered badly from two major deficiencies, poor photocathodes and poor coupling. Between the low quantum yield of the then available photocathodes\* and the losses in coupling, the early image intensifier was a light amplifier whose net gain was less than one.

The development of both cathode and coupling technologies lifted the image intensifier from a not very practical concept to the useful device it now is. The two most important factors were the development of the trialkali cathode (S-20) and fiber optics coupling.

The material below is an abridged historical review of intensifier development supplied by George Morton.

The history of intensifiers cannot be divorced from the history of the signal generating or camera tube itself. Interest in this area began shortly after the formalization of electron optics in the 1920's. Much of this early work had as its ultimate objective the application of electron imaging to the problem of increasing the sensitivity of television camera tubes. The first published articles on image tubes appeared in the middle 1930's and included papers by Holts, deBoer, Teves and Veenemans (Ref. 1), Bruche and Shaffernicht (Ref. 2), Zworykin and Morton (Ref. 3), Heimann (Ref. 4), and others. The image tubes described were, in general, single stage converter tubes employing S-1 semitransparent cathodes. Their sensitivity to near infrared radiation was one of the features of interest at the time.

The concept of image intensification by cascading stages was suggested independently by a number of workers in the field during the same period. It is impossible to establish priority for the idea at this date. An early patent in this area was issued to Barthelemy and Leithine (Ref. 5) (31 August

---

\* Photocathodes will sometimes be called cathodes in the remainder of this report.



1936). This type of device is also described, not as original, in the book, "Electron Optics," by L. M. Meyers (1936) (Ref. 6). These intensifiers employed a phosphor screen closely coupled to a photocathode as the two-dimensional space current amplifier. However, at this time, the technology of photocathodes and phosphors had not developed to a point where image intensification could be achieved. The best cathode available was the Ag-O-Cs (S-1) photoemitter. Even if all the electrons from an S-1 cathode could be focused into the most efficient phosphor of that period, the amount of light generated would be less than the light on that cathode.

During World War II, a good deal of effort went into the development of image converter tubes for infrared imaging. In Great Britain, the work was directed toward proximity focused tubes, while in the United States (Ref. 7) and in Germany (Ref. 8), electrostatically focused image tubes were developed into practical production-type devices.

The period following World War II witnessed greatly accelerated research on image intensifiers. It was during this period that the cesium antimony cathode was developed by P. Goerlich (Ref. 9). This, together with advances in phosphors, made it possible to obtain a current gain with the combination of a fluorescent screen and photocathodes. Work had begun at RCA as early as 1941 on investigating the current gain that can be obtained with an intensifier screen consisting of a thin glass or mica supporting membrane coated on one side with a phosphor layer and on the other with a photocathode. The first practical image intensifier utilizing this principle was completed in 1949 (Ref. 10). In Germany, a similar development was reported in a review, "The Development of Infrared Techniques in Germany," by Krezik and Vand in 1946 (Ref. 8). The exact date and performance of this tube are not known, but it is believed that it was built by Schaffernicht.

Image brightness intensification by fractional magnification had been used even in the early infrared image tubes (Ref. 7). This principle was successfully applied to visible light image intensifiers to be used in fluoroscopic diagnosis by Westinghouse in the United States and by Philips in Holland.

Transmission secondary emission was made feasible for image intensification by the work of Sternglass

(Ref. 11) at Westinghouse who found that aluminum oxide supported potassium chloride layers would yield as many as 8 or 10 secondary electrons when bombarded with 6- to 8-kv primary electrons. Attempts to employ such films in a multi-stage intensifier were rather unsuccessful until about 1959 when Wilcock, at the Imperial College of London, succeeded in building spectacularly successful tubes. This brought this form of intensifier to a point where it was a fairly serious competitor for intensifiers using cascaded phosphor-photocathode screens.

A third type of intensifier which received a small amount of attention over most of this period and which recently has gained considerable prominence is the multichannel secondary emission intensifier now usually called the microchannel plate intensifier. Each picture element of this type of intensifier is a minute multi-stage secondary emission multiplier. The first experiments were low-resolution devices fabricated element by element using tubular multiplier structure. Work along these lines was done at RCA Laboratories, the Imperial College of London (Ref. 12), Chicago Midway Laboratories (Ref. 13) and other laboratories. This was followed by attempts to use registered plates of metal (dynode material) and insulator, with arrays of shaped holes, to give the dynode geometries. More recent work grew out of that by the Bendix Aviation group (Ref. 14) in the late 1950's.

Fiber optics is another development which has resulted in a considerable advance in the intensifier art. The development of fiber optics was contributed by a number of optical companies. The role played by the American Optical Company was a major one in the initial stages, and later Mosaic Fabrications continued this work.

Fiber-optic discs facilitate efficient optical coupling of intensifier tubes to other intensifiers or to camera tubes and permit construction of the modern modular cascade image intensifiers described in Ref. 15.

The development of low-light-level television as we know it today really began with the advent of the image orthicon tube in 1946. The orthicon became the "queen of the television studio" and was universally adopted for all quality programming. The usual practice in

studio lighting made the S-10 cathode quite suitable for orthicons and thus formed a basis upon which later technology could build.

The combination of the spectral response of the S-10 cathodes used in most orthicons designed for commercial television and studio lighting gave rise to an overall spectral response that was not too far different from that usually attributed to the photopic eye. Thus, technicians proceeded to use visual-response light meters with television tubes, although this was known to be improper theoretically.

The advent of better cathodes such as the modern S-20, S-20VR,\* S-25, and related surfaces has made such practices not only theoretically wrong but practically inappropriate, but then so are most of the commercially published specifications.

Manufacturers of television tubes (and also manufacturers of photographic films) are quick to point out that they use data measured with visual-response light meters for their own purposes in quality control and that it is not their fault if systems people misinterpret and misuse their data.

Figure I-1, taken from a manufacturer's pamphlet, has been crossed out as a warning not to use such a method of computation. It is wrong and very misleading.

The nomogram in Fig. I-1 has basic flaws and leads one astray for two reasons:

1. The chart is based upon  $2854^{\circ}\text{K}$  radiation, whereas  $3000^{\circ}$  to  $5000^{\circ}\text{K}$  indoors or  $2000^{\circ}$  to  $15,000^{\circ}\text{K}$  outdoors (Ref. 16) under conditions of starlight or north light in daytime can very well be representative of usual lighting.
2. The footcandle is a unit by which one judges human visual performance. It is normalized to the human eye and IS INDEPENDENT OF SPECTRAL DISTRIBUTION. This normalization

---

\* S-20VR is not a term of the Joint Electron Device Engineering Council (JEDEC) but is applied to the recent better cathodes by Varo, Inc., and others.

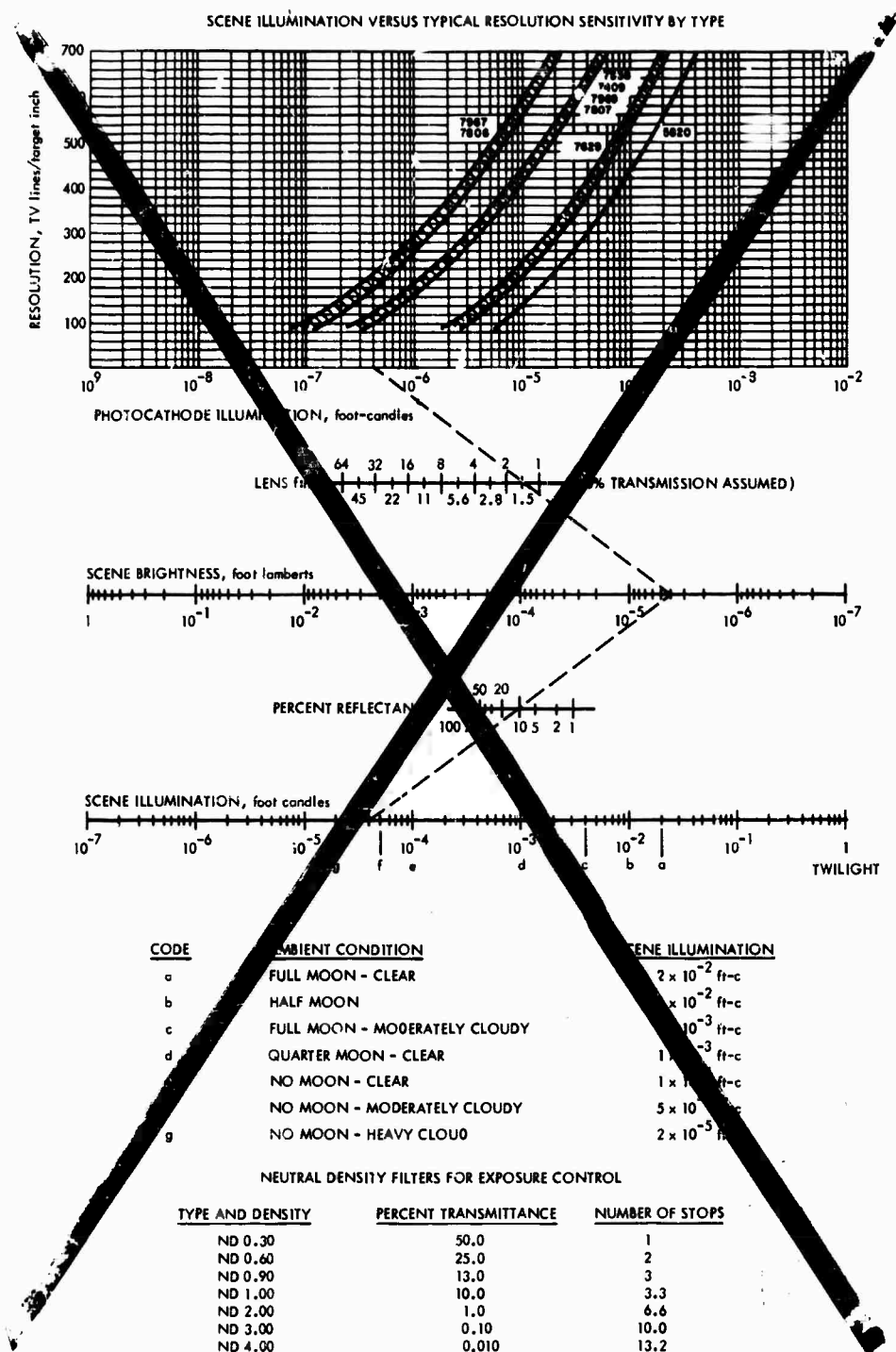


FIGURE I-1. Camera Tube Data Typical of Manufacturers' Literature

does not apply to camera tubes unless they are specifically normalized to the human visual response by the use of color filters, and very few camera tubes are.

Although the data in the nomogram of Fig. I-1 are based on 2854°K radiation, the table at the bottom of the figure definitely infers that it applies to sunlight or moonlight of a specified number of footcandles. THAT INFERENCE IS INVALID. Results calculated as these were are erroneous. One of the purposes of this report is to dispel the popular misconception that Fig. I-1 represents.

Until quite recently, very little engineering information on television camera tubes was available. About the best to be found was in the data sheets put out by General Electric. One could find in such sheets data on the "luminous sensitivity" or the signal current in amperes per lumen, and if one knew that what was meant was not really a lumen but rather the number of 2854°K watts of radiant power when an illuminometer registered one lumen, then one could, from the data shown on the relative spectral response, calculate the absolute response of the tube in question (Refs. 17, 18). From that, one could then go on to calculate such things as the limiting resolution for different levels of light and for different spectral distributions.

Certainly, the above is far different from the process indicated in the nomogram of Fig. I-1. After all these computations, however, one would know only the limiting resolution. Could one perhaps infer that one tube would produce a better picture than another if its limiting resolution were better than the other's? For seemingly identical tubes off the same production line that would probably be true, but for different types of tubes that would be a dangerous assumption--sometimes true, often not.

Thus it is clear that to use the nomogram one must know not only how many footcandles are involved but also what kind of footcandles they are (i.e., from what source) and what kind of cathode will sense

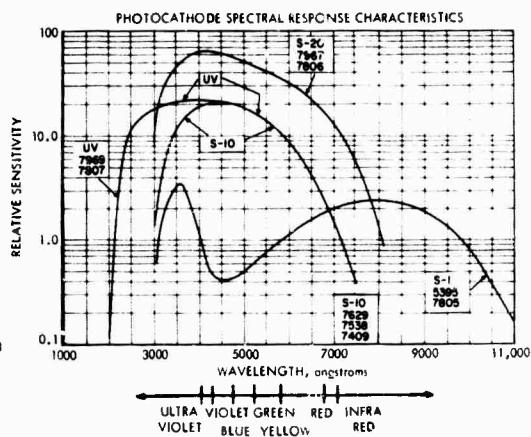
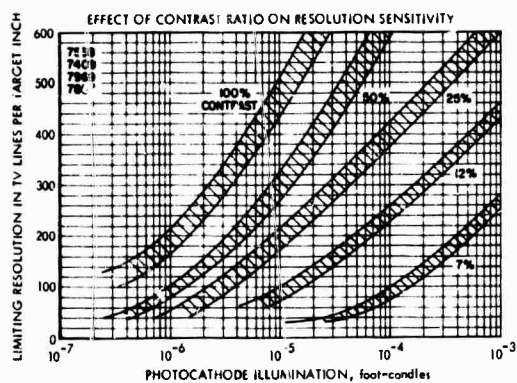
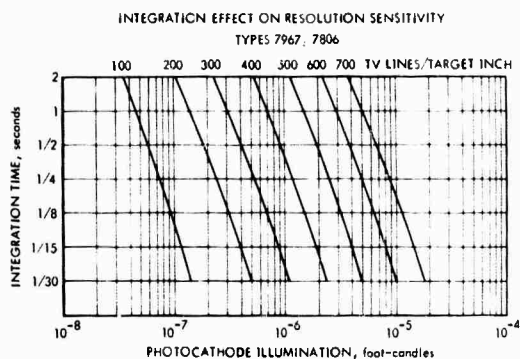
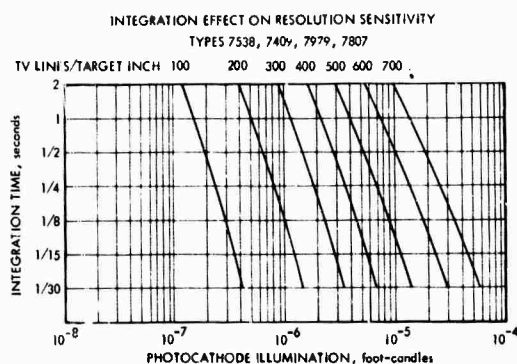
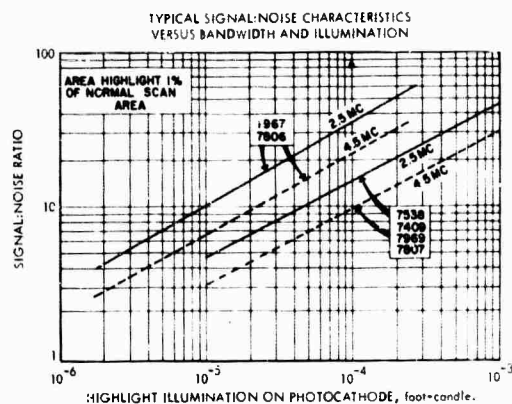
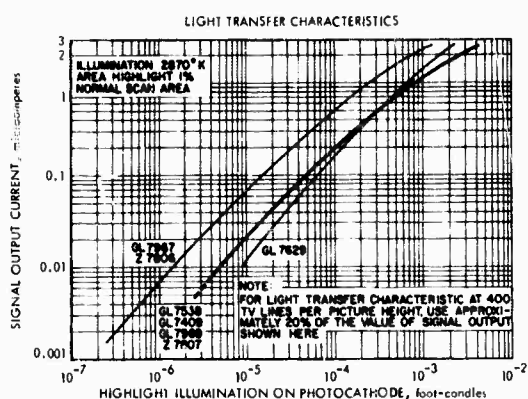
them. One must then perform all the necessary numerical integrations. The footcandle was conceived to make such calculations unnecessary in visual problems and to make the eye independent of the spectral composition of the illumination when measured in footcandles. The footcandle obviously does not fit television sensors. THE FOOTCANDLE SHOULD NOT BE USED IN SPECIFICATIONS OR COMPUTATIONS FOR THE DESIGN OR EVALUATION OF LOW-LIGHT-LEVEL DEVICES.

Figures I-1 and I-2 illustrate camera tube specifications of a reputable manufacturer. To the uninitiated they look technical, logical, and factual. The fact that they do not enable one to compute the probability of seeing a target (or even a bar chart) has not yet stopped the use of such inappropriate data as a basis for procurement.

The nomograph in Fig. I-1 is in fact erroneous and misleading because it allows one to use scene illumination without regard to color or color temperature, i.e., spectral distributions. The rest of the data, while factual, is logical and useful only to the tube manufacturer--not to the user.

In the preceding material, the inference is that manufacturers do not know better than to use footcandles and other photometric terms in describing electrooptical device performance. Though this may be partially true, it was encouraged by early military requests for comparisons to be made against unaided visual performance. The question was usually asked, "How well can I see with my eyes in varying degrees of darkness, and how well can your low-light-level television see?" Thus, the darkness was measured with a photometer to give a subjective measure, and this was propagated into military practice.

This history does not justify the present situation but does explain why it is difficult to eradicate or change. One should ask the same procurement or specification people how they specify the sensitivity of infrared mapping equipment, a FLIR, or a radar receiver--in lumens or watts? Low-light-level devices are primarily near-infrared devices--visual units and measures do not apply.



S 3-17-71-5

FIGURE I-2. Camera Tube Data Typical of Manufacturers' Literature

#### D. CRITERIA FOR SYSTEM QUALITY

There are currently three important classes of high-resolution night sensors:

1. Forward-looking infrared (FLIR)
2. Direct-view image intensifiers
3. Low-light-level television (LLTV)

Normally FLIR and LLTV devices use a picture tube display, while the direct-view image intensifier devices use an eyepiece focused on the intensifier phosphor.

Systems of all three classes, but principally FLIR and LLTV systems, suffer from the lack of a suitable output or display. This problem is most severe for FLIR and LLTV systems for two main reasons:

1. In many applications, it is difficult to find room for a display tube of adequate size, so that often the performance of the entire sensor system is compromised because its display tube presents a picture too small to permit visibility of the detail that is present. The directly viewed image intensifier device presents a "virtual" image that appears large and thus permits detail present on the phosphor to be seen by the observer.
2. The television raster, with its line structure, tends to bother the observer when he is looking for details that approximate the dimensions of the raster structure. Directly viewed devices do not generate rasters, and the corresponding problem due to the fiber optics pattern or phosphor grain does not occur until much higher levels of spatial frequency (resolution) are considered.

Images of rectangular objects parallel to the raster lines tend to lose their horizontal boundaries (but not their vertical boundaries) because they blend with the raster lines. Ohmart (Ref. 19) has shown that this effect increases the required search time for such objects



by a very significant amount. The general case of image reproduction by a line raster process is discussed in the second article in Part II.

The problem of display size has long been understood. Steedman and Baker (Ref. 20) analyzed it long ago, but their work has been ignored because their data complicate the problem of systems design. More of the early airborne systems were deficient because of inadequate display size than for almost any other reason.

One early LLLTV device for a helicopter was judged to have resolution too poor for operational use. That was true, but the deficiency was due neither to the camera nor to the display. The 8-in. display was good enough and big enough for the quality of the camera used. To maintain the status quo in the cockpit, however, the display had been mounted on the deck next to the pilot's left ankle. At that distance, the television screen, as seen by the pilot's eyes, had insufficient resolution. An eyepiece focused on a 1-in. display tube would have given the pilot an apparent image about 20 in. in diameter and about 20 in. away--an image about ten times as large. Thus, the pilot would have had a tenfold improvement in his visual ability.

But eyepieces--even those with rubber eye cups and forehead braces--are less than enthusiastically received by aircrews. Thus one gets good display quality with uncomfortable and unloved eyepieces, or one gets compact display tubes that are far too small to permit recognition of the detail that the sensors are designed to produce. As a result, there are some fine systems under design or in production that overmatch the human eye by factors of 4 to 10. That is, the detail displayed by the sensor is of good quality, but a magnifying glass of 4 to 10 power is required to enable an airborne observer to see it.

This topic has been treated by many authors (Refs. 21-26), including the present one, with but little effect upon those project officers who try to replace an existing radarscope with a universal display tube to provide a multisensor display. The usual result of

such attempts is not a multipurpose display but a fractionally effective display connected to multiple sensors in a manner that degrades image quality to a level of near uselessness. Moreover, there is little understanding of the image quality needed to perform the functions of search, detection, identification, and recognition. It is upon such image quality that design specifications should be based.

John Johnson, of the Night Vision Laboratories, did research on image quality and published his findings in a 1958 report (Ref. 27) that is used as the present-day Bible on the subject. Unfortunately, the important diagrams and tables in Johnson's report are separated from the explanatory text. Thus, where the text states that "for a target to be recognizable, there must be system 'resolution' sufficient to place  $4.0 \pm 0.8$  line pairs\* across the critical dimension of that target," the related table and diagram show "resolution across minimum dimension" and make no reference to "line pairs," which is the universal standard of resolution terminology EXCEPT in the television industry, which talks about "TV lines."\* Further, Johnson assumes a knowledgeable readership and so does not explain the implicit relationships between resolution and contrast.

As a result, designers commonly misuse Johnson's data, referring to "lines on target" instead of line pairs in the minimum dimension at a contrast considerably above liminal. This confusion of "line pairs" with "TV lines" often results in systems that are underdesigned or underspecified by a factor of 2. Confusion of "lines on target" with "line pairs per minimum dimension" leads not only to the line-pair error but also to neglect of the length-to-width ratio of typical targets.\*\* These two errors result in a typical underdesign factor of 4. Further, specification and acceptance procedures are so inappropriate and so casual that there is little reason to believe that the image

---

\* One line pair equals two "TV lines." For further discussion of image quality see Part II.

\*\* The similarities and differences between the detection of single isolated signals and the detection of periodic signals (e.g., bar targets) are treated in detail in Section V-A.

quality the contracting officer thinks he has specified will ever emerge.

The preparation of formal specifications must be based upon a sound understanding of principles of operation and of the principal parameters that govern performance. This report attempts to give the reader that understanding. Specification and acceptance test procedures for low-light-level devices are covered quite fully in Ref. 15, and that coverage will not be duplicated here.

Corresponding material on FLIR has been published as IDA Paper P-676.

A committee has at last been set up at the Air Force Avionics Laboratory (AFAL), Wright-Patterson Air Force Base, to see that, beginning in FY 1970, procurements originating at AFAL provide meaningful specifications in accordance with at least these four guidelines:

1. Input flux level will be defined radiometrically and spatially.
2. Output flux level will be defined photometrically and spatially.
3. Specification will call for output/input functions rather than single-number designators.
4. Specifications will call for signal-to-noise performance functions at input, output, and various pertinent points in between.

The really big procurements come not from R&D organizations such as AFAL, however, but from system engineering groups or special project offices that have not heard about these guidelines or may not have understood their significance.

As a case in point, present understanding of the FLIR (and LLLTV) problem is well documented in a pair of papers presented in May 1969 at the 17th National Infrared Information Symposium (IRIS) by John M. Lloyd and Robert Sendall (Refs. 28, 29), who were largely responsible for getting the Army's Passive Infrared Night Equipment (PINE) specification written in accordance with the above guidelines. Further

work by Lloyd and Joseph R. Moulton (Refs. 30, 31) was presented at the 18th National IRIS in May 1970. Sendall, Moulton, and Lloyd have attempted to relate specifications to those factors demonstrated to be important to man's visual performance, such as the area between the modulation transfer function (MTF) of the equipment and the demand modulation function (DMF) of the observer, to be discussed in Part II of this report.

As a further example of such factors, other studies reported elsewhere\* conclude that the curve of probability versus range for the detection of targets at a known location is independent of the speed at which the observer approaches the target. Under such conditions, the probability data indicate that the observer will see the target just as soon as the target image size and brightness are sufficient to fulfill the observer's acuity requirements. There is essentially no delay for search, as the observer has narrowed his attention to that specific place where the target will appear. Data indicate that this independence of closing rate applies from rates of zero to at least 350 knots.

When the observer does not know where to expect targets, the range is shortened by the product of the observer's search function time and his approach velocity. For example, the search of a display for high-contrast objects subtending about 15 minutes of arc is about 10 sec for about 50 percent probability. Thus, in an aircraft moving at 500 ft/sec, the ability to find a target in a unknown location at a distance of 2 miles is reduced to half that range, or 1 mile, due to the time expended in search.

The quality of the camera little affects this kind of range degradation. For a system of poor image quality, however, the already poor range performance can become useless or nearly useless in fast-aircraft search tasks.

---

\* In IDA Study S-346 (classified), Vol. II, Appendix D, p. 69, December 1969.

The relationship between an observer's performance and the performance of the image-forming system he is using is expressed by the difference between the MTF of the equipment and the DMF of the observer, as mentioned earlier. The DMF\* is not very well known except for a few isolated tasks such as recognition of standard USAF three-bar test target patterns.

Tests in which targets are immersed in varying degrees of clutter indicate that the search function takes so long that the observer has closed to such a short range before he detects the target that he detects it and recognizes it simultaneously. In fact, under some conditions, detection, recognition, and identification occur almost simultaneously.

The proper design of low-light-level devices starts, therefore, with an understanding of the difficulty of the visual task and thus with an understanding of the form of the DMF. The MTF of the system or, more important, the signal-to-noise ratio versus spatial frequency must then be matched to that demand curve to ensure, at least theoretically, before detailed design begins, that a real and useful device can be produced. Had this process been carried out in the past, it is quite probable that the vast majority of low-light-level systems designed to meet specific requirements would have been recognized as inadequate before they became hardware.

The form and performance of such devices are closely related to the application, that is, to the character of the scene--its spectral composition, contrast, and radiance--to the difficulty and the degree of detail in the visual task to be performed, and to the required speed of performance. The time the observer has in which to make his observation and the detail required in his observation are factors usually overlooked in discussing the capabilities of these devices.

---

\* Sometimes called the aerial image modulation (AIM) curve.

Because of neglect of such factors, many attempts have been made to use for technical or military purposes an inappropriate family of parameters that have gained acceptance in entertainment television. These attempts have led to gross misestimates of system capability.

## PART I. REFERENCES

1. Hoist, de Boer, Teves and Veenemans, "An Apparatus for the Transformation of Light of Long Wavelength into Light of Short Wavelength," Physica, Vol. 1, p. 297, February 1934.
2. E. Bruche and W. Schaffernicht, "Bericht ueber Elektronenoptische Fragen auf dem Fernsehgebiet," Elektrische Nachrichten-Technik, Vol. 12, p. 381, 1935.
3. V.K. Zworykin and G.A. Morton, "Applied Electron Optics," J. Opt. Soc. Am., Vol. 26, p. 181, April 1936.
4. W. Heimann, "Elektronenoptische Abbildung von Photokathoden als Grundlage fuer Fernsehuebertragung," Elektrische Nachrichten-Technik, Vol. 12, p. 68, 1935.
5. French Patent No. 802244.
6. L.M. Meyers, Electron Optics, Chapman, London, 1939.
7. G.A. Morton and I.E. Flory, "An Infrared Image Tube and its Military Applications," RCA Review, Vol. 7, p. 385, September 1946.
8. V. Krezik and V. Vand, "The Development of Infrared Technique in Germany," Elect. Engrg., Vol. 18, p. 316, October 1946.
9. P. Gorlich, Zeitschrift fuer Physik, Vol. 101, p. 335, 1936; Z. Physik, Vol. 106, p. 374, 1938; "Photoelectric Cells for the Visible Spectral Range," J. Opt. Soc. Am., Vol. 31, p. 504, July 1941.
10. On Navy Contracts NObrs-3937 (1948-50) and NObrs-52198 (1951-52) with RCA Laboratories.
11. E.J. Sternglass, "High Speed Electron Multiplication by Transmission Secondary Electron Emission," Rev. Sci. Instr., Vol. 26, p. 1202, December 1955.
12. J.D. McGee, E.A. Flinn and H.D. Evans, "An Electron Image Multiplier," Advances in Electronics and Electron Physics, Vol. XII, p. 87, Academic Press, New York, 1960.

13. J. Burns and M.J. Neumann, "The Channeled Image Intensifiers," Advances in Electronics and Electron Physics, Vol. XII, p. 97, Academic Press, New York, 1960.
14. W.C. Wiley and C.F. Hendee, "Electron Multipliers Utilizing Continuous Strip Surfaces," IRE Trans. on Nuclear Science, NS-9, No. 3, p. 103, June 1962. (Proceedings of the Eighth Scintillation Counter Conference, Washington, D.C., March 3, 1962.)
15. Lucien M. Biberman and Sol Nudelman, eds., Photoelectronic Imaging Devices: Vol. II, Devices and Their Evaluation, Plenum Press, New York, January 1971.
16. John W.T. Walsh, The Science of Daylight, MacDonald, London, 1961.
17. R.W. Engstrom, "Calculations of Readout Sensitivity from Luminous Sensitivity," RCA Review, 1955.
18. E.H. Eberhardt, "Source Detector Spectra Matching Factors," Applied Optics, Vol. 1, p. 2037, 1968.
19. Martin Marietta Corporation, Orlando, Florida, James G. Ohmart et al., Target Acquisition Studies: Fixed Television Fields of View, Report No. OR 9656, Contract No. N00014-67-C-0340, October 1968.
20. Wright Air Development Division, Wright-Patterson AFB, W.C. Steedman and C.A. Baker, Target Size and Visual Recognition, Technical Report 60-93, February 1960.
21. J.W. Miller and Elek Ludvich, "Time Required for Detection of Stationary and Moving Objects as a Function of Size in Homogeneous and Partially Structured Visual Fields," Visual Search Techniques, Washington, D.C., National Academy of Sciences, National Research Council, 1960 (Pub. 712).
22. Lucien M. Biberman, "The Specification of Low-Light-Level System Performance," Proceedings of the DoD-NSIA Symposium on Night Combat Operations, April 30-May 2, 1968.
23. Lucien M. Biberman, "Display Size, Brightness Level and Observer Response Time," Proceedings of the Symposium on Image Display and Recording (SIDAR), Air Force Avionics Laboratory, Wright-Patterson AFB, April 8-10, 1969.
24. Lucien M. Biberman, "Specifications for Electronic Image Forming Devices," Proceedings of the Worldwide USAF Aeronautical Reconnaissance Review, October 8-9, 1968.



25. Institute for Defense Analyses, Specifications for Electronic Image-Forming Devices, IDA Research Paper P-467, Lucien M. Biberman, March 1969.
26. R.H. LaSalle, Tactical Reconnaissance Display Technology, Rome Air Development Center, Griffiss Air Force Base, New York.
27. John Johnson, in Proc. Image Intensifier Symposium, Fort Belvoir, Virginia, October 6-7, 1958. (No report number.)
28. J.M. Lloyd, "Laboratory Evaluation of the Noise-Limited Performance of Infrared Imaging Systems," presented at the 17th National Infrared Information Symposium, May 20-22, 1969.
29. R.L. Sendall, "The Definition and Analysis of the Noise-Limited Performance of an Infrared Imaging System," presented at the 17th National Infrared Information Symposium, May 20-22, 1969.
30. J.M. Lloyd, "The Optical Transfer Function of Real-Time Infrared Imaging Systems," presented at the 18th National Infrared Information Symposium, May 1970.
31. J.R. Moulton, "Two Port Evaluation Techniques for Framing Thermal Imaging Systems," presented at the 18th National Infrared Information Symposium, May 1970.

## II. IMAGE QUALITY

Here in Part II we discuss the performance of low-light-level devices. The ultimate measure of their performance is how well people perform visual tasks with the assistance of these devices.

Actually, low-light-level devices can be classified according to the form of the imagery. Image intensifiers produce images that are like photographs in their continuity along both the vertical and horizontal axes. Television devices sample the imagery and present it in sequential lines written at very high speed by a single tiny, moving spot, relying upon the persistence of the phosphor and the human eye to integrate the flying spot into an image. Forward-looking infrared imaging devices sample in two dimensions and use the flying spot to paint a series of dots of varying brightness that, again, are integrated by the eye into a picture.

The problems of sampling\* strongly affect system design and the human perception process.

In the first of the following two articles, Harry Snyder examines the relationship between image quality in nonsampled image systems and human operator performance. In the second article, Otto Schade discusses the process of image formation by a raster (sampling) process.

This material is in turn followed by a detailed description of nonsampling low-light-level devices in Parts III and IV and then by a description of raster-forming devices in Part V.

---

\*Institute for Defense Analyses, Selected Papers on Image Quality in Sampled Data Systems, IDA Paper P-741, Lucien M. Biberman et al., in publication.

# PHOTOGRAPHIC IMAGE QUALITY AND OPERATOR PERFORMANCE

by Harry L. Snyder

## A. INTRODUCTION

The purpose of this section is to describe the present state of knowledge about the ability of a trained observer to obtain target-relevant information from an imaging system display, and to relate this information-extraction performance to design characteristics of the imaging system. Unfortunately, as shall be noted below, the research pertaining to this relationship for low-light-level systems is somewhat ambiguous, and one must rely upon the related definitive data from the imagery developed by hard-copy photographic systems and then develop an analytical generalization to raster-scan systems.

During the past two decades, over 300 laboratory and analytical studies have been performed to assess the relationship between variation in line-scan display image parameters and observer performance. Conclusions drawn from critical reviews of these studies (e.g., Refs. 1-4) have indicated that cross-study comparisons are virtually impossible. Variation in specific system design parameters, or in the manner by which display image quality is synthetically manipulated, is often incompletely controlled, so that concomitant variation in the several contributing sources of image quality results. Table II-1 lists some of the experimental variables which have been shown to have a significant effect upon operator information-extraction (e.g., target-acquisition) performance. It should be noted that individual experiments have tended to examine the effects of one, two, and sometimes three such variables. However, due to the inherent interaction (nonindependence) among these variables in their effects upon operator performance, quantitative combination of the results is hazardous even in the presence of good experimental control and measurement. In the absence of such control, any a posteriori attempt to combine the results is merely foolish.

TABLE II-1. SOME OF THE VARIABLES AFFECTING INFORMATION  
EXTRACTION PERFORMANCE

<u>Atmosphere</u>	<u>Scene</u>
Aerosol Content	Target Characteristics
Cloud Cover	Background Characteristics
Illumination Level	Terrain Masking
	Clutter Level
<u>Sensor</u>	<u>Display</u>
Bandwidth	Luminance
Number of Scan Lines	Size
Field of View	Number of Scan Lines
Field/Frame Rate	Contrast
Aspect Ratio	Scene Movement
S/N Level	Dynamic Range
Integration Time	Gamma
	S/N Level
	Aspect Ratio
<u>Image Processing</u>	
Edge Enhancement	
Gamma	
Spatial Filtering	

Because of these gross conflicts and inconsistencies in the experimental literature dealing with the effects of individual system parameters, recent efforts have been oriented toward the development of (1) analytical expressions of overall image quality, such as those discussed in Part V of this volume, and (2) experimental evaluations of logically derived summary measures of image quality. The remainder of Part II will discuss the present content and limitations of data pertaining to summary measures of image quality and operator performance.

#### B. MODULATION TRANSFER FUNCTION AREA (MTFA)

Any summary measure of image quality, to be useful, must be (1) easily measured for existing imaging systems, (2) quantitatively predictable, analytically, for future imaging systems at the paper design stage, and (3) highly correlated with (or validated by) empirically

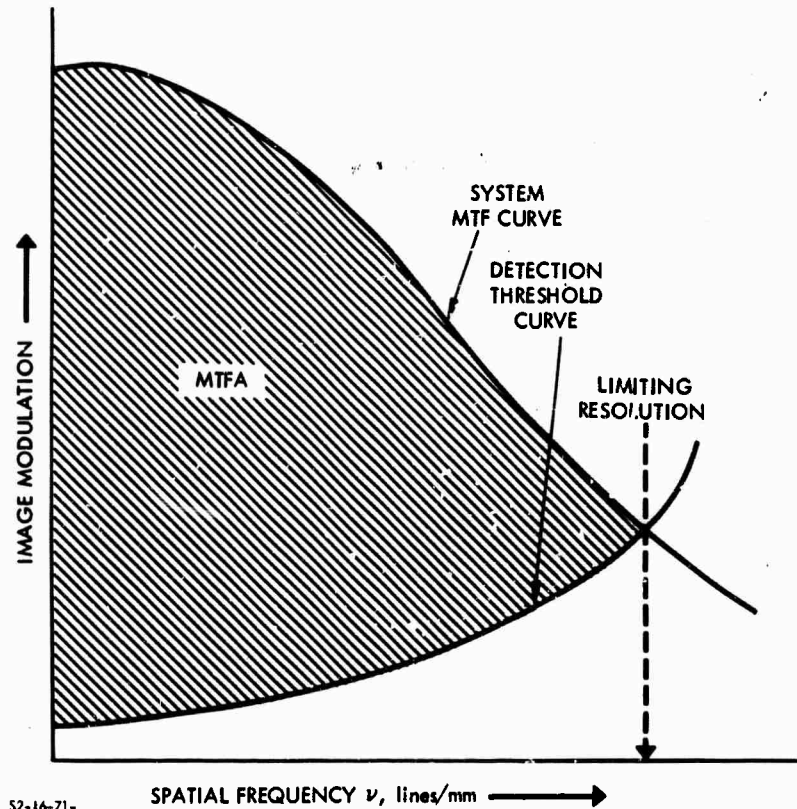
determined operator performance under the operational conditions of interest for the specified mission. To date, the summary measure of image quality which shows the greatest promise for meeting these criteria is the modulation transfer function area (MTFA).

Originally proposed by Charman and Olin (Ref. 5), who termed it the threshold quality factor, and renamed by Borough et al. (Ref. 6), the MTFA concept has been evaluated in two experimental situations and demonstrated to relate strongly to the ability of image interpreters to obtain critical information from reconnaissance photographic imagery. In its original form, the MTFA was proposed as a unitary measure of photographic image quality which contains "the cumulative effect of the various stages of the atmosphere-camera-emulsion-development-observation process, the 'noise' introduced in the perceived image by photographic grain, and the limitations imposed by the physiological and psychological systems of the observer" (Ref. 5, p. 385). While this measure was originally developed for direct photographic systems, its generalization to electrooptical systems is analytically straightforward.

The MTFA is derived in such a manner as to make use of the modulation transfer function (MTF) of the imaging system, thereby retaining the analytical convenience of component analysis based upon sine-wave response characteristics. In addition, it attempts to take into account other variables critical to the imaging and interpreting problem, such as exposure, the characteristic curve, granularity, the human observer capabilities and limitations, and the nature of the interpretation task. For the electrooptical system, the first three of these variables can be considered analogous to detector irradiance level, gamma (typically unity), and noise, respectively.

Figure II-1 shows that the MTFA is the area bounded by the imaging system MTF curve and the detection threshold curve of the total system, including the eye. The MTF curve for the imaging system is obtained in the conventional manner, while the detection threshold curve requires several assumptions regarding the human operator. Specifically, it is

assumed that the viewing conditions are optimum, and that threshold detection of any target in the imaged display is a function of the target image contrast modulation, the noise in the observer visual system, and the noise in the imaging system exclusive of the observer. It should be noted that the crossover of the two curves in Fig. II-1 represents the limiting resolution of the system for a sine-wave target.



52-16-71-

FIGURE II-1. Modulation Transfer Function Area (MTFA)

At low spatial frequencies, the threshold detection curve is dependent upon the properties of the human visual system, as shown in Fig. II-2. At higher spatial frequencies, the effect of imaging system noise becomes important. For the photographic case, this imaging system noise is equivalent to granularity. It is assumed further that the eye's contrast threshold is 0.04, so that this target image contrast modulation must be realized at the display for the target to be detected, regardless of the contrast modulation of the target object.

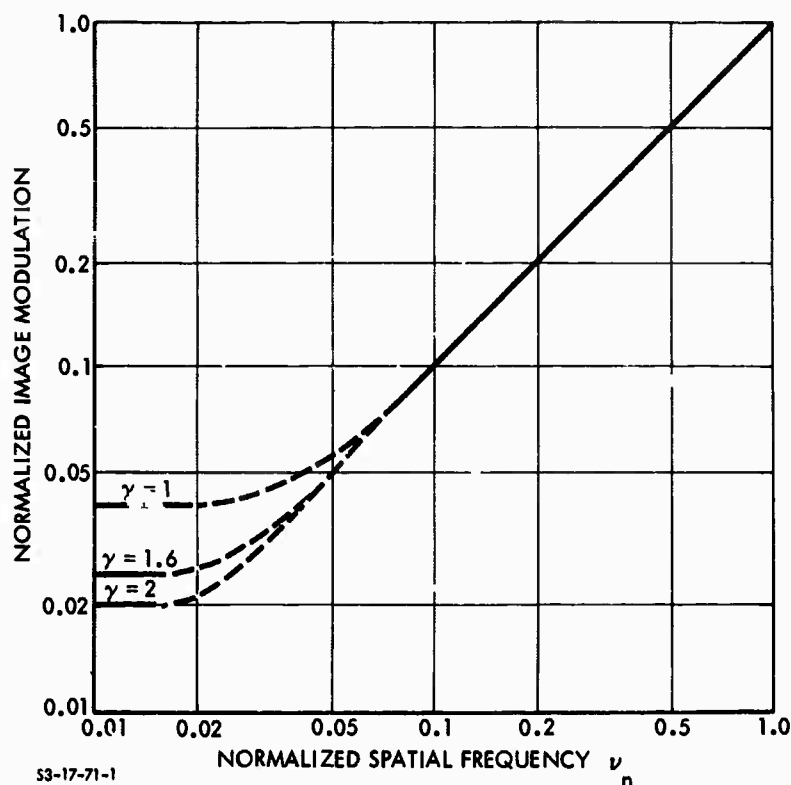


FIGURE II-2. Generalized Detection Threshold

Figure II-2 illustrates the normalized detection threshold curve, which must be adjusted both vertically and horizontally for a specific set of conditions. First, the curve is positioned vertically by increasing the normalized ordinate scale by  $\frac{M_t(\nu)}{M_o}$ , where  $M_t(\nu)$  is the normalized value as shown in Fig. II-2 and  $M_o$  is the object contrast modulation. Note that the lower portion of the threshold curve (at the lower spatial frequencies) is also adjusted by the system gamma, which, if greater than unity, enhances the modulation recorded at the display (e.g., the film) so that the minimum detectable threshold modulation decreases by  $\frac{0.04}{\gamma}$ .

Next, the detection threshold curve is positioned horizontally by multiplying the scale of the abscissa in Fig. II-2 by  $\frac{2}{C\sigma(D)}$ , where  $C$  is an empirically derived constant [0.03 for fine-grained films and

0.04 for coarser grained films (Ref. 7)] and  $\sigma(D)$  is equal to the rms granularity measured with a 24-micron scanning aperture, as used in the Kodak handbooks.

Algebraically, the detection threshold curve for a photographic system is therefore (Ref. 5):

$$M_t(\nu) = 0.034 \left[ \frac{dD}{d(\log_{10} E)} \right]^{-1} \left[ 0.033 + \sigma(D)^2 \nu^2 S^2 \right]^{1/2}$$

in which

$\nu$  = any spatial frequency, in lines per millimeter

0.034 = an empirically derived constant\*

$D$  = mean film density

$E$  = exposure

0.033 = an empirically derived constant\*

$\sigma(D)$  = rms granularity for a 24  $\mu$  scanning aperture

$S$  = signal-to-noise ratio necessary for threshold viewing, assumed to be about 4.5 (Ref. 14).

$\frac{dD}{d(\log_{10} E)}$  = film characteristic slope, including effects of development

When the MTF curve and the detection threshold curve are plotted on log-log coordinates (Ref. 6), the expression for the MTFA becomes:

$$\begin{aligned} \text{MTFA (log-log)} &= \int_{\log \nu_0}^{\log \nu_1} (\log T_\nu) d \log \nu - \int_{\log \nu_0}^{\log \nu_1} \left( \log \frac{M_t(\nu)}{M_0} \right) d \log \nu \\ &= \int_{\log \nu_0}^{\log \nu_1} \left( \log \frac{M_0 T_\nu}{M_t(\nu)} \right) d \log \nu \end{aligned}$$

---

\* For derivation, see Charman and Olin (Ref. 5). Generation of these values is considered unimportant in the present context.



where

$\nu_0$  = the low spatial frequency limit, in lines/millimeter

$\nu_1$  = the spatial frequency at which the MTF curve crosses the detection threshold curve (limiting resolution)

$T_\nu$  = the MTF value at spatial frequency  $\nu$

$M_0$  = the object contrast modulation

$M_t(\nu)$  = the normalized detection threshold curve value, as taken from Fig. II-2.

When the MTF curve and the detection threshold curve are plotted on linear coordinates, the area of interest is given by (Ref. 6):

$$\text{MTFA (linear)} = \int_0^{\nu_1} \left( T_\nu - \frac{M_t(\nu)}{M_0} \right) d\nu.$$

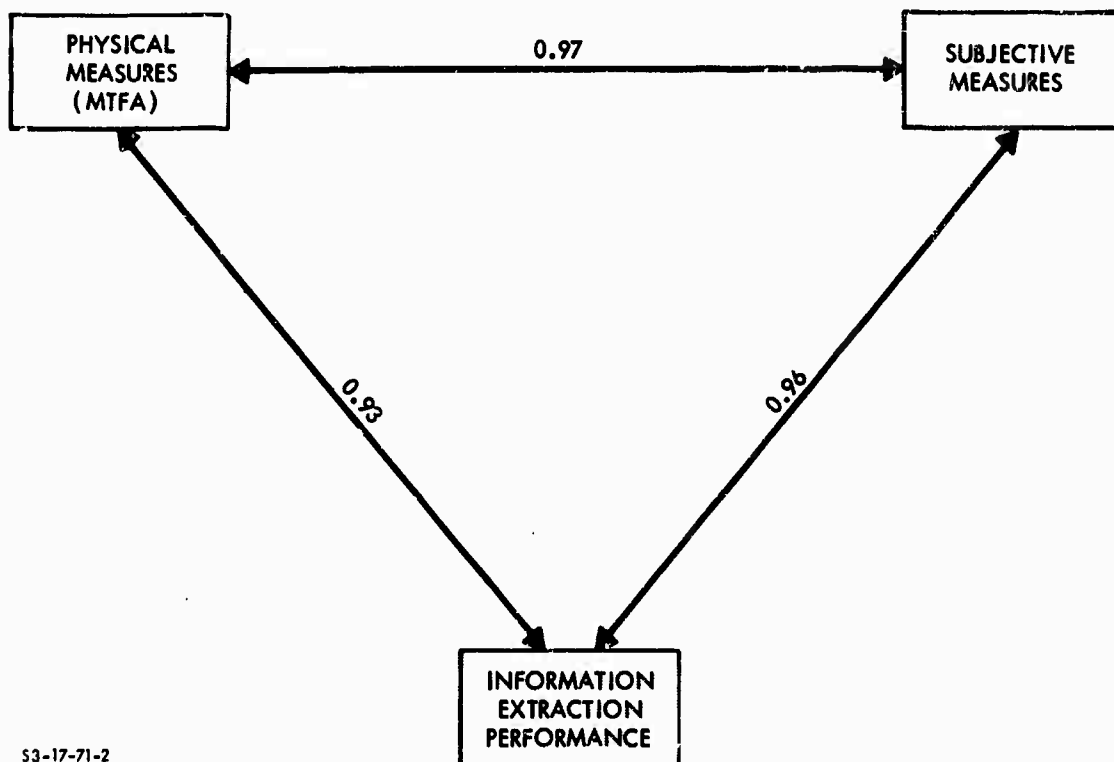
The linear form computation utilizes no lower frequency cutoff, whereas the log-log formulation employs an arbitrary cutoff at, say, 10 lines/millimeter. The reason for this difference is simply that the log-log plot integration would place an inappropriately large weight upon integration over the lower spatial frequencies were this cutoff eliminated. The nature of the linear plot avoids the need for such an arbitrary cutoff.

It might also be noted, parenthetically, that the detection threshold curve, as described here, is akin to such concepts as contrast sensitivity (Ref. 8), sine-wave response (Refs. 9-11), and demand modulation function (DMF).

### C. EVALUATION OF THE MTFA

To date, two empirical evaluations of the MTFA concept have been conducted, both using photographic imagery. In the first study (Ref. 6), an attempt was made to relate MTFA to subjective estimates of image quality obtained from a large number of trained image interpreters. In the second of these experiments, actual information-extraction performance data were obtained, as well as subjective

estimates of image quality, and both measures were compared with the MTFA values of the imagery. Schematically, these relationships can be thought of as those depicted in Fig. II-3. While it is desirable from an operational viewpoint to have a quick judgment of subjective image quality to serve as an indicant of the quality of any source of imagery for, say, rapid screening purposes, the critical measure of goodness of any imaging system is the ability of the observer to perform the required information-extraction tasks.



S3-17-71-2

FIGURE II-3. Indices of Image Quality

In the first study to evaluate MTFA, the purpose was to determine whether a strong relationship existed between MTFA and subjective image quality. This limited evaluation was imposed simply to reduce data

collection costs in the event that the MTFA measure proved fruitless. In this experiment performed by Borough et al. (Ref. 6), nine photographic reconnaissance negatives were used as the basis for laboratory-controlled manipulation of image quality. Each of the scenes was printed in 32 different MTFA variants, determined by four different MTF's, three levels of granularity, and three levels of contrast, as illustrated in Fig. II-4. Four cells of the matrix were deleted because their MTFA values corresponded to others in the 32-cell matrix. The MTF curves are illustrated in Fig. II-5.

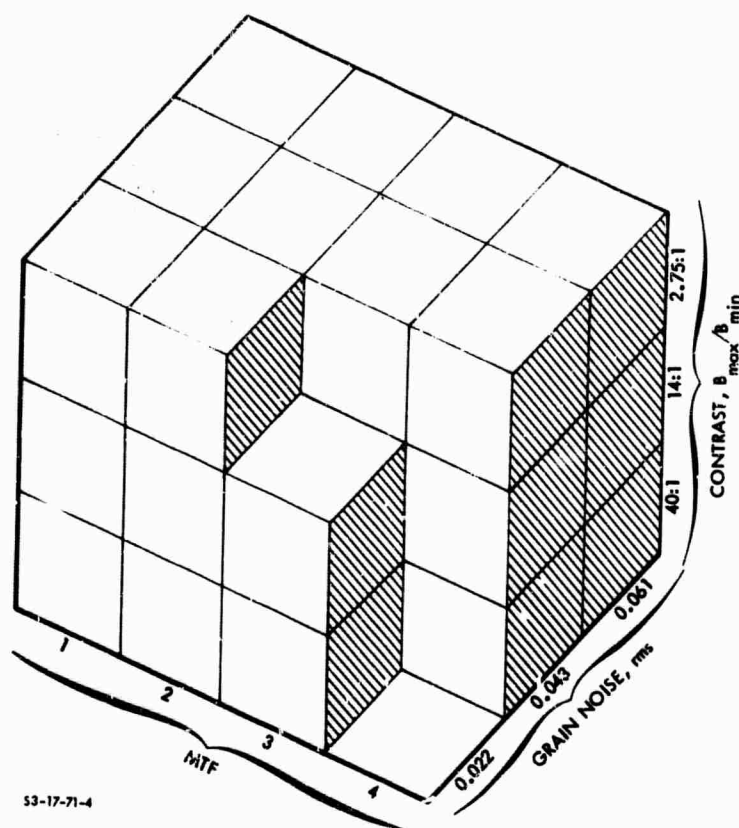
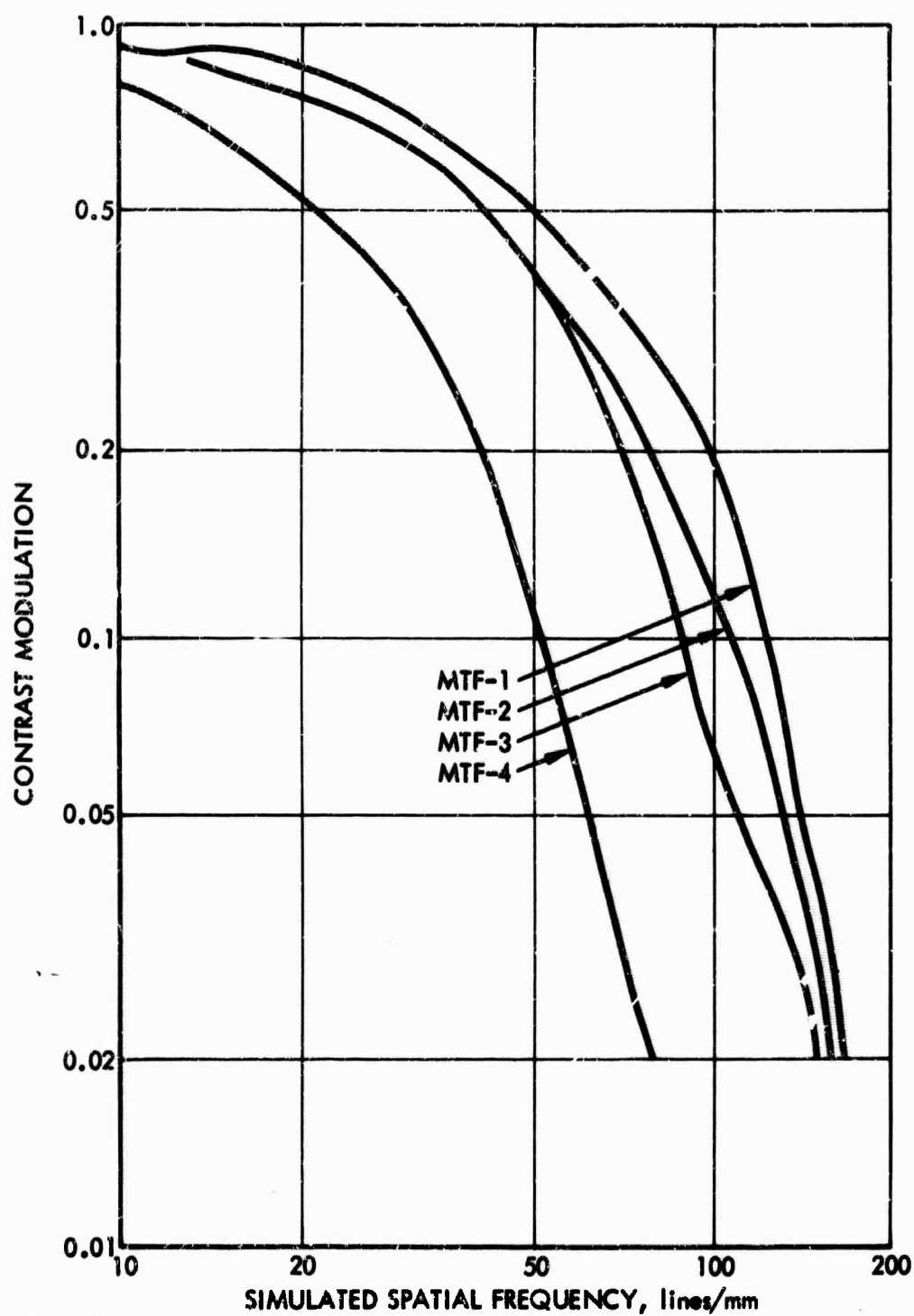


FIGURE II-4. Production of MTFA Values

The resulting 288 transparencies (9 scenes by 32 variants/scene) were used in a partial paired-comparison evaluation by 36 experienced photointerpreters. The subjects were asked to select the photo of each pair that had the best quality for extraction of intelligence



53-17-71-3

FIGURE II-5. Average Modulation Transfer Functions Measured by Edge-Response Method

information. All pairs were composed of two variants of the same scene; each subject made a total of 256 comparisons, for a grand total for all subjects of  $36 \times 256 = 9216$  judgments.

Correlations were obtained between the subjective image quality rating (derived from the paired comparisons) for each of the 32 variants and several physical measures of image quality. Table II-2 shows the results. Most important to this discussion is the mean correlation of 0.92 between MTFA (linear) and subjective image quality, which indicates that MTFA is strongly related to subjective estimates of image quality.

TABLE II-2. CORRELATIONS OF PHYSICAL VARIABLES WITH SUBJECTIVE IMAGE QUALITY SCALE VALUE

Physical Variables	Scene Number									Mean $r^*$
	1	2	3	4	5	6	7	8	9	
MTFA (Linear)	0.921	0.927	0.900	0.925	0.935	0.919	0.919	0.920	0.913	0.920**
Modulation	0.220	0.641	0.511	0.618	0.680	0.699	0.497	0.698	0.632	0.576
MTF	0.698	0.529	0.580	0.660	0.579	0.608	0.697	0.469	0.542	0.601
Granularity	-0.543	-0.632	-0.618	-0.450	-0.516	-0.428	-0.505	-0.589	-0.577	-0.543
MTFA (Log-Log--2 Cycle)	0.666	0.863	0.866	0.821	0.874	0.890	0.749	0.902	0.876	0.846
MTFA (Log-Log--10 Cycle)	0.768	0.923	0.923	0.867	0.920	0.921	0.824	0.941	0.920	0.900
Acutance	0.599	0.448	0.526	0.568	0.564	0.599	0.625	0.440	0.602	0.555

\* These mean values were determined by transforming the correlations to Fisher's Z values. Such a transformation is necessary when correlations are being combined to obtain a mean correlation.

\*\* This mean value was significantly greater ( $p < 0.01$ ) than all of the other mean correlation values except the value for MTFA (Log-Log--10 Cycle). This latter value was still significantly less than the MTFA linear value at the 0.05 level of significance.

The next experiment, by Klingberg, Elworth, and Filleau (Ref. 12), examined the relationship between objectively measured information-extraction performance and the MTFA values. As a check on the results of Borough et al., Klingberg et al. also obtained subjective estimates

of image quality, so that all three correlations suggested by Fig. II-3 were evaluated.

The imagery used for this experiment was the same as that used by Borough et al. (Ref. 6). A group of 384 trained military photointerpreters served as subjects. Each subject was given one variant of each of the nine scenes and asked to (1) rank the image on a nine-point interpretability scale, using utility of image quality for information extraction as the criterion, and (2) answer each of eight multiple-choice questions dealing with the content of the scene. The interpretability scale values were used to develop a subjective image quality measure for the 288 images, while scores on the multiple-choice interpretation questions were used to measure information-extraction performance.

Figure II-6 shows the scattergram between information-extraction performance and MTFA for the 32 MTFA values. The resulting correlation, averaged across the nine scenes, is -0.93. (The minus value is due to the use of number of errors, which is inversely related to MTFA, as a measure.)

Individual correlations among performance, MTFA, and subjective quality (rank) are shown in Table II-3. It is apparent that the relationship between MTFA and performance is not as high for some scenes (e.g., 6 and 9) as for others, but that the mean correlation  $\bar{r}$  across scenes (0.72) is quite high. Further, if one disregards scene content and places all scenes on a common performance continuum, the correlation of -0.93 accounts for over 86 percent of the variance in information-extraction performance. Further, the 0.97 correlation of MTFA with subjective quality (rank) agrees quite well with the correlation of 0.92 obtained by Borough et al.

A further comparison among these measures is given in Table II-4, which compares the paired-comparison subjective quality values  $V$  of Borough et al. with the other measures obtained by Klingberg et al. both for individual scenes and all nine scenes combined. As the summary matrix indicates, information-extraction performance, MTFA, and

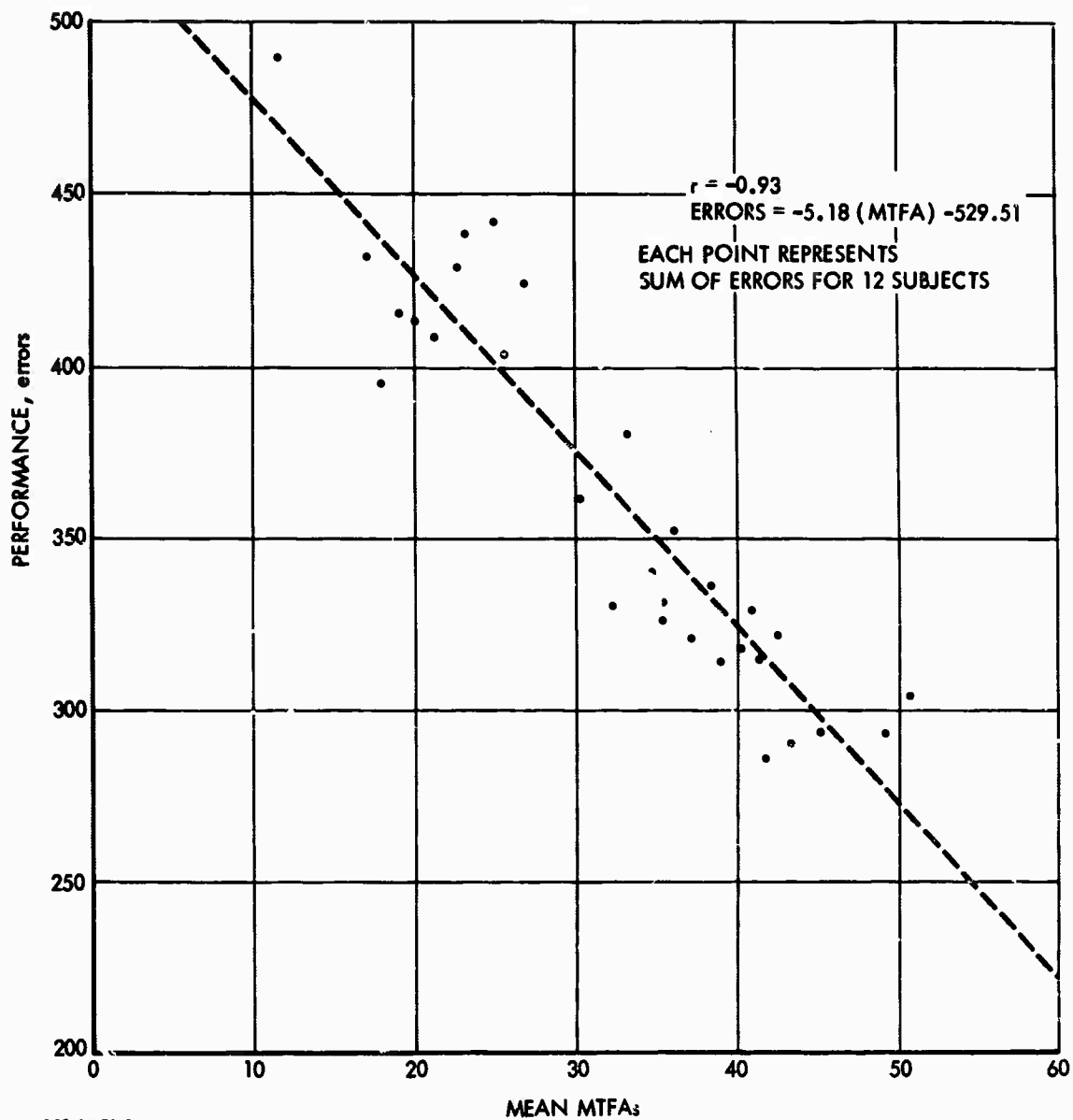


FIGURE II-6. Scattergram of Information Extraction Performance Versus MTFA

subjectively scaled image quality (obtained by either absolute judgments or paired comparisons) intercorrelate highly. These resulting values are shown on the appropriate lines in Fig. II-3.

TABLE II-3. CORRELATIONS (PEARSON  $r$ 's) BETWEEN IMAGE QUALITY, INTERPRETER PERFORMANCE AND SUBJECTIVE JUDGMENTS

Scene	1	2	3	4	5	6	7	8	9	$\bar{r}^*$	$r_m^{**}$
Performance/MTFA	0.69	0.66	0.80	0.65	0.78	0.55	0.84	0.86	0.46	0.72	0.93
Performance/Rank	0.71	0.67	0.89	0.60	0.80	0.42	0.78	0.76	0.42	0.70	0.96
MTFA/Rank	0.90	0.87	0.90	0.93	0.94	0.87	0.92	0.86	0.83	0.90	0.97

N = 32 image quality levels (MTFA)

\* $\bar{r}$  = Average of  $r$ 's using Z scores.

\*\* $r_m$  = Values averaged across scenes before computing correlation.

#### D. CONCLUSIONS AND CAUTIONS

These data show that a measure of image quality based upon the excess of MTF over the threshold detection level correlates highly with the ability of observers to obtain critical operational information from the imagery.\* As will be shown in Part V of this report, there are other ways to define the same (or a very similar) quantity. For example, Rosell's display signal-to-noise ratio ( $SNR_D$ )\*\* is essentially the same quantity as MTFA when appropriate alterations are made in the calculations to account for the differences between photographic imaging system variables and electrooptical line-scan system variables. In both cases, the general value of interest is the excess of signal over noise as a function of spatial frequency. Viewed in that context, the data reported here demonstrate that MTFA (or  $SNR_D$ ) is an extremely useful and valid measure of the figure of merit of an imaging system. At the same time, however, some cautions must be noted.

\*Where the objects of interest range broadly in the target size spectrum.

\*\*Discussed in Sections V-A-2 and V-G.



TABLE II-4. INTERCORRELATIONS OF ALL MEASURES BY SCENE

<u>SCENE 1</u>				<u>SCENE 2</u>				<u>SCENE 3</u>			
	R	M	V		R	M	V		R	M	V
Performance (P)	0.71	0.69	0.68		0.67	0.66	0.67		0.89	0.80	0.83
Ranks (R)		0.90	0.92			0.87	0.87			0.90	0.91
MTFA (M)			0.92				0.93				0.88
Paired-Comparison Values (V)											

<u>SCENE 4</u>				<u>SCENE 5</u>				<u>SCENE 6</u>			
	R	M	V		R	M	V		R	M	V
Performance (P)	0.60	0.65	0.64		0.80	0.78	0.76		0.42	0.55	0.70
Ranks (R)		0.93	0.92			0.94	0.92			0.87	0.83
MTFA (M)			0.92				0.93				0.92
Paired-Comparison Values (V)											

<u>SCENE 7</u>				<u>SCENE 8</u>				<u>SCENE 9</u>			
	R	M	V		R	M	V		R	M	V
Performance (P)	0.78	0.84	0.82		0.76	0.86	0.82		0.42	0.46	0.43
Ranks (R)		0.92	0.90			0.86	0.87			0.83	0.77
MTFA (M)			0.92				0.92				0.91
Paired-Comparison Values (V)											

<u>ALL SCENES COMBINED</u>			
	R	M	V
Performance (P)	0.97	0.93	0.93
Ranks (R)		0.96	0.97
MTFA (M)			0.97
Paired-Comparison Values (V)			

First, the specification of the detection threshold curve (or Rosell's 50 percent probability-of-detection S/N level) implies that optimum viewing conditions are obtained. In the studies reported here, the observer was ground based, supplied with an ample nonglare display luminance, and was not time-restricted in his responses. Similarly,

in the data used to develop the concept of  $SNR_D$ , observers were not severely hampered by operational constraints. In both cases, therefore, the detection threshold curves represent the best performance of which the well-trained observer is capable. If, for the sake of argument, this threshold were to be uniformly elevated by adverse operational circumstances for all spatial frequencies of the display, no changes in the relationships presented here would occur--the relative magnitudes of MTFA would remain unchanged. If, on the other hand, operational requirements caused a nonuniform elevation of the detection threshold curve across all usable spatial frequencies, then inversions could occur in the MTFA values for systems having different MTFs.

This is not a minor consideration when it is realized that the eye's contrast threshold varies not only with spatial frequency but also with display signal-to-noise, overall image luminance, adaptation level (mean surround luminance), and such environmental parameters as glare, vibration, glint, and time stress. As the MTFA concept is applied to electrooptical systems, it is particularly important to note that the MTF is defined specifically in the absence of noise, so that at low detector irradiance (and hence low S/N) levels, a display may have a considerable amount of "snow" and thereby produce poor target acquisition performance, even though the system MTF remains unchanged. For this reason, it is vital that the display S/N level be included as a determinant of the detection threshold curve used in MTFA calculation, and that other conditions under which the MTFA is defined (e.g., display luminance and operating environment) also be specified to avoid ambiguity. Otherwise, the MTFA obviously cannot be used to predict observer performance over a wide range of electrooptical system operating conditions.

Secondly, it is likely that, upon further analysis, we must learn how to weigh the excess signal over the noise at various spatial frequencies, rather than integrate uniformly as in the current MTFA or  $SNR_D$  concepts, for the following reason. It has been shown that noise of a spatial frequency similar to the spatial frequency of the target

of interest has the most deleterious effect upon threshold detection performance (Ref. 13). Thus, because various missions might require acquisition of targets of predominantly specific spatial frequencies, and because various imaging system designs might produce noise power at certain spatial frequency bands, one cannot simply conclude that the excess of signal above noise can be assumed to be of equal importance at all spatial frequencies. That is, there are undoubtedly spatial frequency bands which are more important for some missions than others, and appropriate weighting of these bands should be considered when evaluating a particular system (by MTFA or  $SNR_D$ ) for that mission, and that uniform integration across all spatial frequencies from zero to limiting resolution might produce nonrepresentative results.

Finally, although the author is convinced that the MTFA approach (or, equivalently, the  $SNR_D$  to be discussed in Part V) presents the most valid figure of merit for present and near-future imaging systems, cautions must be noted as to the representativeness of the data which lead to this conclusion. The data of Borough et al. (Ref. 6) and Klingberg et al. (Ref. 12) were obtained for non-time-limited, non-stressed viewing conditions; the display of the imagery was nearly optimal; and the imagery itself was continuous-image photographic negative material, not line-scanned, cathode-ray-tube presentations under dynamic conditions. Clearly, verification of these results is indicated for conditions more representative of the operational mission in which the typical line-scan system is employed.\*

---

\* EDITOR'S NOTE: After this material by Snyder was written, experimental work by Rosell and Willson, the results of which are shown in Fig. V-A-3 et seq., firmly established the value of  $SNR_D$  as a figure of merit.

**BLANK PAGE**

## REFERENCES

1. Air Force Avionics Laboratory, Low Light Level TV Viewfinder Simulation Program. Phase A: State-of-the-Art Review, Report AFAL-TR-67-293, H.L. Snyder et al., November 1967.
2. B. Hillman, "Human Factor Considerations in Real-Time Airborne Target Acquisition," in Air-to-Surface Missile Technology, 1975-1980, IDA Report R-133, December 1967.
3. The Boeing Company, Night and All-Weather Target Acquisition: State-of-the-Art Review. Part III: Television and Low-Light-Level Television Systems, Boeing Company Report D162-10116-3, H.W. Hairfield, May 1970.
4. The Boeing Company, Night and All-Weather Target Acquisition: State-of-the-Art Review. Part II: Infrared and Laser Systems, Boeing Company Report D162-10116-2, C.R. Filleau, April 1970.
5. W.N. Charman and A. Olin, "Image Quality Criteria for Aerial Camera Systems," Phot. Sci. and Eng., Vol. 9, pp. 385-397, December 1965.
6. The Boeing Company, Quantitative Determination of Image Quality, Boeing Company Report D2-114058-1, H.C. Borough, R.F. Fallis, T.H. Warnock and J.H. Britt, May 1967.
7. F. Scott, in Image Evaluation for Reconnaissance, Proceedings of a Symposium, Itek 9048-6, April 9-17, 1963.
8. F.W. Campbell and D.G. Green, "Optical and Retinal Factors Affecting Visual Resolution," J. Physiol., Vol. 181, pp. 576-593, 1965.
9. J.J. DePalma and E.M. Lowry, "Sine-Wave Response of the Visual System. II. Sine-Wave and Square-Wave Contrast Sensitivity," J. Opt. Soc. Am., Vol. 52, pp. 328-335, 1962.
10. E.M. Lowry and J.J. DePalma, "Sine-Wave Response of the Visual System. I. The Mach Phenomenon," J. Opt. Soc. Am., Vol. 51, pp. 740-746, 1961.

11. C. Bryngdahl, "Characteristics of the Visual System: Psychophysical Measurements of the Response to Spatial Sine-Wave Stimuli in the Photopic Region," J. Opt. Soc. Am., Vol. 56, pp. 811-821, 1966.
12. The Boeing Company, Image Quality and Detection Performance of Military Interpreters, Final Report, Air Force Office of Scientific Research Contract F44620-69-C-0128, C.L. Klingberg, C.L. Elworth, and C.R. Filleau, April 1970.
13. B.H. Eckhardt, "Application of Spatial Frequency Data to the Prediction of Imaging System Effectiveness," in CIRADS: Supplementary Proceedings, Human Factors Conference, Advanced Research Projects Agency, January 12, 1967.
14. P.D. Carman and W.N. Charman, "Detection, Recognition, and Resolution in Photographic Systems," J. Opt. Soc. Am., Vol. 54, pp. 1121-1130, 1964.

## IMAGE REPRODUCTION BY A LINE RASTER PROCESS

by Otto H. Schade, Sr.

### A. THE SAMPLING PROCESS OF A LINE RASTER

The intensity function  $I(\rho, \theta)$  of images formed by optical or electron lens systems is continuous in any radial direction  $(\rho, \theta)$  of the format area. The modulation transfer functions  $MTF(\theta, \rho)$  are generally isotropic for small radial distances  $(\rho)$  but may become anisotropic for larger radial distances because of point-image distortion by astigmatism or coma. Isotropy requires a point-image or sampling "aperture" of circular symmetry.

The conversion of continuous intensity functions  $I(\rho, \theta)$  into one-dimensional time functions  $I(t)$  and reconversion into continuous two-dimensional intensity functions in a television system involves scanning of the format area with an "aperture" along uniformly spaced parallel lines termed a "line raster." The raster process yields a set of continuous intensity functions  $I(x)$  along the lines, whereas intensity functions  $I(y)$  are transmitted as discrete amplitude samples taken at intervals  $\Delta y$  determined by the raster line spacing. It follows at once that continuity in the displayed image requires a display aperture having a particular spread  $S(y)$  to fill the interline spaces of the raster and establish continuity in  $y$ , whereas the aperture spread  $S(x)$  could be very much smaller, making the resolution in the image anisotropic. Similarly, the effective spread  $S(y)$  of the sampling aperture in the camera must have a particular value to prevent loss of information contained in the interline spaces of the raster, indicating a "flat field" requirement\* in the camera.

---

\*The "flat field" requirement refers to a structure-free reproduction of a continuous field of uniform intensity by a line raster process. It specifies a uniform charge readout in the camera, leaving no interline charges on the storage surface, and is satisfied when the sum of the effective line image cross sections of the scanning aperture spaced at raster line distances yields a constant intensity function  $I(y)$ .

An isotropic image requires apertures of circular symmetry. Continuity in  $y$  can be obtained by selecting a raster line density to provide a large overlap of aperture positions in successive line scans. A high raster line density, however, is wasteful in terms of the electrical frequency channel and raises two questions: Is a flat, i.e., uniform, field necessary? What is the optimum aperture size and shape to achieve uniformity?

Most television displays have a visible line structure on the screen, and increased viewing distances are required to effect integration by the eye into a flat or structureless field. An image containing a visible line structure may appear to be sharper, but more detail becomes visible when the line structure is removed. This can be demonstrated convincingly by modulating a CRT with wide-band noise. It will be observed that the noise is much more visible when the interfering line structure is removed by defocusing the CRT spot or by increasing the viewing distance. The line structure is an interfering signal which, like noise, prevents detection of small detail.

Various other effects occur when the effective sampling apertures of the camera and display are too small relative to the raster line spacing. Diagonal lines become staircases, spurious diamond-shaped patterns appear in horizontal line wedges, low-frequency beat patterns occur in "vertical" resolution charts of parallel lines at higher frequencies, and the reproduction of significant detail depends on position relative to the raster lines.

Quantitative specifications can be derived by convolution of intensity functions in the space and time domains. An analysis in the frequency domain, however, is more convenient.

The discontinuous intensity function  $I(y)$  obtained by the raster process in the camera represents a pulse carrier wave with infinitesimal pulse width of spatial frequency  $f_r$ , amplitude modulated by the spatial frequencies  $f_m$  contained in the image, which are limited by the  $MTF_c$  of the camera aperture  $\delta_c$ . The fundamental frequency  $f_r$  of the spatial carrier wave is equal to the number of raster lines per unit length.



The spatial intensity functions  $I(y)$  are converted by the sequential scanning process into time functions  $I_y(t)$  contained in the video signal, which can be displayed with an electrical sampling circuit on an oscilloscope. The time signals are converted back into spatial modulated carrier waves in the display system by a synchronized scanning process. The pulse carrier must now be demodulated by a low-pass filter, the MTF of the display aperture  $\delta_d$ , to restore a continuous undistorted modulation envelope from the transmitted samples. The solution for optimum low-pass MTF's is known from modulation theory and states that the MTF of both input and output filters must be limited to frequencies  $f_m \leq 0.5 f_r$  to eliminate all raster carrier components and unwanted modulation products. The MTF's should be constant for maximum utilization of the frequency channel. This optimum solution may not be realizable in a practical system. We therefore examine the general expression for the intensity function  $I(y)$  resulting from a carrier modulation by a frequency  $f_m$ , given by the following equation:

$$I(y) = \bar{I} (1 + 2 \sum \tilde{r}_{d,kf_r} \cos(k \cdot 2\pi f_r y)) \quad (C)$$

$$+ \hat{I}_{f_m} \tilde{r}_c \tilde{r}_d \cos(2\pi f_m y + \theta) \quad (f_m)$$

$$+ \hat{I}_{f_m} \tilde{r}_c \cdot \sum^k \left[ \tilde{r}_{d,(kf_r + f_m)} \cos(2\pi(kf_r + f_m)y + \theta) \right] \quad (S) \quad (II-1)$$

$$+ \hat{I}_{f_m} \tilde{r}_c \cdot \sum^k \left[ \tilde{r}_{d,(kf_r - f_m)} \cos(2\pi(kf_r - f_m)y + \theta) \right] \quad (D)$$

where

$$k = 1, 2, 3, \dots$$

$f_m$  = modulation frequency, cycles/unit length

$f_r$  = raster frequency, number of sampling points/unit length

$y$  = distance along y-coordinate

$\bar{I}$  = mean intensity of test object wave form

$\hat{I}_{f_m}$  = crest intensity of sine-wave test object

$\tilde{r}_c$  = sine-wave response factor of camera at  $f_m$

$\tilde{r}_d$  = sine-wave response factor of display system at  $f_m$

$\tilde{r}_{d,(\text{index})}$  = sine-wave response factor of display at index frequency

$\theta$  = phase displacement between  $\hat{I}_{f_m}$  and raster lines

The first term (C) contains the dc level ( $\bar{I}$ ) and an infinite number of steady carrier frequency components  $k f_r$  ( $k$  is an integer) with amplitudes  $2\bar{I} \tilde{r}_d$  depending only on the  $MTF_d$  of the display system. The second term ( $f_m$ ) is the normal MTF product ( $\tilde{r}_c \tilde{r}_d$ ) of the system as obtained without raster process at any modulation frequency.

The third and fourth terms (S) and (D) are modulation products (sidebands) generated by sum and difference frequencies with the carrier components.

The entire frequency transfer characteristic for the y-coordinate of the television process is shown by the graphic representation in Fig. II-7. The  $MTF_c$  under the input frequency scale of the raster characteristic is the product of the MTF's of all two-dimensional aperture processes preceding the raster process and including the scanning beam in the camera.

The MTF of the video system is unity for the y-samples and need not be shown. The transfer functions of the raster itself are a network of diagonal lines with constant transfer factors ( $\tilde{r} = 1$ ) for the frequency  $f_m$  and the sum and difference frequencies (D,S). The carrier frequencies ( $C_1, C_2, \dots$ ) are represented by horizontal lines because their existence depends only on the dc term and on the attenuation by the output filter.

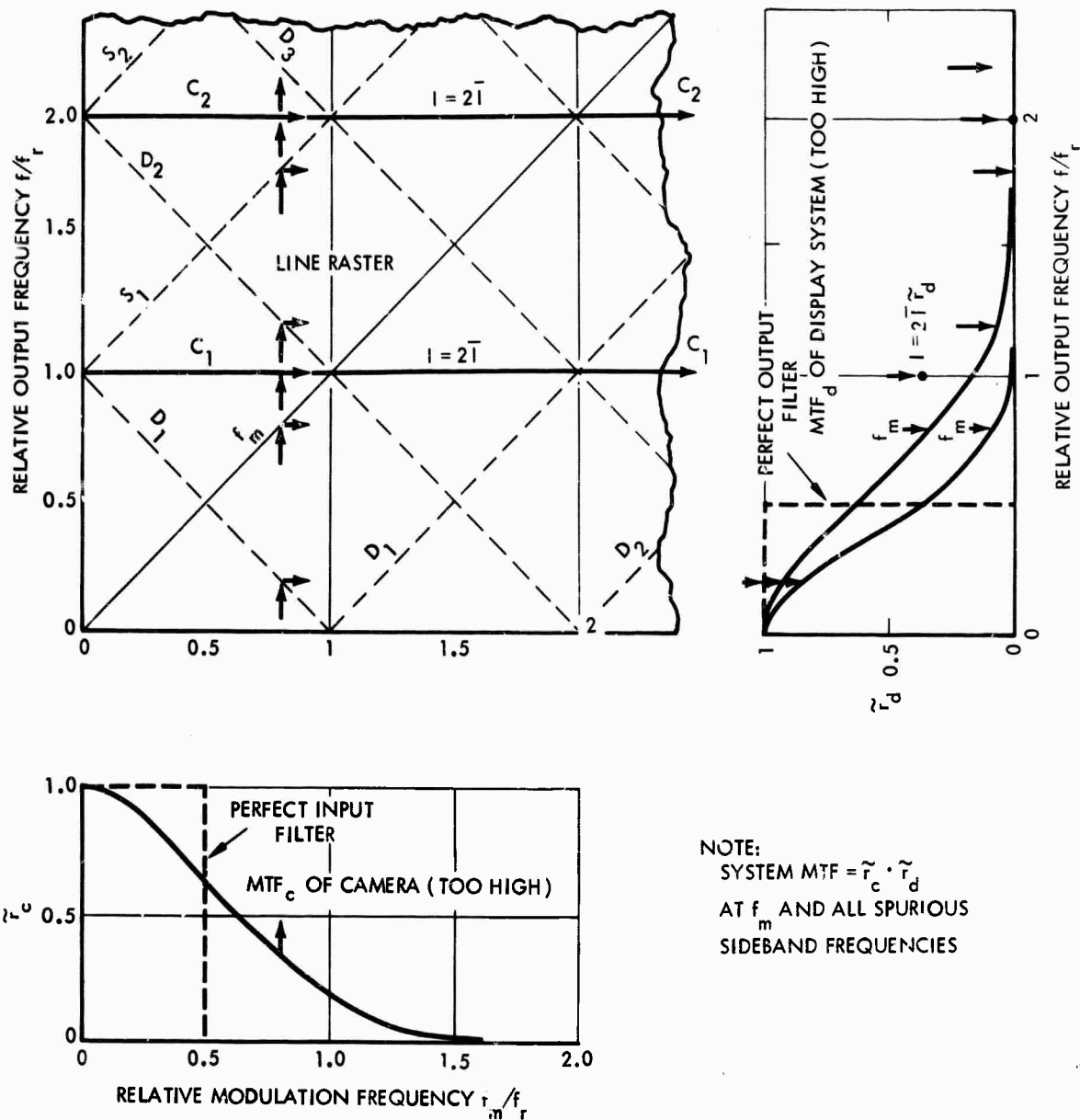


FIGURE II-7. Frequency and Modulation Transfer Characteristic in y-Coordinate of Television Systems with Line Raster Process

The  $MTF_d$  of the display system is drawn parallel to the output frequency scale of the raster characteristic. It is the product of the MTF's of all two-dimensional aperture processes following the raster process and includes, therefore, the MTF's of copying systems and the eye. Unless eliminated by adequate magnification, the MTF of the eye must obviously be considered in MTF specifications of display systems designed for a specific viewing distance.

The use of the diagram is simple. A vertical projection of an input frequency  $f_m$  (see arrows) locates the output frequencies of the raster process at the intersections with the various transfer lines. Horizontal projections from these points onto the output  $MTF_d$  indicate the attenuation ( $2\bar{I} \tilde{r}_d$ ) of the carrier frequency components and the response factors  $\tilde{r}_d$  for determining the relative amplitudes ( $\tilde{r}_c \tilde{r}_d$ ) of the modulation products. The example illustrates that the higher  $MTF_d$  reproduces the carrier C, with a modulation amplitude of 36 percent, representing a 72 percent peak-to-peak variation in a uniform field ( $\bar{I}$ ). The lower  $MTF_d$  reproduces a substantially flat field, but the raster generates a low difference frequency  $f_D = 0.2 f_r$  of amplitude  $\tilde{r}_c \tilde{r}_d = 0.27$  from a modulation frequency  $f_m = 0.8 f_r$  of 32 percent amplitude because the input  $MTF_c$  exceeds the value  $f_m = 0.5 f_r$ . It is seen at a glance that a complete elimination of all spurious modulation frequencies restricts the MTF's to the spatial frequency bands indicated by the broken line rectangle; i.e., to frequencies  $f_m \leq 0.5 f_r$ . In other words, a minimum of one sample per half cycle is necessary to transmit a continuous sine wave by a sampling process.

#### B. RASTER LINE FREQUENCIES AND MTF COMBINATIONS FOR LOW SPURIOUS RESPONSE

The inverse transform of a rectangular frequency spectrum is a  $(\sin x)/x$  impulse function or line image which can be realized with the coherent light of laser-beam image reproducers by using a rectangular lens stop. Similar functions can be synthesized from the Gaussian-type impulses by vertical aperture correction with tapped delay lines for noninterlaced or interlaced scanning (Ref. 1). Such

corrections may not be feasible in many cases that are then restricted to the MTF's of normal cameras and display systems, which are approximated in the illustrations by Gaussian functions.

A substantially flat field is obtained when the  $MTF_d$  at  $f_r$  is 2.5 percent or less. The carrier amplitude for the upper limit is  $2\bar{I}r_d = 0.05 \bar{I}$ , producing a peak-to-peak ripple of 10 percent. The numerical evaluation of cross products is illustrated by Fig. II-8. Curves 1 through 5 represent the  $MTF_c$  of various cameras. The MTF of the display system repeats for the sum and difference frequencies of the side bands  $MTF_D$  and  $MTF_S$ , as shown in Fig. II-8. The spurious modulation products  $\tilde{r}_c \tilde{r}_{D1}$  and  $\tilde{r}_c \tilde{r}_{S1}$  are easily evaluated\* and shown by curves 1 through 5 in Fig. II-9a for the five camera MTF's of Fig. II-8. Note that the zero frequency of the cross products occurs at the modulation frequency  $f_m = f_r$  and that the modulation frequencies generate higher spurious frequencies for  $f_m < 0.5 f_r$  and lower frequencies for  $f_m > 0.5 f_r$ . The maximum values of the spurious response are plotted in Fig. II-9b as a function of the camera response ( $\tilde{r}_c$ ) at the theoretical frequency limit  $f_m = 0.5 f_r$ . The straight line shows the overall MTF ( $\tilde{r}_c \tilde{r}_d$ ) of the system.

A spurious response  $\tilde{r}_{sp}$  of 10 percent may be considered an upper limit for good system design. This value is a worst case and occurs occasionally for 100 percent contrast in the scene. Spurious frequencies occur in the range indicated by a curve intermediate for curves 2 and 3 in Fig. II-9a and do not include low-frequency beats, which are most visible. It follows that the raster frequency (number of raster lines) should be

$$f_r \cong 2 f_{m(0.26)} \quad (II-2)$$

where  $f_{m(0.26)}$  is the spatial frequency at which the camera has a sine-wave response factor  $\tilde{r}_c = 0.26$ . An overall system response  $\tilde{r}_c \tilde{r}_d = 0.10$  is then obtained with a flat field display system having a sine-wave response  $\tilde{r}_d = 0.38$  at the theoretical frequency limit  $f_m = f_r/2$ .

\* The remaining products are very small or zero and can be neglected.

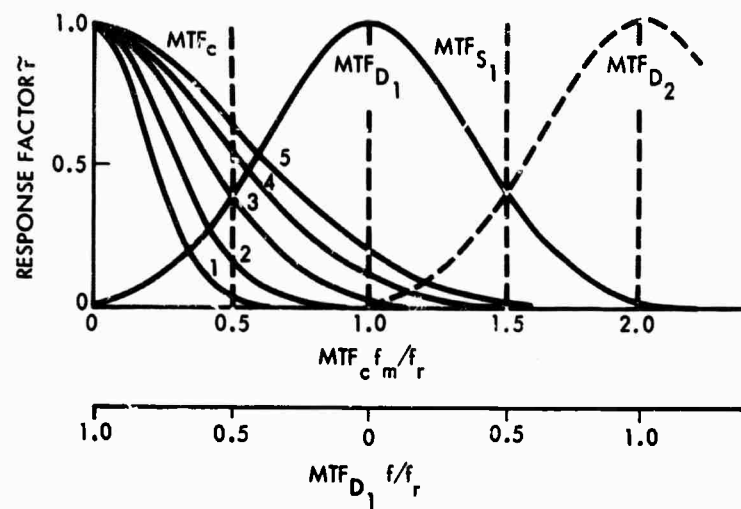


FIGURE II-8. Evaluation of Cross Products for an  $MTF_D$  Producing a Flat Field

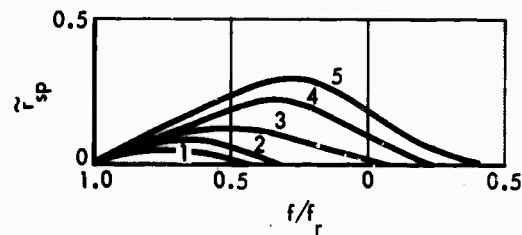


FIGURE II-9a. Cross Products  $\tilde{r}_{sp}$  for  $MTF_S = MTF$  No. 3 and Various  $MTF_c$  Curves 1  $\rightarrow$  5

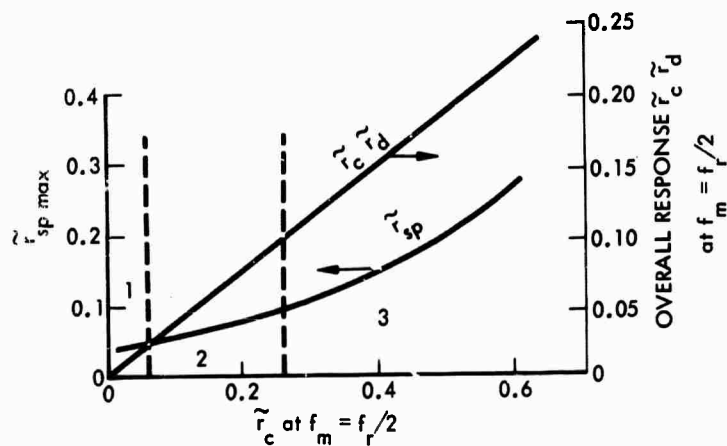


FIGURE II-9b. Maximum Spurious Response  $\tilde{r}_{sp}$  and Overall Response  $\tilde{r}_{cd}$  for  $MTF_d = MTF$  No. 3 and Various Camera MTF's at  $f_m = f_r/2$

There is, of course, an upper limit for the raster frequency  $f_r$  because a frequency  $f_m = f_r/2$  with negligible amplitude need not be sampled as expressed by

$$2f_{m(0.05)} \geq f_r \geq 2f_{m(0.26)} \quad (\text{II-3})$$

The index numbers specify the camera response ( $\tilde{r}_c$ ) at  $f_m$ . The upper limit  $f_r = 2f_{m(0.05)}$  provides a very low level of spurious signals but requires a wide video passband.

### C. SYSTEM DESIGN

The  $\text{MTF}_c$  of the camera determines the constants of the television system or vice versa. Equation II-3 states that the raster frequency should be in the range  $f_r = 2f_{0.26}$  to  $2f_{0.05}$ , where  $f_{0.05}$  and  $f_{0.26}$  are the spatial frequencies at which the camera response is 26 percent and 5 percent, respectively. A design for best utilization of the electrical frequency channel would select the lower raster frequency ( $2f_{0.26}$ ) whereas a design for maximum resolving power requires the upper limit. In terms of television line numbers ( $N$ ) and the raster line number ( $n_r$ ), Eq. II-3 specifies the range  $n_r = N_{0.26}$  to  $N_{0.05}$ . A commercial 525 line system, for example, has an active raster line number  $n_r = 490$  lines and the vertical camera response at this line number ( $N$ ) is generally less than 26 percent.

A flat field and low spurious response dictate a display system designed for an  $\text{MTF}_d$  of 2.5 percent or less at the raster frequency ( $f_r$ ). The  $\text{MTF}$  of a good commercial CRT is in the order of 27 percent at  $f_r = 490$  cycles and, at a luminance  $B = 40$  ft-L, the  $\text{MTF}$  of the eye (Ref. 2) is 5 percent for a relative viewing distance  $d/V = 4$  and about 0 percent for  $d/V = 6$ . The  $\text{MTF}_d$  of the display system is thus 1.35 to 0 percent. The peak-to-peak ripple is 4 times higher and still visible at the shorter viewing distance. The line structure is very pronounced at close viewing distances and should be eliminated by vertical "spot wobble." The spot-wobble frequency should be outside the frequency spectrum of the system; about 20 MHz for standard

CRT's, 50 MHz for a 20-MHz video system and 140 MHz for 100-MHz systems and very high-resolution CRT's. Spot wobble is particularly recommended when the CRT image is magnified by overscanning the normal format. A laser-beam image recorder designed for a substantially rectangular frequency spectrum and a flat field increases the  $MTF_d$  and overall MTF of the system. It does, however, increase also the amplitude of the spurious response products. Figures II-7 and II-8 illustrate by rectangular broken lines that portions of the sidebands (D) are reproduced with unity response by a rectangular  $MTF_d$ . The modulation products shown in Fig. II-9a are zero for  $f/f_r > 0.5$  and have amplitudes equal to  $r_c$  for  $f/f_r < 0.5$ , which are the portions of curves 1 to 5 in Fig. II-8 inside the rectangular first sideband. This condition recommends the use of higher raster frequencies  $f_r \approx 2 f_{m(0.10)}$  to reduce spurious low frequencies. The MTF's of the camera and display system are products of a number of components. It may thus occur that the MTF of the scanning aperture (beam) in the camera is much higher than the product, for example, when a high-resolution beam is used in combination with a light intensifier and a high-aperture lens. Calculation of the raster frequency with Eq. II-3 may indicate a relatively low raster frequency at which the scanning beam leaves unscanned interline spaces. Although sufficient integration of the image flux occurs in the stages preceding scanning, the efficiency of signal conversion is reduced by interline charges not contacted by the beam and can result in undesirable secondary effects recommending the use of a larger beam or a higher raster frequency. A similar situation may occur in a display system containing several "copying" stages which "diffuse" the image of the actual scanning spot to provide a flat field. The current or light density in the scanning spot may then become excessive, which can result in saturation effects.

A "perfect" television system having equal rectangular MTF's in  $x$  and  $y$ , producing a structureless field, is anisotropic because the effective apertures  $\delta_c$  and  $\delta_d$  have a square base, causing an increase of the spatial frequency spectrum by  $\sqrt{2}$  in the diagonal directions.



The same anisotropy occurs in optical images formed with monochromatic light by a lens having a square lens stop. A practical television system in which the MTF is bandwidth limited in  $x$  by the video system is similarly anisotropic, as is readily confirmed by observation. The system becomes isotropic when the raster frequency has twice the value at which the camera response is 5 percent, the MTF of the display system is 2 percent or less at the raster frequency, and the video system has unity response up to the resolution limit of the overall MTF product because the MTF of the system is then limited in all radial directions by the isotropic response of its two-dimensional circular apertures. This is the preferred system design for high resolving power. It should be pointed out that the MTF of a charge storage camera can become anisotropic because of "self-sharpening" of a low-velocity beam in  $x$  or  $y$ , which depends on a low or excessively high raster line density, respectively. The  $MTF_c$  in the  $y$ -direction is readily measured with a horizontal pulse gating circuit, and isotropy in the reproduced image can be tested visually by comparing the contrast of vertical and horizontal resolution bars in a standard Air Force test object, which can be made equal by adjusting the MTF of the video system by aperture correction circuits.

#### REFERENCES

1. Otto H. Schade, Sr., Patent 3,030,440, Vertical Aperture Correction.
2. Otto H. Schade, Sr., "Optical and Photoelectric Analog of the Eye," J. Opt. Soc. Am., Vol. 46, No. 9, p. 721, 1956.

### III. LOW-LIGHT-LEVEL PERFORMANCE OF VISUAL SYSTEMS

by

Alvin D. Schnitzler

**BLANK PAGE**

### PART III. SYMBOLS

A	area of aperture
B	luminance
e	magnitude of electric charge, coulombs
F	luminous flux
H	raster height
$i_s$	primary photoelectric current
$j_s$	electric current density at photocathode
$M_D$	modulation amplitude on display
$M_S$	modulation amplitude on photocathode
$m$	subjective magnification
m	magnification
N	number of television lines per raster height
$n_s$	photoelectron flux density
$P_\lambda$	spectral radiant power
$R(\lambda)$	relative spectral response
S	separation between display and observer
$T(\nu)$	sine-wave response, frequency response, modulation transfer function
t	effective integration time of eye
$\epsilon$	effective length-to-width ratio of half period of test frequency
$\lambda$	wavelength of radiation

$\nu$	sine-wave spatial frequency
$\nu_D$	spatial frequency on display
$\nu_s$	spatial frequency on photocathode
$\sigma(\lambda)$	responsivity of photocathode, amperes per watt
$\Omega$	solid angle

### III. LOW-LIGHT-LEVEL PERFORMANCE OF VISUAL SYSTEMS

by Alvin D. Schnitzler

#### A. LOW-LIGHT-LEVEL PERFORMANCE OF THE EYE

A full appreciation of the principles of operation of photoelectric imaging (PEI) systems depends on knowledge of certain features of the visual process. For this purpose it is useful to examine and compare the operation of visual systems such as the unaided eye and binoculars on the one hand with PEI systems on the other. However, in any comparison of visual systems, in which the retina of the eye is the primary radiation sensor, with physical devices, in which some other radiation-sensitive layer is the primary sensor, one is confronted with the relation between the subjective and objective effects of radiation in the visible and adjacent regions of the spectrum. This relation is particularly important in examining the operation of visual systems incorporating PEI systems, since their overall performance depends on both the physical properties of the input radiation and the subjective properties of the output radiation.

The problem arises because the eye, as shown in Fig. III-1, is so selective in its spectral response that radiant power expressed in watts is an inadequate measure of the subjective effect of a flux of radiant energy. Two alternative procedures are available:

1. a. Specify the spectral response of the eye,  
b. Specify the spectral content of the flux, and  
c. Perform a numerical integration of their product over all wavelengths within the passband of the eye.
2. Define an arbitrary unit of luminous flux, spectrally normalized to the peak of human visual response, as an overall measure of the subjective effect of the flux of radiant energy

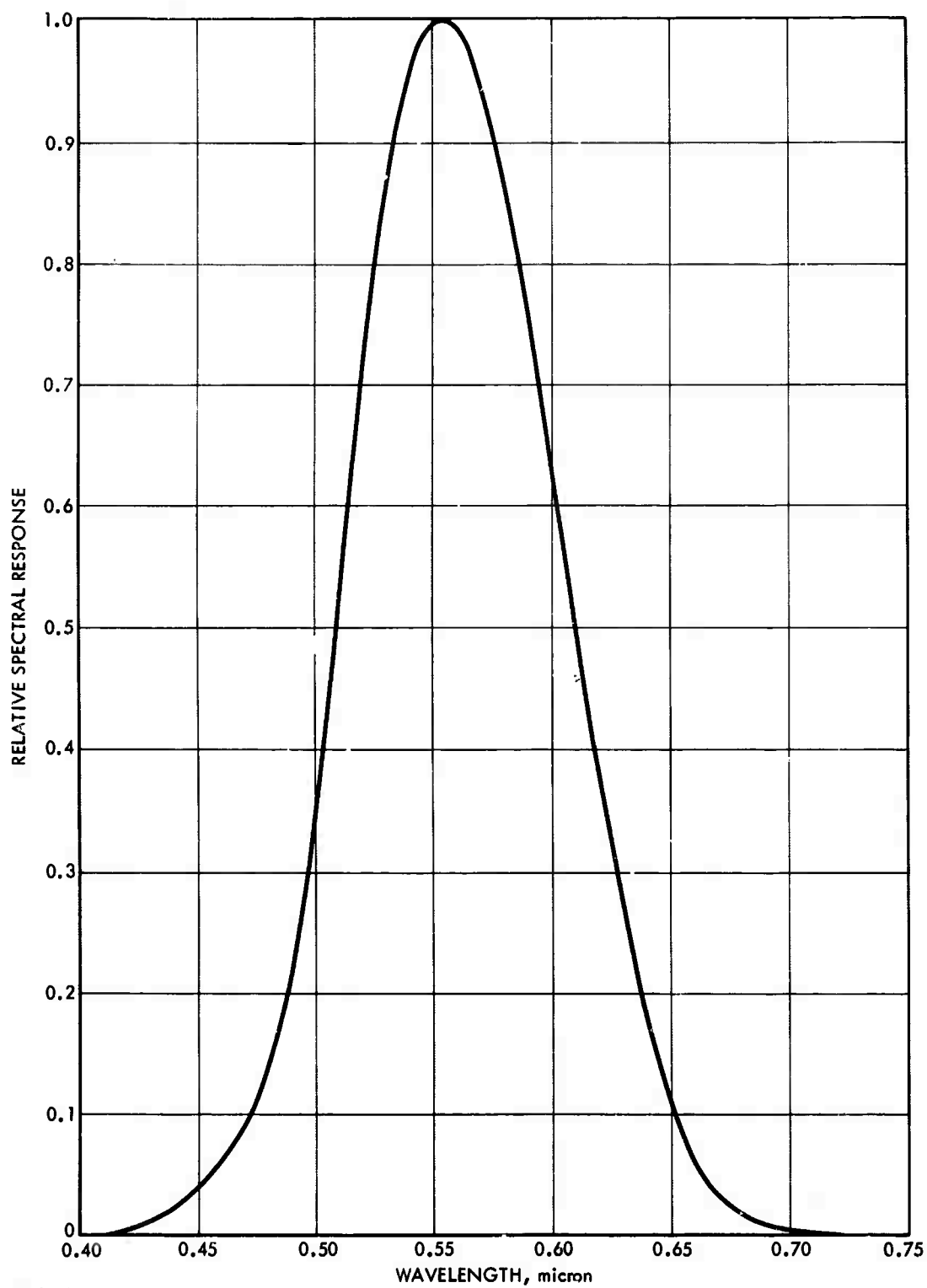


FIGURE III-1. Standard Visibility Curve of the Photopic Eye



without explicit concern for its spectral content and the spectral response of the eye.

The second procedure requires the establishment of a standard of luminous flux as a reference to determine the value of unknown luminous flux by comparison. In practice, it is easier to maintain a standard of luminous intensity rather than a standard of luminous flux. The standard of luminous intensity, the candela, is defined as one-sixtieth of the luminous intensity per square centimeter of a blackbody radiator at the temperature of solidification of platinum (approximately 2042°K). The unit of luminous flux, the lumen, is the amount of luminous flux emitted within a unit solid angle by an isotropic point source of luminous intensity equal to one candela. For an extended source of luminous flux, the luminance of an element of surface is defined as the luminous flux that leaves the surface per unit solid angle and unit projected area of the element of surface. If the surface is a perfectly diffuse radiating (or reflecting) surface, the total luminous flux leaving the surface per unit area is equal to  $\pi$  times the luminance. The amount of luminous flux incident per unit area of a surface is the illumination of the surface. The unit of illumination, lumen per unit area, depends on the unit of area chosen.

Since the procedure of establishing a unit of luminous flux as an overall measure of the subjective effect of a flux of radiant energy is implicitly dependent on the spectral response of the Commission Internationale de l'Eclairage (CIE) "standard observer," this procedure does not apply to radiation sensors with other spectral responsivities. For general application to all radiation sensors, the first procedure, explicitly taking into account the spectral response of the radiation sensor (e.g., the eye), is superior, for then the radiant power can be expressed in watts without loss of rigor. In the case of the eye, for any spectral distribution of radiant power, one has

$$F = 680 \int_0^{\infty} y(\lambda) P_{\lambda} d\lambda \quad (\text{III-1})$$

where  $F$  (in lumens) may be viewed either as a luminous flux (i.e., the visual content of the flux of radiant energy) or as a measure of the amount of visual sensation evoked by the radiant power,  $y(\lambda)$  is the relative spectral response (better known as the "standard observer" function) of the eye, and  $P_\lambda$  is the spectral radiant power in watt/nm. The numerical factor 680 is the luminous equivalent of one watt of radiant power at the peak of the visibility curve [ $y(\lambda) = 1$ ], which for photopic vision occurs at 555 nm.

If a photoelectronic sensor is employed rather than visual sensation, the output is a directly measurable electric current. In this case, one has

$$I = \sigma(\lambda_p) \int_0^\infty R(\lambda) P_\lambda d\lambda \quad (\text{III-2})$$

where  $I$  is the electric current in amperes,  $\sigma(\lambda_p)$  is the absolute radiant responsivity of the sensor at the peak wavelength in amperes/watt,  $R(\lambda)$  is the relative spectral response of the sensor, and  $P_\lambda$  is again the spectral radiant power.

The physical quantities corresponding to luminance and illuminance are radiance and irradiance. They are based on radiant power in watts. The unit of radiance, depending on the choice of unit of area, is watt per unit area per unit solid angle. Likewise, the unit of irradiance is watt per unit area. A table of some of the corresponding subjective (photometric) and physical (radiometric) quantities is given on the next page. For a more extensive treatment of photometric and radiometric quantities, see, for example, Refs. 1 and 2, among other sources.

Photometric		Radiometric	
Quantity	Unit	Quantity	Unit
Luminous flux	lumen	Radiant flux	watt
Luminous intensity	candela*	Radiant intensity	watt/steradian
Luminance	candela/ meter <sup>2</sup>	Radiance	watt/meter <sup>2</sup> - steradian
Illuminance	lumen/ meter <sup>2</sup>	Irradiance	watt/meter <sup>2</sup>

In the text below, wherever it is appropriate to take explicit note of the spectral response of the eye or wherever photoelectronic sensors are under consideration, the quantities used will be radiometric.

At low light levels, to compensate for the loss of visual stimuli, the eye automatically undergoes various adjustments. These adjustments include:

- Increasing photon collection by dilation of the pupil.
- Integrating the signal over larger areas on the retina by extracting the signal from larger clusters of elemental sensors.
- Increasing the sensitivity of the retina by means of dark adaptation, which includes switching from less sensitive to more sensitive sensors as well as lowering the sensitivity thresholds of both.
- Integrating the signal over a longer time.

The area of the pupil of the eye is controlled by the iris, a ring-shaped involuntary muscle adjacent to the anterior surface of the lens. It has been shown (Ref. 3) that the pupil area increases by

---

\*The candela is defined to yield one lumen per steradian. Thus the unit solid angle is implicit in the definition.

approximately a factor of 10 as the light level decreases from bright sunlight at  $10^3 \text{ cd/m}^2$  to the darkness of an overcast night at  $10^{-5} \text{ cd/m}^2$ .

The amount of light collected by a circular aperture such as the entrance pupil of the eye is given by

$$F = AB \Omega \quad (\text{III-3})$$

where  $A$  is the area of the aperture,  $B$  is the luminance of a paraxial object, and  $\Omega$  is the solid angle subtended by the object at the aperture. Since an increase in the area of the entrance pupil has no effect on the magnification of the eye, the area of the image on the retina remains unchanged. Hence, by dilation of the pupil retinal illumination increases, image brightness increases, and visual perception at low light levels is improved.

The ability of the eye to integrate the signal over increasing areas of the retina with decreasing light level is shown (Ref. 4) in Fig. III-2. The threshold luminance  $B_t$  required for perception of an object subtending an angle  $\alpha$  at the entrance pupil of the eye decreases with increasing  $\alpha^2$ , which is proportional to the area of the image on the retina. Data such as are shown in Fig. III-2 differ little, whether a disk or a Landolt C-ring is projected on a screen, and for a given  $\alpha$  the luminance is increased until the viewer perceives the location of either the disk or the gap in the C-ring. The two portions of the curve in Fig. III-2 are due to the presence of two types of sensors: (1) the rods, which respond at low light levels, and (2) the cones, for daylight and color vision.

According to Eq. III-3, the luminous flux collected from an object by the eye is proportional to the product of  $B_t$  and  $\alpha^2$  (since  $\Omega \propto \alpha^2$ ). However, Fig. III-2 shows that at low light levels, where vision depends on the rod sensors, the eye becomes quite ineffective at integrating the signal from elements separated from the center of the object by distances which subtend angles larger than 4 or 5 deg. Thus, as  $\alpha$

approaches 4 or 5 deg, the threshold flux increases rapidly. This limitation is shown in Section III-B to be of special significance for the application of large-aperture binoculars or night glasses to increase visual perception at low light levels.

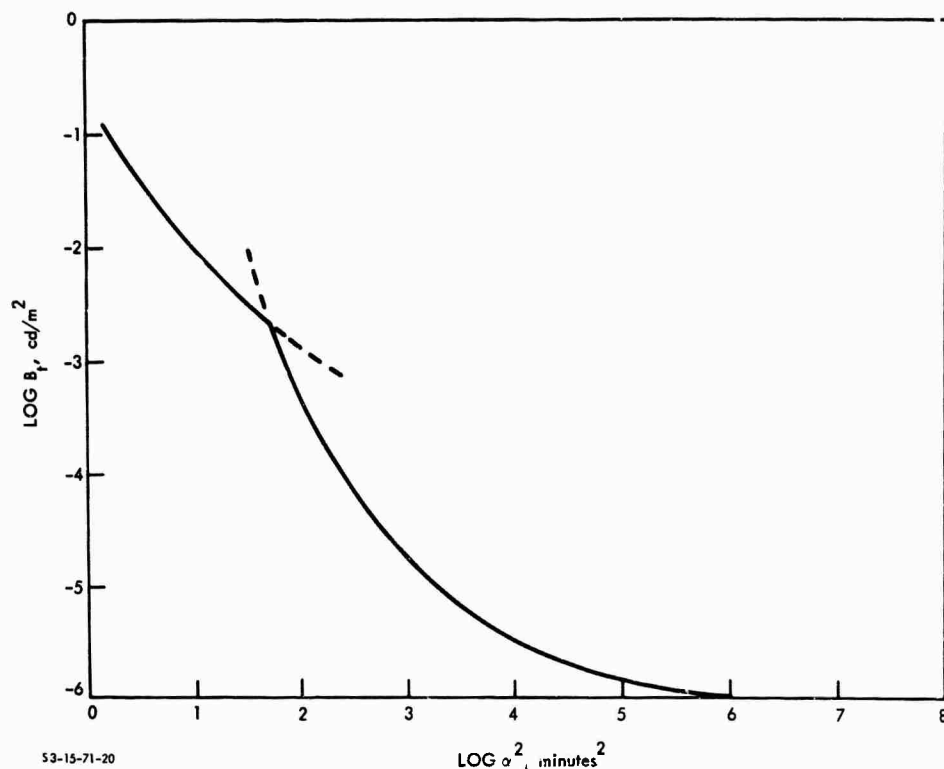


FIGURE III-2. Threshold Luminance as a Function of Angle Subtended at Eye Pupil by Disk or Gap in Landolt C-Ring (Ref. 4)

The increase in sensitivity (reduction in visual threshold) that occurs with increasing dark adaptation is illustrated in Fig. III-3 (Ref. 5), where the logarithm of threshold luminance versus time of dark adaptation is plotted. The experiments were conducted by pre-adaptation with approximately  $5000 \text{ cd/m}^2$  of white light and then determination of the threshold luminance required by the observer to resolve the lines of a grating. In these experiments, vision is dominated by the cone sensors during the first 7 or 8 min of dark adaptation before the visual threshold of the rod sensors, decreasing more

rapidly, becomes dominant. The effect of area on visual threshold, as discussed above, is also evident in Fig. III-3. It is interesting to note that the rod sensors cannot resolve lines subtending an angle of 4 min, while the cone sensors can resolve objects of less than 1 min.

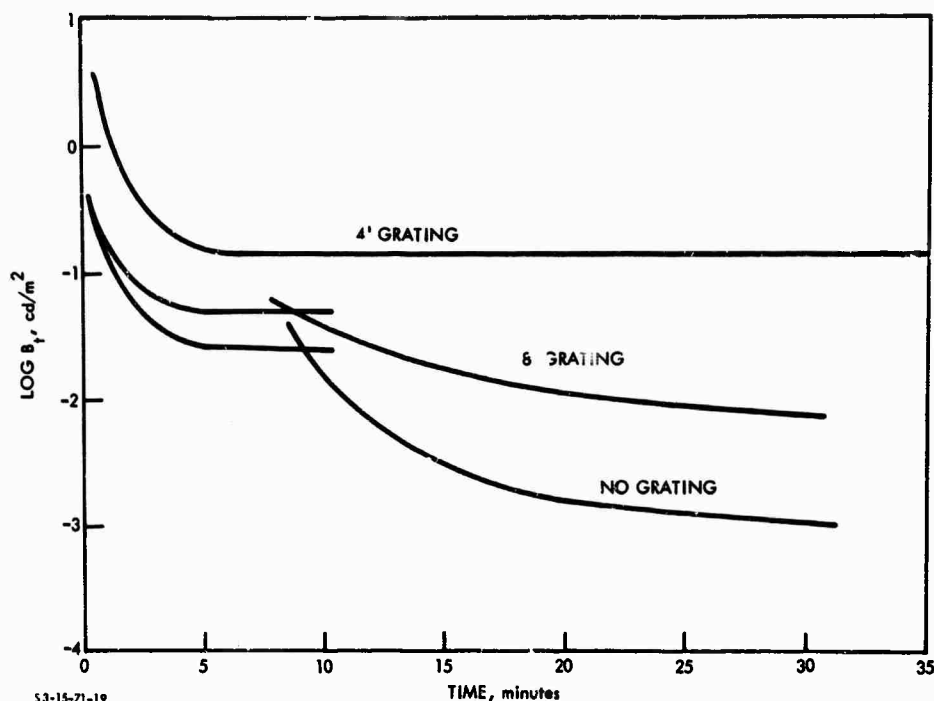


FIGURE III-3. Threshold Luminance as a Function of Time During Dark Adaptation Following Preadaptation to  $5000 \text{ cd/m}^2$  (Ref. 5)

The relatively slow progress of dark adaptation shown in Fig. III-3 poses a severe problem for sensitive vision at night if an observer is required to pass from a brightly illuminated artificial environment into a dimly illuminated natural environment or if dark adaptation is destroyed by flashes or occasional sources of light in an otherwise dark scene. For example, under the conditions applying to Fig. III-3, if the object luminance were  $10^{-2} \text{ cd/m}^2$ , the observer would have to wait nearly 11 min to become sufficiently dark-adapted to perceive a gross unlined object, and approximately 22 min to resolve

a line grating in which a line subtends an angle of 8 min at the eye. Image-intensifier and television systems can be of great value under such conditions, since it is unnecessary to wait for dark adaptation if the output image is presented at sufficient brightness.

The ability of the eye to integrate the signal over a longer time at low light levels appears to be the least important of the response parameter adjustments made to compensate for the decreased photon flux. Rose (Ref. 6), for example, claims that the effective storage or integration time of the eye is close to 0.2 sec and that it varies little from extremely low to high light levels. Schade (Ref. 7), on the other hand, claims that the effective storage time decreases from approximately 0.2 sec at the threshold of vision towards a plateau of approximately 0.05 sec at high illumination.

#### B. LOW-LIGHT-LEVEL PERFORMANCE OF BINOCULARS

Limited aid to visual performance at low light levels can be provided by means of purely geometric optic devices such as binoculars. Special care is taken in the design and construction of such devices to ensure maximum transfer of radiation collected by the objective to the retina of the eye. It is essential that the exit pupil of the device is large enough to match the large entrance pupil of the dark-adapted eye. In this case, binoculars will produce the subjective impression of increased image brightness and permit the detection of targets not visible to the unaided eye. This increase in visual performance, the well-known night-glass effect, is shown below to result from the increased size of the image on the retina provided by the subjective magnification of the binoculars. It does not result from more irradiance in the image. Indeed, an increase in image radiance by purely geometric optics would violate the second law of thermodynamics.

The other parameters upon which the detection of a target image depends, such as wavelength, exposure time, contrast, and requirement for dark adaptation, are little affected by night-vision binoculars.

The aid to visual performance provided by night-vision binoculars depends solely on the spatial integration capability of the dark-adapted eye, which was described in Section III-A as relatively ineffective for images viewed in the eyepiece subtending more than 4 to 5 deg at the entrance pupil of the eye.

In any well-designed visual instrument, such as night-vision binoculars, the eye is placed so that the entrance pupil of the eye nearly coincides in position with the exit pupil of the instrument, since placing the eye elsewhere merely introduces an additional stop that may unnecessarily reduce the field of view. A diagram of the complete visual system is shown in Fig. III-4. A detailed discussion of the binocular is given in Ref. 8. A detailed discussion of the limitation of rays by apertures will be found in Chapter V of Ref. 3.

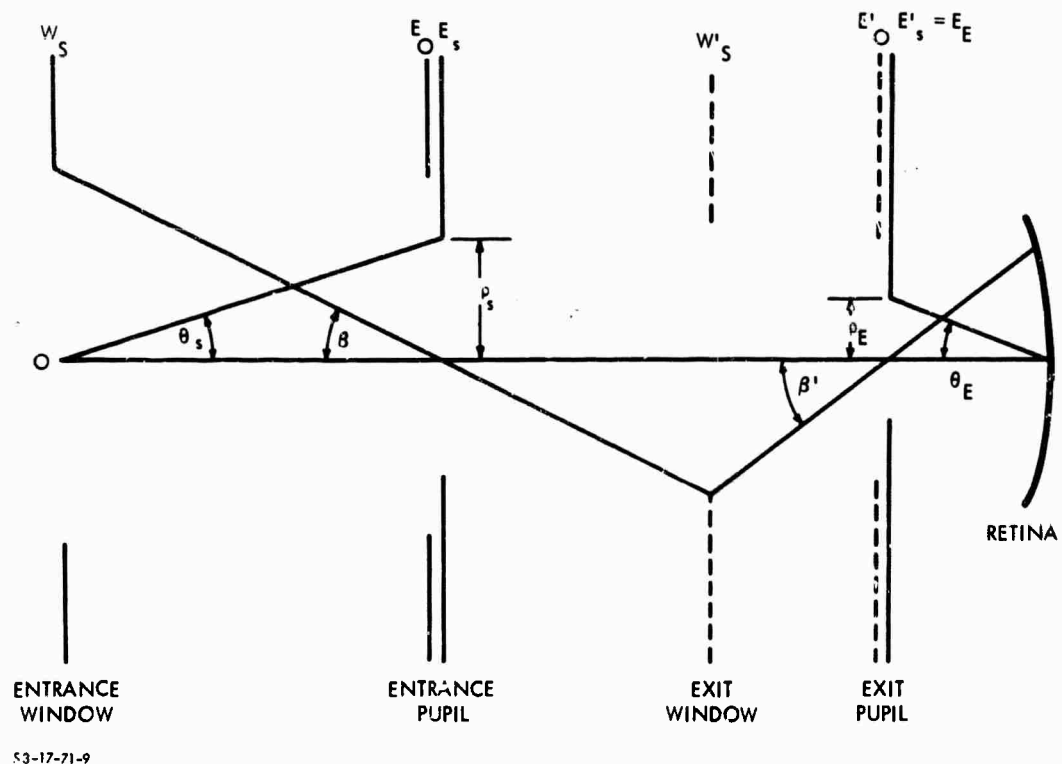


FIGURE III-4. Schematic Diagram of Binocular Visual System



The increase in visual perception at low light levels realized with binoculars may be attributed to the increase in image area on the retina produced by the subjective magnification and depends on the limited ability of the eye to integrate the signal over the increased image area. High subjective magnification is required for target detection, but the field of view, which is of major importance in visual search operations, is reduced in proportion to the increase in retinal image area. Thus, binoculars increase the probability of detection if the object is within the field of view but decrease the probability that the visual field includes the object to be detected.

## C. BASIC PARAMETERS AND THEORY OF PERFORMANCE OF PHOTOELECTRONIC IMAGING SYSTEMS

### 1. Optical Parameters and Principle of Operation

The incorporation of PEI devices in visual systems permits the manipulation of design parameters with far greater flexibility than allowed with binoculars. Image-intensifier night-vision systems incorporate an objective for collecting and focusing the radiant flux emanating from the scene onto the fiber-optic faceplate of an image-intensifier tube, an image-intensifier tube usually containing three stages of intensification, and an eyepiece presenting an enlarged virtual image of the intensifier display. Low-light-level television systems incorporate the following: an objective, one or more intensifier modules, a camera tube, fiber-optic couplers, a video signal amplifier, and a monitor containing a kinescope for displaying a real image for viewing. The incorporation of PEI devices in visual systems has the effect of decoupling the input and output radiant fluxes, removing some of the optical constraints encountered in binocular systems, such as those on:

- The utilization of radiant flux outside the visible spectrum and generally the use of more efficient image sensors than the eye.

- Independent adjustments of subjective magnification and flux collection power.
- The use of integration times longer than that of the eye.
- The time required for dark adaptation (dark adaptation is not required).
- The independent choice of optimum image brightness for high visual acuity and freedom from eyestrain.

In addition, PEI systems may provide greater flexibility of viewing through the use of remote-view television techniques. In practice, limitations on the performance of PEI systems arise because of imperfect technology and practical restrictions on size, weight, and cost.

a. Image-Intensifier Systems. In visual systems incorporating image intensifiers, the three parameters, (1) subjective magnification, (2) collection power, and (3) field of view, can be adjusted independently in contrast to binocular visual systems. In addition, the threshold sensitivity, quantum efficiency, and integration time of the system are subject to optimization to increase visual perception at low values of scene radiance.\*

In image-intensifier systems, if sufficient gain is provided, the appearance of a scintillation on the display will educe a visual sensation in the retina. Hence, the quantum efficiency of a visual system incorporating an image intensifier is characteristic of the quantum efficiency of the image-sensing surface of the intensifier.

If the duration of a scintillation produced on the display of an image intensifier is considerably longer than the integration time of the eye, the effective integration time of the complete visual system is characteristic of the integration time of the intensifier. Generally, however, image intensifiers are designed with integration

---

\* Each of the parameters is considered in turn, beginning with subjective magnification, in Ref. 2.

times comparable to that of the eye to avoid loss of visual perception for moving targets.

b. Television Systems. Television systems for low-light-level applications offer some additional degrees of design flexibility not available to direct-view image-intensifier systems. Besides the possibility of separating the position of the image sensor from the image display, it is possible to perform contrast enhancement and other forms of image processing by means of associated optical and computer systems with the long-range possibility of a completely automatic photoelectronic imaging and decision-making system.

These additional degrees of design flexibility in remote-view television systems result from the incorporation of an additional conversion process not found in direct-view image intensifiers--the conversion of the two-dimensional electron image generated at the primary photocathode into a video signal current by means of sequential readout of the image elements of the electron image on the camera-tube charge storage target. The conversion of the electron image into a video signal and subsequent amplification may introduce a limit on sensitivity not associated with the parameters of the eye. The minimum detectable signal current will be determined by the video preamplifier noise unless sufficient electron multiplication of the primary photoelectron is provided. In practice, it has been found that an electron multiplication of about  $10^4$  is required. Electron multiplication may be achieved with image-intensifier modules and/or internal electron multiplication by means of electron bombardment of the storage target.

If sufficient electron multiplication ahead of the storage and readout system is provided, the video current will consist of a coarse-grained signal current of large pulses reflecting the Poisson distribution and its noise in the signal current--large pulses compared to the usual fine-grained noise current of the preamplifier. The luminous image formed on the display by conversion of the video current will consist of bright scintillations forming the image and a dim background randomly generated by the video noise current. Under

these conditions, the quantum efficiency of the total visual system comprising the remote-view television system and the operator will be characteristic of the primary photocathode. Threshold sensitivity and integration time, as in direct-view image-intensifier systems, will be at the disposal of the designer subject to whatever restrictions are imposed by operational requirements, size, weight, and cost.

The same flexibility in design of subjective magnification and radiant flux collection power exists in remote-view television systems as in direct-view image-intensifier systems. However, the subjective magnification is not so rigidly specified. The difference lies in the fact that the magnification between the display and the retina depends on the distance, which may not be rigidly controlled.

The field of view of a television system is determined by the size of the primary photocathode and the focal length of the objective.

## 2. Spectral Response of Photocathodes

The effectiveness of a photocathode employed in a low-light-level photoelectronic imaging (PEI) system largely depends on the match between the spectral content of the input image irradiance and the spectral responsivity of the photocathode. The principal sources of passive nighttime radiant power in the order of decreasing magnitudes are the full moon, the hydroxyl emissions of the upper reaches of the atmosphere known as airglow, and the stars. The spectral content of moonlight, of course, is somewhat similar to that of sunlight. The airglow, whose integrated spectral radiant power (in the range from 0.6 to 1.8 microns) is only a factor of 10 less than full moonlight, exhibits roughly an exponentially increasing spectral radiant power dependence on wavelength. In addition, since both the contrast of many military targets against vegetation increases and the loss of contrast in transmission via atmospheric scattering decreases with increasing wavelength from the visible into the near infrared, it is valuable in low-light-level PEI systems to employ photocathodes with high near-infrared response.

The spectral responses of several typical photocathodes used as image sensors in PEI systems are shown in Fig. III-5. The S-1 surfaces are sensitive well into the near infrared and have been used in conjunction with auxiliary near-infrared scene irradiators designed to achieve operational covertness. One application during World War II was the sniperscope. Although the S-10 surface has been used extensively in commercial broadcast applications, where the similarity between its spectral response and that of the eye (shown in Fig. III-1) is prized, it is of no interest in the design of low-light-level PEI systems. The S-20 and its derivatives, the S-25 and S-20VR,\* with their high responsivity in both the visible and near-infrared portions of the spectrum, are the standard photocathodes employed in low-light-level PEI systems.

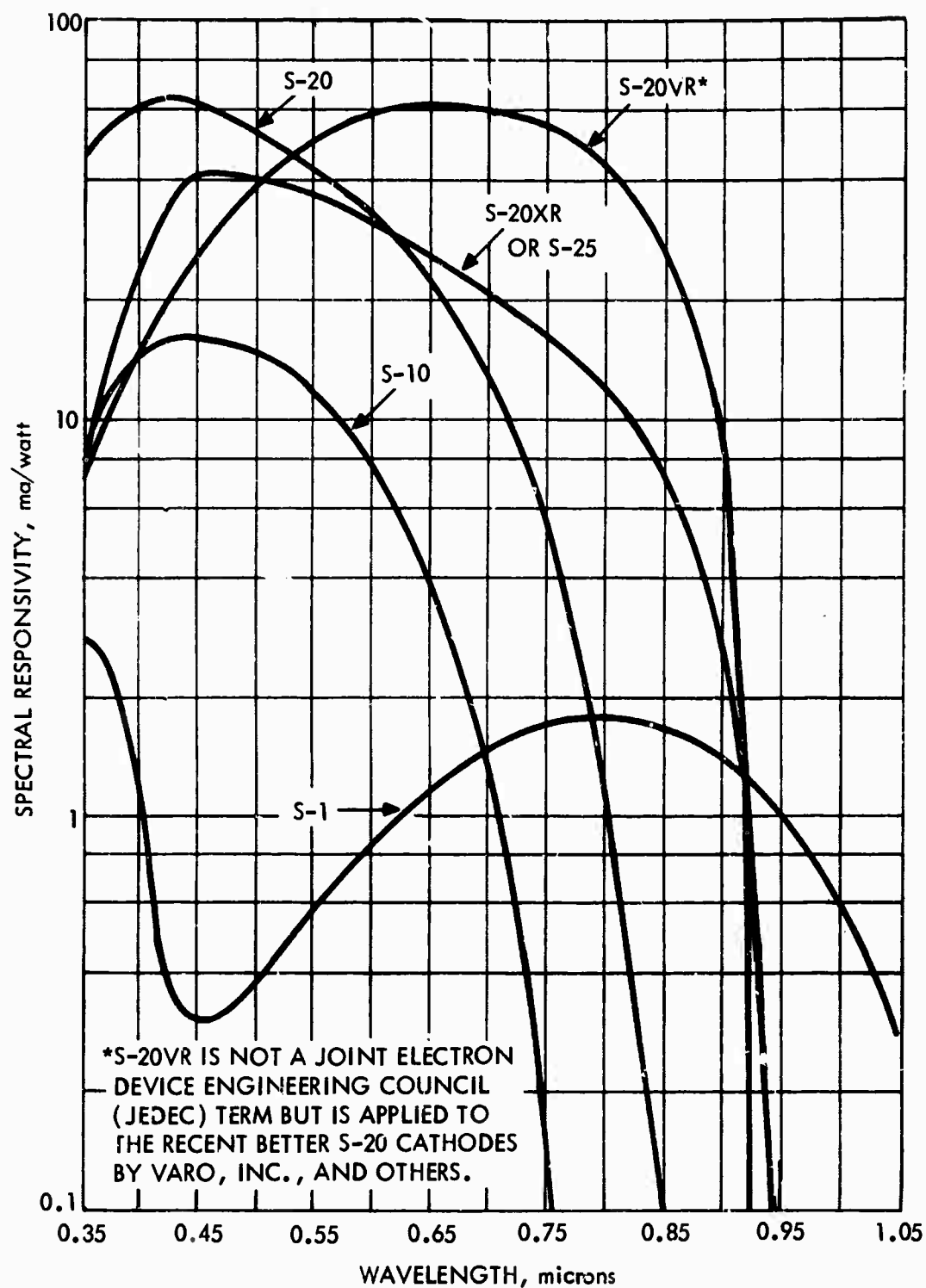
The value of the mean responsivity  $\alpha_T$  of an S-10 surface measured with a 2854°K lamp is typically 0.8 ma/watt.

One of the first steps forward in low-light-level imaging was the development of the S-20 surface with a  $\alpha_T$  of typically 3 ma/watt. This surface was gradually improved by extending its red response so that by the mid-1960's values of  $\alpha_r$  equal to 4 ma/watt became quite commonplace, with occasional values as high as 5 to 6 ma/watt. As the S-20 was improved, it became known as the S-20XR (XR for extended red) and was finally type-classified as the S-25. More recently even further improvements have resulted in a surface which is tentatively described as the S-20VR (VR for very red), whose mean responsivity is reported to vary from 5 to 9 ma/watt. The responsivity of the S-20VR in the near infrared is especially notable. Both the S-25 and the S-20VR will be used in calculations, although the S-20VR is not now as commonly available.

If the thermionic emission or dark current of a photocathode is comparable to or higher than the photoelectric current, contrast in

---

\* S-20VR is not a Joint Electron Device Engineering Council (JEDEC) term but is applied to the recent better S-20 cathodes by Varo, Inc., and others.



53-15-71-15

FIGURE III-5. Spectral Responsivity Versus Wavelength for Several Photoemissive Photocathodes

the output image of a scene is reduced. The thermionic emission or dark current of the S-1 is quite high, being  $10^{-11}$  to  $10^{-12}$  amp/cm<sup>2</sup> at room temperature. In many cases it is necessary to cool this surface to avoid excessive contrast loss. The dark current of the S-10 is considerably better at  $10^{-13}$  to  $10^{-14}$  amp/cm<sup>2</sup> but is still higher than desired for low-light-level applications. For the S-20 and S-25 surface, dark current is extremely low ( $10^{-15}$  to  $10^{-16}$  amp/cm<sup>2</sup>) and is not ordinarily a problem. The dark current of the S-20VR is similarly low.

### 3. Luminous Conversion Factor

In the operation of a low-light-level PEI system, the photoelectric current density generated at the primary photocathode is first amplified and then focused onto an output phosphor where a radiant image is generated. For a given set of electrode potentials the spectral radiant conversion factor of an image intensifier or kinescope is constant over a range of incident current densities  $j_p$  from near zero to near a saturation value. The saturation current density of zinc sulphide phosphors such as the P-20 is approximately 0.1 ma/cm<sup>2</sup>, independent of the incident electron energy.

The relative spectral radiant conversion factor as a function of  $\lambda$  is shown in Fig. III-6 for the typical modified P-20 phosphor used in most modern image-intensifier tubes. Comparison of the spectral radiant conversion factor of the modified P-20 with the relative spectral response curve of the eye shown in Fig. III-1 and the photocathode spectral responsivity curves shown in Fig. III-5 reveals that efficient optical coupling exists between this phosphor and both the human eye and the photocathodes S-20 and S-25.

### 4. Temporal Response

If an image system has a temporal response longer than that of the eye, the effect is to smear together image detail when an input image moves across the photocathode. In an intensifier some lag due to phosphor decay can be expected. One such measurement of temporal response performed with a modulated light source is shown in Fig. III-7.

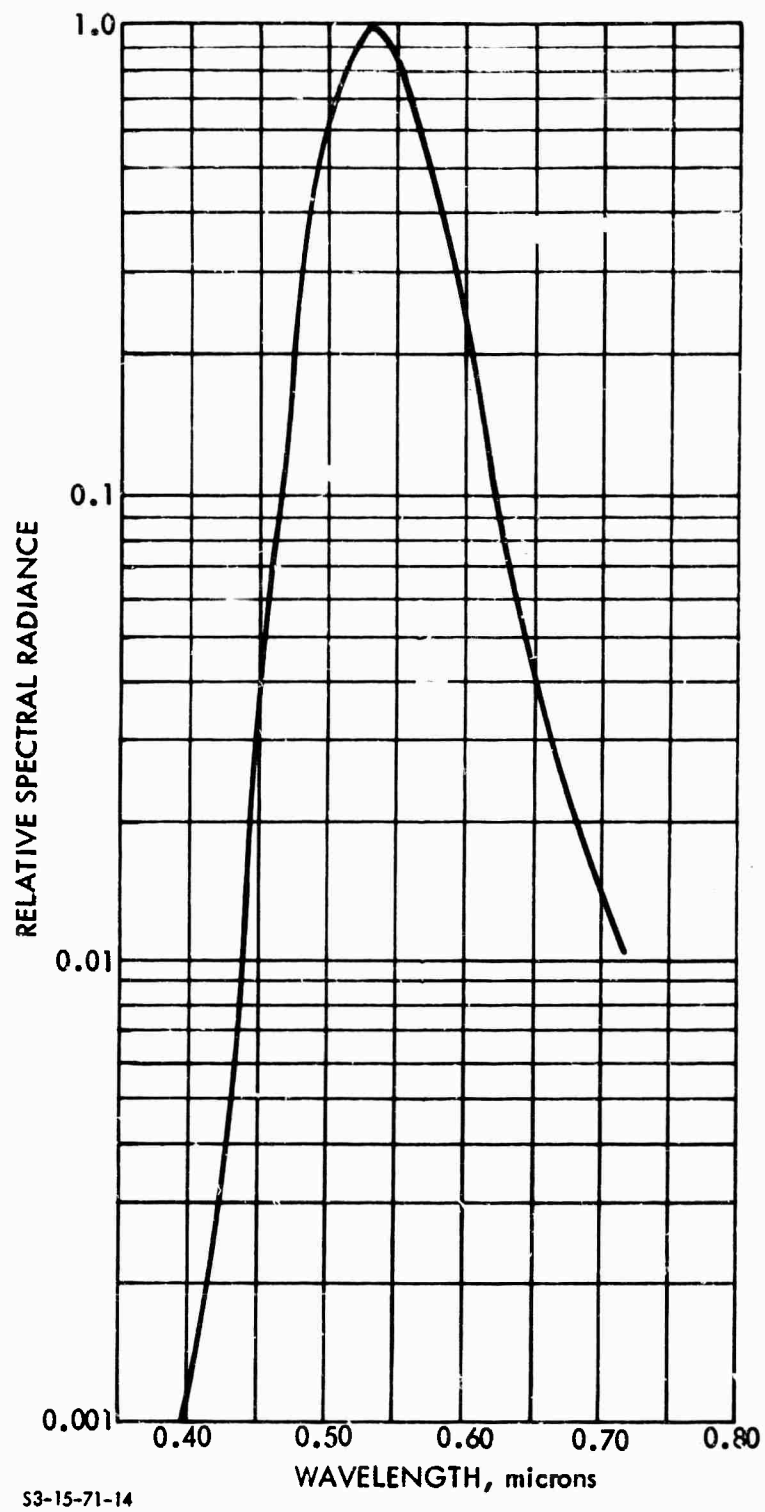


FIGURE III-6. Relative Spectral Radiance of a Modified P-20 Phosphor



The temporal response at the normal TV frame rate (30 frames/sec) is seen to be quite high for a single-stage intensifier but is appreciably lower for three-stage intensifiers. Methods of measuring and specifying temporal responses are not well known, but such measurements and specifications can be quite important, as will be discussed in connection with TV camera tubes.

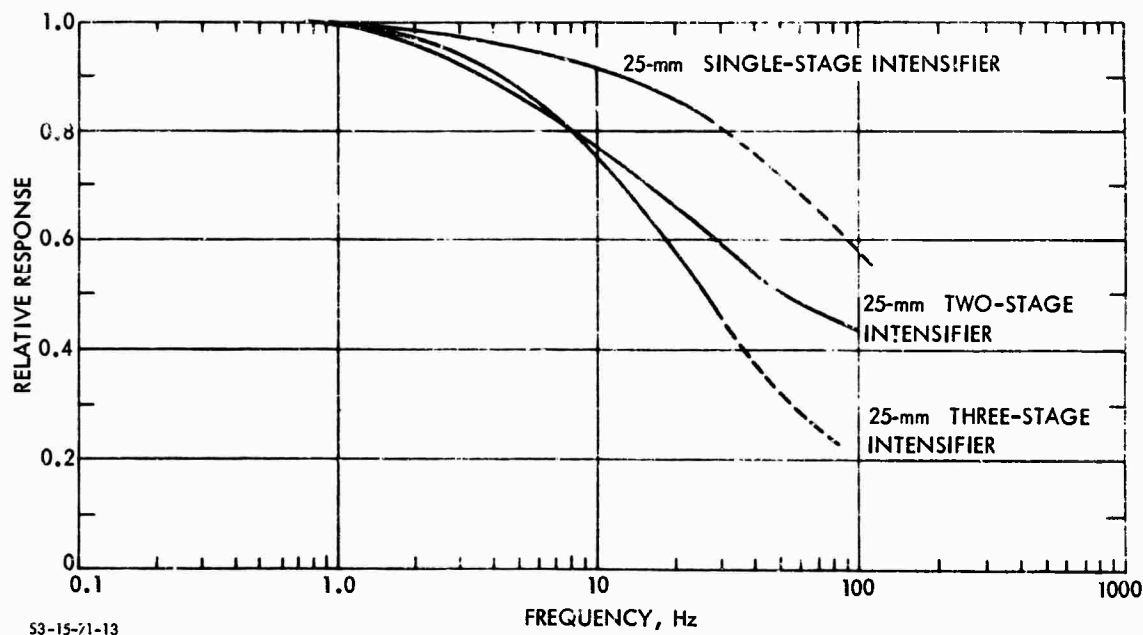


FIGURE III-7. Temporal Response of Image Intensifiers

Although intensifiers do exhibit lag effects of their own, their addition to a system can reduce overall system lag. Most camera tubes, in particular, have lag characteristics that depend on light level. That is, lag increases as light level decreases. By increasing light level on the camera tube, the increase in lag due to an added intensifier is usually more than offset by the decrease in camera lag.

## 5. Spatial Frequency Response

In the process of detecting the input image, converting it into electrons, focusing it onto the phosphor, and recreating a visible image, contrast is lost at each step for the reason that aberrations cause an overlapping of the radiance pattern on the display produced by the input image irradiance. In the limit of small-image element sizes, as contrast falls below a few percent, detection probability approaches zero.

Rather than reproduction of contrast on the display as a function of image element size, it is customary to consider the reproduction of the modulation amplitude of a sinusoidal, spatially modulated, radiant test pattern as a function of spatial frequency. The relation between contrast and modulation amplitude is described below. The modulation transfer function (MTF) or sine-wave response of a PEI system is defined as the ratio of the modulation amplitude of the display image to the modulation amplitude of the input image on the photocathode as a function of spatial frequency--normalized to unity as the frequency approaches zero. The sine-wave response can be measured by projecting a sine-wave pattern with 100 percent modulation onto the photocathode. First, a sine-wave pattern of low spatial frequency is employed and the peak-to-peak output amplitude is noted. With this amplitude as a reference, the pattern spatial frequency is increased in discrete steps. At each step, the new peak-to-peak amplitude is measured and the ratio of this amplitude to that measured at the low spatial frequency is formed. The plot of these amplitude ratios as functions of pattern spatial frequency constitutes the sine-wave response.

The sine-wave spatial frequency is described quantitatively in terms of  $\nu$ , the number of cycles (or line pairs) per millimeter or, alternatively, the number of half cycles (or lines) in some dimension such as the photocathode diameter or height of the display. The sine-wave responses of a typical single-intensifier module and of two- and three-intensifier modules, respectively, in cascade with unity magnification are shown in Fig. III-7. In general, the overall sine-wave response of several components in cascade is given by

$$T(v_{1s}, v_{nD}) = T_1(v_{1s}/m_1)T_2(v_{1s}/m_1m_2)\dots T_n(v_{1s}/m_1m_2\dots m_n) \quad (\text{III-4})$$

where  $T(v_{1s}, v_{nD})$  is the overall sine-wave response on the output phosphor at frequency  $v_{nD}$  to an input sine-wave pattern at frequency  $v_{1s}$ ;  $T_1(v_{1s}/m_1)$  is the sine-wave response of the first component, etc.;  $m_1$  is the image magnification in the first component, and so on. Equation III-4 results from observing that:

- The spatial frequency on the display is related to the spatial frequency on the sensor by  $v_D = v_s/m$ .
- The modulation amplitude  $M$  at the input to the second component is equal to the modulation amplitude at the output of the first component.
- The modulation amplitude at the output of each component is related to the modulation input by  $M_D = T(v/m)M_s$ .

It is apparent, on referring to Fig. III-8, that care must be exercised in cascading components that the expected increase in performance due to increased intensifier gain at the desired frequency is not cancelled by the reduced sine-wave response of cascaded stages at that spatial frequency.

The case of a zoom intensifier merits special attention. If the zoom-intensifier sine-wave response were unity at all spatial frequencies, resolution would be unlimited in both wide-angle and narrow-angle modes. Since the wide-angle mode also covers more viewfield, there would be little point to zoom with consequent reduction of viewfield. As a practical matter, the sine-wave response of the intensifier is limited by aberrations in the electron optics and the phosphor particle sizes. The sine-wave response of a zoom intensifier in both wide- and narrow-angle modes is shown in Fig. III-9. As the viewfield is decreased, going from the wide- to the narrow-angle modes, image magnification increases from  $m_W$  to  $m_N$  in the same ratio. Consequently, the spatial frequency scale of the sine-wave response curve is compressed by the factor  $m_N/m_W$  or, alternatively, on the same frequency

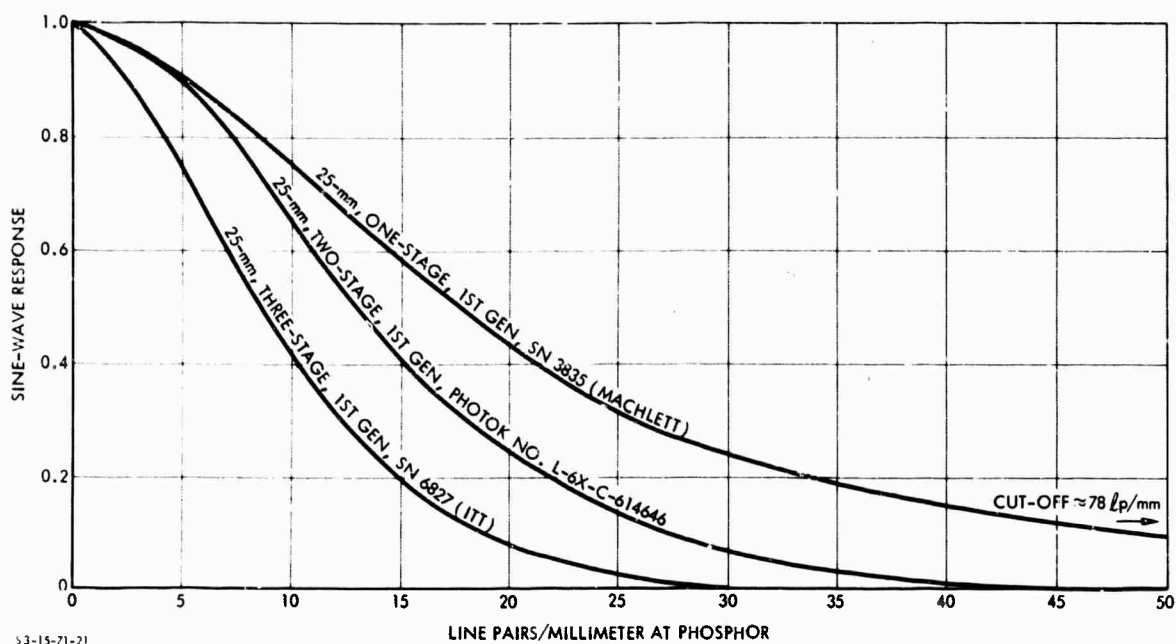


FIGURE III-8. Modulation Transfer Function of Image Intensifiers

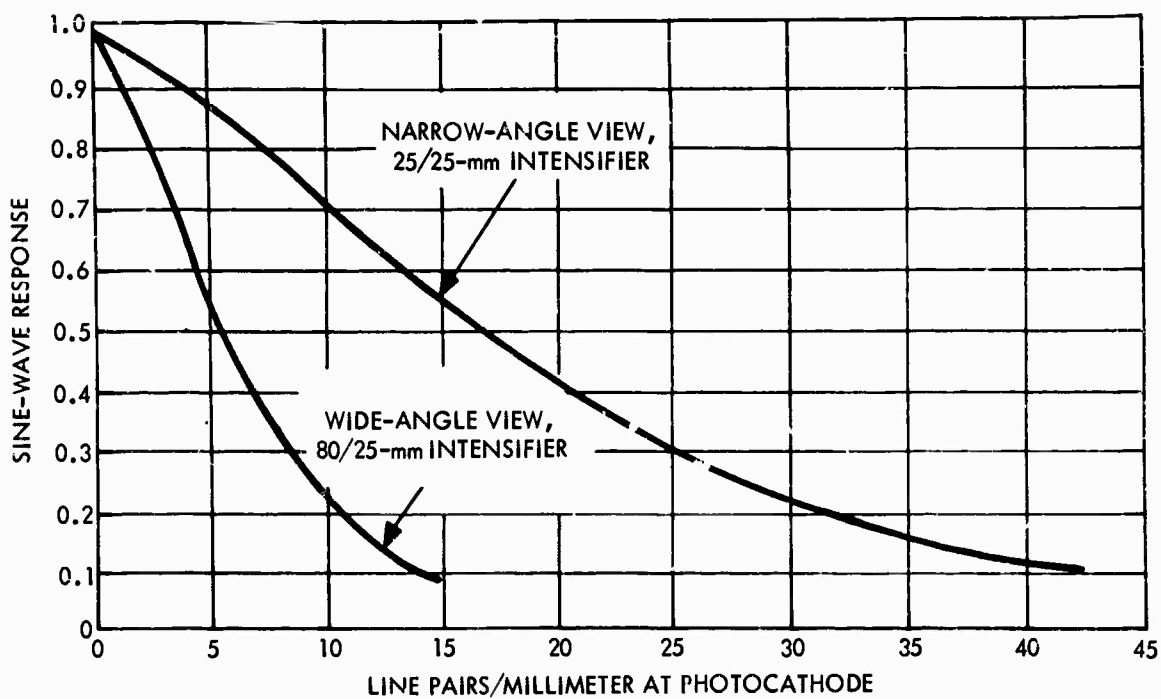


FIGURE III-9. Response of a Zoom Intensifier Referred to the Input Photocathode

scale the abscissa of points on the curve may be multiplied by  $m_N/m_W$ , shifting the entire curve as indicated in Fig. III-9. Specifically, for an 80/25-mm zoom tube, the magnification increases from approximately 1/3 to unity as the viewfield is decreased, and the abscissa of points on the wide-angle curve at a given response is shifted in the narrow field mode by approximately three times the frequency. Thus, some of the higher sine-wave response at a given target spatial frequency in the narrow-angle mode is sacrificed in the wide-angle mode for the sake of wider viewfield. On the other hand, greater brightness gain is realized and, if sufficient brightness gain is not otherwise provided, may provide some improvement in performance.

For evaluation of the overall performance of a complete visual system comprising both the human operator and the PEI system, it is also necessary to consider the spatial frequency response of the eye and the relation between frequency on the display and on the retina. Since it is not feasible to monitor the spatial dependence of the electrical signals generated in the eye as a function of spatial variations in the irradiance of the retina, it is not possible to make a direct measurement of the spatial frequency response. Rather, spatial frequency response can only be indirectly inferred from measurements of the modulation amplitude of a sine-wave test pattern required by the eye for some specified detection probability and the signal-to-noise ratio theory of detection probability. The dependence of detection probability on the signal-to-noise ratio at the decision centers of the brain, because it involves such parameters as the quantum efficiency and the temporal and spatial bandwidths of the eye, is incomplete. However, the required modulation function alone is sufficient to make predictions of the overall performance of a PEI system and its operator.

The frequency scale of the required modulation function depends on the distance from the eye to the display of a television monitor or the subjective magnification ( $m$ ) of an eyepiece. For example, if the viewing distance were 30 inches,  $m$  would be 1/3.

The required modulation as a function of frequency in cycles per inch calculated from retinal modulation sensitivity curves published by A. van Meeteren (Ref. 9) is shown in Fig. III-10 for a subjective magnification of unity and three luminance levels. These curves were determined under conditions such that for a given display luminance the signal-to-noise ratio is maximum, and hence the curves represent the minimum required modulation functions. The curve at  $0.52 \text{ cd/m}^2$  or  $0.15 \text{ ft-L}$  corresponds approximately to the usual luminance working level of an image intensifier display. Figure III-10 reveals that reduction of display luminance below  $0.52 \text{ cd/m}^2$  has a dramatic effect on the required modulation function, while increases in display luminance have a much smaller relative effect.

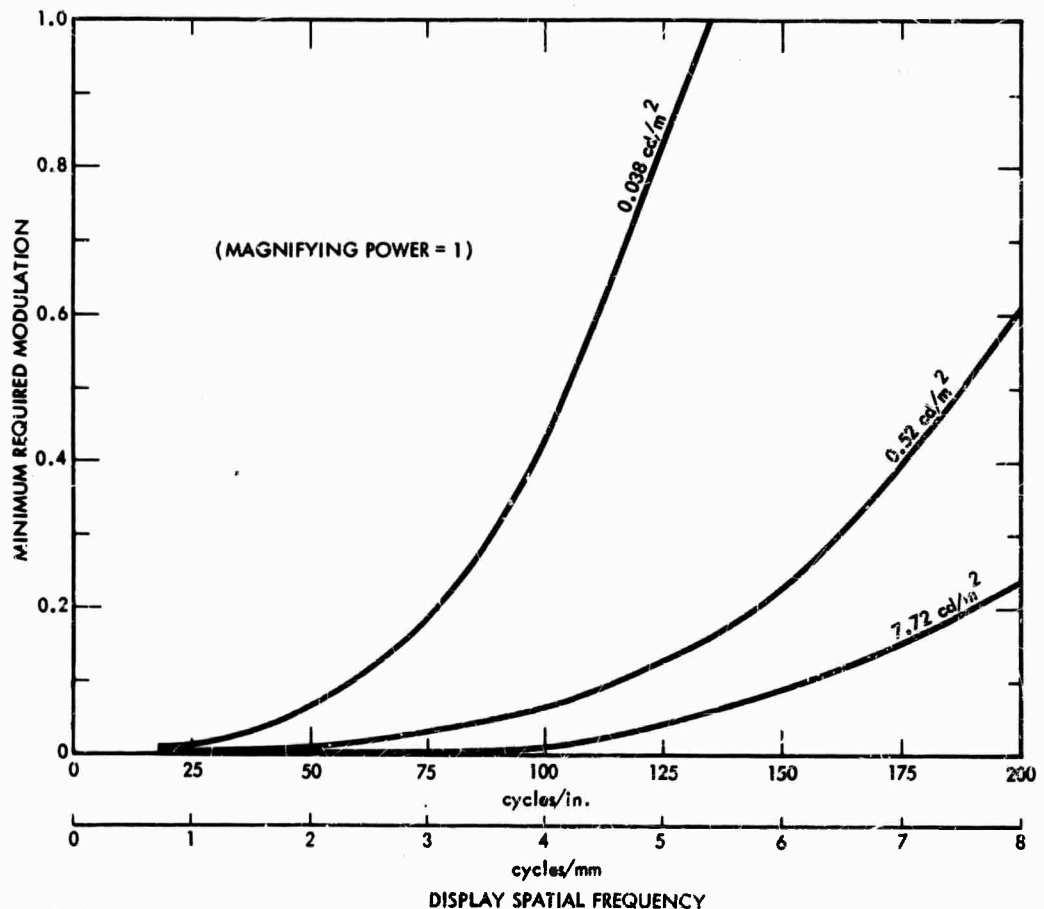


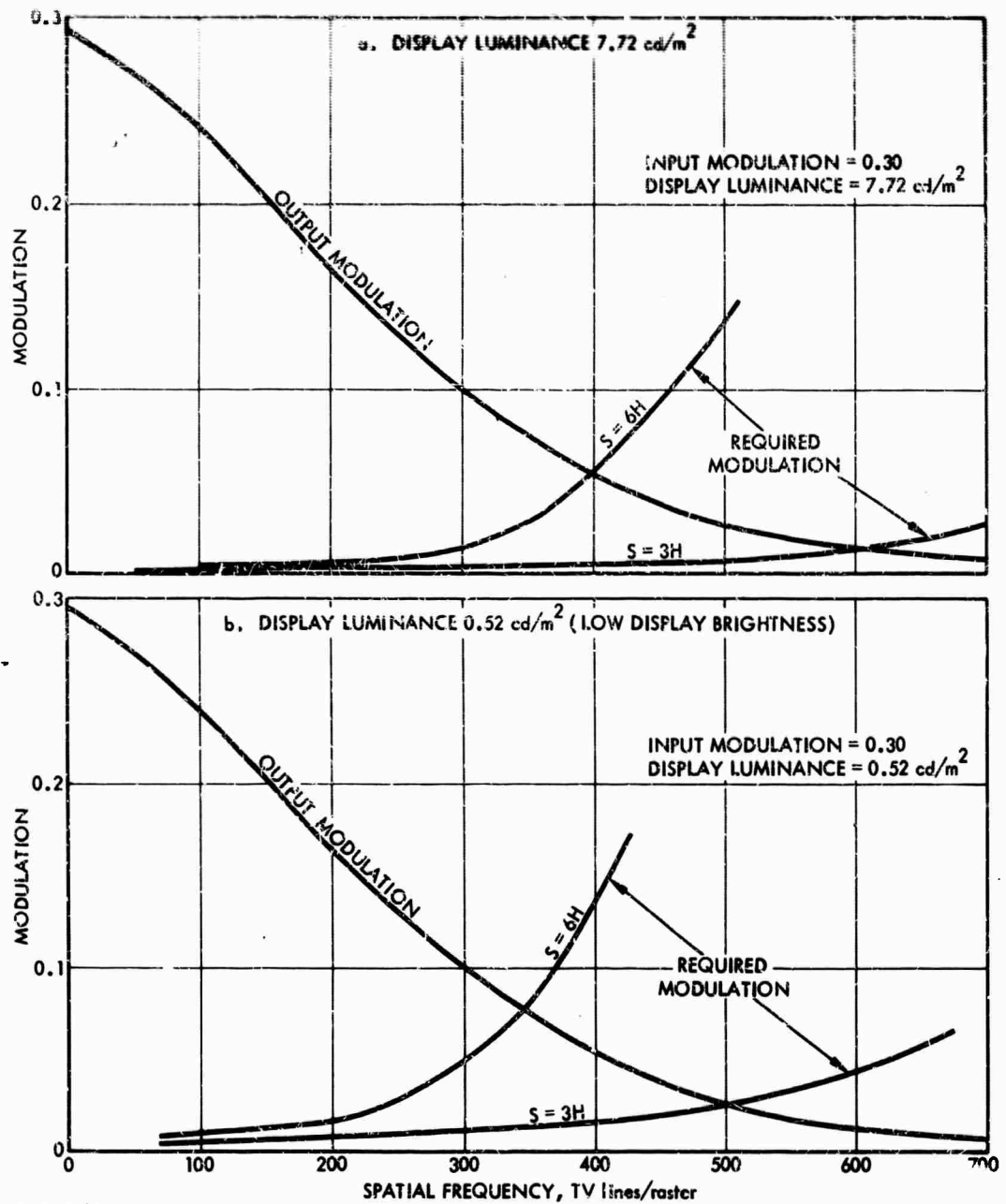
FIGURE III-10. Minimum Required Modulation for Detection of Sine-Wave Pattern by Eye (Ref. 9)

The relation between the minimum required modulation functions and the output modulation of a typical low-light-level television system is shown in Fig. III-11a and b at two display luminances, as indicated. In Fig. III-11a and b, for 30 percent input modulation, the output modulation of a single-stage noise-free but otherwise typical low-light-level television tube as a function of spatial frequency is shown in conjunction with the required modulation at viewing distances equal to six and three times the raster height. The frequencies at the intersections of the required modulation and output modulation curves are the resolution values of the eye-display combination under the assumed conditions. In Fig. III-11b, increasing the viewing distance from three to six times the raster height reduces the resolution from roughly 500 to 350 television lines per raster height.

In image-intensifier systems the subjective magnification of the eyepiece is typically seven times, which is equivalent to a viewing distance of only 1.4 in. Therefore, both the required modulation of the eye and the resolution are determined by the output luminance fluctuations. However, an exception may arise in single-stage demagnifying image intensifiers, where both  $M$  and the display luminance may become low compared to their corresponding values in a conventional multistage image intensifier.

It is important in the design of both remote-view television and direct-view image-intensifier systems to present the output image to the eye at sufficient luminance and angular size that the required modulation is little affected by the optical properties of the eye and the neurological organization of the retina but rather by the fundamental effects of output luminous fluctuations on the decision process.

It has been determined empirically (Part II) that excellent correlation exists between the subjective quality of aerial photographs and the modulation transfer function area (MTFA) bounded by the ordinate axis, the image modulation function of the photograph, and the required modulation function of the eye. The rationale for the choice (Ref. 10) of the MTFA as an overall measure of picture quality and



53-15-71-12

**FIGURE III-11. The Ultimate Limit for Visibility as a Function of Brightness and Viewing Distance. (Output Modulation for 30 Percent Input Modulation to a Noise-Free but Otherwise Typical Low-Light-Level Television Tube and Required Modulation for Viewing Distance  $S$  Equal to Six and Three Times Raster Height  $H$ . The Noise Level for the Data is Determined Only by the Electric Noise Generated in the Eye Due to the Photon Nature of the Display Luminance.)**



observer performance is based on the observation that easy detection of a particular spatial frequency requires that the modulation should be as high as possible (conspicuous) above that required by the eye, for, say, 50 percent detection probability with unlimited viewing time. In aerial photographs, all spatial frequencies are generally of interest. Hence, the MTFA was proposed as an overall measure of observer performance and picture quality. In the visual observation of photographs, the modulation required by the eye at low spatial frequencies depends on the properties of the visual system. At higher spatial frequencies, fluctuations in grain size set the requirement and cause the required modulation to rise.

In the case of low input image irradiance to PEI systems, a rise in required modulation with increasing frequency is observed that is due to fluctuations in the output luminance produced by scintillations on the display. While the required modulation function depends on the optics and neurological organization of the eye at high-input irradiance, at low-input irradiance the required modulation function is largely determined by the effects of luminance fluctuations at the display on the decision process. A different required modulation curve occurs at low-input irradiance for each photocathode at each input irradiance. The effect of fluctuations on the required modulation function of the eye is discussed further below.

## 6. Theory of Performance of Photoelectronic Imaging

The probability of correctly identifying a known signal in the presence of noise is a function of the signal-to-noise ratio. It has been demonstrated by Rose (Ref. 6), Schade (Ref. 11), Coltman (Ref. 12), and Coltman and Anderson (Ref. 13) that the probability of detecting simple targets, such as disks on a uniform background, bar patterns, and sine-wave patterns, depends on the signal-to-noise ratio of the image formed on the display. They concluded that in an image formed by scintillations (under low brightness conditions, when fluctuations in intensifier gain and internal sources of noise can be neglected), the signal is proportional to the average difference in

the number of scintillations generated at adjacent image elements per sampling time (the effective integration time of the eye), and the noise is proportional to the root-mean-square value of the fluctuations in the difference.

The primary source of noise at the input of a PEI system arises from shot noise inherent in the photoelectric current generated at the photocathode by random absorption of the incident photon flux. It is observed that the numbers arriving on a small area of the sensor in equal intervals of time obey the Poisson distribution function. The root-mean-square value of the fluctuations about the average number is equal to the average number. Such temporal fluctuations constitute noise that inhibits image perception and reduces detection probability per glimpse.

For a given input-image element size and sampling time, the signal-to-noise ratio of the output image is determined by four properties of the PEI system:

1. The size of the entrance pupil of the objective.
2. The quantum efficiency of the photocathode.
3. The internal generation of noise, such as shot noise in thermionic current (fluctuations in electron multiplication processes and Johnson noise in the input resistor of the video amplifier).
4. The degree to which the input image can be reproduced on the display without overlap of the luminance of adjacent image elements, i.e., the modulation transfer function.

- In image-intensifier tubes, thermionic current and fluctuations in electron multiplication are generally negligible compared to the shot noise of the photocathode current. In low-light-level television systems, if high intensifier gain is provided, the video amplifier output current consists of a coarse-grained current of large pulses and a fine-grained noise current. The large pulses result from charge pulses evoked by emission of an electron from the photocathode and by

electron multiplication increased to several thousand electrons before the video amplifier. The fine-grained noise current in tubes without electron multipliers largely results from random thermal generation in the first stage of the video preamplifier. Intensification of a primary photoelectron by a factor of approximately  $10^4$  at static and scan rates is sufficient to overcome the effect of video noise in the output image.

As an example, if the storage target comprises  $5 \times 10^5$  storage elements and the frame time is 1/30 sec, the readout time of one storage element is  $6.7 \times 10^{-8}$  sec. For a readout time of  $6.7 \times 10^{-8}$  sec and primary electron intensification of  $10^4$ , the average pulse current due to a single photoelectron will be roughly 24 na, providing an average pulse-current signal-to-video amplifier noise ratio of 10 at the input to a good video preamplifier. Primary electron intensification of  $10^4$  can be easily obtained with a combination of a one-stage image intensifier and SEBIR tube, can be just barely obtained with a one-stage image intensifier and SEC vidicon combination, and cannot be realized with a double image intensifier and plumbicon or vidicon combination. The required factor of  $10^4$  requires three cascaded intensifiers for an intensifier vidicon camera. However, more intensification, at a sacrifice in frequency response, is obtained by cascading more intensifier stages.

The steps followed in the analysis of photoelectronic imaging systems consist in calculating the signal and the noise, forming the signal-to-noise ratio, setting it equal to unity, and solving for the modulation, i.e., the noise-equivalent modulation (NEM). The modulation required by the eye is then determined by multiplying the NEM by the signal-to-noise factor  $k$  required by the observer to make correct decisions of a given probability.

The chief result of the analysis of image intensifiers is given by the following equation\* for the required modulation  $M_t$ :

---

\*The derivation of Eq. III-5 is given in Section IV-F of Ref. 8.

$$M_t = 3.8 \pi v_{os} / (2 e \bar{n}_s t)^{\frac{1}{2}} \quad (\text{III-5})$$

where 3.8 is the S/N factor  $k$  (Ref. 14),  $\epsilon$  is the length-to-width ratio of a half period of a sine-wave test pattern,  $v_{os}$  is the spatial frequency of the test pattern at the photocathode in cycles/mm,  $\bar{n}_s$  is the photoelectron emission of the primary photocathode in electrons/mm<sup>2</sup>-sec, and  $t$  is 0.2 sec--the effective integration time of the eye and phosphor. Higher values of  $M_t$  would be required if higher detection probability, shorter detection time, or detection under field conditions rather than laboratory conditions were required.

For low-light-level television systems, it is convenient to express the modulation required by the eye in the form

$$M_t = 3.8 \pi N / [6 \epsilon (i_s / e) t]^{\frac{1}{2}} \quad (\text{III-6})$$

where  $N$  is the number of television lines per raster height,  $\epsilon$  is the length-to-width ratio of a half period of the test pattern,  $t$  is 0.2 sec, the integration time of the eye,  $e$  is the magnitude of the electron charge in coulombs,  $i_s = e \bar{n}_s (4/3) H^2$  is the total primary photocathode current, and  $H$  is the height of a raster on the photocathode. Equation III-6 applies to low-light-level television systems with sufficient intensifier gain that the output signal-to-noise ratio is negligibly affected by the video preamplifier noise.

The overall performance of a low-light-level PEI-human eye system at a given scene radiance is essentially specified by the frequency response (modulation transfer) function and the required modulation function of the eye. For example, output modulation functions for several values of input modulation, calculated curves of required modulation for several values of primary photocathode current, and minimum required modulation functions at display luminances of 0.52 cd/m<sup>2</sup> and 7.72 cd/m<sup>2</sup> are shown in Fig. III-12 for a typical triple image intensifier and in Fig. III-13 for a typical low-light-level television system.

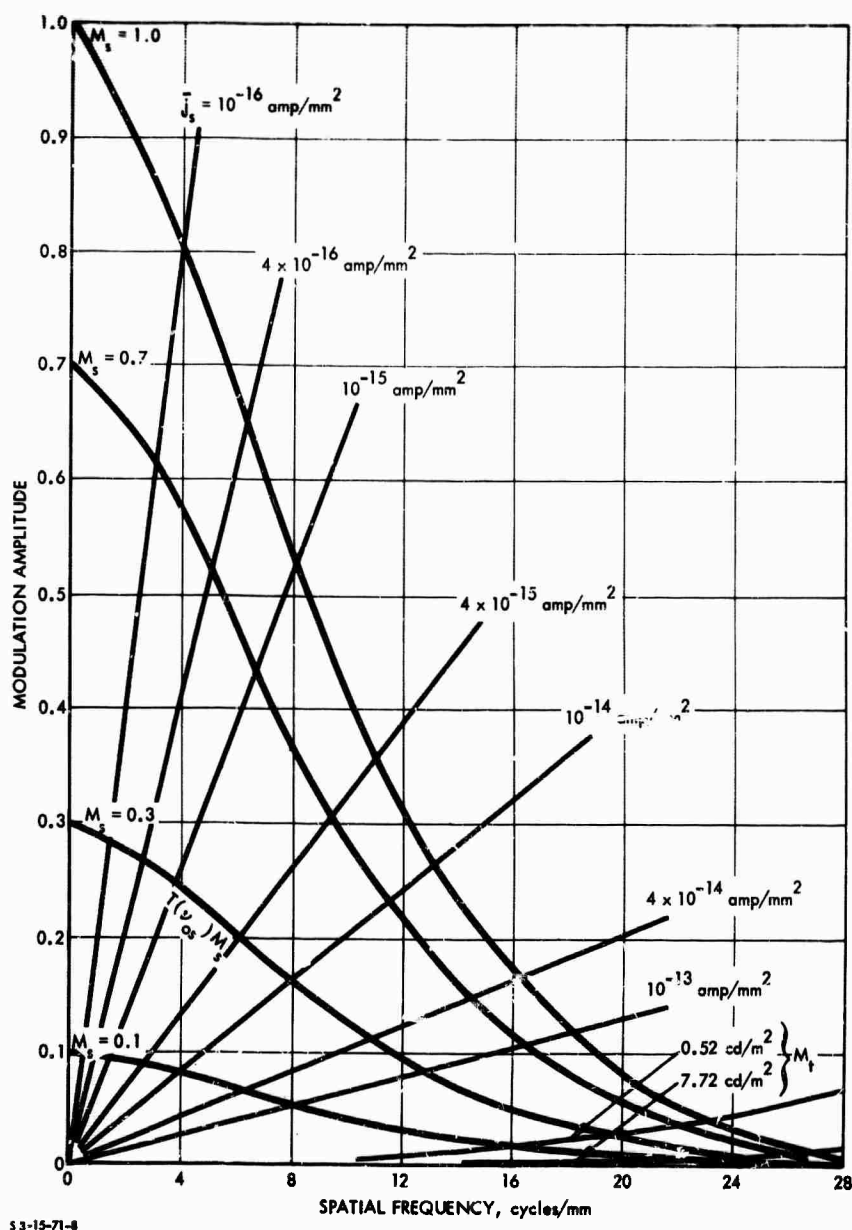


FIGURE III-12. (a) Output Modulation of Typical Triple Image Intensifier for Input Modulation Values  $M_s$  of 1.0, 0.7, 0.3, and 0.1 and (b) Theoretical Modulation  $M_t$  Required by the Eye for Values of Photocathode Current Density  $\bar{J}_s$  of  $10^{-16}$ ,  $4 \times 10^{-16}$ ,  $10^{-15}$ ,  $4 \times 10^{-15}$ ,  $10^{-14}$ ,  $4 \times 10^{-14}$ , and  $10^{-13}$  amp/mm<sup>2</sup>. Experimental Limiting Required Modulation Curves, Labeled  $0.52 \text{ cd/m}^2$  and  $7.72 \text{ cd/m}^2$ , are for an  $M = 7$  Ocular.

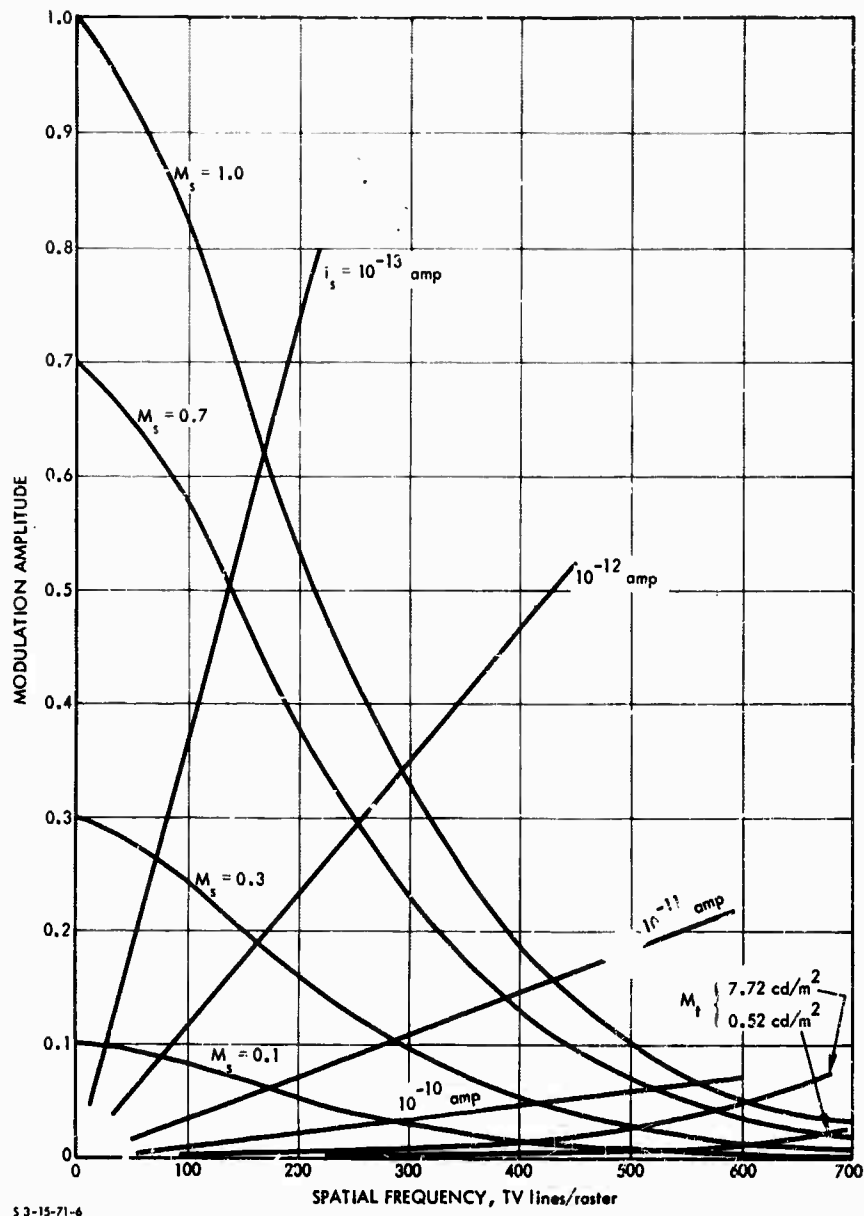


FIGURE III-13. (a) Output Modulation of Typical Low-Light-Level Television for Input Modulation Values  $M_s$  of 1.0, 0.7, 0.3, and 0.1 and (b) Theoretical Modulation Required by the Eye for Primary Photocathode Current  $i_s$  of  $10^{-13}$ ,  $10^{-12}$ ,  $10^{-11}$ , and  $10^{-10}$  amp. Experimental Limiting Required Modulation Curves, Labeled  $0.52 \text{ cd/m}^2$  and  $7.72 \text{ cd/m}^2$ , are for a Viewing Distance Equal to Three Times the Raster Height.

These figures depict the following information:

- The ratio of the output modulation to the required modulation at a given spatial frequency, equal to  $1/3.8$  times the output signal-to-noise ratio.
- At the intersection of a given output modulation and required modulation curve, the value of the output signal-to-noise ratio is just 3.8, the minimum required for 50 percent detection probability. Hence, the corresponding value of spatial frequency at the point of intersection is the resolution frequency of the PEI-human eye system for test patterns of a given modulation and radiance.

It is interesting to note, first, that the value of required modulation\* at the resolution frequency is not 1.5 percent, as commonly supposed, but depends on the primary photocathode current density determined by the "apparent" radiance of the test pattern, the f-number of the objective, and the mean responsivity of the photocathode. Second, it is interesting to note that the limiting resolution frequency at low input irradiance is not proportional to the square root of the primary photocathode current density but rather is relatively insensitive to it.

The common assumption that resolution frequency is proportional to the square root of the mean responsivity owes its origin to the earliest papers (Refs. 6, 12) on the signal-to-noise theory of resolution, in which the authors did not include consideration of the frequency-response function. This, in effect, amounts to assuming an ideal flat frequency-response function. For example, in Fig. III-12 this assumption would result in the output modulation curves becoming horizontal lines. The intersections of the required modulation curves with these horizontal lines of output modulation would then yield the

---

\* At low modulation, the contrast is about twice the modulation value. For the relation between modulation amplitude and contrast, see Eq. 52, Ref. 8.

proportionality of resolution frequency on the square root of mean responsivity. However, due to the rapid roll-off of frequency response with increasing frequency, the resolution frequency is quite insensitive to responsivity.

The relative importance of responsivity and frequency response to performance is discussed further in Part IV, where specific image intensifier tube structures are described.



### PART III. REFERENCES

1. Jurgen R. Meyer-Arendt, "Radiometry and Photometry: Units and Conversion Factors," Appl. Opt., Vol. 7, No. 10, p. 2081, October 1968.
2. Institute for Defense Analyses, Luminance, Radiance, and Temperature, IDA Research Paper P-339, Lucien M. Biberman, August 1967.
3. A.C. Hardy and F.H. Perrin, The Principles of Optics, McGraw-Hill, New York, 1932.
4. C.H. Graham, Vision and Visual Perception, John Wiley and Sons, Inc., New York, 1965.
5. J.L. Brown, C.H. Graham, H. Leibowitz, and H.B. Ranken, "Luminance Thresholds for the Resolution of Visual Detail During Dark Adaptation," J. Opt. Soc. Am., Vol. 43, No. 3, p. 197, March 1953.
6. A. Rose, "The Sensitivity Performance of the Human Eye on an Absolute Scale," J. Opt. Soc. Am., Vol. 38, No. 2, p. 196, February 1948; "Television Pickup Tubes and the Problem of Vision," Advances in Electronics, Vol. 1, p. 131, 1948.
7. Otto H. Schade, Sr., "Optic and Photoelectric Analog of the Eye," J. Opt. Soc. Am., Vol. 46, No. 9, p. 721, 1956.
8. Institute for Defense Analyses, Low-Light-Level Performance of Visual Systems, IDA Paper P-741, Alvin D. Schnitzler, March 1971.
9. A. van Meeteren, Modulation Sensitivity and Spatial Bandwidth of the Eye at Low Luminances, paper presented at Optical Society of America meeting, Chicago, Ill., October 21-24, 1969.
10. W.N. Charman and A. Olin, "Image Quality Criteria for Aerial Camera Systems," Phot. Sci. and Eng., Vol. 9, p. 385, December 1965.
11. Otto H. Schade, Sr., "The Resolving-Power Functions and Quantum Processes of Television Cameras," RCA Review, Vol. 28, p. 460, September 1967.

12. J.W. Coltman, "Scintillation Limitations to Resolving Power in Imaging Devices," J. Opt. Soc. Am., Vol. 44, No. 3, pp. 234-237, March 1954.
13. J.W. Coltman and A.E. Anderson, "Noise Limitations to Resolving Power in Electronic Imaging," Proc. IRE, Vol. 48, p. 858, May 1960.
14. Richard Legault, "Visual Detection Process for Electrooptical Images: Man--The Final Stage of an Electrooptical Imaging System," Chapter 4 in L.M. Biberman and S. Nudelman, eds., Photo-electronic Imaging Devices, Vol. I, Plenum Press, New York, 1971.

#### IV. IMAGE-INTENSIFIER TUBE STRUCTURES

by Alvin D. Schnitzler

##### A. BASIC SINGLE-STAGE STRUCTURE

Night-vision systems incorporate a variety of image-intensifier devices, often in combinations, designed to meet various operational conditions and military requirements. The physical electronic functions performed in image intensifiers include:

- Conversion of the radiant image formed on the image-sensor surface into an electron image,
- Intensification of the electron image, and
- Conversion of the intensified electron image formed on the display surface into a visual image

By far the most sensitive image-intensifier devices--and the only ones found to be useful at low radiation levels--rely on photoelectron emission in vacua for radiant-to-electron image conversion, though photoemission is not as efficient a conversion process as the internal photoelectric effect in photoconductors. Photoemissive devices are superior because in the internal electron-multiplication process, the mean free path of hot electrons is so short that the high electric field required to achieve multiplication results in background current exceeding the photoelectric current at low radiation levels by many orders of magnitude. Another essential advantage of vacuum photoemission is that the process is extremely fast and free of the capacitive lag problem inherent in photovoltage-dependent image sensors such as the vidicon and the velocity selector tube.

In addition to brightness gain, image intensifiers can be used to provide viewfield zoom by simple electronic means. They are also simply coupled to television pickup tubes to increase their sensitivity.

The simplest and earliest developed (publications on them appeared in the 1930's) image intensifiers (Ref. 1) consist of a photocathode, an electron lens, and a phosphor screen. The power that provides the possibility for image intensification comes from that absorbed by the electrons falling through the potential difference between cathode and phosphor. If the potential difference is several thousand volts, the high-energy electrons impinging on the phosphor screen will produce many electron-hole pairs, which subsequently recombine to yield many output light quanta. Focusing of the electron image, generated by the radiant image incident on the photocathode, onto the phosphor screen by either (1) proximity focusing, (2) electrostatic focusing, or (3) magnetic focusing gives rise to three types of basic image-intensifier tubes.

Proximity focusing depends on accelerating the photoemitted electrons in their parabolic paths so that the transit time from cathode to phosphor is so short that the transverse distance traveled by the electrons is negligible. Disadvantages of this method of electron focusing are:

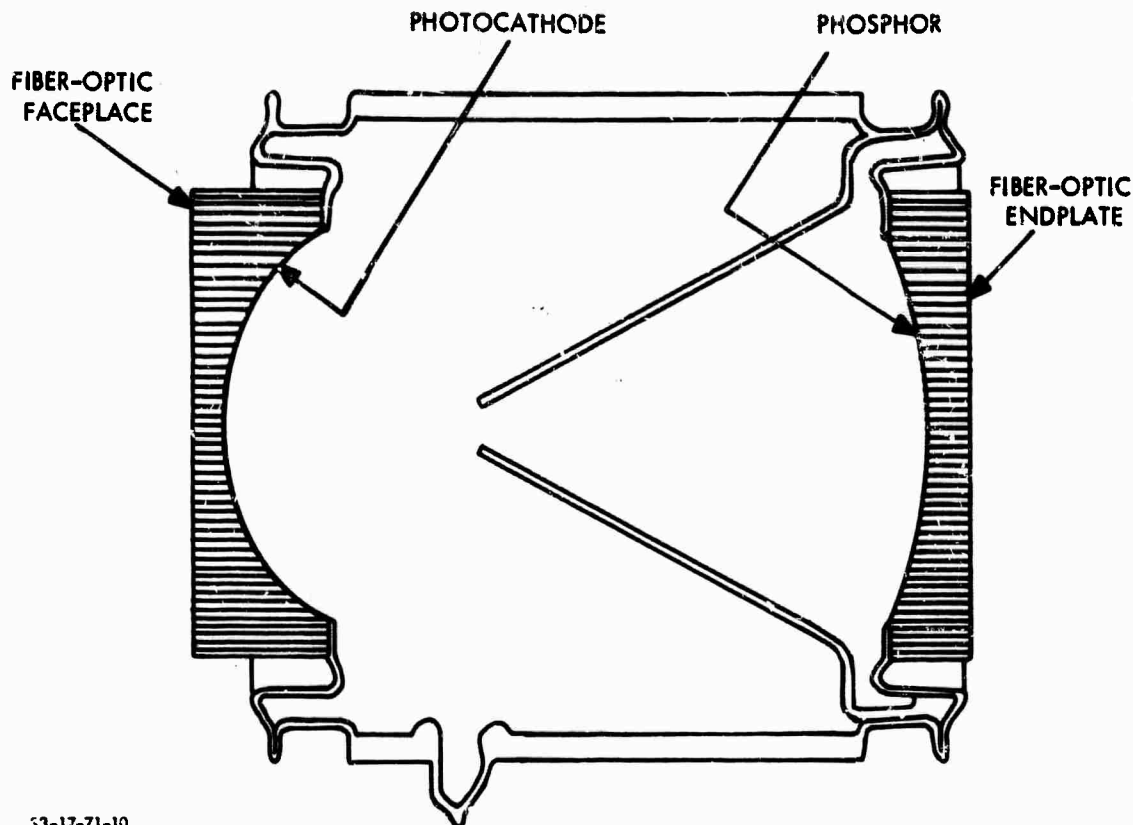
- The high electric fields required tend to cause cold-electron emission, which exhibits shot noise and reduces contrast in the image produced at the screen.
- The close spacing required makes the preparation of the photocathode difficult.

Electrostatic focusing of electrons results from superposition of a radially symmetric field and the longitudinal electric field in the space between cathode and screen. Such an electrostatic lens is capable of forming a first-order image and is analogous to a glass lens with variable index of refraction (the square root of the electric potential at each point corresponding to the index of refraction). Unfortunately, electrostatic lenses are subject to severe aberrations, including curvature of the image field, astigmatism, and radial distortion. It has not been found practical to design electrostatic lenses to provide a good extended image when a flat cathode is employed.

However, by proper curvature of the cathode, both curvature of image field and radial distortion can be reduced so that the resolution over an extended image several centimeters in diameter exceeds the phosphor capabilities.

Magnetic focusing of electrons emitted by the photocathode results from superposition of a strong, uniform axial magnetic field and the electric field in the space between cathode and screen. Emitted electrons traverse helical paths under the influence of the uniform parallel electric and magnetic fields, and, independent of their initial lateral velocities, all electrons emitted from a point come together to form image points periodically after each complete cycle. The phosphor screen is generally placed at the first image point. The chief advantage of the magnetic lens is that high resolution can be obtained with a flat photocathode. However, exact adjustment and regulation of the electric and magnetic fields are necessary for good resolution requiring well-regulated power supplies. Moreover, magnetic lenses are generally bulky. Therefore, the most commonly used method of electron focusing in image intensifiers of low to moderate resolution is electrostatic focusing.

A typical module of an electrostatically focused image intensifier is shown in Fig. IV-1. It consists of an evacuated glass envelope with a photocathode on the inner surface of one fiber-optic plate and a phosphor on the other. The inner surface of the fiber-optic plates are curved to minimize image distortion. The photoelectron image is greatly accelerated and focused onto the phosphor, which recreates the original image in correct spatial correspondence, except that the image is inverted top for bottom and right for left. To prevent feedback of phosphor light to the photocathode, the internal cone-shaped electrode is blackened and the inner surface of the phosphor is aluminized. The light that emanates from the output plate is diffused, so that when coupling to other intensifiers, both first-stage output and second-stage input plates must be optically flat and tightly joined.



53-17-71-10

FIGURE IV-1. Schematic of a Single-Stage Image Intensifier

The maximum accelerating voltage is typically 15 kv. At higher voltages, the dark current rapidly increases, and difficulties with positive-ion bombardment of the photocathode may be encountered. Some control over image brightness can be achieved by reducing the accelerating voltage (about 10 to 15:1), but at voltages much below 2 to 3 kv the image will lose focus and rotate.

If the magnification is made variable and an increase in magnification is accompanied by a decrease in viewfield, then one has electronic zoom. This can be accomplished by reducing the effective area of the input photocathode while maintaining the same size of the image field on the phosphor. A zoom intensifier in which the input photocathode area is variable is shown in Fig. IV-2. In this tube, the amount of photocathode area that is imaged on the phosphor is electronically

variable by changing potentials on various internal focus electrodes. In current practice, a zoom of up to 3:1 viewfield can be provided while maintaining the image field on the phosphor at full size.

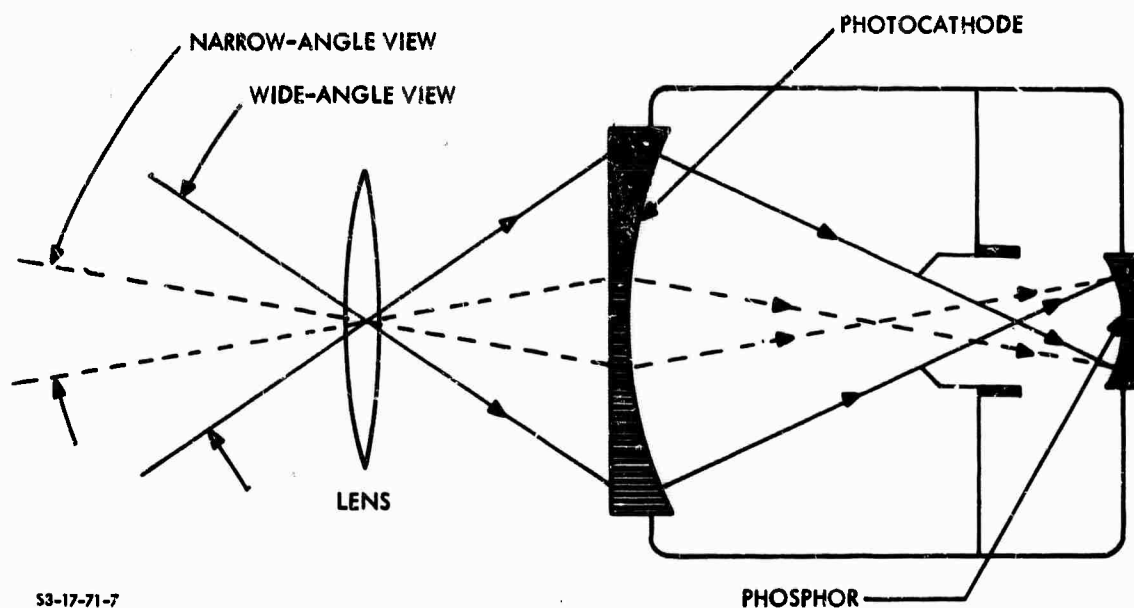


FIGURE IV-2. Schematic of an "Electronic Zoom" Intensifier

The most common intensifier module sizes are 16/16, 18/18, 25/25, 40/18, 40/25, 40/40, 60/18, 80/25, and 80/40 mm, where the first number refers to the photocathode diameter and the last refers to the phosphor diameter. The approximate dimensions are given in Table IV-1. These sizes vary considerably from manufacturer to manufacturer but may be thought of as representative.

TABLE IV-1. TYPICAL INTENSIFIER DIMENSIONS

Intensifier Photocathode/Phosphor Dia., mm	Zoom Range	Length, in.	Diameter,* in.
16/16	1:1	1.65	1.16
18/18	1:1	2.0	1.35
25/25	1:1	2.4	2.0
40/25	1:1	5.4	4.0
40/40	1:1	3.7	3.0
60/18	3:1	6.0	3.7
80/25	3:1	8.0	6.0
80/40	3:1	8.0	6.0

\* Exclusive of high-voltage insulation

#### B. CASCADE IMAGE INTENSIFIERS

Early interest in image intensifiers was stimulated by concern for increasing the sensitivity of television camera tubes. However, the technology of photocathodes and phosphor screens had not then developed to the point where intensification could be achieved. The best available cathodes at the time were the silver-oxygen-caesium photoemitters, and their sensitivity to near-infrared radiation stimulated an interest in infrared image conversion. During World War II, infrared image-converter tubes were manufactured and incorporated into Snooperscopes for use by the Army. Conversion efficiencies were too low for passive operation, and it was necessary to irradiate the scene with infrared.

With the development of the cesium antimony cathode (Ref. 2) and advances in phosphor technology, it became possible in the 1940's to



achieve intensifier gain with a simple photocathode-phosphor screen tube. Dating from the 1930's, the concept of achieving high intensifier gains by cascading stages was now technically feasible. As a result of the loss of resolution due to lateral diffusion of light as it passes through the glass windows between the phosphor screen of one tube and the photocathode of the next, it was not feasible to simply cascade single-stage tubes. Rather, it was necessary to fabricate dynodes consisting of a thin supporting membrane of glass or mica coated on one side with a phosphor layer and on the other with a semi-transparent photocathode for mounting in a single glass tube envelope. The chief drawback to these phosphor-photocathode multistage tubes, besides their expense, was the necessity of applying magnetic focusing between the flat dynodes to avoid curvature of the electron image field and radial distortion. An important application of phosphor-photocathode multistage tubes is to astronomy, where size and expense are not considered to be a serious hindrance to their acceptance.

Another tube, somewhat similar in nature, became feasible with the development in the 1950's of transmission secondary emission multiplier dynodes (Ref. 3), consisting of an aluminum oxide supporting film coated on one side with a thin metal film electrode on which is deposited a semiconductor of low electron affinity, such as potassium chloride, which serves as the secondary emitter. Photoexcited electrons emitted from the cathode gain sufficient energy from an applied electric field between the cathode and dynode to penetrate the aluminum oxide, the metal film electrode, and the semiconductor where most of the energy is absorbed. Typically 4 to 8 transmission secondary electrons are emitted into the vacuum from the semiconductor and, in turn, are accelerated to impinge on a second dynode. As many as 4 or 5 dynodes may be used to achieve electric current gains of the order of 10,000. Due to the difficulty of obtaining the right curvature of the thin dynodes for electrostatic focusing, flat dynodes are used and magnetic focusing is required. Consequently, these tubes, like phosphor-photocathode multistage tubes, are bulky and expensive to fabricate.

Further advances in photocathode technology resulted from the development (Ref. 4) of trialkali antimony photoemitters in 1955. With their enhanced response, these cathodes, incorporated in suitable high-gain image-intensifier tubes, offered the possibility of passive viewing under nighttime conditions of only partial moonlight or starlight. To be easily handled and to receive wide acceptance by potential users, tubes incorporating trialkali antimony cathodes could not rely on bulky magnetic lenses and would have to be much less expensive to build than the two high-gain image-intensifier tubes described above. The development (Ref. 5) of fiber-optic plates in the 1950's was to play an important role in the subsequent development of cascade image intensifiers of modular form, which go a long way toward fulfilling the above tube requirements.

Fiber-optic plates used in image intensifiers are made of an array of tiny fibers fused together, each fiber consisting of a core of glass having a high index of refraction, coated with a sheath of glass having a lower index of refraction. The individual fibers behave as dielectric waveguides, transmitting the light entering at one end to the opposite end. If an image is focused on one side of a fiber-optic plate, it will be efficiently transmitted through the plate with very little lateral diffusion. However, because most phosphors have a considerably higher index of refraction than available optical glasses, a certain fraction of the light emitted by a phosphor strikes the fiber sheath at an angle less than critical and refracts out of the fiber into neighboring fibers. This problem is avoided either by coating the fibers with a second sheath of absorbing material or by strategically locating discrete absorbing fibers in the interstices.

The chief value of fiber optics for cascade image intensifiers is that it permits the selection of faceplates of sufficient thickness to be mechanically strong, subject to any shape desired, and yet no loss of resolution occurs due to lateral diffusion of light as it passes through the faceplate. In particular, the outside of a plate can be flat, while the inside face on which either the cathode or the phosphor may be deposited is curved to meet the requirements of electrostatic

focusing. Thus, two or more single-stage tubes can be optically coupled together efficiently by simply placing the flat outside faces of the fiber optic plates in contact. The coupling efficiency in this instance can be as high as 50 to 80 percent, depending on the type, diameter, and cladding of the fiber used. A practical advantage in using fiber optics is that each single-stage tube can be constructed, processed, and tested separately for high performance before being incorporated into a complete cascade image intensifier.

A typical three-stage modular cascade image intensifier tube is shown in Fig. IV-3. The three modules are mechanically and optically coupled together and completely encapsulated with the voltage multiplier sections of the high-voltage power supply. Electrostatic focusing with approximately unity magnification is employed in each module. Image inversion, occurring in each of the electrostatically focused modules, is canceled by image inversion in the objective of complete visual systems. Cascade image-intensifier tubes are generally made in three standard sizes: one with an 18-mm cathode, one with a 25-mm cathode, and one with a 40-mm cathode. Limited numbers of single and multiple modular image-intensifier tubes of other sizes are made for special applications. The 18-mm tube is approximately 5.8 in. in length and 2.1 in. in diameter; the 25-mm tube is approximately 7.6 in. in length and 2.75 in. in diameter; the 40-mm tube is approximately 12 in. in length and 3.7 in. in diameter.

Manufacturers' performance data for representative single-stage and three-stage cascade image-intensifier tubes are presented below in Tables IV-4 through IV-10. Where performance data are measurements of input radiation, radiometric units are used. The use of photometric units based on the lumen as measures of input radiation to a physical detector is to be discouraged, since the lumen, by definition, depends implicitly on the spectral responsivity of the eye.

Photocathode responsivity is specified in milliamperes per watt of total blackbody input radiation from a 2854°K tungsten source. It has sometimes been customary to specify photocathode responsivity in

microamperes per lumen of input luminous flux from a  $2854^{\circ}\text{K}$  tungsten source. The conversion factor from microamperes per lumen to milliamperes per watt of total blackbody radiation from a  $2854^{\circ}\text{K}$  tungsten source is approximately  $2 \times 10^{-2}$ , i.e.,  $200 \mu\text{A/L} \sim 4 \text{ mA/watt}$ .

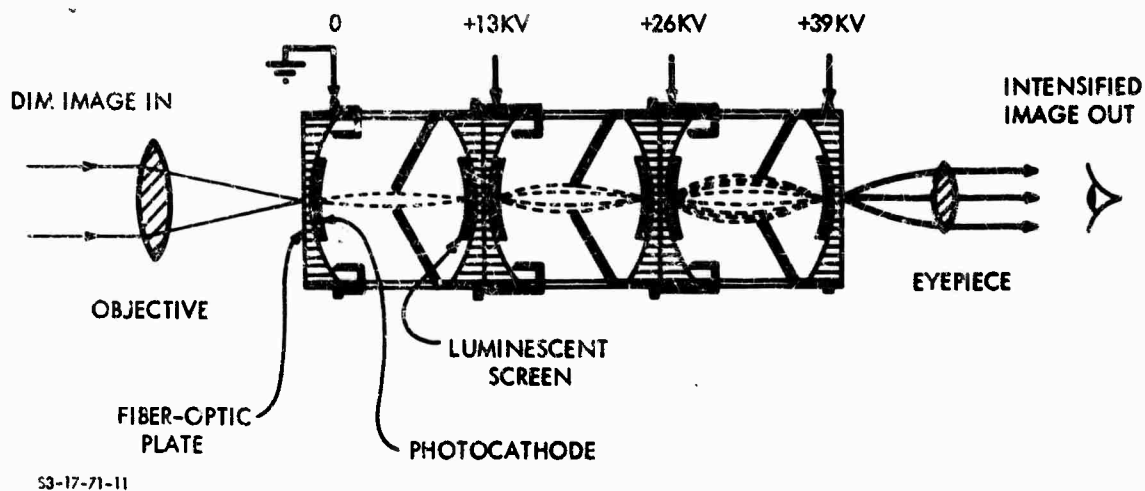


FIGURE IV-3. Schematic Diagram of Modular Cascade Image Intensifier

Gain, or more precisely the luminous conversion factor, is specified as the ratio of output luminance in candela per square meter to input irradiation in watts per square meter from a  $2854^{\circ}\text{K}$  source. It is sometimes customary to specify gain as the ratio of the output luminance in foot-lamberts to input illumination in footcandles or lumens per square foot from a  $2854^{\circ}\text{K}$  source. The conversion factor from foot-lamberts/footcandles to  $(\text{cd/m}^2)/(\text{watts/m}^2)$  is approximately  $20/\pi$  for a  $2854^{\circ}\text{K}$  source.

TABLE IV-2. SINGLE-STAGE IMAGE-INTENSIFIER PERFORMANCE DATA (MACHLETT LABORATORIES, INC.)

	Photocathode/Phosphor Diameter, mm					
	18/18		25/25		40/40	
	Typical	Minimum	Typical	Minimum	Typical	Minimum
Photocathode Responsivity, ma/watt						
(a) To 2854 <sup>0</sup> K Lamp	4.2	3.5	4.2	3.5	4.2	3.5
(b) At 800 nm	13	10	13	6	13	6
(c) At 850 nm	7	3	7	1	7	1
Gain,* (cd/m <sup>2</sup> )/(watt/m <sup>2</sup> )	754	446	754	446	754	446
Equivalent Background Input,* watl/cm <sup>2</sup>	2.5x10 <sup>-13</sup>	1x10 <sup>-12</sup> (max)	2.5x10 <sup>-13</sup>	1x10 <sup>-12</sup> (max)	2x10 <sup>-13</sup>	1x10 <sup>-12</sup> (max)
Contrast Transfer Ratio**						
(a) 5 line pairs/mm	0.95	0.85	0.93	0.86	0.91	0.87
(b) 10 line pairs/mm	0.83	0.69	0.81	0.69	0.76	0.70
(c) 15 line pairs/mm	0.69	0.52	0.63	0.52	0.60	0.53
Resolution, line pairs/mm on output face						
(a) Center	64	57	64	57	64	57
(b) Edge (80% dia.)	57	45	57	45	51	45
Magnification						
(a) Center	0.97 ± 0.03		0.96	1.0(max)	0.95	1.0(max)
(b) Edge	1.02	1.08(max)	1.02	1.08(max)	1.01	1.08(max)
Operating Voltage, kv	13		15		15	

\* With 2854<sup>0</sup>K lamp.

\*\* Square-wave test pattern.

TABLE IV-3. CASCADE (THREE-STAGE) IMAGE-INTENSIFIER PERFORMANCE DATA  
(MACHLETT LABORATORIES, INC.)

	Photocathode/Phosphor Diameter, mm					
	18/18		25/25		40/40	
	Typical	Minimum	Typical	Minimum	Typical	Minimum
Photocathode Responsivity, ma/watt						
(a) To 2854 <sup>0</sup> K Lamp	4.2	3.5	4.2	3.5	4.2	3.5
(b) At 800 nm	13	10	13	6	13	6
(c) At 850 nm	7	3	7	1	7	1
Gain,* (cd/m <sup>2</sup> )/(watt/m <sup>2</sup> )	365,000	206,000	411,000	240,000	480,000	--
Equivalent Background Input,* watt/cm <sup>2</sup>	2.5x10 <sup>-13</sup>	1x10 <sup>-12</sup> (max)	5x10 <sup>-12</sup>	2x10 <sup>-11</sup> (max)	2.5x10 <sup>-13</sup>	1x10 <sup>-12</sup> (max)
Modulation Transfer Function**						
(a) 5 line pairs/mm	0.84	0.90	0.84	0.76	0.80	0.74
(b) 10 line pairs/mm	0.59	0.53	0.57	0.34	0.52	0.38
(c) 15 line pairs/mm	0.38	0.31	0.38	0.12	0.36	0.14
Resolution, line pairs/mm on output face						
(a) Center	32	30	29	25	32	25
(b) Edge (80% dia.)	29	25	25	23	25	23
Magnification						
(a) Center	0.87	1.0(max)	0.87	1.0(max)	0.87	1.0(max)
(b) Edge (80% dia.)	1.01	1.06(max)	1.01	1.06(max)	1.01	1.06(max)
Operating Voltage, kv		36		45		45

\* With 2854<sup>0</sup>K lamp.  
\*\* Sine-wave test pattern.

TABLE IV-4. CASCADE (THREE-STAGE) IMAGE-INTENSIFIER PERFORMANCE DATA (VARO, INC.)

	Photocathode/Phosphor Diameter, mm		
	<u>18/18</u>	<u>25/25</u>	<u>40/40</u>
Photocathode Responsivity, ma/watt			
(a) To 2854°K Lamp	3.5(min)	3.5(min)	3.5(min)
(b) At 800 nm	6-30	6-30	6-30
(c) At 850 nm	1-25	1-25	1-25
Gain,* (cd/m <sup>2</sup> )/(watt/m <sup>2</sup> )	206,000(min)	240,000(min)	240,000(min)
Equivalent Background Input,* watt/cm <sup>2</sup>	1x10 <sup>-12</sup> (max)	1x10 <sup>-12</sup> (max)	1x10 <sup>-12</sup> (max)
Modulation Transfer Function**			
(a) 5 line pairs/mm	0.84(min)	0.75(min)	0.75(min)
(b) 10 line pairs/mm	0.50(min)	0.36(min)	0.36(min)
(c) 15 line pairs/mm	0.28(min)	0.23(min)	0.23(min)
Resolution, line pairs/mm			
(a) Center	32(min)	25(min)	25(min)
(b) Edge (80% dia.)	28(min)	23(min)	23(min)
Magnification	0.86-1.0	0.84-1.0	0.82-1.0
Operating Voltage, kv	38	45	45

\* With 2854°K lamp.

\*\* Sine-wave response.

TABLE IV-5. CASCADE (THREE-STAGE) IMAGE-INTENSIFIER PERFORMANCE DATA (RCA)

	Photocathode/Phosphor Diameter, mm		
	18/18		40/40
	Typical	Minimum	Typical Minimum
Photocathode Responsivity, ma/watt			
(a) To 2854°K Lamp	4.2	3.5	- 4.0
(b) At 800 nm	13	10	22 20
(c) At 850 nm	7	3	15 12
Gain,* (cd/m <sup>2</sup> )/(watt/m <sup>2</sup> )	206,000	343,000	159,000 -
Equivalent Background Input,* watt/cm <sup>2</sup>	2.5x10 <sup>-13</sup>	1x10 <sup>-12</sup> (max)	- 1x10 <sup>-12</sup> (max)
Modulation Transfer Function**			
(a) 5 line pairs/mm	0.86	0.82	0.82 0.75
(b) 10 line pairs/mm	0.58	0.50	0.42 0.36
(c) 15 line pairs/mm	0.35	0.28	0.22 0.15
Resolution, line pairs/mm			
(a) Center	36	32	35 25
(b) Edge (80% dia.)	36	30	30 23
Magnification, Center		0.82-1.0	0.82-1.0
Operating Voltage, kv		36	45

\* With 2854°K lamp.

\*\* Sine-wave response.



TABLE IV-6. SINGLE-STAGE IMAGE-INTENSIFIER PERFORMANCE DATA (VARIAN ASSOCIATES)

	Photocathode/Phosphor Diameter, mm			
	80/25 ZOOM		80/40 ZOOM	
	<u>Typical</u>	<u>Minimum</u>	<u>Typical</u>	<u>Minimum</u>
Photocathode Responsivity, ma/watt				
(a) To 2854 <sup>0</sup> K Lamp	3.7	2.9	3.7	3.4
(b) At 800 nm	15	10	15	10
(c) At 850 nm	10	6	10	6
Gain,* (cd/m <sup>2</sup> )/ watt/m <sup>2</sup> )	789	532	789	532
Equivalent Background Input,* watt/cm <sup>2</sup> .	1.2x10 <sup>-13</sup>	1.2x10 <sup>-12</sup> (max)	1.2x10 <sup>-13</sup>	1.2x10 <sup>-12</sup> (max)
Modulation Transfer Function**				
(a) 5 line pairs/mm	0.93	0.90	0.93	0.90
(b) 10 line pairs/mm	0.83	0.80	0.83	0.80
(c) 15 line pairs/mm	0.70	0.65	0.70	0.65
Resolution, line pairs/mm on output face				
(a) Center	80	65	80	65
(b) Edge (80% dia.)	55	45	55	45
Magnification	0.32 to 1.0		0.5 to 1.0	
Operating Voltage, kv	15		15	

\* With 2854<sup>0</sup>K lamp; gain for unity magnification.

\*\* Sine-wave test pattern.

TABLE IV-7. SINGLE-STAGE IMAGE-INTENSIFIER PERFORMANCE DATA (VARO, INC.)

	Photocathode/Phosphor Diameter, mm							
	40/18 Zoom		60/18 Zoom		80/25 Zoom		80/40 Zoom	
	Typical	Minimum	Typical	Minimum	Typical	Minimum	Typical	Minimum
Photocathode Responsivity, ma/watt								
(a) To 2854 <sup>0</sup> K Lamp	5	3.5	5	3.5	5	3.5	5	3.5
(b) At 800 nm	20	10	20	10	20	10	20	10
(c) At 850 nm	10	3	10	3	10	3	10	3
Gain,* (cd/m <sup>2</sup> )/(watt/m <sup>2</sup> )	687	412	687	412	687	412	687	412
Equivalent Background Input,* watt/cm <sup>2</sup>	1x10 <sup>-12</sup>		1x10 <sup>-12</sup>		1x10 <sup>-12</sup>		1x10 <sup>-12</sup>	
Modulation Transfer Function**								
(a) 5 line pairs/mm	0.97		0.97		0.97		0.98	
(b) 10 line pairs/mm	0.90		0.92		0.90		0.90	
(c) 15 line pairs/mm	0.75		0.85		0.76		0.75	
Magnification	0.45 to 1.0		0.3 to 1.0		0.3125 to 1.0		0.5 to 1.0	
Resolution, line pairs/mm on input face								
(a) Center	30	70	25	75	20	65	32	65
(b) Edge (80% dia.)	25	60	15	60	15	50	25	50
Operating Voltage, kv								
(a) Screen	15		15		15		15	
(b) Zoom	2-13		2-13		2-13		2-13	
(c) Focus	0.5-0		0.5-0		0.5-0		0.5-0	

\* With 2854<sup>0</sup>K lamp; gain for unity magnification.

\*\* Sine-wave test pattern.

TABLE IV-8. SINGLE-STAGE IMAGE-INTENSIFIER PERFORMANCE DATA (AEROJET DELFT)

	Photocathode/Phosphor Diameter, mm	
	80/25 Zoom	25/125 Magnifying
Photocathode Responsivity, ma/watt		
(a) To 2854°K Lamp	3.8	3.0
(b) At 800 nm	10	--
(c) At 850 nm	6	--
Gain,* (cd/m <sup>2</sup> )/(watt/m <sup>2</sup> )	687	1140
Equivalent Background Input,* watt/cm <sup>2</sup>	1x10 <sup>-12</sup> (max)	1x10 <sup>-12</sup> (max)
Modulation Transfer Function,** On Screen		
(a) 5 line pairs/mm	0.94	0.80
(b) 10 line pairs/mm	0.83	0.45
(c) 15 line pairs/mm	0.60	0.22
Resolution, line pairs/mm on output face		
(a) Center	65	24
(b) Edge (80% dia.)	40	20
Magnification	0.33-1.0	5
Operating Voltage, kv	15	--

\* For 2854°K lamp; gain for unity magnification.

\*\* Square-wave input to 80/25 zoom. Sine-wave input to 25/125 magnifying.

TABLE IV-9. SINGLE-STAGE INTENSIFIERS (WESTINGHOUSE)

	Photocathode/Phosphor Diameter, mm											
	25/16			40/25			80/25			80/25 Zoom		
	Typical	Minimum		Typical	Minimum		Typical	Minimum		Typical	Minimum	Typical
Photocathode Responsivity, ma/watt												
(a) To 2854 <sup>0</sup> X Lamp	--	2.4	4.5	3.5	--	3.5	--	--	3.5	--	--	3.5
(b) At 800 nm	--	--	12	6	--	6	--	--	6	--	--	6
(c) At 850 nm	--	--	7	1	--	1	--	--	1	--	--	1
Gain, * (cd/m <sup>2</sup> )/(watt/m <sup>2</sup> )	--	373	782	521	672	--	636	--	586	--	636	--
Equivalent Background Input, * watt/cm <sup>2</sup>	--	2.5x10 <sup>-11</sup> (max)	1x10 <sup>-12</sup>	2.5x10 <sup>-12</sup> (max)	--	2.5x10 <sup>-12</sup> (max)	--	2.5x10 <sup>-12</sup> (max)	--	2.5x10 <sup>-12</sup> (max)	--	2.5x10 <sup>-12</sup> (max)
Contrast Transfer Ratio**												
(a) 5 line pairs/mm	0.93	--	0.89	0.84	0.96	--	0.95	--	0.93	--	0.93	--
(b) 10 line pairs/mm	0.75	--	0.68	0.62	0.90	--	0.85	--	0.82	--	0.82	--
(c) 15 line pairs/mm	0.50	--	0.41	0.35	0.80	--	0.65	--	0.66	--	0.66	--
Magnification	0.625	--	0.64	--	0.30	--	0.30 to 1.00	--	0.48	--	0.50 to 1.00	--
Resolution, line pairs/mm on Input Face												
(a) Center	--	--	25	23	--	--	--	--	--	--	--	--
(b) Edge (80% dia.)	--	--	20	18	--	--	--	--	--	--	--	--
Operating Voltage, kv	--	--	15	--	15	--	15	--	15	--	15	--

\* With 2854<sup>0</sup>X lamp; gain for unity magnification.

\*\* Square-wave test pattern.

TABLE IV-10. CASCADE (THREE-STAGE) IMAGE-INTENSIFIER (VARIAN)

	Photocathode/Phosphor Diameter, mm	
	Typical	Minimum
Photocathode Responsivity, ma/watt		
(a) To 2854°K Lamp	3.7	2.9
(b) At 800 nm	15	10
(c) At 850 nm	10	6
Gain,* (cd/m <sup>2</sup> )/(watt/m <sup>2</sup> )	240,000	159,000
Equivalent Background Input,* watt/cm <sup>2</sup>	1.2x10 <sup>-13</sup>	1.2x10 <sup>-12</sup> (max)
Modulation Transfer Function**		
(a) 5 line pairs/mm	0.92	0.90
(b) 10 line pairs/mm	0.75	0.70
(c) 15 line pairs/mm	0.50	0.45
Resolution, line pairs/mm on output face		
(a) Center	35	35
(b) Edge (80% dia.)	35	30
Magnification	0.28 to 0.87	
Operating Voltage, kv	43	

\* With 2854°K lamp; gain for unity magnification.

\*\* Sine-wave response.

Equivalent background input is defined as the irradiance of the input face required from a 2854°K source to produce an additional output luminance equal to the mean background luminance existing when the primary photocathode is masked. The conversion factor from photometric units of lumens per square centimeter to watts of total blackbody radiation per square centimeter is approximately equal to 1/20 with a 2854°K source.

The modulation transfer function, synonymous with spatial frequency response or sine-wave response, is measured with a sine-wave test pattern. In some cases the available data are for response to a bar pattern or a square-wave-modulated test pattern. Response to square-wave-modulated test patterns is specified in the tables as contrast transfer ratio. It must be noted that response to square-wave test patterns is higher (except at zero line pairs/millimeter, where it is normalized to unity) than response to sine-wave test patterns (Ref. 6).

#### C. SECOND-GENERATION IMAGE INTENSIFIERS

The exploitation of electrooptical technology, principally by the Army Night Vision Laboratory, culminated in the development of the "first-generation" night-vision instruments employing the cascade image-intensifier tubes. It was recognized even at the beginning of this development effort that the size, performance, and cost of first-generation night-vision equipment would fall short of desirable specifications. Hence, a second generation was envisioned that hopefully would meet the desired specifications.

The second-generation night-vision instruments would employ a single stage intensifier tube incorporating a high-gain microchannel-plate (MCP) dynode. It was believed that the use of a single high-gain stage would diminish the loss of modulation transfer occurring in the three stages of the cascade image-intensifier tubes. It was further believed that the method of fabrication of the channel plates would lead to high production volumes and low cost.

Unfortunately, of the three objectives of the MCP image-intensifier tube development, only the desirable size specification has been achieved. The gain characteristics and image quality have not reached expectations. Further, reliability (life) and cost remain problems.

Recent research results (Ref. 7) on the silicon transmission secondary-electron multiplier (TSEM) dynode structure (Section IV-C-3) as an alternative to microchannel plates strongly indicate for the first time that sufficient gain can be achieved in a single stage without the severe degradation of the spatial frequency response that occurs in the MCP tubes. Thus, the silicon TSEM is a serious candidate to replace the MCP in the presently proposed family of second-generation devices.

#### 1. Rationale for Image-Intensifier Performance Improvement

The performance of image intensifiers is chiefly determined by three tube parameters:

1. The frequency response or modulation transfer function (MTF).
2. Responsivity of the photocathode.
3. Noise introduced by the gain mechanism.

Of these, at the present time, greater improvement in image-intensifier performance at useful low light levels can be achieved by improvements in the MTF than by likely improvements in photocathode responsivity.

The resolution of image-intensifier tubes even at very low illumination levels is strongly dependent on the MTF and not merely dependent on the responsivity of the photocathode. This is because the MTF of an image tube (unlike the frequency response of an electronic amplifier, which is essentially flat out to some cut-off frequency) begins to fall off at less than one line pair per millimeter. A graphic illustration is shown in Fig. IV-4. The lower curve is the frequency dependence of the modulation on the screen, produced by a three-stage, first-generation image intensifier tube with a sine-wave test pattern of 30 percent modulation. To estimate the relative importance of MTF and responsivity on resolution frequency, consider the

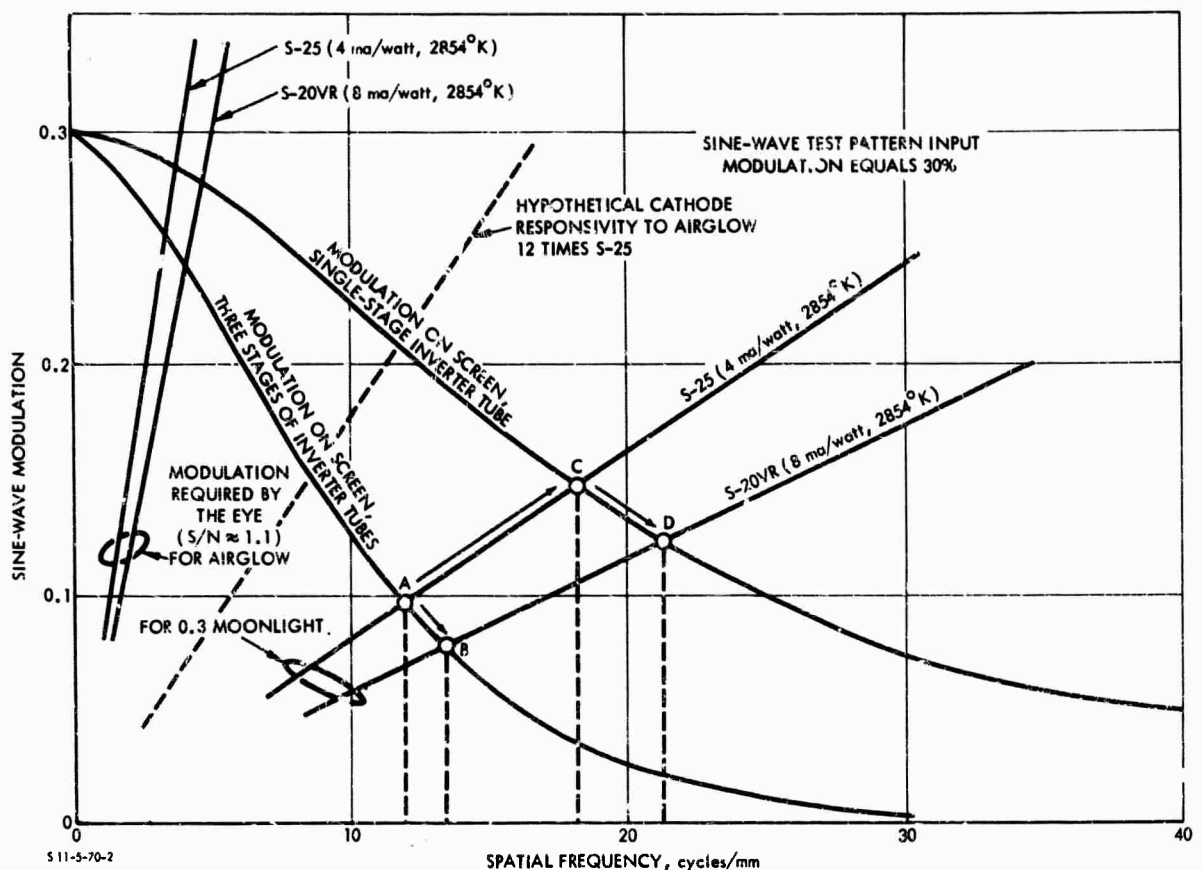


FIGURE IV-4. Predicted Effect of Cathode Responsivity Versus MTF on Image-Intensifier Performance

line representing the modulation required to provide a signal-to-noise ratio of 1.1, as required by the eye for perception of the image of the pattern on the screen of an image intensifier with an S-25 (4 ma/watt) photocathode and irradiance of the test pattern by 0.3 moonlight. All of the curves representing the modulation required by the eye versus the number of lines per millimeter were calculated by assuming the average reflectivity of the scene being viewed to be 20 percent, the objective to be effectively  $f/2$ , and the signal-to-noise ratio required by the eye for this one-dimensional variation in luminance to be approximately 1.1. The intersection of the required modulation line for an S-25 cathode and 0.3 moonlight with the three-stage modulation on the screen curve at point A indicates that the resolution is approximately 12 cycles/mm or line pairs/mm. With this point of intersection as a reference, consider two alternatives for increasing resolution:



1. Choose an S-20VR photocathode with double the responsivity (measured under illumination from a standard 2854°K tungsten lamp).
2. Develop a gain structure that will allow reduction of the number of intensifier stages from three to one, with the consequence that the MTF is increased as shown by the two curves of modulation on the screen (Fig. IV-4).

In the first case, higher photocathode responsivity, the resolution would increase from 12 to 13.4 cycles/mm, as indicated by the arrow from A to B. In the second case, better MTF, the resolution would increase from 12 to 18.2 cycles/mm, as indicated by the arrow from A to C. It is clear in this example that of the two alternatives for increasing resolution, increasing the MTF is the most effective. Furthermore, by comparison of the arrows from C to D and from A to B, it is evident that increases in MTF enhance the effect of subsequent increases in cathode responsivity on resolution.

Figure IV-4 also shows the effects on resolution of changes in responsivity and MTF at the low value of scene irradiance provided by airglow alone (clear night sky, no moonlight). As the irradiance decreases from 0.3 moonlight to airglow, the resolution of a three-stage image intensifier with an S-25 photocathode decreases to such a low value (3 cycles/mm or 75 cycles per diameter with the 25-mm tube used in the starlight telescope) that little improvement can be realized by improving the MTF alone. It is generally acknowledged that with the presently available S-25 photocathodes "quarter" moonlight is required for satisfactory operational performance. Theoretically, the present quarter moonlight performance could be achieved at airglow by increasing the photocathode responsivity to airglow by a factor of approximately 50. Such a large increase in responsivity is not in the offing. However, the dashed line in Fig. IV-4, representing the required modulation with a hypothetical photocathode 12 times more responsive to airglow than the S-25, indicates that by improving the MTF the required improvement in responsivity could be relaxed. An improvement in the MTF to that of a single-stage tube would reduce the required increase in photocathode responsivity from 50 to approximately 12. Thus, it seems clear that the required resolution and operational performance currently realized at quarter

moonlight could be achieved with airglow alone in the foreseeable future only if both the responsivity and the MTF were greatly improved.

## 2. Microchannel-Plate (MCP) Image Intensifier

The microchannel-plate (MCP) image intensifier is based on a concept that received little attention for many years but has recently gained considerable prominence. In the MCP image intensifier, a mosaic of microscopic hollow channels in a thin glass plate forms an array of continuous secondary-electron multipliers that amplify the photoemission current from elemental segments of the photocathode.

The first efforts to make an array of secondary-electron multipliers suitable for image intensification were made on low-resolution devices, fabricated element by element, using tubular multiplier structures. Work along these lines was done by RCA Laboratories, the Imperial College of London, Chicago Midway Laboratories, and others. Later attempts were made to use registered plates of metal (dynode material) and insulators with arrays of shaped holes to give the dynode geometries. The latest and most promising efforts to make an array of microscopic secondary-electron multipliers was initiated at Bendix Aviation in the late 1950's, and has led to the development of MCP secondary-electron multiplier arrays, that are of sufficient fineness to be of interest for imaging.

Development of MCP secondary-electron multiplier arrays capable of producing images of moderate resolution aroused interest in the possibility of a simple single-stage, high-gain image-intensifier tube replacement of the three-stage modular cascade image intensifier. It was anticipated that MCP intensifiers would offer the advantages not only of smaller size, lighter weight, and lower cost but also of better performance (i.e., higher target detection probability due to better spatial frequency response). However, the performance of MCP image intensifiers to date has generally been considerably less than was initially anticipated because a number of problems peculiar to these devices (to be discussed later) have arisen during development.

a. Principles of Operation. The MCP image-intensifier tube, shown schematically in Fig. IV-5, consists of a fiber-optic faceplate, on the back side of which is formed a photocathode, an electrostatic

image-inverting electron lens, an MCP secondary-electron multiplier, and a second fiber-optic plate on the front side of which is formed a phosphor screen with the usual aluminum film required to prevent light feedback to the photocathode. Image transfer from the MCP to the phosphor depends on the close proximity of these two elements. As shown in Fig. IV-5, the electron image generated at the photocathode is focused on the MCP by means of an electrostatic lens. These MCP image intensifier tubes are customarily called inverter tubes. It is necessary to employ a decelerating electric field to correct the flat image plane presented by the front surface of the MCP. Besides the inverter tubes employing electrostatic focusing between the photocathode and the MCP, considerable effort has been expended in the development of proximity focusing in what is customarily called a wafer tube. Development of the wafer tube has not been as successful as development of the inverter tube.

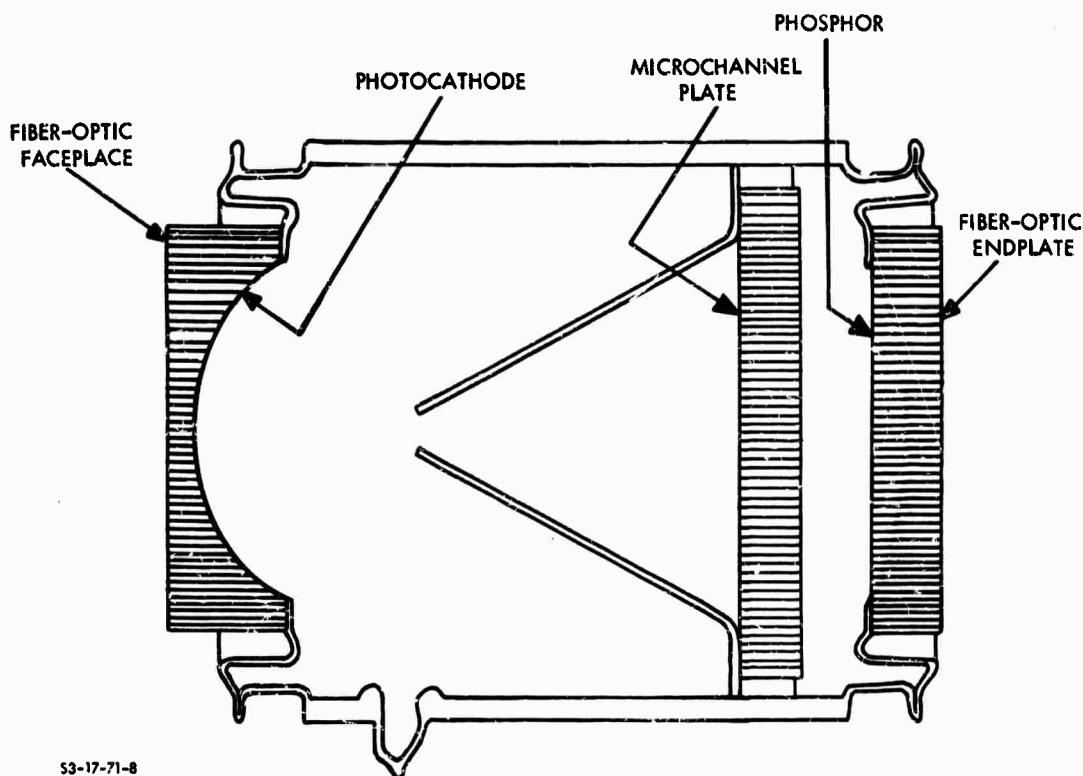


FIGURE IV-5. Schematic of an MCP Image Intensifier

Although the additional length of the inverter tube is a disadvantage in systems such as night-vision goggles, this disadvantage is offset by at least two advantages in systems where size is less critical. The larger volume of the inverter tube facilitates the inclusion of gettering material needed to adsorb gasses that are constantly desorbed from the glass channels during operation. Outgassing by the MCP has the adverse effects of reducing the lifetimes of both the photocathode emission and the secondary-electron multiplication, as well as yielding high ion noise. A second advantage of the inverter is the partial light shielding provided by the cone forming the electrostatic lens between the photocathode and the MCP. In the wafer tube, radiation transmitted through the semitransparent photocathode is partially reflected and scattered back to the photocathode from the front surface of the MCP and the channels. The resultant background current reduces the contrast in the output image produced on the phosphor screen.

Operation of the MCP depends on a large number of factors.\* A single channel consists of a glass tube with a length equal to about fifty diameters. The inside surface of the channels is made semiconducting with a resistance in the range from  $10^8$  to  $10^{14}$  ohms (typically  $10^9$  ohms), depending on the output current to be drawn from the channel. The output secondary-electron emission current, which can be drawn from a channel while maintaining linearity between the output current and the input photoelectric current, is approximately 10 percent of the strip current flowing in the walls of the channel.

The MCP operates with a potential applied between electrodes formed by evaporating a thin metallic coating at an oblique angle over the two polished surfaces of the glass plate. Electrons emitted from the photocathode enter the channels and strike the walls to produce secondary electrons, which are accelerated axially by the strong applied axial electric field. The transverse energy of emission possessed by the secondary electrons causes them to traverse the channel

---

\* These are thoroughly discussed in Ref. 8.

as they are accelerated axially, so that they, in turn, strike the wall, producing additional secondary electrons. The process is repeated many times along the channel until a large pulse of electrons emerge from the high potential end.

b. MCP Gain Function. The gain, equal to the average number of electrons in an output pulse, depends on the length-to-diameter ratio of the channel, the secondary emission ratio of the channel, and the applied potential. With 1 kv applied, the gain will typically be several thousand. It is observed that with constant applied potential the gain passes through a maximum at a particular voltage approximately equal to 22 times the length-to-diameter ratio. This is a desirable operating point because the gain variation from channel to channel then will be least dependent on differences in channel diameter. The saturation effect on the gain caused by drawing output current in excess of 10 percent of the strip current will act to limit the maximum brightness at the center of an output image but, of course, has little effect on the extent of image spread, which is described by either the modulation transfer function or point spread function.

c. Spatial Frequency Response. It has been noted (Section III-C-5) that the frequency response of a multiple-component optical system is equal to the product of the frequency responses of each component and thus is reduced by cascading more and more components. It would appear, therefore, that an MCP image intensifier would have an improved frequency response function compared to that of a three-stage modular cascade image intensifier. In point of fact, this has not been true, although recent development efforts have yielded considerable improvement.

The failure of the frequency response function of MCP image intensifiers to measure up to earlier expectations is due to a number of factors, which include the use of proximity focusing between the MCP and the phosphor screen, the relatively high applied potential between the MCP and the phosphor screen required for efficient electron-to-luminant-image conversion in the phosphor, and the relatively high

transverse energies of the secondary electrons emerging from the channels of the MCP.

The distribution of the points of impact on the phosphor of electrons emerging from a channel has not been calculated. However, some appreciation of the problem with proximity focusing between the MCP and the phosphor screen can be gained by considering the path of a single electron as a function of the relevant parameters. In the uniform electric-field region between the MCP and phosphor screen, each emerging electron will follow a parabolic path, eventually striking the screen at a transverse distance  $d$  from the channel exit point given approximately by

$$d = L \sin\theta / (V/V_0)^{1/2} \quad (\text{IV-1})$$

provided that  $V/V_0 \gg 1$ , where  $V$  is the applied potential,  $V_0$  is the initial energy of the emerging secondary electron in electron-volts,  $L$  is the separation between the MCP and the screen, and  $\theta$  is the angle made by an emerging electron relative to the direction of the applied electric field. It is clear from Eq. IV-1 that the transverse displacement of an electron is reduced by decreasing the separation and increasing the applied potential between the MCP and the screen, i.e., increasing the applied electric field. However, it is found in practice that the maximum applied electric field is limited to approximately  $6 \times 10^4$  v/cm, and the applied potential required for efficient electron-to-luminant-image conversion is approximately 6,000 v. Thus, the separation between the MCP and the screen is approximately 1 mm. The energies of the emerging electrons will exhibit a distribution in which 100 ev is a typical value. If one substitutes the above values for the parameters in Eq. IV-1, one finds that the transverse displacement will range from zero to roughly one-eighth of a millimeter, depending on the value of  $\theta$ . One would expect few electrons to achieve the maximum displacement, since they would have to originate from emission points near the end of a channel. Electrons emitted from points not

so near the end of a channel will emerge with smaller values of  $\theta$  and hence smaller transverse displacements.

A practical method for limiting the maximum transverse displacement of electrons striking the phosphor is the deposition of the back electrode of the MCP a distance equal to several diameters into the channels. This creates a field-free region of low secondary emission ratio near the ends of the channels and thus restricts the maximum value of  $\theta$ , at which electrons emerge from the MCP.

A more fundamental limitation on frequency response stems from the mosaic structure of the MCP. This limitation depends on the relative spatial phase of the regular array of channels and the periodic test pattern used to measure the frequency response. For example, if the test-pattern frequency equals the reciprocal of twice the channel center-to-center spacing and if the phase is such that the adjacent crossover points of the sine-wave modulation about the mean fall at the center of adjacent channels, the frequency response will be zero. For a typical channel center-to-center spacing of 16  $\mu\text{m}$ , this spatial frequency is 31 cycles/mm. At the same frequency, but at a phase relation such that adjacent maxima and minima of the sine-wave modulation fall at the center of adjacent channels, the frequency response will be  $2/\pi$ . For other phase relations the frequency response will be between 0 and  $2/\pi$ . If the frequency of the test pattern is equal to the reciprocal of the center-to-center spacing of adjacent channels, the frequency response will be zero, independent of phase. For the 16- $\mu\text{m}$  spacing this latter test-pattern frequency is 62 cycles/mm. At other test-pattern frequencies, beats will occur in the output sine-wave pattern produced on the phosphor screen. These interference effects have rarely been observed in MCP intensifiers because they are masked by the overlapping due to the distributions of emission angles and transverse energies of the electrons emerging from the channels. With improvements in the frequency-response function by end spoiling and by closer positioning of the MCP and the phosphor screen, closer micro-channel center-to-center spacing will be required to avoid the interference effects.

d. Signal and Noise in MCP Image Intensifiers. Loss of image signal-to-noise ratio occurs in MCP image intensifiers because of a number of factors in addition to those common to all PEI systems, such as the photoelectric quantum efficiency of the photocathode and the spatial frequency response of the electron optics and phosphor screens (Section III-C-6).

Firstly, some of the photoelectric current generated by the input irradiance on the photocathode is lost at the input to the MCP. The loss has been reported to be less than would be expected from the fraction of MCP cross-sectional area occupied by glass. Although only 60 to 70 percent of the MCP area is open to them, apparently 80 to 85 percent of the photoelectrons enter the channels.

Secondly, the secondary electron multiplication process in the channels introduces fluctuations in the number of secondary electrons in the output pulses. Fluctuations in the output pulse heights are due to fluctuations in the secondary emission yield, fluctuations in secondary electron escape energy, and fluctuations in escape direction. For a given secondary electron, the escape energy and direction are initial conditions that, in conjunction with the applied axial electric field, determine its trajectory. The trajectory of the electron, in turn, determines how far it will be accelerated toward the exit end of the channel before striking the wall opposite its origin. Longer path lengths will result in greater striking energy at a more nearly grazing angle of incidence and will produce, on the average, higher yield. For a given channel length, however, longer path lengths result in fewer wall impacts. Thus, fluctuations in escape energy and direction give rise to fluctuations in yield and in the number of electron collisions with the channel walls.

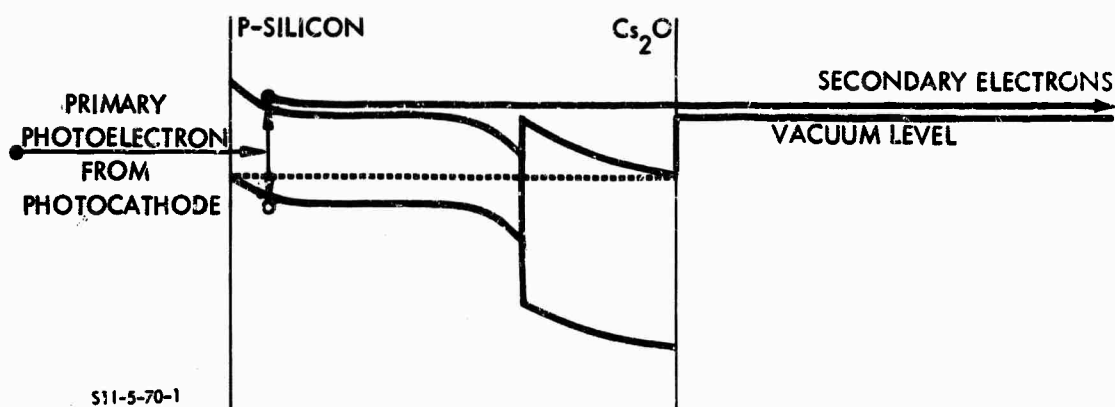
Other sources of noise (Ref. 9) are local variations in the emission properties of channel walls, ionic feedback due to outgassing from the glass surfaces, and electrons either reflected or emitted from the front electrode of the MCP.



The magnitude of the reduction in signal-to-noise ratio in MCP image intensifiers due to each of the above factors is difficult to measure. Wide variations are observed from one tube to another. Efforts to determine the fluctuations in the electron multiplication process have often been masked by the overwhelming effects of ionic feedback noise. Typical values of signal-to-noise ratio reduction are not yet available.

### 3. Silicon Transmission Secondary-Electron Multiplier (TSEM) Dynode

The silicon TSEM dynode (Ref. 7) consists of a thin (approximately 5 microns--sufficient thickness to be self-supporting) wafer of low-resistivity, P-type silicon having one surface carefully cleaned and treated with cesium and oxygen to reduce the potential difference between the bulk and vacuum (the effective bulk electron affinity) to zero or less. The resulting energy-level structure is shown schematically below:



The dynode is mounted in a vacuum-tube image intensifier with the untreated surface facing the photocathode and the cesium-oxide-treated surface facing the phosphor. Photoelectrons generated by the radiant image of the scene focused on the photocathode are accelerated and focused to strike the silicon TSEM dynode with the energy of several thousand electron volts. As the primary electrons penetrate the silicon

to a depth of a few thousand angstroms, energy is primarily lost via electron-hole pair production at the rate of approximately 3.6 ev per pair. Some of the resulting excess holes recombine with electrons supplied to an ohmic contact at the periphery of the silicon wafer, while an equal number of excess electrons rapidly thermalize to the temperature of the wafer, diffuse toward the silicon-cesium oxide interface, and escape into the vacuum to maintain current continuity. In a first effort (Ref. 7), 750 secondary electrons per primary electron have been measured at 20 kv, and 230 at 10 kv. Slightly heavier acceptor concentration at the front surface to reduce surface recombination will increase the yield. Photoemission measurements reported earlier (Ref. 10) indicate that the escape probability of excited electrons from cesium- and oxygen-treated, P-type silicon surfaces can be 20 percent or higher.

A transmission secondary-emission ratio of at least 500 at 10 kv can be expected. This TSEM gain of 500, multiplied by a diode gain of 50 due to the photocathode-phosphor combination, yields an overall gain of 25,000. An overall gain of 25,000 is ample to view scenes of low radiance down to the limit determined by the photoelectron shot noise without dark adaptation.

#### 4. Comparison of Silicon TSEM and Glass MCP Dynodes

The silicon TSEM dynode offers the following advantages over the glass MCP dynode:

1. Silicon, unlike glass (a notoriously "dirty" material), is a single element, completely stable chemically, susceptible to ultrahigh purification via zone refining, and susceptible to high-temperature bakeout during tube fabrication to remove any and essentially all adsorbed gasses that could damage the photocathode during tube operation. The compatibility of silicon with photocathodes of the S-20 type has been amply demonstrated in the camera tube employing the silicon-dicde-array charge-storage target.

2. The solid structure of the TSEM dynode, in contrast to the porous MCP structure, greatly facilitates surface cleansing and removal of adsorbed gases during bakeout, and it reduces the surface-to-volume ratio of the dynode.
3. Gain in a silicon TSEM dynode is essentially noiseless. In general, the mean square fluctuation  $\sigma^2$  in the number of secondary electrons per incident photoelectron observed for a large number of incident photoelectrons is given by  $\sigma^2 = F\bar{N}$ , where  $F$  is a parameter sometimes called the Fano factor and  $\bar{N}$  is the mean number of secondary electrons per incident photoelectron. If the distribution of yields is Gaussian or Poissonian,  $F$  is unity. For the MCP dynode,  $F$  is generally acknowledged to be greater than unity--approximately 2. For secondary-electron multiplication in semiconductors,  $F$  is known to be in the range of 0.1 to 0.2.
4. The silicon TSEM dynode does not require deposition of an electrode over a portion of the front surface of the dynode. Hence, the collection efficiency for incident photoelectrons is essentially 100 percent, compared to 70 to 80 percent for the MCP dynode. For a 70 percent collection efficiency, the effective responsivity of a 4-ma/watt photocathode is reduced to 2.8-ma/watt.
5. Degradation of image-tube MTF by the silicon TSEM dynode ought to be nil compared to the degradation produced by a MCP dynode. The causes of MTF degradation in MCP intensifiers are the broad spread in secondary-electron exit trajectories from adjacent microchannels and the finite size of the microchannels making up the MCP structure. The effect of the broad spread in secondary-electron trajectories is to produce poor proximity focusing in the space between the MCP and the phosphor screen. The origin of the broad spread in secondary-electron trajectories is the high secondary-electron energies coupled with the required accelerating voltage for good phosphor

conversion efficiency and limited breakdown field observed in any electron vacuum tube. Typical values of the energy of electrons emerging from a MCP are in the range 10 to 100 ev. On the other hand, in a silicon TSEM dynode, the transmission secondary electrons emerge via thermal diffusion to and across a surface treated with cesium oxide to reduce the electron affinity to zero with thermal energy equal to only 1/40 ev at room temperature. While some improvement in the MTF of MCP tubes has been achieved via "end spoiling" the channels to restrict the angles of the exiting electrons, the MTF remains comparable to that of a three-stage, first-generation intensifier, despite earlier predictions of a better MTF than even that of a single-stage inverter tube.

Without the broad spread in secondary-electron trajectories, the finite size of the microchannels would ultimately limit the MTF of an MCP tube in accordance with the well-known sampling theorem of communication theory. At a center-to-center spacing of 16 microns, for example, the MTF falls to zero at a spatial frequency in the range 31.2 to 62.4 line pairs/mm, depending on the relative phase between the microchannel array and the periodicity of the test pattern. Efforts to make finer microchannel plates with smaller channels are met with greater difficulties in technology and result in small gains. Guided by experience with the silicon-diode-array camera-tube target and present technology which allows the use of targets 2 to 3 microns thick, it is safe to predict that lateral diffusion of excited electrons in the continuous silicon TSEM structure will not significantly degrade the MTF of a single-stage image intensifier.

It is clear that the microchannel approach should be considered to be only one of two competing technologies for second-generation image-intensifier tubes, and that the silicon TSEM offers a much greater overall improvement. Barring unforeseen problems, the silicon TSEM approach should be pursued as the basis for a better and cheaper technology.

#### PART IV. REFERENCES

1. G.A. Morton, "Image Intensifiers and the Scotoscope," Appl. Opt., Vol. 3, No. 6, p. 651, June 1964.
2. P. Gorlich, "Ueber Zusammengesetzte Durchsichtige Photokathoden," Z. Physik, Vol. 101, p. 335, 1936.
3. E.J. Sternglass, "High-Speed Electron Multiplication by Transmission Secondary Electron Emission," Rev. Sci. Instr., Vol. 26, No. 12, p. 1202, December 1955.
4. A.H. Sommer, "New Photoemissive Cathodes of High Sensitivity," Rev. Sci. Instr., Vol. 26, No. 7, p. 725, July 1955.
5. R.J. Potter and R.E. Hopkins, paper presented at Image Intensifier Symposium, Fort Belvoir, Virginia, October 6 & 7, 1958.
6. J.W. Coltman, "The Specification of Imaging Properties by Response to a Sine Wave Input," J. Opt. Soc. Am., Vol. 44, No. 6, p. 468, June 1954.
7. R.U. Martinelli, "Reflection and Transmission Secondary Emission from Silicon," Appl. Phys. Letters, Vol. 17, No. 8, p. 313, 15 October 1970.
8. C.E. Catchpole, "The Channel Image Intensifier," Chapter 8 in L.M. Biberman and S. Nudelman, eds., Photoelectronic Imaging Devices, Vol. II, Plenum Press, New York, 1971.
9. W.M. Sackinger, "Noise Performance of the Channel Electron Multiplier," Chapter 9 in L.M. Biberman and S. Nudelman, eds., Photoelectronic Imaging Devices, Vol. I, Plenum Press, New York, 1971.
10. R.U. Martinelli, "Infrared Photoemission from Silicon," Appl. Phys. Letters, Vol. 16, No. 7, p. 261, 1 April 1970.

V. TELEVISION CAMERA TUBE PERFORMANCE AND DATA

by

Frederick A. Rosell

## PART V. SYMBOLS

A	effective (illuminated) photocathode area, $m^2$ , usually a 3x4 rectangle inscribed in the circular photocathode
G	scatter gain of isocon readout, dependent on target material employed
a	scene elemental area imaged on the first photosurface by the lens
$A_I$	effective intensifier photocathode area, $m^2$
$A_P$	effective phosphor area, $m^2$
$A_V$	effective vidicon photocathode area, $m^2$
$A_1/A_2$	ratio of first-stage (input) photocathode area to second-stage photocathode area
C	contrast
$D_V$	viewing distance
E	photocathode (highlight) irradiance, $watt/m^2$
e	electron charge, coulombs
$e_h$	horizontal scan efficiency
$E_I$	intensifier photocathode (highlight) irradiance, $watt/m^2$
$E_{min}$	minimum detectable (highlight) irradiance for a sensor-augmented observer when the input image is a square of unit contrast, $watt/m^2$
$E_P$	radiant emittance of phosphor, $watt/m^2$

$E_T$	total photocathode irradiance due to a 2854°K source, watt/m <sup>2</sup>
$E_{T \text{ max}}$	maximum total photocathode irradiance due to a 2854°K source, watt/m <sup>2</sup>
$E_V$	vidicon photocathode (highlight) irradiance, watt/m <sup>2</sup>
$e_v$	vertical scan efficiency
$E_{\lambda \text{ max}}$	maximum spectral irradiance, watt/m <sup>2</sup> -micron
$E_{\lambda \text{ min}}$	minimum spectral irradiance, watt/m <sup>2</sup> -micron
$E(\lambda, 2854^\circ\text{K})$	spectral irradiance due to a 2854°K source, watt/m <sup>2</sup> -micron
$\mathcal{F}$	the Fourier transform of ...
$F_L$	lens focal length, mm
$G$	gain of any signal-amplifying devices within the camera tube prior to the preamplifier
$G_{ET}$	electron gain at the various intensifier-phosphor/intensifier-photocathode interfaces
$G_{E,1-2}$	electron gain of phosphor/photocathode (or intensifier-phosphor/intensifier-photocathode) combination, electrons in/electrons out
$G_I$	electron gain due to an added intensifier
$G_{IV}$	apparent gain at the phosphor/photosurface interface for an intensifier vidicon of radiant sensitivity equal to $\sigma_0$ amp/watt
$G_L$	apparent light gain due to the addition of an intensifier in front of a second intensifier (or a camera tube)
$G_{L,IV}$	apparent light gain due to a single intensifier of unit magnification coupled to a vidicon
$G_M$	electron multiplier gain
$G_{M,1}$	gain of first dynode stage



$G_{M,4}$	gain of stages following first dynode stage
$G_P$	gain at intensifier-phosphor/image orthicon photocathode
$G_T$	target gain
$g(x)$	image wave shape weighting function in x dimension
$g(x,y)$	image wave shape weighting function in x and y dimensions
$g(y)$	image wave shape weighting function in y dimension
$H$	display height, inches
$i_b$	total electron beam current, amp
$i_d$	dark current, amp
$\bar{I}_B$	rms beam noise, amp
$\bar{I}_{BD}$	rms beam noise due to dark current, amp
$\bar{I}_{BH}$	rms beam noise proportional to signal level, amp
$\bar{I}_{Bo}$	rms beam noise with optimum beam, amp
$\bar{I}_D$	rms first dynode noise, amp
$\bar{I}_e$	rms photoelectron noise, amp
$\bar{I}_N$	total rms noise, amp
$\bar{I}_{NF}$	total rms noise with fixed beam current, amp
$\bar{I}_{No}$	total rms noise with optimum beam current, amp
$\bar{I}_{PA}$	rms preamplifier noise, amp
$i_{refl}$	portion of electron beam that is specularly reflected and does not reach target, amp
$I_S$	signal current output (input to preamplifier), amp

$i_s$	highlight signal current; image signal; photocurrent, amp
$i_{sI}$	highlight signal current for isocon, amp
$I_{S \max}$	maximum signal current output, amp
$i_{s \max}$	maximum photocurrent, amp
$i_{s \min}$	minimum photocurrent, amp
$i_{\text{scat}}$	portion of electron beam scattered by interaction with target, amp
$I_{SF \max}$	maximum highlight signal current obtainable from the isocon when operated near the knee of the signal transfer curve, amp
$i_{sv}$	SEC camera tube photocurrent, amp
$\bar{I}_T$	rms target noise, amp
$K_D$	that fraction of highlight signal current which is dark current, amps
$k_p$	radiant power conversion gain of a phosphor at peak $\lambda$ , watt/amp
$k_{pl}$	radiant power conversion gain of a phosphor, including coupling losses to second-stage photocathode, watt/amp
$K_S$	signal reduction factor variously attributed to field mesh transmittance or incomplete separation of reflected and scattered electrons
$K_V$	proportionality constant related to photoconductor sensitivity
$m$	beam modulation factor
$N$	spatial frequency, TV lines/picture height
$N_c$	frequency at which MTF becomes negligible, TV lines/picture height

$\bar{n}_b$	mean number of photoelectrons in background flux from an equivalent area adjacent to the image of the primary object
$N_H$	maximum horizontal resolution, TV lines/raster height
$N_h$	number of horizontal TV lines per picture height = $Y/x_0$
$N_{hc}$	cutoff frequency, TV lines/picture height
$N_{hl}$	spatial frequency of square-wave input image, half-cycles per picture height = $1/x_0$ , when $x_0$ is measured in units of picture height
$N_{LP}$	spatial frequency, line pairs/millimeter
$\bar{n}_o$	mean number of photoelectrons generated by a photosurface in time $t$ by the image of an object in the scene whose image area is $a$
$N_{TV}$	frequency, TV lines/picture height
$N_{TVP}$	number of line pairs/picture height
$N_{TVP/W}$	number of line pairs/picture width
$N_V$	number of active scanning lines
$N_v$	number of vertical lines per picture height = $\gamma/y_0$
$n_v$	height of bar in terms of number of bar widths
$\dot{n}_{xy}$	number of photoelectrons generated by a photosurface per unit area and time
$P_{min}$	minimum detectable power, watts
$R$	vacuum range
$R_o(N_{TV})$	MTF or sine-wave response in $x$ direction for frequency $N_{TV}$
$R_o(N_h)$	MTF or sine-wave response in $x$ direction for frequency $N_h$
$r_o(x,y)$	sensor response at a point $x,y$ with an impulse input

$R_o(\omega_x, \omega_y)$	Fourier transform of the impulse response, known as the complex steady-state frequency response, the optical transfer function, the sine-wave response, or the modulation transfer function (MTF)
$R_{SQ}(N)$	square-wave amplitude response for frequency $N$
$R_{SQ}(N_h)$	square-wave amplitude response for frequency $N_h$
$R(\lambda)$	relative spectral response of photosurface
$R_\omega$	sine-wave response at spatial frequency $\omega$
$SNR_D$	display signal-to-noise ratio
$SNR_D/C$	display signal-to-noise ratio to contrast $C$
$SNR_{D,T}$	threshold display signal-to-noise ratio (that needed to obtain a detection probability of 0.5)
$SNR_{D/A}$	display signal-to-noise ratio per unit image area
$SNR_{D/A,T}$	threshold display signal-to-noise ratio per unit image area
$SNR_{D/E}$	display signal-to-noise ratio per element $E$
$SNR_{D/E,T}$	threshold display signal-to-noise ratio per element $E$
$SNR_V$	video signal-to-noise ratio
$SNR_{VM,T}$	measured value of threshold video signal-to-noise ratio
$SNR_{V,N,C}$	video signal-to-noise ratio measured or calculated by using a bar pattern of frequency $N_{TV}$ lines/picture height and contrast $C$
$SNR_{V,RMS}$	root-mean-square video signal-to-noise ratio
$SNR_{V,0,C}$	broad-area video signal-to-noise ratio at near-zero spatial frequency and contrast $C$
$SNR_{V,0,1}$	video signal-to-noise ratio at near-zero spatial frequency and unity contrast
$Sq(N)$	Fourier transform of a square wave

$t_e$	integration time of the eye, sec
$T_M$	mesh transmittance
$W$	picture width
$X$	picture width
$\chi_g$	scene "ground" resolution
$x_o$	input pulse width
$Y$	picture height
$y_o$	input pulse height
$Z$	random variable = $SNR_D - SNR_{D,T}$
$Z(\lambda)$	relative spectral distribution of phosphor radiance
$\alpha$	horizontal-to-vertical picture aspect ratio; width-to-height aspect ratio of CRT display, commonly 4:3
$\gamma$	slope of log-log plot of signal-to-noise ratio versus signal irradiance, normally specified along the linear portion of the curve
$\Delta f$	video bandwidth, Hz
$\Delta y$	linear dimension of bar width; bar spacing
$\delta_o(x,y)$	unit volume impulse
$\lambda$	wavelength of radiation, microns
$\sigma$	photocathode radiant sensitivity, amp/watt, to a given source such as a tungsten lamp operated at 2854°K
$\sigma_I$	radiant sensitivity of intensifier photocathode, amp/watt
$\sigma_p$	absolute radiant sensitivity of photosurface at peak $\lambda$ , amp/watt
$\sigma_T$	total photocathode radiant sensitivity to a 2854°K source, amp/watt

$\alpha_i$	photocathode radiant sensitivity of vidicon
$\phi(\omega_x)$	phase transfer function in horizontal direction, radians
$\phi(\omega_y)$	phase transfer function in vertical direction, radians

## V. TELEVISION CAMERA TUBE PERFORMANCE AND DATA

by Frederick A. Rosell

### A. INTRODUCTION

New and different types of television camera tubes are becoming available at an ever-increasing rate. While these new sensors must inevitably lead to improved imaging systems, the process of sensor selection becomes more demanding and, should the traditional methods of comparative laboratory evaluation be followed, costs will become prohibitive to all but the largest laboratories. To evaluate a single new developmental sensor can often require an investment of tens of thousands of dollars and many months of time, with no assurance that the result, based on a single sample, will be representative.

In many cases, however, the need for competitive evaluation can be greatly reduced by the use of analytical performance prediction methods. These methods have been developed to the point where the computed performance of a sensor such as a television camera tube is found to be in good, if not perfect, agreement with measured capability. Indeed, in most instances, the difference between computed and measured performance is less than the expected error in measurement. Significant differences, where they exist, are being rapidly resolved, and the results now being obtained are quite usable in their present form. This is particularly true in making sensor comparisons because, as far as is known, the calculations do not significantly favor one type of sensor over any other. The principal shortcomings of the analyses are these:

- The methods of describing image lag are quite primitive.
- Defects such as picture nonuniformity, graininess, and blemishes, which are sometimes lumped under the elusive term, "picture quality," are largely undefined.

Thus, while one can greatly narrow tube selection for any application analytically, one cannot escape laboratory evaluations.

The following discussion will first review the evolution of low-light-level television (LLLTV) sensors and then proceed to describe the analytical prediction methods and apply them to five different television sensor types:

1. The vidicon,
2. The secondary electron conduction (SEC) camera tube,
3. The image orthicon (IO),
4. The image isocon (II), and
5. The silicon electron bombardment induced-response (SEBIR)\* tube.

These tubes will be considered singly and in combination with one or more intensifiers. While the primary emphasis will be on tubes that have low-light-level potential, the performance of tubes such as the vidicon, which are only suitable at high light levels, will be analyzed.

#### 1. Evolution of Low-Light-Level Television

By day, the unaided human eye can resolve a small high-contrast object which subtends an angle of only 0.15 milliradians. At night, the same object must subtend 15 milliradians or more to be equally detectable. This corresponds to a hundredfold loss in resolving power. In recent times, it has been found possible to restore an observer's night vision to its daytime value by means of electrooptical sensory systems such as LLLTV.

---

\* Or SEBIR. Also variously known as the silicon diode array storage tube, the silicon intensifier tube (SIT) (RCA), the electron-bombarded silicon (EBS) tube (Westinghouse), and the intensified diode array camera (IDAC) tube (Army Electronics Command).



The history of LLLTV probably begins with the development of the image orthicon in 1946. This tube, when equipped with a suitable lens of moderate speed, could provide resolving power comparable to that of the unaided human eye. In format, the IO consists of a photoemissive photocathode followed by a target-mesh assembly that both amplifies and stores the image during the periods between signal readout by a scanning electron beam. The IO incorporates, in addition, an integral return-beam electron multiplier that serves as a low-noise preamplifier. The primary improvements in the IO in the years following 1946 were in the photocathode and the target.

In the early 1950's, a new photocathode--the S-20 photoemitter--was developed. The S-20 was four times more sensitive than what had previously been available. Further inroads on sensitivity were made in the mid-1950's with the development of a new thin-film metal-oxide target that provided a signal amplification three to five times greater than that of the glass target originally used.

To achieve true low-light-level capability, an image intensifier had to be added to the image orthicon. This device converts an input photon image into a photoelectron image, which is then accelerated to a phosphor. The phosphor recreates a visible image of greater brightness than the image incident on the input. This brighter image is fiber-optically piped to the image orthicon and provides an additional light gain of between 30 and 50. With this increased gain, the intensifier image orthicon (I-IO) very nearly achieves the so-called photoelectron-noise-limited condition for stationary broad-area images. This means that the primary noise at the output of the tube is due to the inherent fluctuations in the primary photoprocess due to the conversion of photons to electrons. This noise represents a fundamental limitation, and since the fundamental limits had apparently been reached, it might be thought that the development of LLLTV had been completed. However, because of other defects, this was not the case.

In low-light-level imaging, it is necessary to amplify the input photoelectron noise to a level well above that of any tube- or system-generated noise. In the case of the I-IO, the primary system noise is

that of the scanning-electron-beam noise at the input of its internal electron multiplier preamplifier. This is very low, and therefore the gain needed for photoelectron noise to overwhelm the beam noise is not large. For the I-IO, the gain needed and provided is about 500. One result of this low gain, however, is that the beam current is very small as well, which makes the time constant long. While target capacitance is made as small as possible, there are limits to capacitance reduction because signal storage capability is reduced correspondingly. The net result is that the I-IO tends to be of limited dynamic range and somewhat laggy. The effect of lag is to decrease signal for scenes in motion.

In the early 1960's, the intensifier secondary electron conduction (I-SEC) camera was developed. The secondary electron conduction (SEC) target provides a tenfold increase in gain before readout by the beam and is, therefore, much less laggy. Because the SEC tube uses an external preamplifier that is noisier than the internal electron multiplier preamplifier of the IO, the higher gain is needed to acquire sensitivity for the I-SEC comparable to that of the I-IO. Both the I-IO and I-SEC fall somewhat short of photoelectron noise limits at the very lowest light levels, but the deficiency is not serious. Besides being less laggy, the I-SEC is less complicated to operate and has a wider dynamic range. Thus, by the mid-1960's, the I-SEC had substantially replaced the I-IO in LLLTV systems.

The I-SEC also has its faults, however. The time constant, though much improved, becomes marginal at the very lowest light levels. Also, some increase in sensitivity would be desirable. Both the IO and SEC targets were initially subject to damage by extreme overexposure to about the same degree, although both could usually be protected by electronic means. More recently, a mesh-supported SEC target has been developed that is many factors of ten less prone to damage and that should be proof against all but the most severe environments. Even with extreme overexposure, the damage to the new SEC target is localized to the overexposed area rather than to a general area, as before.

Sufficient gain to make any TV sensor photoelectron noise limited can always be provided by adding a sufficient number of intensifiers to its input. Unfortunately, this involves a number of imaging and reimaging steps, and, at each step, resolving power is lost. Thus, every effort is made to minimize the number of intensifiers. In current practice, most high-quality LLLTV systems employ one image-intensifier stage, which is sufficient to provide the needed gain and usually does not degrade overall resolving power by a large amount. With only one intensifier, the principle resolution-limiting element in an LLLTV camera is the combination of the target and the electron scanning beam in the TV pickup tube. For the I-SEC, the principal problem is the interaction of the electron beam with a suppressor mesh needed to prevent an image-runaway condition. Because of this interaction, about the only way to improve resolving power is to increase the SEC target size, but this increases target capacitance, lag, and tube size.

The most promising new sensor becoming available is the intensifier silicon electron bombardment induced response (I-SEBIR) tube, which, except the target, is identical in construction to the I-SEC. In the I-SEBIR, the target is a matrix of silicon diodes. The principal features of this new target are a twentyfold higher gain than the I-SEC and an immunity to damage by overexposure. The gain is more than sufficient to ensure that I-SEBIR cameras will be photoelectron noise limited at all light levels of interest and to ensure an adequate speed of response.

The current-resolving power of the I-SEBIR is comparable to that of the I-SEC camera. It is expected that the resolving power will increase with time as target size is increased. Because no suppressor mesh is needed in the I-SEBIR, there is none to form a fundamental limit to resolution as there is in the I-SEC. Also, the absence of a suppressor mesh results in a tube that has lower shunt capacitance and is less subject to microphonics. Because lag should be smaller than it needs to be, some increase in lag, which would accompany increases in target size, can be permitted.

The I-SEBIR shows high promise. Good tubes have been constructed and tested. Blemishes and uniformity problems, though not completely solved, are tolerable for military applications. A target lifetime problem due to soft X rays has been encountered, but this problem appears manageable.

To recapitulate, the four principal LLLTV pickup systems employed to date or expected to be used in the near future are given in Table V-A-1.

TABLE V-A-1. PRINCIPAL LLLTV PICKUP SYSTEMS AND DATES OF USE

<u>System</u>	<u>Dates</u>
Image Orthicon (IO)	1946-1961
Image Isocon (II)*	1949-
Intensifier - Image Orthicon (I-IO)	1961-1965
Intensifier - Secondary Electron Conduction (I-SEC) Camera	1965-
Intensifier - Image Isocon (I-II)**	1969-
Intensifier - Silicon Electron Bombardment Induced Response (I-SEBIR) Camera	1971-

\* Though introduced in this year, the II has not been used extensively.

\*\* Used for evaluation only.

The improvements obtained in low-light-level imaging are illustrated in Fig. V-A-1.

As can be seen, the image orthicon improved by a factor of 100 in the 1946-1961 time span. It was gradually replaced by the I-SEC camera, which by 1965 gave roughly equal sensitivity, somewhat higher resolving power, and lower lag. The I-SEC continued to improve both in sensitivity and resolving power until a fairly high order of capability was achieved in 1969. The I-SEBIR became available in very limited quantity in 1969. At the lower line numbers, its sensitivity

is outstanding, but its maximum resolving power is limited. The projected improvement in the I-SEBIR is also shown in Fig. V-A-1. This projection is based on increase in target size only. Other technological improvements can also be expected.

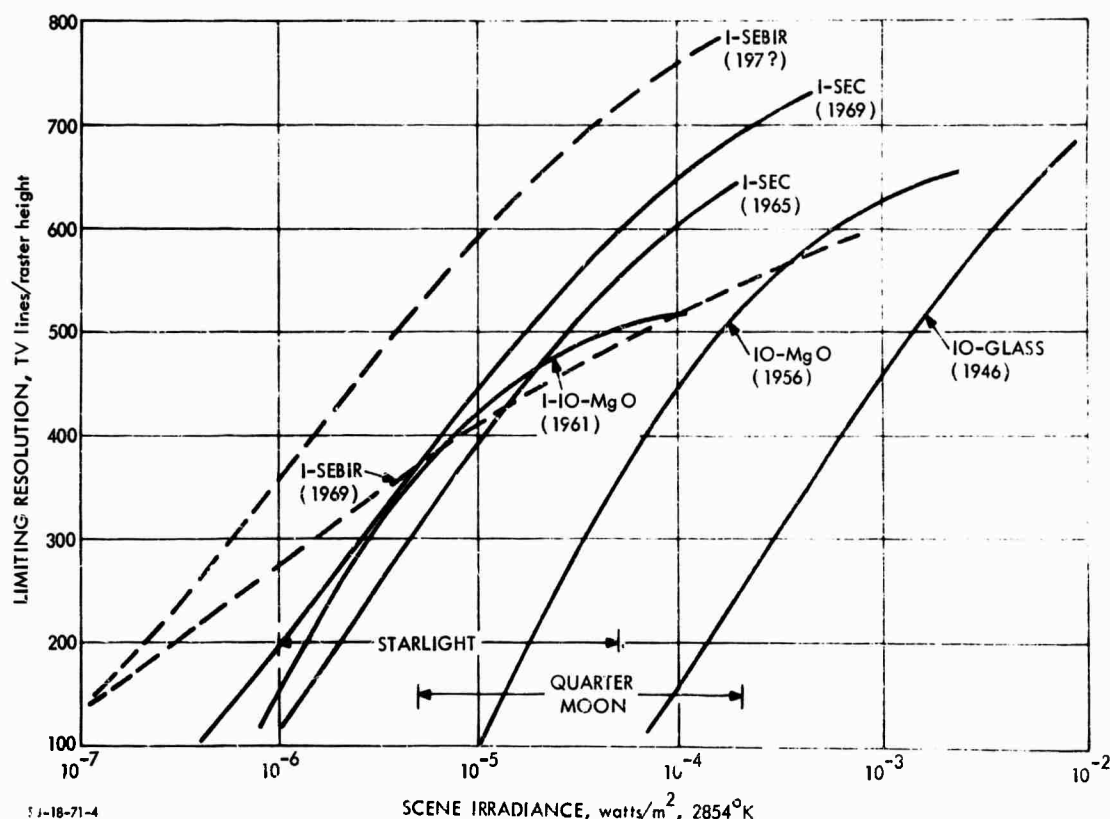


FIGURE V-A-1. Limiting Resolution Versus Scene Irradiance for Various 40-mm Low-Light-Level Television Cameras. An F/1.5 Lens is Assumed

Photocathodes have also improved steadily in quality and sensitivity over the years. The earliest television camera tubes employed the S-1 photoemitter, which was characterized by a very high dark current of  $10^{-11}$  to  $10^{-12}$  amp/cm<sup>2</sup>, a wide spectral response of from 0.4 to 1.2 microns, and a rather low radiant sensitivity to tungsten light of 0.25 ma/watt. This surface is now used only in conjunction with auxiliary scene illuminators. The first image orthicons available in 1946 employed an S-10 photoemitter, which had a lower dark current of

$10^{-13}$  to  $10^{-14}$  amp/cm<sup>2</sup>, a more restricted spectral bandpass of from 0.4 to 0.7 microns, and a larger radiant sensitivity of 0.5 ma/watt. This surface is prized mainly for its ease of manufacture and the similarity of its spectral response to that of the human eye.

The S-20 photoemitter, developed in the early 1950's, had a very low dark current of  $10^{-15}$  to  $10^{-16}$  amp/cm<sup>2</sup>, improved spectral bandpass of from 0.4 to 0.8 microns, and a much larger radiant sensitivity of 3.0 ma/watt. By the early 1960's, the red response of the S-20 improved and, along with that, the radiant sensitivity increased to 4-4.5 ma/watt. This surface became known informally as the S-20XR (XR for extended red). Even further improvements in the mid-1960's led to sensitivities of the order of 4.5-5.5 ma/watt. This version of the S-20 was type classified as the S-25.

In the late 1960's, the S-20 was once again improved. This new surface, now known as the S-20VR (VR for very red), shows appreciable response at 0.85 microns and radiant sensitivities in the 6-9 ma/watt region. It is understood that dark current has not significantly increased as the S-20 has been successively improved.

The spectral responses of these various surfaces as they currently exist are shown later in Fig. V-B-2 (p. 248) and the other parameters are shown in Table V-A-2.

Improved photocathodes lead to increased sensitivity. The increase in sensitivity is directly proportional to photocathode sensitivity if the sensor is preamplifier or system noise limited. If the sensor is photoelectron noise limited, as is the case for LLLTV, the increase in sensitivity is proportional to the square root of photocathode sensitivity. However, target-to-background contrast is often significantly higher at the longer wavelengths to which the new, improved sensors are sensitive.

To achieve real-time, low-light-level imaging, it is necessary to substantially amplify the photoelectron signal generated by the photocathode prior to readout by the electron beam. A large gain serves two useful purposes:

1. A large gain raises the photoelectron signal and noises to levels well above that of the video preamplifier that directly follows the readout process.
2. A large gain reduces the readout time constant, since a high gain implies a high reading beam current.

Indeed, a higher gain is often needed to achieve a satisfactory time constant than is needed simply to eliminate the preamplifier as a noise source.

TABLE V-A-2. PARAMETERS OF VARIOUS PHOTOCATHODES

Period	Type	Dark Current, <u>amp/cm<sup>2</sup></u>	Radiant Sensitivity @ 0.85 micron, <u>ma/watt</u>	Radiant* Sensitivity, <u>ma/watt</u>
--	S-1	10 <sup>-11</sup> -10 <sup>-12</sup>	1.5-2.5	0.25
1946	S-10	10 <sup>-13</sup> -10 <sup>-14</sup>	--	0.5
Early 1950's	S-20	10 <sup>-15</sup> -10 <sup>-16</sup>	--	3.0
Early 1960's	S-20XR	10 <sup>-15</sup> -10 <sup>-16</sup>	1-2.5	4-4.5
Mid- 1960's	S-25	10 <sup>-15</sup> -10 <sup>-16</sup>	5-9	4.5-5.5
Late 1960's	S-20VR	10 <sup>-15</sup> -10 <sup>-16</sup>	20-25	5.5-9.0

---

\* For tungsten sources operated at 2854°K.

One method of achieving large gains is simply to cascade a number of image intensifiers in front of the TV pickup tube. While any amount of gain can be provided in this manner, a severe loss in resolving power will be incurred because at each imaging and reimaging step,

signal amplitude modulation due to image detail is lost.. Thus, the effort is to achieve the requisite gain with a minimum number of components.

Most of the more sensitive TV pickup tubes employ signal storage targets that also have gain. While these gains can be appreciable, all of these tubes, in current practice, require at least one additional image-intensifier stage either to obtain the necessary gain or to sufficiently reduce the time constant or to do both. Ordinarily, the intensifier provides an additional gain of about 40.

It can be observed in Table V-A-3 that the gain of the intensifier image orthicon is not large. Even so, it is known that this tube is a quite capable performer. The reason for this apparent discrepancy is that the image orthicon employs a return-beam electron multiplier as a preamplifier. From a sensitivity viewpoint, it is sufficient to have enough gain to overcome preamplifier noise, and the noise of an electron multiplier is very low compared to that of an external preamplifier. One rough measure or indicator of the adequacy of the gain is the ratio of gain to preamplifier noise, as is shown in Table V-A-3. It should be noted that it is possible to have too much gain, which is the case for the I-SEBIR tube. However, gain can be quite easily reduced.

Also shown in Table V-A-3 is an estimate of lag characteristics. While the I-IO with MgO target is very acceptable from a sensitivity viewpoint, its low gain before readout results in an overly large lag. The 1-SEC, though slightly less sensitive, is much less laggy. However, even the I-SEC must be considered marginal at the lowest light levels. The I-SEBIR should not have these problems.

## 2. Performance Criteria for Sensor Analysis

Camera tube manufacturers routinely supply certain data. Ordinarily, this includes a signal transfer curve, a bar-pattern amplitude response function, and sometimes a limiting resolution versus light level characteristic. Certain other auxiliary data, such as interelectrode



capacitance, photocathode response, and residual signal characteristics, may also be provided.

TABLE V-A-3. COMPARISON OF GAIN-TO-PREAMPLIFIER-NOISE RATIO

<u>Period</u>	<u>Tube Type</u>	<u>Target Type</u>	<u>Product of Target and Intensifier Gain</u>	<u><math>I_{PA}</math> Preamp Noise, na</u>	<u><math>G/I_{PA}</math></u>	<u>Lag: Ratio of Actual to Acceptable at Very Low Light Levels</u>
Early 1950's	I-IO	Glass	120	0.25*	480	100
Late 1950's	I-IO	MgO	400	0.25*	1,600	10
Early 1960's	I-SEC	SEC	4,000	3.0	1,333	2
Late 1960's	I-SEIR	Silicon Matrix	80,000**	3.0	26,666**	0.5

\* With fixed beam current, noise is at the input to the internal electron multiplier.

\*\* In practice, gain will be reduced to between 10,000 and 20,000, and therefore the gain-to-preamplifier noise ratio  $G/I_{PA}$  will range from 3,300 to 6,600.

The signal transfer characteristic is a plot of signal current at the camera tube's output as a function of the input photocathode irradiance or illuminance as shown in Fig. V-C-2. This is measured using a broad-area test image which is not degraded by any sensor aperture. Under certain conditions, the signal transfer curve may be indicative of relative sensor sensitivity, but many exceptions can be noted. In fact, the extension of the transfer characteristic to lower photocathode irradiance levels by means of intensifiers, for example, may result in either sensitivity improvement or merely a reduction in dynamic range. Also, the signal transfer characteristic contains information regarding neither sensor noise nor its resolving power.

The bar-pattern amplitude response function is a measure of a camera tube's ability to resolve fine image detail if the signal-to-noise ratio available is otherwise high enough. Its primary function is to determine the extent to which the finite apertures of the camera tube degrade the signal generated by the input photocathode. To measure it, a bar pattern of known amplitude and of very low spatial frequency is projected on the photocathode and the output signal amplitude is noted. Next, the spatial frequency of the bar pattern is increased step by step, and the ratio of the output signal amplitude at the high spatial frequency to that measured at the low reference frequency is computed. A typical result is shown in Fig. V-C-3 (p. 263). Ordinarily, the amplitude response function conveys no sensitivity or noise information.

While the signal transfer and amplitude modulation curves are related to sensor performance, performance cannot be inferred from them directly.

The video signal-to-noise ratio obtainable from the sensor as a function of the input photocathode irradiance is a somewhat better indicator of performance. Usually, it is measured for broad-area images at fairly high light levels and extrapolated to lower light levels analytically. Also, the results can be extrapolated to bar-pattern images of fine detail in many cases by appropriately multiplying the broad-area video signal-to-noise ratio by the amplitude response. This ratio is of some interest in applications where the video signal is used directly, as in contrast trackers. However, the video signal-to-noise ratio does not translate directly into resolving power. Furthermore, it is a function of video bandwidth, which is not fundamental to the detection process as performed by a human observer.

From the viewpoint of the human observer, a new measure, the display signal-to-noise ratio, will be defined in the following. This represents the signal-to-noise ratio associated with the image on the cathode-ray tube display. Since the image signals and noises have been so highly amplified and magnified before being displayed, it has

been shown that the display signal-to-noise ratio will not be significantly degraded by the eye over a wide range of conditions. Therefore, the signal-to-noise ratio at the observer's retina will be essentially identical to that on the display. The display signal-to-noise ratio is very nearly independent of video bandwidth. A further merit of the display signal-to-noise ratio as defined is that it has been experimentally determined that the ratio needed to detect a given type of image liminally is approximately constant, as shown in Fig. V-C-5 (p. 269). Since the display signal-to-noise ratio includes the camera tube's signal transfer characteristic, its amplitude response,\* and all of the noises generated either in the primary photoprocess or in subsequent signal processing, it represents a reasonably good means of comparing various camera tubes.

The intersection of the display signal-to-noise ratio obtainable with that needed by the observer as shown in Fig. V-C-5 (p. 269) can be used to determine the limiting resolution versus light level characteristic such as is shown in Fig. V-C-6 (p. 271). This characteristic can be measured directly by an observer by projecting a bar pattern of known spacing and irradiance level on the photocathode and reducing the irradiance level until the pattern becomes barely discernible. While not as versatile as the display signal-to-noise ratio curves, the resolution versus irradiance level characteristic has some utility in that it can be roughly related to the maximum scene resolution to be expected at a given scene radiance level.

### 3. Electrooptical Imaging Sensor Analysis

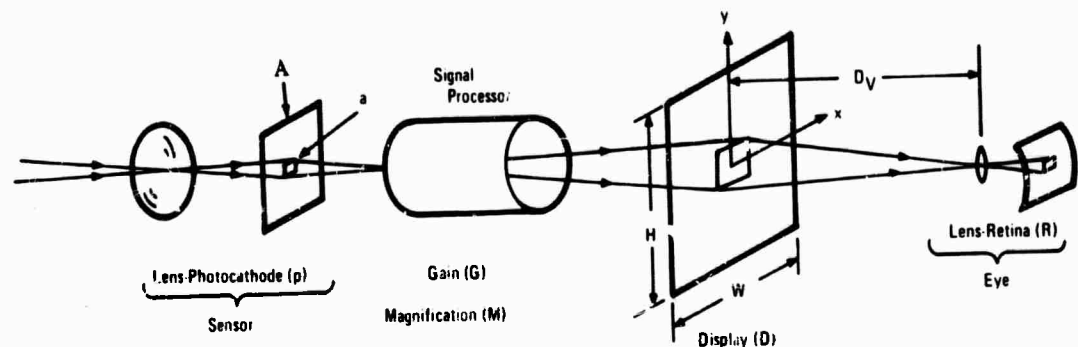
In viewing a scene indirectly on the display of an electrooptical sensor, the lens and photosurface of the sensor replace the lens and retina of the eye as the primary phototransducer. The purpose of replacing the eye in this manner is to provide the observer with capability he does not ordinarily have. For example, the sensor can have greater aperture and longer focal length to increase light gathering

---

\* Square-wave amplitude response as currently defined.

capability and resolution of scene detail. Photocathodes of greater quantum efficiency than the eye can be obtained in the visible region, and, if desired, imaging at wavelengths far beyond the visible can be provided. Even without these attributes, the sensor may be of some use, since it can be remotely located.

The essentials of an electrooptical imaging sensor are shown in Fig. V-A-2. The scene, consisting of a small area  $a$  in this case, is imaged on the photosurface by the lens. The photosurface converts the scene photon image to a photoelectron image that is amplified and magnified by a signal processor and focused on a phosphor that creates a visible light image. Finally, photons from the displayed image are collected by the observer's lens and projected onto his retina, which converts the image to sensory impulses for subsequent processing and interpretation by the brain.



70-1283-VA-1

FIGURE V-A-2. Electrooptical Image Process

In the following discussion, the degree to which the sensor can aid the observer will be determined. The main emphasis will be on the overall sensor sensitivity and resolving power. The observer will be as an integral part of the overall system. We will show that the capability of the sensor-augmented observer can be analytically predicted

for simple scene test patterns such as disks, rectangles, and bar patterns and that these predictions correlate closely with measured results. However, sensory system performance prediction must still be regarded as an art needing considerable development to achieve greater precision and to extend the results to more complicated (and more realistic) imaging situations. To the extent that the analysis applies at all, it applies equally well to any electrooptical sensor, including low-light-level television and real-time forward-looking infrared scanners.

In most electrooptical sensory systems, the designer has some latitude in selecting the sensor objective lens and input photodetector type. For present purposes, both the lens and phototransducer can be considered to be design parameters. Then, the beginning point of the analysis is the output of the photosurface, which may be considered to be the source of a photoelectron image. System elements, including the observer, will be generally unaware of the source of this image. We do observe, however, that the photon-to-electron conversion process is noisy and that there is a signal-to-noise ratio associated with the primary photoprocess that inherently limits its information content.

The function of the signal processor is to amplify the signal and magnify it as necessary to preclude the possibility that the eye will be acuity-limited by either image size or luminance. Were the sensor ideal, the signal and noises generated by the input photosurface would be equally amplified so that the signal-to-noise ratio generated by the input photosurface would be identical to that at the phosphored screen and, in turn, would be identical to that generated by the eye retina. In real sensors, the signals may be distorted or smeared by the signal-processor finite apertures and display elements, and noises may be added.

a. Detection of Isolated Rectangular Images. In the beginning of this analysis, it will be assumed that the image is large relative to the sensor point image spread function, so that the finite sensor apertures can be neglected and the signal processor is noise free.

The eye viewing the display also has limitations, depending on the display brightness, video gain, image size, and viewing distance. Fluctuation noises are associated with the conversion of display photons to sensory impulses, and both the eye and the retina have finite apertures. However, we shall assume that the display luminance is sufficient and that the image is large enough, relative to the viewing distance, to preclude either retinal fluctuation noise or acuity limitations on image detection. On the other hand, the image will not be so large as to exceed the spatial integration capability of the eye. With these assumptions, the signal-to-noise ratios at the output of the photosurface display and at the retina will be equal. Linearity of all processes is assumed in the following.

The elementary model describing the effect of photoconversion-fluctuation noise is ordinarily attributed to Rose (Ref. 1), who, in turn, attributes it to deVries (Ref. 2). The basic model assumes that the photon-to-photoelectron conversion process is random in space and time and that the randomness can be characterized by the Poisson probability distribution law. According to Poisson statistics, if the photosurface generates  $\dot{n}_{xy}$  photoelectrons per unit area and time, then the average or mean number  $\bar{n}_0$  generated in time  $t$  by an area  $a$  will be

$$\bar{n}_0 = \dot{n}_{xy} (at) \quad (V-A-1)$$

Also, the standard deviation or rms fluctuation noise associated with  $\bar{n}$  is equal to  $(\bar{n})^{\frac{1}{2}}$ , so that the signal-to-noise ratio becomes  $\bar{n}/(\bar{n})^{\frac{1}{2}}$ , provided that there is no background flux. With background, the Rose model assumes that the incremental signal becomes  $\bar{n}_0 - \bar{n}_b$  and that the signal-to-noise ratio becomes

$$SNR_D = (\bar{n}_0 - \bar{n}_b) / (\bar{n}_b)^{\frac{1}{2}} \quad (V-A-2)$$

Note that the symbol D is added to the signal-to-noise ratio SNR to indicate that the calculations are referenced to an idealized, hypothetical

display without line structure and an MTF of 1. This is convenient when the effects of observer viewing distance are to be taken into account.

In a later model, Coltman and Anderson (Ref. 3) assumed that the noises from the background and the object should be quadratically summed, so that Eq. V-A-2 becomes

$$SNR_D = (\bar{n}_o - \bar{n}_b) / (\bar{n}_o + \bar{n}_b)^{1/2} \quad (V-A-3)$$

This model appears to be more consistent with the statistical detection model discussed below. In both models, the inference is that the eye compares the area with signal to some other area of equal size in which the signal is absent. Before proceeding, we define contrast as

$$C = (\bar{n}_{xy \max} - \bar{n}_{xy \min}) / \bar{n}_{xy \max} \quad (V-A-4)$$

So that contrast is always positive and varies only from 0 to 1. Further, we will assume that signals are always positive, so that combining Eqs. V-A-1, V-A-3, and V-A-4 yields

$$SNR_D = C(\bar{n}_{xy \max} \cdot at) / [(2-C)\bar{n}_{xy \max} \cdot at]^{1/2} \quad (V-A-5)$$

In the above, we have set  $t$  equal to the integration time of the eye  $t_e$ .

As the next step, we note that the photoelectron rate can be written in terms of the photocurrent  $i_s$ , as

$$\bar{n} = i_s / (eA) \quad (V-A-6)$$

where  $e$  is the charge of an electron and  $A$  is the effective area of the photocathode. Now, Eq. V-A-5 may be written as

$$\text{SNR}_D = \left[ t a / A \right]^{1/2} \cdot C i_{s \text{ max}} / \left[ (2-C) e i_{s \text{ max}} \right]^{1/2} \quad (\text{V-A-7})$$

Now, we multiply the numerator and denominator of Eq. V-A-7 by  $\Delta f$ , the video bandwidth, with the result that

$$\text{SNR}_D = \left[ t \Delta f a / A \right]^{1/2} \cdot \left[ C i_{s \text{ max}} / \left[ (2-C) e \Delta f i_{s \text{ max}} \right]^{1/2} \right] \quad (\text{V-A-8})$$

The second term in the above can be recognized by those familiar with television signal-to-noise analysis as the broad-area video signal-to-noise ratio  $\text{SNR}_{V,0,C}$ . "Broad-area" means that the image used to make the measurement is large compared to the point spread or impulse response of the sensor.

The original formulation of fluctuation noise limitations to imaging, as formulated by de Vries in 1943, gave the image signal-to-noise ratio (or  $\text{SNR}_D$ , as we define it here) as

$$\text{SNR}_D = \frac{\Delta n}{(n_o + n_b)^{1/2}}$$

while Schade prefers

$$\text{SNR}_D = \frac{\Delta n}{[(n_o + n_b)/2]^{1/2}}$$

When an independent source of noise  $n_s$  is added, the de Vries formulation leads to

$$\text{SNR}_D = \frac{\Delta n}{(n_o + n_b + 2n_s)^{1/2}},$$



while Schade's formulation led to

$$\text{SNR}_D = \frac{\Delta n}{[(n_o + n_b)/2 + n_s]^{1/2}} .$$

Written in terms of a photocurrent, the de Vries model gives

$$\begin{aligned} \text{SNR}_D &= \frac{\Delta i \cdot (at)^{1/2}}{[e(i_o + i_b) + 2 e i_s]} \\ &= \frac{\Delta i (at)^{1/2}}{[2 e \bar{i} + 2 e i_s]} , \end{aligned}$$

whereas the Schade model gives

$$\text{SNR}_D = \frac{\Delta i (at)^{1/2}}{(e \bar{i} + e i_s)^{1/2}}$$

In order to convert the de Vries model to a form recognizable in terms of a video signal-to-noise ratio as used in this document, the numerator and denominator were multiplied by  $\Delta f$ , the video bandwidth, whereas, to achieve the same result with the Schade model, the numerator and denominator are multiplied by  $2\Delta f$ . With this understanding, both models are similar in the noise expression but differ by the  $\sqrt{2}$  in the signal expression. However, in the analysis reported herein, we have used a value of 0.2 sec (following Rose) for the eye's integration time, while Schade prefers a value of approximately 0.1 sec for the usual range of display luminances (0.2 to 1 ft-L). With this adjustment both the de Vries model and the Schade model give the same numerical result. In future work Schade's model will be used and 0.1 sec used as the eye integration time.

In passing, it should be observed that in using  $\bar{i}$ , the average current, the apparent dependence of noise on image contrast is eliminated, since

$$(2 - C) i_{\max} = 2 \bar{i}$$

The only purpose of the use of  $i_{\max}$  is that it converts directly to highlight irradiance, which is the quantity usually plotted in resolution-versus-irradiance characteristics.

With these observations, Eq. V-A-7 is written as

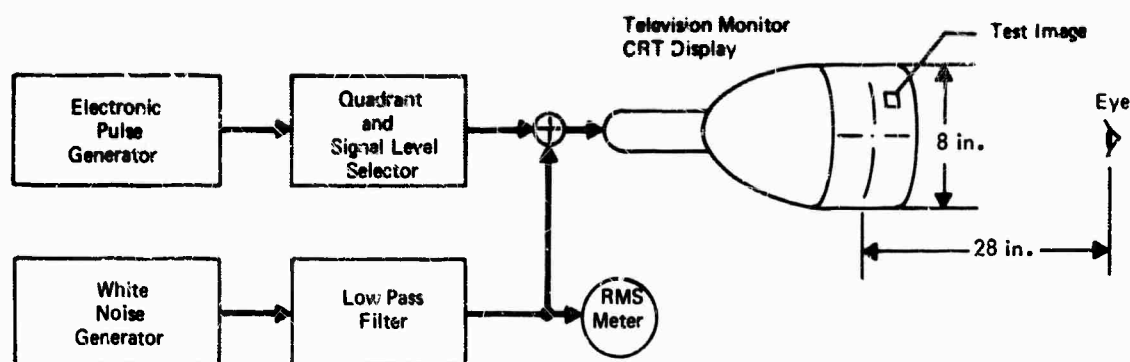
$$\text{SNR}_D = [t \Delta f a/A]^{\frac{1}{2}} \cdot \text{SNR}_{V,0,C} \quad (\text{V-A-9})$$

If our premise is correct, and if Eq. V-A-9 is correct, then we should be able to demonstrate that for a series of image sizes a constant level of probability of detection will require larger video signal-to-noise ratios ( $\text{SNR}_V$ ) for small images than for large images. Further, we should be able to show that a given value of  $\text{SNR}_D$  is associated with a given value of probability of detection--over a very broad range of image sizes.

These predictions were well borne out in the experiment described below, wherein a rectangular image is electronically generated, mixed with band-limited white noise,\* and displayed on a television monitor (Fig. V-A-3). A selector was devised so that the image could appear in any one of four quadrants.

---

\* In the experiments reported herein, the noise was Gaussian rather than Poisson distribution. In the Coltman and Anderson experiment (Ref. 3), however, the results obtained using noise of either Gaussian or Poisson distribution appear to correlate closely.



53-18-71-5

FIGURE V-A-3. Equipment for Display Signal-to-Noise Ratio Experiment

Response was forced (i.e., the observer had to pick a quadrant whether he saw an image or not). The probability of detection obtained in this way was then corrected for chance. The ratio of viewing distance to display height was  $D_V/H = 3.5$ , with the displayed scene being 8 in. high and 28 in. distant. In the first experiment, the image was a series of rectangles of different sizes. Their dimensions were expressed in terms of scan line widths, and a 525-line total vertical scan with 490 active lines was assumed. Thus, the image size in terms of scan lines became

$$n_x n_y = (490)^2 \cdot \alpha(a/A) \quad (V-A-10)$$

where  $\alpha$  is the width-to-height aspect ratio of the CRT display, 4:3 in this case. The image chosen was 4 scan lines high and from 4 to 180 scan lines wide. Next, the probability of detecting the image was determined as a function of the video signal-to-noise ratio at a video bandwidth of 7.1 MHz. The result is shown in Fig. V-A-4a. Observe that the larger the rectangle, the smaller the  $SNR_V$  needed.

The display signal-to-noise ratio required was computed from Fig. V-A-4a and the equation

$$SNR_D = (1/490) (n_x n_y t \Delta f / \alpha)^{1/2} \cdot SNR_V \quad (V-A-11)$$

which was derived using Eqs. V-A-8 and V-A-9 and is plotted in Fig. V-A-5 for  $t = 0.2$  sec. As can be seen, the display signal-to-noise ratio required for a given probability of detection is a constant independent of image size over a wide range of image aspect ratios. It should be noted that the angular extent of the image relative to the observer's eye varied from  $0.13 \times 0.13$  deg for the rectangle of 1:1 length-to-width ratio to  $0.13 \times 6.2$  deg for the 45:1 ratio. The eye-and-brain combination can apparently integrate over large areas in space.

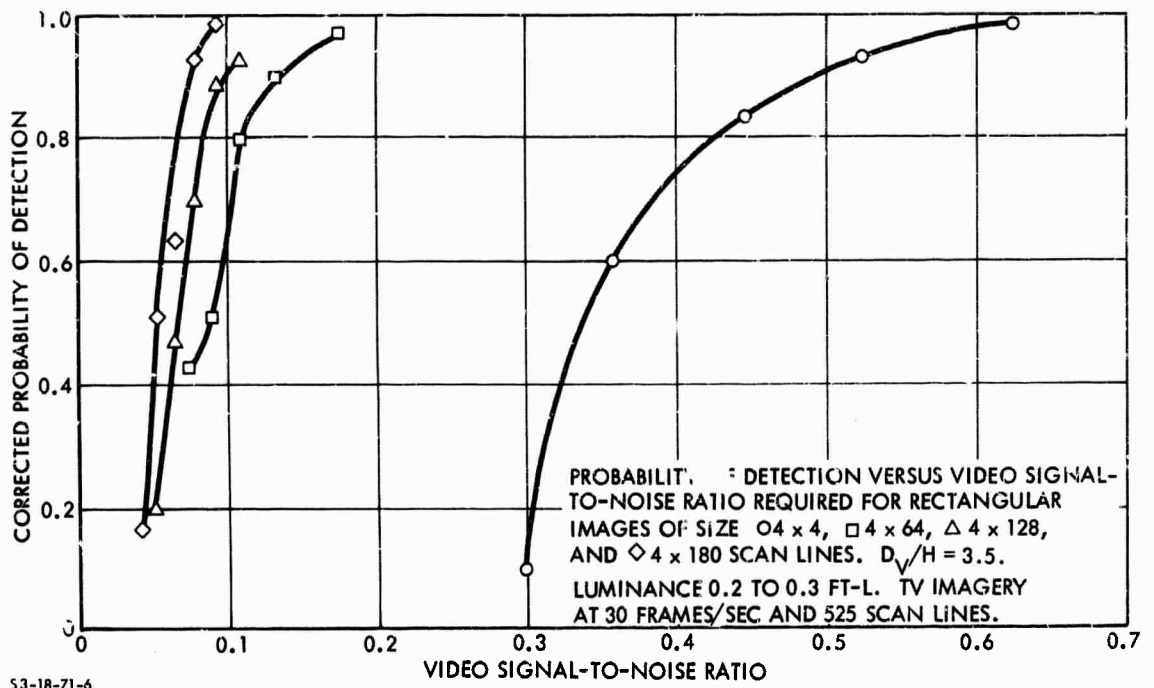


FIGURE V-A-4a. Corrected Probability of Detection Versus Video Signal-to-Noise Ratio for Rectangular Images

It has been observed that the long, thin rectangles in Fig. V-A-4a are nearly "all edge" and that the eye is more sensitive to edges than to areas. As a preliminary test of this concept, various squares were used as test images. These squares were  $2 \times 2$ ,  $4 \times 4$ ,  $8 \times 8$ ,  $16 \times 16$ ,  $32 \times 32$ , and  $64 \times 64$  scan lines in size and varied in angular subtense at the eye from  $0.06 \times 0.06$  deg to  $2 \times 2$  deg. The

result is shown in Fig. V-A-4b. As can be seen, the  $SNR_D$  required to detect the images  $2 \times 2$  to  $16 \times 16$  scan lines in size (angular subtense from 0.06 to 0.5 deg) is approximately constant. However, the  $SNR_D$  required to detect the squares of larger angular extent (1 and 2 deg) increases. This lends some support to the "edge" theory. Since the large areas are of less importance to the user of a system, it is felt that the notion of a constant  $SNR_D$  based on image area is appropriate for most system prediction purposes.

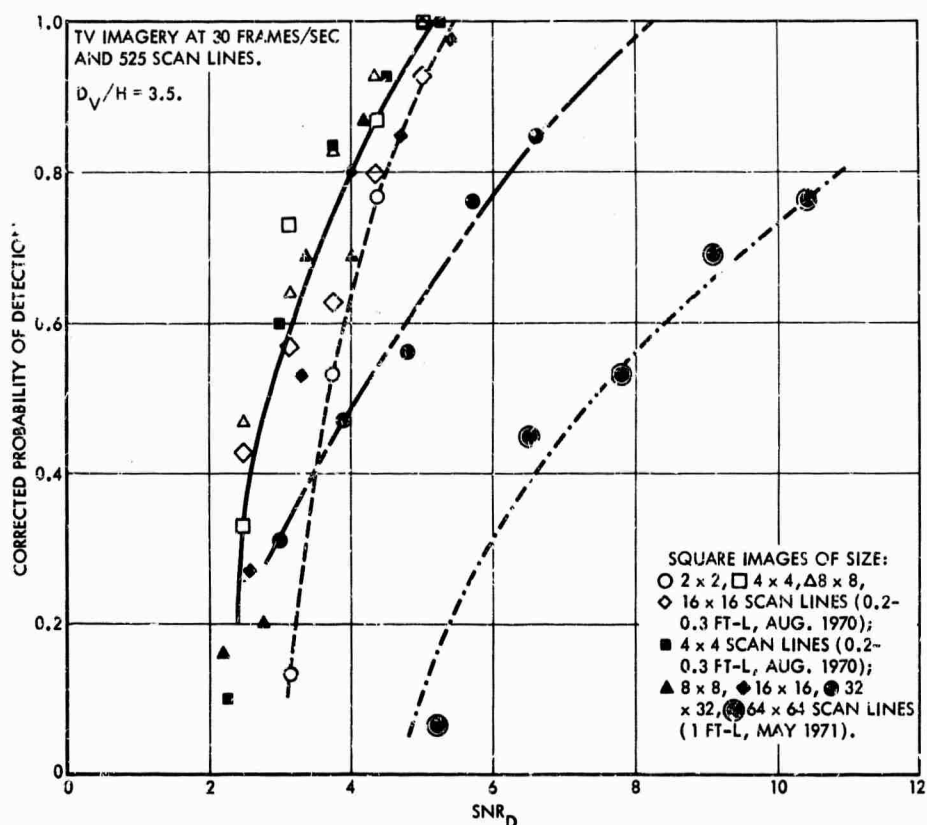


FIGURE V-A-4b. Corrected Probability of Detection Versus Display Signal-to-Noise Ratio for Square Images

We have also observed that the detectability of a displayed image is almost entirely a function of its  $SNR_D$ , not of its displayed contrast, unless the contrast becomes so low that the eye becomes acuity-limited by the fluctuations generated in the retina by the display background luminance. However, this only means that the noise generated in the retinal photoprocess should have been included in the

analysis. Had it been, detectability would probably have been independent of the displayed contrast, as before. The  $SNR_D$  is, of course, a strong function of the image contrast at the input photocathode, which can be far different from the displayed image contrast.

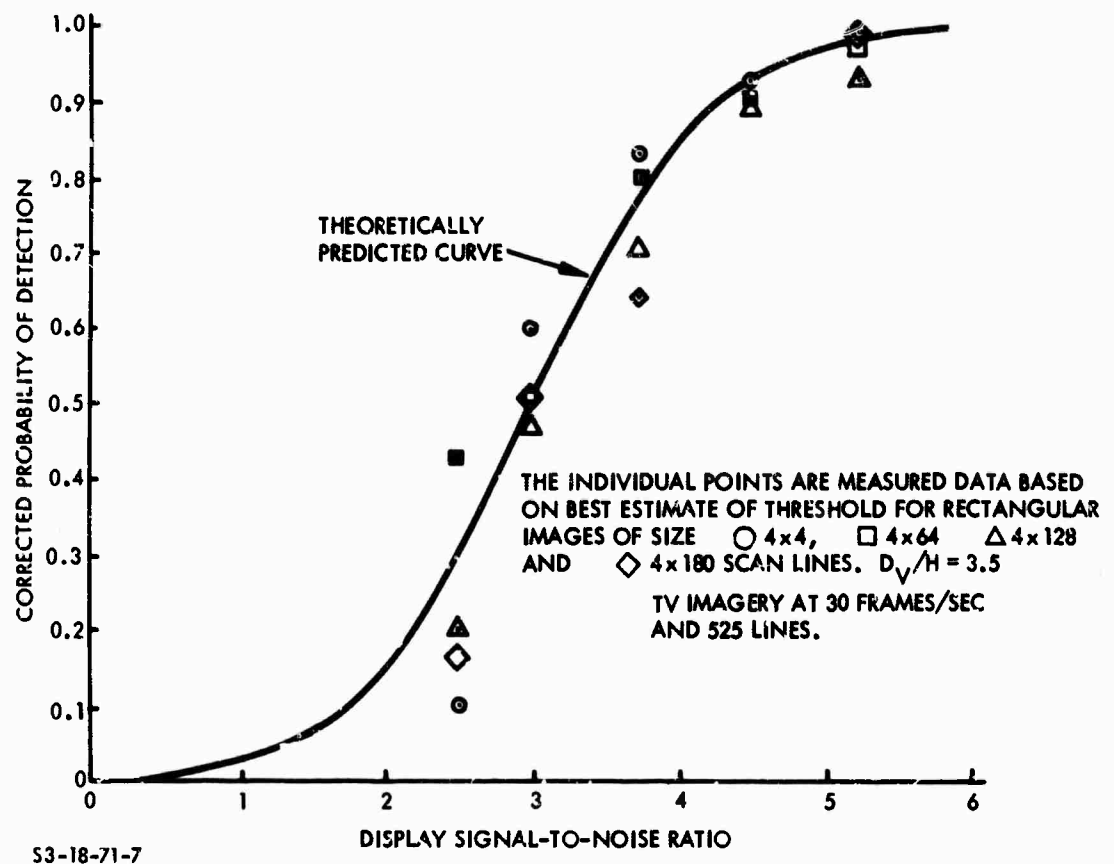


FIGURE V-A-5. Measured and Predicted Probability of Detection

The curve used to fit the experimental points is based on a probability model originally suggested by Legault (Ref. 4). In this model, which is derived in the Appendix, it is assumed that the mean number of photoelectrons within the sampling interval has become sufficiently large that the Gaussian or normal probability distribution given by

$$f_z(z) = \exp [-z^2/2]/(2\pi)^{\frac{1}{2}} \quad (V-A-12)$$

becomes a good approximation of the Poisson distribution law, which actually represents the signal and noise processes. In the above,  $Z$  is a random variable shown to be numerically equal to

$$Z = \text{SNR}_D - \text{SNR}_{D,T} \quad (\text{V-A-13})$$

where  $\text{SNR}_{D,T}$  is the display signal-to-noise ratio needed to obtain a detection probability of 0.5, which is generally considered to be the threshold of detection as indicated by the subscript T. Other values of  $\text{SNR}_D$  are obtained from the formula

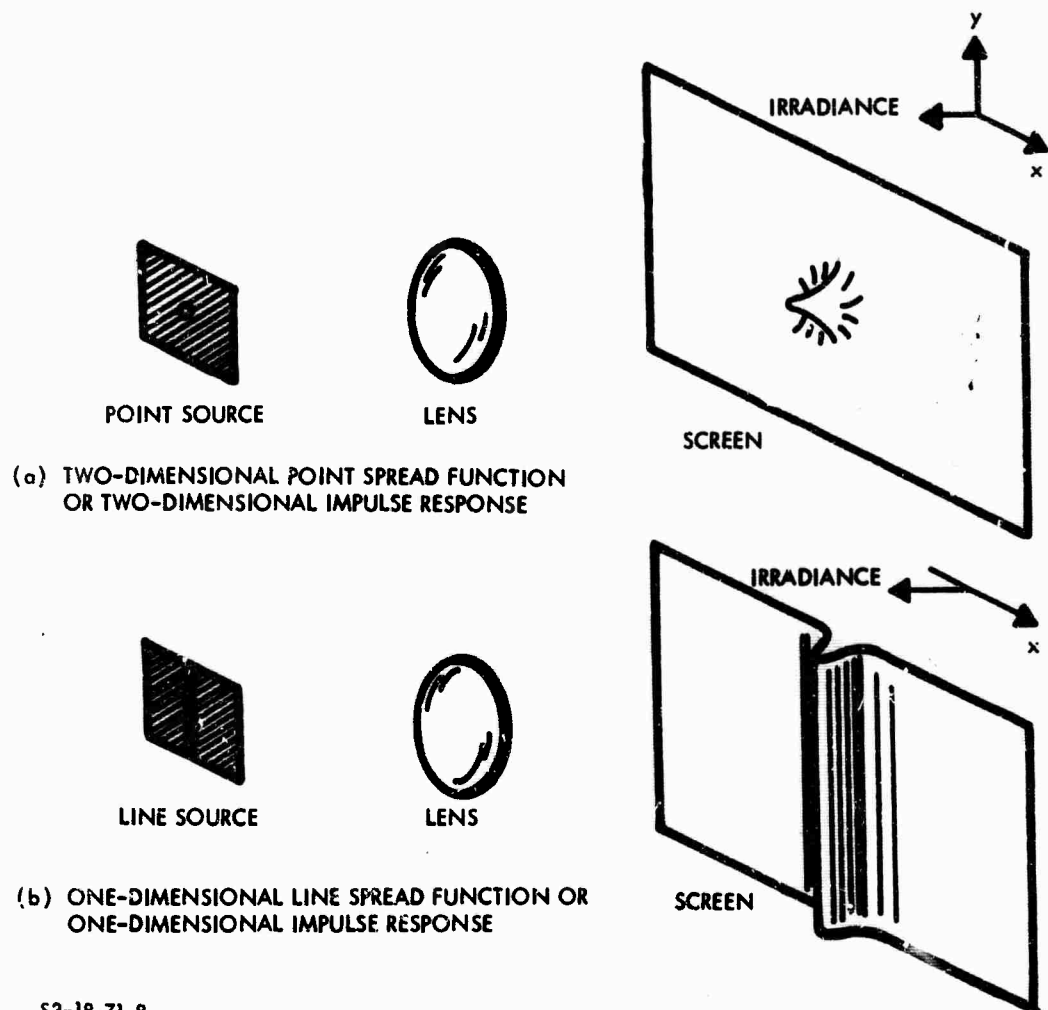
$$P_d (-\infty < Z < z_2) = \frac{1}{(2\pi)^{1/2}} \int_{-\infty}^{z_2} \exp \left[ -z^2/2 \right] dz \quad (\text{V-A-14})$$

which cannot be integrated in closed form, but is widely available in standard mathematical tables.

In the foregoing, a model was developed for the SNR developed at the output of the input photocathode in a perfect system in which the image's spatial fidelity is preserved at each reimaging step, and the only noise is that generated in the primary photoprocess. In this case, the SNR developed by the photocathode is identical to that at the display and the observer's retina. In psychophysical experiments that approximate the perfect sensor case, it was shown that the SNR required to detect rectangular targets is relatively a constant over a wide range of image sizes and that probabilities of detection can be associated with the display signal-to-noise ratios developed.

b. Effect of Finite Apertures on Aperiodic Image Detection. The rectangular images discussed in the previous section were aperiodic images. However, it was assumed that they were reproduced at the retina and converted to sensory impulses with perfect spatial fidelity. In real sensors, the images at the display may be distorted in amplitude, shape, position (phase), or all three. These distortions are

due to finite imaging apertures such as the objective lens, any fiber-optic coupling plates, electron lenses, electron scanning beams, finite phosphor particles, and the like. The effect of these apertures is to smear image detail in a manner directly analogous to that of electrical filter networks, except that the sensor apertures can result in both one- and two-dimensional filtering effects, as shown in Fig. V-A-6. This analogy can be put to good use.



S3-18-71-8

FIGURE V-A-6. Impulse Responses



In the discussion that follows, all of the various system elements, including the observer, are considered to be linear and amenable to Fourier analysis, wherein complicated input signals are decomposed into simpler signals for which the system response is known, and then the total response is found by summing the individual responses in linear combination. The requirements and properties of linearity are well known (Ref. 5) and will not be belabored further here, except to note that, without the mathematical simplifications made possible by assuming linearity, analysis becomes all but impossible in many cases. Also, in the interest of focusing on fundamental principles, it will be assumed that, where two-dimensional apertures are involved, the two dimensions are independent and separable. With this assumption, complicated two-dimensional problems can be reduced to the more familiar one-dimensional problems.

In the Fourier analysis of sensors, it is convenient to employ a certain set of input test signals known as the singularity test signals. The most useful singularity test signal is the unit volume impulse  $\delta_0(x,y)$ , which is of zero amplitude everywhere except at one point, where its amplitude is infinite. However, its volume (or its area, in the one-dimensional case) is always unity. The sensor response with an impulse input is designated as  $r_0(x,y)$  and is known either as the impulse response or the point spread function. The Fourier transform of the impulse response is designated as  $R_0(\omega_x, \omega_y)$  and is known as either the complex steady-state frequency response or the optical transfer function. If either  $r_0(x,y)$  or  $R_0(\omega_x, \omega_y)$  are known for the sensor, the response to any other input can be determined.  $R_0(\omega_x, \omega_y)$  may be written as

$$\begin{aligned} R_0(\omega_x, \omega_y) &= \mathcal{F}[r_0(x,y)] \\ &= |R_0(\omega_x, \omega_y)| \exp [j\phi(\omega_x) + j\phi(\omega_y)] \end{aligned} \quad (V-A-15)$$

where  $\mathcal{F}$  implies "the Fourier transform of."  $R_O(\omega_x, \omega_y)$  is known as either the sine-wave response or the modulation transfer function (MTF), while  $\phi(\omega_x)$  and  $\phi(\omega_y)$  are the phase transfer functions. By the use of the separability assumption (Ref. 6),

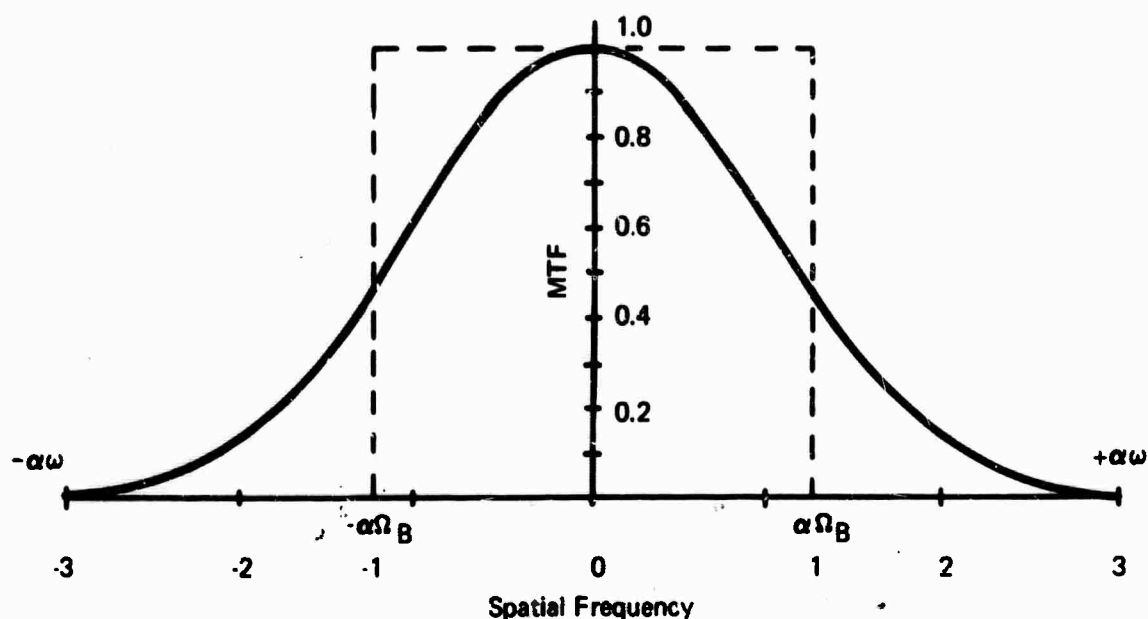
$$\begin{aligned} R_O(\omega_x, \omega_y) &= \mathcal{F}\{r_O(x) \cdot r_O(y)\} \\ &= \mathcal{F}_x[r_O(x)] \cdot \mathcal{F}_y[r_O(y)] \end{aligned} \quad (\text{V-A-16})$$

A typical one-dimensional MTF curve is shown in Fig. V-A-7. This curve happens to be a Gaussian or error curve filter, which closely approximates the MTF of many sensors and is given quantitatively by

$$|R_O(\omega)| = \exp \left[ -\frac{\omega^2 \sigma^2}{2} \right] \quad (\text{V-A-17})$$

If phase shift is zero, then  $|R_O(\omega)| = R_O(\omega)$ , and we can find the filter's response to any input signal. Suppose the input signals to be rectangular pulses, as shown by the dashed curves of Fig. V-A-8. It is seen that, as the input pulse is made progressively narrower, the output pulse becomes progressively wider relative to the input pulse width, and its amplitude eventually drops to well below that of the input pulse. Nevertheless, the area under the output pulse curve is identical to that under the input pulse. This is the nature of the error curve filter and of many optical apertures encountered in nature. Apertures of this type are dissipationless. Suppose that the eye is viewing an image that has first passed through a dissipationless filter. The effect of the filter would be expected to be that of smoothing the noise and smearing the signal. In the rectangle experiment, it was shown that, as images get larger, the eye expands the distance over which it integrates. If this is so, and there is every reason to believe that it is, then it could be inferred that, since the integrated signal in the filtered signal is the same and the noise

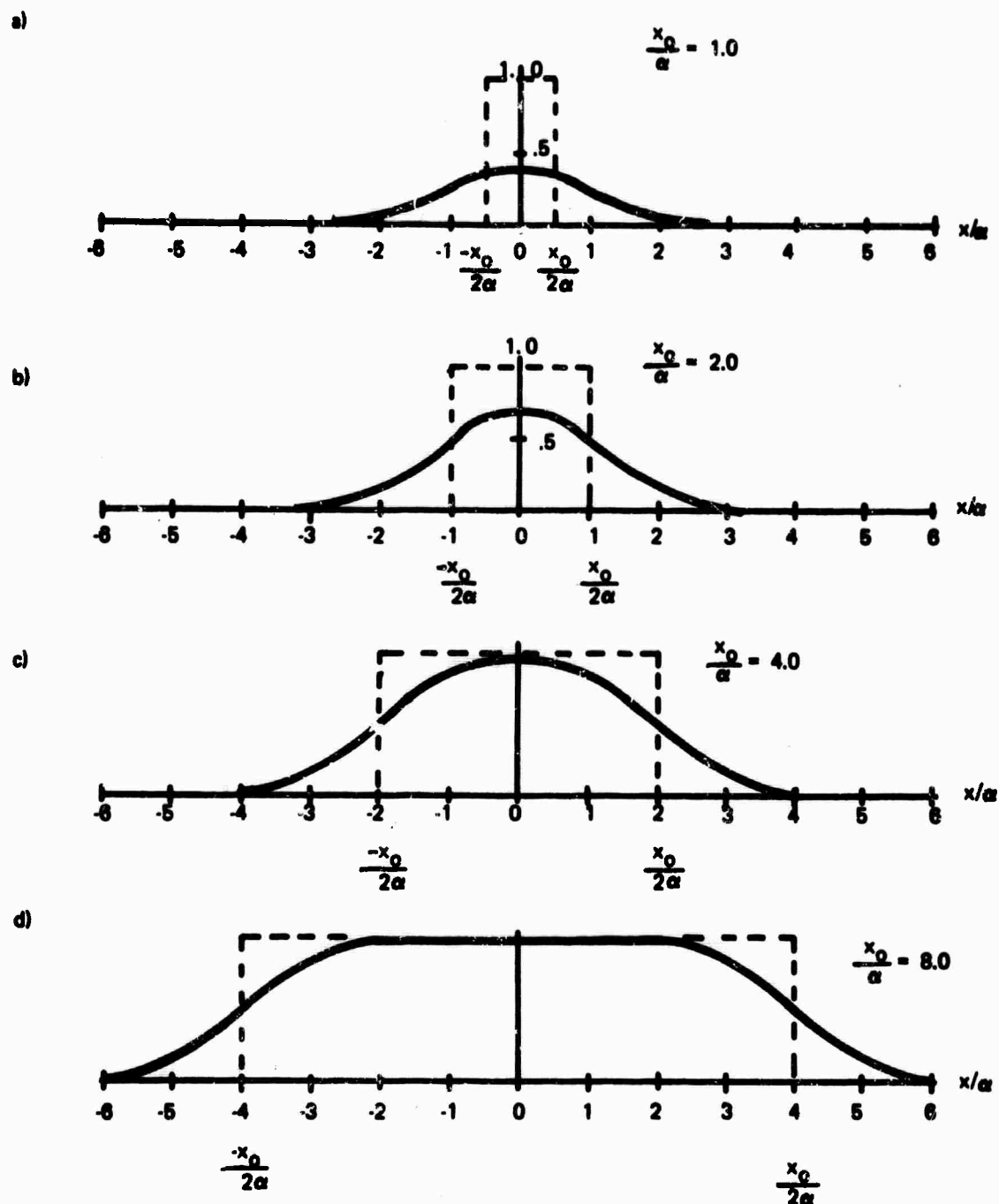
is reduced, the image detectability is enhanced by the filtering, or, as a minimum, the detectability remains unchanged.



70-1283-VA-6

**FIGURE V-A-7. Modulation Transfer Function and Effective Bandwidth for Error Curve Filter in Dimensionless Coordinates**

We find this result unpleasing. While it is possible to improve a signal-to-noise ratio by filtering, this seems unlikely when the signal and noise occupy the same spatial area and frequency band, as is the case here. Also, it is a common experience that finite apertures degrade images; they do not enhance them. The following solution to this dilemma is proposed. As the output pulse is smeared, the amplitude of the signal in the tails of the pulse becomes small. We presume these small signals to be less effective than the higher amplitudes near the peak of the pulse. Thus, an analytical model that weights the higher amplitudes in favor of the lower amplitudes would seem to be desired. This can be obtained by viewing the eye as an energy detector and by applying the Fourier energy integral, which represents the equivalence between energy in the space and the spatial frequency domains. In two dimensions, the Fourier energy integral is equal to



70-1253-VB-7

FIGURE V-A-8. Output Pulse (-) for an Error Curve Filter as the Width of a Unit Amplitude Rectangular Input Pulse (---) is Varied

$$\iint_{-\infty}^{\infty} f^2(x,y) dx dy = \frac{1}{\pi} \iint_0^{\infty} |F(\omega_x, \omega_y)|^2 d\omega_x d\omega_y \quad (V-A-18)$$

By using this formulation, which is also known as Parseval's relation and Plancherel's theorem (Ref. 7), the  $SNR_D$  of Eq. V-A-5 is modified to read

$$SNR_D = \frac{c(\bar{n}_{xy} t)^{\frac{1}{2}} \iint_{-\infty}^{\infty} g^2(x,y) dx dy}{\left[ (2-C) \iint_{-\infty}^{\infty} g^2(x,y) dx dy \right]^{\frac{1}{2}}} \quad (V-A-19)$$

In the above,  $[\bar{n}_{xy} t g(x,y)]$  represents the signal envelope at the output of the filter. Alternatively, the result of Eq. V-A-19 can be expressed in the spatial frequency domain or

$$SNR_D = \frac{c}{\pi} \frac{(\bar{n}_{xy} t)^{\frac{1}{2}} \iint_{-\infty}^{\infty} |G(\omega_x, \omega_y)|^2 d\omega_x d\omega_y}{\left[ (2-C) \iint_{-\infty}^{\infty} |G(\omega_x, \omega_y)|^2 d\omega_x d\omega_y \right]^{\frac{1}{2}}} \quad (V-A-20)$$

In general,

$$\iint_{-\infty}^{\infty} g^2(x,y) dx dy \leq \iint_{-\infty}^{\infty} g(x,y) dx dy \quad (V-A-21)$$

for positive signals, and

$$\iint_0^\infty |G(\omega_x, \omega_y)|^2 d\omega_x d\omega_y \leq \iint_0^\infty |G(\omega_x, \omega_y)| d\omega_x d\omega_y \quad (\text{V-A-22})$$

The result, in the new formulation, is that a photoelectron image passed through an aperture will be less detectable than one that is not.

To illustrate the effect of the new proposed model, we will calculate the minimum detectable power  $P_{\min}$  and the minimum detectable highlight irradiance  $E_{\min}$  for a sensor-augmented observer when the input image is a square of unit contrast. First, suppose the sensor MTF to be unity. The photoelectron current  $i_{s \max}$  may be written as

$$i_{s \max} = \sigma A E \quad (\text{V-A-23})$$

where  $\sigma$  is the photocathode's sensitivity (in amp/watt) to a given source such as a tungsten lamp operated at  $2854^\circ\text{K}$ , and  $E$  is the photocathode's highlight irradiance (in watt/m<sup>2</sup>) due to the same given source. Using Eq. V-A-23 in Eq. V-A-7, we obtain

$$\text{SNR}_D = \left[ \frac{\sigma a E t}{e} \right]^{1/2} \quad (\text{V-A-24})$$

For threshold detection (50 percent probability of detection),  $\text{SNR}_{DT} = 2.8$ . With this value for  $\text{SNR}_{D,T}$ ,  $E$  becomes  $E_{\min}$ , and thus, for the perfect sensor with unity MTF,

$$E_{\min} = (2.8)^2 e / (\sigma a t) \quad (\text{V-A-25})$$

and

$$P_{\min} = (2.8)^2 e / (\sigma t) \quad (\text{V-A-26})$$

These equations are plotted in Figs. V-A-9 and V-A-10 for  $\sigma = 4.10^{-3}$  amp watt and  $t = 0.2$  sec. We include the effect of the apertures, assuming that the apertures in  $x$  and  $y$  are independent and separable, so that Eq. V-A-16 holds. The impulse response in  $x$  (or  $y$ ) is given by

$$r_0(x) = \exp \left[ -x^2/2\alpha^2 \right] / \left( 2\pi\alpha^2 \right)^{\frac{1}{2}} \quad (\text{V-A-27})$$

and  $\alpha$  is taken to be  $2.31 \times 10^{-2}$  mm. For a square image,  $g(x)$  or  $g(y)$  is given by

$$g(x) = \frac{1}{2} \operatorname{erf} \left[ \frac{x + x_0/2}{(2\alpha^2)^{\frac{1}{2}}} \right] - \frac{1}{2} \operatorname{erf} \left[ \frac{x - x_0/2}{(2\alpha^2)^{\frac{1}{2}}} \right] \quad (\text{V-A-28})$$

where  $\operatorname{erf}$  is the error function and  $x_0$  is the input pulse width. Now,

$$E_{\min} = \frac{(2.8)^2}{e\sigma t_e} \frac{\left[ \int_{-\infty}^{\infty} g^2(x) dx \int_{-\infty}^{\infty} g^2(y) dy \right]^2}{\int_{-\infty}^{\infty} g^2(x) dx \int_{-\infty}^{\infty} g^2(y) dy} \quad (\text{V-A-29})$$

where  $g(x)$  is given by Eq. V-A-28 and  $g(x) = g(y)$ .  $P_{\min}$  is found from Eq. V-A-29, and

$$P_{\min} = E_{\min} \cdot a \quad (\text{V-A-30})$$

where  $a$  is the input image area. The impact of the assumed apertures can be observed from the curves shown in Figs. V-A-9 and V-A-10. It is seen that, with unity MTF,  $E_{\min}$  is proportional to  $1/a$ , while  $P_{\min}$  is constant. With the assumed MTF,  $E_{\min}$  increases at a much faster

rate as image size is diminished, while  $P_{\min}$  is no longer a constant but increases as image size decreases.

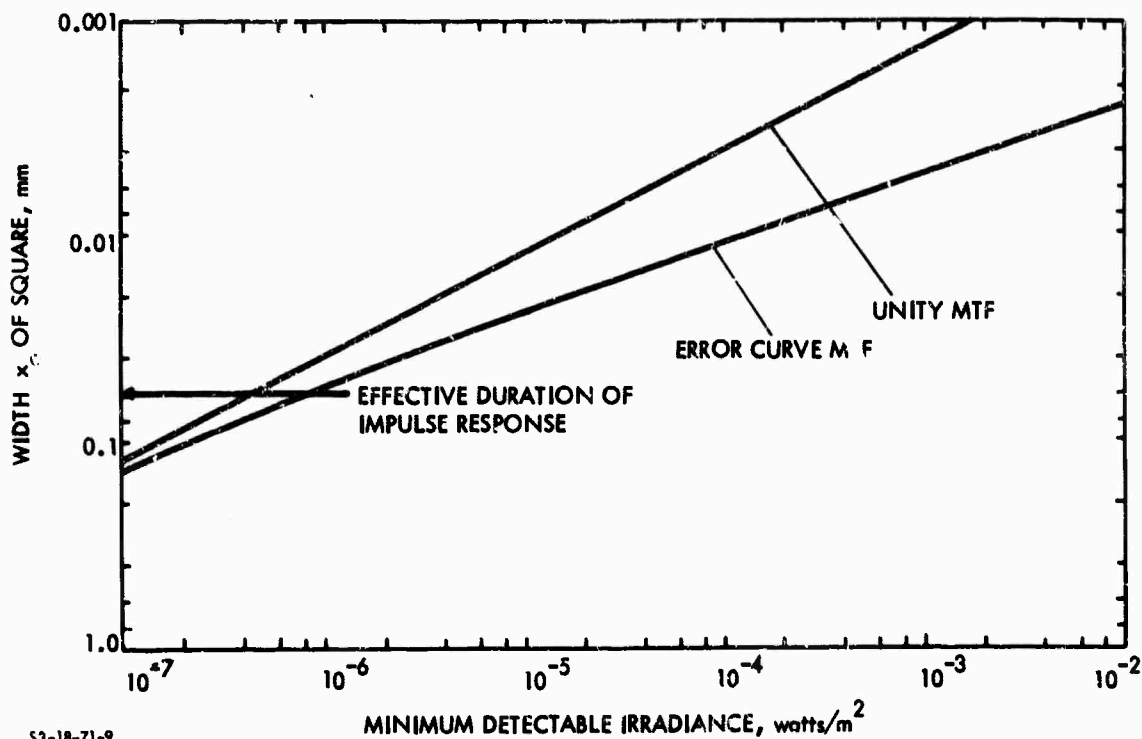
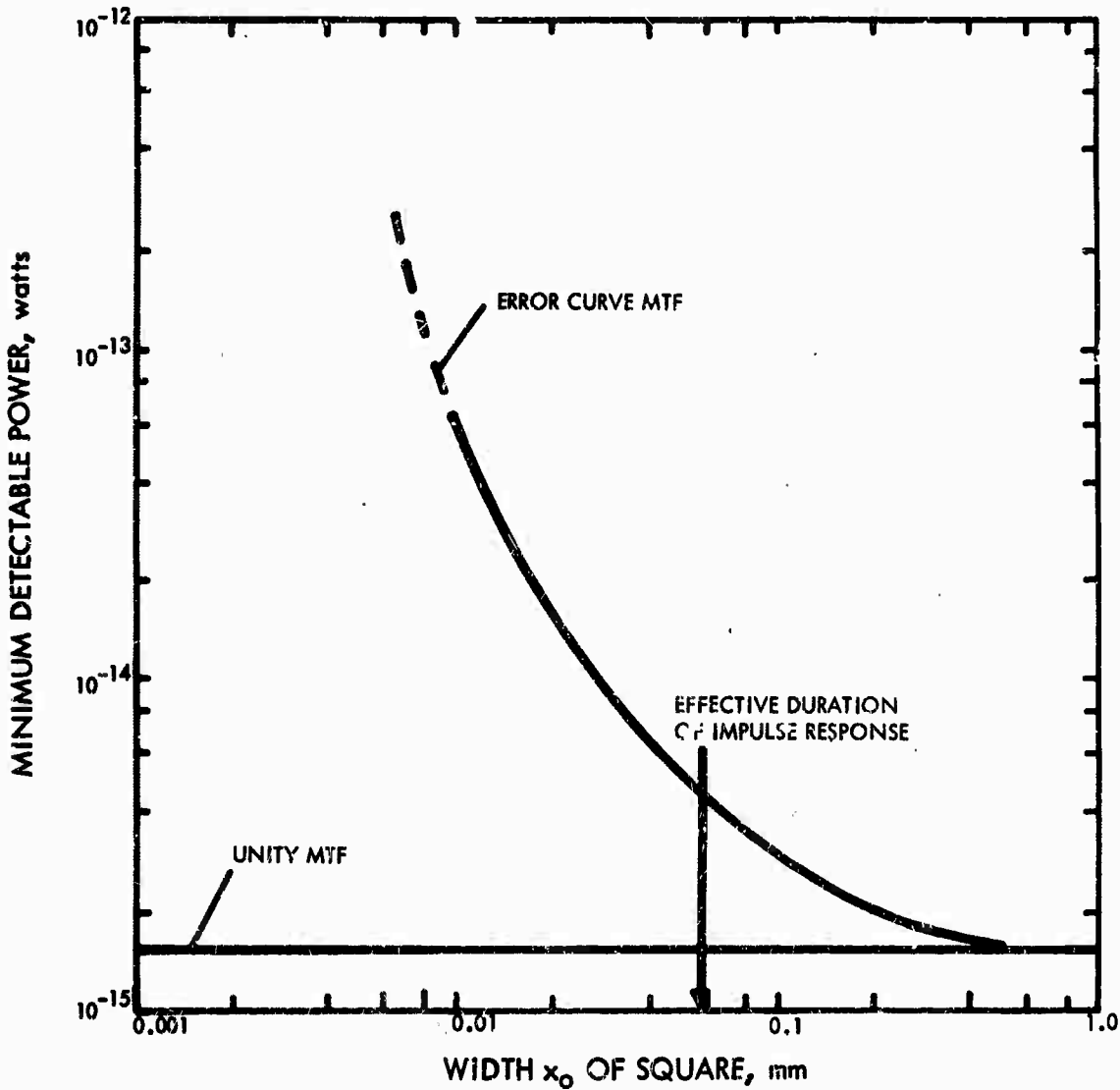


FIGURE V-A-9. Minimum Detectable Irradiance

c. Detection of Periodic Signals. Rectangular images are not ordinarily used in measuring and specifying image-forming sensors. Instead, it is more usual to employ periodic images of various forms and types, including sine waves, bars, bursts of bars, and circular sectors or wedges. A typical bar-burst pattern (Ref. 8) is shown in Fig. V-A-11. Whatever the pattern form, the thought is to project patterns of various spatial frequencies onto the sensor photocathode and to measure sensor response both electrically and psychophysically. The electrical tests are mainly to obtain the MTF and the signal current transfer characteristics. In psychophysical tests, an observer is requested to determine the pattern of highest spatial frequency that can be just barely detected as the highlight irradiance of the

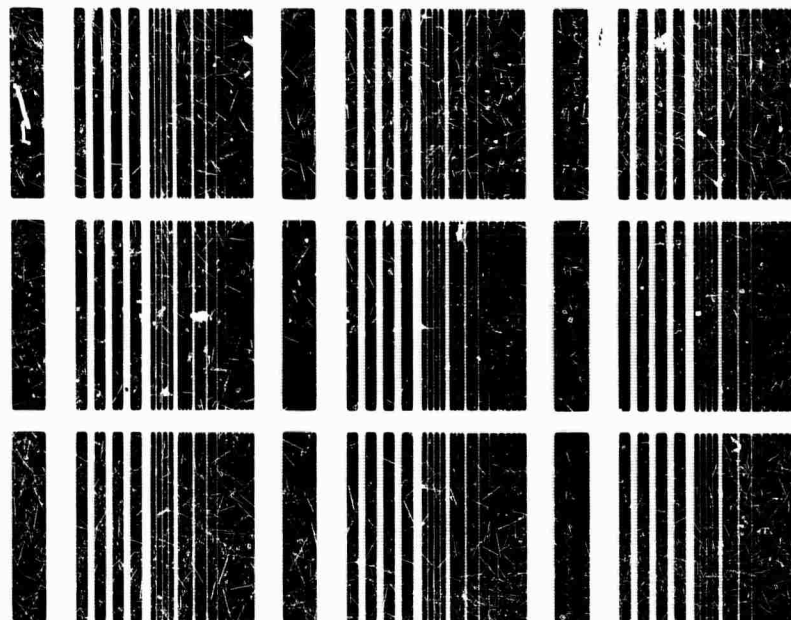


pattern image is varied. The highest spatial frequency that can be just barely detected at a given irradiance is designated as the limiting resolution, and its plot as a function of irradiance is called its limiting resolution versus photocathode irradiance level characteristic.



S3-18-71-10

FIGURE V-A-10. Minimum Detectable Power.



COPYRIGHT © 1967 BY WESTINGHOUSE ELECTRIC CORPORATION 70-1288-PA-10

FIGURE V-A-11. Resolution Test Chart

This characteristic is widely used by all sensor manufacturers to specify and compare the performance of their products with others, even though the patterns and methods of measurement have not been standardized in any form, and widely different techniques are used. Surprisingly, fairly close correlations have been experienced between various manufacturers and laboratories, but, as we shall see, this result is mainly fortuitous. As sensors improve, substantial errors can be encountered unless standards are adopted.

The original experimentations and analyses relating to the detectability of sine-wave and bar patterns displayed on a CRT were performed by Coltman and Anderson (Ref. 3) using an electronic setup similar to that in Fig. V-A-3. The main difference is that vertically oriented sine-wave patterns that filled the entire screen were used instead of squares and rectangles. However, the early analysis proceeds along the lines followed in the previous section. The bar-pattern

image being viewed is divided into square elements of size  $\Delta y$ , where  $\Delta y$  is numerically equal to the bar spacing (which is also equal to the bar width). Then,  $SNR_D$  is calculated for this single square element, which eventually results in Eq. V-A-9. Next, we note that if we define bar spacing  $\Delta y$  in terms of the number  $N_{TV}$  of squares that can be fitted into a picture height, then

$$N_{TV} = \frac{Y}{\Delta y} \quad (V-A-31)$$

Also, if  $X$  is the picture width, which is equal to  $\alpha Y$ , and  $\alpha$  is the picture aspect ratio, then  $A = \alpha Y^2 = \Delta y^2 \times N_{TV}^2$ . Note further that  $a = \Delta y^2$ , so that Eq. V-A-9 becomes

$$SNR_{D/E} = \frac{[t \Delta f / \alpha]^{\frac{1}{2}}}{N_{TV}} \cdot SNR_{V,0,C} \quad (V-A-32)$$

This equation, which is designated the per-element display signal-to-noise ratio, was derived for the photoelectron-noise-limited case, where the noise is white and the sensor MTF is unity. This situation was simulated in the laboratory by Coltman and Anderson (Ref. 3). Their formulation was somewhat different, in that they set up the equation in the form

$$N_{TVP/W} = k [\Delta f']^{\frac{1}{2}} \cdot SNR_{V,RMS} \quad (V-A-33)$$

and then they evaluated  $k$  experimentally for threshold identification of the pattern. Their value was found to be equal to 615 when  $\Delta f'$  was given in MHz,  $N_{TVP/W}$  was given in line pairs/picture width, and the  $SNR_{V,RMS}$  was in terms of rms signal to rms noise. Converting the Coltman and Anderson nomenclature to that used here, we have

$$N_{TV} = \frac{2 \times N_{TVP/W}}{4/3} \frac{\text{lines}}{\text{picture height}}, \quad (V-A-34a)$$

$$\text{SNR}_{V,0,C} = 2.82 \text{ SNR}_{V,\text{RMS}} \frac{\text{peak signal}}{\text{rms noise}}, \quad (\text{V-A-34b})$$

and

$$\Delta f = 10^{-6} \Delta f' (E_z). \quad (\text{V-A-34c})$$

Inserting these results, along with the constant  $k = 615$ , into Eq. V-A-33, we find

$$N_{TV} = 3.27 (\Delta f)^{\frac{1}{2}} \cdot \text{SNR}_{V,0,C} \quad (\text{V-A-35})$$

Next, we solve Eq. V-A-33 for  $N_{TV}$ :

$$N_{TV} = \frac{[t/\alpha]^{\frac{1}{2}}}{\text{SNR}_{D/E}} (\Delta f)^{\frac{1}{2}} \cdot \text{SNR}_{V,0,C} \quad (\text{V-A-36})$$

By comparison of Eqs. V-A-35 and V-A-36, we find that equality would result if

$$\frac{[t/\alpha]^{\frac{1}{2}}}{\text{SNR}_{D/E}} = 3.27 \quad (\text{V-A-37})$$

If  $t = 0.2$  sec and  $\alpha = 4/3$ , then

$$\text{SNR}_{D/E,T} = 1.18 \quad (\text{V-A-38})$$

The inference is that threshold display signal-to-noise ratio  $\text{SNR}_{D/E,T}$  is a constant and is equal to about 1.18. Actually, the constant  $k = 615$  was determined for sine-wave patterns. In an earlier experiment, Coltman (Ref. 9) found  $k$  to be 640 for square waves, which would make  $\text{SNR}_{D/E,T} = 1.23$ . However, in the earlier experiment the bars were of limited extent, which will be found to make a difference.

Somewhat later, Parton and Moody (Ref. 10) gave an equation that is rewritten in the nomenclature used in this paper and rearranged as follows:

$$\text{SNR}_{D/E} = \left[ \frac{t}{\alpha} \right]^{\frac{1}{2}} \frac{C}{N_{TV}} \left[ \frac{\sigma AE}{e} \right]^{\frac{1}{2}} \quad (\text{V-A-39})$$

By multiplying numerator and denominator by  $\Delta f$  and noting that  $[\sigma AE/e \Delta f]^{\frac{1}{2}} = \text{SNR}_{V,0}$ , we find that

$$\text{SNR}_D = \frac{[t \Delta f / \alpha]^{\frac{1}{2}}}{N_{TV}} C \cdot \text{SNR}_{V,0} \quad (\text{V-A-40})$$

which is essentially Eq. V-A-32. Parton and Moody gave a value of 1.2 for threshold  $\text{SNR}_{D/E,T}$ . This number has been used since that time, although, we believe, incorrectly.

Coltman and Anderson also suggested that the effect of the sensor MTF could be taken into account by simply modifying the  $\text{SNR}_V$  obtainable from the photocathode by the MTF. In the nomenclature of this report, this modification becomes

$$\text{SNR}_D = \frac{[t \Delta f / \alpha]^{\frac{1}{2}}}{N_{TV}} \cdot |R_O(N_{TV})| \cdot \text{SNR}_{V,0,C} \quad (\text{V-A-41})$$

where  $|R_O(N_{TV})|$  is the senso. sine-wave response or MTF. This equation has been used extensively to calculate the limiting resolution of sensors, and the results so computed are in very good agreement with measured results. We believe that this is so not because the equation is right, but because it is not too far wrong and because of compensating errors.

That Eq. V-A-41 holds so well is surprising for several reasons. First, the  $\text{SNR}_D$  derived is for a single element of size

$1/N_{TV} \cdot 1/N_{TV}$ , where  $N_{TV}$  is the width of a single bar, and the results are reputed to hold for the detection of the entire bar pattern. The height of the bar pattern is stipulated to be large with respect to the bar spacing, but otherwise no account is taken of it. The threshold  $SNR_{D/E,T}$  is supposedly a constant independent of the height. That would infer that the height is of no moment. A bar pattern is presumably a one-dimensional pattern if the bars are very long compared to their spacing; yet, the derivation assumes a two-dimensional element. This assumption does not seem physically reasonable.

To show the impact of reducing the number of bars available to the observer, Coltman and Anderson devised the experiment shown in Fig. V-A-12. The displayed pattern was left fixed, and a series of cardboard apertures were employed to vary the number of lines seen by the observer (Ref. 2, p. 862). The mask was of square aspect ratio. The results as shown in Fig. V-A-12 "show that the observer probably uses no more than seven line pairs in making an identification. As the number which he is permitted to see is decreased, the signal required rises rapidly, being greater by a factor of four when only one line pair is presented" (Ref. 2, p. 862).

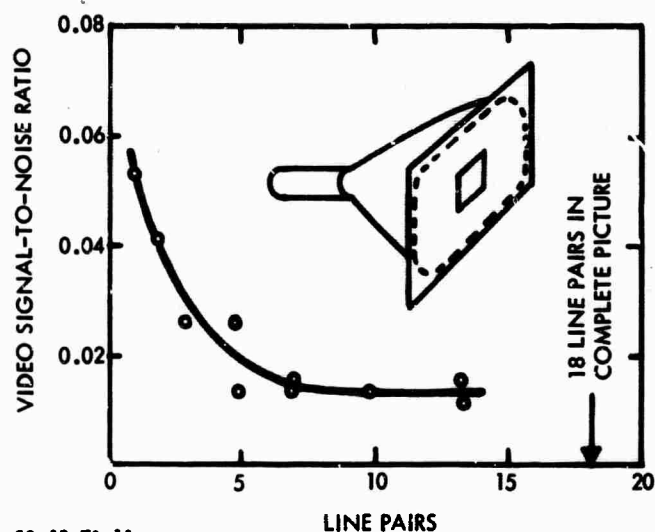


FIGURE V-A-12. Number of Line Pairs Seen Through Mask (Adapted from Ref. 3)

Schade (Ref. 11, p. 731) also notes that "the sampling aperture of the eye for lines and edges is its line image, limited in length to fourteen equivalent point image diameters." These two observations give a possible explanation for the use of the elemental image of size  $1/N_{TV} \cdot 1/N_{TV}$ . However, if this is to hold over a wide range of spatial frequencies, it is necessary to conclude that, as the pattern spacing changes, the eye's ability to integrate along the line changes in direct proportion, or else it reaches some limit. This is at considerable variance with the results obtained in the rectangle experiment, where, in Fig. V-A-5, it was shown that the eye could integrate a line of length-to-width aspect ratio from 1:1 to at least 45:1 and perhaps even more, since no end point was determined.

Since the notion of using an elemental image to describe a one-dimensional bar pattern conflicts with physical intuition, and since the notion of a limited but variable integrating capability, or even of a fixed integrating capability, for the eye conflicts with measured data on a television display (Fig. V-A-4a, p. 206), it was decided to take a new approach. First, we will define detection. By detection, it is implied that the observer must be able to determine that a bar pattern is actually present. We will further stipulate that the observer makes this determination on the basis of a single line pair. Thus, the problem reduces to the two-dimensional rectangle detection problem discussed earlier, except that we feel that a higher signal-to-noise ratio is needed because the identification of a bar must be positive. For this reason, and because the result will be found to fit well, we will assume that the bar must be detected with nearly 100 percent probability. From Fig. V-A-5 this will be seen to require an  $SNR_{DT}$  of 5.3. Let the dimensions of the bar be given in terms of the reciprocal distances  $N_v \cdot N_h$ , where

$$N_h = \frac{Y}{\Delta y} \quad (V-A-42a)$$

$$N_v = \frac{Y}{n_v \cdot \Delta y} \quad (V-A-42b)$$

in which  $Y$  is the picture height,  $\Delta y$  is the linear dimension of the bar width, and  $n_v$  is the height of the bar measured in terms of a number of bar widths. The image area relative to the total effective photocathode area is then

$$\frac{a}{A} = \frac{n_v \Delta y^2}{\alpha_y^2} \quad (\text{V-A-43a})$$

$$= \frac{1}{\alpha N_v \cdot N_h} \quad (\text{V-A-43b})$$

$$= \frac{n_v}{2 N_{TV}} \quad (\text{V-A-43c})$$

where  $N_{TV} = Y/\Delta y$  lines per picture height. The result is that Eq. V-A-41 becomes either

$$\text{SNR}_{D/A} = \frac{[t \Delta f / \alpha]^{\frac{1}{2}}}{[N_v \cdot N_h]^{\frac{1}{2}}} \cdot \text{SNR}_{V,0,C} \quad (\text{V-A-44})$$

or

$$\text{SNR}_{D/A} = [t \Delta f / \alpha]^{\frac{1}{2}} \cdot \frac{n_v^{\frac{1}{2}}}{N_{TV}} \cdot \text{SNR}_{V,0,C} \quad (\text{V-A-45})$$

These equations become the new trial models for the recognition of bar patterns. They are called the area models. The  $\text{SNR}_{D/A,T}$  required is taken to be 5.3, as previously discussed.

Next, we focus our attention on Eq. V-A-45, which is very similar to Eq. V-A-32, which was previously used for bar-pattern detection. The right sides of the two equations would, in fact, be identical if Eq. V-A-45 were divided by  $(n_v)^{\frac{1}{2}}$ , which would result in the formula



$$\frac{\text{SNR}_{D/A}}{(n_v)^{\frac{1}{2}}} = \frac{[t \Delta f / \sigma]^{\frac{1}{2}}}{N_{TV}} \cdot \text{SNR}_{V,0,C} \quad (\text{V-A-46})$$

Consider  $\text{SNR}_{D/A}/(n_v)^{\frac{1}{2}}$  to be a new display signal-to-noise ratio that has a threshold value for bar patterns of frequency  $N_{TV}$  and of

$$\text{SNR}_{D/E,T} = (\text{SNR}_{D/A,T})/(n_v)^{\frac{1}{2}} \quad (\text{V-A-47})$$

This equation is plotted as the solid line in Fig. V-A-13. We note that the per-element  $\text{SNR}_{D/E,T}$  drops quickly to a value of about 1.2 at a bar height-to-width ratio of about 20 lines (or 10 line pairs) and decreases slowly thereafter. This appears to be the origin of the value of  $\text{SNR}_{D/E,T} = 1.2$  for bar or sine-wave patterns. It is not 1.2 but is nearly so over a fairly broad range of bar heights. When other effects are taken into account, it will probably be found that the apparent range of validity of  $\text{SNR}_{D/E,T} = 1.2$  will be even larger.

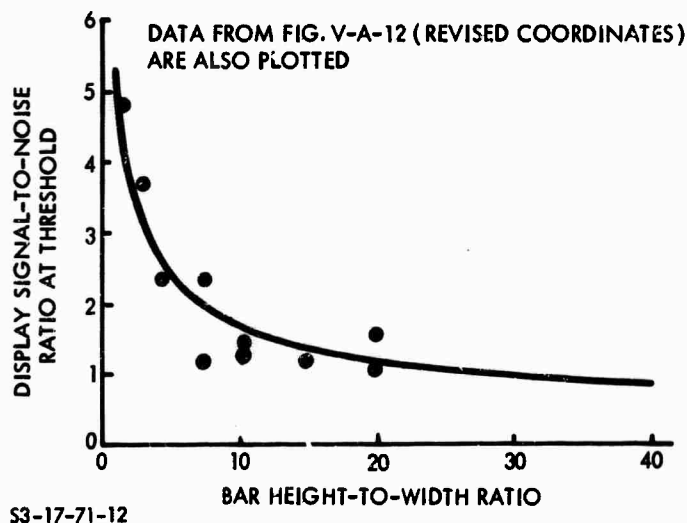


FIGURE V-A-13. Threshold Display Signal-to-Noise Ratio Required to Identify Bar Pattern as a Function of Bar Height-to-Width Ratio

It is of considerable interest to replot the Coltman and Anderson data in Fig. V-A-12 on Fig. V-A-13, using the relation

$$\text{SNR}_{D/E,T} = \frac{[0.15 \Delta f]^{\frac{1}{2}}}{N_{TV}} \cdot \text{SNR}_{VM,T} \quad (\text{V-A-48})$$

where  $\text{SNR}_{VM,T}$  is now the measured value of threshold video signal-to-noise ratio after the conversion factors of Eq. V-A-34 are applied to the data. The fit of the Coltman and Anderson data to the predicted curve, using Eq. V-A-46, is seen to be well within the experimental measurement errors. It is concluded that the effect of the cardboard apertures was mainly to decrease the bar height over which the eye can integrate. Attempts to show that the eye uses only seven line pairs in making an identification have proved unfruitful. Similarly, the premise that the eye can integrate over a small portion of the bar length is not borne out.

In a preliminary experiment, the  $\text{SNR}_D$  required to identify a bar pattern was determined for three bar length-to-width ratios with the result shown in Fig. V-A-14. The  $\text{SNR}_D$  was calculated on the basis of the area of a single bar in the pattern. As can be seen, the probability of detection is the same for all three patterns when plotted versus  $\text{SNR}_{D/A}$ .

We next turn to the formulation of a model that, though it will require considerable modification and verification, represents the most accurate representation of the fundamentals of imaging as we know them and is felt to be the best point of departure for further model development. In the beginning of this model development, it is assumed that the input test pattern is a sine wave and that the sensor MTF is unity.

Recall that we have hypothesized that the eye uses only a single line, or line pair, in identifying a bar pattern. For this analysis, the displayed pattern is taken to be an infinitely long train

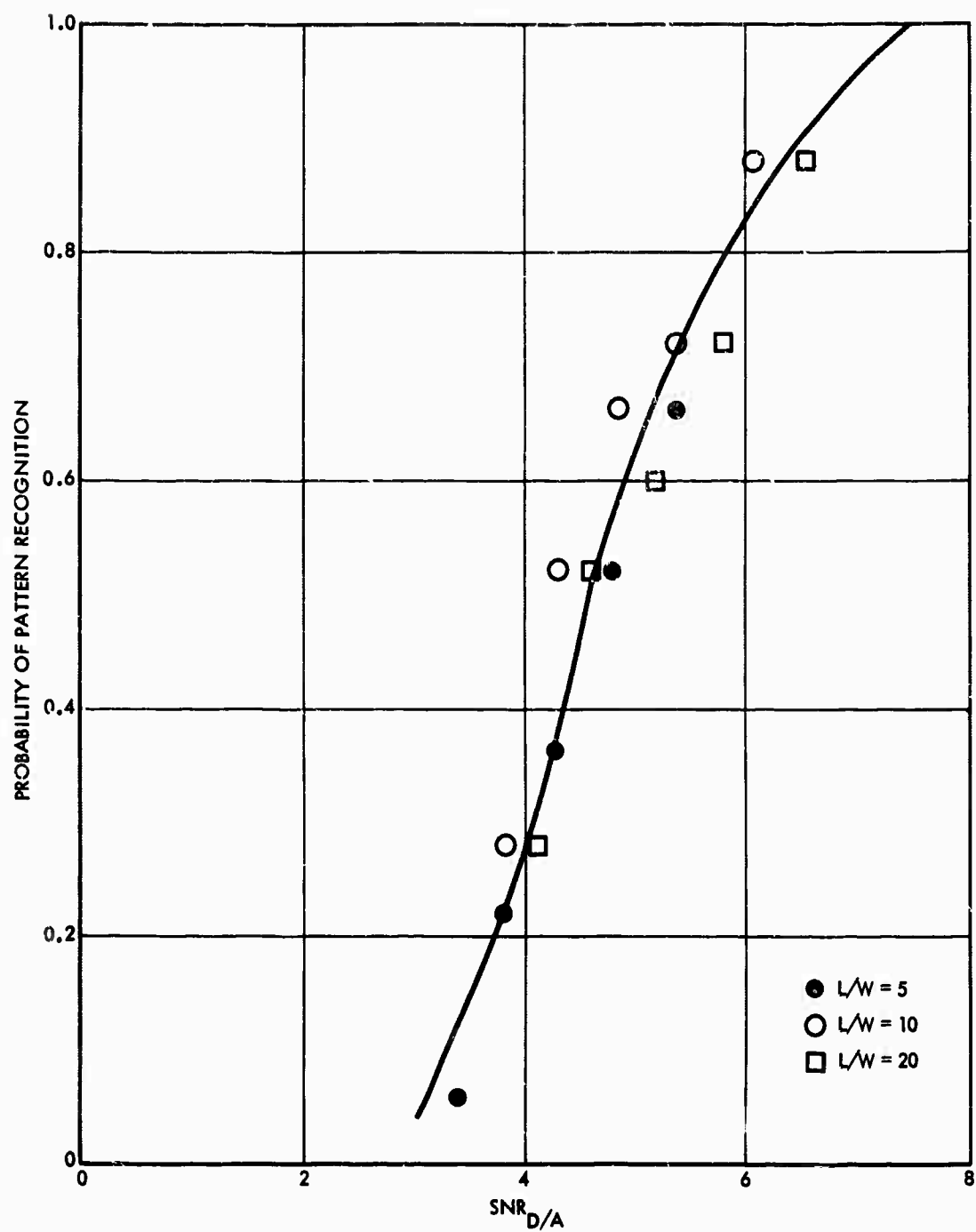


FIGURE V-A-14. Probability of Pattern Recognition Versus  $SNR_{D/A}$  for 372-Line Bar Pattern for Three Length-to-Width Ratios ( $L/W$ )

of cosine waves in the x direction and a rectangle in the y direction, but only the single cycle shown in Fig. V-A-15 used for the pattern identification. Quantitatively, the wave form used by the eye will be assumed to be

$$g(x) = \begin{cases} 0 & -\infty < x < -x_0 \\ \frac{1}{2} (1 + \cos \pi x/x_0) & -x_0 \leq x \leq x_0 \\ 0 & x_0 < x < \infty \end{cases} \quad (\text{V-A-49})$$

$$g(y) = \begin{cases} 0 & -\infty < y < -y_0/2 \\ 1 & -y_0/2 \leq y \leq y_0/2 \\ 0 & y_0/2 < y < \infty \end{cases} \quad (\text{V-A-50})$$

and

$$g(x,y) = g(x) \cdot g(y) \quad (\text{V-A-51})$$

The basic  $\text{SNR}_{D/A}$  expression to be used will be Eq. V-A-7, rearranged to read:

$$\begin{aligned} \text{SNR}_{D/A} &= \left[ \frac{t}{A} \right]^{\frac{1}{2}} \frac{C i_{s \max} a}{\left[ (2-C) i_{s \max} a \right]^{\frac{1}{2}}} \\ &= \left[ \frac{t/a}{y^2} \right]^{\frac{1}{2}} \frac{C i_{s \max} a}{\left[ (2-C) i_{s \max} a \right]^{\frac{1}{2}}} \end{aligned} \quad (\text{V-A-52})$$

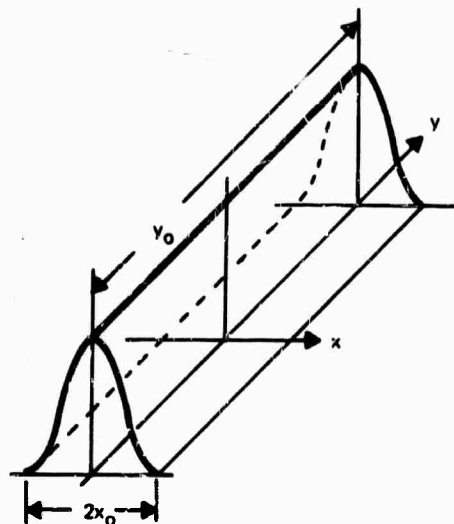
where A, the effective photocathode area, is equal to  $\alpha^2$ , as previously noted. The area a in Eq. V-A-52 will be treated according to the Fourier energy integral of Eq. V-A-18. Thus,

$$a = \iint_{-\infty}^{\infty} g^2(x, y) dx dy \quad (V-A-53)$$

and, because of the independence and separability assumption,

$$a = \int_{-\infty}^{\infty} g^2(x) dx \int_{-\infty}^{\infty} g^2(y) dy \quad (V-A-54)$$

The appeal of this formulation is that it is identical to that used for the aperiodic rectangle detection problem, that it eliminates the problem of deciding what to do about images that have both positive and negative components, that it treats signals and noise alike, that integration limits become fairly well defined, that it gives results that are in good agreement with those obtained by other investigators, and that the results predicted using this concept correlate well with measured results.



70-1283-VA-13

FIGURE V-A-15. Portion of Wave Train Assumed Used by the Eye to Recognize Wave Pattern.

The result of applying Eq. V-A-54 to Eqs. V-A-49 and V-A-50 is that

$$a = 3 y_o x_o / 4 \quad (\text{V-A-55})$$

and Eq. V-A-52 becomes

$$\text{SNR}_{D/A} = \left[ \frac{t/\alpha}{y_o^2/x_o y_o} \right]^{1/2} \frac{0.75 C i_{s \max}}{\left[ 0.75 (2-C) e i_{s \max} \right]^{1/2}} \quad (\text{V-A-56})$$

Also, since  $N_v = Y/y_o$  and  $N_h = Y/x_o$ , where  $N_v$  and  $N_h$  are expressed in TV lines per picture height,

$$\text{SNR}_{D/A} = \left[ \frac{t/\alpha}{N_v \cdot N_h} \right]^{1/2} \frac{0.75 C i_{s \max}}{\left[ 0.75 (2-C) e i_{s \max} \right]^{1/2}} \quad (\text{V-A-57})$$

which is very similar to the trial models postulated in Eq. V-A-44.

Suppose, next, that the sensor MTF is either unity in the  $y$  direction or that the image is so long in the  $y$  vertical that it can be considered to be unity. In the  $x$  direction, let the MTF be  $|R_o(N_h)|$ . Then Eq. V-A-57 is revised to read

$$\text{SNR}_{D/A} = \left[ \frac{t/\alpha}{N_v \cdot N_h} \right]^{1/2} \frac{0.75 C |R_o(N_h)| i_{s \max}}{\left[ 0.75 (2-C) |R_o(N_h)| e i_{s \max} \right]^{1/2}} \quad (\text{V-A-58})$$

The use of  $|R_o(N_h)|$  in this form is somewhat unusual. It stems from the following reasoning. If the input image to a linear filter (or optical aperture) is a one-dimensional train of sine or cosine waves, then the output waveform will be a train of sine or cosine waves of identical spatial frequency but of reduced amplitude. The image wave-shape weighting function  $g(x)$  remains unchanged. The effect of the

aperture is then only one of decreasing the signal and mean square noise equally in the sampling area. In other cases, however, the wave shape is altered, as, for example, for square-wave (or bar-pattern) image inputs.

For the case of a square-wave input, suppose that the sensor MTF is unity once again. Also, let  $g(y)$  be given by Eq. V-A-50 as before, but  $g(x)$  is

$$g(x) = \begin{cases} 0 & -\infty < x < -x_0/2 \\ 1 & -x_0/2 < x < x_0/2 \\ 0 & x_0/2 < x < \infty \end{cases} \quad (\text{V-A-59})$$

Proceeding as before, we find that

$$a = x_0 y_0 = Y^2 / N_h \times N_v \quad (\text{V-A-60})$$

and

$$\text{SNR}_{D/A} = \left[ \frac{t/\alpha}{N_v \cdot N_h} \right]^{1/2} \frac{C i_{s \max}}{\left[ (2-C) e i_{s \max} \right]^{1/2}} \quad (\text{V-A-61})$$

(for square-wave image inputs)

Thus, for a photoelectron-noise-limited sensor, the area form of the display signal-to-noise ratio is larger for a unit amplitude square-wave image than for a unit amplitude sine-wave image by a factor of  $1/(0.75)^{1/2}$ , or 1.15, presuming both to be of equal spatial frequency. Intuitively, we would expect square waves to be more detectable.

To consider the effects of the MTF on a periodic square wave, we will first decompose the square-wave input image to a series of sine waves, using the Fourier series representation

$$\text{sq}(x) = \frac{4}{\pi} \sum_k \frac{\sin(\pi k N_{hl} x)}{k} \quad (\text{V-A-62})$$

$$k = 1, -3, 5, -7, 9, \dots$$

where  $N_{hl}$  is the spatial frequency of the square wave in half-cycles per picture height and is equal to

$$N_{hl} = 1/x_0 \quad (\text{V-A-63})$$

for  $x_0$  measured in units of picture height. If the sine-wave response or MTF is given by  $|R_o(N_h)|$ , the square-wave amplitude response may be written as

$$R_{SQ}(N_h) = \frac{4}{\pi} \sum_k R_o(N_h)/k \quad (\text{V-A-64})$$

$$k = 1, -3, 5, -7, 9, \dots$$

The MTF of a typical television sensor is plotted in Fig. V-A-16. Also, the square-wave amplitude response, or MTF, is plotted for a typical television sensor, which here happens to be an I-SEBIR camera tube with a 25-mm target. The assumed MTF curve is seen to go to 0 at 900 TV lines. Thus, at  $N_h > N_{hc}/3$ , where  $N_{hc}$  is the cutoff frequency, the displayed image is a sine-wave input. At higher frequencies, the square-wave amplitude is  $4/\pi$  times the value of MTF for a unit amplitude square-wave input. Indeed, this result holds with fair accuracy down to frequencies of  $N_{hc}/4$  or  $N_{hc}/5$ . At lower frequencies, the square-wave amplitude response approaches unity. However, the energy keeps increasing, being  $4/3$  that of a unit amplitude sine wave at zero frequency. This effect is shown as the dashed curve in Fig. V-A-16. We see the following interesting result. At frequencies above  $N_{hc}/3$ , a square-wave input yields a sine-wave output of amplitude  $4/\pi$  times the input amplitude. Thus, one could treat it as a sine wave, using Eq. V-A-58. The  $3/4$  factor of Eq. V-A-58 becomes  $3/4 \times 4/\pi = 0.955 \approx 1.0$ . At lower spatial frequencies, the energy relation must be used,

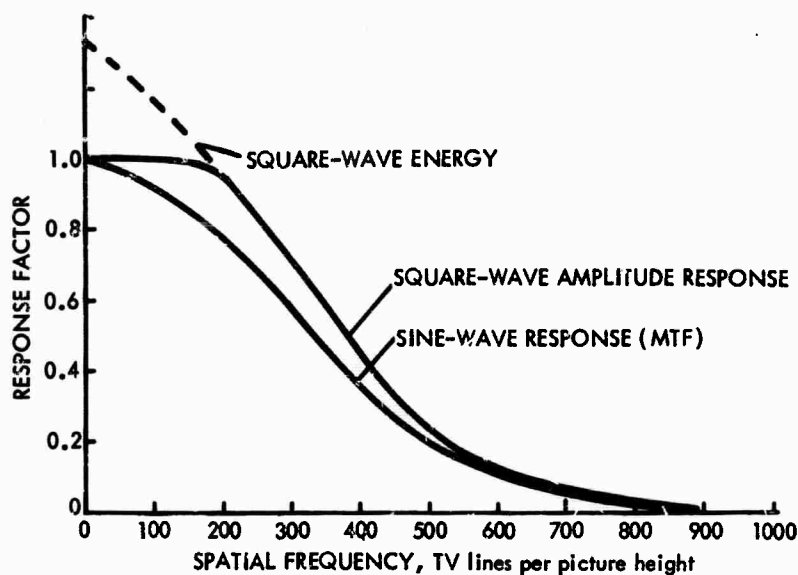


but the only effect will be that  $4/\pi$  becomes  $4/3$  at zero frequency. Thus, to a good approximation, we can write

$$\text{SNR}_{D/A} = \left[ \frac{t/\alpha}{N_v \cdot N_h} \right]^{\frac{1}{2}} \frac{C |R_o(N_h)| i_{s \max}}{\left[ (2-C) |R_o(N_h)| e i_{s \max} \right]^{\frac{1}{2}}} \quad (\text{V-A-65})$$

(for square-wave image inputs)

where  $|R_o(N_h)|$  is the sine-wave response or MTF, as before. Similarly, the square-wave amplitude response times 0.75 is a reasonable approximation for spatial frequencies from cutoff down to  $N_{hc}/4$  or  $N_{hc}/5$ . Alternatively, the threshold value of  $\text{SNR}_{D/A}$  can be adjusted when making limiting resolution predictions. Equation V-A-65 is recommended for general calculations of  $\text{SNR}_D$ .



S3-18-71-13

FIGURE V-A-16. MTF and Square-Wave Response for an I-SEBIR TV Camera

#### 4. Comparison of Current Low-Light-Level Television Camera Tubes

The various measures discussed above will now be used to compare various camera tubes.

There are more similarities than differences between the performances of the various low-light-level television cameras to be discussed. No obvious best choice for even a majority of applications will be evident. The bulk of the comparisons are based on performance in viewing a stationary scene, the main factors being sensitivity and resolution. Nevertheless, at any point in time, other factors such as cost, size, weight, power, or even availability may be overriding considerations. Also, performance specifications are continuously subject to change.

On the other hand, comparisons that are reasonably valid at this point in time can be made. In the comparisons that follow, some attempts to rank currently available sensors on the basis of sensitivity and pattern resolution are made mainly for the purpose of summarizing the results obtained. It must be understood that methods of ranking are rather poorly defined, so that complete objectivity is not entirely possible.

The first method of ranking is to construct Tables V-A-4, -5, -6 and -7, which show the display signal-to-noise ratio as a function of intensifier photocurrent for various resolutions expressed in television lines/raster height. (The abbreviations used in these tables are given in Table V-A-8.) As has been discussed, the display signal-to-noise ratio has the merit of being independent of video bandwidth and of relating to observer performance directly. The use of input photocurrent as a parameter has the desirable feature of being independent of the input intensifier's photocathode type, area, or sensitivity. Thus, the results apply equally well to intensifiers with other types of photocathodes and to intensifiers of the minifying type. However, the tables include the photocathode irradiance levels that would be associated with a photocathode of the extended red S-20 type with a radiant sensitivity of 4 ma/watt to a tungsten source operated at 2954°K. The most questionable parameter in the tables is the use of resolving power in terms of TV lines/raster height, which tends to favor TV camera tubes that have largest photocathodes. Rating

TABLE V-A-4. DISPLAY SIGNAL-TO-NOISE RATIO VERSUS INTENSIFIER PHOTOCURRENT FOR VARIOUS LOW-LIGHT-LEVEL TELEVISION CAMERAS

Camera Type	I <sup>2</sup> -pV	I <sup>3</sup> -V		I-SEC		I-IO	I-II	I-SEBIR		
TV Tube Photocathode Diameter	21.4mm	16 mm	25 mm	25 mm	40 mm	40 mm	40 mm	16 mm	25 mm	40 mm
Input Photocathode Irradiance* for an Intensifier Photocurrent of 10 <sup>-13</sup> Amp										
80 mm	1.1x10 <sup>-8</sup>	--	8.15x10 <sup>-9</sup>	8.15x10 <sup>-9</sup>	8.15x10 <sup>-9</sup>	8.15x10 <sup>-5</sup>	8.15x10 <sup>-9</sup>	--	8.15x10 <sup>-9</sup>	8.15x10 <sup>-9</sup>
40 mm	4.44x10 <sup>-8</sup>	--	3.25x10 <sup>-8</sup>	3.25x10 <sup>-8</sup>	3.25x10 <sup>-8</sup>	3.25x10 <sup>-8</sup>	3.25x10 <sup>-8</sup>	--	3.25x10 <sup>-8</sup>	3.25x10 <sup>-8</sup>
25 mm	1.14x10 <sup>-7</sup>	--	8.33x10 <sup>-8</sup>	8.33x10 <sup>-8</sup>	--	--	--	--	8.33x10 <sup>-8</sup>	--
16 mm	--	2.04x10 <sup>-7</sup>	--	--	--	--	--	2.04x10 <sup>-7</sup>	--	--
Resolution, TV Lines/ Raster Height	Display Signal-to-Noise Ratio									
10	9.05	25.8	25.8	13.1	13.2	16.6	17.0	34.5	34.6	34.7
100	0.712	1.72	2.0	1.09	1.13	1.52	0.3	2.57	2.73	2.82
200		0.126	0.63	0.414	0.46	0.59		0.761	0.885	0.976

Rank Ordering of Cameras on the Basis of Sensitivity for a Photocurrent of 10<sup>-13</sup> amp:  
1. 40-mm I-SEBIR  
2. 25-mm I-SEBIR  
3. 16-mm I-SEBIR  
4. 25-mm I<sup>3</sup>-V  
5. 16-mm I<sup>3</sup>-V  
6. 40-mm I-IO  
7. 40-mm I-SEC  
8. 25-mm I-SEC  
9. 21.4-mm I<sup>2</sup>-PV  
10. 40-mm I-II

\* For intensifier photocathode sensitivities of  $4 \times 10^{-3}$  amp/watt.

TABLE V-A-5. DISPLAY SIGNAL-TO-NOISE RATIO VERSUS INTENSIFIER PHOTOCURRENT  
FOR VARIOUS LOW-LIGHT-LEVEL TELEVISION CAMERAS

Camera Type	I <sup>2</sup> -pV	I <sup>3</sup> -V		I-SEC		I-IO	I-II	I-SEBIR	
TV Tube Photocathode Diameter	21.4mm	16 mm	25 mm	25 mm	40 mm	40 mm	16 mm	25 mm	40 mm
Intensifier Photocathode Diameter	Input Photocathode Irradiance* for an Intensifier Photocurrent of 10 <sup>-12</sup> Amp								
80 mm	1.11x10 <sup>-7</sup>	--	8.15x10 <sup>-8</sup>	8.15x10 <sup>-8</sup>	8.15x10 <sup>-8</sup>	8.15x10 <sup>-8</sup>	--	8.15x10 <sup>-8</sup>	8.15x10 <sup>-8</sup>
40 mm	4.44x10 <sup>-7</sup>	--	3.25x10 <sup>-7</sup>	3.25x10 <sup>-7</sup>	3.25x10 <sup>-7</sup>	3.25x10 <sup>-7</sup>	--	3.25x10 <sup>-7</sup>	3.25x10 <sup>-7</sup>
25 mm	1.14x10 <sup>-6</sup>	--	8.33x10 <sup>-7</sup>	8.33x10 <sup>-7</sup>	--	--	--	8.33x10 <sup>-1</sup>	--
16 mm	--	2.04x10 <sup>-6</sup>	--	--	--	--	--	2.04x10 <sup>-6</sup>	--
Resolution, TV Lines/Raster Height	Display Signal-to-Noise Ratio								
10	64.4	82.4	82.4	77.2	77.5	83.	104.	104.3	104.5
100	5.08	5.65	6.35	6.5	6.64	8.16	7.75	8.82	8.48
200	1.52	1.27	2.0	2.44	2.69	3.44	2.29	2.66	2.92
300	0.525	0.315	0.74	1.16	1.38	1.73	0.798	1.04	1.22
400				0.59	0.762	0.88		0.403	0.523
Rank Ordering of Cameras on the Basis of Sensitivity for a Photocurrent of 10 <sup>-12</sup> amp: 1. 40-mm I-IO 2. 40-mm I-SEC 3. 40-mm I-SEBIR 4. 25-mm I-SEC 5. 25-mm I-SEBIR 6. 16-mm I-SEBIR 7. 40-mm I-II 8. 25-mm I <sup>3</sup> -V 9. 21.4-mm I <sup>2</sup> -pV 10. 16-mm I <sup>3</sup> -V									

\* For intensifier photocathode sensitivities of 4x10<sup>-3</sup> amp/watt.

TABLE V-A-6. DISPLAY SIGNAL-TO-NOISE RATIO VERSUS INTENSIFIER PHOTOCURRENT FOR VARIOUS LOW-LIGHT-LEVEL TELEVISION CAMERAS

Camera Type	I <sup>2</sup> -pV	I <sup>3</sup> -V		I-SEC		I-IO		I-II		I-SEBIR	
TV Tube Photocathode Diameter	21.4mm	16 mm	25 mm	25 mm	40 mm	40 mm	40 mm	40 mm	16 mm	25 mm	40 mm
Intensifier Photocathode Diameter	Input Photocathode Irradiance* for an Intensifier Photocurrent of 10 <sup>-11</sup> Amp										
80 mm	1.11x10 <sup>-6</sup>	--	8.15x10 <sup>-7</sup>	8.15x10 <sup>-7</sup>	8.15x10 <sup>-7</sup>	8.15x10 <sup>-7</sup>	8.15x10 <sup>-7</sup>	8.15x10 <sup>-7</sup>	--	8.15x10 <sup>-7</sup>	8.15x10 <sup>-7</sup>
40 mm	4.44x10 <sup>-6</sup>	--	3.25x10 <sup>-6</sup>	3.25x10 <sup>-6</sup>	3.25x10 <sup>-6</sup>	3.25x10 <sup>-6</sup>	3.25x10 <sup>-6</sup>	3.25x10 <sup>-6</sup>	--	3.25x10 <sup>-6</sup>	3.25x10 <sup>-6</sup>
25 mm	1.14x10 <sup>-5</sup>	--	8.33x10 <sup>-6</sup>	8.33x10 <sup>-6</sup>	--	--	--	--	--	8.3x10 <sup>-6</sup>	--
16 mm	--	2.04x10 <sup>-5</sup>	--	--	--	--	--	--	2.04x10 <sup>-5</sup>	--	--
Resolution, TV Lines/Raster Height	Display Signal-to-Noise Ratio										
10	301.	259.	286.	311.90	312.	308.	170.	329.	330.	331.	
100	23.70	17.3	20.10	25.9	26.7	28.3	15.7	24.5	26.9	26.9	
200	7.08	3.98	6.3	9.81	10.8	11.9	7.0	7.25	8.35	9.32	
300	2.45	0.425	2.32	4.68	5.56	6.0	3.8	2.52	3.28	3.88	
400	0.826		0.877	2.37	3.08	3.04	2.05	0.855	1.25	1.66	
500	0.252			1.16	1.67	1.52	1.05		0.405	0.585	
600				0.514	0.832	0.675					
700											

Rank Ordering of Cameras on the Basis of Sensitivity for a Photocurrent of 10<sup>-11</sup> amp:

1. 40-mm I-SEC
2. 40-mm I-IO
3. 25-mm I-SEC
4. 40-mm I-II
5. 40-mm I-SEBIR
6. 25-mm I-SEBIR
7. 16-mm I-SEBIR
8. 21.4-mm I<sup>2</sup>-pV
9. 25-mm I<sup>3</sup>-V
10. 16-mm I<sup>3</sup>-V

\* For intensifier photocathode sensitivities of 4x10<sup>-3</sup> amp/watt.



in line pairs/millimeter would, in many instances, favor tubes that have smaller photocathodes, and could change the rank ordering in some cases.

TABLE V-A-8. ABBREVIATIONS

	<u>Camera Type</u>
$I^2$ -PV	Double Intensifier Lead-Oxide Vidicon
$I^3$ -V	Triple Intensifier Vidicon
I-SEC	Intensifier Secondary Electron Conduction Camera Tube
I-IO	Intensifier Image Orthicon
I-II	Intensifier Image Isocon
I-SEBIR	Intensifier Silicon Electron Bombardment Induced Response Camera Tube

At the lowest photocurrents, tubes with the largest signal amplification have the advantage because their preamplifier noise is made negligible thereby, and resolving power is so low that amplitude response is of no concern (except in the case of the intensifier image isocon). As photocurrents are increased, tubes with the highest square-wave response prevail.

As can be seen, the I-II ranks lowest at the lower photocurrents and highest at the higher. The I-SEBIR is top ranked at the lowest photocurrents, but only attains middle rank at the higher levels. This is due to its currently limited modulation transfer function (MTF). This characteristic is expected to improve with time, however. The I-SEC and I-IO currently rank high for all but the very lowest photocurrents. The converse is true for the  $I^3$ -V, which has more than adequate gain, but a severely limited square-wave response. The  $I^2$ -PV in its present form is handicapped by its 21.4-mm photocathode. With

a 25-mm photocathode, it should attain middle rank at the moderate to high photocurrent levels.

To further illustrate, the results of Tables V-A-5 and V-A-7 are plotted in Figs. V-A-17 and V-A-18. The first figure corresponds to operation at a moderately low light level, while the second pertains to operation at nearly maximum light levels.

The  $SNR_D$  tables and noise figure curves apply only to static imaging of scenes. When even moderate scene motion is involved (scene speeds as slow as 20 sec per horizontal field of view), lag effects will dominate. As previously noted, the measurement and specification of lag is poorly understood. A rank ordering is shown in Table V-A-9, based on the author's experience with lag characteristics such as are shown in this section and with other dynamic resolution measurements that have not been reviewed.

TABLE V-A-9. RANK ORDER ESTIMATED FOR LOW-LIGHT-LEVEL TELEVISION TUBES ON THE BASIS OF LAG

<u>Lag</u>	<u>Camera Type</u>
Very low	I-SEBIR
Low to moderate	I-SEC
Moderate	I-II
	I-IO
Moderate to high	I <sup>2</sup> -PV
	I <sup>3</sup> -V

Combining the lag tables with the  $SNR_D$  tables, we can draw certain conclusions that appear to be consistent with general practice. The I-IO ranks quite high with regard to sensitivity and low lag, and for many years it was the mainstay of LLLTV. It has been gradually replaced by the I-SEC, which has comparable sensitivity and lower lag, in addition to being simpler to operate. The I<sup>3</sup>-V has been used in low-cost miniature systems where image motion effects are not too



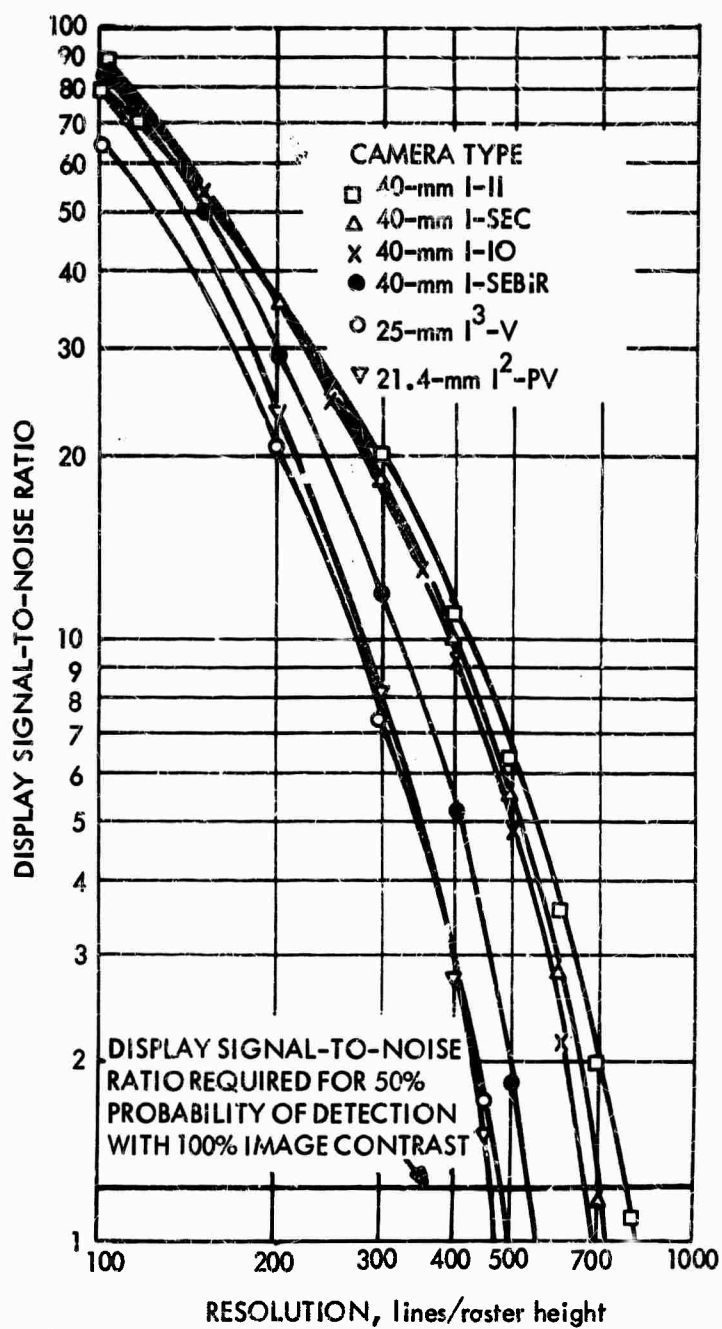
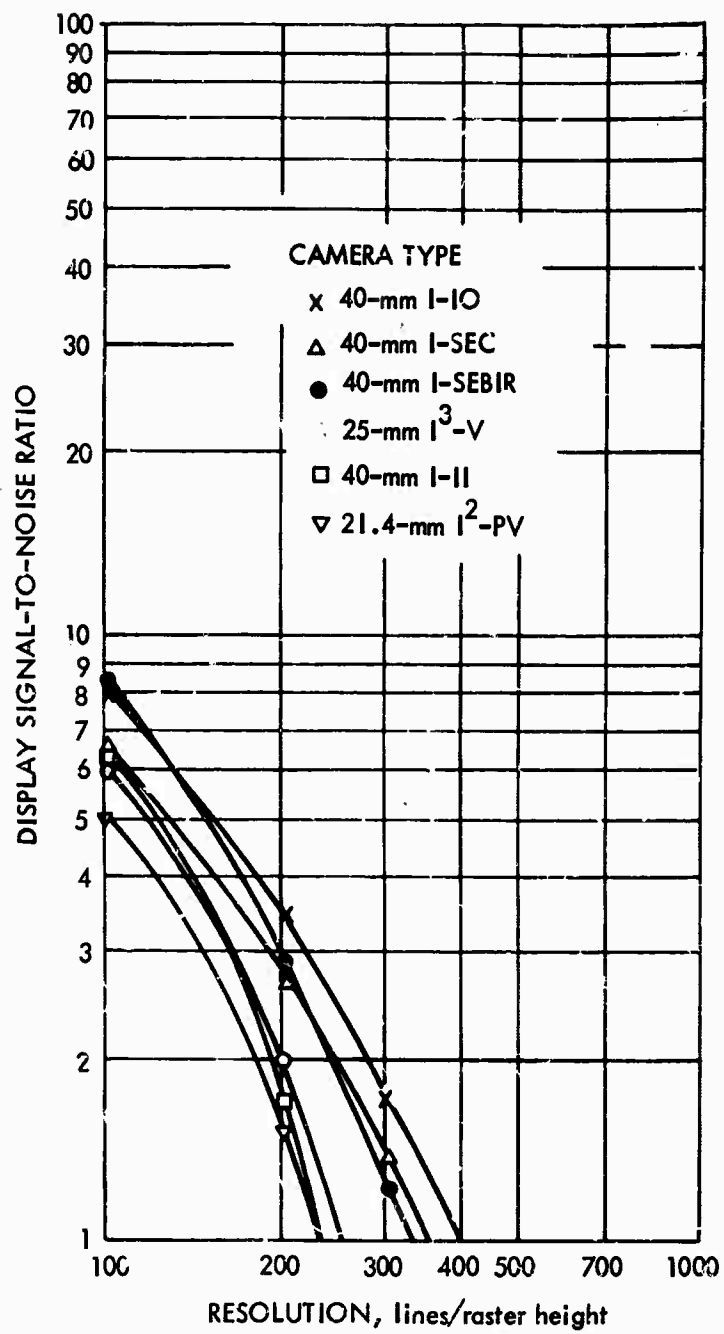


FIGURE V-A-17. Display Signal-to-Noise Ratio Versus Resolution for Various Low-Light-Level Cameras with an Input Photocathode Current of  $10^{-10}$  Amp.



53-18-71-15

FIGURE V-A-18. Display Signal-to-Noise Ratio Versus Resolution for Various Low-Light-Level Cameras with an Input Photocathode Current of  $10^{-12}$  Amp.

demanding. The I<sup>2</sup>-PV remains to be field evaluated. In the larger sizes, this combination may have promise. The I-II is of recent origin from a practical viewpoint and provides capability not too far different from the I-SEC, being somewhat superior at high light levels and somewhat inferior at lower light levels. It is also somewhat laggier, and the cameras using it are somewhat larger and more complex, although complexity has decreased in recent models. One major advantage of the I-II is that it is relatively immune from damage by extreme overexposure. The I-IO requires some protection against extremely bright lights, as does the I-SEC, although the new mesh-supported SEC target offers some relief in this regard. The I-SEBIR is very new, but shows the most promise from the viewpoints of both sensitivity and lag. It is also reported to be immune to overexposure difficulties and should become the mainstay of future LLLTV systems.

#### B. IMAGE CONVERTERS AND IMAGE INTENSIFIERS\*

An image converter is a sensor whose function is to detect a two-dimensional photon image, convert it into a photoelectron image, and then reconvert the photoelectron image back into a photon image. An image intensifier is a special case of an image converter. This term is used to describe an image converter whose input and output images are primarily in the visible spectrum and whose output image is much brighter than that of the input. The output of an image intensifier may be viewed directly or it may be coupled to other image intensifiers to provide even larger image-brightness gains. Image intensifiers may be coupled by means of lenses interposed between individual intensifier stages, but the efficiency of such coupling is usually less than 5 percent. In modern intensifiers, the input photocathodes and output phosphors are deposited on fiber-optic plates so that tubes can be directly coupled by simply butting one against the next. The coupling

---

\* In the interest of making this discussion self-sufficient, some of the material in Section V-B duplicates material that appeared in Parts III and IV.

efficiency in this case can be as high as 50 to 80 percent, depending on the type, diameter, and cladding of the fibers used.

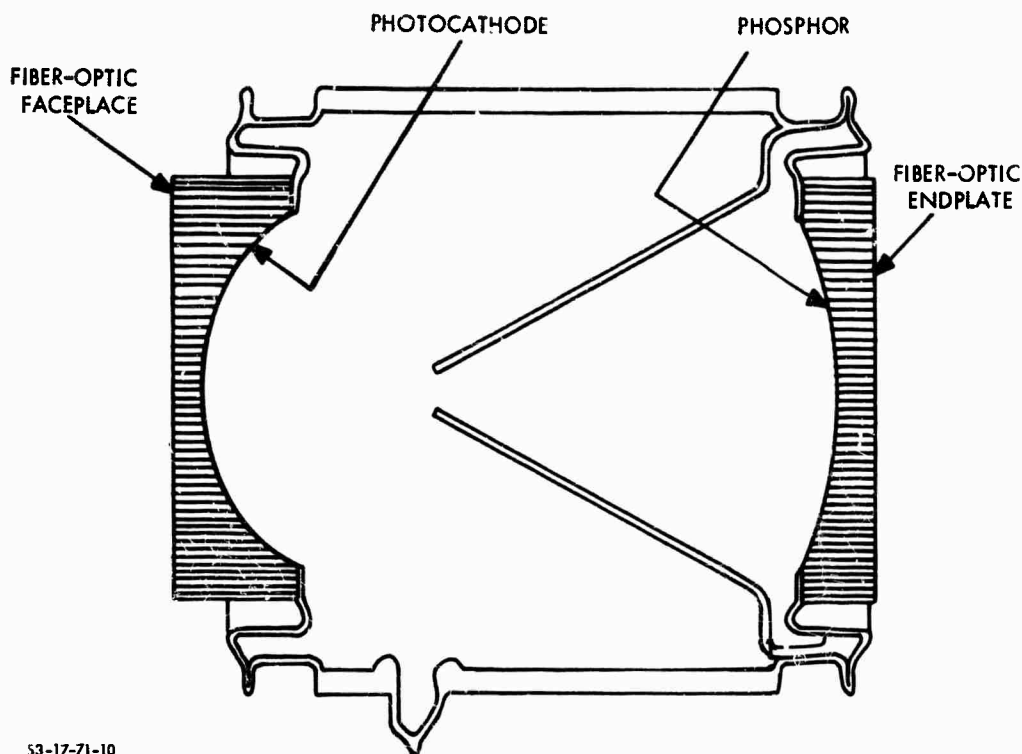
In addition to brightness gains, image intensifiers can be used to provide viewfield zoom by simple electronic means. They are also coupled to television pickup tubes to increase their sensitivity.

#### 1. Principles of Operation

A typical electrostatically focused image intensifier is shown in Fig. V-B-1. It consists of an evacuated glass envelope with a photocathode on the inner surface of one fiber-optic endplate and a phosphor on the other. The inner surfaces of the endplates are curved to minimize image distortion. The photoelectron image is greatly accelerated and focused onto the phosphor, which recreates the original image in correct spatial correspondence, except that the image is inverted top for bottom and right for left. To prevent feedback of phosphor light to the photocathode, the internal cone-shaped electrode is blackened and the inner surface of the phosphor is aluminized. The light that emanates from the output endplate is diffused so that, when coupling to other intensifiers, both first-stage output and second-stage input endplates must be optically flat and tightly joined.

The maximum accelerating voltage is typically 15 kv. At higher voltages, the dark current rapidly increases, and difficulties with positive ion bombardment of the photocathode may be encountered. Some control over image brightness can be achieved by reducing the accelerating voltage (about 10:1 to 15:1), but at voltages much below 2 or 3 kv the image will lose focus and rotate.

The spectral responses of several typical photoemitters are shown in Fig. V-B-2. The S-1 surfaces are sensitive mainly in the near infrared and are used in conjunction with auxiliary near-infrared scene illuminators. One application during World War II was the sniperscope. The S-10 surface has been used extensively in commercial broadcast applications, where the similarity of its spectral response to that of the human eye is prized. The radiant sensitivity of the photoemitters, which respond mainly in the visible, is sometimes expressed in the form



53-17-71-10

FIGURE V-B-1. Schematic of a Single-Stage Image Intensifier

of response to a tungsten source operated at  $2854^{\circ}\text{K}$ . Quantitatively, the specific radiant sensitivity  $\sigma_T^*$  due to this source is given by

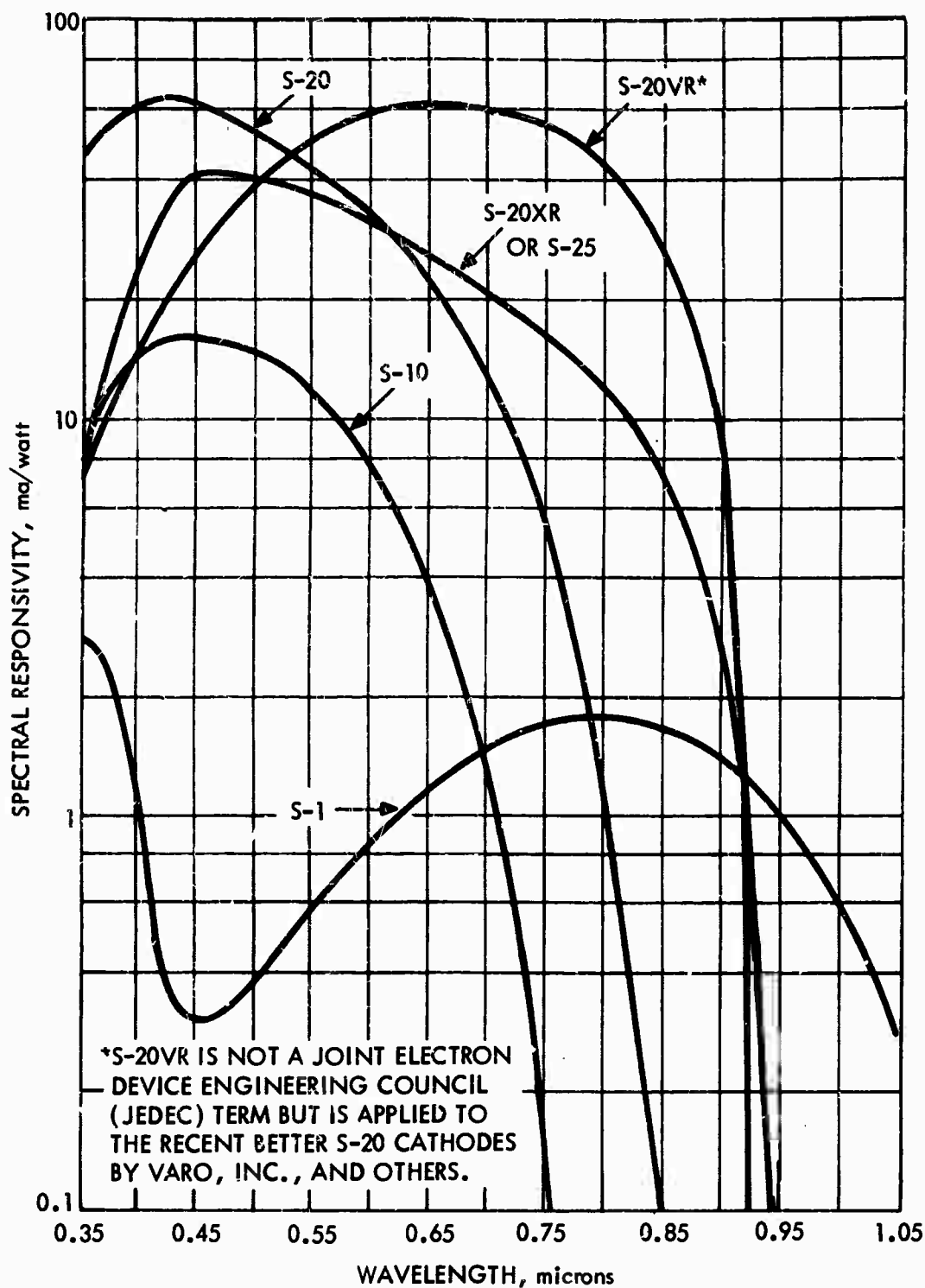
$$\sigma_T = \frac{\int_{\lambda} \sigma_p R(\lambda) E(\lambda, 2854^{\circ}\text{K}) d\lambda}{\int_{\lambda} E(\lambda, 2854^{\circ}\text{K}) d\lambda} \quad (\text{V-B-1})$$

where

$\sigma_p$  = the absolute radiant sensitivity of the photosurface at peak  $\lambda$  (amp/watt),

$R(\lambda)$  = the relative spectral response of the photoemitter,

\*This usage of  $\sigma_T$  is common, if not universal.



S3-15-71-15

FIGURE V-B-2. Spectral Responsivity Versus Wavelength for Several Photoemissive Photocathodes. (S-20VR Substrate on Fiber Optics, Others on Lime Glass.)

$E(\lambda, 2854^{\circ}\text{K})$  = the spectral irradiance due to the tungsten source operated at  $2854^{\circ}\text{K}$  (watt/m<sup>2</sup>), and

$\lambda$  = the wavelength of the radiation in microns.

Measured in these terms, the  $\alpha_T$  of the S-10 surface is about 0.8 ma/watt. One of the first steps forward in low-light-level imaging was the development of the S-20 surface with a typical specific radiant response  $\alpha_T$  of 3 ma/watt. This surface was gradually improved by extending its red response, and by the mid-1960's 4 ma/watt became quite commonplace, with occasional values as high as 5 to 6 ma/watt. As the S-20 was improved, it became known as the S-20XR (XR for extended red), and it was finally type classified as the S-25. More recently, even further improvements have resulted in a surface which is tentatively described as the S-20VR (VR for very red), whose sensitivity is reported to vary from 5 to 9 ma/watt. The sensitivity of the S-20VR in the near infrared is especially notable. The S-20VR is not now as commonly available as the S-25, and hence the latter will be used here for calculations. In all that follows, the radiant sensitivity of a photoemitter used in an intensifier will be assumed to be 4 ma/watt.

The thermionic emission or dark current of the S-1 is quite high, being  $10^{-11}$  to  $10^{-12}$  amp/cm<sup>2</sup> at room temperature. In many cases, it is necessary to cool this surface to avoid excessive contrast loss. The dark current of the S-10 is considerably better at  $10^{-13}$  to  $10^{-14}$  amp/cm<sup>2</sup>, but is still higher than desired for low-light-level applications. For the S-20 and S-25 surface, dark current is extremely low ( $10^{-15}$  to  $10^{-16}$  amp/cm<sup>2</sup>) and is not ordinarily a problem. It is understood that the dark current of the S-20VR is similarly low.

## 2. Intensifier Gain

The input photocathode current  $i_s$  due to an input irradiance  $E(\lambda)$  is given by

$$i_s = A\sigma_p \int_{\lambda} R(\lambda) E(\lambda) d\lambda \quad (\text{V-B-2})$$

where  $A$  is the effective or usable area of the photocathode and the other terms are as before. Alternatively, when the source is tungsten at  $2854^{\circ}\text{K}$ , one may write the simpler equation,

$$i_s = \alpha_T A E_T. \quad (\text{V-B-3})$$

The photocurrent is accelerated to the phosphor, which recreates an image of radiant power distribution equal to

$$E_p(\lambda) = i_s k_p Z(\lambda)/A_p \quad (\text{V-B-4})$$

where  $k_p$  is the radiant power conversion gain of the phosphor at peak  $\lambda$  in watts/amp,  $A_p$  is the phosphor area, and  $Z(\lambda)$  is the relative spectral distribution of the phosphor's output radiation.  $Z(\lambda)$  for a typical modified P-20 phosphor as used in most modern intensifiers is shown in Fig. V-B-3. The modified P-20 phosphor represents a good spectral match both with the human eye and with S-20 and S-25 photoemitters. In addition, it is a good compromise between high gain and resolving power. When one's eye views the output of the phosphor directly, one is concerned with brightness gain, which is the ratio of output to input image brightness. This can be a factor of 100 or more for intensifiers of equal input and output image areas. This high gain is due in part to the phosphor's green color, to which the eye is most sensitive.

The apparent light gain  $G_L$  due to adding an intensifier in front of a second intensifier will be different from the brightness gain because the spectral response of a second-stage photocathode is different from that of the eye. In the cascaded intensifier case, it is convenient to define the light gain relation as

$$G_L = \frac{A_1}{A_2} \frac{\alpha_{T,1}}{\alpha_{T,2}} G_{E,1-2}, \quad (\text{V-B-5})$$



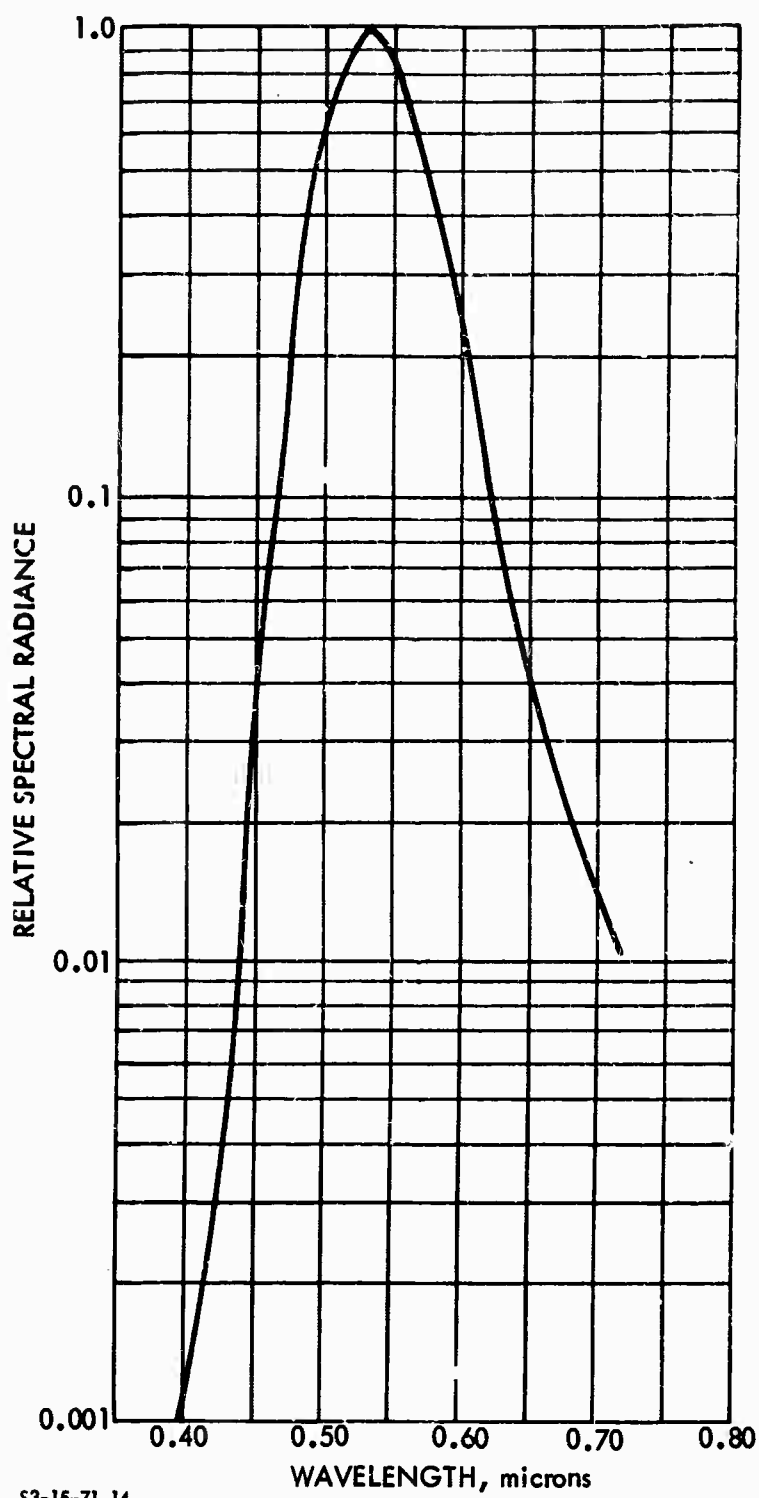


FIGURE V-B-3. Relative Spectral Radiance of a Modified P-20 Phosphor

where the subscript 1 refers to the input stage and the subscript 2 refers to the output stage. The quantity  $A_1/A_2$  is the ratio of first- to second-stage photocathode areas,  $\sigma_{T,1}/\sigma_{T,2}$  is the ratio of photocathode radiant sensitivities, and  $G_{E, 1-2}$  is the electron gain at the input intensifier's phosphor/output intensifier's photocathode. Specifically, the electron gain is equal to the ratio of photocurrents in stage 1 to photocurrents in stage 2. Thus,

$$G_{E,1-2} = \frac{i_{s,2}}{i_{s,1}} = \int_{\lambda} K_{p,1} Z_1(\lambda) \times \sigma_2 R_2(\lambda) d\lambda \quad (V-B-6)$$

In this formulation,  $K_{p,1}$  includes any coupling losses that may take place between the two intensifiers. The value of  $G_E$  is variable from tube to tube but is usually in the range of 30 to 50, 40 being typical for tubes with P-20/S-20 phosphor/photocathode combinations.

In Eq. V-B-5, one observes first that the electron gain should correlate with the value of  $\sigma_{T,2}$ , i.e., a high value for  $\sigma_{T,2}$  should result in a high value for  $G_{E,1-2}$ . This is not necessarily true, because the phosphor's spectral output is quite narrow spectrally and is centered at about 0.51 or 0.52 microns. Therefore, the sensor sensitivity at only this wavelength is of concern. The more sensitive photocathodes get their sensitivity mainly from a wider spectral band-pass, which is of no use when coupling to a phosphor. Indeed, the old S-20 may be somewhat superior to the S-25 in this regard, as can be seen by comparing Figs. V-B-2 and V-B-3.

One observes next that the input intensifier's phosphor must match the photocathode that follows it in size, while the input photocathode need not. This is shown as the area ratio gain  $A_2/A_1$ . A zoom intensifier in which the input photocathode area is variable is shown in Fig. V-B-4. In this tube the amount of photocathode imaged on the phosphor is electronically variable by changing the potentials on various internal-focus electrodes. In current practice, up to a 3:1 viewfield zoom can be provided while maintaining the image on the

phosphor at full size. As will be discussed, an increase in viewfield through electronic zoom is generally accompanied by an increase in sensitivity and a decrease in scene resolving power.

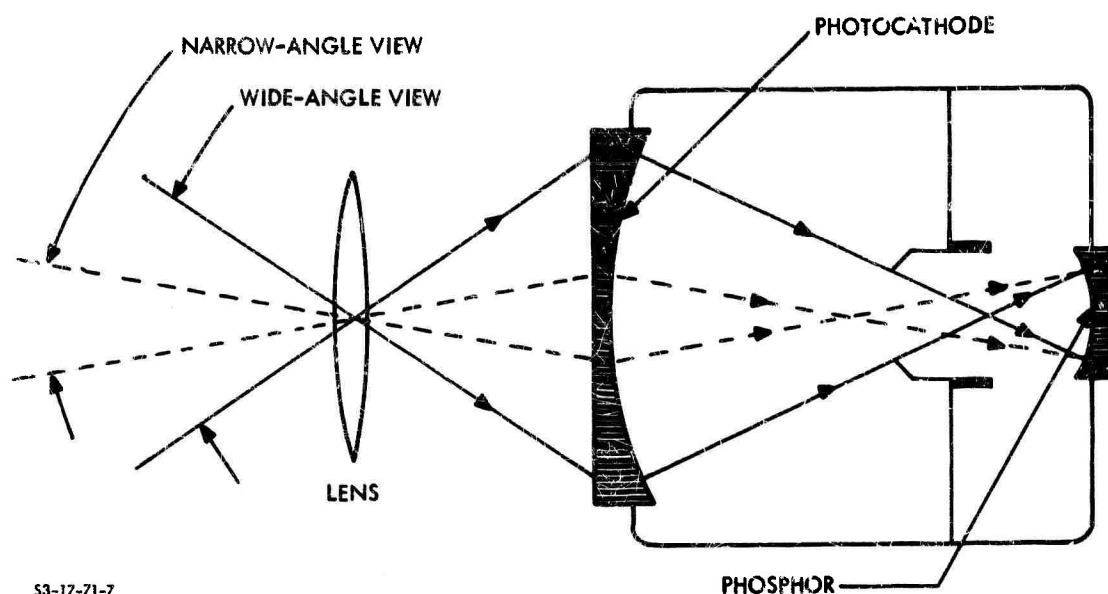


FIGURE V-B-4. Schematic of an "Electronic Zoom" Intensifier

### 3. Intensifier Sine-Wave Response\*

In detecting the image, converting it to electrons, focusing it onto the phosphor, and recreating a visible image, resolving power is lost at each step. It has become customary to describe the overall loss in resolving power by means of the sensor's sine-wave response  $R_w(N)$ . This can be measured by projecting a sine-wave bar pattern on the photocathode. First, a sine-wave pattern of low spatial frequency is employed and the peak-to-peak output amplitude is noted. Using this amplitude as a reference, the pattern spatial frequency is increased in discrete steps. At each step, the new peak-to-peak output amplitude is measured and the ratio of this amplitude to that measured at the low spatial frequency is formed. The plot of these amplitude

\*The MTF of a system is the product of the MTF of each component. In this report, we discuss electrooptical components, and nowhere in the following material do we include the MTF of the optical lens used in a camera.

ratios as a function of pattern spatial frequency constitutes the sine-wave response.

The sine-wave spatial frequency is described quantitatively in terms of the number of cycles (or line pairs) per millimeter or in terms of the number of half cycles (or lines) per some dimension--the photocathode diameter, for example. The sine-wave response of a typical intensifier is shown in Fig. V-B-5. Also shown are the sine-wave responses of two and of three intensifiers in cascade, unit magnification being assumed (equal input photocathode and phosphor diameters in each stage). These responses are calculated from the relation

$$R_w (LP) = R_{w,1} (N_{LP}) \times R_{w,2} (N_{LP}) \dots R_{w,n} (N_{LP}) \quad (V-B-7)$$

where the term  $R_w (N_{LP})$  is the overall sine-wave response and the terms  $R_{w,n} (N_{LP})$  are the sine-wave responses of the individual intensifiers. When combining responses in this form, it is necessary to reference the spatial frequency to the area where the individual elements are physically coupled in each case. For two intensifiers in cascade, the appropriate area is the phosphor/photocathode interface. Where the intensifiers are of unit magnification the point of reference is of no concern, but where zoom intensifiers are involved case must be exercised.

The special case of a zoom intensifier merits some attention. If the intensifier were of unlimited resolving power, which implies a unit sine-wave response, the scene resolution would be the same in both the wide-angle and narrow-angle modes. Since the wide-angle mode also covers more viewfield, there would then be little point to zoom. As a practical matter, the intensifier's resolving power is limited by the phosphor particle sizes. Thus, as viewfield is increased, the amount of scene detail per phosphor particle increases. When the detail becomes smaller than the particles, the detail must inevitably be lost. The consequence is that a viewfield increase is accompanied by a loss in scene detail. On the other hand, the photoelectron density

per particle increases with an increase in photocathode size, and hence the smaller, less detailed scene object becomes brighter.

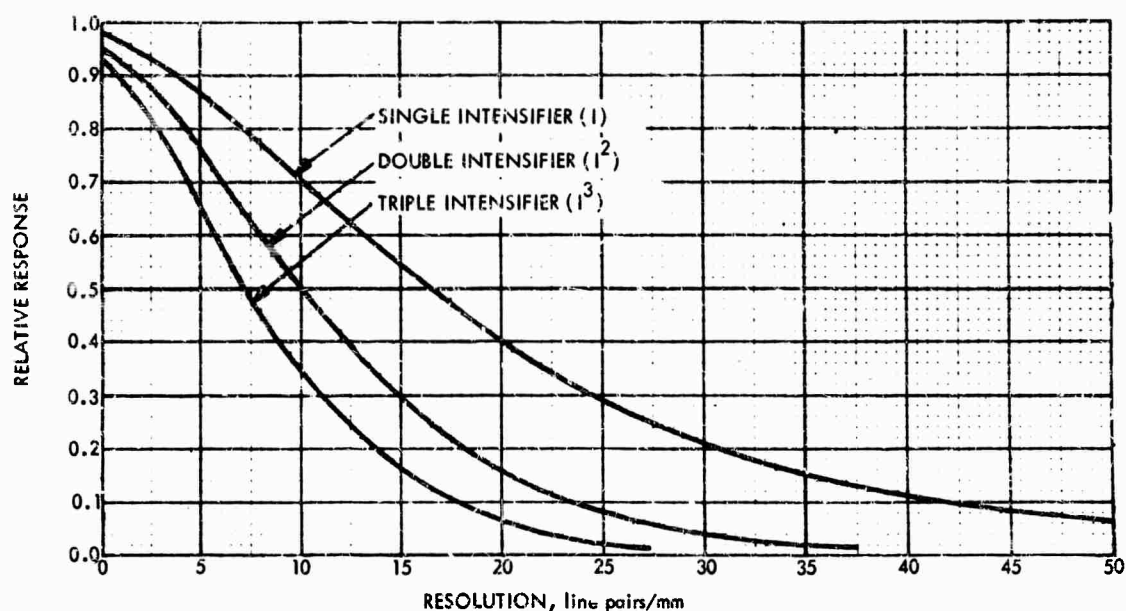


FIGURE V-B-5. Sine-Wave Amplitude Response for a Single, a Double, and a Triple Intensifier. (These Curves are Independent of Intensifier Size to a First Approximation.)

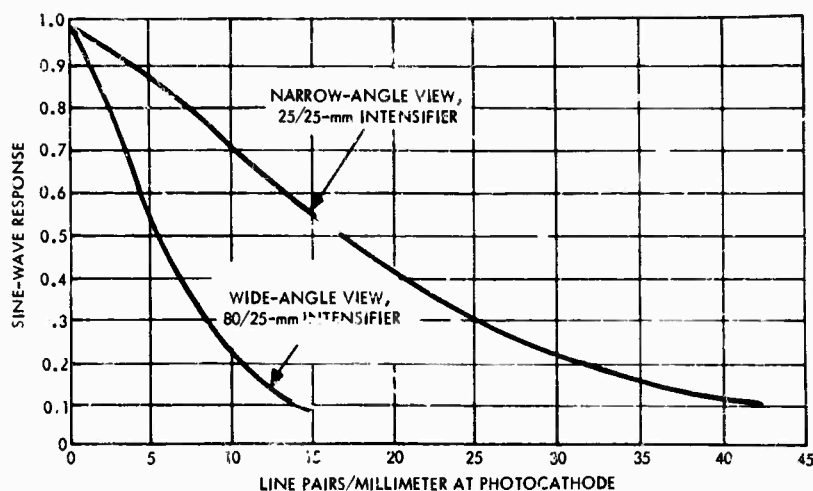
To illustrate this result more graphically, the sine-wave response of a zoom intensifier is plotted in Fig. V-B-6, referred to the input photocathode. It is interesting to observe that the photocathode is ordinarily of very high resolving power compared to the phosphor. Hence, the sine-wave response referred to the phosphor is very nearly the same in either the wide-angle or narrow-angle view.

#### 4. Lag Effects

The effect of image lag is to smear together scene detail when scene image moves across the input photocathode. In an intensifier, some lag due to phosphor decay can be expected. One measurement of such lag, performed with a modulated light source, is shown in Fig. V-B-7. The lag at the normal TV frame rate (30/sec) is seen to be quite small for a single intensifier but is appreciable for three-stage sensors. Methods of measuring and specifying lag effects are

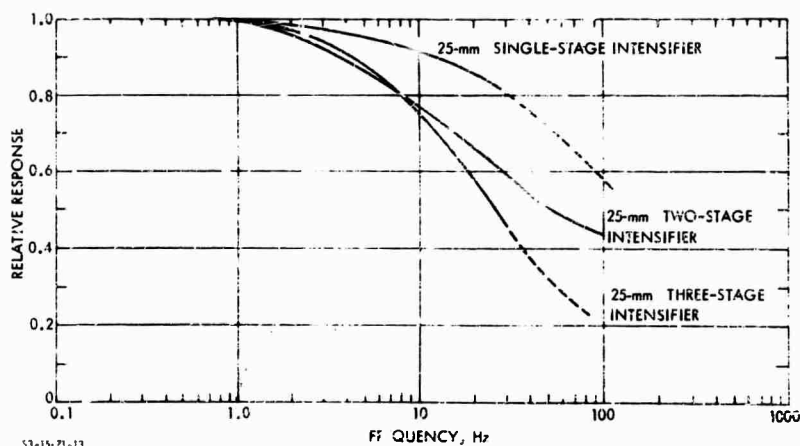
not well known but can be quite serious, as will be discussed in connection with TV camera tubes.

Although intensifiers exhibit lag effects of their own, their addition can reduce overall system lag. Most camera tubes, in particular, have lag characteristics which are dependent on light level. That is, lag increases as light level decreases. By increasing the light level on the camera tube, the increase in lag due to an added intensifier is usually more than offset by the decrease in camera tube lag.



53-15-71-16

FIGURE V-B-6. Sine-Wave Response of a Zoom Intensifier Referred to the Input Photocathode



53-15-71-13

FIGURE V-B-7. Temporal Response of Image Intensifiers

## C. VIDICON CAMERA TUBES

The term vidicon is used generically to describe those television camera tubes that employ a photoconductive photosurface, but it is also used to describe many other types of tubes in which the photosurface acts both as a photon-to-electron transducer and as the signal storage medium. In this section, the term vidicon, when unmodified by other descriptors, will mean a tube in which the surface is a porous antimony-trisulfide photoconductor. The next most prevalent type of vidicon at present is one using a lead-oxide layer as its photosurface. This surface behaves like a reverse-biased p-i-n diode. The principal advantage of the lead-oxide vidicon is a lower lag versus light level characteristic, while vidicons in general are capable of higher maximum resolving power. Neither the vidicon nor the lead-oxide vidicon is capable of low-light-level performance unless aided by two or more intensifiers in cascade.

As is well known, photoconductors and other photosensitive semiconductors can provide photon conversion efficiencies larger than unity, but when the additional requirements of signal storage and a reasonable time constant are imposed, this capability is precluded for practical purposes. Because of this lack of gain in the photosurface, the limiting noise becomes that of the camera's video preamplifier. While considerable care should be exercised in the design of the preamplifier, the extraordinary measure of incorporating a low-noise internal secondary-emission preamplifier such as a return-beam electron multiplier (Ref. 12) or isocon readout is seldom warranted, except in very special applications when slow scan rates can be tolerated. This is due to the fact that the lag characteristics of these tubes are dependent on light levels. At the light levels where the reduced noise of the electron multiplier is effective, the lag far exceeds that tolerable for real-time imaging of scenes in motion. These lag effects are more serious for the vidicon than for the lead-oxide vidicon but are of concern for both.

## 1. The Lead-Oxide Vidicon (PV)\*

The lead-oxide vidicon, which will be abbreviated hereafter as PV, is of more recent vintage than the vidicon, but its analysis is simpler, and therefore discussing it first better serves to illustrate the analytical performance presentation techniques that will be used throughout Section V-C. The photosurface of the PV consists of a layer of reverse-biased p-i-n photodiodes. In operation, this surface is similar to that in a vidicon, except that the discharge of the layer capacitance by light takes place by means of hole-electron pairs photogenerated in the i layer. Nearly all of the target potential is impressed across this layer, and the resulting electric field rapidly sweeps the holes generated to the electron gun or p side and the electrons to the input window or n side. The p and n contacts act as blocking electrodes, preventing the injection of carriers, so that only thermally generated hole-electron pairs can contribute to the dark current. These are generated at a very low rate due to the 1.9-ev bandgap of PbO.

The advantages claimed for the PV are that dark current is intrinsically very low, that the dark current reaches a saturation at a low level as target potential is increased, that the signal and dark currents are independent of temperature over a quite wide range about room temperature, and that the lag is quite small compared to that of a vidicon. The gamma of the PV is near unity, as opposed to the value of 0.65 typical of vidicons. This is claimed to be an advantage in color TV and in radiometric applications. The PV is understood to be relatively immune to damage by bright lights.

a. Principles of Operation. The vidicon and the lead-oxide vidicon operate in a similar manner except for the details of the primary photoprocess. The schematic of a typical vidicon is shown in Fig. V-C-1. A transparent signal electrode is deposited on the inner surface of the faceplate. The faceplate can be either glass or a fiber-optic plate. The photosurface or "target" is deposited on the signal electrode. Ordinarily, the signal electrode is biased 15 to 40

\*Commercially typified by the Plumbicon<sup>®</sup> (Phillips), oxicon (GEC), vistacon (RCA), and lead-oxide vidicon (GE).



volts positive with respect to the electron gun. The side of the photocathode facing the electron gun is periodically charged to the electron gun potential by the action of the scanning electron beam. If light is incident on a resolution element of the photosurface during the interval between successive scans, electrons are generated within the photosurface and move in an appropriate direction so as to discharge the charge stored on it. However, current cannot flow in the external target lead resistor until the beam once again passes the illuminated point. The function of the beam is to recharge the photocathode point by point back to gun-cathode potential, and the resulting charging current flowing through the target lead constitutes the video signal. Signal storage results from the fact that scene light impinging on a point on the photosurface continually discharges it between successive passes of the beam. The charge replaced by the beam is the total integrated amount of charge discharged during the period between scans. This period is called the frame time. In commercial practice the frame time is 1/30 sec.

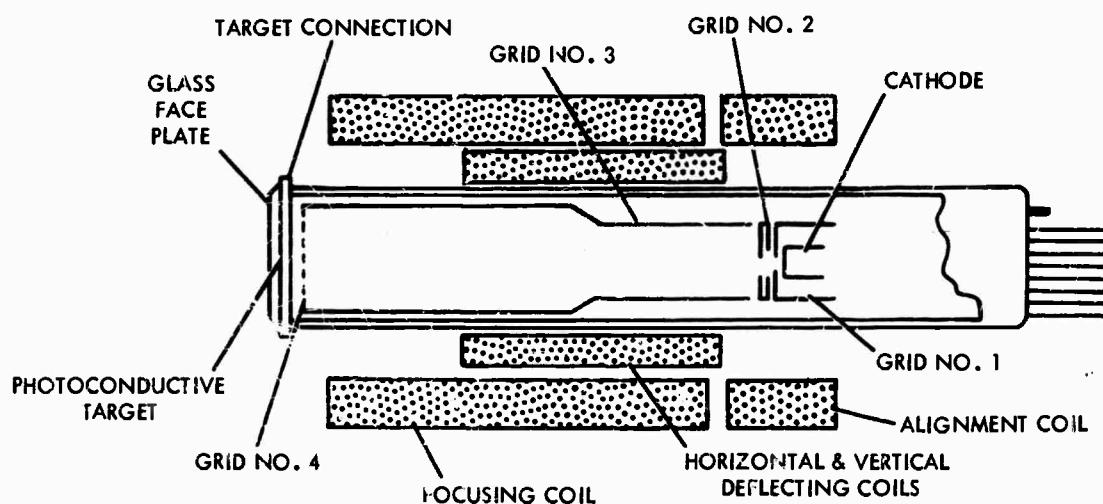


FIGURE V-C-1. Schematic of Vidicon and Associated Focus, Deflection, and Alignment Coils

There are usually three important time constants in the operation of the tube. First, there is a signal-storage time constant or dielectric relaxation time consisting of the RC time constant of the layer. This time constant should be long compared to the frame time. A second time constant is associated with the photoprocess itself and has to do with the mobility of charge carriers. The third time constant, called the readout time constant, is a product of the beam resistance times the photoconductor capacitance. Both the second and third time constants, which collectively limit the speed and efficiency of signal readout, should be short. In the PV, both the photoprocess and readout time constants are short. For slow-scan applications, however, the signal storage time constant of the PV tends to be somewhat short.

b. Signal Transfer Characteristic. The signal transfer characteristic of a TV pickup tube is an experimentally measured plot of signal current at the output of the tube as a function of the input photosurface irradiance as shown in Fig. V-C-2. This curve is obtained with the photosurface uniformly irradiated. For the PV, the slope or gamma of the  $\log I_S$  versus  $\log E_T$  curve is unity. Hence, one may write the signal current equation as

$$I_S = \sigma_T A E_T / e_v e_h \quad (V-C-1)$$

where the terms are as defined in Section V-B,\* except that one must include here  $e_v$  and  $e_h$ , the vertical and horizontal scan efficiency terms. The value of  $e_v e_h$  for commercial broadcast TV is about 0.79. These terms stem from the fact that the electron beam, in scanning a raster pattern from right to left and from top to bottom, needs some time to return to the left to begin a new line and some time to return to the top to begin a new field. Because of this "dead" time in the

---

\*  $\sigma_T$  is the radiant sensitivity of the photoemitter, expressed as response to the total radiation from a tungsten source operated at 2854°K.

picture, the beam must scan each line more quickly, which increases the rate of charge readout. Thus, signal current increases. Reductions in scan efficiencies can result in increased sensitivity at the expense of other parameters such as video bandwidth, area scanned, or maximum resolving power, depending on the scan mechanism used.

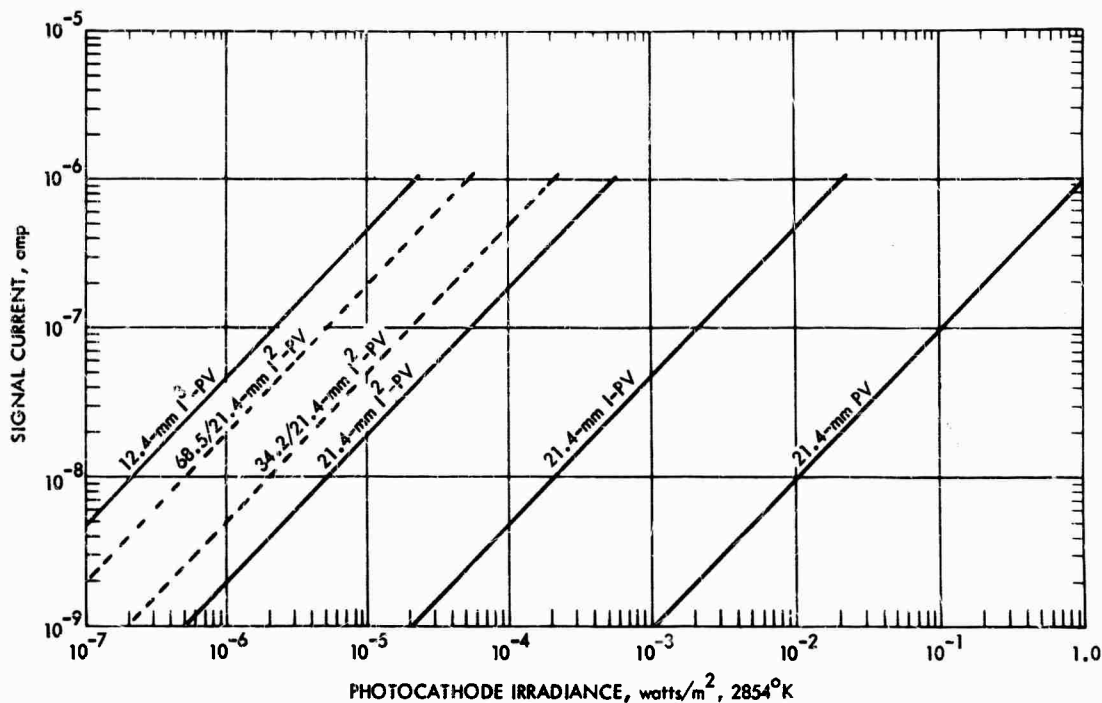


**FIGURE V-C-2. Signal Current Versus Photocathode Irradiance Characteristic for the Lead-Oxide Vidicon and its Combination with Various Intensifiers**

The PV signal-transfer curve shows no discernable "knee" or leveling off characteristic as photosurface irradiance increases, although a knee may be artificially introduced by electronic means to increase dynamic range. The spectral response of the more common lead-oxide photocathode resembles that of the S-10 photoemitter, but has a photosurface sensitivity of the order of 3 to 6 ma/watt. An extended-red-sensitive surface is also available with sensitivities in the 6- to 9-ma/watt range. The signal-transfer curve applies to a "standard" lead-oxide surface deposited on a fiber-optic faceplate.

For this case, it is estimated that the specific radiant sensitivity to tungsten light will be 3.42 ma/watt. In the fiber-optic version of the PV, the current photocathode diameter is 21.4 mm and the effective area is  $2.2 \times 10^{-4} \text{ m}^2$ , if one assumes the usual 4 horizontal to 3 vertical picture aspect ratio.

c. Amplitude Response. The square-wave amplitude response of a TV camera tube is obtained by imaging a bar pattern of 100 percent contrast and noting the output amplitude as the bar widths and spacings are reduced. The number of black and white bars, counted individually, is expressed in terms of the raster height dimension (TV lines/raster height) or, alternatively, in line pairs per millimeter, as discussed in Sec. V-B. The advantage of the former definition is that resolving power expressed in these terms is independent of the variations in image dimensions that may take place from point to point within the tube. At low line numbers (broad bars), the bar pattern will be reproduced quite faithfully without any appreciable degradation of signal amplitude. As the bar number is increased, the signal amplitude decreases due to a smearing together of detail, as in the case of the intensifier previously discussed. The amplitude or square-wave response of the TV pickup tube is obtained by taking the ratio of the signal amplitude due to the high-line-number bar pattern to that at the low-line-number pattern. A typical result for a PV is shown in Fig. V-C-3.

Although the bar pattern used is specified in terms of the number of bars/raster height, the bar pattern is oriented vertically in the manner of a picket fence. The quantity measured, therefore, is the square-wave response in the horizontal. The vertical square-wave response will be different from the horizontal response, but it is neither measured nor specified in most cases.

The main effect of the square-wave (or sine-wave) response of the sensor is to decrease the available signal. This results chiefly in loss of the picture's high-frequency content, i.e., detail. In high-performance sensors, it may also filter noises generated prior to the limiting sensor apertures.

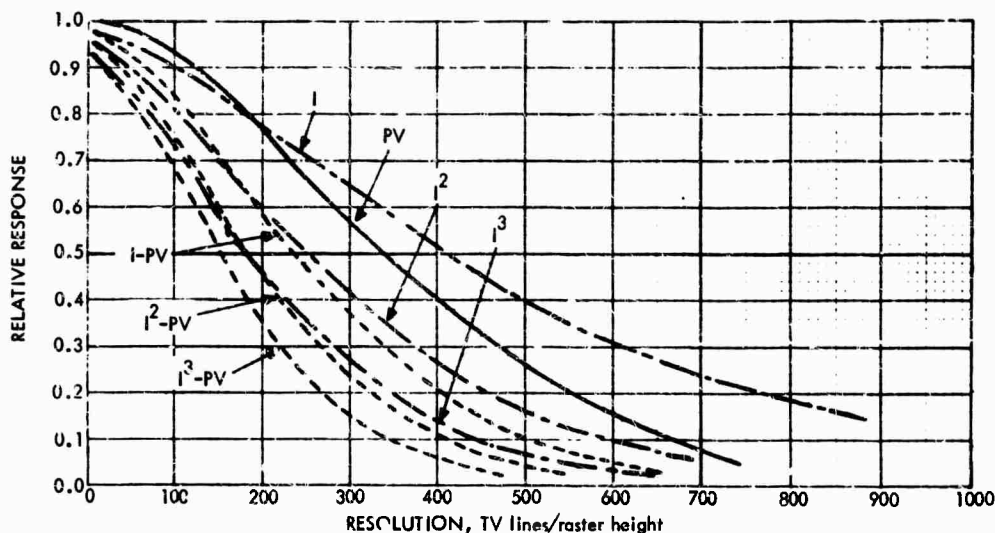


FIGURE V-C-3. Uncompensated Sine- or Square-Wave Responses for the Lead-Oxide Vidicon and its Combination with Intensifiers with 21.4-mm Phosphors. (Intensifier Response is Sine Wave; Lead-Oxide Vidicon and Intensifier Lead-Oxide Vidicon Response is Square Wave.)

d. Video and Display Signal-to-Noise Ratios. The methods of analyzing the performance of television camera tubes are derived in Section V-A-3, and the procedures described therein are generally employed, with certain exceptions as will be noted.\* Before proceeding further, please observe that the contrast definition used herein will be the following:

$$C = (E_{\max} - E_{\min})/E_{\max}. \quad (\text{V-C-2a})$$

And, since  $i_{s \max}$  is the signal produced by  $E_{\max}$  and  $i_{s \min}$  is the signal produced by  $E_{\min}$ ,  $C$  may also be equated as follows:

\* Section V-A-3 represents recent work performed subsequent to the analysis contained in this section, and the analytical models derived therein are believed to be more accurate. However, the errors resulting from the use of the earlier model are in most cases within the usual errors in making measurements.

$$C = \frac{i_{s \max} - i_{s \min}}{i_{s \max}} \quad (\text{V-C-2b})$$

The analysis that follows will use the concept of display signal-to-noise ratio as developed in Section V-A-3. In this treatment, it is assumed that the image signal-to-noise ratio appearing on the display is identical to that appearing at the output of the retina of the eye, if one takes into account the ability of the eye to integrate in space and time. This display is presumed perfect, a condition that can be approximated in practice by making the display sufficiently large and by incorporating appropriate gamma correction. The observer is permitted to adjust his viewing distance and display brightness so that he is not acutely limited by either display luminance or image size.

The basic analytical formulation used will be that of Eq. V-A-46, modified slightly to read:

$$\frac{\text{SNR}_{D/A}}{(n_v)^{\frac{1}{2}}} = \frac{[t_e \Delta f / \alpha]^{\frac{1}{2}}}{N} \times \text{SNR}_{V,N,C} \quad (\text{V-C-3})$$

The test pattern is presumed to be a bar pattern containing a sufficient number of bars so that any wave-shape distortions due to system transients are eliminated, and the bars are of height-to-width ratio  $n_v$ . The bars are also assumed to be long enough so that the sensor's modulation transfer function in the vertical is near unity. In the above equation,  $\text{SNR}_{D/A}$  is the display signal-to-noise ratio based on the image area,  $t_e$  is the integration time of the eye,  $\Delta f$  is the video bandwidth,  $\alpha$  is the horizontal-to-vertical picture aspect ratio,  $N$  is the spatial frequency of the bar pattern expressed in terms of the number of bars that can be fitted into a picture height, and  $\text{SNR}_{V,N,C}$  is the video signal-to-noise ratio measured (or calculated) by using a bar pattern of frequency  $N_{TV}$  lines/picture height and contrast  $C$ .

As a further simplification, the bar height-to-width ratio  $n_v$  is assumed to be a constant equal to approximately 20. As discussed in Section V-A-3, the exact value of  $n_v$  is not very critical, since the resolving power of the sensor is not a strong function of this ratio. In the following, the notation

$$\text{SNR}_D = \text{SNR}_{D/A} / n_v^{\frac{1}{2}} \quad (\text{V-C-4})$$

will be used. Here,  $\text{SNR}_D$  is identical to the per-element signal-to-noise ratio discussed in Section V-A-3.

Suppose next that the test pattern is a sine wave rather than a bar pattern. Then Eq. V-A-58 applies. This equation is modified by multiplying the numerator and denominator by the video bandwidth  $\Delta f$  and by noting that  $N_v = n_v N_h = n_v N$ , so that the equation becomes

$$\begin{aligned} \text{SNR}_D &= \text{SNR}_{D/A} / n_v^{\frac{1}{2}} \\ &= \frac{(t \Delta f / \alpha)^{\frac{1}{2}}}{N} \times \frac{0.75C |R_O(N)| i_{s \max}}{[0.75(2-C) |R_O(N)| e i_{s \max} \Delta f]^{\frac{1}{2}}} \end{aligned} \quad (\text{V-C-5})$$

where  $|R_O(N)|$  represents the sensor's modulation transfer function (MTF). By analogy with Eq. V-C-3,

$$\text{SNR}_{V,N,C} = \frac{0.75C |R_O(N)| i_{s \max}}{[0.75(2-C) |R_O(N)| e i_{s \max} \Delta f]^{\frac{1}{2}}} \quad (\text{V-C-6})$$

At spatial frequencies  $N$  larger than  $N_c/3$ , where  $N_c$  is the frequency at which the MTF becomes negligible,  $|R_O(N)| = (\pi/4) R_{SQ}(N)$ , where  $R_{SQ}(N)$  is the square-wave amplitude response. The result of substitution in Eq. V-C-6 is

$$\text{SNR}_{V,N,C} \approx \frac{C R_{SQ}(N) i_{s \max}}{[(2-C) R_{SQ}(N) e i_{s \max} \Delta f]^2} \quad (\text{V-C-7})$$

While this equation is only a good approximation for  $N > N_C/3$ , the error at line numbers as low as  $N_C/5$  is not much more than 5 to 10 percent in principle and is probably less in practice. The effect of using  $R_{SQ}(N)$  at low line numbers, instead of the square-wave energy approach discussed in Section V-A-3, is to give a pessimistic value for  $\text{SNR}_{V,N,C}$ . In practice (for reasons not now clear), the resolution predictions at low line numbers using Eq. V-C-7 tend to be optimistic rather than pessimistic. Thus, the use of the square-wave amplitude response rather than the sine-wave response (or MTF) appears reasonable.

Two other approximations were made in the earlier analysis on which the calculations in this section are based. One was an assumption that the photoelectron noise is white rather than spatially filtered, as indicated in Eq. V-C-7. This is of no consequence for sensors that are limited by preamplifier noise rather than photoelectron noise, and it is of only modest concern where the preamplifier noise is of a magnitude comparable to the photoelectron noise. The most serious error occurs for tubes that are photoelectron-noise limited, such as the I-SEBIR of Section V-F. Again, however, one notes that the error is proportional to only the square root of the MTF, which is not a strong function. Also, in the earlier model, it was recognized that photoelectron noise is spatially filtered, and a partial compensation was made by dropping the  $(2-C)$  term under the radical in the denominator. This has the largest effect for images of low contrast, where photoelectron noise is a more important factor than it is for images of high contrast.

In spite of the deficiencies cited above, results calculated by using the earlier model correlate well with measured results. Indeed, the methods of measurement probably have more deficiencies than the model, since manufacturers have not standardized methods and



procedures of measurement, nor do they provide any details of the test patterns and measurement procedures used. Consequently, sensors produced by different manufacturers cannot be reliably compared from catalog data. Even with its problems, the analytical approach has the advantage of being consistent and correctable.

Equation V-C-7 applies only to sensors that are photoelectron-noise limited. If other noise, such as preamplifier noise, is a factor, this equation must be rewritten in the form

$$\begin{aligned} \text{SNR}_{V,N,C} &= \frac{CG i_{s \max} R_{SQ}(N)}{(G^2 e \Delta f i_{s \max} + \bar{I}_{PA}^2)^{\frac{1}{2}}} \\ &= \frac{CG \alpha_T A E_{T \max} R_{SQ}(N) / e_v e_h}{\left[ \underbrace{(G^2 e \Delta f \alpha_T A E_{T \max} / e_v e_h)}_{\text{mean square photoelectron noise}} + \bar{I}_{PA}^2 \right]^{\frac{1}{2}}} \end{aligned} \quad (\text{V-C-8})$$

where  $G$  is the gain of any signal-amplifying devices within the camera tube prior to the preamplifier,  $\bar{I}_{PA}$  is the rms preamplifier noise, and Eq. V-C-1 is used.

In the specific case of the PV unaided by intensifiers, the preamplifier noise and the gain  $G$  are unity, so that  $\text{SNR}_{V,N,C}$  becomes

$$\text{SNR}_{V,N,C} = \frac{C \alpha_T A E_{T \max} R_{SQ}(N) / e_v e_h}{\bar{I}_{PA}} \quad (\text{V-C-9})$$

It is quite common to measure or calculate the video signal-to-noise ratio  $\text{SNR}_{V,N,C}$  at a low spatial frequency ( $\sim 0$ ) and at unit contrast. The calculated result for  $\text{SNR}_{V,N,C}$  using Eq. V-C-9 is shown in Fig. V-C-4 for an rms preamplifier noise of  $3 \times 10^{-9}$  amp and a video bandwidth of 7.5 MHz. The  $\text{SNR}_D$  for images of unit contrast becomes

$$\text{SNR}_D = \frac{(t_e \Delta f / \alpha)^{1/2}}{N} \times \frac{R_{SQ} \alpha_T A E_T / e_v e_h}{I_{PA}} \quad (\text{V-C-10})$$

and is plotted in Fig. V-C-5 as a function of  $N$ , the spatial frequency for various values of  $E_T$ . The eye integration time  $t_e$  used is 0.2 sec,  $\alpha = 4/3$ , and  $\sigma = 3.42$  ma/watt.

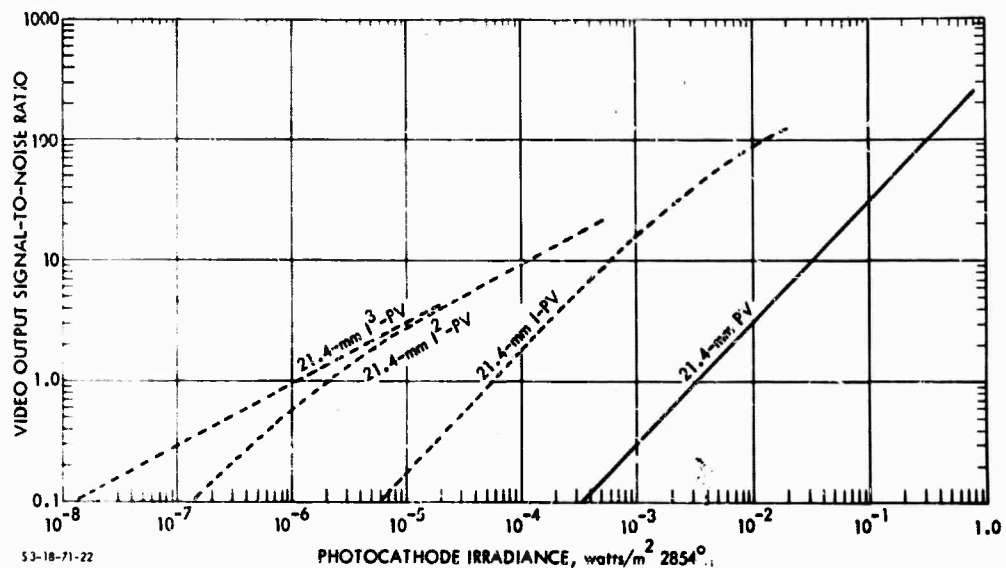


FIGURE V-C-4. Video Output Signal-to-Noise Ratio Photocathode Irradiance Characteristic for the 21.4-mm Lead-Oxide and Intensifier Lead-Oxide Vidicons with a 7.5-MHz Video Bandwidth

It has been experimentally determined that the  $\text{SNR}_D$  required to detect a bar pattern of the type assumed with 50 percent probability is approximately 1.2, as discussed in Section V-A-3. Thus, one sets  $\text{SNR}_{D,T} = 1.2$  and plots in Fig. V-C-5. The intersection of the  $\text{SNR}_D$  obtainable from the sensor with the  $\text{SNR}_D = 1.2$  curve gives a value for  $N$  that is designated the limiting bar-pattern resolution.

Observe that the  $\text{SNR}_D$ -obtainable curves are plotted for unity contrast. For lower values of contrast, new  $\text{SNR}_D$  curves should

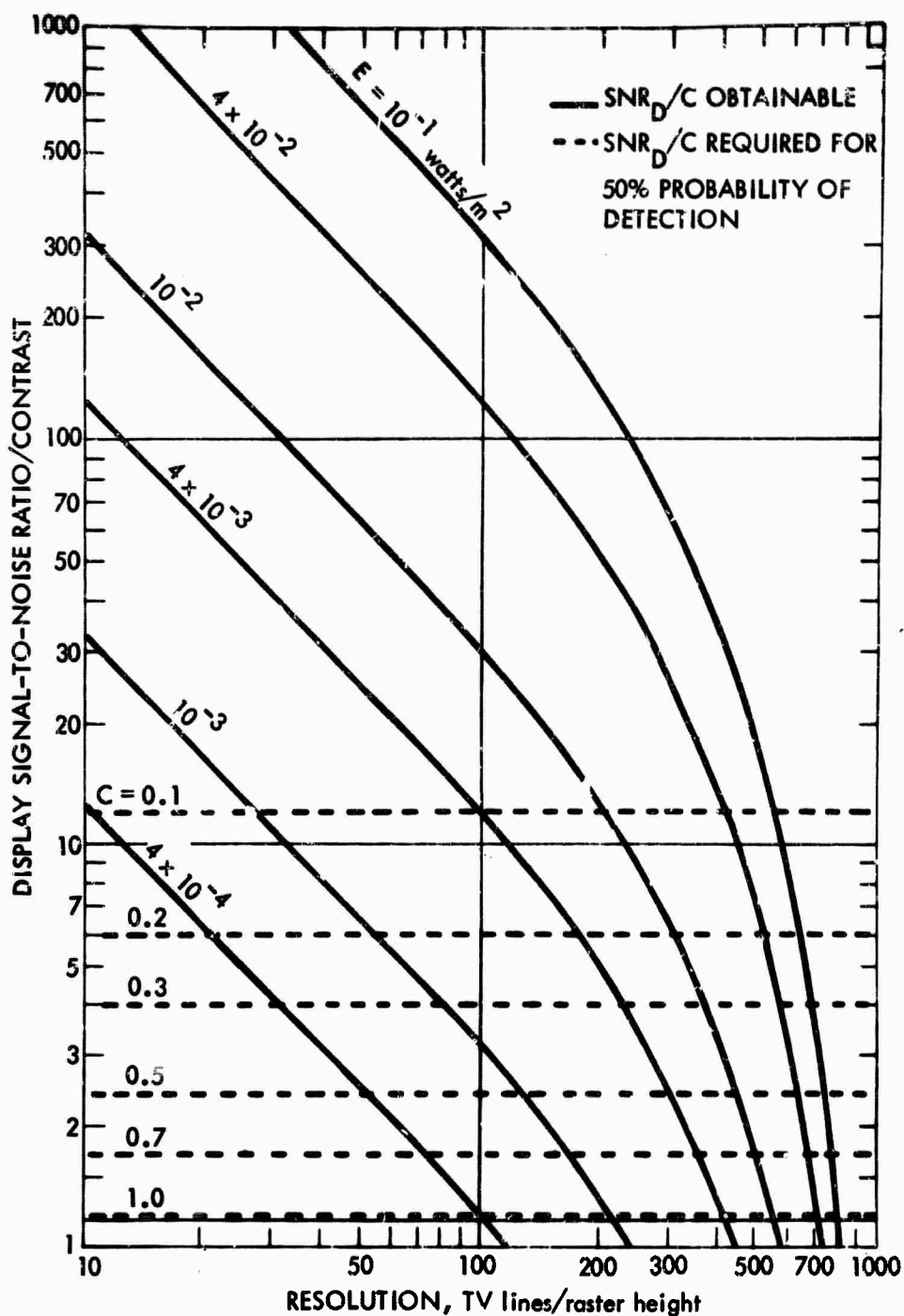


FIGURE V-C-5. Display Signal-to-Noise Ratio Versus Resolution for the Lead-Oxide Vidicon for Various Image Highlight Irradiances

be plotted, but instead it is convenient to adjust the threshold value of  $SNR_D$  so that the "new threshold" becomes

$$SNR_{D,T} = 1.2/C \quad (V-C-11)$$

This equation is plotted for various values of  $C$  in Fig. V-C-5.

e. Limiting Bar-Pattern Resolution. The limiting bar-pattern resolution as derived from Fig. V-C-5 is plotted in Fig. V-C-6. Observe that as contrast is decreased, image irradiance must be increased by a factor of  $1/C$  to maintain resolving power at the same level. This is characteristic of imaging tubes that are system or preamplifier-noise limited (as opposed to photoelectron-noise limited).

f. Computed versus Measured Results. The resolution versus image-irradiance-level characteristics are not ordinarily quoted for the PV. However, one set of data obtained for images of 100 percent contrast shows the computed result to be pessimistic by a constant amount of 30 TV lines at each irradiance level. However, the photocathode of the measured tube was considerably better (6 ma/watt versus 3.42 ma/watt). If the better photocathode were used in the calculations, the computed results would then be optimistic. However, no really fair comparison can be made without knowing the preamplifier noise, upon which the resolution light-level characteristic is quite dependent, or the test pattern dimensions. It is felt that the calculated result is probably within the experimental error inherent in the measured result.

g. Lag Characteristic. The current, most difficult data to obtain and interpret is that of lag although the lag is generally as significant a parameter in real-time imaging as preamplifier noise or amplitude response. Two methods of specifying lag characteristics have recently been devised. The most usual method is to quote the lag in terms of the residual signal remaining on the third field after removal of the image. To be acceptable from a commercial broadcast viewpoint, this residual should be less than 5 percent, but longer lags

are probably acceptable in industrial or military systems. The effect of lag is to reduce signal modulation for images in motion. This reduces resolving power in turn. Lag could probably be specified in the form of an amplitude response function, but it would be quite complicated to measure because it is dependent on the image-irradiance level.

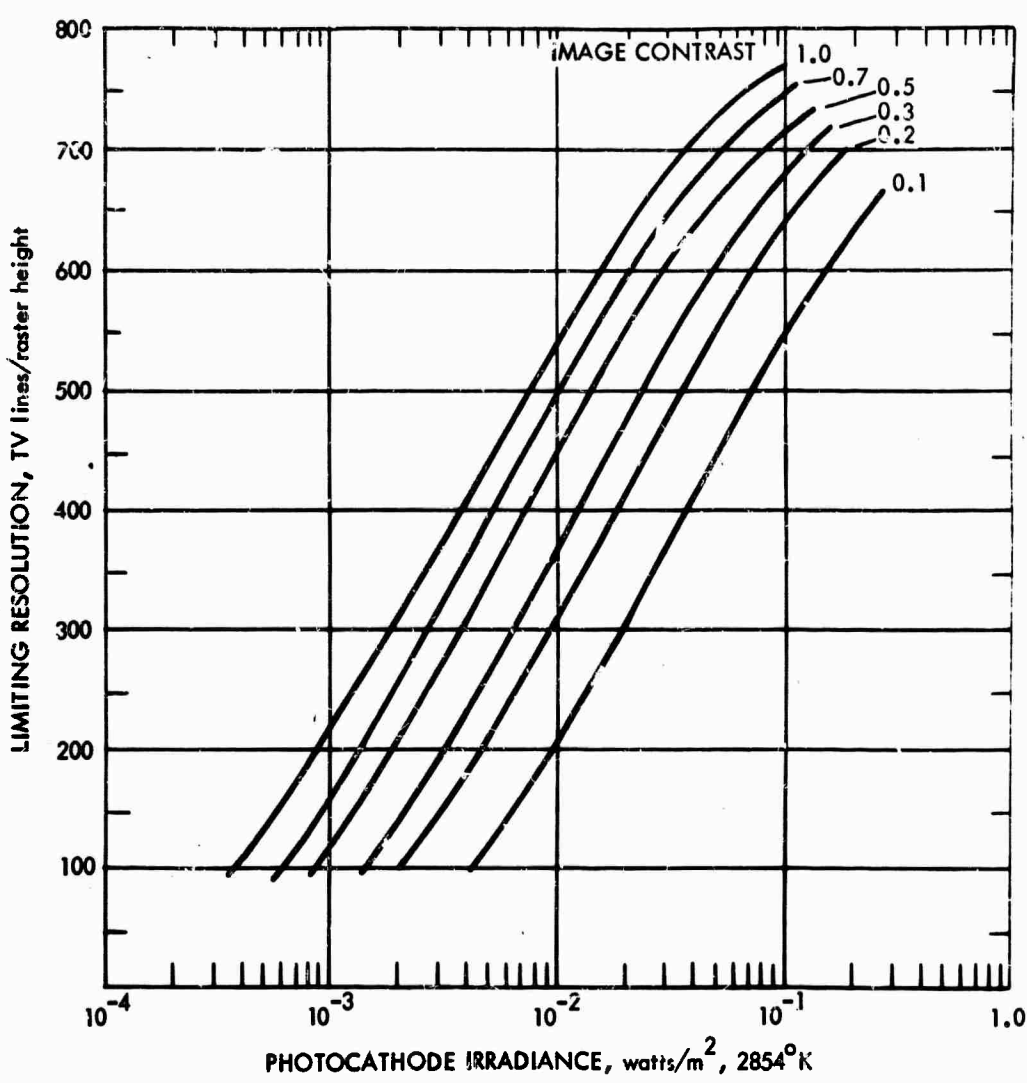


FIGURE V-C-6. Limiting Resolution Versus Photocathode Irradiance for the 21.4-mm Lead-Oxide Vidicon for Various Image Contrasts

A second way of specifying lag is to measure limiting resolution versus irradiance level as the bar pattern is slowly moved across the horizontal field of view.

The residual signal in the third field is shown as a function of photocathode irradiance in Fig. V-C-7. This curve is estimated from current data, but, as will be generally true, these estimates are of rather uncertain reliability. No dynamic limiting resolution versus irradiance level characteristics are currently available for the PV.

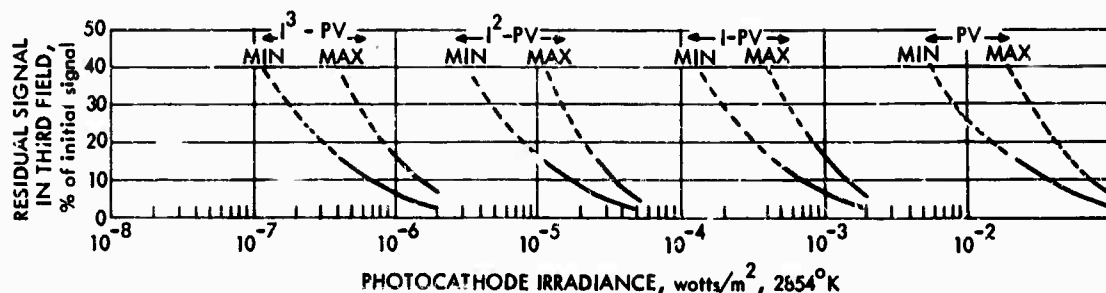


FIGURE V-C-7. Signal Lag Versus Photocathode Irradiance Characteristic Estimated for the 21.4-mm Lead-Oxide Vidicon and the 21.4-mm Intensifier Lead-Oxide Vidicon Combinations

h. Form Factor. The Plumbicon <sup>(F)</sup> is the most available type of lead-oxide vidicon (Table V-C-1). It has been produced with photocathodes of usable diameters of 10, 16, and 21.4 mm, and it is understood that a 40-mm tube may soon become available. The smallest Plumbicon <sup>R</sup> is approximately 0.65 in. in OD by 4.7-in. long, and the 21.4-mm tube is approximately 1.2 in. in OD by 7.5-in. long. In a camera, the outside dimension will become larger due to the focus and deflection coils necessary to operate the tube.

## 2. Intensifier Lead-Oxide Vidicons

To achieve low-light-level capability, two or more intensifiers must be added to the PV. As will be seen, two intensifiers are nearly sufficient to achieve the photoelectron-noise-limited condition, but it is uncertain whether lag is sufficiently reduced thereby. In either event, the intensifier-aided PV is regarded as a valid approach

TABLE V-C-1. TYPICAL PROPERTIES OF PLUMBICONS<sup>(R)</sup> FOR NORMAL OPERATION  
(UNDER 2870°K ILLUMINATION)

Property <sup>a</sup>	Type						
	21XQ <sup>bc</sup>	XQ1070	19XQ <sup>bd</sup>	XQ1020	XQ1023 <sup>c</sup>	7XQ <sup>be</sup>	40XQ <sup>be</sup>
Size: diameter/length, in.	0.65/5.1	1.0/6.25	1.0/6.25	1.2/8.0	1.2/8.0	1.2/8.0	2.0/12.25
Target diagonal, mm	10.5	16	16	21.4	21.4	21.4	40.0
Output capacitance, pf	2.5	4.5	2.5	4.8	4.8	5.0	~10
Radiant sensitivity to 2854°K, ma/watt	8.4	8.0	8.0	8.0	8.8 <sup>f</sup>	6.0 (150 ma/watt <sub>P-11</sub> ) <sup>g</sup>	4.0 (100 ma/watt <sub>P-11</sub> ) <sup>g</sup>
Peak radiant sensitivity, amp/watt	~0.29	~0.27	0.27	0.27	0.29	~0.20	~0.14
Dark current, na	~1.5	0.5	0.3	0.8	1.6	0.5	~5.0
Gamma	0.95	0.95	0.95	0.95	0.95	0.95	0.95
Resolution: central modulation depth, 400 TV lines, %	~25	30	40	43	53	40	~70
Limiting resolution, mod. depth = 10%, TV lines	550	~650	~725	~750	900	~675	~1200
(i <sub>sig</sub> /i <sub>beam</sub> ) for resolution values, na	(150/300)	(150/300)	(200/400)	(300/600)	(300/600)	(300/600)	(300/600)
Layer capacitance, pf	~300	~550	600	800	~1100	~900	~4000
Lag: 3rd field, %	4.0	3.0	2.5-1.5	3.5	7.0	6.0	~6.0
12th field, %	2.0	1.2	~1.0	1.1	2.0	2.0	--
(i <sub>sig</sub> /i <sub>beam</sub> ) for lag values, na	(50/100)	(100/300)	(100/300)	(100/300)	(100/300)	(100/200)	(300/600)

<sup>a</sup>Gamma is the average value of the slope of curve of lag signal current versus lag (faceplate illumination over the range of signal currents from 10 to 300 na. The maximum of radiant sensitivity is that which occurs at the wavelength  $\lambda_p$ , approximately 5000 Å. Resolution and modulation depth are measured at the center of the target. Lag is the percentage of signal remaining in the third field and the twelfth field, the target illumination (white light) being removed in the zeroth field.

<sup>b</sup>Type under investigation.

<sup>c</sup>Extended-red layer type.

<sup>d</sup>With anti-comet-tail (ACT) gun and "light pipes" to provide a bias photosignal that has the effect of reducing lag.

<sup>e</sup>With clad fiber-optic faceplate.

<sup>f</sup>With IR-absorbing filter, Balzer type BL/K1.

<sup>g</sup>watt<sub>P-11</sub> indicates wattage from a P-11 phosphor.

<sup>(R)</sup> Trademark, N.V. Philips of Holland.

to low-light-level imaging, worthy of further field and laboratory evaluation. As far as is known, this tube combination has not yet been extensively employed in either industrial or military applications.

a. Principles of Operation. Any number of intensifiers can be coupled to the PV. If one intensifier is added, the combination will be designated the I-PV, with two, the combination is the I<sup>2</sup>-PV, and so on. The apparent light gain due to a single intensifier of unit magnification coupled to a PV will be designated  $G_{L,IV}$  and is equal to

$$G_{L,IV} = \frac{\sigma_I}{\sigma_V} G_{IV} \quad (V-C-12)$$

where  $\sigma_I$  and  $\sigma_V$  are the photocathode radiant sensitivities of the intensifier and lead-oxide vidicons, respectively, and  $G_{IV}$  is the electron gain of the intensifier-phosphor/lead-oxide vidicon-photosurface combination. If two intensifiers of unit magnification are added, the total electron gain is equal to  $G_{E,1-2} \times G_{IV}$ , where  $G_{E,1-2}$  is the electron gain of the intensifier-phosphor/intensifier-photocathode combination, it being assumed that both intensifiers have equal photocathode sensitivities. The square-wave response of the total tube combination is the product of the sine-wave responses of the individual intensifiers with the square-wave response of the PV.

b. Signal Transfer Characteristic. The apparent light gain due to the addition of a single intensifier of unit magnification is inferred from the experimentally measured shift in signal transfer characteristic, as shown in Fig. V-C-2. In this particular case, the shift gives a gain factor of 50. If the intensifier is assumed to have a photocathode sensitivity of 4 ma/watt and the PV to have a sensitivity of 3.42 ma/watt, the electron gain is about 42.6. If two intensifiers of unit magnification are added, the overall light gain is assumed to be 2000, and for three a value of 50,000 is arbitrarily taken. If, in addition, the input intensifier has a larger photocathode,



an additional light gain proportional to the ratio of its area to that of the PV is obtained. This is illustrated for the  $I^2$ -PV case in Fig. V-C-2. Note that, in adding a zoom intensifier, use will ordinarily be made of an 80/25-mm or 40/25-mm intensifier, but, because of the 21.4-mm photocathode, not all of the input photocathode is used. This is only a matter of current manufacturing practice, however, and not a fundamental limitation.

c. Amplitude Response. The sine-wave response of a single, a double, and a triple intensifier is obtained in units of TV lines/raster height by changing the scale of the abscissa of Fig. V-B-5. This is done by multiplying the number of line pairs/millimeter by twice the picture height ( $2 \times 0.6 \times 21.4$  mm, or 25.6, in this case). The square-wave response of the combined sensors is obtained by multiplying the sine-wave response of the appropriate intensifier(s) with the square-wave response of the PV, with the result as shown.\* It is seen that each additional intensifier has a considerable impact on response.

d. Video and Display Signal-to-Noise Ratio. The video signal-to-noise ratio for images of low spatial frequency and unit contrast  $SNR_{V,0,1}$  is given by

---

\* If  $R_{O,1}(N)$ ,  $R_{O,2}(N)$ , ... are the complex steady state frequency responses for various linear sensor apertures, and if  $R_{SQ}(N)$  is the complex steady state square-wave response, then

$$\begin{aligned} R_{SQ}(N) &= Sq(N) \times R_{O,1}(N) \times R_{O,2}(N) \dots \\ &= [Sq(N) R_{O,1}(N)] \times R_{O,2}(N) \dots \\ &= [Sq(N) R_{O,2}(N)] \times R_{O,1}(N) \dots \end{aligned}$$

where  $Sq(N)$  is the Fourier transform of a square wave.

$$\text{SNR}_{V,0,1} = \left[ \frac{G_{IV}^2 \sigma_I A_I E_{\max}}{e_v e_h} + \bar{I}_{PA}^2 \right]^{1/2} \quad (\text{V-C-13})$$

where  $\Delta f$  is as defined in Eq. V-C-17, p. 285.

Overall light gain was assumed to be 2000, for which the electron gain is about 1700. The specification in terms of input photocurrent is quite convenient because it permits curves of resolving power versus irradiance level to be generated for other values of photocathode or sensitivity by using Eq. V-B-2 or V-B-3. However, for convenience, irradiances corresponding to various values of photocurrent are tabulated on the figure for a number of photocathode areas.

e. Limiting Bar-Pattern Resolution. The limiting resolution versus photocathode irradiance characteristic is derived, as previously described, from Fig. V-C-8 and is plotted in Fig. V-C-9. For comparison, the limiting resolution of the unaided PV is shown as well. In Fig. V-C-10, limiting resolution is plotted in terms of line pairs/millimeter versus irradiance level for two values of contrast. For these curves, the input intensifier is assumed to be of the zoom type wherein the input photocathode area can be varied. The use of the line pairs/millimeter scale is quite convenient because it relates directly to scene resolving power and range. If one assumes no atmospheric degradation of contrast, vacuum range is equal to

$$R = 2X_g N_{LP} F_L \quad (\text{V-C-14})$$

where  $X_g$  is the scene "ground" resolution,  $N_{LP}$  is the resolving power in line pairs/millimeter, and  $F_L$  is the lens focal length in millimeters.

It is worthy to note that the largest input photocathode provides some advantage in resolving power at the very lowest scene irradiance levels, but the smaller photocathodes prevail over most of

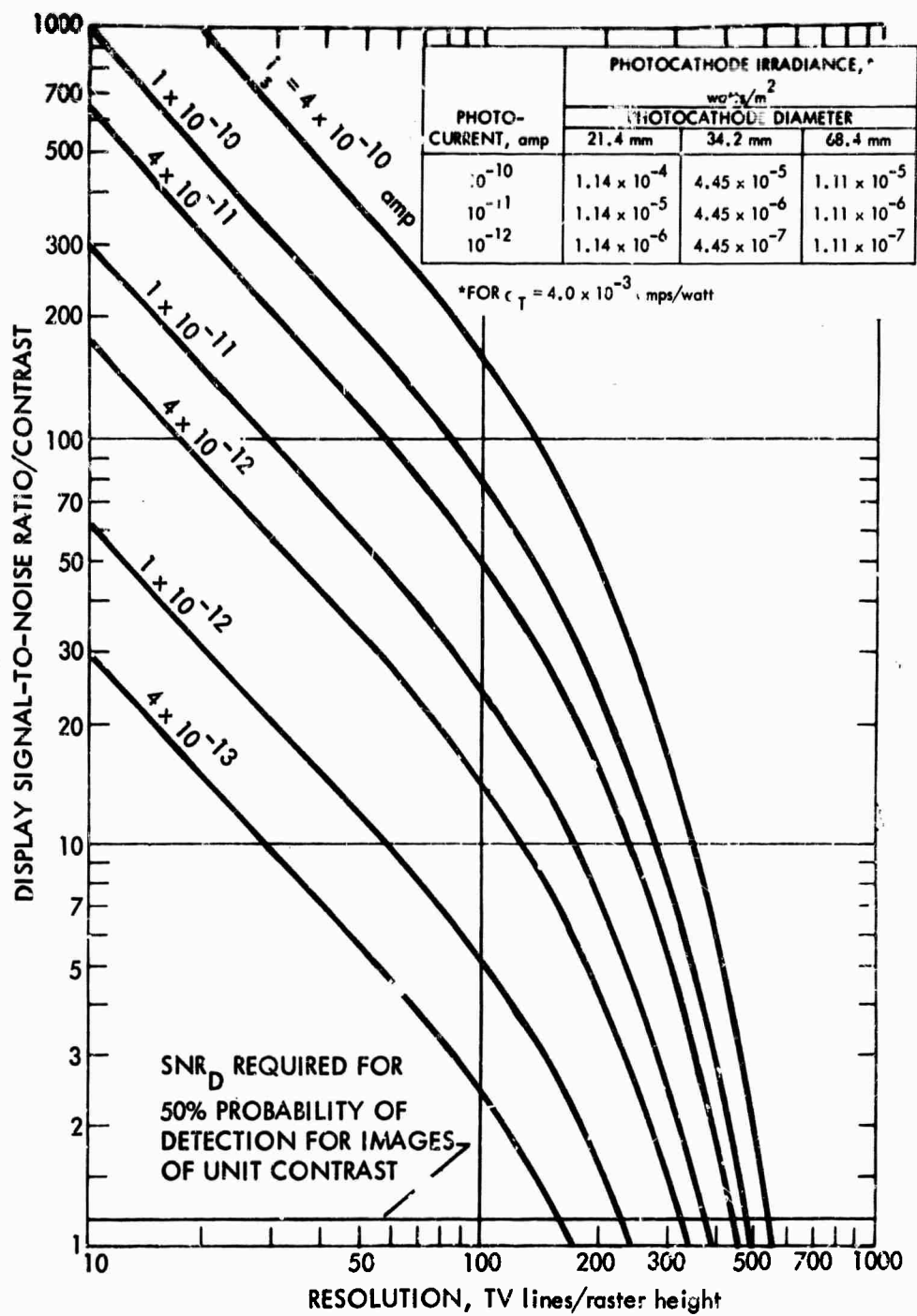


FIGURE V-C-8. Display Signal-to-Noise Ratio Versus Resolution for the Double-Intensifier Lead-Oxide Vidicon for Various Input Photocathode Currents

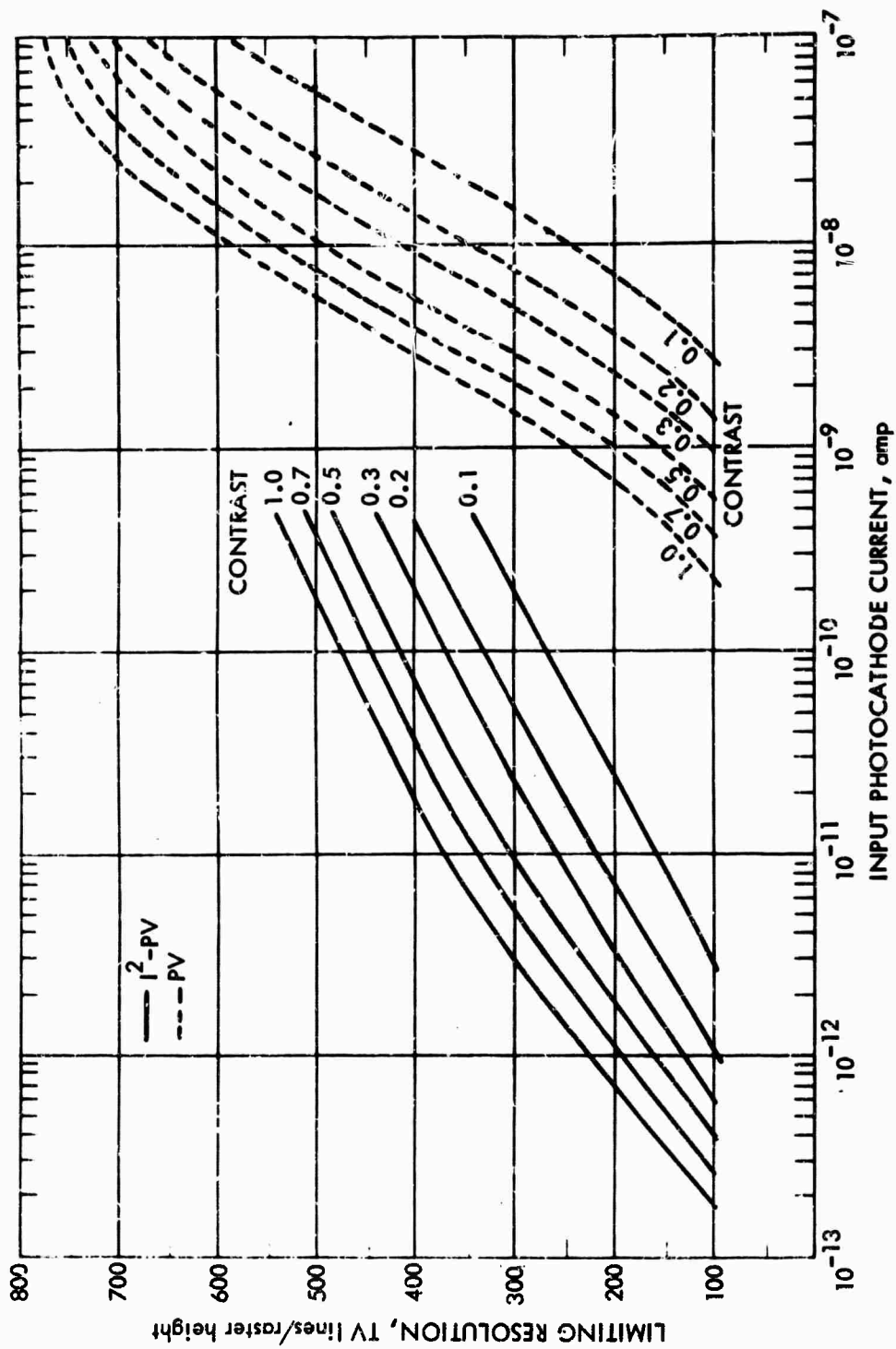


FIGURE V-C-9. Limiting Resolution Versus Input Photocathode Current for the 21.4-mm Lead-Oxide Vidicon and the Intensifier Lead-Oxide Vidicon for Various Input Image Contrasts

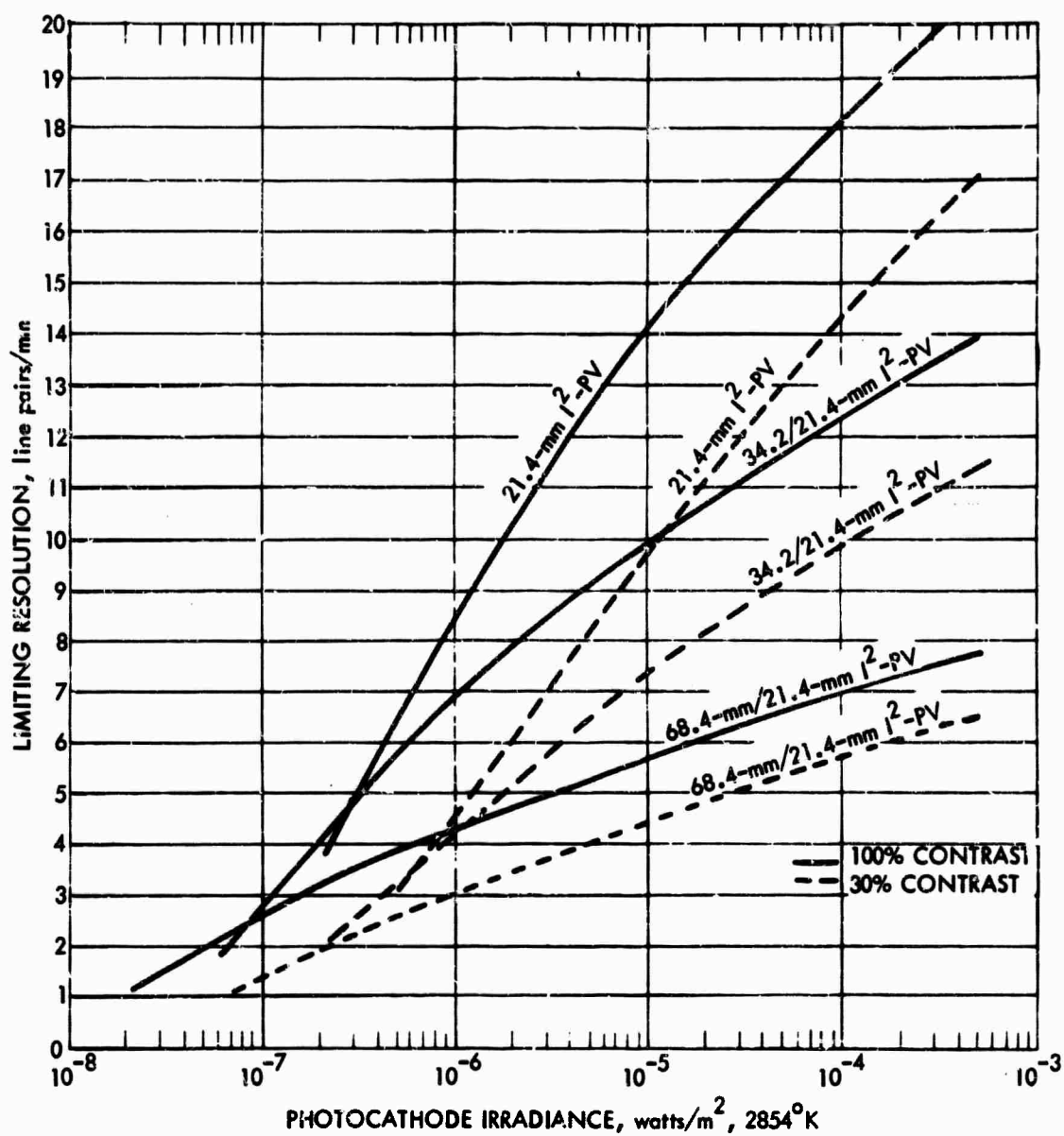


FIGURE V-C-10. Limiting Resolution Versus Photocathode Irradiance for the Double-Intensifier Lead-Oxide Vidicon

the operating range. The main merit of the larger photocathodes is that they provide a larger field of view.

f. Computed versus Measured Results. Measured results have not been obtained for intensifier lead-oxide tube combinations.

g. Lag Characteristics. The lag characteristics for multiple-intensifier lead-oxide vidicon combinations are estimated and shown in Fig. V-C-7. The method of estimation was simply to shift the lag characteristic of the PV by the amount of the apparent light gain provided by the intensifiers involved. This is probably optimistic because the intensifiers add lag of their own. Under starlight scene irradiance levels, sensor photocathode irradiance levels of  $10^{-6}$  watt/m<sup>2</sup> would not be unusual. As can be seen, the I<sup>2</sup>-PV appears to be marginal under these conditions, while an I<sup>3</sup>-PV would be acceptable. However, the relationships between lag, expressed as residual signal versus irradiance, and imaging of scenes in motion are not well known.

h. Form Factor. The 21.4-mm lead-oxide vidicon is approximately 7½ in. long and 1.2 in. in diameter. Adding two 25-mm intensifiers will increase length by about 5 in. and outside diameter to 2.5 or 3 in., including the high-voltage insulation. The use of a zoom intensifier together with a 25-mm intensifier would add 10.5 in. in length and increase outside diameter to 6 in.

### 3. The Vidicon

As previously stated, the term vidicon is restricted herein to mean those tubes in which the photosurface is an antimony-trisulfide photoconductor.

a. Principles of Operation. Except for the detailed photon-to-electron conversion mechanism in the primary photoprocess, the operation of the vidicon is identical to that of the PV. The main differences due to the photoconductor are that the gamma of the vidicon's signal transfer characteristic is 0.65, the lag due to the photoprocess is appreciable, and the dark current can be quite large. The vidicon's gamma of 0.65 is sometimes an advantage because it increases

dynamic light-latitude range and compensates somewhat for the larger-than-unity gammas of a cathode-ray tube display.

The lag of a vidicon can be reduced by making its photoconductor fluffy and thus thicker. However, this decreases sensitivity as well. In some applications, the lag is intentionally made long because this increases the signal storage capability of the surface and permits slow-scan operation. Another way to decrease lag, aside from control of the photocathode's physical dimensions, is by increasing the voltage across the photocathode. Actually, lag at a given photocurrent may increase somewhat as photosurface voltage is increased, but the increase in photosurface sensitivity obtained thereby usually results in a lower lag for a given value of input irradiance. Along with increased sensitivity, a larger photocathode potential results in an increase in dark current, which modulates surface nonuniformities and decreases picture quality.

b. Signal Transfer Characteristics. The vidicon is available in a wide variety of sizes, but only two will be treated here. The most common tubes available are those with a 16-mm or a 25-mm input photocathode diameter. The experimentally derived signal transfer curves are shown in Fig. V-C-11 for two dark currents, two types of faceplates, and two types of photocathode irradiance.

A fiber-optic faceplate version is available for use in conjunction with cascaded intensifiers. The transmission of the fiber-optic faceplate is lower than that of the usual glass faceplate and is variable, depending on the type of light incident. When the fiber-optic vidicon is used in conjunction with lenses of long focal length, the incident radiation approximates collimated light. When the input is the output of an intensifier phosphor, the incident radiation is diffuse. For a vidicon unaided by intensifiers, the glass faceplate version is appropriate and will be used here.

As can be seen, the gamma or slope of the signal transfer curve is less than unity and variable with irradiance, but it ordinarily falls in the 0.6- to 0.7-range. The curves of Fig. V-C-11 apply

equally to 16-mm or 25-mm vidicons, whereas one would ordinarily expect the larger tube to produce a larger current at a given irradiance level. The tube designers have apparently elected to decrease sensitivity as photoconductor size is increased to keep lag within bounds.

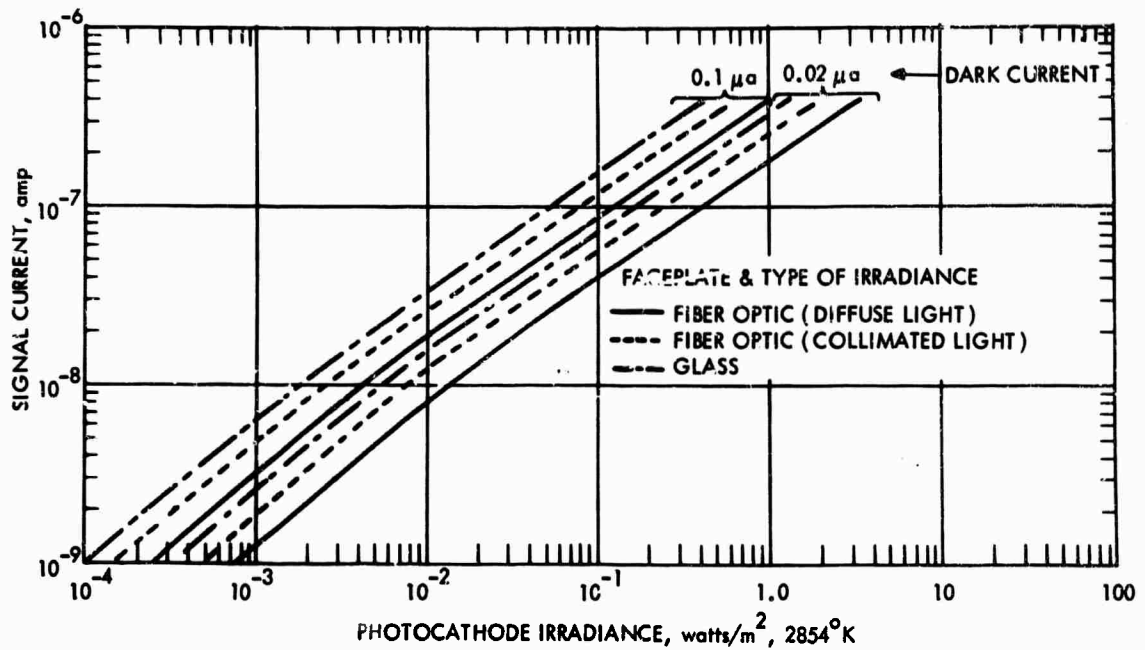


FIGURE V-C-11. Signal Current Versus Photocathode Irradiance Characteristic for the 16-mm or 25-mm Vidicon

The signal current from the vidicon, if one assumes a constant gamma  $\gamma$ , is given by the relation

$$I_S = (A_V K_V H)^\gamma / e_v e_h \quad (\text{V-C-15})$$

The incremental signal due to two unequally irradiated areas is given by

$$\begin{aligned} \Delta I_S &= (A_V K_V)^\gamma (E_{\max} - E_{\min})^\gamma / e_v e_h \\ &= [1 - (1-C)^\gamma] [A_V K_V E_{\max}]^\gamma / e_v e_h \end{aligned} \quad (\text{V-C-16})$$



where use has been made of the contrast relation of Eq. V-C-2. In the above expressions,  $K_V$  is a proportionality constant related to the photoconductor's sensitivity and  $A_V$  is the effective photocathode area.

c. Amplitude Response. The square-wave response of the 16-mm vidicon is shown in Fig. V-C-12, and the response for the 25-mm tube is shown in Fig. V-C-13. These curves apply either to high-quality magnetically focused and deflected vidicon cameras or to mixed-field types of vidicon of the "FPS" or "immersed deflection" types. The resolving power of the vidicon is seen to be quite good, the primary limitation being the finite diameter of the electron beam. In the case of the lead-oxide vidicon, the photocathode itself is limiting. In using the line pairs/millimeter scales shown for curves such as those in Fig. V-C-13, it is important to note that they apply to resolving power referred to the input photocathode only. Thus, the input photocathode diameter must be matched to the appropriate resolution scale.

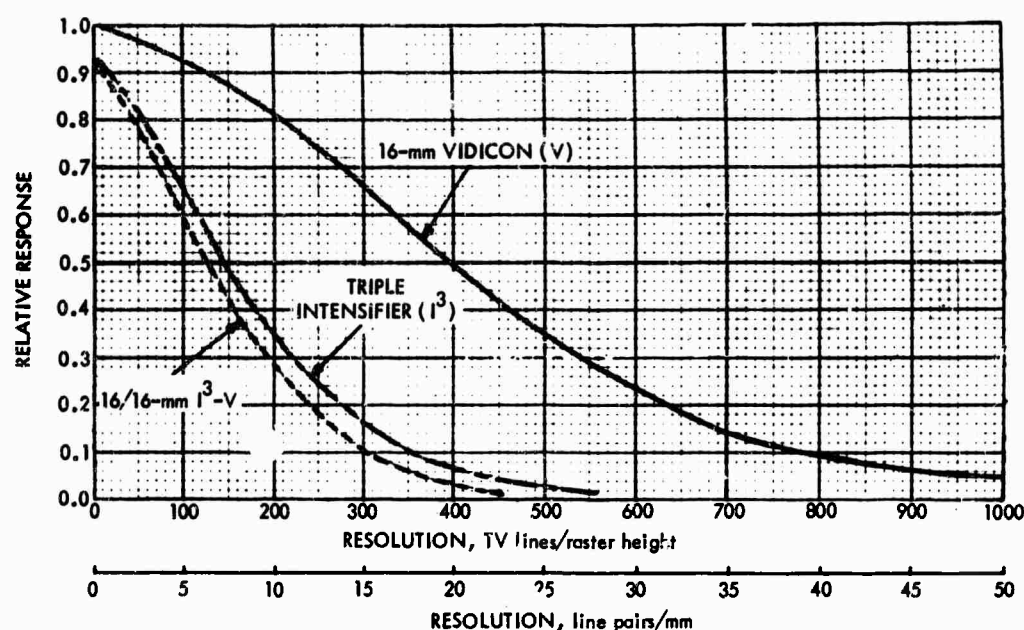


FIGURE V-C-12. Uncompensated Horizontal Square-Wave or Sine-Wave Response for the 16-mm Vidicon and 16/16-mm Triple Intensifier Vidicon. Intensifier Response is Sine Wave; Vidicon and Intensifier Vidicon Response is Square Wave

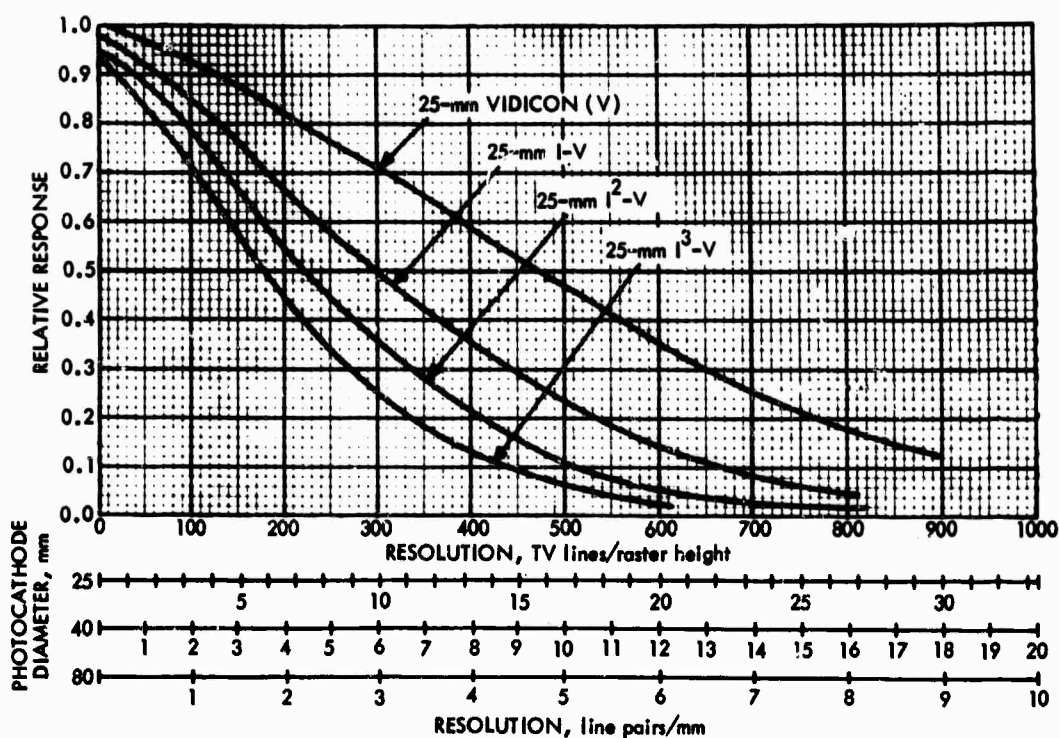


FIGURE V-C-13. Uncompensated Horizontal Square-Wave Response for the 25-mm Vidicon and its Intensifier Variants

d. Video and Display Signal-to-Noise Ratio. The unaided vidicon is preamplifier-noise limited over its entire operating range. Thus, the video signal-to-noise ratio becomes

$$SNR_{V,0,1} = \frac{[1 - (1 - (1 - C)^Y)] [A_V K_V E_{max}]^Y / e_v e_h}{\bar{I}_{PA}}$$

This ratio is plotted in Fig. V-C-14, in which a video bandwidth of 10 MHz and an rms preamplifier noise of 3 na are assumed.

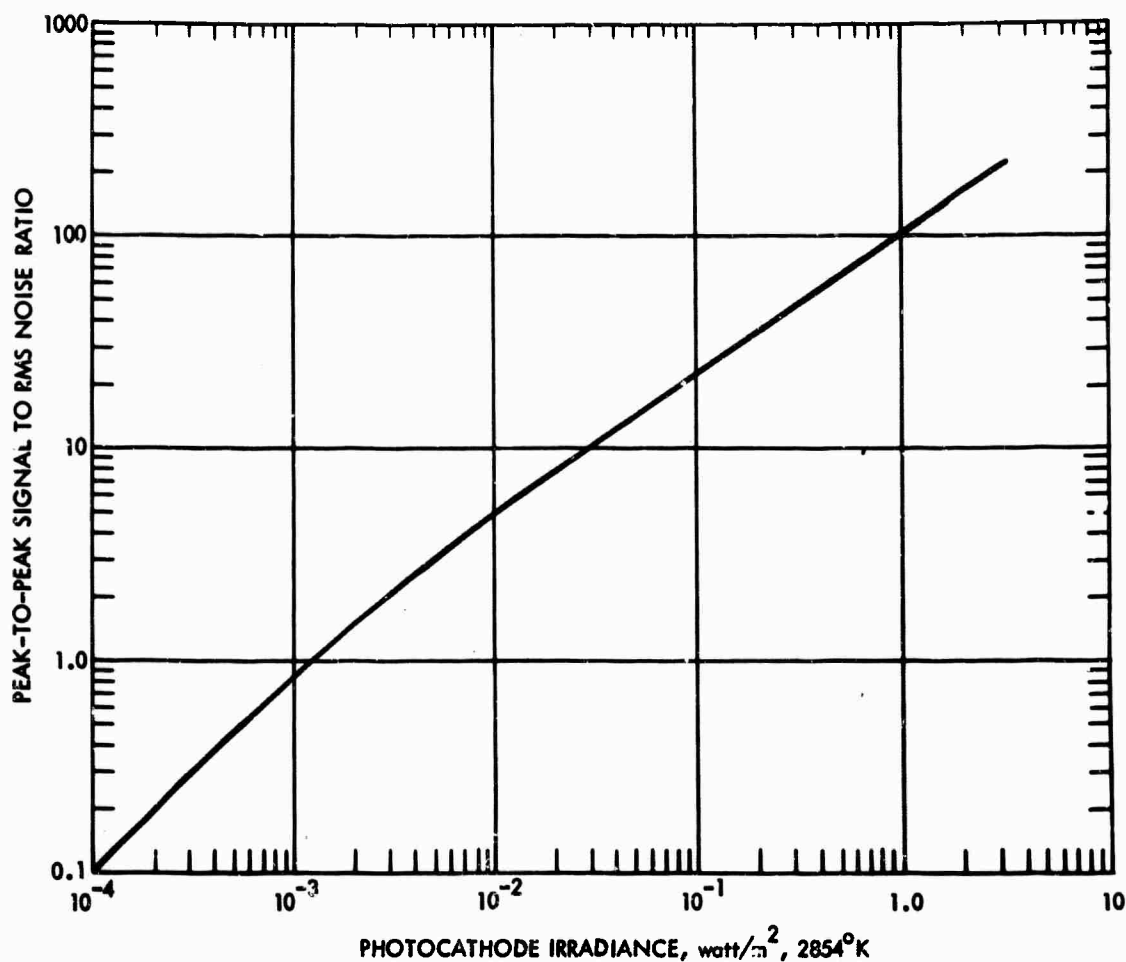


FIGURE V-C-14. Output Video Signal-to-Noise Ratio Versus Photocathode Irradiance Characteristic for the 16-mm or 25-mm Vidicon

The video signal-to-noise ratio is a function of the video bandwidth, as previously noted, because it increases the photoelectron and preamplifier noises. If both noises are white, then the video bandwidth has no effect on  $SNR_D$  and no effect on the resolution-irradiance level characteristics so long as the bandwidth is wide enough to pass the signal frequencies. This bandwidth is numerically equal to

$$\Delta f = \frac{\alpha}{2} \frac{N_H \cdot N_V}{e_v e_h} \quad (V-C-17)$$

where  $\alpha$  is the horizontal-to-vertical picture aspect ratio,  $N_H$  is the maximum horizontal resolution in TV lines/raster height, and  $N_V$  is the number of active scanning lines. For a conventional broadcast TV system, 525 lines are scanned but only 490 are active. The 35-line loss is due to signal blanking to permit the introduction of synchronizing signals into the video.

As a practical matter, the video bandwidth does affect the  $SNR_D$  in some instances because the preamplifier noise is not white but is rather an increasing function of frequency. This is a result of the necessity of compensating for the target's interelectrode capacitance. In this report, two bandwidths are used mainly to show the effect of bandwidth on video signal-to-noise ratio. However, the impact of video bandwidth on the limiting resolution versus irradiance level calculations is comparatively minor, particularly for cameras that approach the photoelectron noise limit.

The display signal-to-noise ratio for the vidicon is calculated as for the PV but is not shown.

e. Limiting Bar-Pattern Resolution. The limiting resolution versus irradiance characteristic for the 16-mm vidicon is determined from the  $SNR_D$  calculation and is plotted in Fig. V-C-15. It is pertinent to observe that it is not customary to report this characteristic because of lag. Like limiting resolution, lag is dependent on light level. By the time that the image irradiance is increased sufficiently to make lag acceptable for the imaging of scenes in motion (above about  $5 \times 10^{-2}$  watt/m<sup>2</sup>), the full resolving power of the vidicon is very nearly realized. Thus, the resolution versus light level characteristic is academic for all but very special applications.

f. Computed versus Measured Resolution. The results above were computed for a vidicon of comparatively high resolving power. The only data available to the author were for a standard "broadcast" vidicon whose amplitude response might be expected to be somewhat below that used in the calculations (but very good, nevertheless). As can be seen in Fig. V-C-16, fairly good correlation is observed at the lower

line numbers, the departure at the higher line numbers being undoubtedly due to the broadcast vidicon's more limited spatial response.

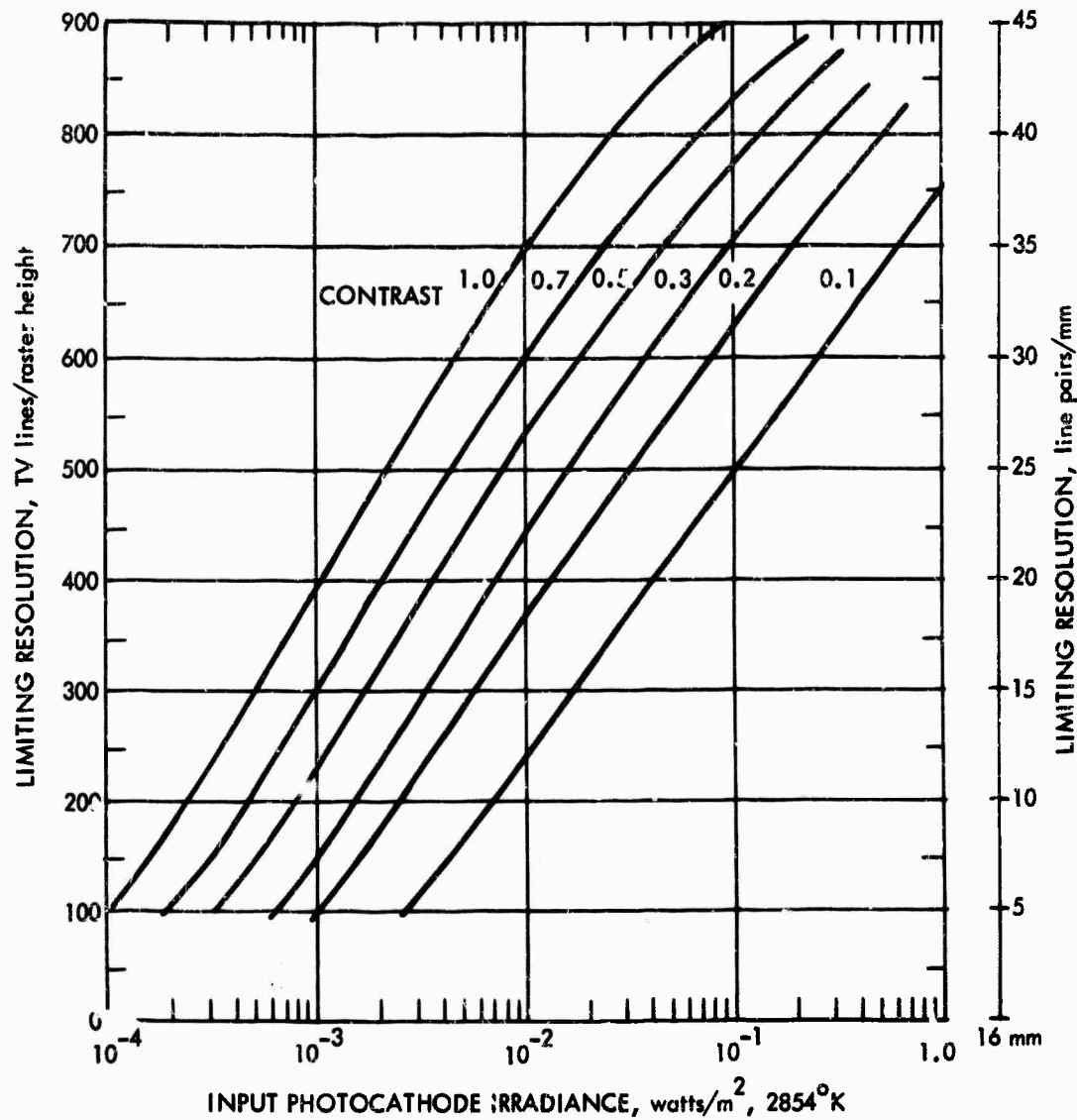


FIGURE V-C-15. Limiting Resolution Versus Input Photocathode Irradiance for the 16-mm Vidicon with 0.02  $\mu$ a Dark Current

-g. Lag Characteristics. The third field lag characteristics for the 16- and 25-mm vidicon are estimated and plotted in Fig. V-C-17. As can be seen, the lag becomes excessively high with photocathode

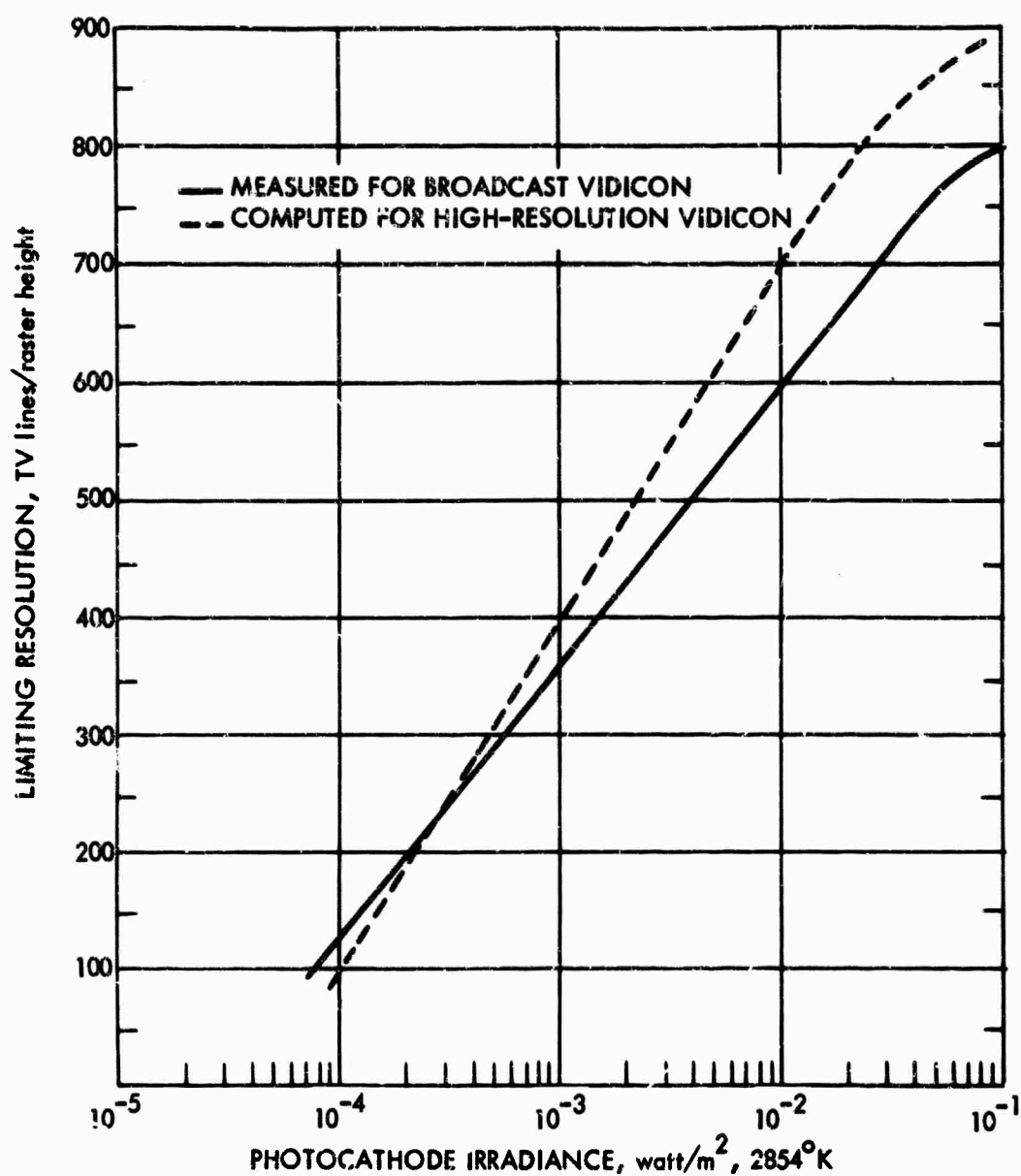
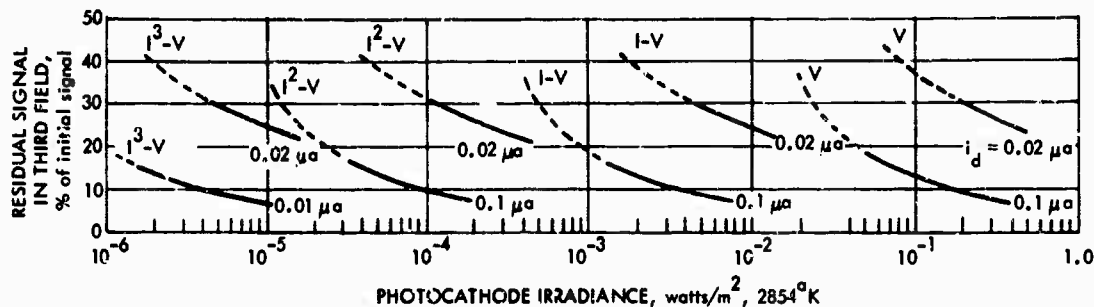


FIGURE V-C-16. Limiting Resolution Versus Input Photocathode Irradiance -- Comparison of Measured and Computed Performance

irradiances in the  $10^{-2}$  to  $10^{-1}$  watt/m<sup>2</sup> range. In Fig. V-C-15, we note that the vidicon still has substantial resolving power at irradiance levels of  $10^{-4}$  to  $10^{-3}$  watt/m<sup>2</sup>, but this sensitivity would not be usable when imaging scenes in motion.



**FIGURE V-C-17. Signal Lag Versus Photocathode Irradiance Characteristic Estimated for Various Vidicons and Intensifier Vidicons with Either 16-mm or 25-mm Input Photocathodes and Two Values of Dark Current**

h. Form Factor. Vidicons are manufactured in a wide variety of configurations and sizes. The 16-mm versions are usually 5 in. to 6.5 in. long and 1-1/8 in. in diameter while the 25-mm versions are 7.5 in. to 8.5 in. long and 1.5 in. to 2 in. in diameter.

i. Manufacturers' Literature. A sample of manufacturers' literature on vidicons will be found in Chart V-3-1.

#### 4. Intensifier Vidicon Cameras

a. Principles of Operation. By coupling a sufficient number of intensifiers to a vidicon with a fiber-optic faceplate, low-light-level capability can be achieved. In general, it will be found that the number of intensifiers needed to achieve an adequate lag characteristic will be greater than the number needed merely to gain sufficient sensitivity. Ordinarily, at least three intensifiers will be needed to image moving night scenes irradiated only by natural sources. In special applications, however, combinations with only one or two intensifiers may be of interest. When an intensifier is used, the primary photoprocess becomes linear rather than sublinear as is the

CHART V-C-1. A SAMPLE OF MANUFACTURERS' LITERATURE  
ON VIDICONS\*

The units, definitions, and methods of measurement specified herein are not necessarily endorsed by the authors but are those used by the manufacturer quoted.

---

\* For table footnotes see page 301.



# Choose from these Categories

**Focus and Deflection Method**  
Magnetic-focus, magnetic deflection vidicons provide highest center and corner resolution but require the most electrical power and result in TV cameras having the most weight.

Magnetic-focus, electrostatic deflection vidicons have resolution capabilities and power requirements essentially equivalent to those of all-magnetic type vidicons. Tubes having this construction feature very short overall length compared with other vidicon structures and in this area provides a unique advantage over the other types.

Electrostatic-focus, magnetic deflection vidicons have intermediate resolution capability, require intermediate electrical power, and find use in compact lightweight cameras.

Electrostatic-focus, electrostatic deflection vidicons require the least electrical power of all vidicon structures and are intended for use in TV cameras that approach the ultimate in package size and weight. The resolution capability of this type vidicon, however, is usually less than that of other type vidicons when operating voltages are the same.

**Separate Mesh Electrode**  
RCA Vidicons are available with

separate mesh connection or with conventional mesh connection. Separate mesh connection vidicons provide higher and more uniform resolution and more uniform signal output when operated at high voltage than do comparable size vidicons having mesh and wall electrodes connected.

**Heater Power**  
RCA Vidicons are available with conventional 3.8 Watt Heaters, with 1.9 Watt Heaters, and with 0.6 Watt "Dark Heaters" for transistorized TV Cameras.

**Tube Diameter**  
Larger tube diameter provides more TV lines per picture height.

Magnetic-Focus Magnetic-Deflection Vidicons					Magnetic-Focus Electrostatic-Deflection Vidicons	Electrostatic-Focus Magnetic-Deflection Vidicons		Electrostatic-Focus Electrostatic-Deflection Vidicons	Heater Power
1/2" Diameter Types	1" Diameter Types	1-1/2" Diameter Types	2" Diameter Types	4-1/2" Diameter Types	1" Diameter Types	1" Diameter Types	1-1/2" Diameter Types	1" Diameter Types	
Conventional Mesh Connection	4427	2048* 7262A 7263A*							≤0.6W
		4478 4500 7038 7735 7735A 7735B							≤3.8W
Separate Mesh Connection	C23104	4542 8541A 8573A C23066 C23136+		C23061A ♦ C23063		C23073A*■	4493 8134 4494 8134/VI 4495 8567*	8490 8490/VI C23033	≤0.6W
		4603A* C23113■						4514*	≤1.9W
		8507A 8572A	8061 8521		C74137A ♦				≤3.8W

\*Ruggedized Type      ♦ Return-Beam Vidicon Type      ■ Vidicon Assembly      + Silicon Target Type

Type numbers with prefix C are developmental types. Each of these C numbers identifies a particular laboratory tube design but the number and the identifying data are subject to change. No obligations are assumed as to future manufacture unless otherwise arranged.

A

Type	Typical Applications	Description Remarks	Focus- ing Method	Deflec- tion Method	Photo- con- ductor <sup>a</sup>	Maximum Overall Length inches	Bulb Dis- meter <sup>b</sup> inches	Typical Operati		
								Operating Mode	Max. Target Voltage for Indicated Dark Current volts	Dark Current microampere

## High-Performance Broadcast-Quality Types for Studio Film Pickup Service

7038	Television Film Pickup	<ul style="list-style-type: none"> <li>High Resistance to Image "Burn-In"</li> <li>Target Stringently Controlled for Blemishes</li> <li>Low Lag</li> </ul>	M	M	I	6.50	1.020 +.030 -.035	Av. Sens. Min. Lag	60 30	0.02 0.004
8572A	TV Film Pickup	<ul style="list-style-type: none"> <li>Similar to the 7038 But Has Separate Mesh Connection</li> <li>High Resolution</li> </ul>	M	M	I	6.375	1.020 +.030 -.035	Av. Sens. Min. Lag	60 30	0.02 0.004
8051	Television Film Pickup and Data Transmission Service	<ul style="list-style-type: none"> <li>Very High Resolution</li> <li>High Resistance to Image "Burn-In"</li> <li>Separate Mesh Connection</li> </ul>	M	M	I	8.00	1.50 +.01	Av. Sens. Min. Lag	50 30	0.02 0.005
8134/V1	Transistorized Cameras in Color Film Pickup Applications	<ul style="list-style-type: none"> <li>A Variant of the 8134 (pgs 8 and 9) Having Extremely Stringent Test Criteria to Guarantee High Performance in Color Cameras</li> </ul>	E	M	II	6.35	1.025 ±.003	High Sens. Av. Sens.	60 48	0.10 0.035
8480	Transistorized Cameras for Broadcast Film Pickup & Data Transmission Applications	<ul style="list-style-type: none"> <li>Low Deflection and Focus Power</li> <li>Very High Resolution</li> <li>Low Power (0.6W) "Dark Heater"</li> <li>Separate Mesh Connection</li> </ul>	E	M	I	10.375	1.500 ±.005	Av. Sens. Min. Lag	60 30	0.02 0.005
8480/V1	Transistorized Cameras in Color Film Pickup Applications	<ul style="list-style-type: none"> <li>A Variant of the 8480 Having Extremely Stringent Test Criteria to Guarantee High Performance in Color Cameras</li> </ul>	E	M	I	10.375	1.500 ±.005	Av. Sens. Min. Lag	60 30	0.02 0.005

## Vidicons for Live TV and Industrial Service

### Non-Critical Closed-Circuit Applications

4478	Non-Critical TV Systems	<ul style="list-style-type: none"> <li>Economy Priced Type</li> <li>Mechanically Similar to 7735B</li> </ul>	M	M	II	6.50	1.020 +.030 -.035	Av. Sens.	70	0.035
------	-------------------------	--	---	---	----	------	-------------------------	-----------	----	-------

1 B

Part Number	Typical Operating Conditions						Typical Resolution at Operating Light Level		Type
	Operating Mode	Max. Target Voltage for Indicated Dark Current volts	Dark Current microampere	Signal Output Current microampere	Illumination		Amplitude Response at 400 TV Lines per cent	Limiting Resolution TV Lines	
					On Tube Face <sup>d</sup> footcandles	On Scene <sup>e</sup> footcandles			
020 030 035	Av. Sens. Min. Lag	60 30	0.02 0.004	0.4 0.3	15 100	— —	30 30	750 750	7038
020 030 035	Av. Sens. Min. Lag	60 30	0.02 0.004	0.3 0.3	10 100	— —	60k 60k	1100k 1100k	8572A
500 01	Av. Sens. Min. Lag	50 30	0.02 0.005	0.5 0.5	10 50	— —	65 65	1500 1500	8051
025 003	High Sens. Av. Sens.	60 45	0.10 0.035	0.10 0.265	0.1 1.0	25 250	25 25	700 700	8134/V1
500 005	Av. Sens. Min. Lag	60 30	0.02 0.005	0.5 0.5	10 50	— —	60 60	1400 1400	8480
500 005	Av. Sens. Min. Lag	60 30	0.02 0.005	0.5 0.5	10 50	— —	60 60	1400 1400	8480/V1
020 030 035	Av. Sens.	70	0.035	0.265	1.0	250	—	650	4478

A

Type	Typical Applications	Description Remarks	Focus- ing Method	Deflec- tion Method	Photo- con- ductor <sup>a</sup>	Maximum Overall Length inches	Bulb Dia- meter <sup>b</sup> inches	Opera- ting Mode
------	----------------------	------------------------	-------------------------	---------------------------	---------------------------------------	--	--	------------------------

### Vidicons for Live TV and Industrial Service (cont'd)

#### General Closed-Circuit Applications

7735	Economy Priced Type For General Closed-Circuit TV Systems	<ul style="list-style-type: none"> <li>• Good Sensitivity</li> <li>• Mechanically Similar to 77358</li> </ul>	M	M	II	6.50	1.020 +.030 -.035	Av. S
7735A	For General Closed-Circuit TV Systems	<ul style="list-style-type: none"> <li>• Good Sensitivity</li> <li>• Low Lag</li> <li>• Mechanically Similar to 77358</li> </ul>	M	M	II	6.50	1.020 +.030 -.035	Av. S

#### High-Performance Broadcast and Industrial Applications

4427	Compact, Transistorized Industrial TV Cameras	<ul style="list-style-type: none"> <li>• Short 1/2" Diameter Type</li> <li>• Uses 8mm Film Lens System</li> <li>• Low Power (0.6W) "Dark Heater"</li> </ul>	M	M	II	3.40	0.520 +.030 -.020	Max.
7262A	Live TV and Industrial Transistorized Cameras	<ul style="list-style-type: none"> <li>• Short Sturdy Type</li> <li>• Low Power (0.6W) "Dark Heater"</li> <li>• Electrical Characteristics Similar to the 77358</li> <li>• Low Microphonics</li> </ul>	M	M	II	5.18	1.020 +.030 -.035	High S Av. S
8573A	Live TV and Industrial Transistorized Cameras	<ul style="list-style-type: none"> <li>• Similar to 7262A but Has Separate Mesh Connection</li> <li>• High Resolution</li> <li>• Low Power (0.6W) "Dark Heater"</li> </ul>	M	M	II	5.18	1.020 +.030 -.035	High Av. S
7735B	High-Quality Live TV and Industrial Cameras	<ul style="list-style-type: none"> <li>• High Sensitivity</li> <li>• Low Lag</li> <li>• High Resolution</li> <li>• Target Stringently Controlled for Blemishes</li> </ul>	M	M	II	6.50	1.020 +.030 -.035	High Av. S
8507A	Live TV and Industrial Pickup Service	<ul style="list-style-type: none"> <li>• High Resolution 1" Diameter Type</li> <li>• Separate Mesh Connection</li> <li>• Supersedes 8507</li> </ul>	M	M	II	6.375	1.020 +.030 -.035	High Av. S

1 B

Photo-tube <sup>a</sup>	Maximum Overall Length inches	Bulb Dia-meter <sup>b</sup> inches	Typical Operating Conditions						Typical Resolution at Operating Light Level		Type
			Operating Mode	Max. Target Voltage for Indicated Dark Current volts	Dark Current microampere	Signal Output Current <sup>c</sup> micro-ampere	Illumination		Amplitude Response at 400 TV Lines per cent	Limiting Resolution <sup>f</sup> TV Lines	
							On Tube Faced <sup>d</sup> footcandles	On Scene <sup>e</sup> footcandles			
6.50	1.020 +.030 -.035	Av. Sens.	55	0.02	0.15 (min.)	1.0	250	—	700	7735	
6.50	1.020 +.030 -.035	Av. Sens.	40	0.02	0.15 (min.)	1.0	250	—	700	7735A	
3.40	0.520 +.030 -.020	Max. Sens.	90	0.05	0.08	0.4	100	5	400	4427	
5.18	1.020 +.030 -.035	High Sens. Av. Sens.	60 40	0.10 0.02	0.10 0.20	0.1 1.0	25 250	30 30	750 750	7262A	
5.18	1.020 +.030 -.035	High Sens. Av. Sens.	60 40	0.10 0.02	0.10 0.20	0.1 1.0	25 250	60 <sup>k</sup> 60 <sup>k</sup>	1100 <sup>k</sup> 1100 <sup>k</sup>	8573A	
6.50	1.020 +.030 -.035	High Sens. Av. Sens.	50 40	0.10 0.025	0.27 0.275	0.5 1.0	125 250	30 30	750 750	7735B	
6.375	1.020 +.030 -.035	High Sens. Av. Sens.	60 40	0.10 0.02	0.10 0.20	0.1 1.0	25 250	60 <sup>k</sup> 60 <sup>k</sup>	1100 <sup>k</sup> 1100 <sup>k</sup>	8507A	

Type	Description  Typical Applications  Remarks	Focus- ing Method	Deflec- tion Method	Photo- con- ductor <sup>a</sup>	Maximum Overall Length inches	Bulb Dia- meter <sup>b</sup> inches	Operating Mode	M V In D vo

## Vidicons for Live TV and Industrial Service (cont'd)

### High-Performance Broadcast and Industrial Applications (cont'd)

8541A	Transistorized Cameras For Live Scene and TV Film Pickup	<ul style="list-style-type: none"> <li>• Low Heater Power Variant of the 8507A</li> <li>• High Resolution 1"-Diameter Type</li> <li>• Separate Mesh Connection</li> </ul>	M	M	II	6.375	1.020 +.030 -.035	High Sens. Av. Sens.
4493 4494 4495	Chroma Channels of Live Pickup Color Cameras	<ul style="list-style-type: none"> <li>• Very Low Lag</li> <li>• High Degree of Signal Uniformity</li> <li>• Precision Outer-Diameter Bulb</li> <li>• Low Power (0.6W) "Dark Heater"</li> </ul>	E	M	II	6.35	1.025 ±.003	Av. Sens.
8134	Transistorized Cameras for Live TV, Industrial, and Color TV Service	<ul style="list-style-type: none"> <li>• Low Deflection and Focus Power</li> <li>• Low Power (0.6W) "Dark Heater"</li> <li>• Precision Outer-Diameter Bulb</li> </ul>	E	M	II	6.35	1.025 ±.003	High Sens. Av. Sens.

### High-Performance Vidicons for Space, Military and Special Industrial Service

4500	Slow-Speed Scan Pickup Systems or Limited-Motion Industrial TV	<ul style="list-style-type: none"> <li>• Very High Sensitivity</li> <li>• Extended Lag Characteristics</li> <li>• Interchangeable in Cameras Using 1" All-Magnetic Vidicons</li> </ul>	M	M	III	6.50	1.020 +.030 -.035	Av. Sens. Slow-Scan
4514	Space, Military, and Special Industrial (For government end use only)	<ul style="list-style-type: none"> <li>• Ruggedized</li> <li>• Separate Mesh Connection</li> <li>• Precision Outer-Diameter Bulb</li> <li>• 1.9 Watt Heater</li> </ul>	E	E	II	5.81	1.013 ±.002	Av. Sens.
4542	Weather Radar and High-Sensitivity Signal Storage Systems	<ul style="list-style-type: none"> <li>• Very Long Lag</li> <li>• Separate Mesh Connection</li> <li>• Low Power (0.6W) "Dark Heater"</li> </ul>	M	M	IV	6.375	1.020 +.030 -.035	High Sens.
8521	Industrial TV Cameras	<ul style="list-style-type: none"> <li>• Very High Resolution</li> <li>• Separate Mesh Connection</li> <li>• High Sensitivity</li> </ul>	M	M	II	8.0	1.50 ±.01	High Sens. Av. Sens.

1 B

Bulb Diameter <sup>b</sup> inches	Typical Operating Conditions						Typical Resolution at Operating Light Level		Type
	Operating Mode	Max. Target Voltage for Indicated Dark Current volts	Dark Current microamperes	Signal Output Current <sup>c</sup> micro- ampere	Illumination		Amplitude Response at 400 TV Lines per cent	Limiting Resolution <sup>f</sup> TV Lines	
					On Tube Faced <sup>d</sup> footcandles	On Scene <sup>e</sup> footcandles			
1.020 +.030 -.035	High Sens. Av. Sens.	60 40	0.10 0.02	0.10 0.20	0.1 1.0	25 250	60k 60k	1100k 1100k	8541A
1.025 ±.003	Av. Sens.	35 35 35	0.01 0.01 0.005	0.0359 0.089 0.0309	1.59 5.09 4.09	— — —	70h 70h 70h	500 500 500	4493 4494 4495
1.025 ±.003	High Sens. Av. Sens.	60 48	0.10 0.035	0.10 0.265	0.1 1.0	25 250	25 25	700 700	8134
1.020 +.030 -.035	Av. Sens. Slow Scan	25 30 typ.	0.005 0.008	0.4 0.07 <sup>i</sup>	1.0 0.25 fc-s <sup>j</sup>	25 —	20 50k	600 —	4500
1.013 ±.002	Av. Sens.	50	0.02	0.20	1.0	250	—	750	4514
1.020 +.030 -.035	High Sens.	65	0.02	0.2	0.1	25	60	1000	4542
1.50 ±.01	High Sens. Av. Sens.	60 35	0.10 0.02	0.2 0.2	0.1 1.0	25 250	65 65	1500 1500	8521

Type	Description	Typical Applications	Remarks	Focus ing Method	Deflec- tion Method	Photo- con- ductor <sup>a</sup>	Maximum Overall Length inches	Bulb Dia- meter <sup>b</sup> inches	Typ	
									Operating Mode	Max. Target Voltage for Indicated Dark Current volts

## High-Performance Vidicons for Space, Military and Special Industrial Service (cont'd)

8480	Transistorized Cameras for Broad- cast Film Pickup and Data Transmis- sion Applications	<ul style="list-style-type: none"> <li>• Low Deflection-and-Focus Power</li> <li>• Very High Resolution</li> <li>• Low Power (0.6W) "Dark Heater"</li> <li>• Separate Mesh Connection</li> </ul>		E	M	I	10.375	1.500 ±.005	Av. Sens. Min. Lag	60 30
2048	Space, Military, & Special Industrial	<ul style="list-style-type: none"> <li>• Short Ruggedized Type</li> <li>• Special Target Connector</li> <li>• Precision Outer-Diameter Bulb</li> <li>• Low Power (0.6W) "Dark Heater"</li> </ul>		M	M	I	5.214	1.025 ±.003	Max. Sens. Av. Sens.	100 60
7263A	Space, Military, & Special Industrial Transistorized Cameras	<ul style="list-style-type: none"> <li>• Short Ruggedized Type</li> <li>• Electrically Similar to the 7262A</li> <li>• Low Power (0.6W) "Dark Heater"</li> </ul>		M	M	II	5.18	1.020 +.030 -.035	High Sens. Av. Sens.	60 40
4503A	Space, Military and Special Industrial	<ul style="list-style-type: none"> <li>• Short Ruggedized Type</li> <li>• High Sensitivity</li> <li>• Low Lag</li> <li>• Low Power (1.0 W) Heater</li> </ul>		M	M	II	5.25	1.025 ±.003	High Sens. Av. Sens.	60 40
8567	Space, Military, & Industrial Transis- torized TV Cameras	<ul style="list-style-type: none"> <li>• Ruggedized</li> <li>• Precision Outer-Diameter Bulb</li> <li>• Low Power (0.6W) "Dark Heater"</li> </ul>		E	M	II	6.35	1.025 ±.003	High Sens. Av. Sens.	60 40

<sup>a</sup>For spectral response characteristics and description of specified photoconductive surface, see page 14. The scanned area of the photoconductive surface for 1/2", 1", and 1-1/2" diameter vidicons is 0.24" x 0.18", 1/2" x 3/8", and 3/5" x 4/5", respectively. However, scanned area for type 4542 is 5/8" x 5/8".

<sup>b</sup>Maximum diameter of target flange for 1/2", 1", and 1-1/2" diameter vidicons is 0.574", 1.135" and 1.60", respectively.

<sup>c</sup>Defined as the component of highlight target current after the dark-current component has been subtracted.

<sup>d</sup>Indicated values of illumination are those required to obtain optimum signal from the tube. Values of illumination t/t<sub>0</sub> of those indicated will still produce a picture of usable quality.

<sup>e</sup>Assumes a lens setting of f/5.6, lens transmission of 80%, and that highlight scene reflectance is 60%.

<sup>f</sup>The resolution capability of all focusing coil current and deflect

<sup>g</sup>These characteristics are measure  
For type 4493 (Rad)  
For type 4494 (Gree)  
For type 4495 (Blue)

<sup>h</sup>Response to a 125 TV line square

<sup>i</sup>For a field time of 2 seconds, no

<sup>k</sup>Values are for high-voltage tube



Typical Operating Conditions						Typical Resolution at Operating Light Level		Type
Operating Mode	Max. Target Voltage for Indicated Dark Current volts	Dark Current microampere	Signal Output Current <sup>c</sup> micro-ampere	Illumination		Amplitude Response at 400 TV Lines per cent	Limiting Resolution <sup>f</sup> TV Lines	
				On Tube Faced <sup>d</sup> footcandles	On Scene <sup>e</sup> footcandles			
Av. Sens.	60	0.02	0.5	10	—	60	1400	8480
Min. Lag	30	0.005	0.5	50	—	60	1400	
Max. Sens.	100	0.20	0.3	2	—	30	750	2048
Av. Sens.	60	0.02	0.3	10	—	30	750	
High Sens.	60	0.10	0.10	0.1	25	30	750	7263A
Av. Sens.	40	0.02	0.20	1.0	250	30	750	
High Sens.	60	0.10	0.10	0.1	25	60 <sup>k</sup>	1100 <sup>k</sup>	4503A
Av. Sens.	40	0.02	0.20	1.0	250	60 <sup>k</sup>	1100 <sup>k</sup>	
High Sens.	60	0.10	0.10	0.1	25	25	700	8567
Av. Sens.	40	0.02	0.20	1.0	250	25	700	

<sup>f</sup> The resolution capability of all vidicons may be increased by operating the tubes at voltages up to the maximum ratings and by increasing the focusing-coil current and deflecting-coil power.

<sup>g</sup> These characteristics are measured using the following standard optical filters, or equivalent

For type 4493 (Red) — Wratten No. 25 (A) with 2 Fish-Shurman No. IR650

For type 4494 (Green) — Wratten No. 58 with 1 Fish-Shurman No. IR650

For type 4495 (Blue) — Wratten No. 47 with 1 Fish-Shurman No. IR650

<sup>h</sup> Response to a 125 TV line square-wave test pattern with 1/4" x 3/16" scan raster.

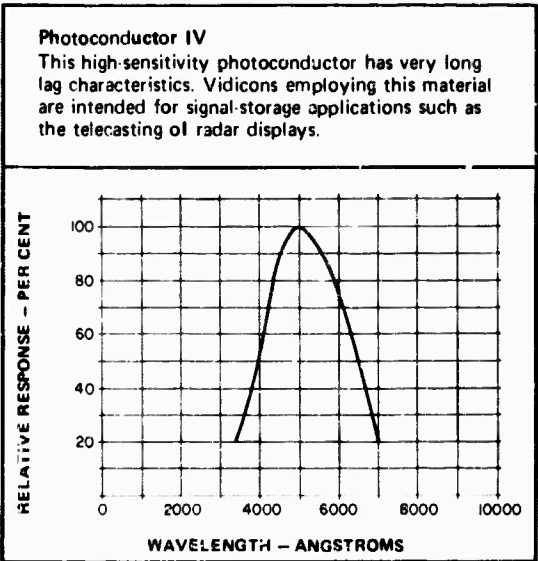
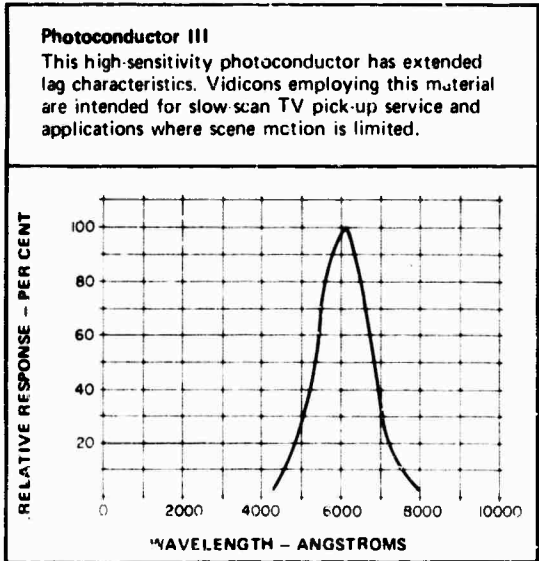
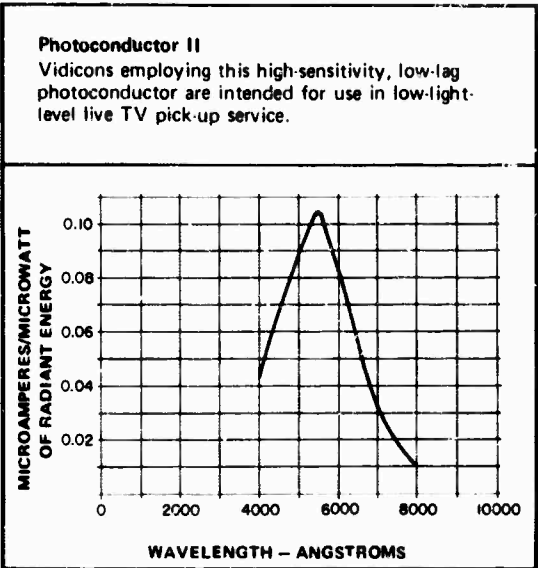
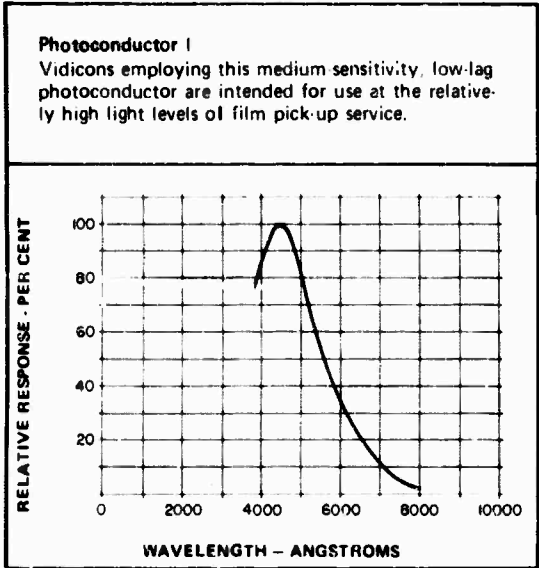
<sup>i</sup> For a field time of 2 seconds, non-interlaced.

<sup>k</sup> Values are for high-voltage tube operation.

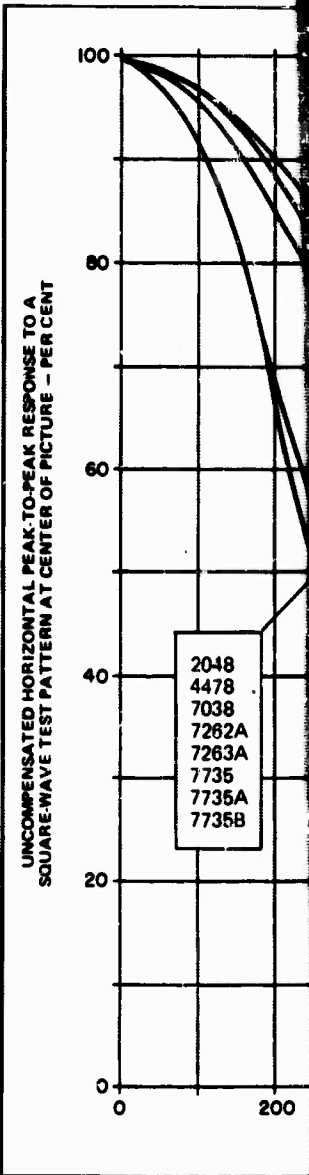
A

# Selected Characteristic Curves

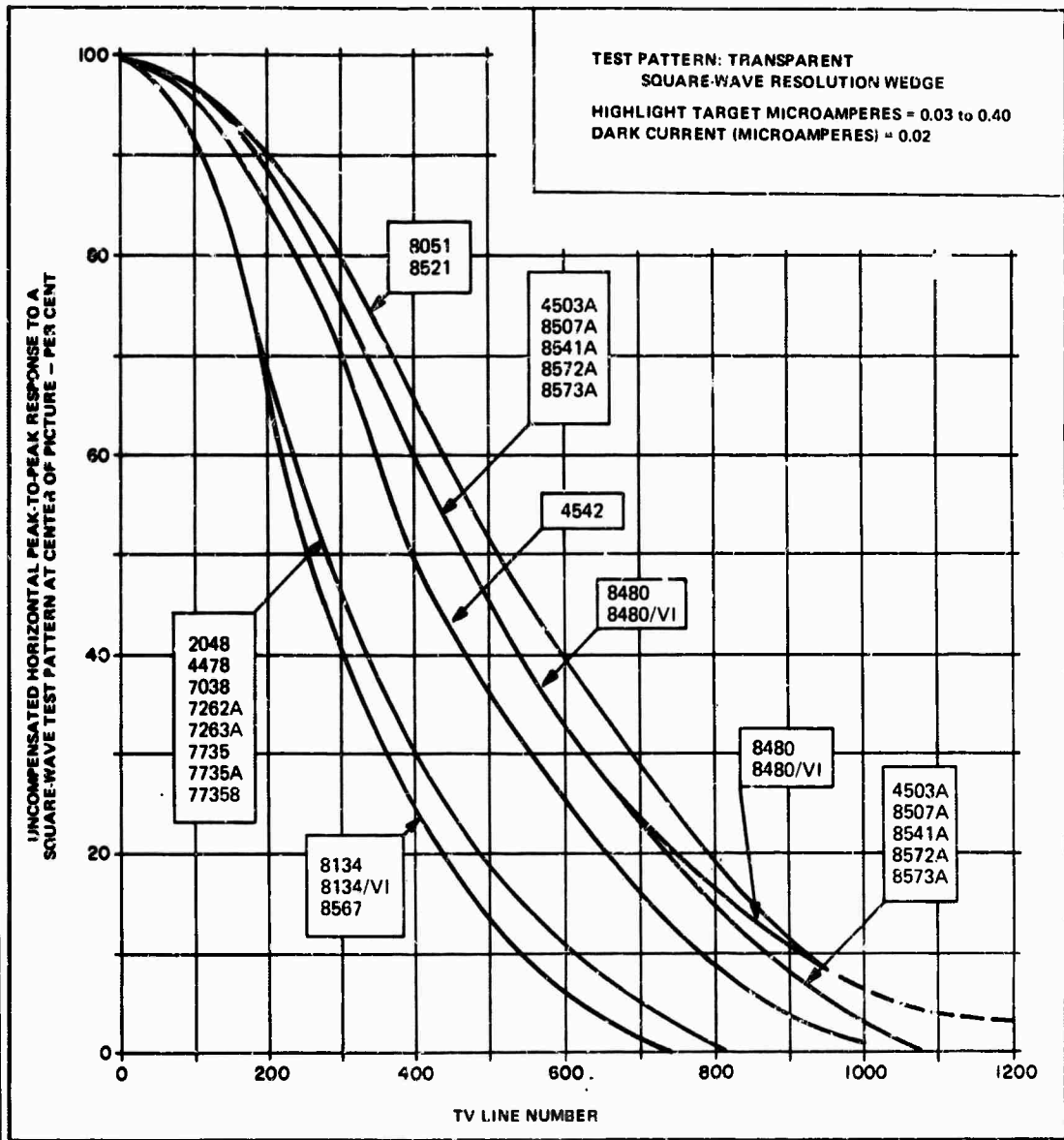
## Spectral Response Curves



## Typical Amplitude Response



# Typical Amplitude Response Curves



**BLANK PAGE**

case for the vidicon alone. The vidicon surface still imparts a gamma to the signal transfer characteristic, but its effect is that of a nonlinear amplifier.

b. Signal Transfer Characteristic. The signal transfer characteristics assumed for the various intensifier vidicon combinations are shown in Fig. V-C-18. The apparent light gain assumed for one stage of intensifier is 45. For two stages the gain is 1800, and for three stages 45,000. The photocathode radiant sensitivity is taken to be  $4 \times 10^{-3}$  amp/watt.

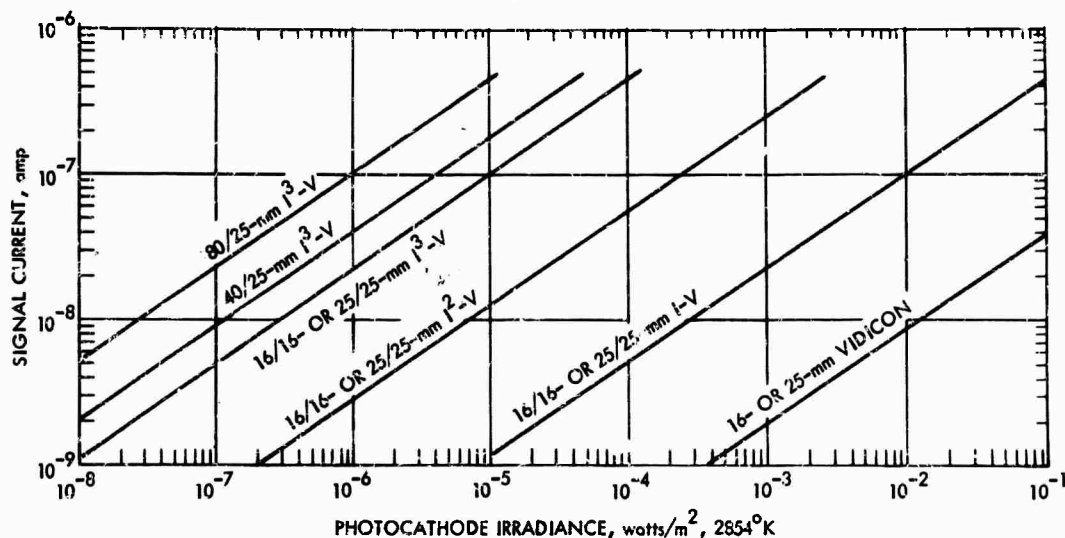


FIGURE V-C-18. Signal Current Versus Photocathode Irradiance Characteristic for the 16-mm and 25-mm Vidicons with their Intensifier Variants

For quantitative purposes, the signal current for the intensifier vidicon may be written by noting that the main effect of the intensifiers is to increase the irradiance on the vidicon. The new apparent value is equal to

$$E_V = \frac{A_I}{A_V} \cdot G_{ET} \cdot \frac{\sigma_I}{\sigma_O} \cdot G_{IV} E_I, \quad (V-C-18)$$

where  $A_I/A_V$  is the ratio of intensifier photocathode area to vidicon photocathode area, and  $G_{ET}$  is the electron gain at the various intensifier-phosphor/intensifier-photocathode interfaces. The quantity  $G_{IV}$  refers to the apparent gain at the intensifier-phosphor/vidicon-photocathode interface with an intensifier of radiant sensitivity equal to  $\sigma_o$  amp/watt, and  $\sigma_I$  is the radiant sensitivity of the intensifier photocathode actually used. With this understanding, the signal output current may be written as

$$I_S = \frac{A_V}{e_v e_h} \left[ K_V \frac{A_I}{A_V} G_{ET} \frac{\sigma_I}{\sigma_o} G_{IV} E_I \right]^Y \quad (V-C-19)$$

To express this in terms of the intensifier photocurrent, we note that  $i_s = \sigma_I A_I E_I$ , so that

$$\begin{aligned} I_S &= \frac{A_V}{e_v e_h} \left[ K_V \frac{A_I}{A_V} G_{ET} \frac{\sigma_I}{\sigma_o} G_{IV} \frac{i_s}{\sigma_I A_I} \right]^Y \\ &= \frac{[A_V]^Y}{e_v e_h} \left[ K_V \frac{G_{ET}}{\sigma_o} G_{IV} i_s \right]^Y \end{aligned} \quad (V-C-20)$$

The gain of the tube combination is obtained by setting the output current

$$I_S = 3 i_s / e_v e_h$$

so that

$$G = \left[ K_V \frac{G_{ET}}{\sigma_o} G_{IV} \right] \left( \frac{i_s}{A_V} \right)^{Y-1} \quad (V-C-21)$$

Thus, gain is a function of the photocurrent itself. It is assumed that the gain nonlinearity introduced thereby does not appreciably alter the noise statistics.

c. Amplitude Response. The amplitude response for a 16-mm triple-stage intensifier vidicon ( $I^3$ -V) is shown in Fig. V-C-12, and the responses of the 25-mm single, double and triple intensifier vidicons ( $I$ -V,  $I^2$ -V, and  $I^3$ -V) are shown in Fig. V-C-13. The 25-mm intensifier's amplitude response is comparable to that of the 25-mm vidicon. Thus, a single intensifier significantly decreases the overall amplitude response of the vidicon camera. With three intensifiers, the intensifiers themselves are primarily limiting for amplitude response.

d. Video and Display Signal-to-Noise Ratio. The video signal-to-noise ratio for the intensifier vidicon may be written as

$$SNR_{V,N,C} = \frac{[1-(1-C)^Y] \cdot R_{SQ}(N) \cdot G i_s / e_v e_h}{[G^2 e \Delta f i_s / e_v e_h + \bar{I}_{PA}^2]^{\frac{1}{2}}}, \quad (V-C-22)$$

where the terms are as before except that  $G$ , the overall sensor gain, is as defined in Eq. V-C-21.

The video signal-to-noise ratios for the various intensifier vidicon combinations are shown in Fig. V-C-19 as functions of input intensifier photocurrent. Observe that the 16-mm  $I$ -V provides a larger signal current for a given photocurrent than does the 25-mm  $I$ -V. This is a consequence of the 16-mm vidicon's higher photoconductor efficiency. Recall that the 25-mm vidicon photocathode sensitivity was sacrificed for a decreased lag. With two intensifiers, the 16-mm vidicon becomes photoelectron noise limited, and the 25-mm vidicon becomes nearly so. The only reason for adding a third intensifier, then, is to decrease lag.

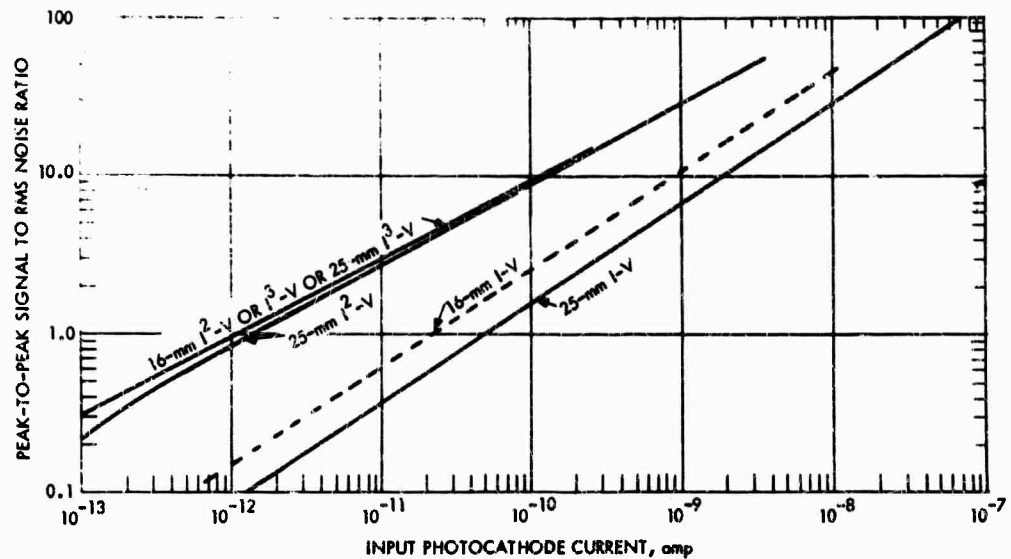


FIGURE V-C-19. Signal Current Versus Input Photocathode Current for Intensifier Vidicons. Video Bandwidth is 10 MHz

The display signal-to-noise ratios are shown for a 16-mm triple intensifier vidicon in Fig. V-C-20 and for a 25-mm triple intensifier vidicon in Fig. V-C-21.

e. Limiting Bar-Pattern Resolution. The limiting resolution versus irradiance characteristic for 25-mm intensifier vidicon combinations are shown in Fig. V-C-22. The 25/25-mm I-V is seen to be preamplifier noise limited, since additional performance can be obtained by adding more intensifiers. The 25/25-mm I-V is very close to being photoelectron noise limited and has a maximum resolving power in excess of 700 lines. With three intensifiers, maximum resolving power drops to the 550-line level. As a rule of thumb, if the 25-mm vidicon becomes marginally unacceptable, from a lag viewpoint, at  $5 \times 10^{-2}$  watt/m<sup>2</sup>, then the I-V becomes marginal at  $10^{-3}$  watt/m<sup>2</sup>, the I<sup>2</sup>-V at  $2.5 \times 10^{-5}$  watt/m<sup>2</sup>, and the I<sup>3</sup>-V at  $10^{-6}$  watt/m<sup>2</sup>. However, the lag characteristics are somewhat variable from tube to tube, depending on the tradeoffs made by the manufacturer.



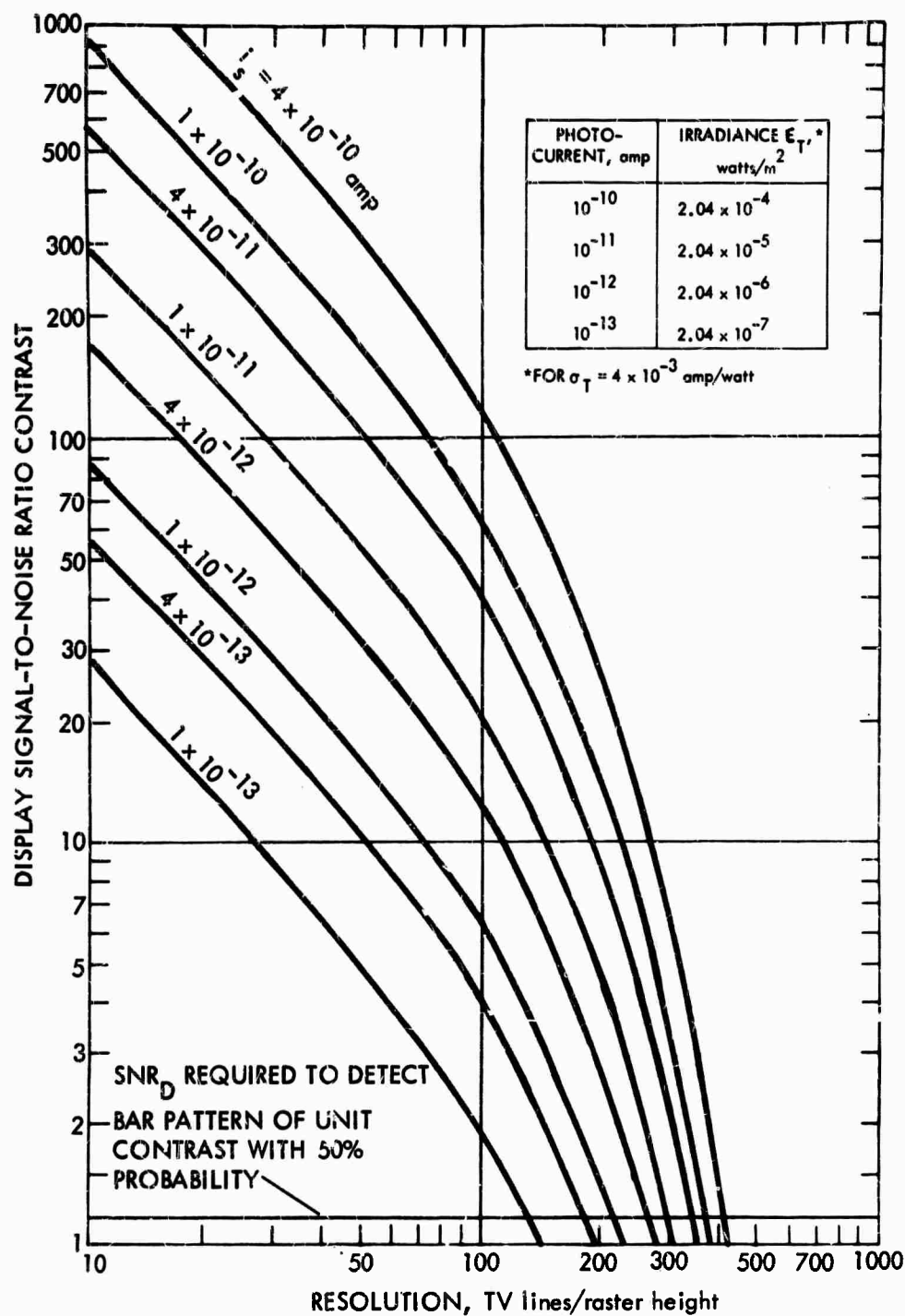


FIGURE V-C-20. Display Signal-to-Noise Ratio Versus Resolution for the 16-mm Triple Intensifier Vidicon for Various Input Photocathode Currents

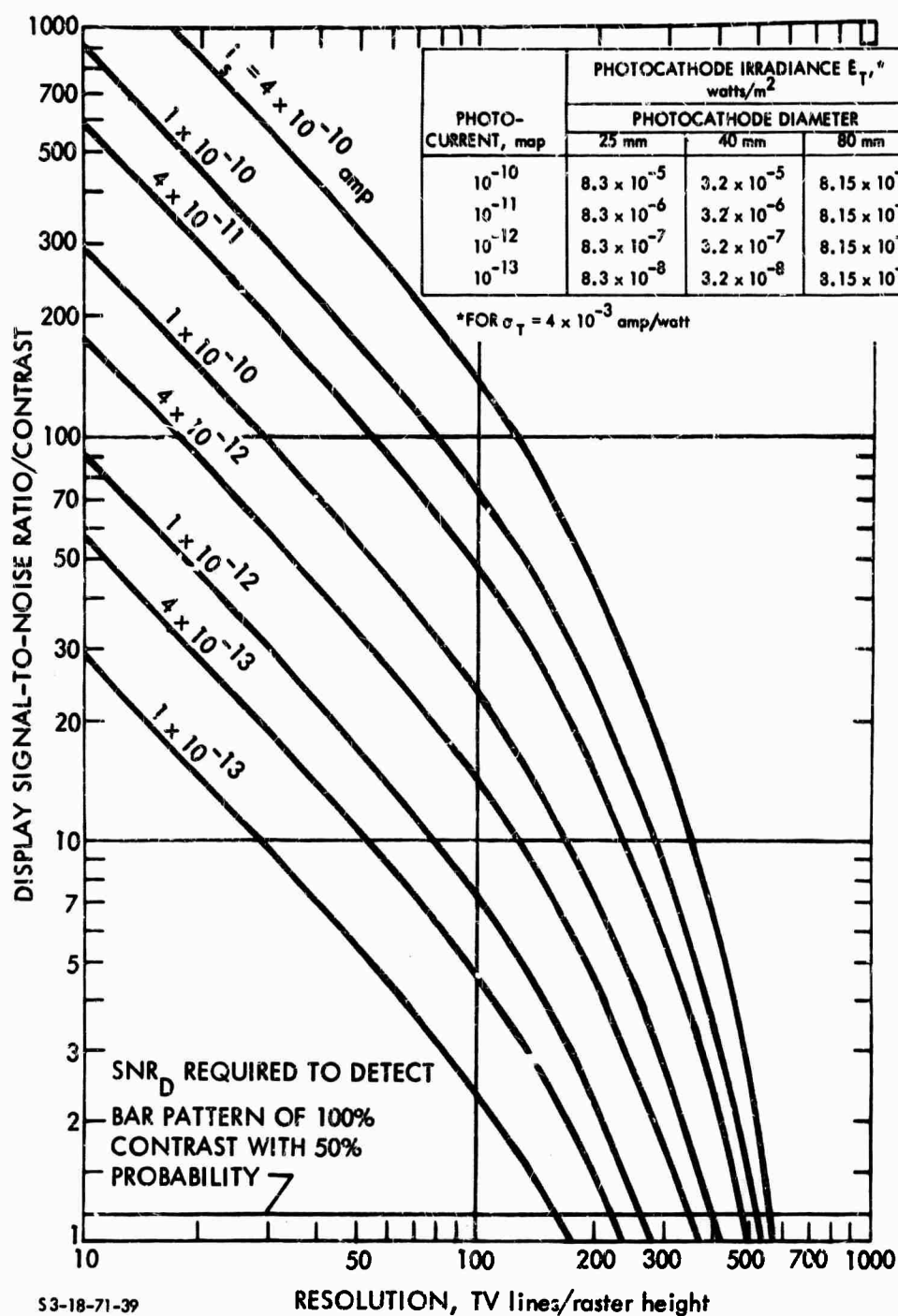


FIGURE V-C-21. Display Signal-to-Noise Ratio Versus Resolution for the Triple Intensifier Vidicon for Various Input Photocurrents, Using a 25-mm Vidicon TV Pickup Tube

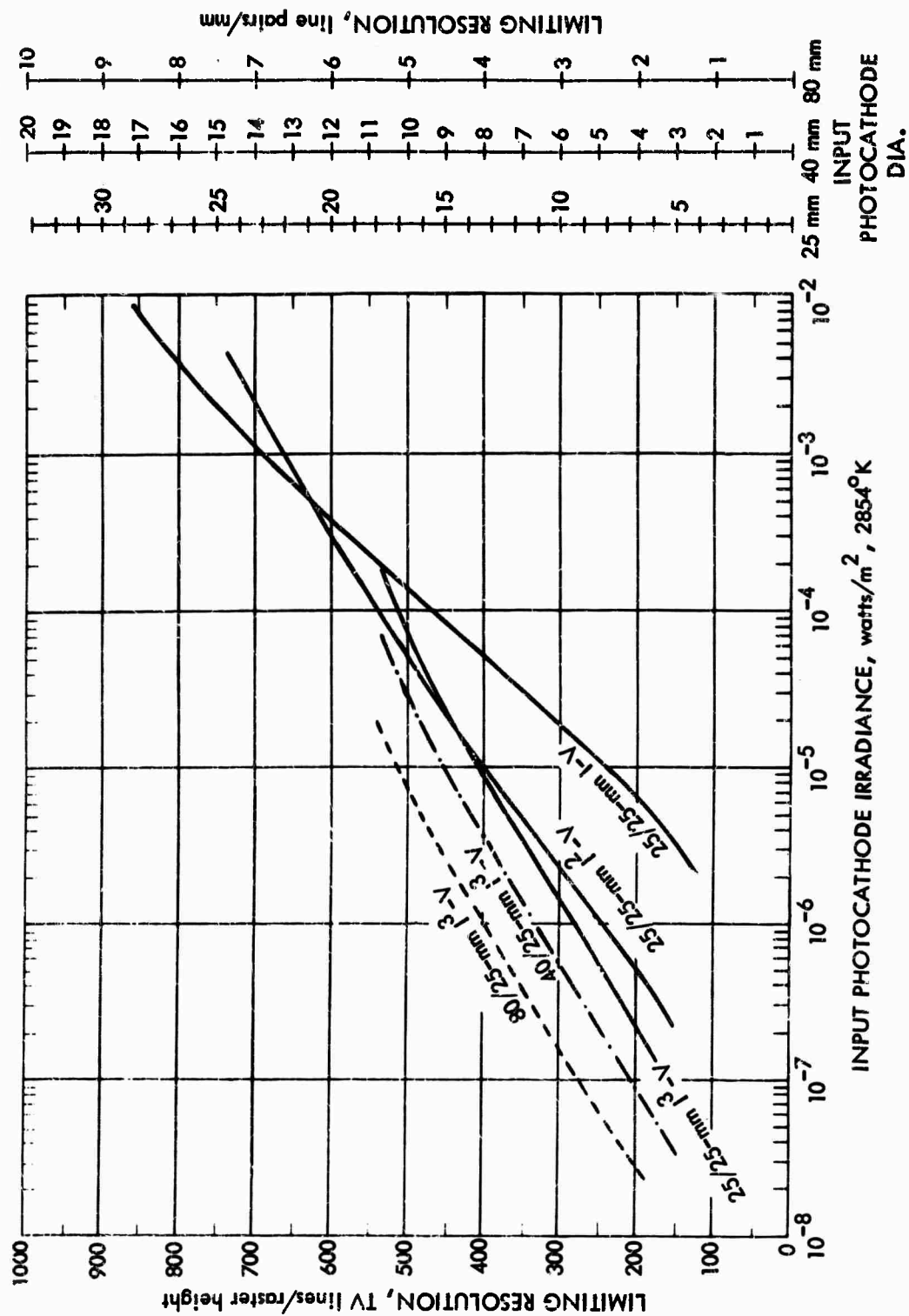


FIGURE V-C-22. Limiting Resolution Versus Input Photocathode Irradiance for 25-mm Intensifier Vidicon Combinations

Limiting resolution versus input photocurrent is shown in Fig. V-C-23 for the 16- and 25-mm\* triple intensifier vidicons. Limiting resolution versus photocathode irradiance is shown in Fig. V-C-24.

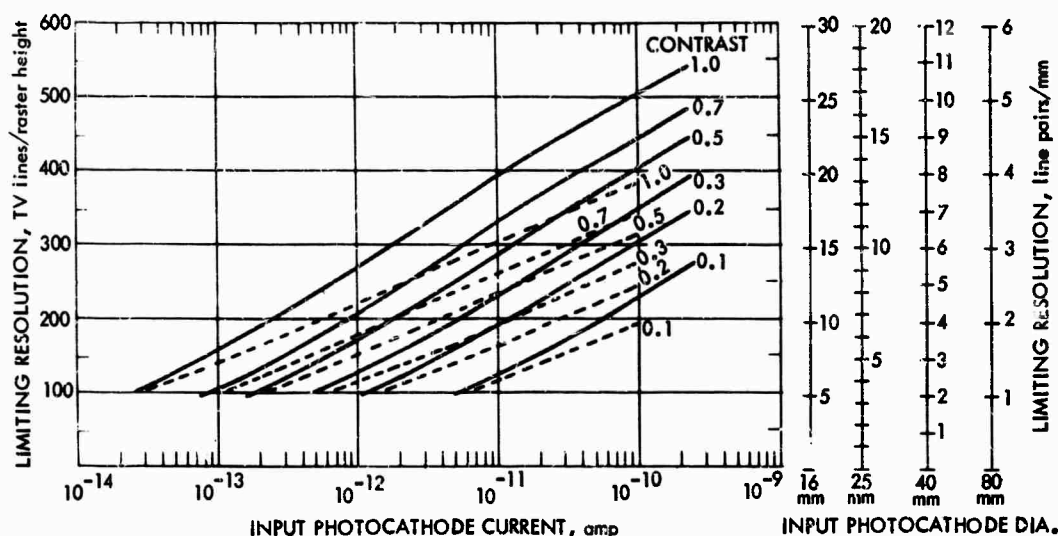


FIGURE V-C-23. Limiting Resolution Versus Input Photocathode Current for the Triple-Intensifier Vidicons at Various Image Contrasts. Solid Curves Apply to Tubes with 25-mm Vidicons; Dashed Curves to Tubes with 16-mm Vidicons

f. Computed versus Measured Results. Only two sets of data are available for the triple intensifier vidicon version. These results are compared to those computed in this section in Fig. V-C-25. As is usually the case herein, the calculations apply to a typical assumed tube and not to the tube actually measured. In most cases, the tubes measured will, however, have parameters not far different from those used in the calculations, and thus fairly good correlation is obtained.

g. Lag Characteristics. The third-field lag characteristics are estimated in Fig. V-C-17 for the various intensifier vidicon combinations. The second method of specifying lag effects are to measure limiting resolution as the pattern is slowly moved across the horizontal

\* A 16-mm tube is normally called a 1-in. vidicon; a 25-mm tube is normally called a 1½-in. vidicon.

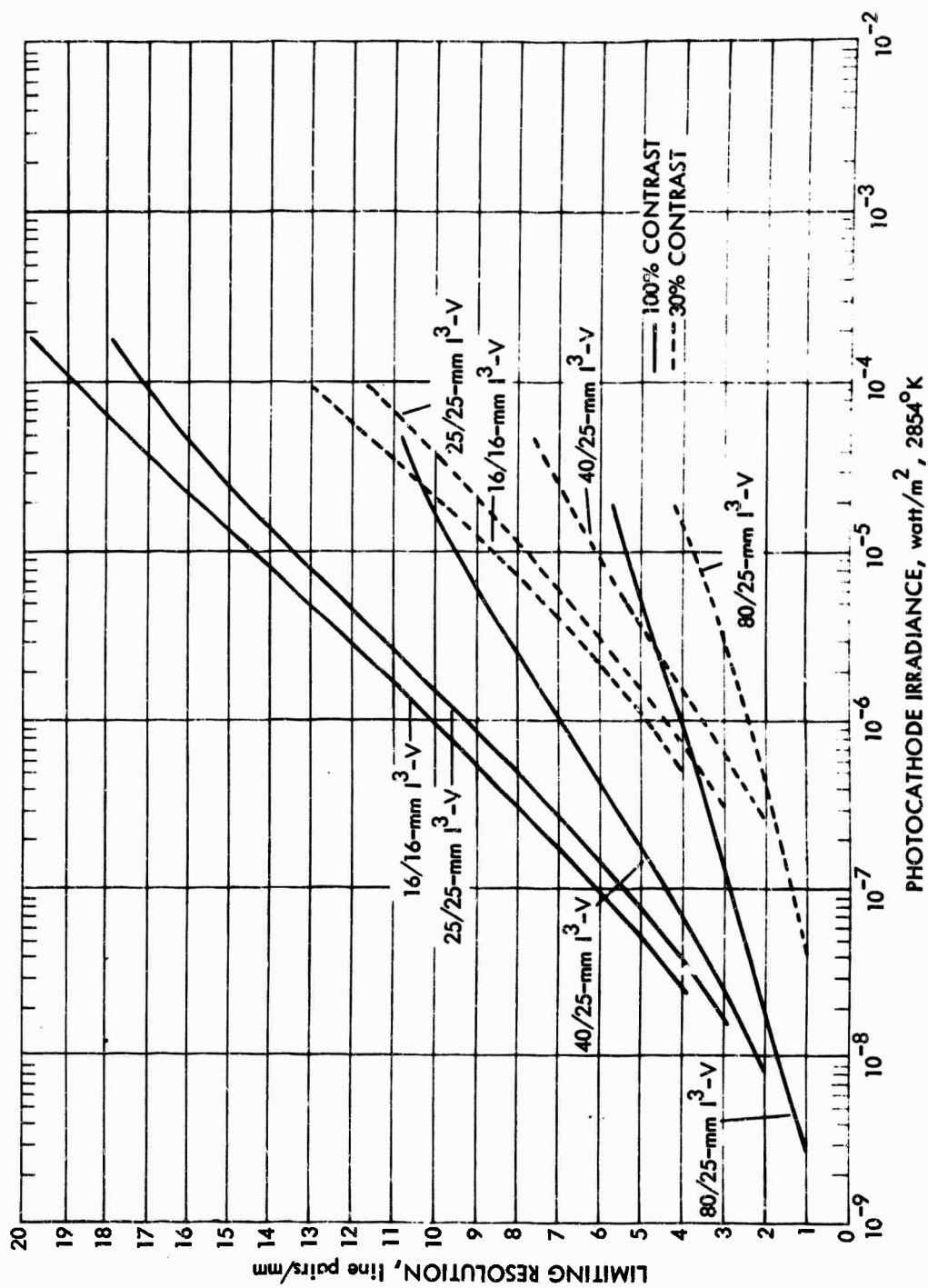


FIGURE V-C-24. Limiting Resolution Versus Photocathode Irradiance for Various Triple Intensifier Vidicons at Two Contrasts

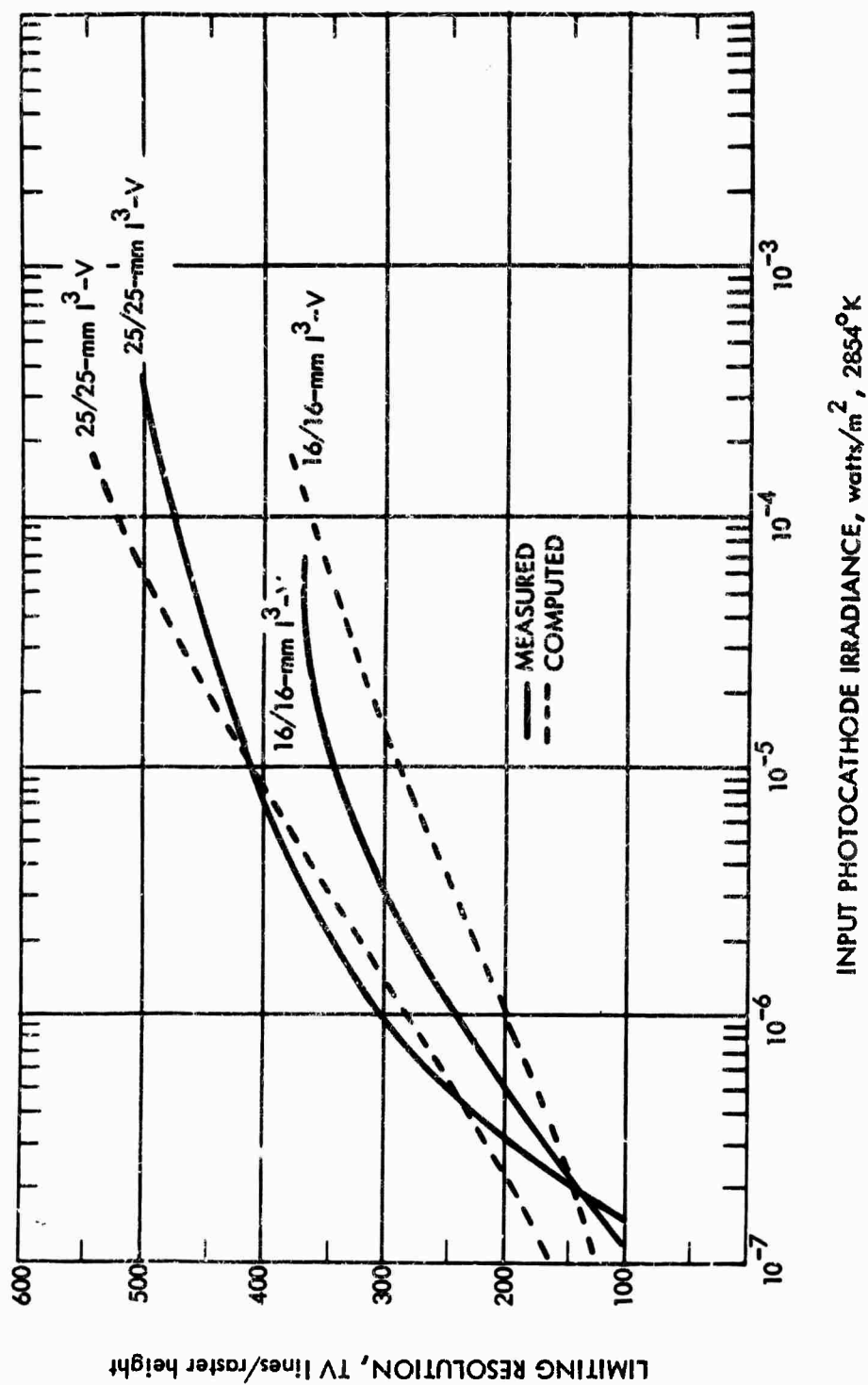


FIGURE V-C-25. Limiting Resolution Versus Input Photocathode Irradiance -- Comparison of Measured and Computed Results for the 16-mm and 25-mm Triple Intensifier Vidicons with 100 Percent Image Contrast

field of view. The effect of such pattern motion on the resolution irradiance level characteristic is shown in Fig. V-C-26 for the 16-mm  $I^3$ -V and in Fig. V-C-27 for the 25-mm  $I^3$ -V, for two pattern speeds in each case.

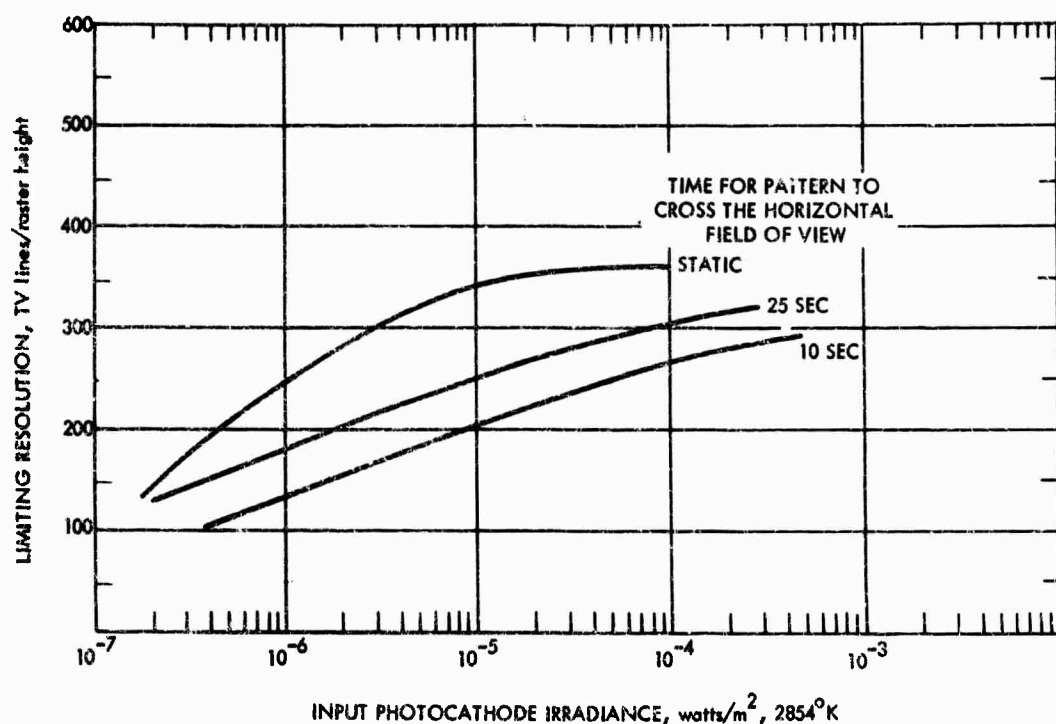


FIGURE V-C-26. Limiting Resolution Versus Input Photocathode Irradiance as a Function of Bar-Pattern Speed Across the Horizontal Field of View for the 16-mm Triple Intensifier Vidicon

h. Form Factor. While the vidicons are not large, length is substantially increased by the three intensifiers required to achieve acceptable low-lag, low-light-level imaging. The length increase with 16-mm intensifiers will be approximately 5 in., and with 25-mm intensifiers it will be 7.2 in. With an 80/25-mm zoom intensifier, length is increased by 12.8 in.

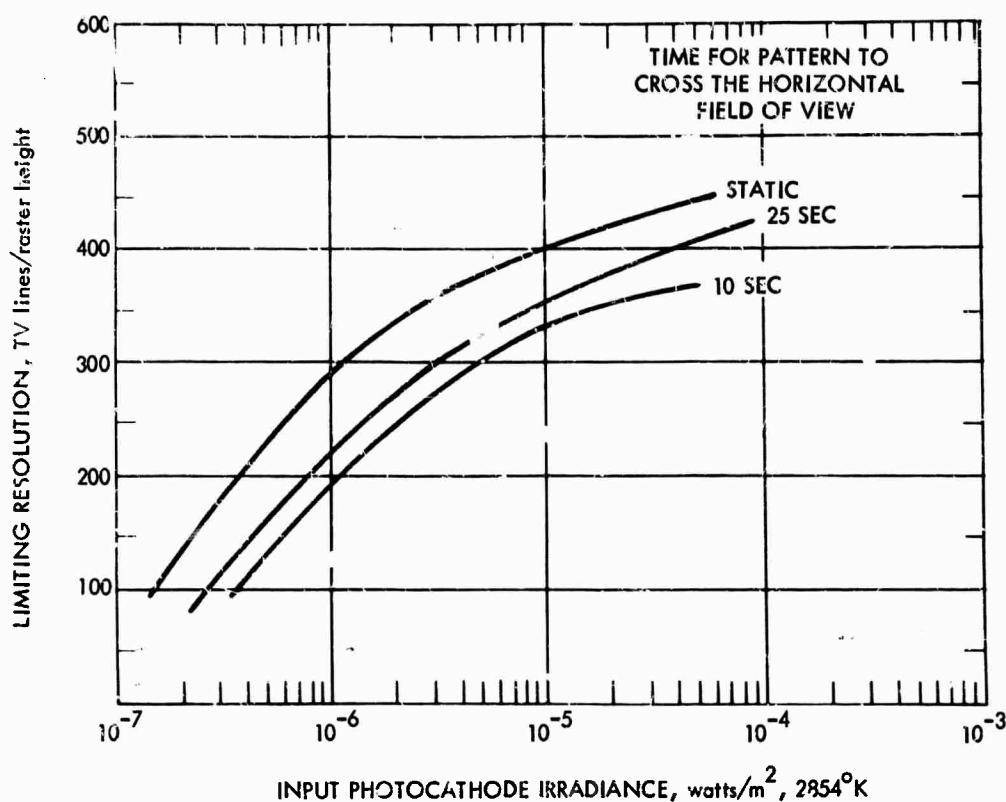


FIGURE V-C-27. Limiting Resolution Versus Input Photocathode Irradiance as a Function of Bar-Pattern Speed Across Horizontal Field of View for the 25-mm Triple Intensifier Vidicon

#### D. THE SECONDARY ELECTRON CONDUCTION CAMERA TUBE AND ITS INTENSIFIED VERSION

The typical secondary-electron-conduction (SEC) television camera tube consists of a diode imaging section, with a photoemitter at one end and the SEC target at the other, and an electron-scanning-beam readout section similar to that used in a vidicon. When the photoemitter is an S-20 surface, the SEC camera is characterized by moderate sensitivity, good resolving power, low image lag, and simplicity of operation. This camera tube was developed in the early 1960's, and in its intensifier version it has been the principal camera tube used in low-light-level cameras from 1965 to the present.

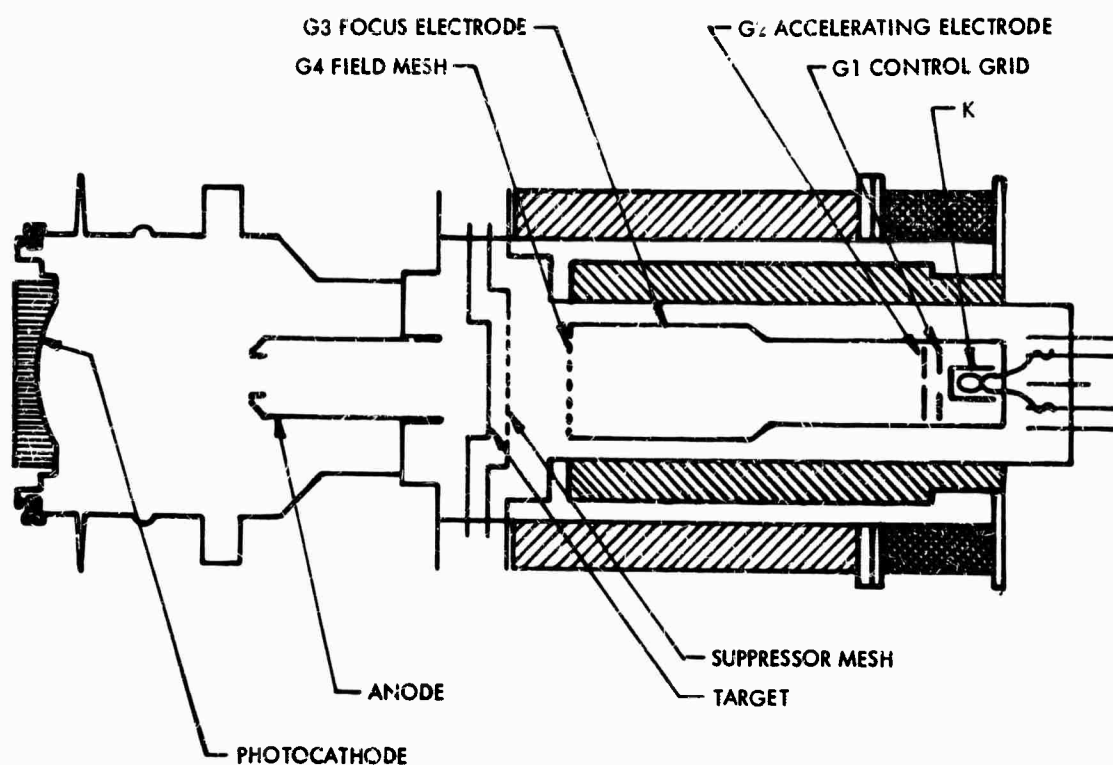


The intensifier SEC (I-SEC) camera approaches the sensitivity of the intensifier image orthicon (I-IO) described in Section V-E, is of lower lag, and is much simpler to operate, since it needs no adjustment over the full range of its light transfer characteristic. The prominent feature of the SEC camera tube is its SEC target, which has high gain, high signal storage capability, and low lag, which permits imaging of both stationary and moving scenes. Information losses in the neighborhood of bright scene highlights due to halation or "blooming," though still a problem, are minimized in this target. Because of the long signal storage capability of the target, the SEC camera can be used to integrate low-light-level images for extended periods or can be used in slow-scan applications. The SEC target, in current tubes, is subject to damage by extreme exposure to about the same degree as the thin-film-targeted image orthicon (IO), but both tubes can be electronically protected in most cases. However, a new mesh-supported SEC target has now been developed that is many factors of 10 less vulnerable to overexposure damage.

#### 1. The Secondary-Electron-Conduction Camera Tube

a. Principles of Operation. A typical SEC camera tube is shown schematically in Fig. V-D-1. The most common tubes employ electrostatically focused image sections and magnetically focused and deflected reading beam sections. However, as is generally the case, many other versions are possible and are even available in some cases. SEC camera tubes have been constructed with all-magnetic image and read sections and with hybrid magnetic/electrostatic read sections.

The SEC camera tube's semitransparent photocathode is deposited on the inner surface of the plano-concave, fiber-optic faceplate in the version of Fig. V-D-1. As in the case of the image intensifier, the photoemitter emits photoelectrons when irradiated. Instead of being accelerated to a phosphor, however, the photoelectrons are accelerated to the SEC target, where they are brought to focus by the electrostatic lens formed between the photocathode surface and the anode cone.



53-18-71-46

FIGURE V-3-1. Cross Section of an SEC Camera Tube

The SEC target consists of a supporting membrane of  $Al_2O_3$  approximately 500 Å thick, followed by a 500 Å layer of aluminum that forms the signal electrode. Deposited on this and facing the reading gun is a highly porous layer of  $KCl$ . The  $KCl$  layer is stabilized at the electron-gun cathode potential by the electron scanning beam, and an electric field is established across the layer by biasing the signal electrode positively.

Photoelectrons arriving at the target with energies of approximately 8 kev penetrate the  $Al_2O_3$  and  $Al$  layers and dissipate most of their energy within the layer by creating free secondary electrons. These electrons are released into the vacuum interstices between the  $KCl$  particles, where they migrate in vacuum toward the signal plate. The electron conduction takes place in the vacuum rather than the

conduction band of the KCl, which avoids the persistence effects caused by the trapping and subsequent release of charge carriers by shallow trapping centers. Also, because of the high resistivity of the low-density target, the charge pattern can be stored for long periods of time.

The function of the SEC target is to amplify and to store the electron image during the period between successive scans by the electron beam. The electron gain within the target is approximately 100, and the storage time is very long compared to the usual frame rates. The video signal is developed directly across the target lead resistor as the electron beam replaces charge on the target point by point.

The low-velocity electron beam that scans the target is produced by an electron gun consisting of an indirectly heated thermionic cathode, a control grid G1, and an accelerating grid G2. The beam is focused at the target by the combined action of the uniform magnetic field of the external coil and the electrostatic field of focus electrode G3. A field mesh G4 provides a uniform decelerating field. A second mesh electrode G5, designated a suppressor mesh, is positioned close to the target surface to control the SEC target potential to just below the KCl "crossover" potential of about 15 volts. In the absence of this mesh, the target exhibits a "runaway" characteristic by charging up to the G4 potential of 400 volts. The maximum resolving power of the SEC target is limited by the interaction of the beam with the suppressor mesh rather than by the SEC target itself.

b. Signal Transfer Characteristics. The main difference between the vidicon and the SEC camera tube, from a signal current viewpoint, is that the SEC target provides a gain  $G_T$  such that the signal current output becomes

$$I_S = G_T i_s / e_v e_h \quad (V-D-1)$$

The signal output current is plotted against photocathode irradiance for several SEC cameras in Fig. V-D-2. The gamma of the curves is shown to be nearly unity, although in practice it is variable from nearly 1 at low light levels to about 0.6 at the higher light levels. This gamma is due to a variation in target gain. At the highest irradiance levels, the target saturates at a surface potential equal to that of the suppressor mesh G5. In the curves shown, a hard "knee" in the signal transfer characteristic is shown, although in fact the characteristic is more rounded. The hard-knee assumption does not appreciably affect the calculations. A soft knee is considered desirable in a real-time system because it extends dynamic range, while at the same time limiting signal excursion. With the SEC image section operated at maximum potential, prolonged exposure at irradiance levels above the knee should be avoided because of the possibility of image burn-in. However, larger irradiances can be tolerated by reducing the photocathode voltage. This can be made automatic by peak-detecting the video signal and using the resulting signal to reduce image section voltage. Dark current in the SEC tube is practically nonexistent.

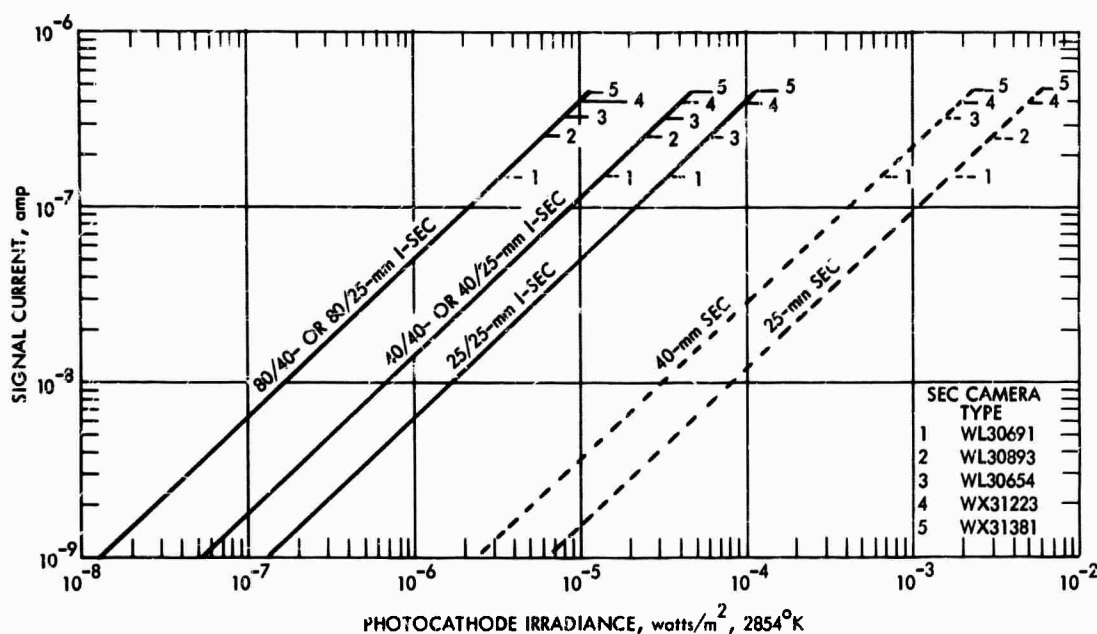


FIGURE V-D-2. Signal Current Versus Photocathode Irradiance Characteristic for the SEC and Intensifier-SEC Cameras as a Function of Input Photocathode Diameter

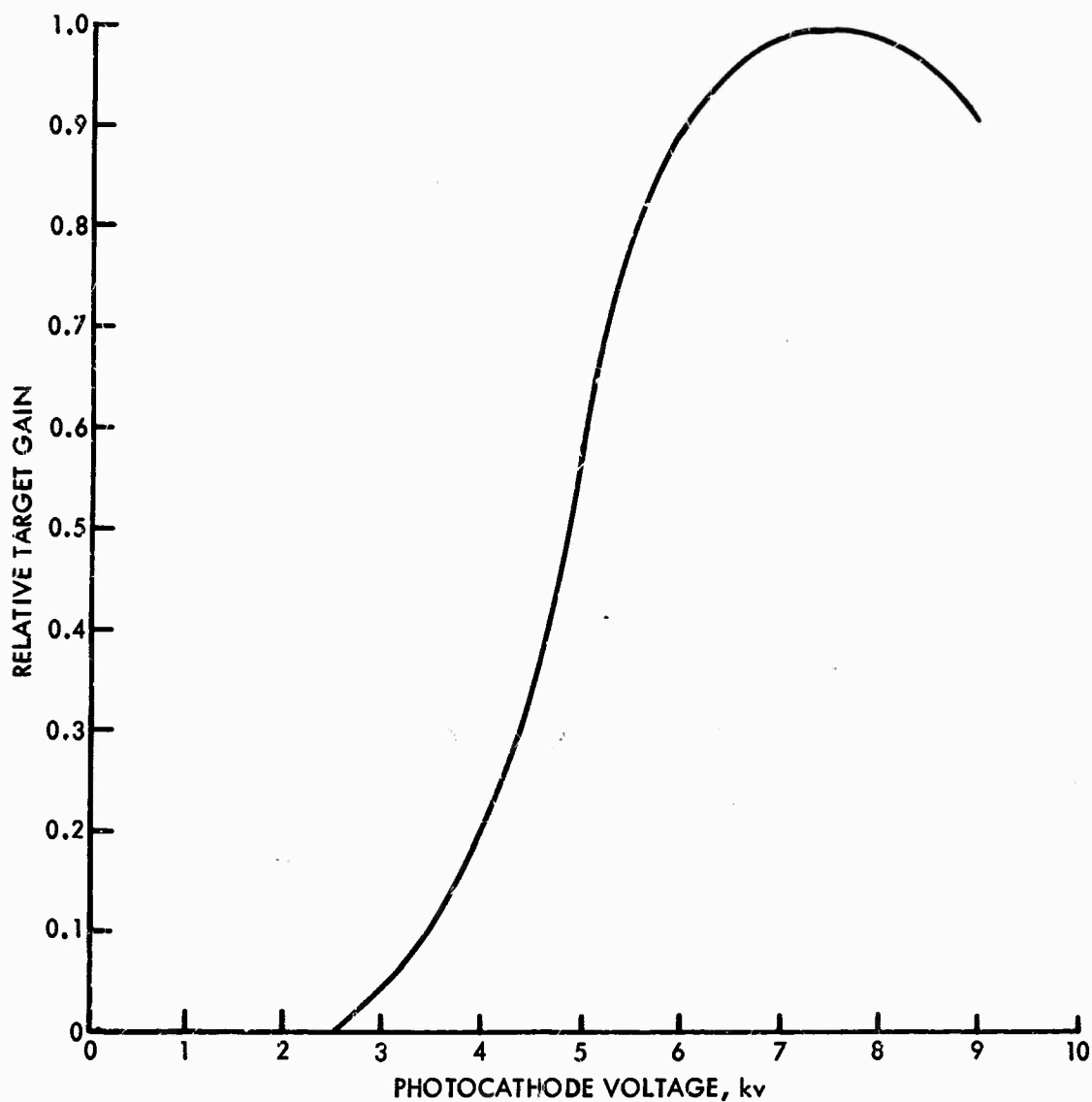


FIGURE V-D-3. Relative SEC Target Gain Versus Photocathode Voltage

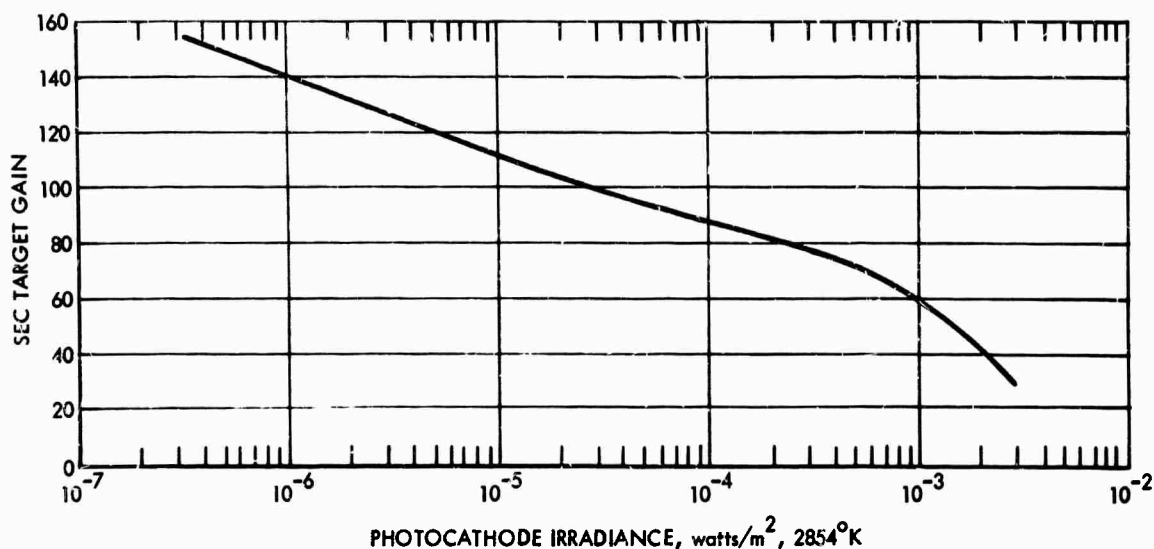
The SEC target gain is proportional to the photocathode voltage, as shown in Fig. V-D-3. The SEC camera gain can also be increased by increasing target voltage, but practical limits to maximum voltage are imposed by the onset of target grain and lag. At lower

voltages, some degree of control can be exercised, but only at the expense of maximum signal storage capability and overall dynamic range. However, effective gain control can be obtained with photocathode voltage control. Over a range of 3.5 to 7.5 kv, a 15-to-1 gain control range can be obtained without loss in resolution, but with an image rotation of about 1 deg at the lower voltage. At even lower voltages, image rotation increases as well as target gain.

The SEC target gain is obtained by solving Eq. V-D-1 for  $G_T$ :

$$G_T = \frac{e_v e_h I_S}{\alpha_T A E_T} \quad (V-D-2)$$

Target gain for a typical real SEC tube is plotted in Fig. V-D-4. As can be seen, the SEC target gain falls off with increasing photocathode irradiance. The droop shown above  $5 \times 10^{-3}$  watt/m<sup>2</sup> is characteristic of a rounded knee rather than the hard knees shown in Fig. V-D-2, which would really correspond to an abrupt drop to zero gain.



53-18-71-49

FIGURE V-D-4. Absolute Target Gain for a Typical 40-mm SEC Camera Tube Versus Photocathode Irradiance

The maximum signal current capability for the various SEC cameras is mainly a function of the SEC target diameter, to which target capacitance is directly proportional. A large target is desirable from two viewpoints: first, the signal storage capability is increased; and second, the amplitude response is improved because the target-mesh assembly is the primary resolution limiting parameter. However, the larger target has a greater interelectrode capacitance, which leads to an increase in preamplifier noise and a larger capacitance, which leads to an increase in readout time constant.

In Fig. V-D-2, a number of knees are shown. The particular knee to use depends on the camera tube type and its target diameter. The WL30691, for example, has a 16-mm target and a maximum signal current of  $1.5 \times 10^{-7}$  amp, while the WX31223 has a 40-mm target and a signal current maximum of about  $4.5 \times 10^{-7}$  amp. Ordinarily, the increase in signal current should be directly proportional to target diameter, but the designer has some latitude in trading lag with other parameters such as target gain.

The parameters of the five most commonly used SEC camera tubes to be discussed herein are given in Table V-D-1. Note also that the rms preamplifier noises are also estimated in this table for the various tubes, a 7.5-MHz video bandwidth being assumed for the WL30691 and a 10-MHz bandwidth for the others.

c. Amplitude Response. The square-wave response of the various SEC cameras are shown in Figs. V-D-5 and V-D-6. Observe that the WX31381 is shown as having both a 25- and a 40-mm-diameter input photocathode. This is accomplished by incorporating an electronic zoom feature within the image section of this tube. In the zoom mode, the input photocathode diameter used is reduced, but the full target diameter is scanned. Since the principal amplitude-response-limiting factors are associated with the scanned target area, the amplitude response is shown to be the same in both the 1:1 and 1.5:1 zoom cases when expressed in terms of TV lines/raster height (but not line pairs/millimeter). The amplitude response of both the SEC and I-SEC cameras

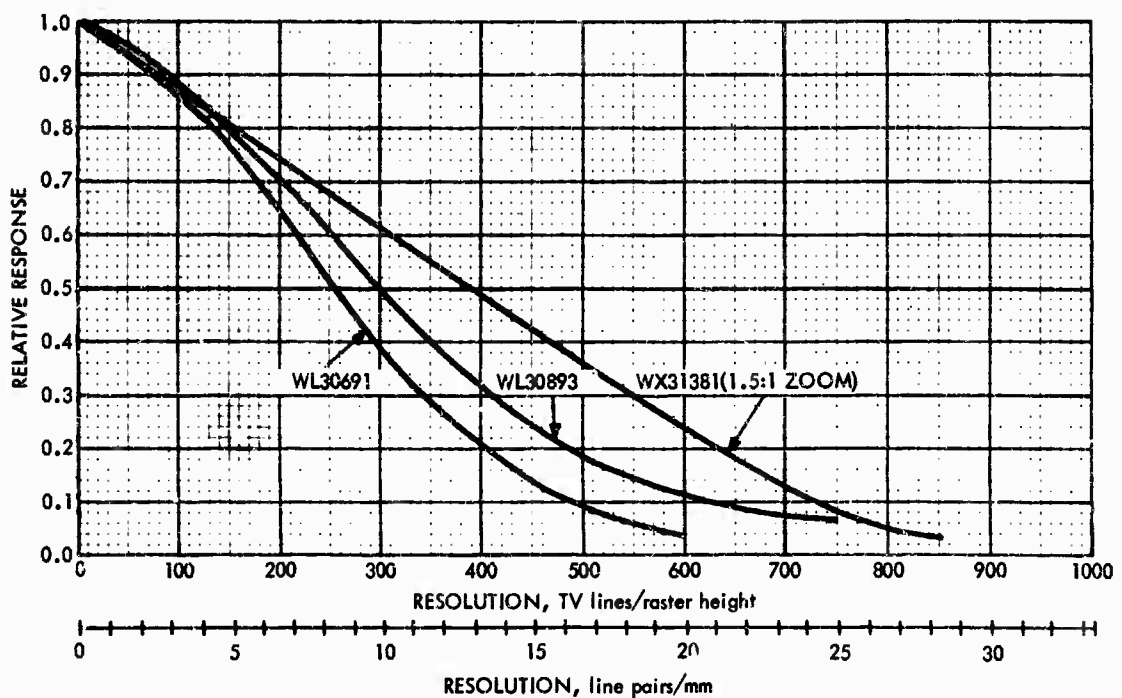
has been found to be independent of light level over the range of light levels for which the characteristic is measurable.

TABLE V-D-1. PHYSICAL CHARACTERISTICS OF VARIOUS SEC CAMERAS

Tube Type	Photocathode Diameter, mm	SEC Target Diameter, mm	Image Section Focus	Estimated RMS Preamp. Noise, na	Max. Tube Diameter, in.	Max. Tube Length, in.
WL30691	25	16	ES*	3.0	2.85	8.6
WL30893	25	21.6	ES	4.5	2.85	9.1
WL30654	40	25	ES	5.0	4.03	13.5
WX31223	40	40	M**	5.5	3.12	16.9
WX31381	40 or 25	33	ES	6.0	4.1	13.9

\* ES = electrostatic

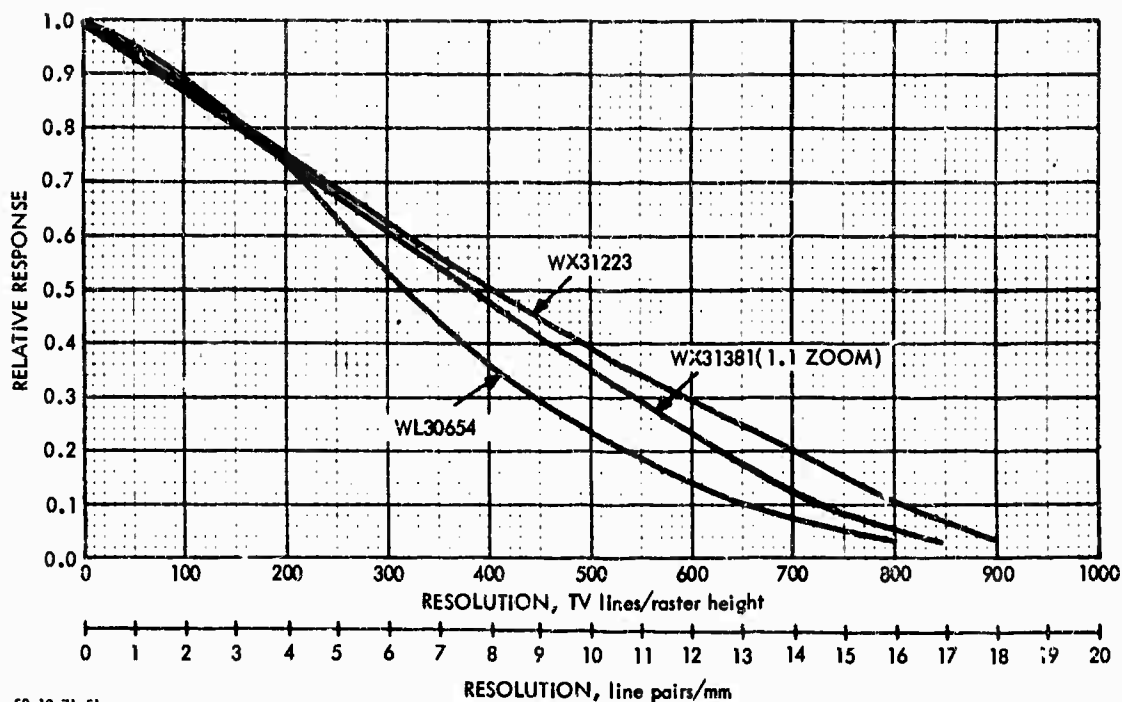
\*\* M = magnetic



S3-18-71-50

FIGURE V-D-5. Uncompensated Horizontal Square-Wave Response for SEC Cameras with 25-mm Input Photocathodes





S3-18-71-51

FIGURE V-D-6. Uncompensated Horizontal Square-Wave Response for SEC Cameras with 40-mm Input Photocathodes

d. Video Signal-to-Noise Ratio. The only noise of consequence for the SEC is the preamplifier noise, except at the very highest light levels, where photoelectron noise has a small but discernible effect. The video signal-to-noise ratio is given by

$$\begin{aligned}
 \text{SNR}_{V,0,1} &= \frac{G_T i_s / e_v e_h}{\left[ \bar{I}_e^2 + \bar{I}_{PA}^2 \right]^{1/2}} \\
 &= \frac{G_T i_s / e_v e_h}{\left[ \frac{G_T^2 e \Delta f i_s}{e_v e_h} + \bar{I}_{PA}^2 \right]^{1/2}},
 \end{aligned}
 \tag{V-D-3}$$

where  $\bar{I}_e^2$  is the mean square photoelectron noise and the other terms are as previously defined. The signal and noise currents for the SEC camera are plotted in Fig. V-D-7 and the signal-to-noise ratio is plotted in Fig. V-D-8. The  $SNR_{V,0,1}$  curves are quite closely spaced. Such spacing as exists is due mainly to the preamplifier noise.

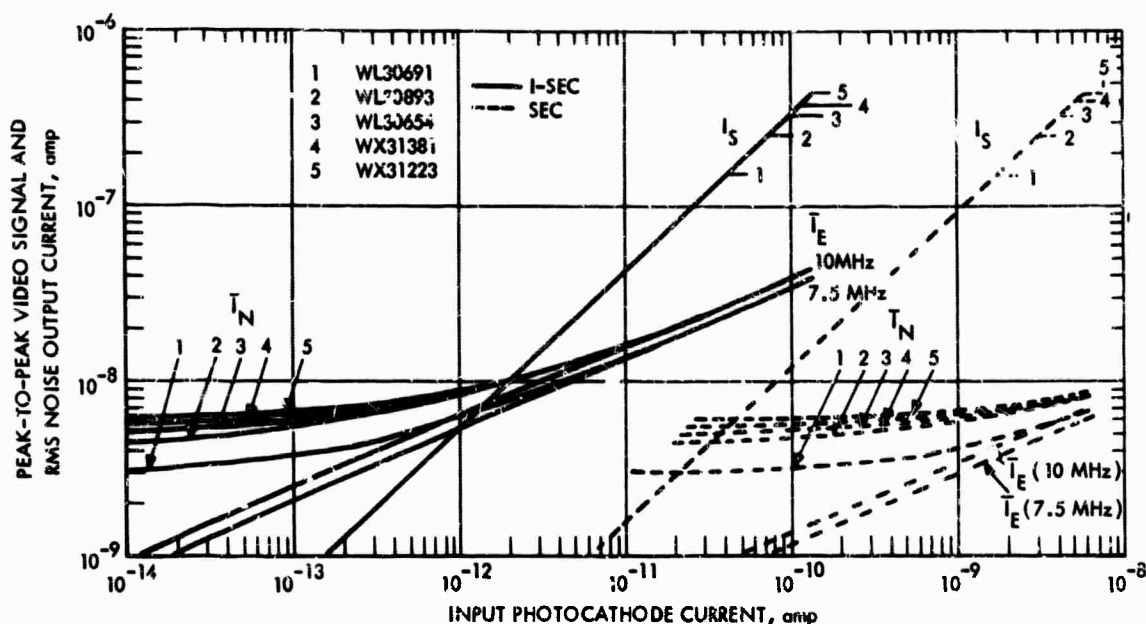
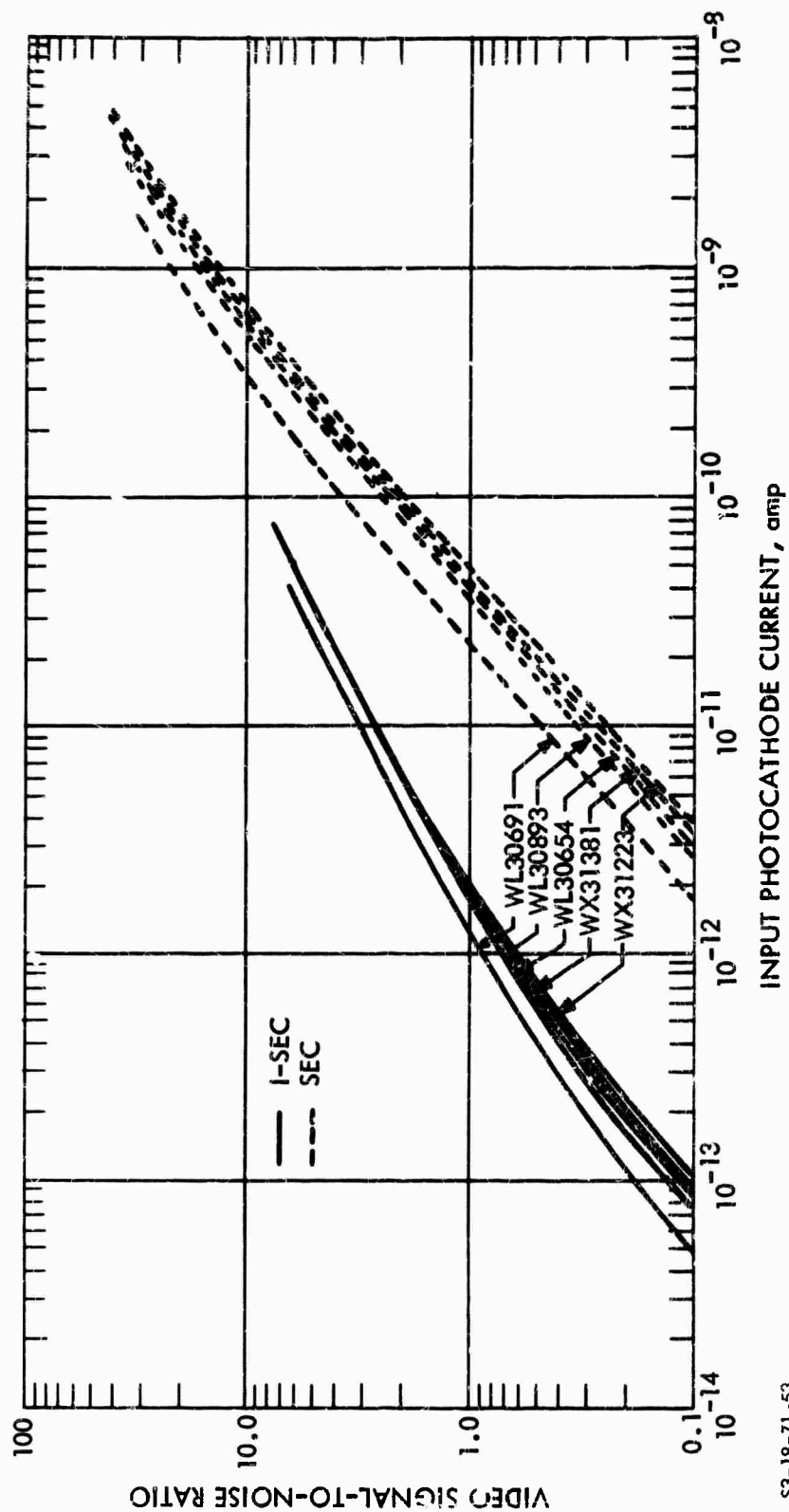


FIGURE V-D-7. Peak-to-Peak Video Signal and RMS Noise Output Currents Versus Input Photocathode Current for Various SEC and Intensifier-SEC Cameras

The display signal-to-noise ratio is determined as before and is plotted in Figs. V-D-9 through V-D-12.

e. Limiting Bar-Pattern Resolution. The limiting resolution versus the input photocathode currents and irradiances are determined from the various  $SNR_D/C$  curves and are plotted in Figs. V-D-13 through V-D-24. Note once again that when resolution is expressed in line pairs/millimeter the scale corresponding to the input photocathode diameter must be used. The appropriate diameter to associate with any tube type is given in Table V-D-1.



53-18-71-53

FIGURE 1-D-8. Peak-to-Peak Signal-to-RMS-Noise Ratio Versus Input Photocathode Current for Various SEC and Intensifier-SEC Cameras. (Video Bandwidth is 10 MHz Except for the WX30691, where it is 7.5 MHz)

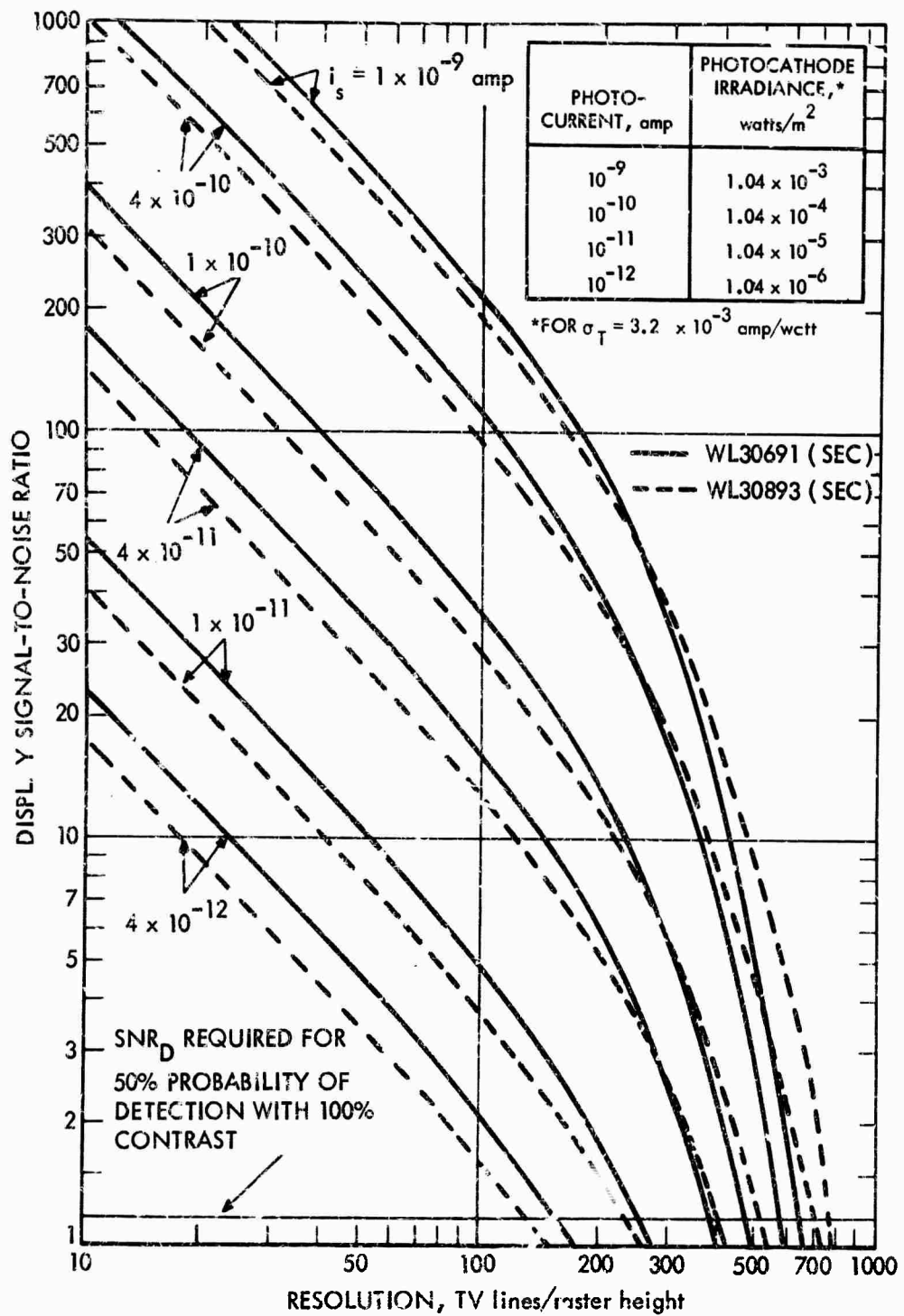


FIGURE V-D-9. Display Signal-to-Noise Ratio Versus Resolution for the WL30691 and WL30893 SEC Cameras for Various Input Photocathode Currents

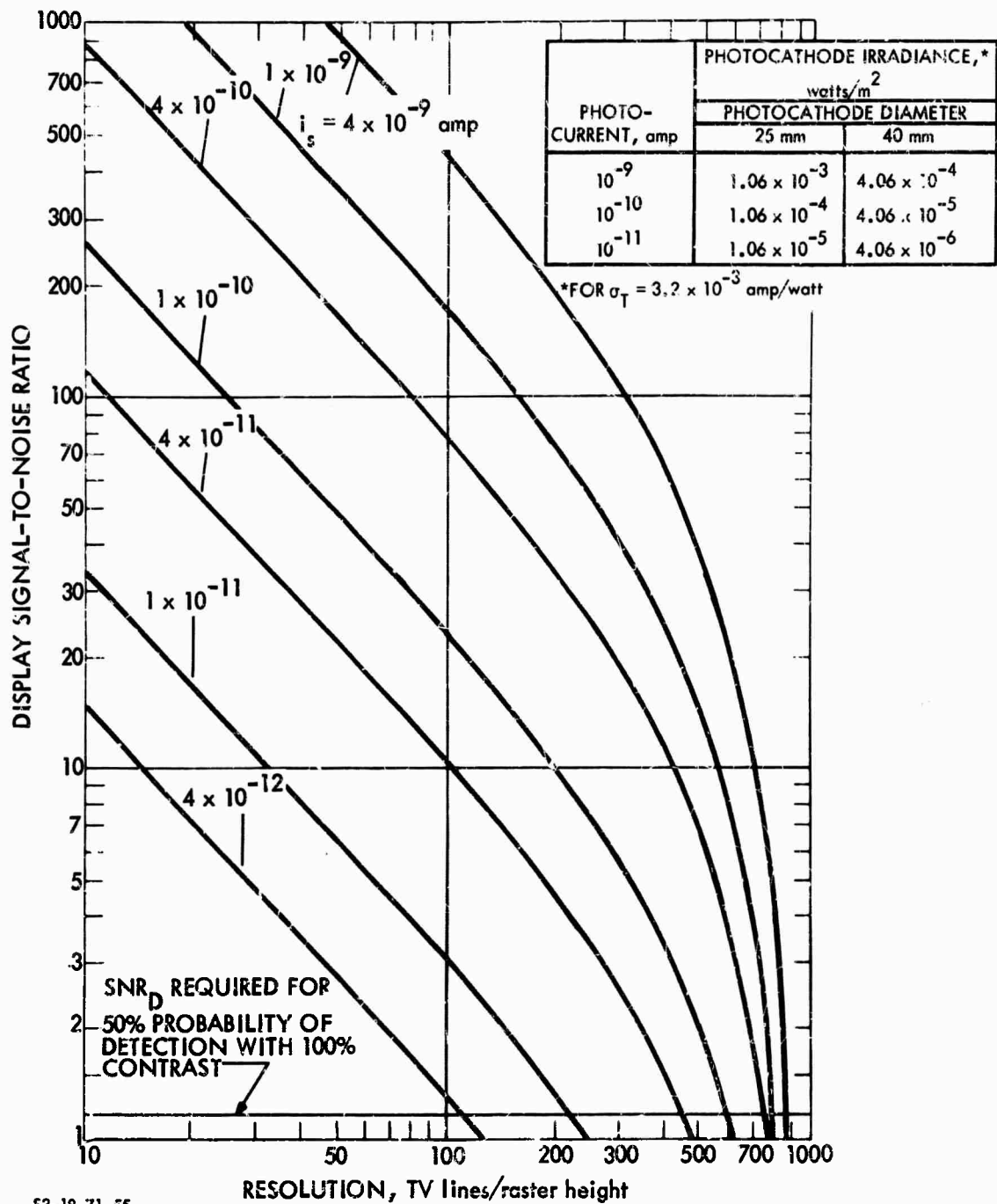


FIGURE V-D-10. Display Signal-to-Noise Ratio Versus Resolution for the WX31381 SEC Cameras in either the 1:1 or 1.5:1 Zoom Made as a Function of Input Photocathode Current

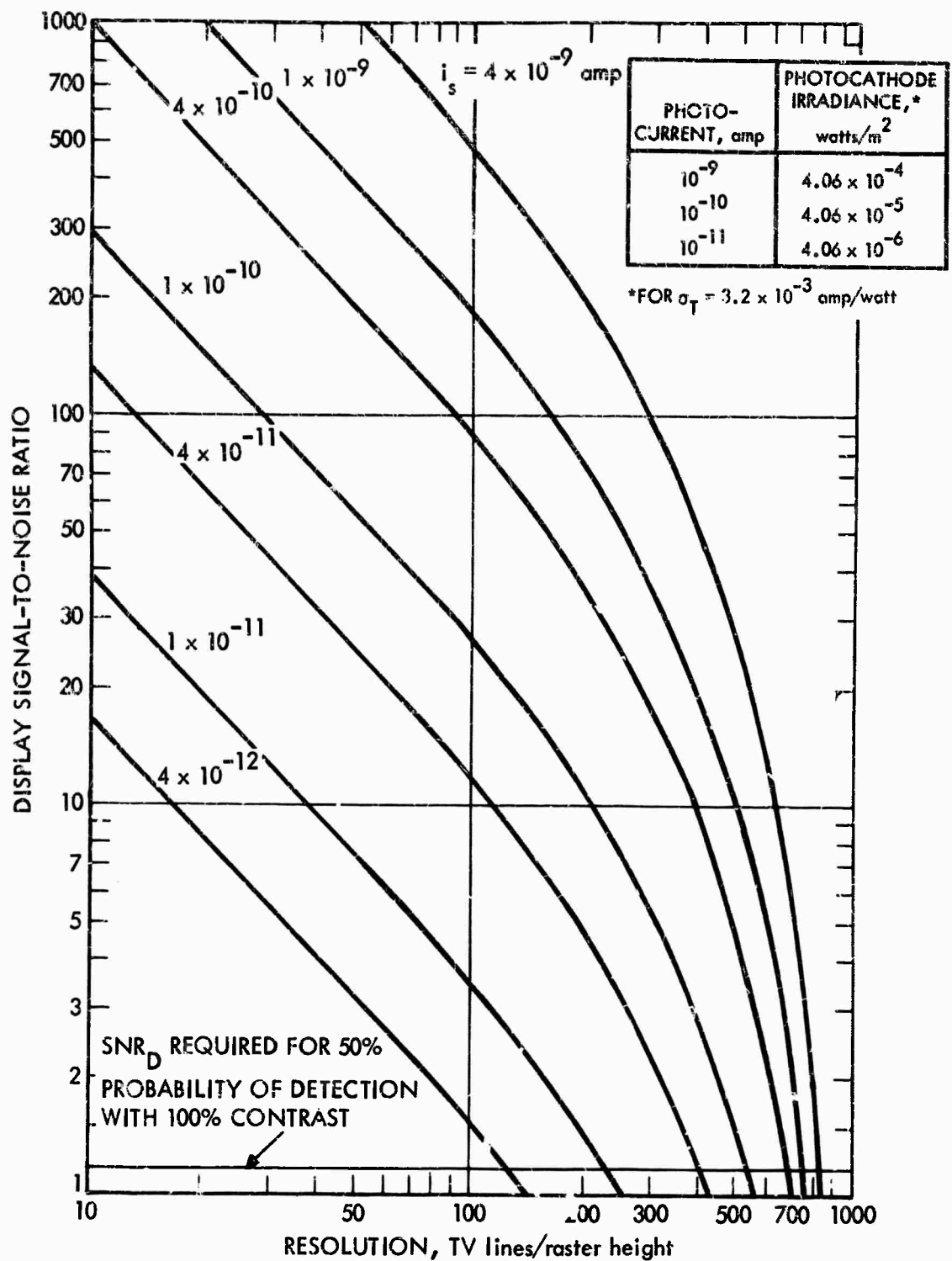
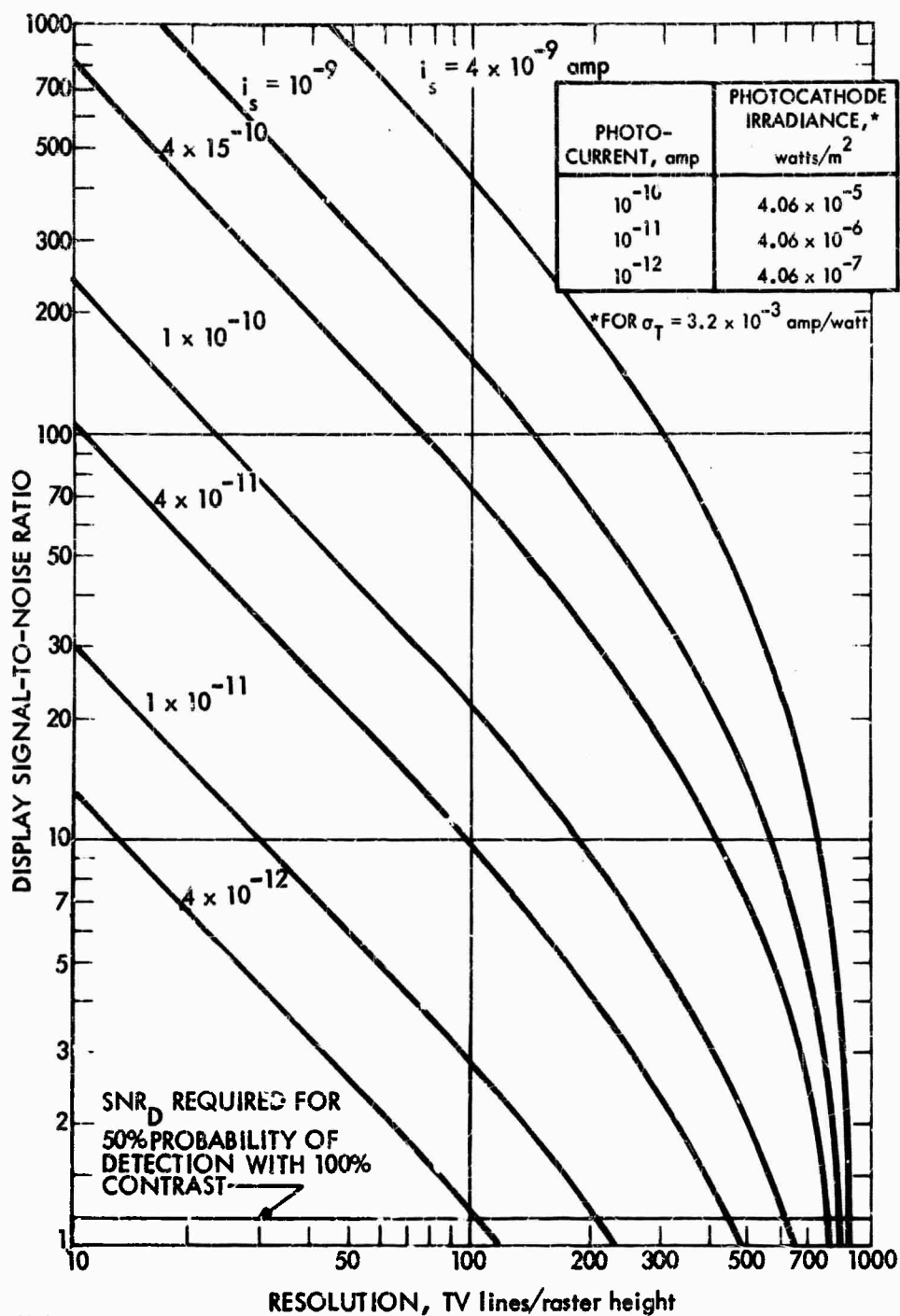


FIGURE V-D-11. Display Signal-to-Noise Ratio Versus Resolution for the WL30654 SEC Camera as a Function of Input Photocathode Current



S3-18-71-57

FIGURE V-D-12. Display Signal-to-Noise Ratio Versus Resolution for the WX31223 SEC Camera for Various Input Photocathode Currents

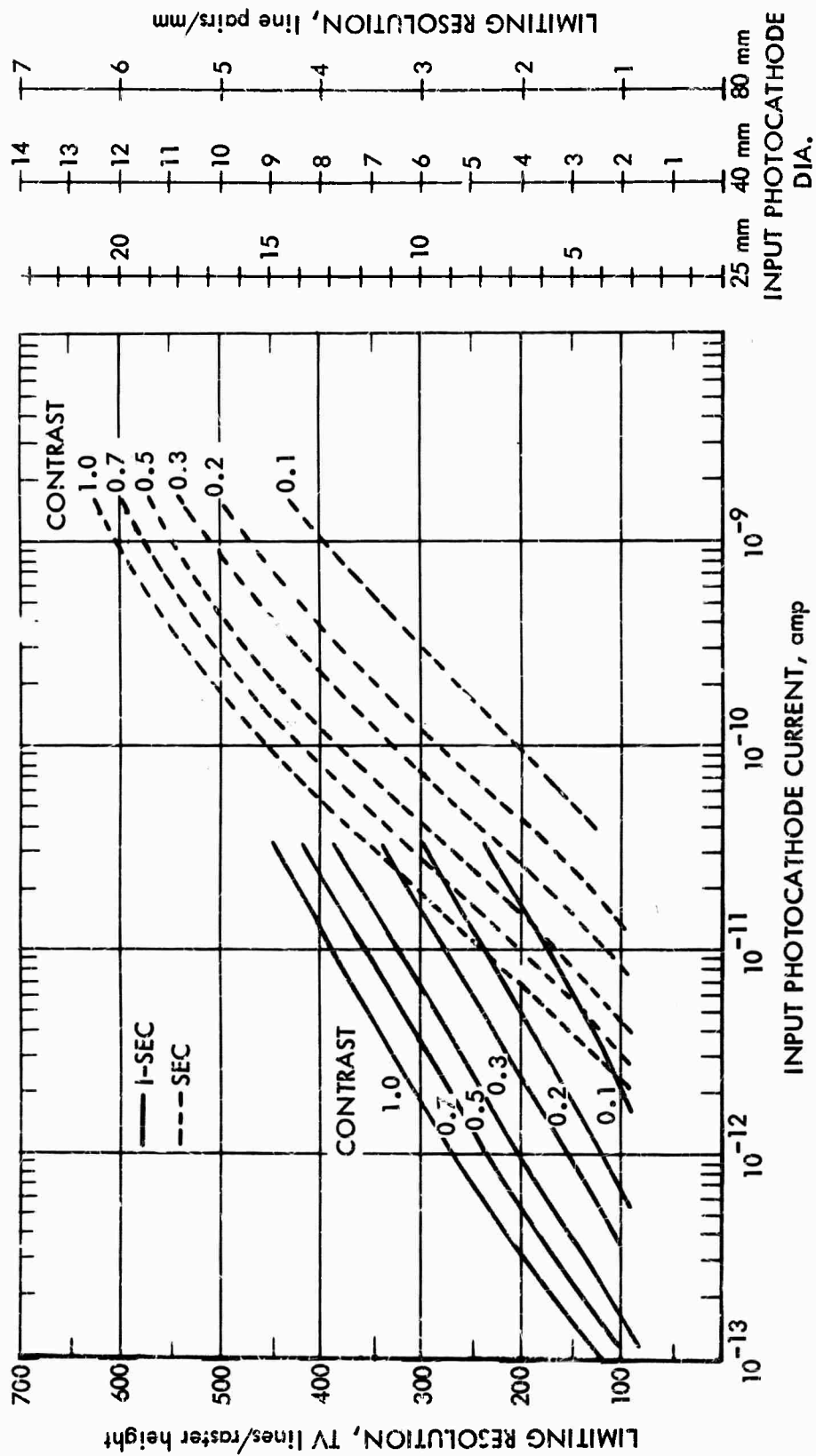


FIGURE V-D-13. Limiting Resolution Versus Input Photocathode Current for the WL30691 SEC and Intensifier-SEC Cameras for Various Image Contrasts



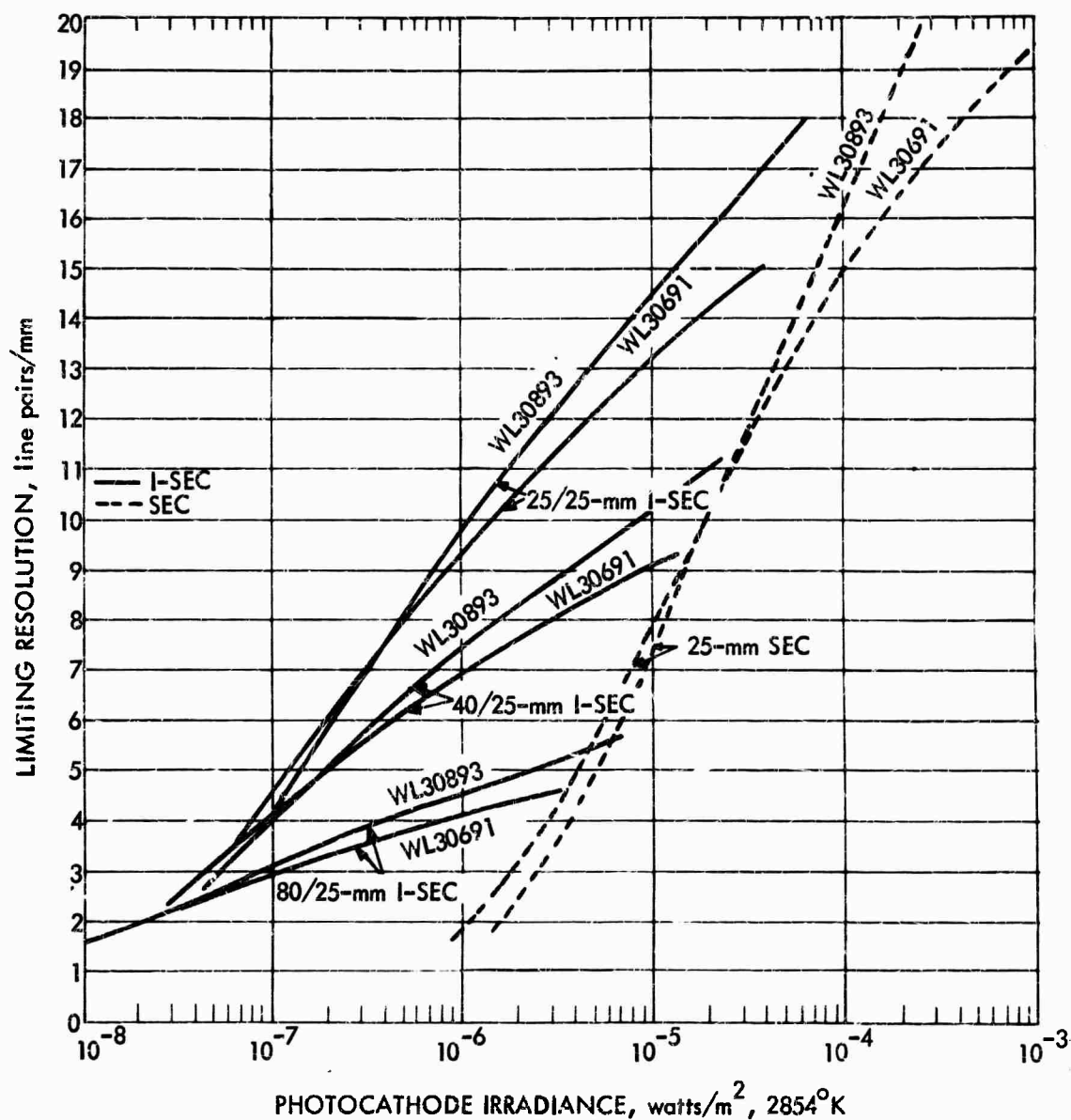


FIGURE V-D-14. Limiting Resolution Versus Photocathode Irradiance, Contrast 100%, for the WL30691 and WL30893 SEC and Intensifier-SEC Cameras

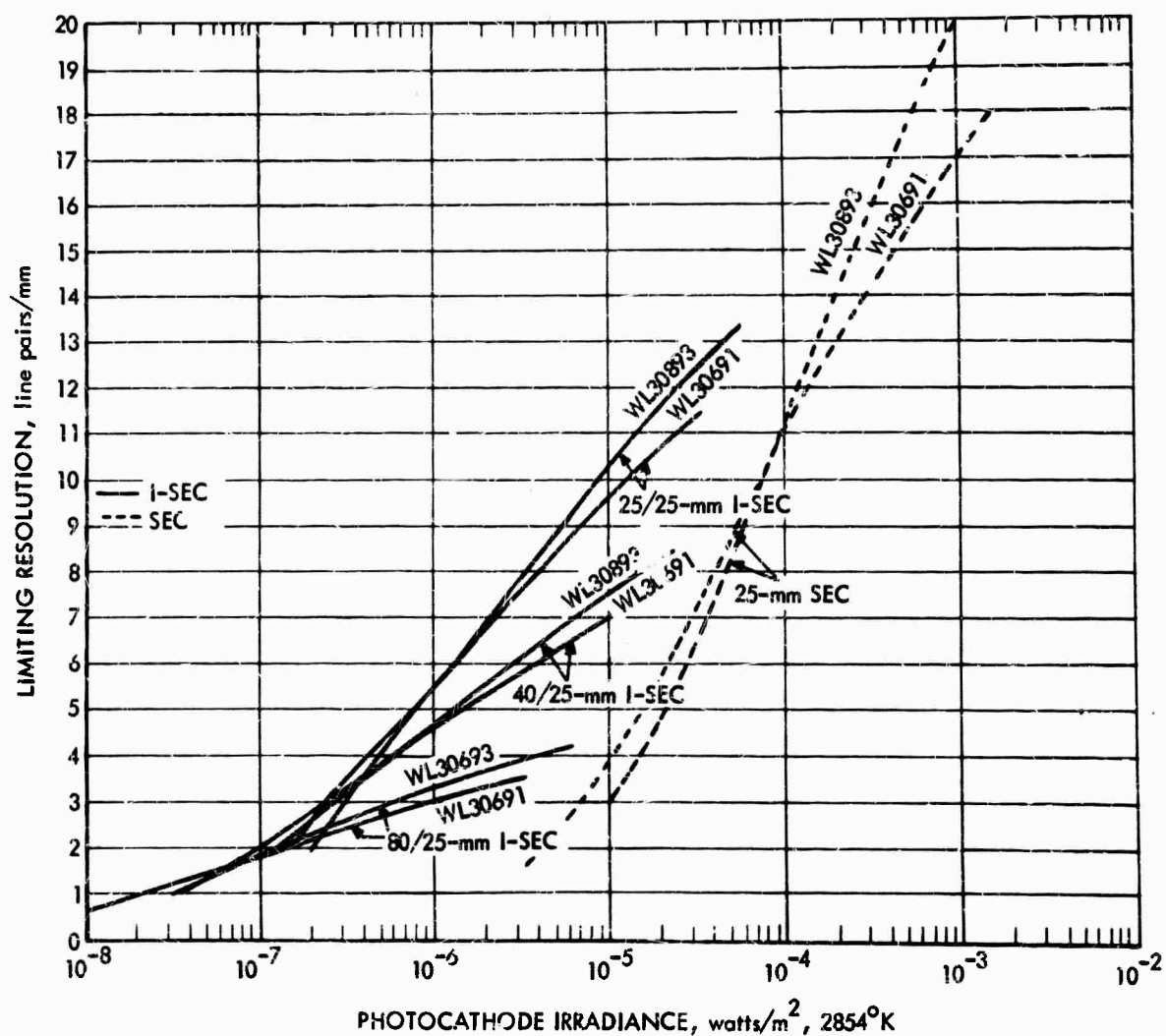


FIGURE V-D-15. Limiting Resolution Versus Photocathode Irradiance, Contrast 30%, for the WL30691 and WL30893 SEC and Intensifier-SEC Cameras

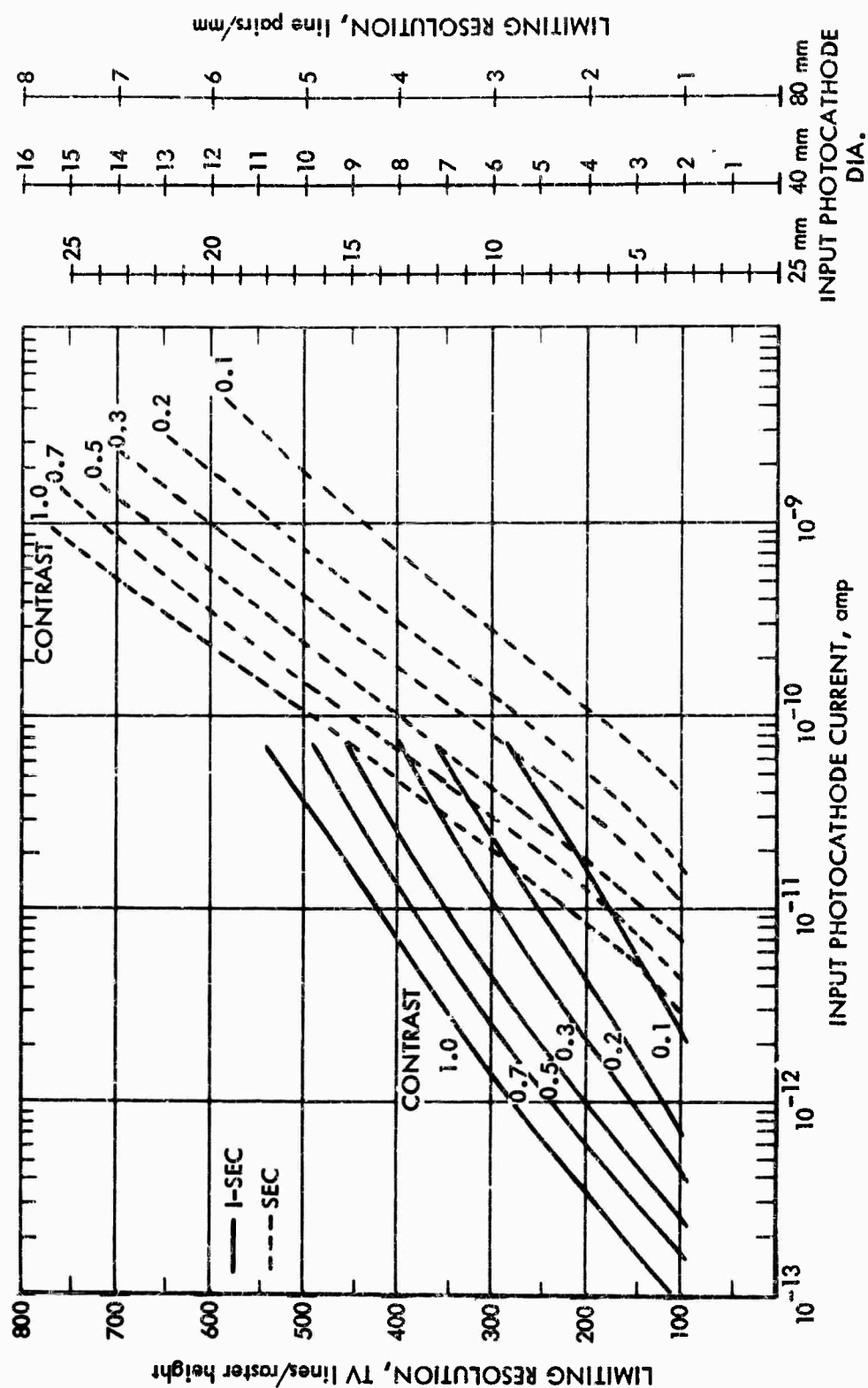


FIGURE V-D-16. Limiting Resolution Versus Input Photocathode Current for the WL30893 SEC and Intensifier-SEC Cameras

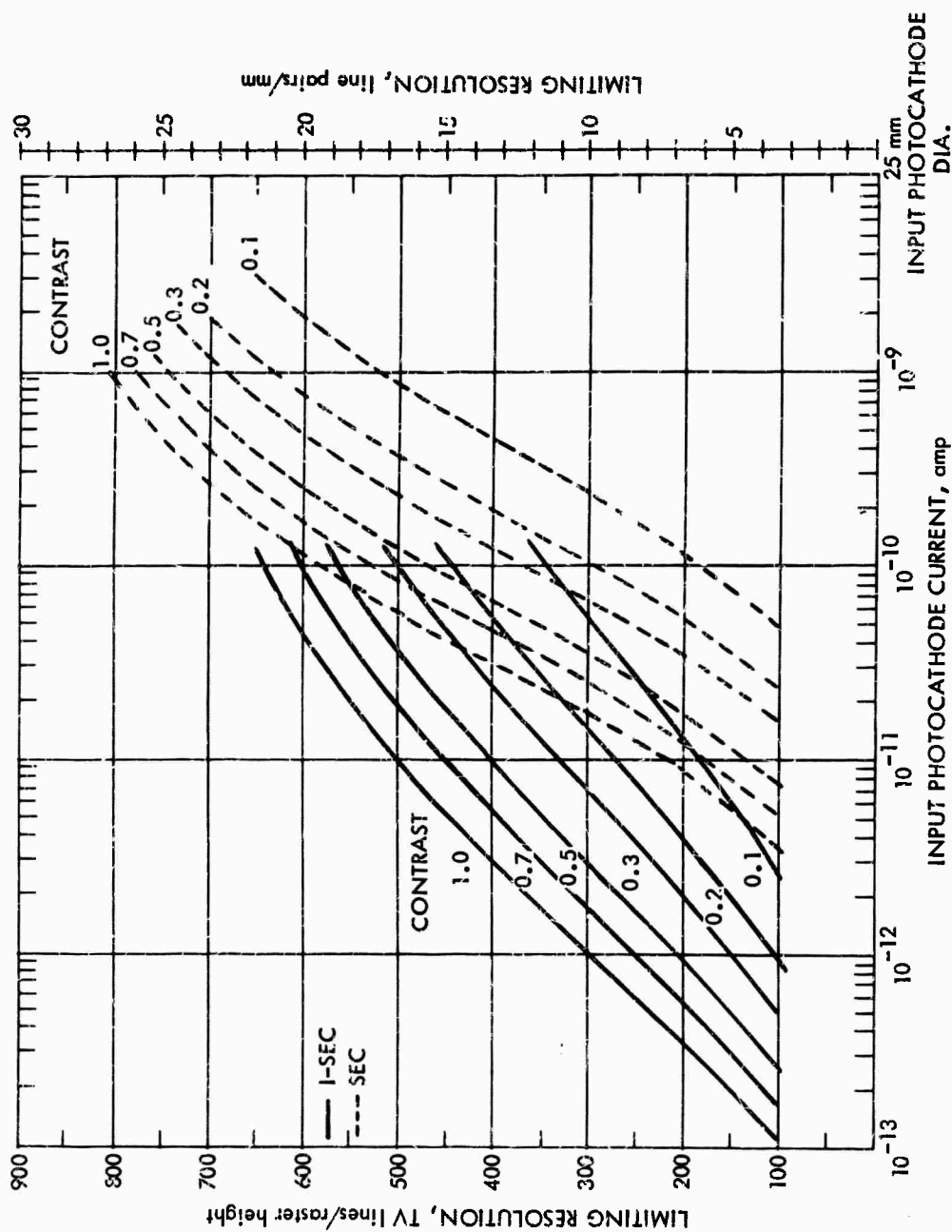


FIGURE V-D-17. Limiting Resolution Versus Input Photocathode Current for the WX31381 SEC and Intensifier-SEC Cameras in the 1.5:1 Zoom Mode (25-mm Input Photocathode) for Various Image Contrasts

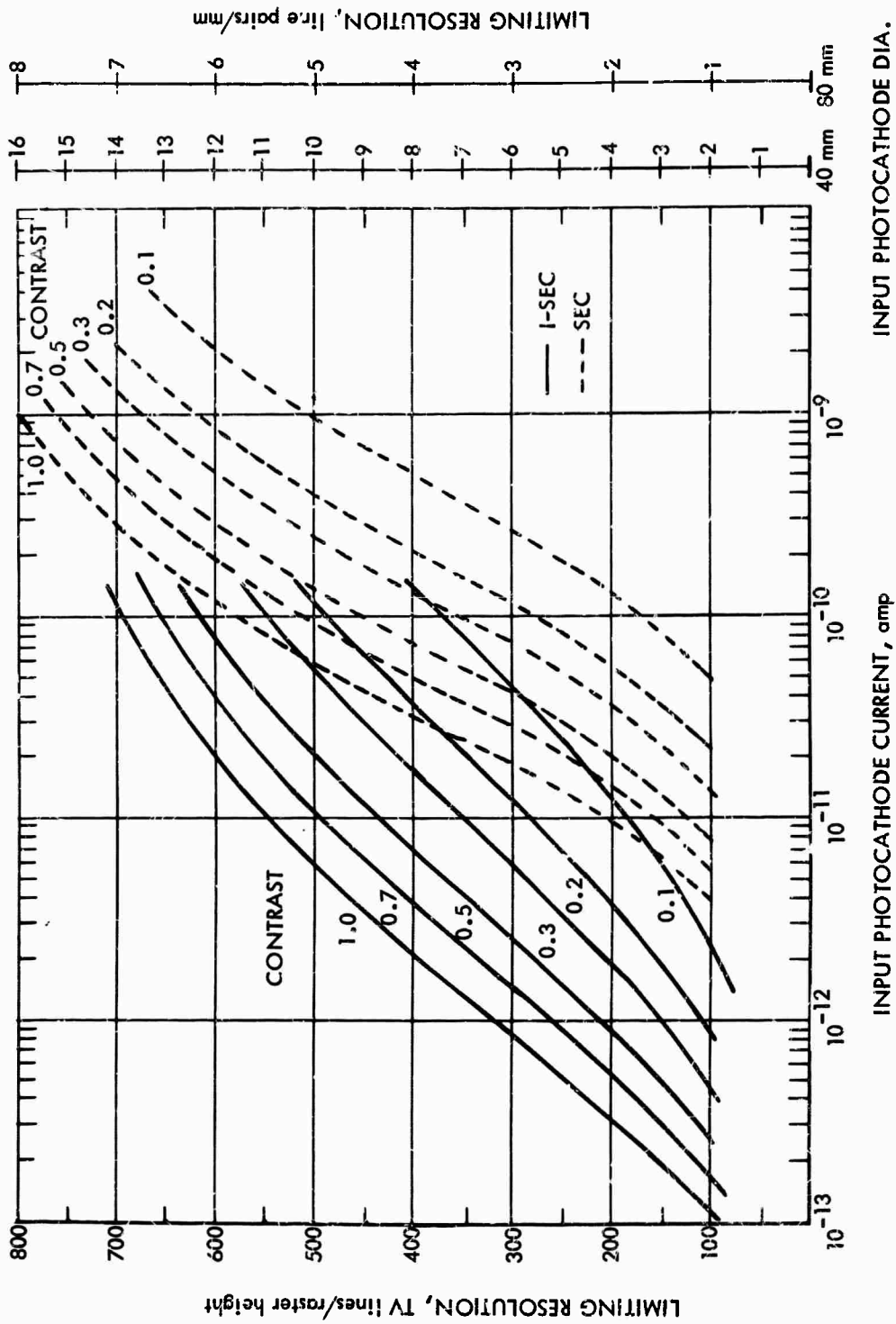


FIGURE V-D-18. Limiting Resolution Versus Input Photocathode Current for the WX31381 SEC and Intensifier-SEC Cameras in the 1:1 Zoom Mode (40-mm SEC Photocathode) for Various Image Contrasts

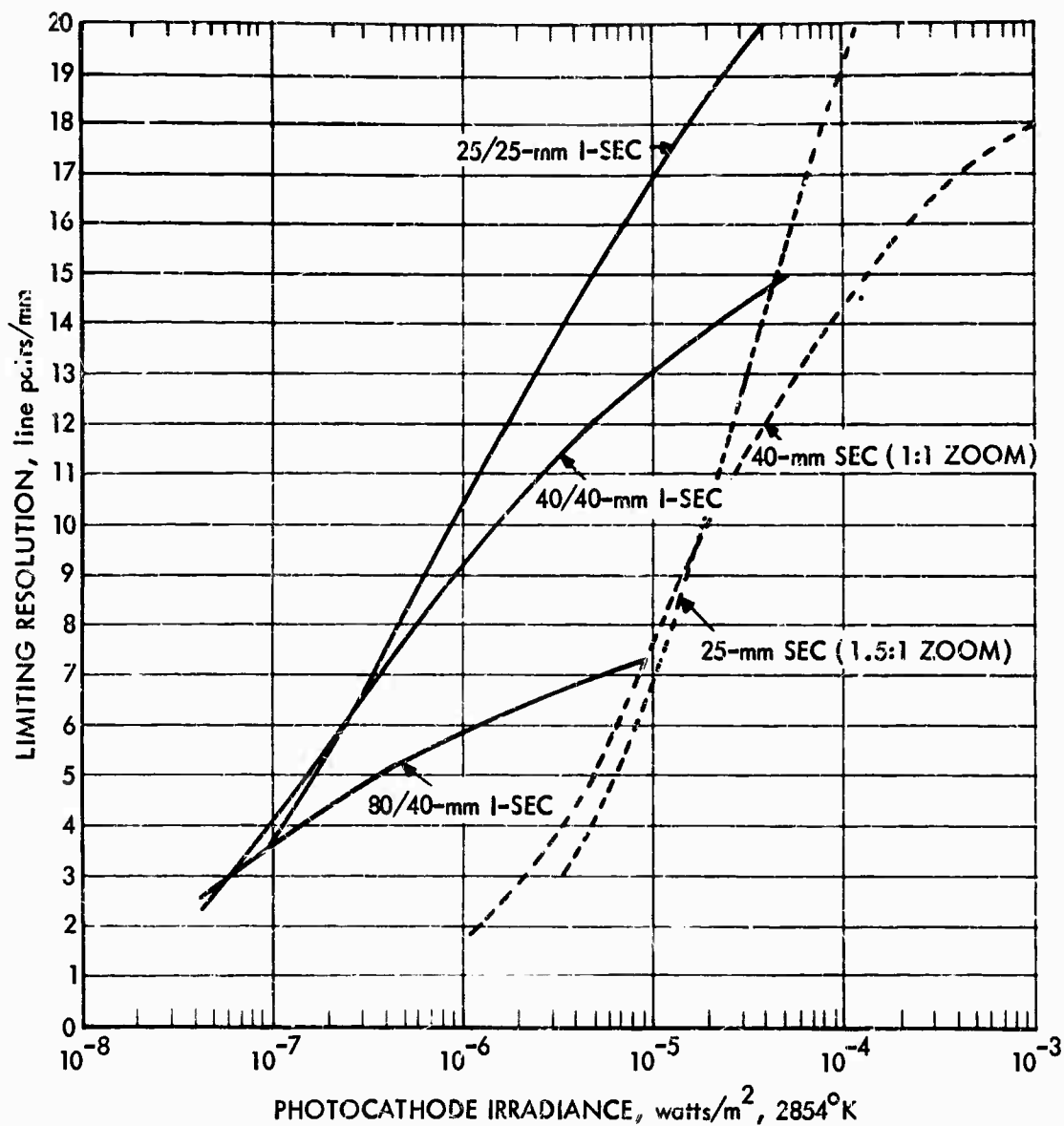


FIGURE V-D-19. Limiting Resolution Versus Photocathode Irradiance, Contrast 100%, for the WX31381 SEC and Intensifier-SEC Cameras

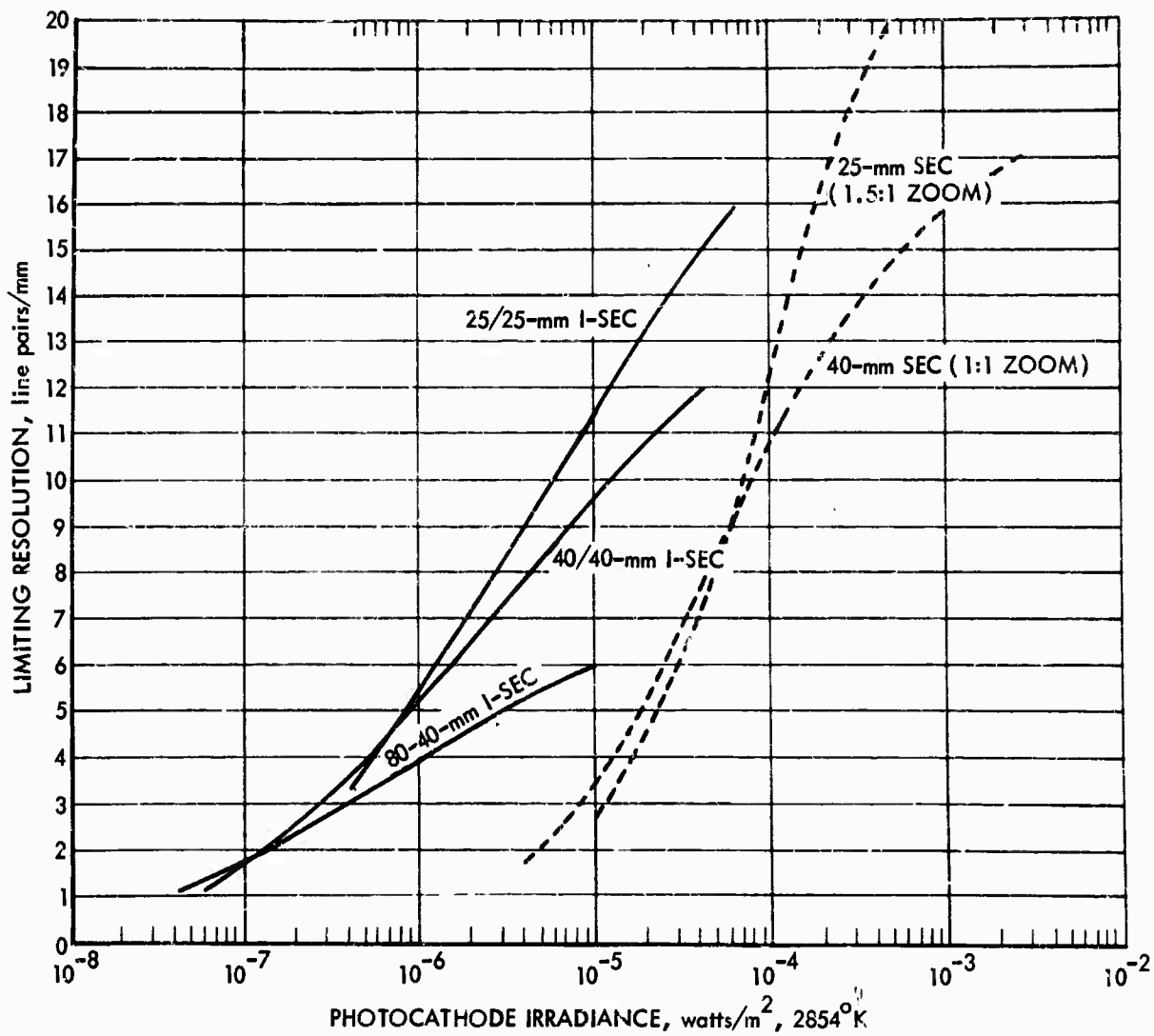


FIGURE V-D-20. Limiting Resolution Versus Photocathode Irradiance, Contrast 30%, for the WX31381 SEC and Intensifier-SEC Cameras

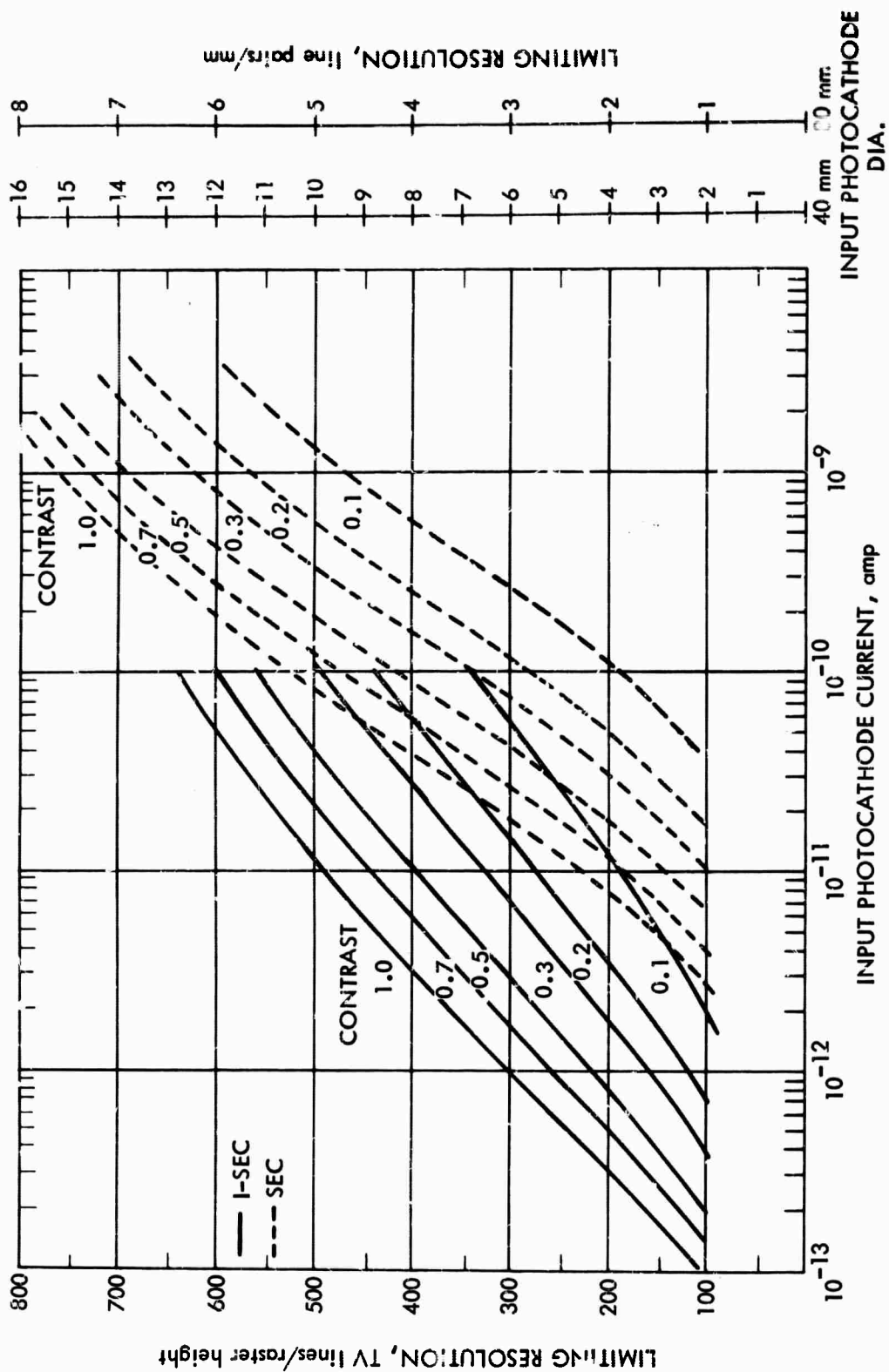


FIGURE V-D-21. Limiting Resolution Versus Input Photocathode Current for the WL30654 SEC and Intensifier-SEC Cameras for Various Image Contrasts



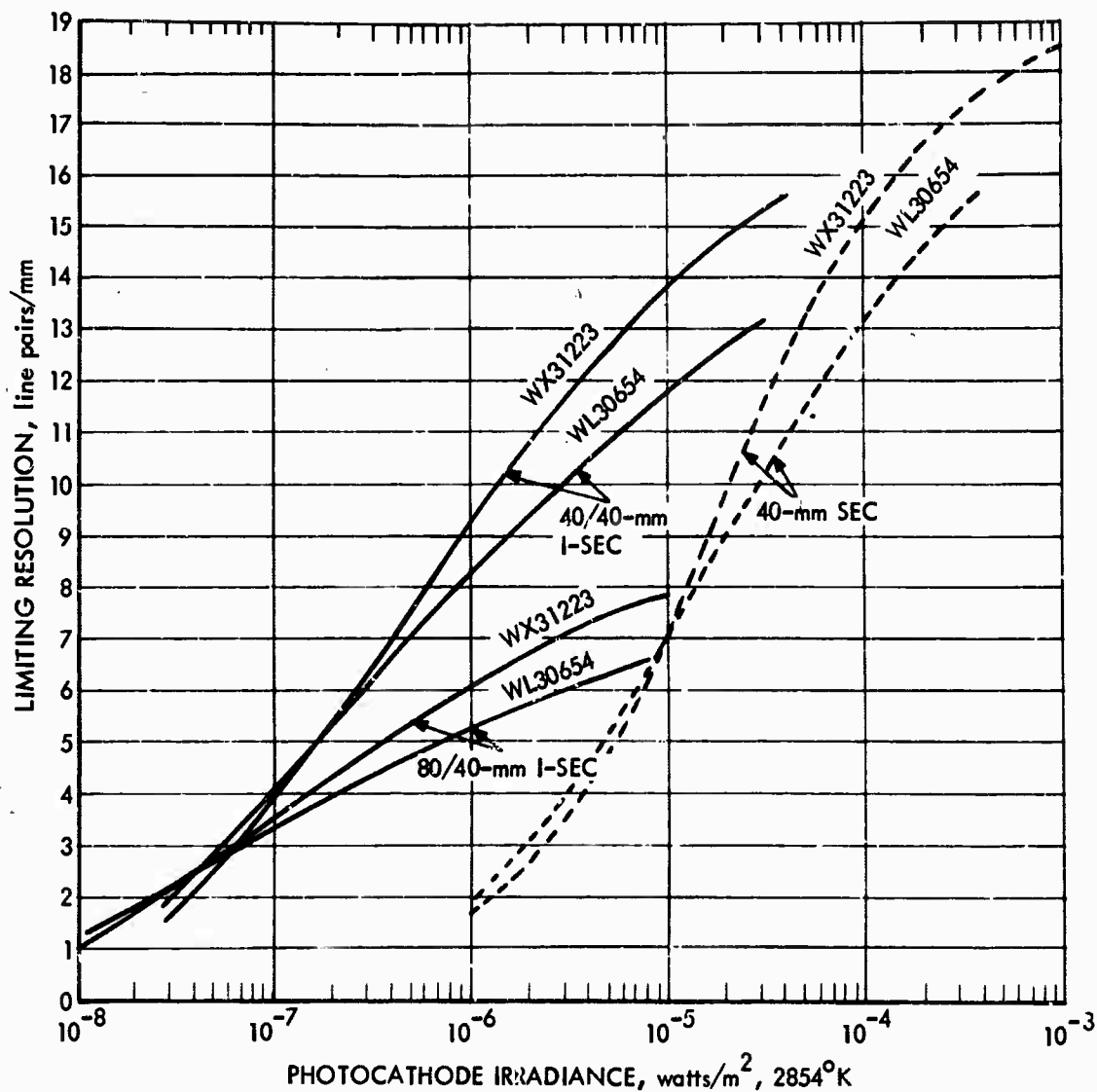


FIGURE V-D-22. Limiting Resolution Versus Photocathode Irradiance, Contrast 100%, for the WL30654 and the WX31223 SEC and Intensifier-SEC

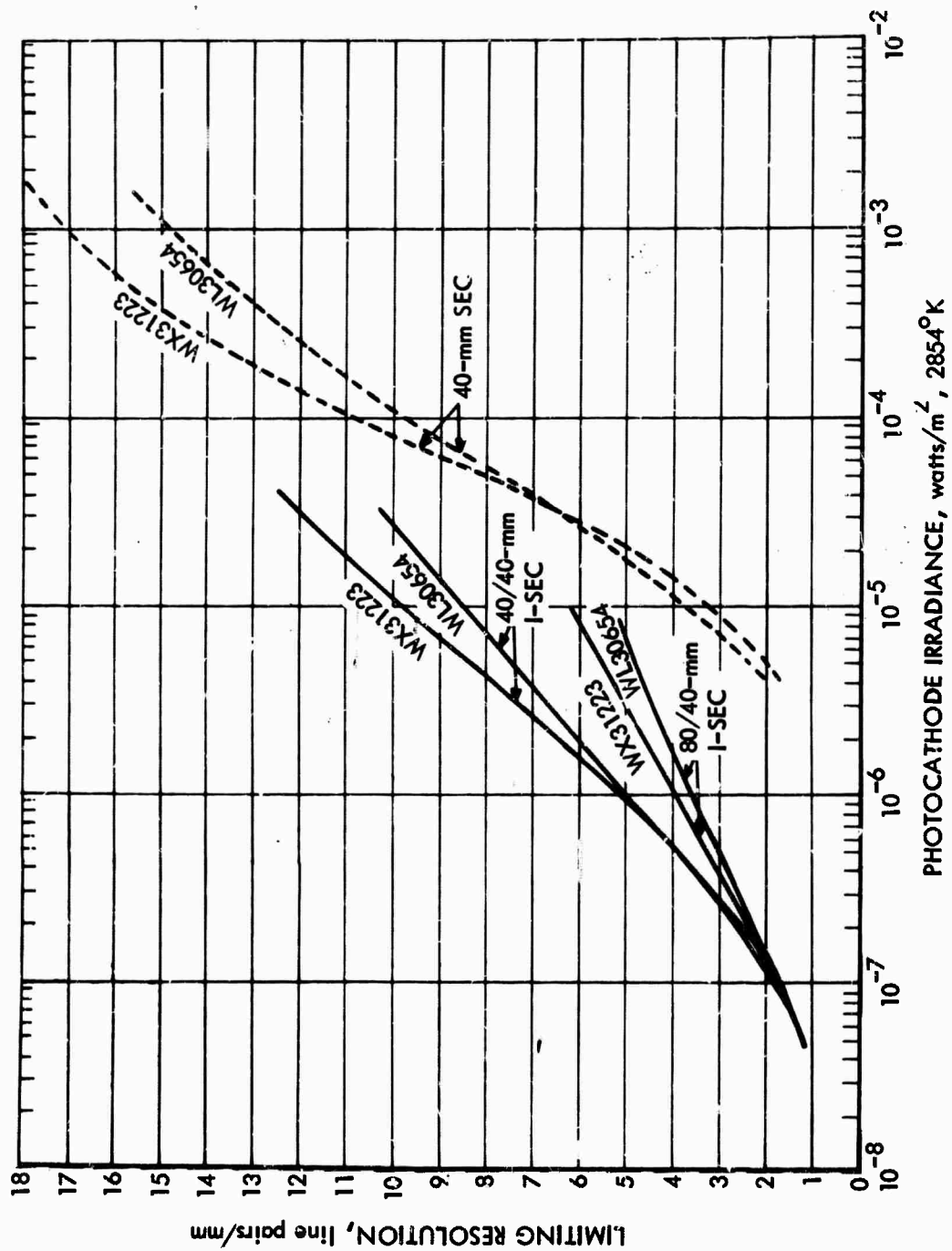


FIGURE V-D-23. Limiting Resolution Versus Photocathode Irradiance, Contrast 30%,  
for the WL30654 and the WX31223 SEC and Intensifier-SEC Cameras

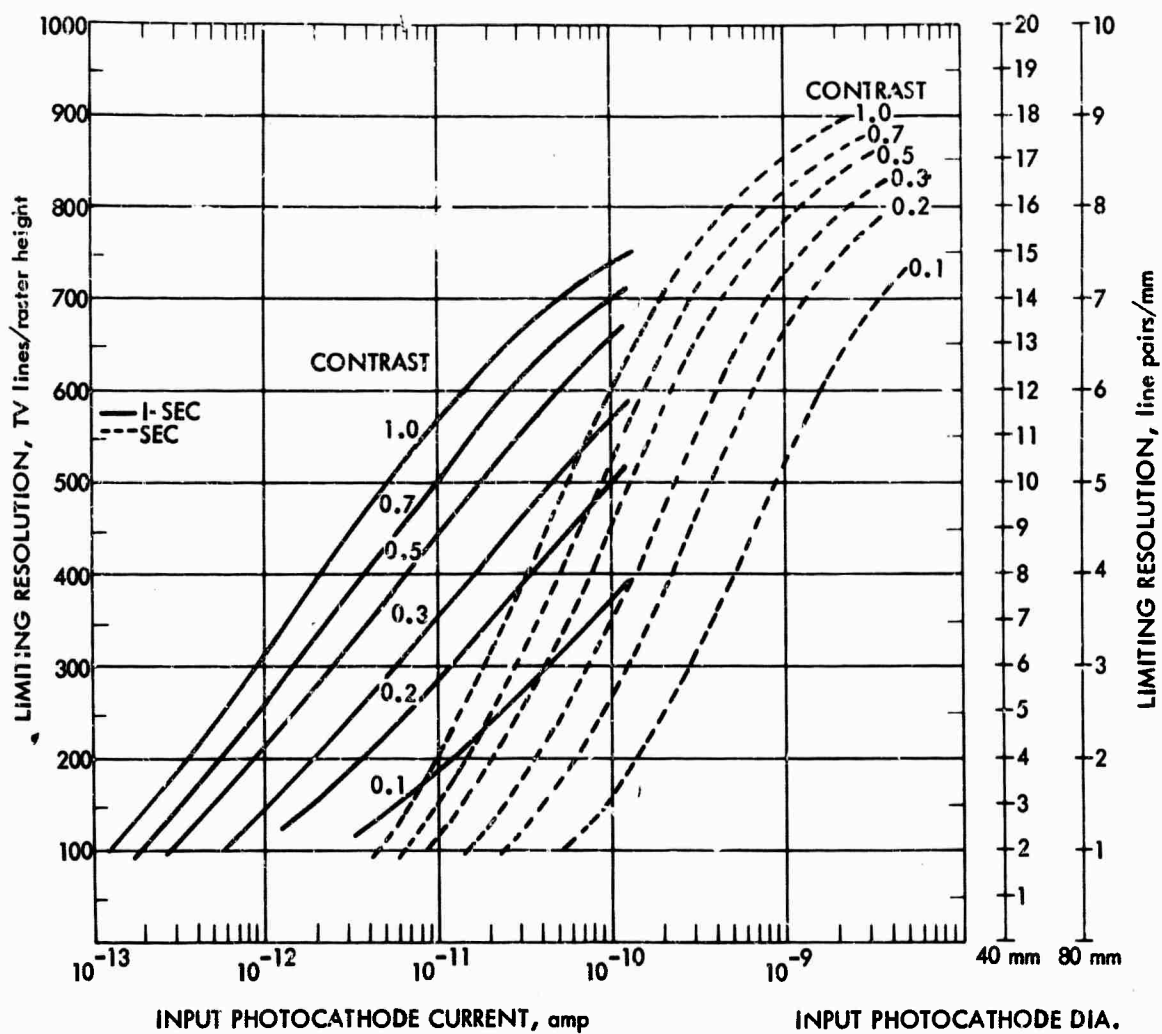


FIGURE V-D-24. Limiting Resolution Versus Input Photocathode Current for the WX31223 SEC and Intensifier-SEC Cameras for Various Input Image Contrasts

f. Computed versus Measured Results. The computed versus measured results correlate quite closely for the SEC cameras. One result is shown for the WL30691 in Fig. V-D-25. The small discrepancy observed is probably due to a somewhat larger preamplifier noise in the real system than was estimated in the analysis.

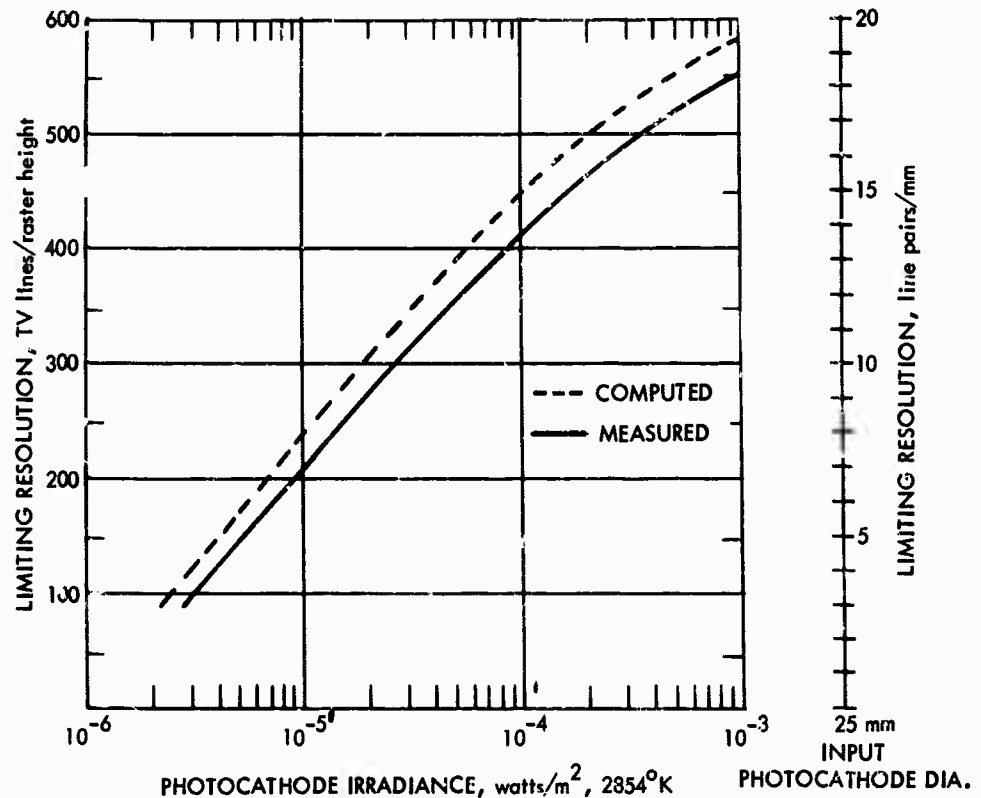


FIGURE V-D-25. Limiting Resolution Versus Photocathode Irradiance. Comparison of Computed Versus Measured Performance for the WL30691 SEC Camera

g. Lag Characteristics. The residual signal versus photocathode irradiance curves are plotted in Fig. V-D-26. Lag is shown in terms of a range of values. In general, tubes with larger photocathodes have larger targets and are therefore laggier, but they are also more sensitive, so that when lag is plotted against irradiance level the

differences tend to cancel out. The dynamic resolution versus photocathode irradiance curves are shown in Fig. V-D-27 for two pattern speeds.

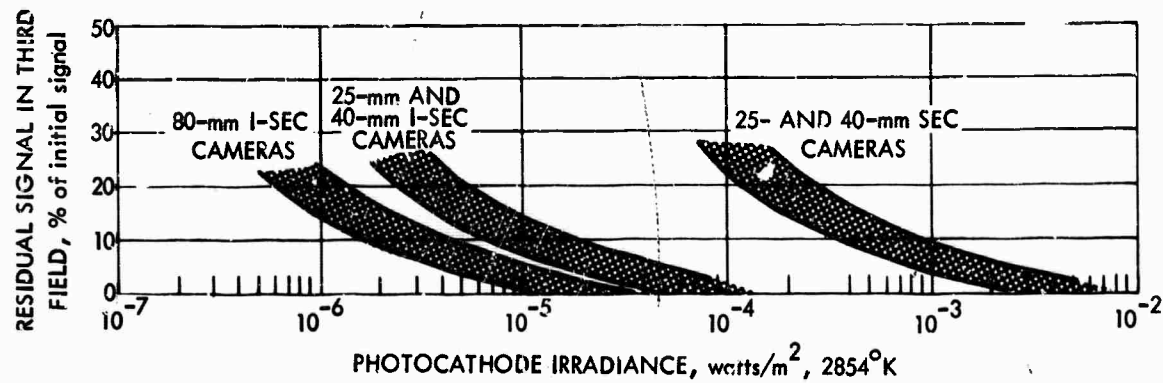


FIGURE V-D-26. Signal Lag Versus Photocathode Irradiance Characteristic for Various SEC and I-SEC Cameras

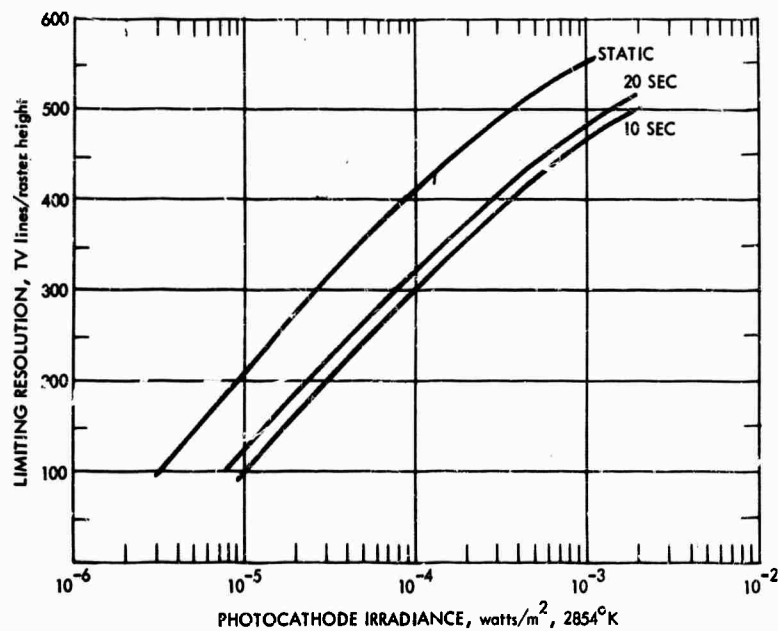


FIGURE V-D-27. Limiting Resolution Versus Photocathode Irradiance as Function of Time for Bar Pattern to Traverse the Horizontal Field of View. (Results are Typical of a WX30691 SEC Camera)

h. Form Factor. The form factors for the various tubes are given in Table V-D-1.

## 2. The Intensifier Secondary-Electron-Conduction Camera

With a single additional intensifier, the SEC camera approaches the photoelectron noise limits at low light levels, and the lag is reduced to an acceptable degree. If it were readily obtainable, an additional gain of between 3 and 5 would be desirable. A second intensifier would provide an additional gain of 30 to 40, which would be more than enough, but the loss in image quality and amplitude response far outweighs the advantage due to increased gain.

a. Principles of Operation. The additional intensifier is directly coupled to the SEC camera by means of the fiber-optic endplate on the phosphor and the fiber-optic faceplate of the SEC camera. Since the SEC target is held at near ground potential, the intensifier faceplate is at - 23 kv when operated at maximum sensitivity. Special precautions to avoid arcing to the lens must be exercised in all current low-light-level cameras, including the I-SEC. It was previously noted that the light-level latitude can be increased by about 10 to 15 by controlling the image section voltage on the SEC. An additional factor of 10 to 15 can be obtained by control of the intensifier voltage, for an overall increase of 100 to 200. By allowing a 10:1 latitude in highlight irradiance in the SEC camera, a total light-level latitude of 1000 to 2000 can be accommodated.

In the following, it will be assumed that the added intensifier will provide an electron gain of 40 and will have a photocathode radiant sensitivity of  $4 \times 10^{-3}$  amp/watt. Intensifiers having unit magnification and zoom capability will be considered.

b. Signal Transfer Characteristics. The signal transfer characteristics of the various I-SEC cameras are shown in Fig. V-D-2. The light gain due to an intensifier of unit magnification is equal to the product of the electron gain and the ratio of intensifier to SEC photocathode sensitivity. This is taken to be 50. When a "zoom" or "minifying" intensifier is used, an additional light gain equal to the ratio

of intensifier to SEC photocathode area is obtained as shown. Thus, the signal current expression becomes

$$\begin{aligned}
 I_S &= G_L G_T i_{sv}/e_v e_h \\
 &= G_I \left[ \frac{\sigma_I}{\sigma_V} \right] \cdot \left[ \frac{A_I}{A_V} \right] \cdot G_T \cdot \frac{\sigma_V A_V E}{e_v e_h} \\
 &= \frac{G_I G_T \sigma_I A_I E}{e_v e_h} \\
 &= G_I G_T i_{sI}/e_v e_h
 \end{aligned}
 \tag{V-D-4}$$

where  $G_I$  is the electron gain due to the intensifier,  $G_T$  is the SEC target gain,  $\sigma_I$  and  $A_I$  are the intensifier's radiant sensitivity and effective photocathode area, respectively, and  $\sigma_V$  and  $A_V$  are the corresponding quantities for the SEC camera.

c. Amplitude Response. The square-wave response for the various I-SEC cameras are shown in Fig. V-D-28 for SEC cameras with 25-mm input photocathodes and in Fig. V-D-29 for SEC cameras with 40-mm photocathodes. The intensifier photocathode areas can be equal to or larger than the SEC photocathode areas. Note that the line pair/millimeter scale applies only to the intensifier's photocathode.

d. Video and Display Signal-to-Noise Ratio. The video signal-to-noise ratio at unit contrast and for patterns of low spatial frequency is equal to

$$SNR_{V,0,1} = \frac{G_I G_T i_s/e_v e_h}{\left[ (G_I G_T)^2 \frac{e \Delta f i_s}{e_v e_h} + \overline{I}_{PA}^2 \right]^{1/2}}
 \tag{V-D-5}$$

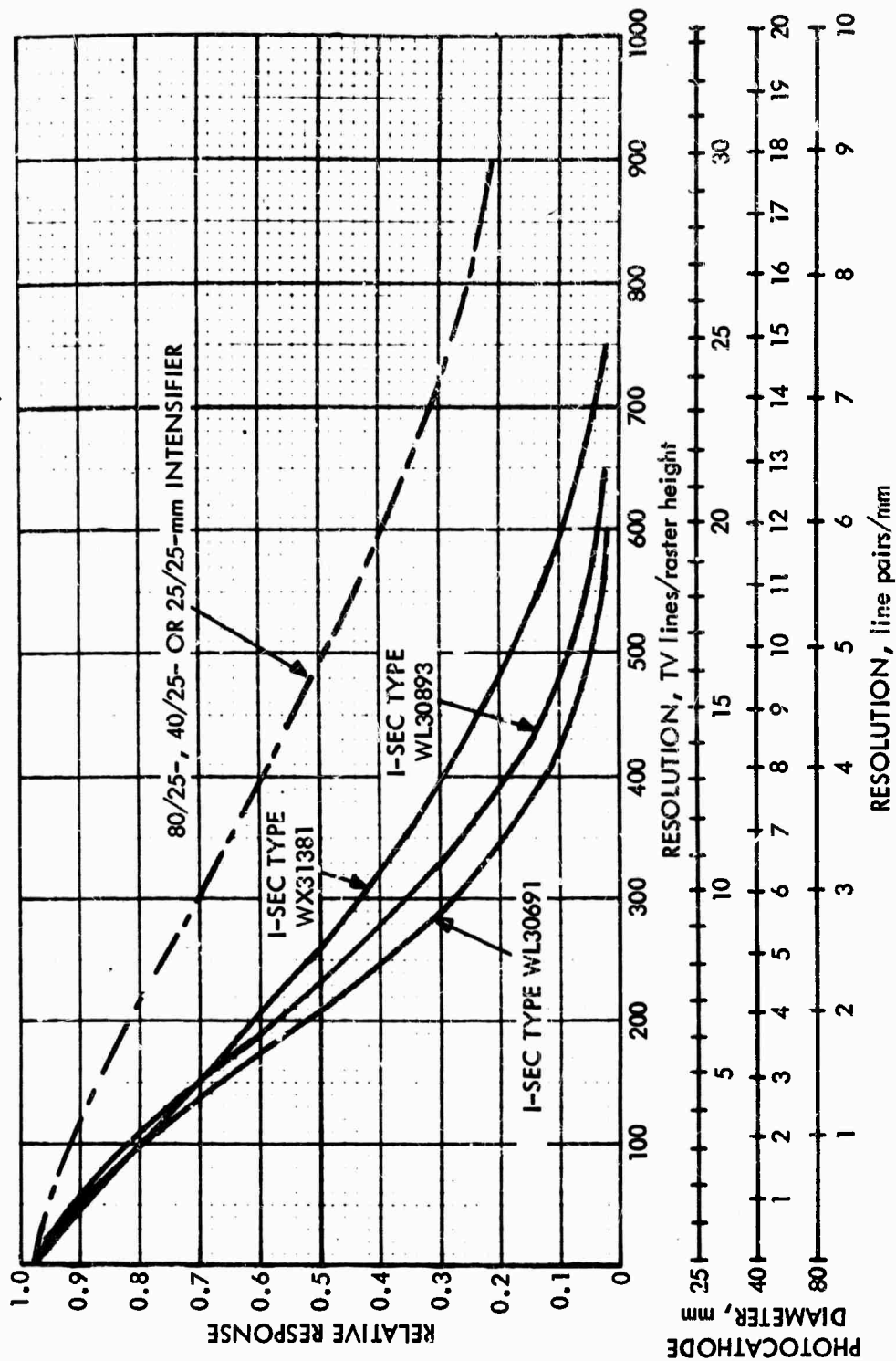


FIGURE V-D-28. Uncompensated Horizontal Square- or Sine-Wave Response of I-SEC Cameras with 25-mm Phosphor-Photocathode Interface Diameters. (Intensifier Response is Sine Wave; I-SEC Response is Square Wave)



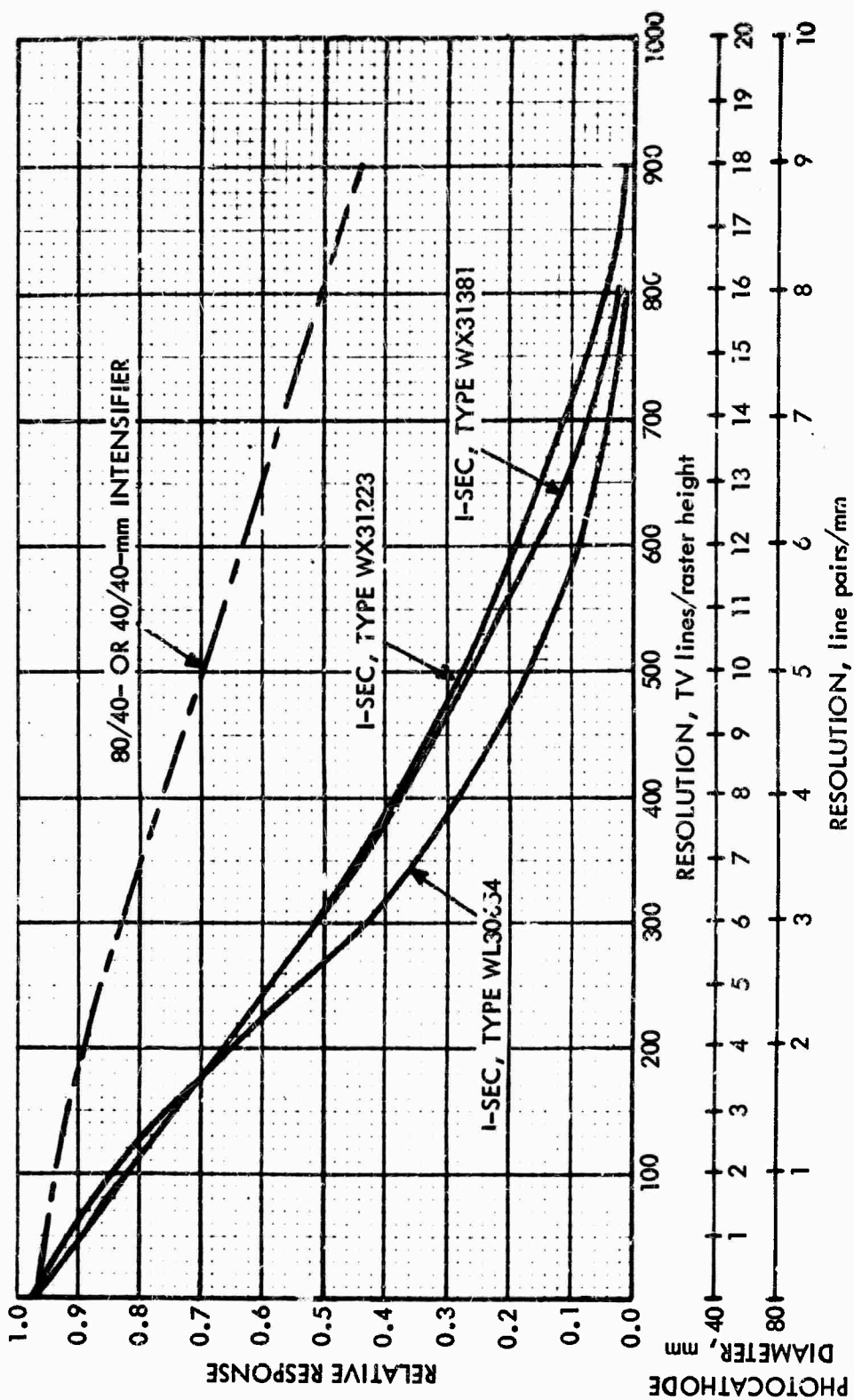


FIGURE V-D-29. Uncompensated Horizontal Square- or Sine-Wave Response for the I-SEC Cameras with 40-mm Phosphor-Photocathode Interfaces. (Intensifier Response is Sine Wave, I-SEC Response is Square Wave)

The various signal and noise currents are plotted in Fig. V-D-7. It is seen that photoelectron noise becomes predominant for photocurrents above about  $10^{-12}$  amp. The video signal-to-noise ratios are plotted in Fig. V-D-8 and the display signal-to-noise ratios are plotted in Fig. V-D-30 through V-D-32.

e. Limiting Bar-Pattern Resolution. The limiting resolution versus photocathode current and irradiance curves are shown in Figs. V-D-13 through V-D-24. As can be seen, the performance of the SEC is considerably extended to the lower irradiance levels by the added intensifier.

f. Computed versus Measured Results. The computed versus measured results are shown for the WL30654 I-SEC in Fig. V-D-33 and for the WX31223 I-SEC in Fig. V-D-34. The results at high contrast are quite close, while low-contrast analytical predictions are pessimistic. This is characteristic of the analysis and stems mainly from the fact that noise filtering by the apertures in the camera tube is only partially taken into account.

g. Lag Characteristics. The third-field residual-signal lag characteristics are shown for the various I-SEC cameras in Fig. V-D-26. The dynamic resolution versus photocathode irradiance curves are shown for the 40-mm WL30654 I-SEC in Fig. V-D-35. With ambient lighting in the quarter-moon-to-starlight range, the corresponding photocathode irradiance will be approximately  $10^{-5}$  to  $5 \times 10^{-7}$ . It can be readily seen that, at the lower irradiance levels, any appreciable scene motion can result in a resolution loss. In practice, it has been found that I-SEC cameras do provide significant capability at starlight levels, but some degradation due to lag is observable.

h. Form Factor. A 25-mm intensifier adds approximately 2 in. to the overall length of the camera-head assembly and nothing to the diameter. An 80-mm intensifier adds 8 in. to the length, and its 6-in. diameter becomes the maximum camera-head diameter.

i. Manufacturers' Literature. A sample of manufacturers' literature on SEC camera tubes will be found in Chart V-D-1.

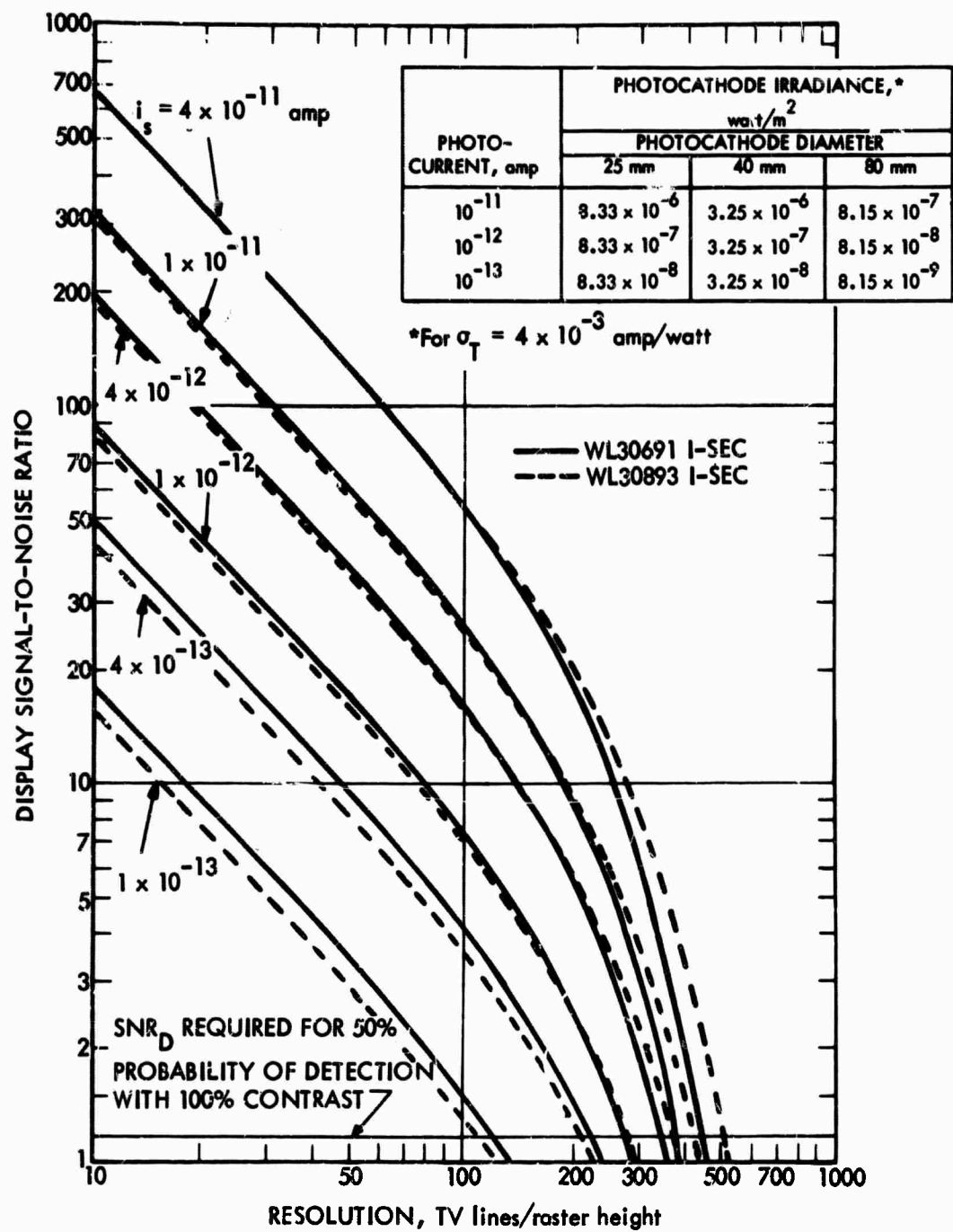


FIGURE V-D-30. Display Signal-to-Noise Ratio Versus Resolution for the WL30691 and WL30893 Intensifier-SEC Cameras as a Function of Input Photocathode Current

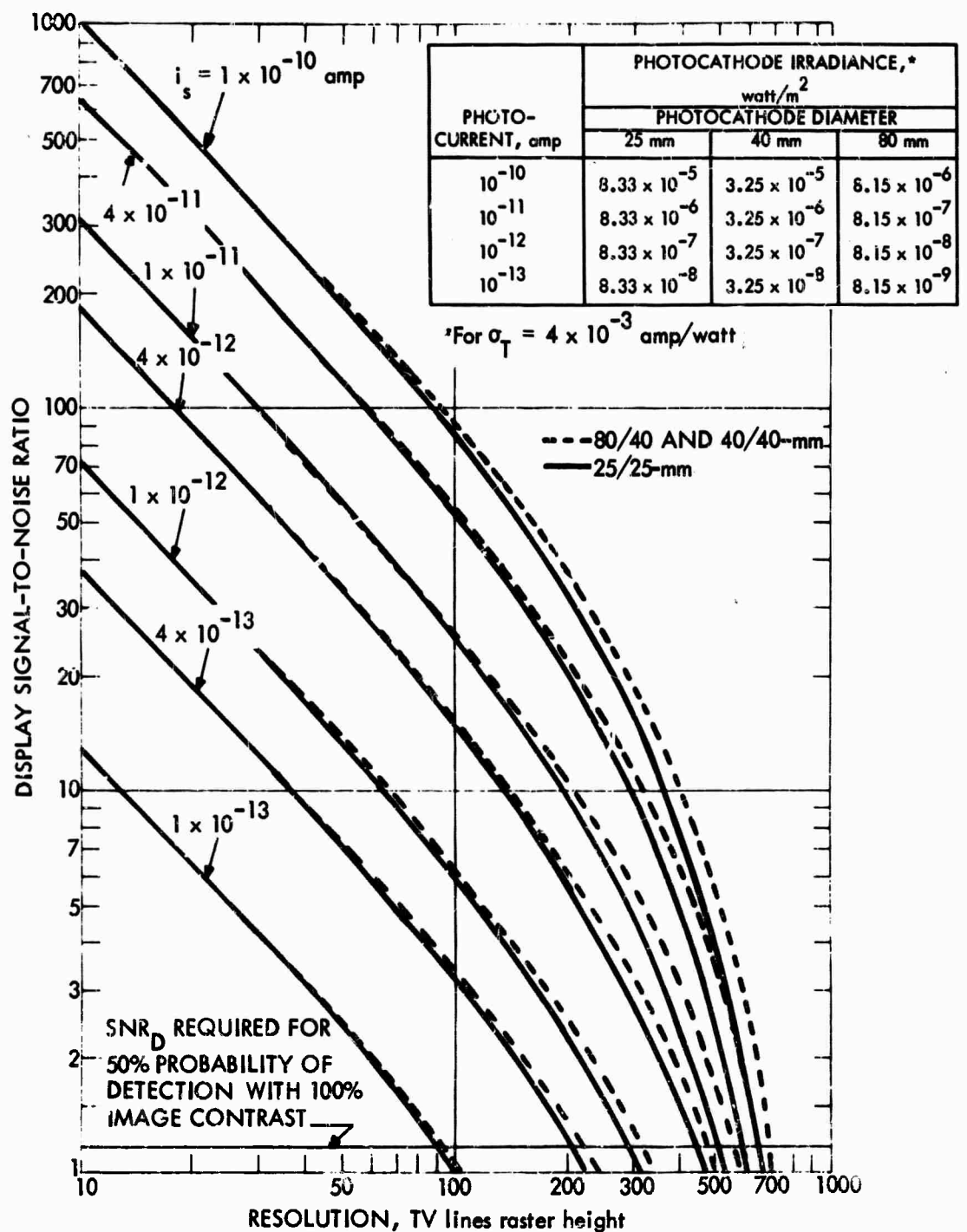


FIGURE V-D-31. Display Signal-to-Noise Ratio Versus Resolution for the WX31381 Intensifier SEC Cameras as a Function of Input Photocathode Current

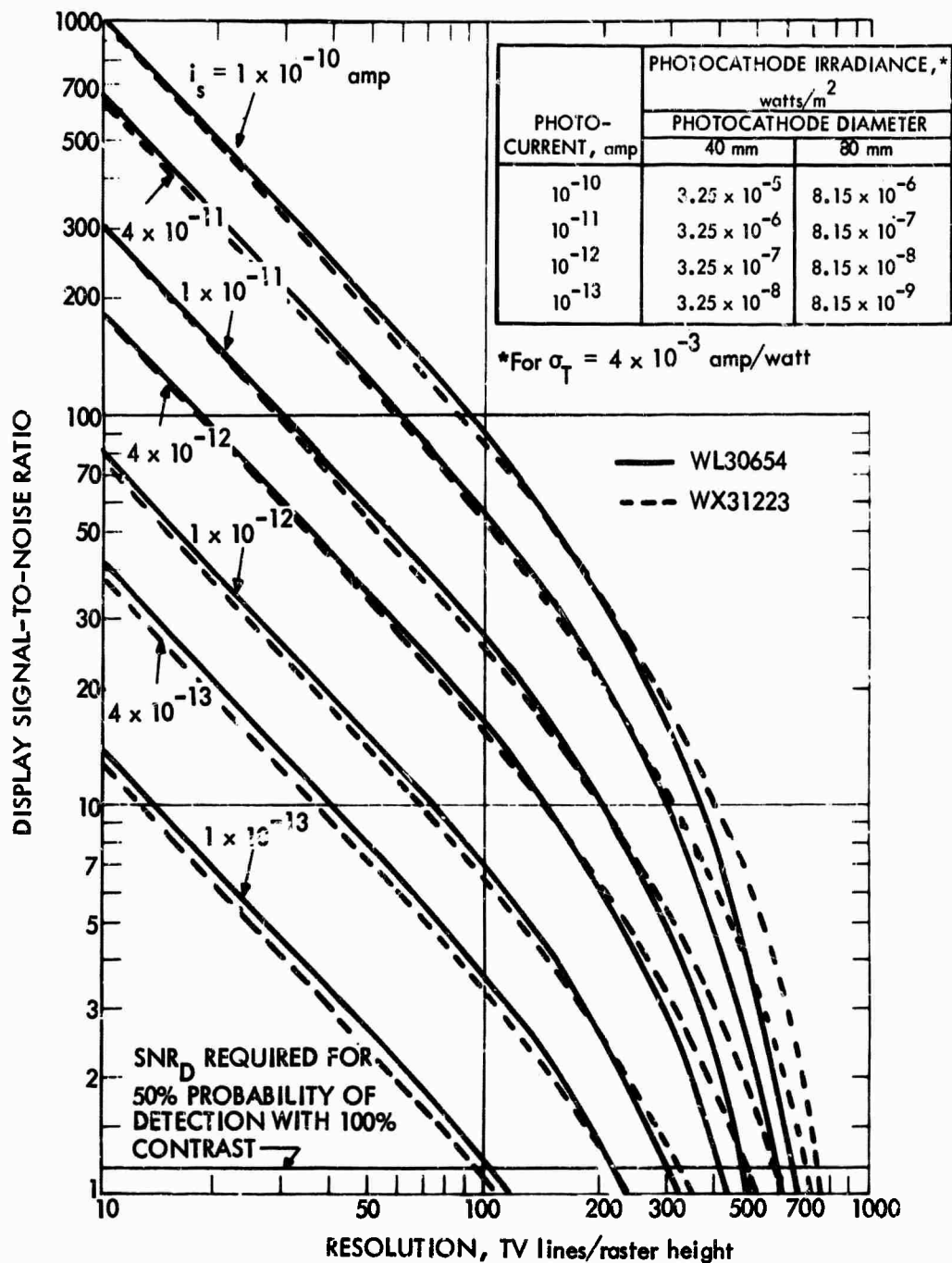


FIGURE V-D-32. Display Signal-to-Noise Ratio Versus Resolution for the WL30654 and WX31223 Intensifier SEC Cameras for Various Input Photocathode Currents

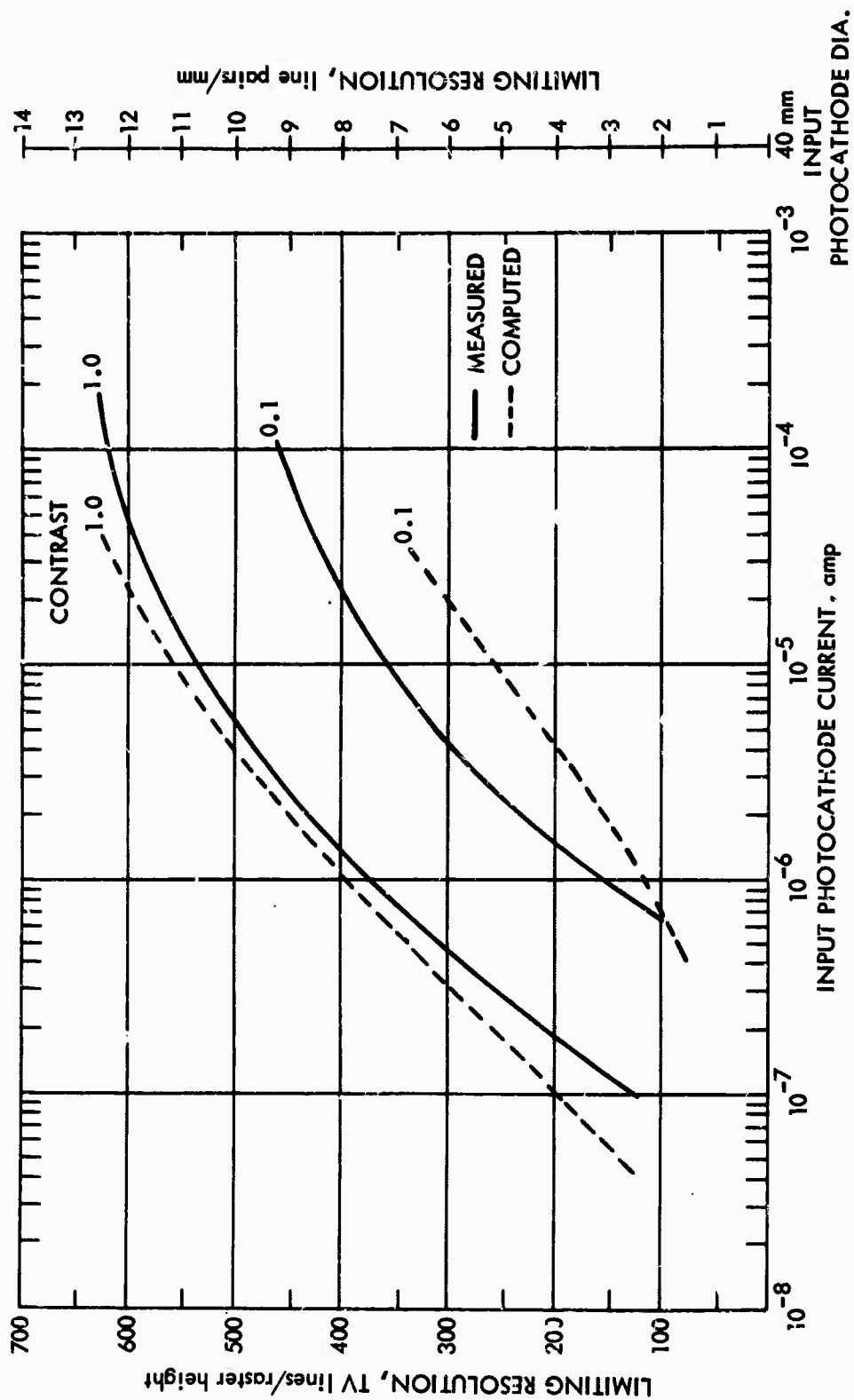


FIGURE V-D-33. Limiting Resolution Versus Photocathode Current --- Comparison of Computed and Measured Performance for the W130654 plus 40-mm Intensifier

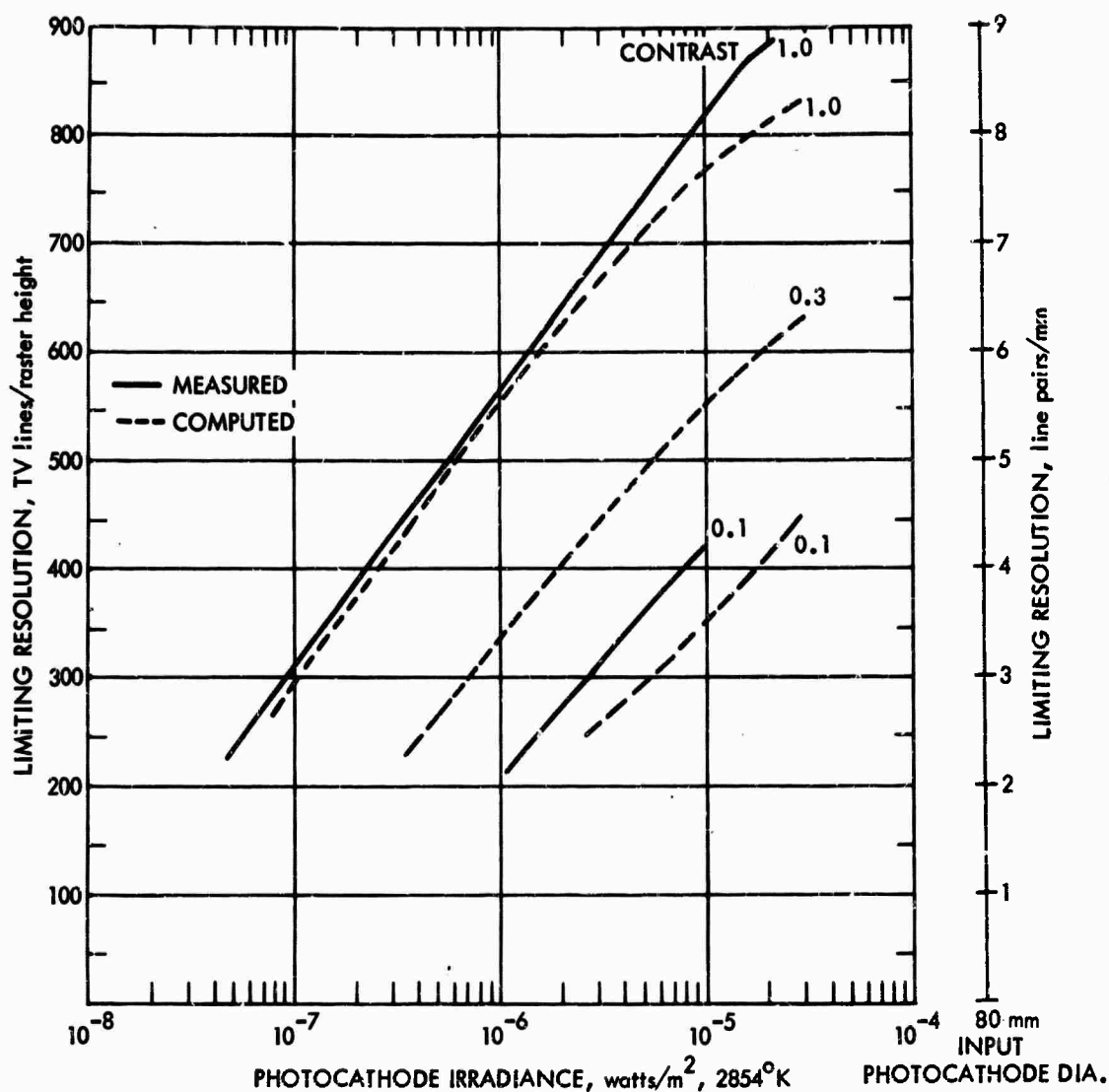


FIGURE V-D-34. Limiting Resolution Versus Photocathode Irradiance -- Comparison of Computed and Measured Performance for the WX31223 plus 80/40-mm Intensifier SEC Camera

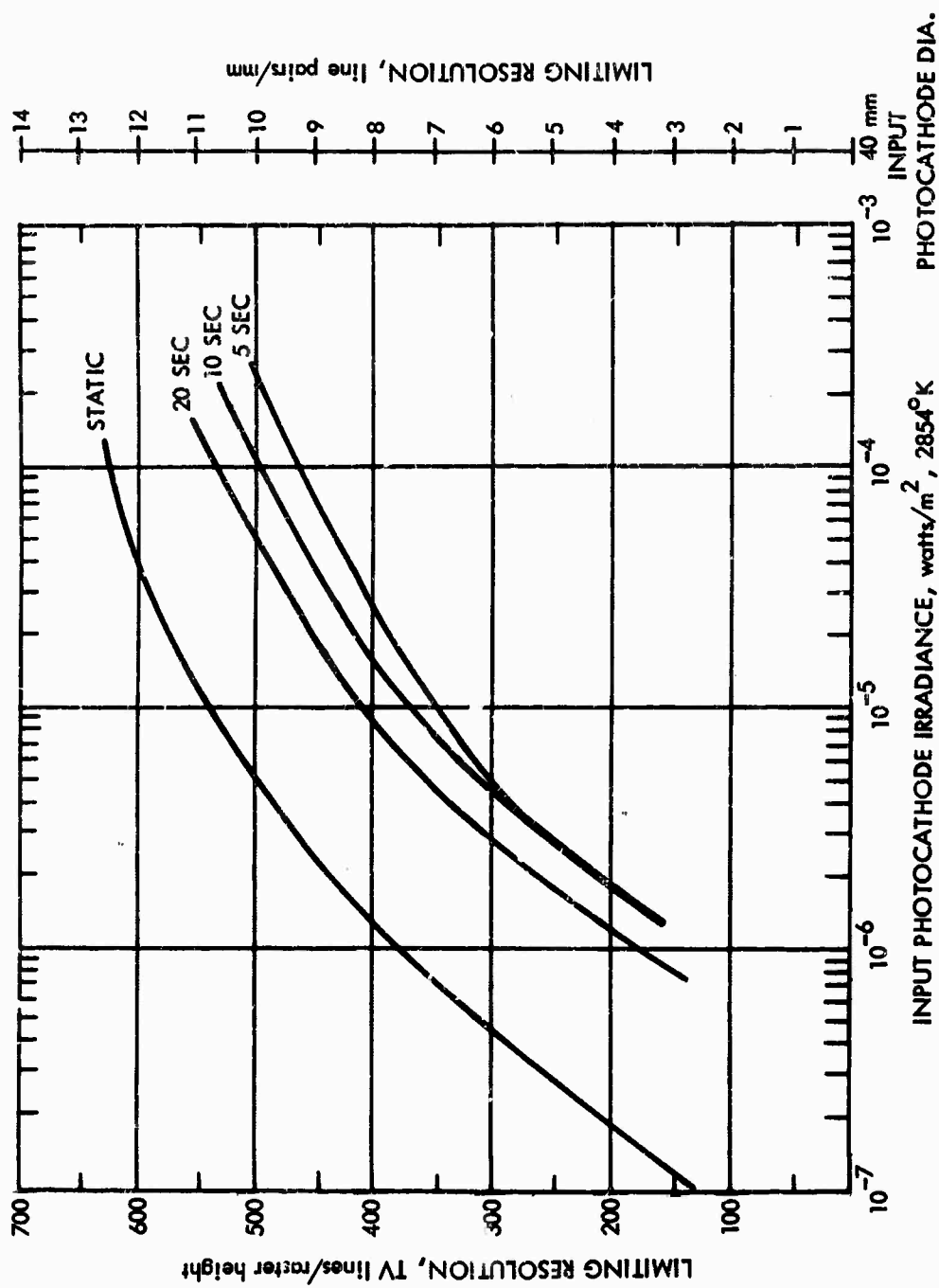


FIGURE V-D-35. Limiting Resolution Versus Photocathode Irradiance as a Function of Time for Bar Pattern to Traverse Horizontal Field of View for the WL30654 plus 40-mm Intensifier SEC Camera



CHART V-D-1. A SAMPLE OF MANUFACTURERS' LITERATURE  
ON SEC CAMERA TUBES

The units, definitions, and methods of measurement specified herein are not necessarily endorsed by the authors but are those used by the manufacturer quoted.

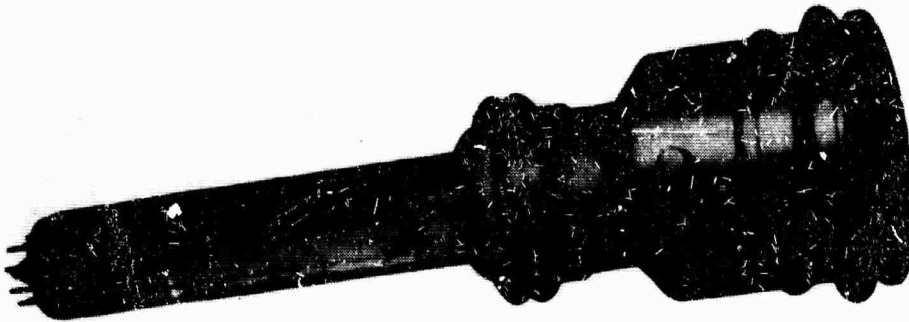
**BLANK PAGE**

Westhouse



## WX-30654 SEC Camera Tube

All Magnetic Gun  
Electrostatic Image Section  
1.6" Image Diagonal



### General Description

The WX-30654 is a rooled-up version of the WL-30591 SEC camera tube. Its larger format provides greater sensitivity, better resolution, and a larger signal-to-noise ratio without compromising other performance parameters. The novel feature of the WX-30654 which distinguishes it and other SEC camera tubes from conventional camera tubes is the Secondary Electron Conduction (SEC) target.<sup>(1)</sup> This target has high gain, excellent storage properties and retains only a very small percentage of its stored signal after a single scan of the reading beam.

Because of the unique properties of the SEC target, the WX-30654 is able to operate over a very wide range of scene illuminations and exhibits excellent sensitivity with moving as well as with stationary scenes. Localized regions of a scene which are sufficiently bright to cause saturation do not produce halation or blooming so that information from surrounding regions is not obscured. The excellent storage characteristics of the SEC target enable the integration of low light level images for extended periods of time. The WX-30654 also performs well at slow scanning rates as well as at the normal scanning rate of 30 frames per second.

The electrostatic image section remains in focus for all photocathode voltages and since the sensitivity of the tube varies with photocathode voltage, this feature provides a convenient means for gain control. Scan power and voltage

- |                                     |                          |
|-------------------------------------|--------------------------|
| • High Static & Dynamic Sensitivity | • Wide Dynamic Range     |
| • Low Lag                           | • Fiber Optic Faceplate  |
| • Excellent Integration & Storage   | • Rugged, Compact Design |
| • No Halation or Blooming           | • Low Power Consumption  |
| • Broad S-28 Spectral Response      | • Simple Operation       |

considerations for the reading gun are similar to those for a standard 1 1/2" all-magnetic vidicon. Suitable deflection yokes and focus coils are commercially available.

The WX-30654 was designed for applications where the limitations of conventional camera tubes (for example, the persistence and lower sensitivity of the vidicon or the operational complexity and lower dynamic range of the image orthicon) either compromise performance or impose unacceptable systems requirements. It may be used, for example, in a color television camera where its high sensitivity permits reduced studio lighting and allows nighttime outdoor broadcasting at normal stadium levels of illumination. The low lag characteristic of the WX-30654 makes possible a field sequential color camera using a single tube,

thus eliminating the present necessity of matching three or four conventional camera tubes. It may also be used in closed circuit television systems for the remote viewing of dimly illuminated scenes. The storage and integration characteristics permit its use, for example, in narrow bandwidth, slow-scan systems and are representative of the versatility which makes the WX-30654 suitable for a wide range of scientific and industrial applications.

The WX-30654 may be used directly with an optical lens system, or may be fiber-optically coupled to an image intensifier in order to achieve remote viewing at extremely low light levels. Alternatively the WX-30654 may be fiber-optically coupled to a suitable image converter to permit detection of X or UV radiation as well as near infrared radiation.

September 1966  
Supersedes TD 86-320 dated September 27, 1964  
96-3A-11C, 96-10C, W1-1300

Preceding page blank

## Westinghouse



## Principles of Operation

The WX-30654 SEC camera tube is schematically illustrated in Figure 1. It consists of an electrostatically focused diode image section, a Secondary Electron Conduction (SEC) target and a magnetically focused and deflected reading section. The semi-transparent S-20 photocathode is deposited on the inner surface of the plano-concave fiber optic faceplate. An optical image focused onto the planar surface of the fiber optic faceplate, is conveyed to the photocathode where photoelectrons are emitted from the illuminated area of the image in direct proportion to the amount of incident radiation.

The photoelectrons are accelerated towards the SEC target where they are brought to focus by the electrostatic lens formed between the photocathode surface and the anode cone. As the electron image is transferred from the photocathode surface to the target, it is reduced in size; the magnification is approximately 0.64.

The SEC target consists of a supporting membrane of  $Al_2O_3$  approximately 500 Å thick followed by a 500 Å layer of aluminum, which forms the signal electrode. Deposited on this, and facing the reading gun, is a highly porous layer of KCl. By applying a positive potential to the aluminum signal plate and stabilizing the potential of the KCl surface at approximately gun cathode potential, (by scanning the KCl surface with the low velocity electron beam), an electric field can be established across the KCl layer.

Photoelectrons arriving at the target with energies of approximately 8 keV penetrate the  $Al_2O_3$  and Al layers and dissipate most of their energy within the KCl layer by generating secondary electrons. An important feature of the SEC target is the release of secondary electrons into the vacuum interstices between the particles of KCl. Under the influence of the internal electric field the secondary electrons migrate in vacuum towards the signal plate. Conduction of the secondary electrons, therefore, takes place in vacuum and not in the conduction band of the KCl, thus avoiding the persistence effects caused by the trapping and subsequent release of charge carriers by shallow trapping centers. The movement of electrons within the KCl layer towards the signal plate creates a positive charge pattern which, in spatial distribution and intensity, corresponds to the optical image focused onto

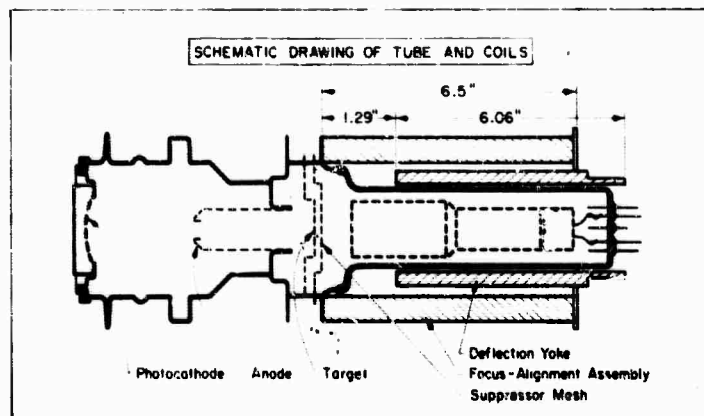


FIGURE 1

the tube faceplate. Because of the high resistivity of the low density target, the charge pattern can be stored for long periods of time.

The charging of the KCl layer is periodically interrupted by the scanning beam, which returns the KCl to gun cathode potential by depositing electrons on the positively charged areas. This current pulse, constituting the video signal, is capacitively coupled to the signal plate. The current flowing in the signal plate is used to develop a voltage across a load resistor which, after amplification, can be used to produce a video picture on a television monitor in the usual manner.

The low velocity electron beam which scans the target is produced by an electron gun consisting of an indirectly heated thermionic cathode, a control grid (G1), and an accelerating grid (G2). The beam is focused at the surface of the target by the combined action of the uniform magnetic field of an external coil and the electrostatic field of G3. A field mesh (G4) serves to provide a uniform decelerating electrostatic field to the target.

A second mesh electrode, G5 (suppressor mesh) is positioned close to the target surface. The purpose of this mesh is to control the potential of the SEC target. It is normally operated at a potential just below the "crossover" potential for KCl (approximately 15 volts). Alignment and deflection of the beam is accomplished by transverse magnetic fields produced by external coils. (See Figure 1).

## Performance Data

## Spectral Response and Sensitivity

The WX-30654 employs an S-20 photosurface deposited on a dark clad, 16µm fiber diameter, fiber optic faceplate. A typical spectral response for this faceplate-photosurface combination is shown in Figure 2. The peak quantum efficiency ranges from 15 to 20% and falls within the wavelength interval of 4200 to 4800 Å.

The high quantum efficiency of the S-20 photocathode, and the high gain of the SEC target provides a typical sensitivity of 120µA/fc, minimum 90µA/fc, at a faceplate illumination of  $10^{-3}$  fc (See Figure 3). Since the optical image size is  $0.96'' \times 1.28''$  this corresponds to a typical sensitivity of 14,000µA/lm.

## Light Transfer Characteristic

The light transfer characteristics of the WX-30654 are shown in Figure 3. The gamma varies from nearly one at lower light levels to about 0.6 at light levels of from  $10^{-3}$  to  $10^{-2}$  fc. At higher light levels, the target saturates at a surface voltage essentially equal to that of the suppressor mesh (G5). Although this provides a "knee" in the transfer curve, the light levels associated with the "knee" may cause image "burn-in" after prolonged exposures (see paragraph titled "Maximum Exposure Levels"). However, the tube may be safely operated at this and higher light levels by reducing the photocathode voltage.

**WX-30654**  
**SEC Camera Tube**

All Magnetic Gun  
Electrostatic Image Section  
1.6" Image Diagonal

The transfer function of Figure 3 applies for a standard 1/30 second frame rate, 525 line interlaced scan with both the photocathode and target voltages adjusted for optimum performance. Under these conditions the tube will provide a typical high-light signal current of 325 nA (minimum 250 nA for extended periods). Using a suitable preamplifier (see section titled "System Considerations") the signal current provides a peak signal to rms noise ratio of about 70. The equivalent visual signal-to-noise ratio<sup>(2)</sup> is about 200 or 48 db. These signal-to-noise ratios correspond to a dynamic range extending over two orders of magnitude in light level.

The excellent storage characteristics of the target makes the WX-30654 ideally suited to slow scan applications. The narrow bandwidths associated with slow scanning provides smaller preamplifier noise currents. However, this advantage is offset by the fact that with continuous slow scanning the highlight signal current is reduced in proportion to the increase in frame time. This reduction in highlight signal current can be avoided by using digital scanning techniques where the beam rapidly scans a single resolution element and is then brought to rest before being pulsed to scan the following resolution element.

The gain of the SEC target increases with target voltage. Dark current is non-existent over the entire range of useful target voltages. Practical limits to the maximum target voltage are imposed by the onset of lag and the appearance of target grain. The optimum target voltage is specified in the test data supplied with each tube. Although some degree of gain control can be achieved by operating the target at lower voltages, this approach is not recommended because the storage capacity and, therefore, the highlight signal current decreases with decreasing target voltage.<sup>(3)</sup>

**Gain Control**

Effective gain control can be accomplished by varying the photocathode voltage. The relative small signal target gain, as a function of photocathode voltage, is shown in Figure 4. Varying the photocathode voltage from 3.5 to 7.5 kV provides a gain control range of at least 16 to 1 with no perceptible loss in resolution and an image rotation of about 1°. A larger range can be obtained by further reducing the photocathode voltage; however, the picture quality is gradually degraded by the appearance of grain.

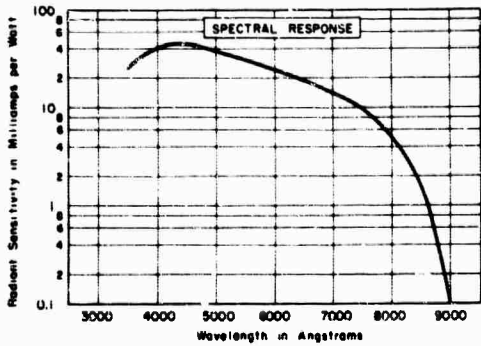


FIGURE 2

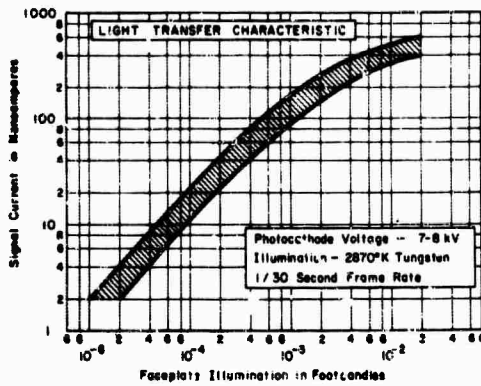


FIGURE 3

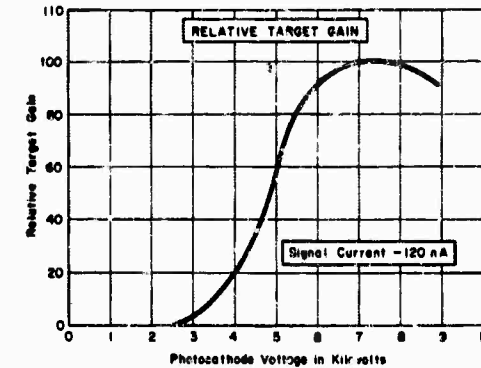


FIGURE 4

# Westinghouse



## Resolution

Figure 5 shows the uncompensated square wave response for the WX-30654. The curve given for the corner<sup>(4)</sup> is obtained when the tube is adjusted for best center resolution. The corner resolution can be improved to approximately match that of the center by dynamically focusing the G3 electrode with a suitable waveform of approximately 10 volts amplitude.

Values for the center square wave amplitude response at 200 and 400 TV lines per picture height are typically 70% and 36% with minimum values of 65% and 30% respectively. No significant variation in the modulation transfer function occurs for photocathode voltages ranging from approximately 3.5 to 8 kV. With a well-designed preamplifier, the typical limiting resolution is 800 TV lines per picture height at the center and 550 TV lines in the corner.

## Lag Characteristics

The signal generating mechanism of the SEC target is essentially lagless because conduction of the secondary electrons across the storage layer takes place in vacuum rather than in the conduction band. The small amount of lag that is observed is believed to be caused by the stored charge residing within the KCI layer rather than on the surface. This limits the beam acceptance resulting in a discharge lag. At higher target voltages, the stored charge penetrates further into the layer resulting in increased lag. Figure 6 shows the lag characteristic for a typical tube operated at optimum target voltage and at a signal current of 200 nA.

In the first frame, more than 95% of the signal is read out, leaving less than 5%, typically 2.5% to be read out in the second frame. In the third and succeeding frames, the residual signal is unperceptible. This performance is significantly better than that of the 1½" vidicon where typically, the signal does not decay to 3% until approximately the tenth frame. The dependence of lag on signal current is shown in Figure 7. At lower light levels, the lag increases primarily because of the poorer beam acceptance associated with the lower voltage excursions on the target surface.

The relative freedom from lag provides the WX-30654 with a dynamic sensitivity which is only slightly less than its static sensitivity. This is illustrated in Figure 8 which shows the limiting resolution as a function of light level for

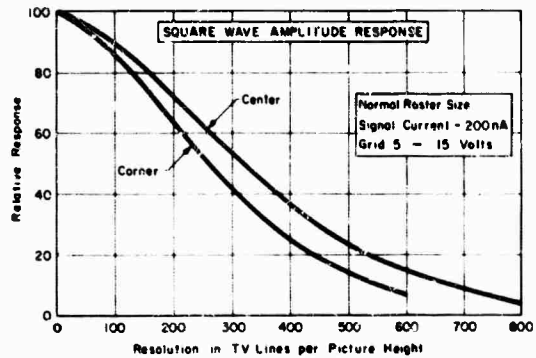


FIGURE 5

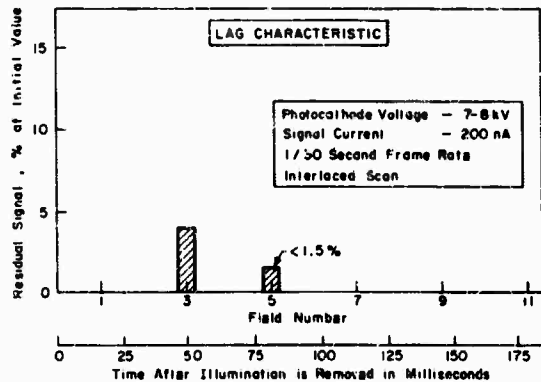


FIGURE 6

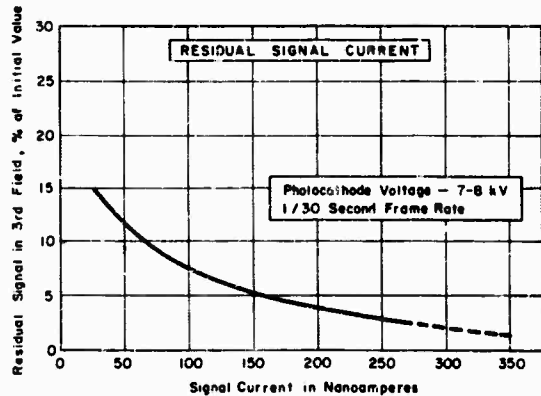


FIGURE 7

WX-30654  
SEC Camera Tube

All Magnetic Gun  
Electrostatic Image Section  
1.6" Image Diagonal

both stationary and moving scenes. In one case, the image moved across the picture width in a 20-second period. In order to obtain the same resolution with the dynamic scene, it is necessary to increase the light level by about a factor of 3.5. Under similar circumstances, the image orthicon requires an increase in light level of about a factor of 100.(5)

Low Contrast Sensitivity

The sensitivity illustrated in Figure 8 was concomitant with a 100% scene contrast. However, in most practical applications, the scene contrast is considerably less than 100% and, in such cases, the sensitivity of the tube to low contrast scenes becomes very important. The low contrast sensitivity of the WX-30654 is excellent and is shown in Figure 9. Over the linear region of the characteristic, where pre-amplifier noise predominates, the illumination required to achieve a given resolution is approximately inversely proportional to the contrast. At higher illuminating levels, where photon shot noise becomes appreciable, this relationship approximates an inverse square dependence. The performance of the WX-30654 compares favorably with that of the image orthicon. For example, at a resolution of 400 TVL/picture height, an increase in illumination of about 14 times is required compared to 4 for the SEC tube when the contrast is reduced from 100% to 25%.

Point Source Imaging

Point source imaging characteristics have been measured for a number of different SEC camera tube types, and have been found to be substantially independent of the tube type.(6) Both the sensitivity, that is the minimum number of radiation quanta sufficient to produce a signal detectable on a television monitor, and the dynamic range of point source detection are important parameters.

The WX-30654, operating in a system with a 3 nA noise current, can detect a signal of about 800 photoelectrons per integration period. For a photocathode with a 15% quantum efficiency, this would correspond to the arrival of 4000 photons at the faceplate of the tube. No significant deviations from perfect reciprocity occur for integration periods of at least several minutes. (See Figure 10). Increased threshold sensitivity may be achieved by increasing the target voltage by approximately 2 volts between integration and read out of the stored signal. In this way the beam resistance is reduced and the co-planar biasing caused by the

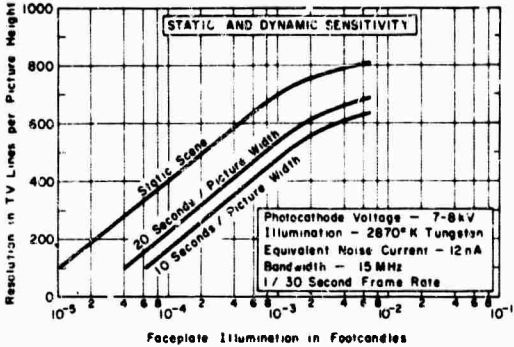


FIGURE 8

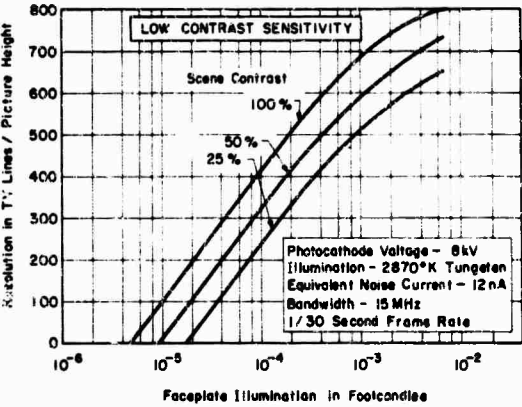


FIGURE 9

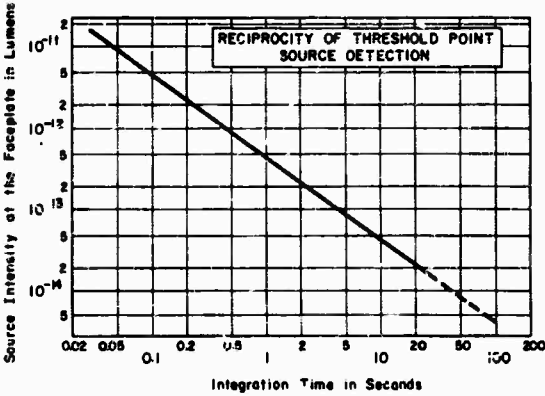


FIGURE 10

Westinghouse



negatively charged unexposed areas of the target can be eliminated.

The dynamic range is limited by the point at which physical spreading or blooming of the point image becomes "objectionable". Figure 11 shows the dependence of the diameter of the image point on the intensity of the source. The curve compounds the results of a number of independent measurements and shows that the diameter of the point image varies approximately with the 0.2 power of the source intensity. For example, the diameter of the point image increases by a factor of approximately six when the source intensity increases from threshold by a factor of four orders of magnitude. This performance may be contrasted with that of the image orthicon where the same degree of point spreading occurs for only one order of magnitude in intensity above the threshold.<sup>(7)</sup>

Integration and Storage

The SEC target used in the WX-3065-4 has an extremely high resistivity. Thus a signal can be integrated over a period of several minutes without degradation due to target leakage. The maximum integration period is limited only by spurious emission in the image section of the tube which, after long periods, can saturate the target. With selected tubes, integration times of up to thirty minutes are possible. Throughout the entire exposure, the tube shows excellent reciprocity in light level and exposure time. The ability to integrate over such long periods effectively increases the sensitivity of the tube by a factor of several thousand without compromising other performance parameters.

Once a signal has been integrated, it can be stored for many hours provided the photocathode voltage is turned off. The stored signal can then be read out in essentially one frame at any convenient scan rate.

Maximum Illumination Levels

If an excessive amount of energy is dissipated in the SEC target, the target suffers a loss of gain, resulting in a permanent negative image (burn-in). Damage can be caused by either an excessive target voltage or by unduly high light levels. In the first case, damage can be avoided by maintaining the target voltage at or below the value recommended in the data supplied with the tube. Damage associated with high light levels also depends on the photocathode voltage and the exposure time. These relationships are illustrated in Figure 12. The curves represent the maximum energy exposure that can be tolerated without danger of permanent target damage for various photocathode voltages. For example, at a photocathode voltage of 5.5 kV, a high light photocathode illumination of 1/5 footcandle can be tolerated for periods of up to 1 minute without "burn-in". For a lens at f/11 this illumination corresponds to a scene brightness of about 120 fL. Longer exposure times may result in permanent damage. It should be noted that, in most cases, exposures at or near those described by the curves of Figure 12, may cause a temporary loss in gain. However, recovery is complete within a period of several minutes.

ships are illustrated in Figure 12. The curves represent the maximum energy exposure that can be tolerated without danger of permanent target damage for various photocathode voltages. For example, at a photocathode voltage of 5.5 kV, a high light photocathode illumination of 1/5 footcandle can be tolerated for periods of up to 1 minute without "burn-in". For a lens at f/11 this illumination corresponds to a scene brightness of about 120 fL. Longer exposure times may result in permanent damage. It should be noted that, in most cases, exposures at or near those described by the curves of Figure 12, may cause a temporary loss in gain. However, recovery is complete within a period of several minutes.

Uniformity and Distortion

Shading in the WX-3065-4 is caused mainly by the slight radial change in magnification in the

image section. The photocurrent density incident on the target varies with the square of the magnification. Since the magnification is slightly larger at the edges, the current density there is reduced, resulting in a lower signal current. The video signal uniformity, defined as the percentage deviation from the maximum signal level, is typically 25% and is always less than 40%. It is measured across a horizontal line at the center of the picture.

Geometric distortion is typically 2% with a maximum of 4%. It is measured with an EIA linearity chart in accordance with IEEE Standard Number 202.<sup>(8)</sup>

Picture Quality

Over the recommended operating ranges of the WX-3065-4, there are no signal redistribution effects so that a signal in a given area is essen-

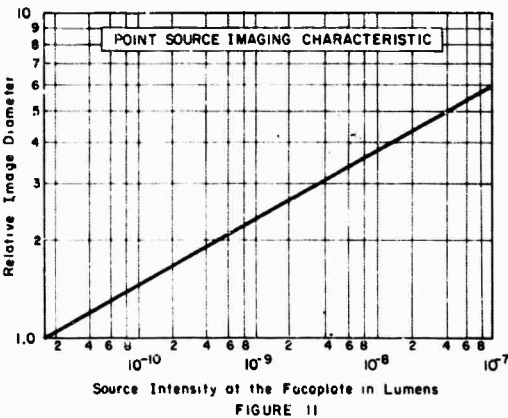


FIGURE 11

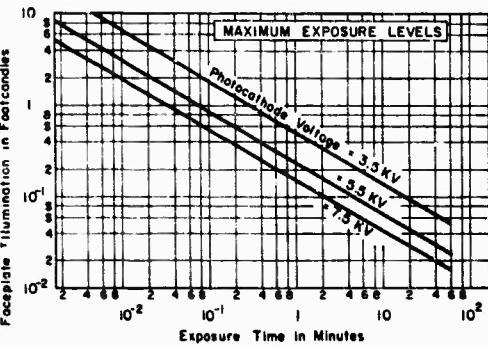


FIGURE 12



WX-30654  
SEC Camera Tube

All Magnetic Gun  
Electrostatic Image Section  
1.6" Image Diagonal

General Data	
Faceplate	Fiber Optic
Fiber Diameter	16 μm
Numerical Aperture	1.1
Useful Diameter	1.6 Inches (40mm)
Photocathode	S-20 (Figure 2)
Image Section:	
Focusing Method	Electrostatic
Configuration	Diode
Target Shunt Capacity:	
Typical	35 pF
Maximum	40 pF
Reading Section:	
Focusing Method	Magnetic
Alignment Method	Magnetic
Focusing-Alignment	
Assembly	t5-VFA-599X* or Equivalent
Deflection Method	Magnetic
Deflection Yoke	15-VY-314* or Equivalent
Cathode	Indirectly Heated
Heater Power	1 Watt
Base	JEDEC No. E8-78
Socket	#208-SBDC (Alden)
Overall Length (maximum)	13.5 Inches
Maximum Diameter	4.0 Inches
Diameter of Reading:	
Gun Bulb	1.5 Inches
Weight	2.19 Pounds
Operating Position	Any

\* Cleveland Electronics, Inc.

tially independent of the signal in a neighboring area. Thus, the tube is free of halation. Slight blooming, or image growth, occurs at very high light levels due to the beam bending associated with excessive voltage excursions at the target surface.

All tubes are free of fixed pattern noise, such as smudges or demarcation lines. The maximum number and distribution of small area blemishes are defined in the table below:

	Zone 1	Zone 2	Zone 3
All Blemishes	1	3	20
Blemishes with a major dimension of 7 or 8 television lines			
	0	1	4

The zones are defined as follows:

Zone 1	Central 10% of raster area.
Zone 2	Central 20% of raster area.
Zone 3	Entire raster area.

Operational Data	Maximum Rating	Typical Operation	Units
<i>Image Size at the Faceplate: 0.96" x 1.28"</i> <i>Direction of Scan: Parallel to a Line Joining Axis of Tube to Target Lead.</i>			
Photocathode Illumination	See Figures 3 and 12		
Photocathode Voltage	-9	-7.5	Kilovolts
Anode Cone Voltage	NA*	Ground	-
Target Voltage (Reference 9)	30	10 to 30	Volts
Grid 5, Suppressor Mesh, Voltage (Reference 10)	40	15	Volts
Grid 4, Field Mesh, Voltage (Reference 11)	1500	500	Volts
Grid 3, Focus Electrode Voltage	1500	480	Volts
Grid 2, Accelerator, Voltage	350	300	Volts
Grid 1 Voltage	-150 ± 0	-40	Volts
Heater Voltage	6.8	6.3	Volts
Peak Heater to Cathode Voltage:			
Heater Negative	125	NA*	Volts
Heater Positive	10	NA*	Volts
Minimum Peak-to-Peak Blanking Voltage Applied To:			
Cathode (Positive Pulse)	NA*	30	Volts
Grid 1 (Negative Pulse)	NA*	80	Volts
Cathode Voltage	NA*	Ground	-
Magnetic Focusing Field (Center of Coil)	NA*	30	Gausses
Magnetic Alignment Field	NA*	0 to 4	Gausses
Peak Deflection Current for Specified Yoke:			
Horizontal	NA*	300	mA
Vertical	NA*	32	mA
Peak Signal Current (Reference 13)	t	NA*	μA

\* Not Applicable

These blemishes are generally bright spots and are defined as any spurious signal whose major dimension covers three or more television lines. No blemish whose major dimension covers nine or more television lines is permitted anywhere in the raster.

**Life and Environmental Characteristics**  
The WX-30654 has been used in various applications and has shown useful life times of 500 hours or more, comparable to vidicons and image orthicons. It does not require an extended warm-up period and shows highly reproducible performance even at operating temperatures as low as -54°C or as high as +55°C. The only performance parameter which may change with extended operation is sensitivity which decreases at most by one f-stop. When stored under suitable conditions, e.g. a clean dry environment at room temperature, the tube remains stable and shows an extremely long shelf-life.

The WX-30654 has been designed for use in systems which must operate under the environmental conditions described in military specification Mil-E-5400J. The rugged design of the tube is compatible with even the most severe vibration levels, (curve IV, of the specification). However, care must be taken in the de-

sign of the camera head to ensure that resonances, which could produce microphonics, are avoided.

**Operating and Handling Considerations**  
**Important Precautions**

1. The tube is supplied with an external voltage limiting device connected between the SEC target and the suppressor mesh (G5). This should not be disconnected, as its purpose is to protect the target from permanent damage which could be caused by the accidental application of a high voltage (e.g. from an electrostatically charging human operator).
2. The target and suppressor voltages recommended with each tube should not be exceeded.
3. The tube should not be operated at exposure levels greater than those illustrated in Figure 12.
4. The horizontal and vertical deflection power should be adjusted to ensure that the target is either normally scanned or over-scanned before the reading beam is turned on. Avoid Underscanning.

## Westinghouse



## Set-up Procedure

As long as the above precautions are taken, the tubes can be set up and operated in a manner similar to that of a vidicon. No special "warm-up" time is required. The sequence given below is recommended as a convenient set-up procedure.

1. Install the tube in the camera head using the focus, deflection, and alignment coil positions shown in Figure 1. The polarity of the focusing coil should be such that an externally positioned north seeking pole is attracted to the target end of the focusing coil. It is also recommended that a 1.6" diagonal rectangular mask with a 4:3 aspect ratio be used to prevent light reaching unused parts of the photocathode.
2. Make connections to all electrodes and apply deflection voltages sufficient to over scan the target.
3. Apply maximum negative bias to G1. Apply voltages to the heater, focusing coil and alignment coils.
4. Apply the recommended voltages to G2, G3, G4, G5, and target.
5. Apply approximately  $10^{-4}$  fc uniform illumination to the faceplate of the tube. Turn on photocathode voltage and adjust the G1 voltage until the beam current is sufficient to discharge the target.
6. Center and focus a test pattern on the faceplate of the tube so that the image size is  $1.28" \times 0.96"$ . The illumination level should be adjusted to about  $10^{-3}$  fc.
7. Adjust the deflection amplitude and centering controls such that the target ring is just visible in the corners of the picture. Then further decrease the deflection power until the test chart completely fills the picture.
8. Adjust the G3 beam focus control and optical focus alternately until no further improvement in picture quality is obtained. The G4 voltage should always be maintained above that of G3 to prevent positive ions generated in the G3 drift space from landing on the target.
9. Adjust alignment currents for best beam landing in the following manner. Reduce the G5 voltage to a value just above the threshold for beam landing. Adjust the alignment current to center and maximize the area over which the beam can land. If a G5 voltage of more than 1 or 2 volts is

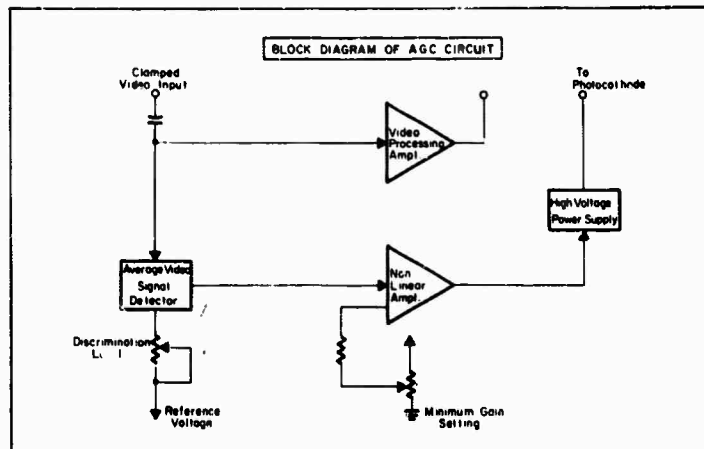


FIGURE 13

needed for beam landing over the entire raster, check the positions of the focusing and deflection coils.

10. Return G5 voltage to recommended value, check G3 and optical focus.

## Note:

If the target "crosses over" during the operation, manifested by the appearance of a black area on the television monitor, the recommended procedure for returning to normal operation is to reduce the G5 voltage temporarily to about 10 volts and either reduce the faceplate illumination or increase the beam current.

## Shutdown Procedure

The only important feature of the shutdown procedure is that the deflection power should be switched off only after the reading beam has been switched off. The recommended sequence is:

1. Turn off all voltages except the deflection supplies.
2. Turn off deflection power.

## Systems Considerations

System requirements for the WX-30654 are similar to those for a standard 1½" magnetically deflected and focused vidicon. Only two additional voltages are required; one for the operation of the electrostatic image section and one for the suppressor mesh electrode

(G5). The mesh, operated at about 15 volts, may be supplied by a voltage divider across the conventional gun supply.

Both this supply and the power supply used for the focus coil should be regulated to a level of 0.1% or less. Similarly, ripple should not exceed 0.1%.

The suppressor mesh should be maintained at AC ground to prevent pick-up of spurious signals. It is recommended that a by-pass network (e.g. a 100K series resistor and a .01 µF capacitor connected directly to G5) be located as closely as possible to the suppressor mesh electrode.

Because the focus of the image section is independent of photocathode voltage, regulation for this supply is not critical. However, ripple is objectionable because it can be coupled into the video signal. It is recommended that the ripple should not exceed 0.1%. Automatic gain control can be accomplished by sampling the video signal and using a feedback network to regulate the photocathode voltage. A block diagram of such a network is shown in Figure 13.

Dynamic focusing and the reduction of shading can be accomplished using techniques similar to those used with standard 1½" all-magnetic vidicons. Dynamic focusing requires a 10 volt wave form applied to G3. Shading can be essentially eliminated by applying a parabolic



Westinghouse



#### Notes & References

An annotated bibliography of published work relating to the SEC target and to SEC camera tubes has been prepared by Westinghouse. Copies may be obtained by writing to Westinghouse Electronic Tube Division, Box 284 Elmira, N.Y. 14902.

1. (a) Boerio, A.H., Beyer, R.R., and Goetza, G.W. - "The SEC Target", *Advances in Electronics and Electron Physics*, Academic Press, Vol. 22A, pp. 229 (1966).
- (b) Goetza, G.W. and Boerio, A.H. - "Secondary Electron Conduction (SEC) For Signal Amplification and Storage in Camera Tubes", *Proc. IEEE*, Vol. 52, pp. 1007 (1964).
- (c) Goetza, G.W. - "Secondary Electron Conduction (SEC) and Its Application to Photoelectronic Image Devices" - *Advances in Electronics and Electron Physics*, Academic Press, Vol. 22A, pp. 219 (1966).
2. The equivalent visual signal-to-noise ratio is the ratio of highlight video signal current to RMS noise current, multiplied by a factor of 3. [CCIR, International Radio Consultative Committee, *Television Standards*, Vol. 5 (1960).] An RMS noise current of 5 nanoamperes is assumed for the video preamplifier operating at a bandwidth of 8 MHz.
3. See Reference (a) of Note 1.
4. The corner resolution is measured at any

point on the circumference of a circle whose diameter is 70% of the raster diagonal and concentric with the tube axis.

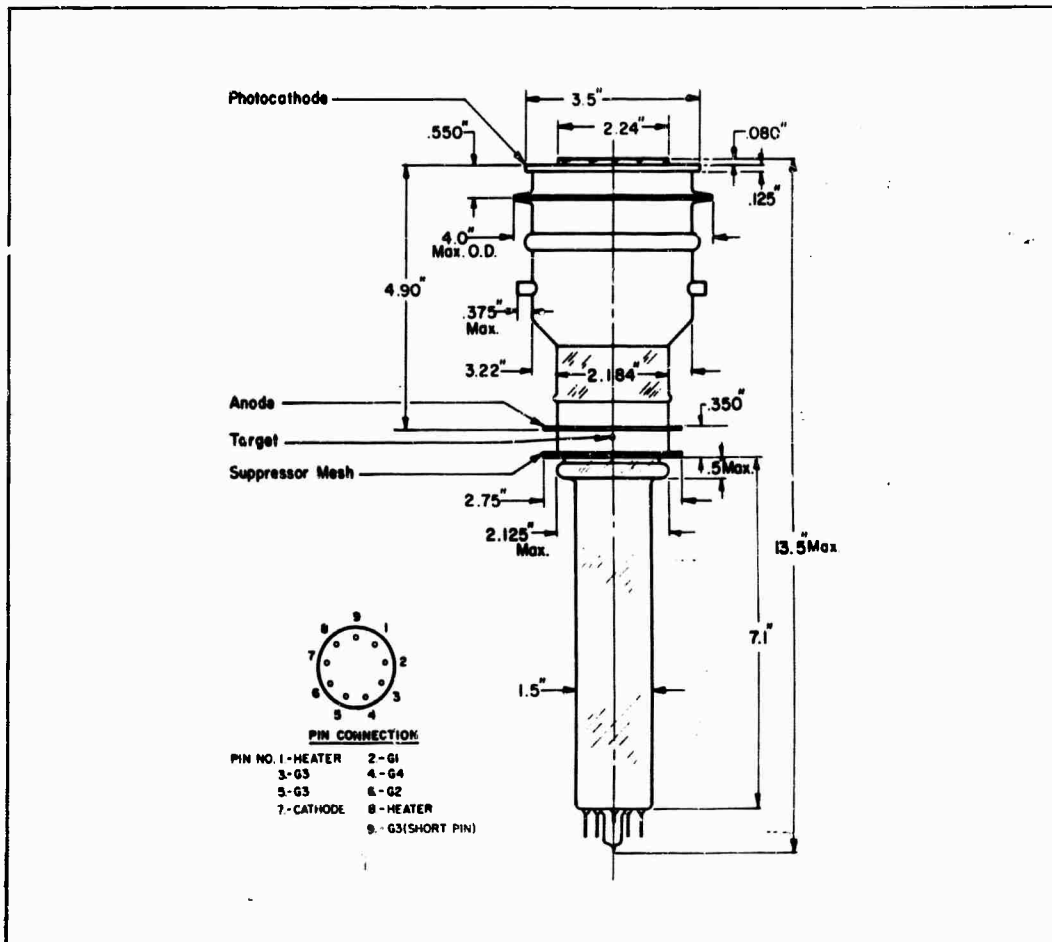
5. Parton, J.S. and Moody, J.C. - "Performance of Image Orthicon Type Intensifier Tubes", *Image Intensifier Symposium*, Fort Belvoir, Virginia, NASA SP (1961).
6. (a) Beyer, R.R., Green, M. and Goetza, G.W. - "Point-Source Imaging with the SEC Target", *Advances in Electronics and Electron Physics*, Academic Press, Vol. 22A, pp. 251 (1966).
- (b) Marshall, F.B. and Roane, G.D. - "Performance Comparison of the SEC Camera Tube and the Image Orthicon" - *Advances in Electronics and Electron Physics*, Academic Press, Vol. 22A, pp. 291 (1966).
- (c) Neel, B. - SEC Vidicons - Sole Site Results. - Unpublished Report.
7. Livingston, W.C. - *Journal of the Society of Motion Picture Television Engineers*, Vol. 72, pp. 771 (1963).
8. IEEE Standards on Television: Methods of Measurement of Aspect Ratio and Geometric Distortion", 202 (54-IRE2351).
9. The recommended target voltage is printed on a data sheet which accompanies each tube.
10. The function of the G5 electrode is to control the potential to which the target surface can rise. If the potential of the G5 electrode is set at a value higher than that

of the crossover potential for KCI (approximately 15 volts) and if, because of a very bright exposure the target surface potential does rise above the crossover, then reading beam electrons will land on the target with sufficient energy to cause a net flow of electrons away from the target until the potential stabilizes at that of G5. The target will then fall to discharge and will produce a black area on the monitor. Operating the target in the "crossed over" mode is not recommended since it can lead to an increase in target grain. In order to discharge the target and resume normal operation, the G5 potential should be temporarily reduced to about 10 V.

11. It is recommended that the potential of the G4 electrode be maintained above the potential of G3.
12. (a) James, I.J.P. - "Fluctuation Noise in Television Camera Head Amplifier", *Proceedings of IEE*, Vol. 99, No. 20 (1957) p. 796
- (b) "Fundamentals of Television Engineering" - G. M. Glasford McGraw Hill, pp. 111 - 124 (1965).
13. The maximum rating of 1  $\mu$ A for the peak signal current should not be confused with the value quoted for the maximum high light signal current (see paragraph entitled Light Transfer Characteristic). The maximum rating quoted here is a figure suggested for the system designers use and is an estimate of the maximum possible signal current that the tube is capable of providing for a short period of time.

# **WX-30664** **SEC Camera Tube**

All Magnetic Gun  
 Electrostatic Image Section  
 1.8" Image Diagonal



**Option**  
 If desired, in order to facilitate mounting, to provide environmental protection against humidity and to reduce the possibility of external voltage breakdown, the WX-30664 can be supplied with the image section encapsulated in a silicon rubber compound. The material used is Dow Corning RTV 511.

**BLANK PAGE**

## E. THE IMAGE ORTHICON AND THE IMAGE ISOCON

The image orthicon (IO) was developed during World War II, and for a period of 20 years thereafter it was the principal camera tube used in all commercial studio broadcasts. It was also the only tube capable of low-light-level operation during most of this period, and it is still a very capable performer. The image isocon (II) is similar to the IO in format and construction, the primary difference being in the readout section. Both tubes use low-velocity electron-beam scanning to extract the video signals and a low-noise return-beam electron multiplier to amplify the signal within the tube. The primary difference is that the II derives its signal only from scattered scanning-beam electrons, while the IO accepts all of the returned beam for amplification. As a result, the noise in the picture lowlights is very small in the II and is a maximum in the IO. While the II provides superior signal-to-noise ratios at moderate photocathode light levels, it has an amplitude response that is light-level dependent. Thus, its low-light-level performance is generally inferior to that of an IO designed for this purpose. However, in practice, it is found that an image intensifier is needed for both the IO and the II to reduce image lag to acceptably low levels. With the added intensifier, the light-level dependence of the amplitude response of the II becomes generally acceptable.

The thin-film, metal-oxide-targeted IO is subject to permanent damage by extreme overexposure, although it can be electronically protected in most applications. The II is reported to be immune to such effects.

### 1. The Image Orthicon

The image orthicon is usually constructed in three sizes, which are described by the diameter of the image section. The three standard sizes are 2, 3, and 4.5 in. The 2-in. size, developed mainly for applications requiring a minimum in size, weight, and power, has been abandoned mainly because of an overly restricted dynamic range and excessive lag. The 4.5-in. version is of main interest for commercial

broadcast use. Its features are a very large signal storage capability and reduced bright-light blooming effects.

The 3-in. IO, which is still of current interest for low-light-level use, has a 40-mm photocathode in the version that is fitted with a fiber-optic faceplate. Ordinarily, the image section consists of an S-20 photoemissive photocathode followed by a target. When struck by accelerated photoelectrons, this target emits secondary electrons in greater numbers than those incident. These electrons are emitted back toward the photocathode, but are collected by a mesh interposed between the photocathode and target. The image section is usually focused magnetically. The readout section consists of a magnetically focused and deflected scanning electron beam. The video signal is not read out at the target, as in the vidicon or the SEC camera tube, but rather the electron beam is returned to an electron multiplier. The signal, which is the difference between the original beam current and that which lands on the target, is greatly amplified by the internal electron multiplier.

The target, whose function is both to amplify and store the signal during the interval between scans, has been fabricated of a number of materials. Originally, the target material was a soda-lime glass whose conductivity was ionic. The net gain of this target was about three. The main problem with soda-lime glass was that the conducting ions always drift in the same direction, causing the glass to become more resistive as the ions become depleted. This caused an increased tendency for images to burn in after a few hundred hours of operation. To extend tube life, it was customary to slowly rotate or "orbit" the image incident on the target.

In the mid-1950's, the thin-film metal-oxide target was developed. The material used was principally magnesium oxide, although other materials were used. The thin-film target is electron conducting, which solves the image burn-in problem. Also, secondary emission gain is increased to as much as 10 to 15, resulting in a sensitivity increase. An even further advantage is that the target is but one-tenth the



thickness of a glass target, and its conductivity, being anisotropic, is higher through the target than along its surface. Thus, these films display a higher resolving power than glass and a longer image storage capability, which is useful in slow scan and in astronomical applications. Being so very thin, the MgO target lacks strength, necessitating a target-to-mesh spacing wider than normal. This reduces signal storage capability to the point where these tubes become marginal for studio broadcast use. Image lag is reduced because of the reduction in capacitance, however, which makes these tubes suitable for low-light-level imaging.

Another target material developed is an electron-conducting glass called "brown glass." This glass usually contains transition metal oxides in both bivalent and trivalent states. The mixture of doubly and triply ionized sites throughout the material permits electron conduction by hopping. This glass eliminates the burn-in problem and the low resolving capability of soda-lime glass, but its gain is no higher (about three).

a. Principles of Operation. The IO is schematically diagrammed in Fig. V-E-1. The photoelectron image is magnetically focused and accelerated to the target through a potential of about 600v. In tubes with magnetically focused image sections, this potential must be precisely maintained, ruling out electronic image-section gain control. Before impinging on the target, the photoelectrons must pass through the mesh, which has a photoelectron transmittance of 0.6 to 0.7.

Upon colliding with the target, the photoelectrons cause secondary electrons to be emitted, as shown in Fig. V-E-2. These secondaries are collected by the mesh, which is biased +2 v. above the target. The capacitance or signal storage capability of the target-mesh assembly is determined by the mesh-to-target spacing, which can be as little as 0.7 mil for glass-targeted tubes and up to 10 mil or more for MgO-targeted tubes.

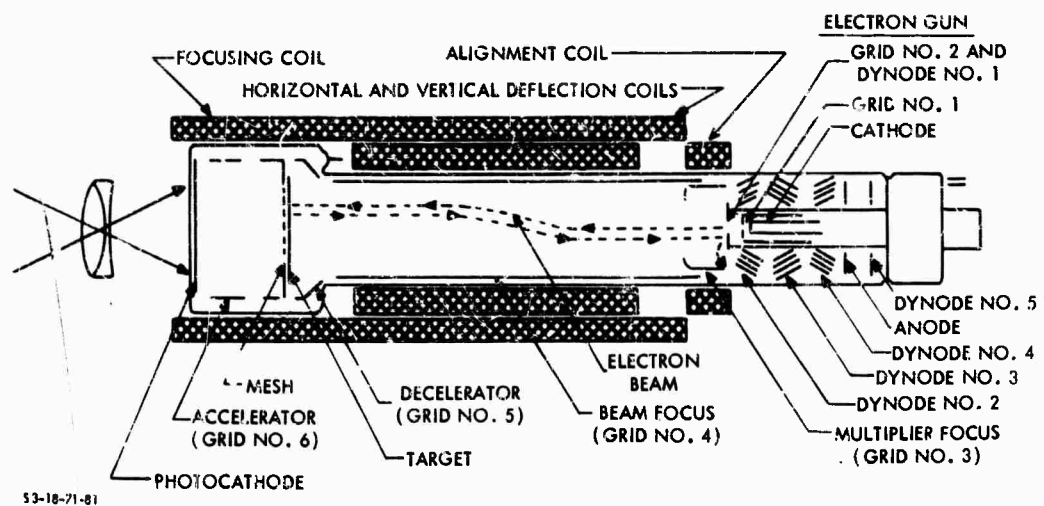


FIGURE V-E-1. Schematic of Image Orthicon

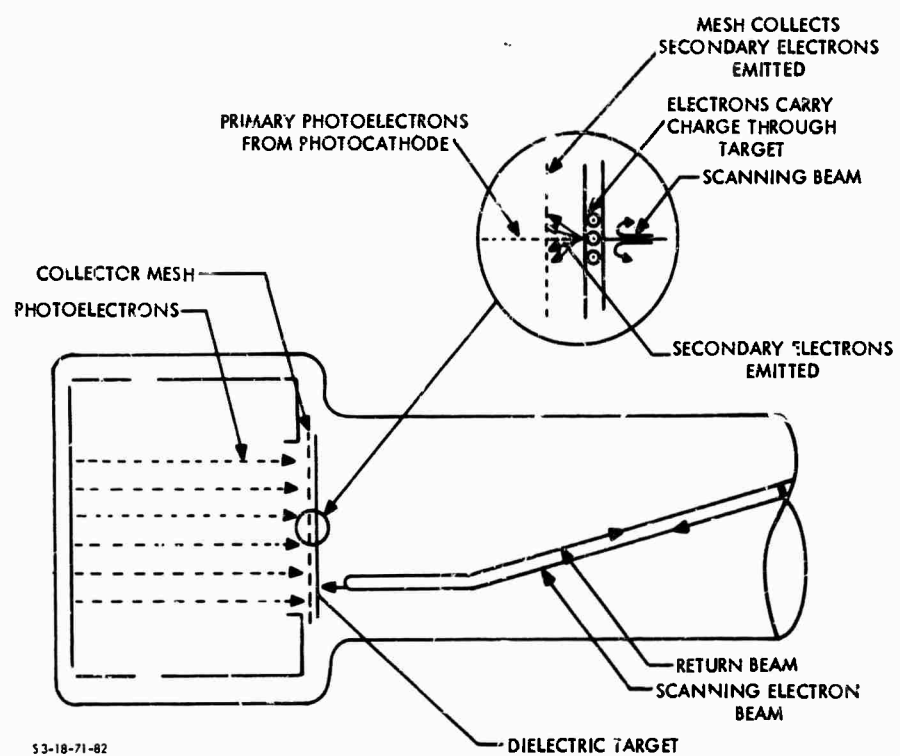


FIGURE V-E-2. Cross Section Showing Action of Image Orthicon Storage Target

The electron beam, formed by the electron gun and the control and accelerating grids 1, 2, and 3, is further accelerated and focused by grid 4 and the focus coil, and then the beam is magnetically deflected into a raster scanning pattern. Next, it is decelerated by grid 5. A portion of the beam lands on the photocathode according to the charge deficiency thereon, and the balance of the beam returns directly to grid 2, dynode 1. Were the focus perfect, the beam would pass back through the original aperture in this structure, but, as a practical matter, it collides with dynode 1, which amplifies the returned portion by a factor of approximately four. The amplified return-beam signal is subsequently amplified further by dynodes 2 through 5. Including the gain of the first dynode, an overall signal amplification of about 500 to 1500 can be achieved. The electron multiplier serves the function of signal preamplifier. While it does not improve the signal-to-noise ratio, it is almost noiseless compared to external preamplifiers. However, one of the principal noises in the IO is the shot noise of the beam.

b. Signal Transfer Characteristic. The signal transfer characteristic for a thin-film MgO-targeted IO is shown in Fig. V-E-3. The gamma of this tube at low irradiance levels is near unity, while at the higher irradiance levels the gamma drops off. In tubes with close-spaced meshes, the transition from unity gamma to zero gamma is quite abrupt. The limitation in this case is mainly target capacitance. In thin-film-targeted tubes with wide-spaced meshes, the transition is more gradual, being a combination of target gain reduction, as photoelectron density increases, and target capacitance.

The signal current output of the IO is given by the relation

$$I_S = CG_M (G_T - 1) T_M i_s / e_v e_h \quad (V-E-1)$$

where terms are as previously defined, except that  $G_M$  is the electron multiplier gain,  $T_M$  is the mesh transmittance, and  $G_T$  is the IO target gain. For calculations, it is usual to assume a constant value for the

multiplier gain, and the net target gain ( $G_T - 1$ ) is computed from the equation

$$(G_T - 1) = \frac{e_v e_h I_S}{G_M T_M \sigma_T A E_T} \quad (V-E-2)$$

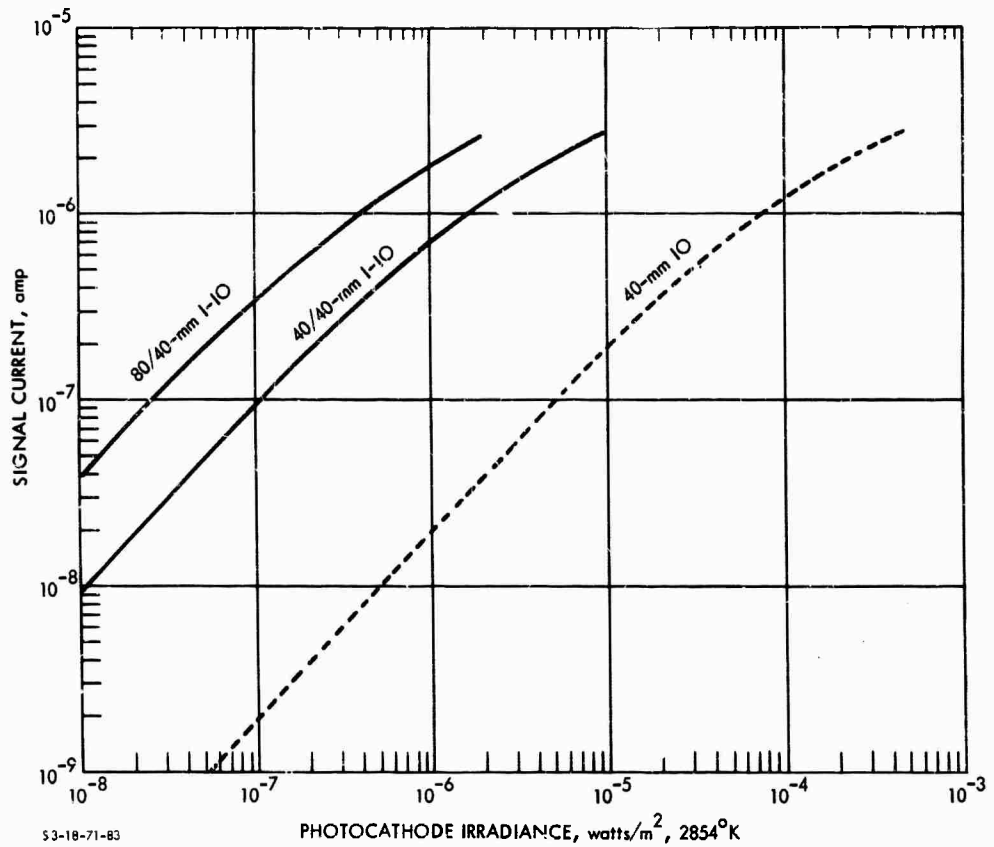


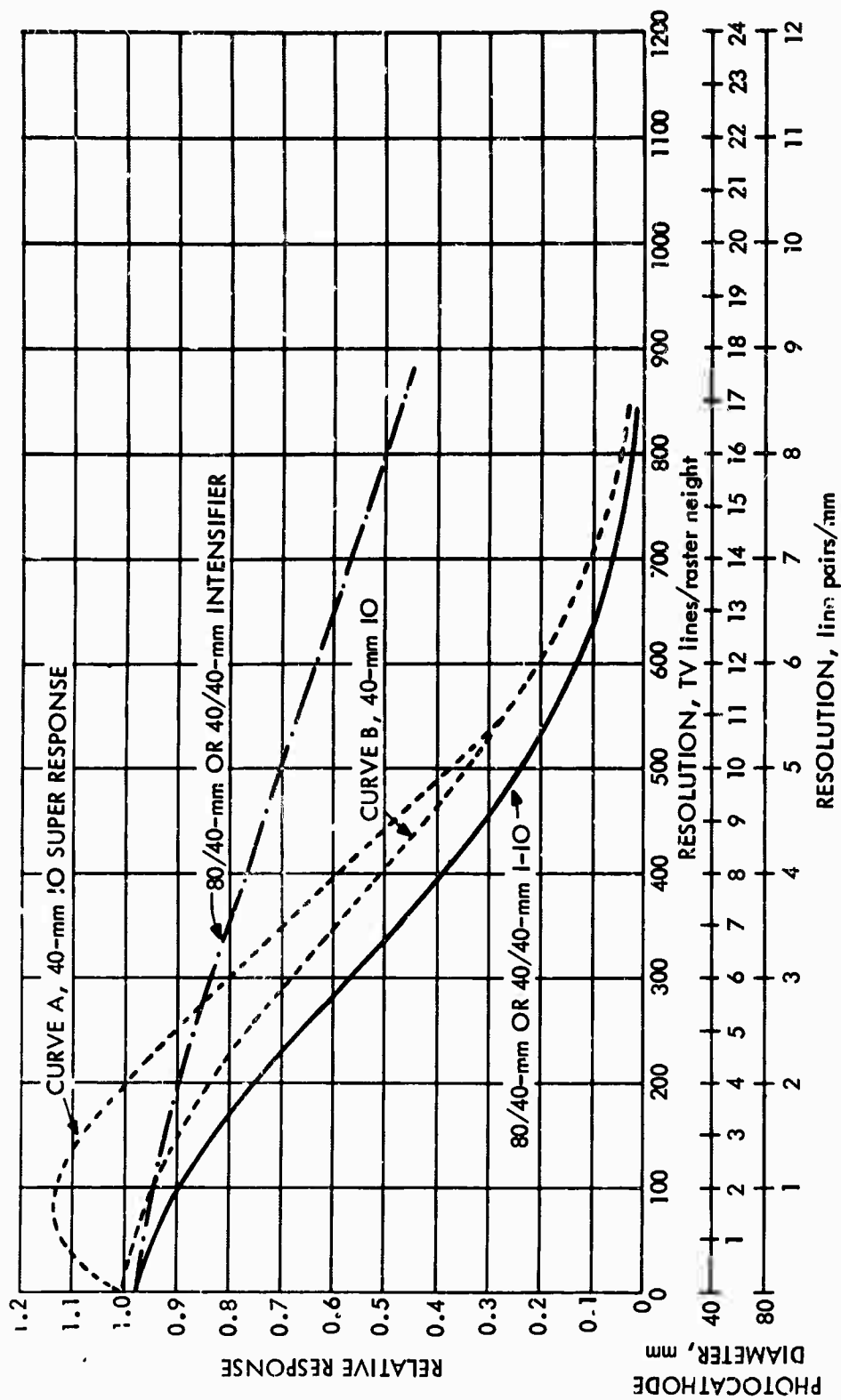
FIGURE V-E-3. Signal Current Versus Photocathode Irradiance Characteristic for the 3-inch, Thin-Film Metal-Oxide-Targeted Image Orthicon with and without an Intensifier

In the linear region of the signal transfer curve,  $(G_T - 1)$  is approximately 10. The effective gain is specified as  $(G_T - 1)$  for the IO because the original photoelectron incident on the target must be discounted. This is only significant near the knee of the signal transfer curve, where the gain becomes quite small. It should be noted that it is quite difficult to measure IO parameters such as beam current, beam modulation, target gain, and electron multiplier gain because not all terminals are brought out of the tube to a measuring point and also because the currents involved are extremely small.

In the calculations that follow, electron multiplier gain is assumed to be 1000, the photocathode radiant sensitivity is  $3.2 \times 10^{-3}$  amp/watt for a 2854°K tungsten source, and the mesh transmittance  $T_M$ , is taken to be 0.66.

c. Amplitude Response. The uncompensated horizontal square-wave response of the IO is not unique, as can be seen in Fig. V-E-4, where a super response and a more conventional response are shown. The super response shown as curve A results from a charge redistribution effect that occurs when the target-mesh assembly becomes fully charged at a point. Secondary electrons from the target are then repelled by the mesh and fall back to the target in areas adjacent to the areas from which they were emitted. In the case of black-and-white bar patterns, the blacks are driven from a normal zero potential to a negative value. This effect is known as black haloing and occurs for bright images of signal level above the knee of the signal transfer curve. Below the knee, the more normal-appearing response shown as curve B is obtained. The resolution is shown in terms of TV lines/raster height and in terms of line pairs/millimeter. For the image orthicon case, use the scale labeled 40-mm photocathode diameter only.

d. Video and Display Signal-To-Noise Ratio. There are several sources of noise in the image orthicon, depending on the mode of operation. Analytically, the video signal-to-noise ratio is written as



53-18-71-84

FIGURE V-E-4. Uncompensated Horizontal Square- or Sine-Wave Response for the 3-inch, Thin-Film-Targeted Image Orthicon with and without an Intensifier. (Note: Intensifier Response is Sine Wave; IO and I-IO Responses are Square Wave.)

$$\text{SNR}_{V,0,1} = \frac{G_M (G_T - 1) T_M i_{s \max}/e_v e_h}{\left( \bar{I}_e^2 + \bar{I}_B^2 + \bar{I}_T^2 + \bar{I}_D^2 + \bar{I}_{PA}^2 \right)^{1/2}} \quad (\text{V-E-3})$$

where the numerator terms are as described above and the noises are:

(a) the mean square photoelectron noise

$$\bar{I}_e^2 = G_M^2 (G_T - 1)^2 T_M e \Delta f i_{s \max}/e_v e_h. \quad (\text{V-E-4})$$

(b) the mean square beam noise

$$\bar{I}_B^2 = 2 G_M^2 (G_T - 1) T_M e \Delta f i_{s \max}/m e_v e_h. \quad (\text{V-E-5})$$

(c) the mean square target noise

$$\bar{I}_T^2 = G_T G_M^2 T_M e \Delta f i_{s \max}/e_v e_h. \quad (\text{V-E-6})$$

(d) the mean square first dynode noise

$$\bar{I}_D^2 = 2 G_{M,1} G_{M,4}^2 \left[ \frac{1-m}{m} \right] (G_T - 1) T_M e \Delta f i_{s \max}/e_v e_h. \quad (\text{V-E-7})$$

(e) the mean square preamplifier noise computed from its measured rms value of  $I_{PA}$ .

In Eq. V-E-6,  $G_{M,1}$  is the gain of the first dynode stage (about four) and  $G_{M,4}$  is the gain of the stages following it (about 250). In both Eqs. V-E-5 and V-E-7,  $m$  is the beam modulation factor. It represents the fact that the beam can never be fully modulated and that, therefore, its value must be set at some value  $1/m$  times higher than the highlight signal current  $i_s$ .

The relationships between peak-to-peak signal output currents are shown as a function of input photocathode current in Fig. V-E-5 for two cases: an optimum beam current and a fixed beam current. In the

optimum beam current case, it is assumed that the beam current is adjusted to be just exactly enough to discharge the scene highlight signal and no more. The beam modulation is assumed to be 0.5. Should the scene increase in brightness even slightly, the tube, when set up for optimum beam at some lower light level, will become beam-current starved, and the image will spread in size over the target until equilibrium between read-in and readout is achieved, if possible.

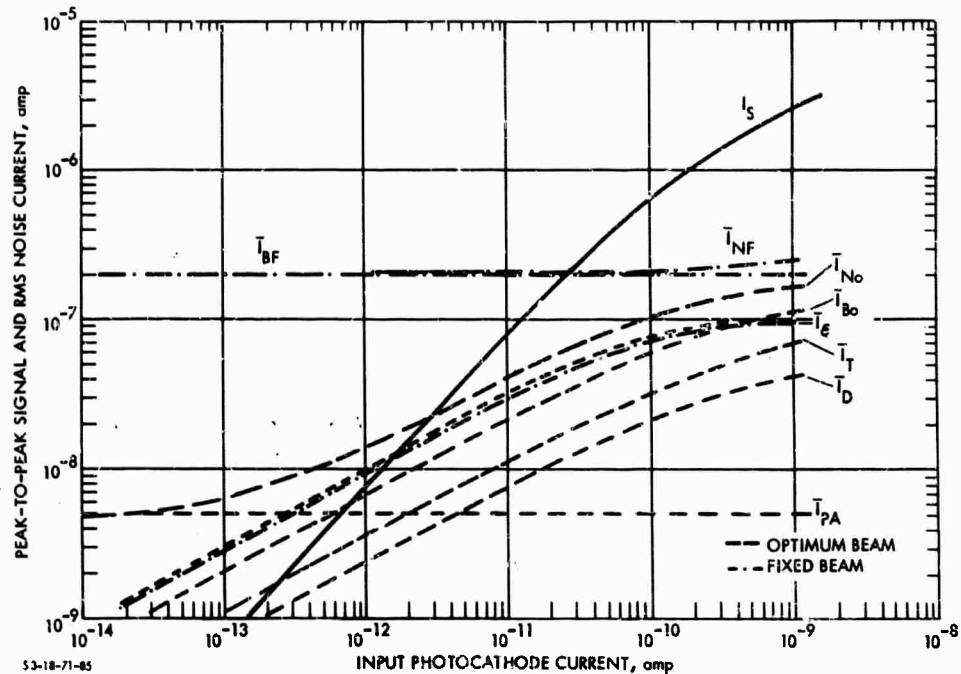


FIGURE V-E-5. Signal and Noise Currents for the 3-inch, Thin-Film-Targeted Image Orthicon Versus Input Photocathode Current with Fixed Beam and Optimum Beam Current

In the optimum beam case, the beam current noise  $I_{Bo}$  and the photoelectron current noise  $I_e$  are roughly comparable. At the very lowest light levels, preamplifier noise exerts some influence, but not much. When operated with optimum beam current, the IO approaches the ideal photoelectron-noise-limited case. Such operation is not generally



possible, however, in imaging a real scene that encompasses a wide range of scene radiances.

In the fixed beam case, the beam is set at some constant value high enough to handle the brightest scene highlight expected. For calculations, it is assumed that the setup is such that the IO will operate with highlights well above the knee of the signal transfer curve. This is the "worst case" from a sensitivity viewpoint, whereas the optimum beam represents the "best case." Actual practical performance will probably be somewhere in between.

The video signal-to-noise ratio  $SNR_{V,0,1}$  for unity image contrast and aperture response is plotted in Fig. V-E-6 for both the fixed beam and the optimum beam by means of Eqs. V-E-3 through V-E-7. The display signal-to-noise ratio  $SNR_D/C$  is calculated in the usual manner and is plotted for the optimum beam (Fig. V-E-7) and for the fixed beam (Fig. V-E-8).

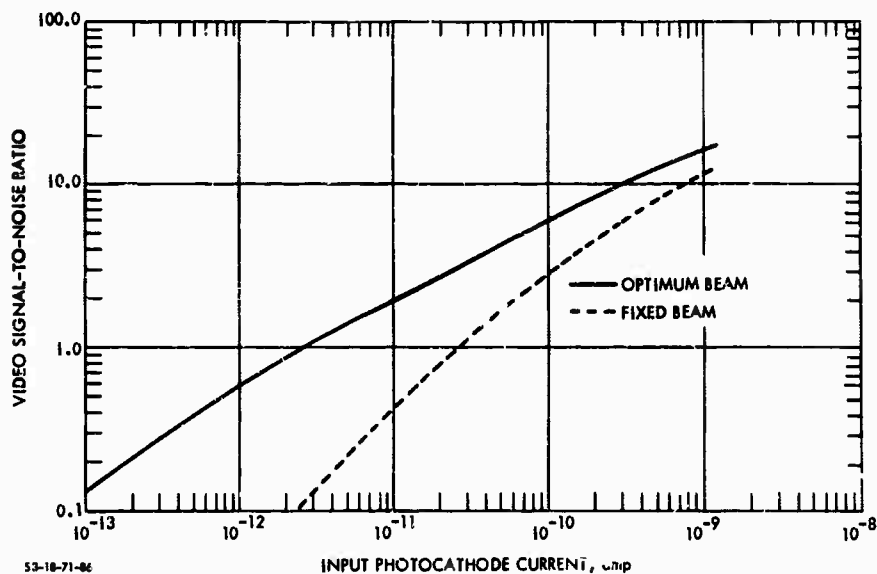


FIGURE V-E-6. Video Peak-to-Peak Signal-to-RMS Noise Ratio for the 3-Inch, Thin-Film-Targeted Image Orthicon Versus Input Photocathode Current for a Video Bandwidth of 10 MHz. (Note: Images are Assumed to be of Unit Contrast and of Low Spatial Frequency.)

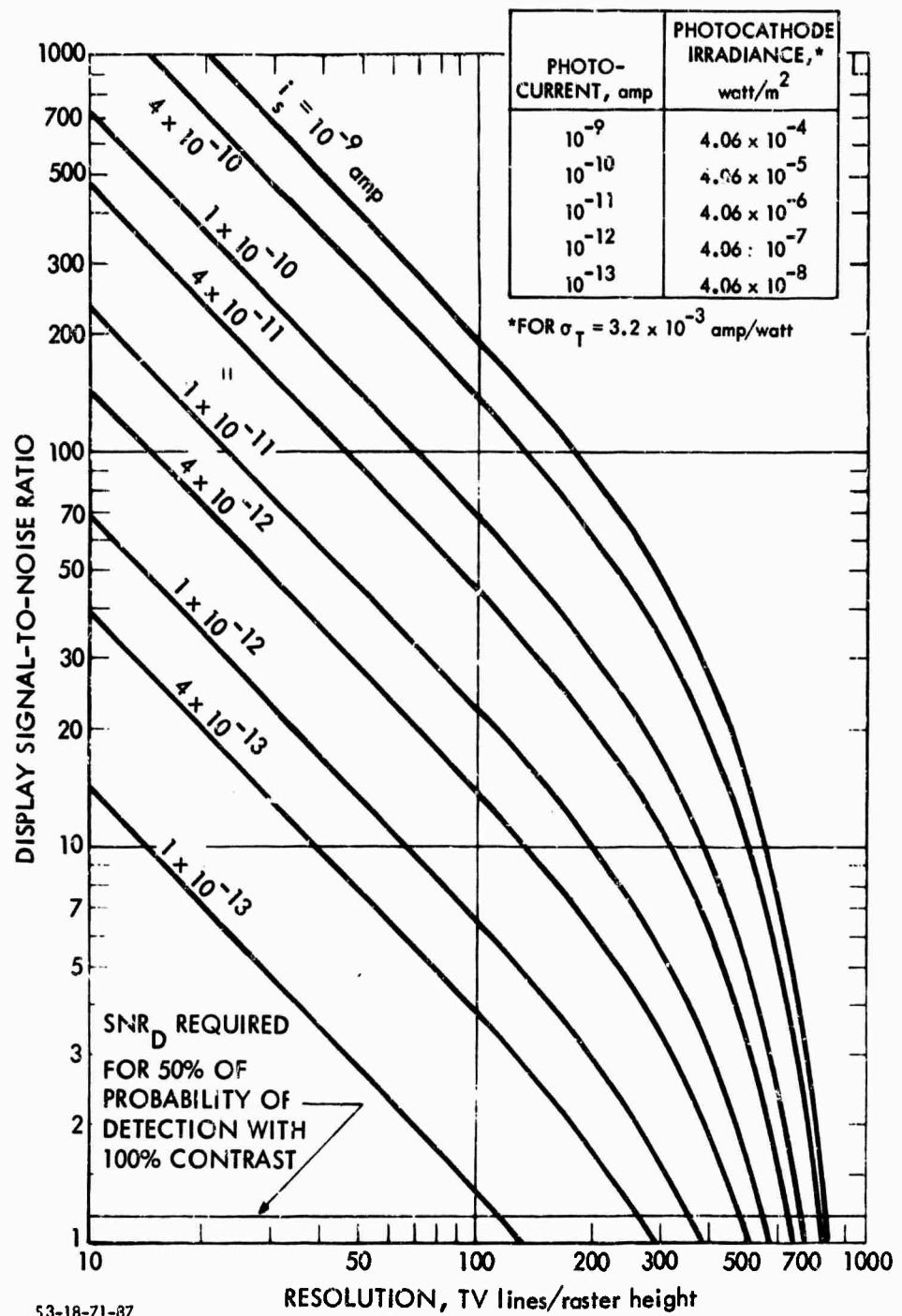


FIGURE V-E-7. Display Signal-to-Noise Ratio Versus Resolution for the Thin-Film Metal-Oxide-Targeted Image Orthicon for Various Input Photocathode Currents (IO Operated with Optimum Beam Current)

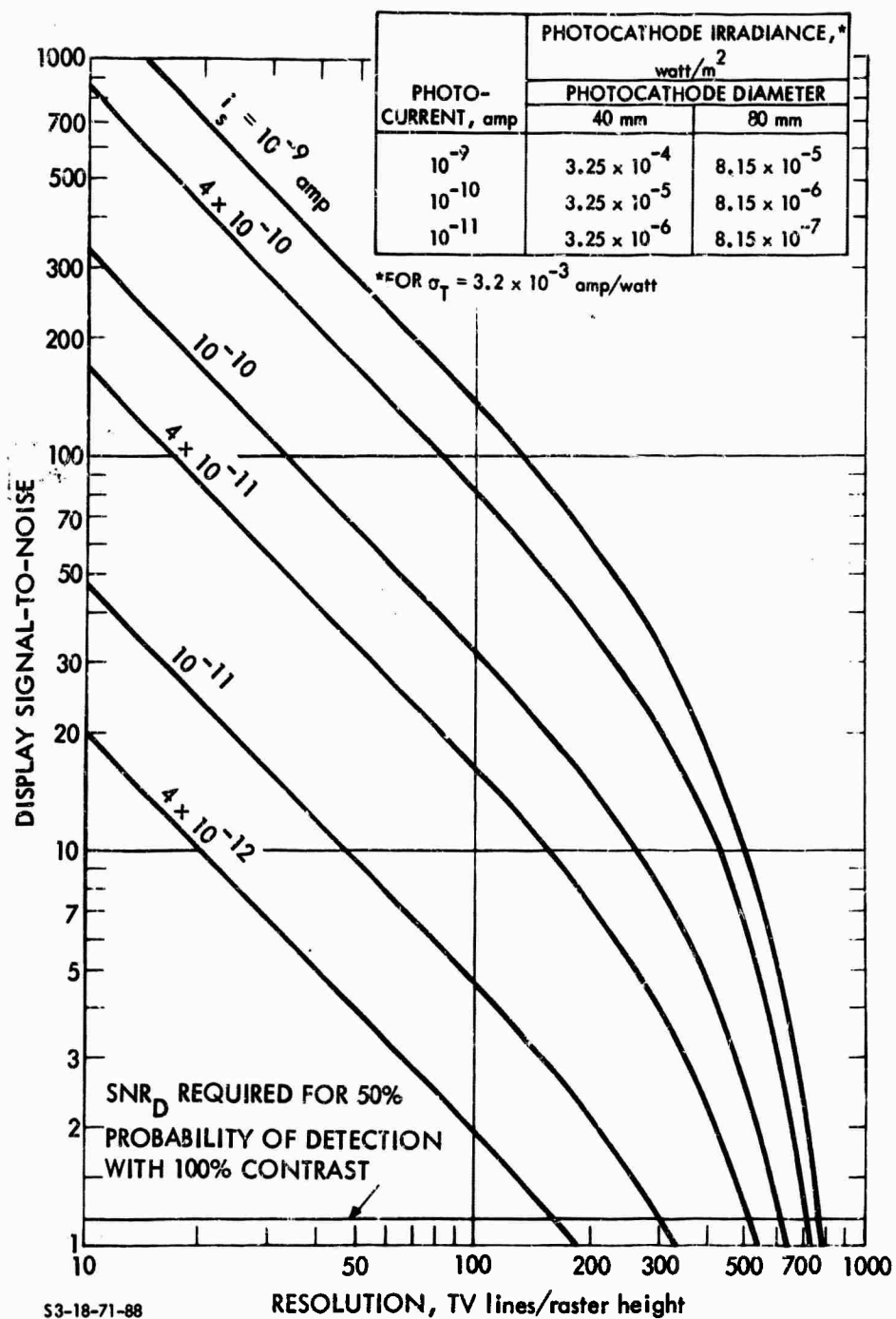


FIGURE V-E-8. Display Signal-to-Noise Ratio Versus Resolution for the Thin-Film Metal-Oxide-Targeted Image Orthicon as a Function of Input Photocathode Current (IO Operated with Fixed Beam Current)

e. Limiting Bar-Pattern Resolution. The limiting bar-pattern resolving power is plotted in Fig. V-E-9 for both the optimum and fixed beams. Another form of the result is plotted in Fig. V-E-10, which gives limiting resolution as a function of photocathode irradiance from a 2854°K tungsten source.

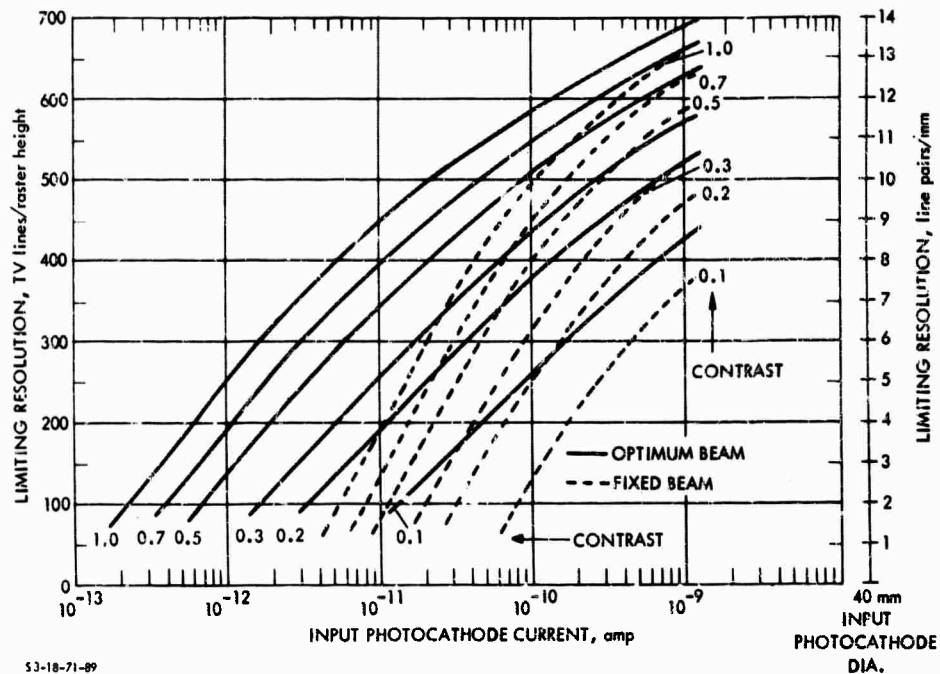


FIGURE V-E-9. Limiting Resolution Versus Input Photocathode Current for the 3-inch, Thin-Film-Targeted Image Orthicon for Various Input Image Contrasts

f. Computed versus Measured Results. The computed resolving power is compared to the data-sheet resolving power in Fig. V-E-11 for 100 percent input image contrast. Fairly good correlation is observed.

g. Lag Characteristics. No lag characteristics are currently available for the thin-film metal-oxide-targeted IO.

h. Form Factor. The standard 40-mm IO is approximately 15.45 in. long and has a maximum diameter of 3.06 in. The outside diameter

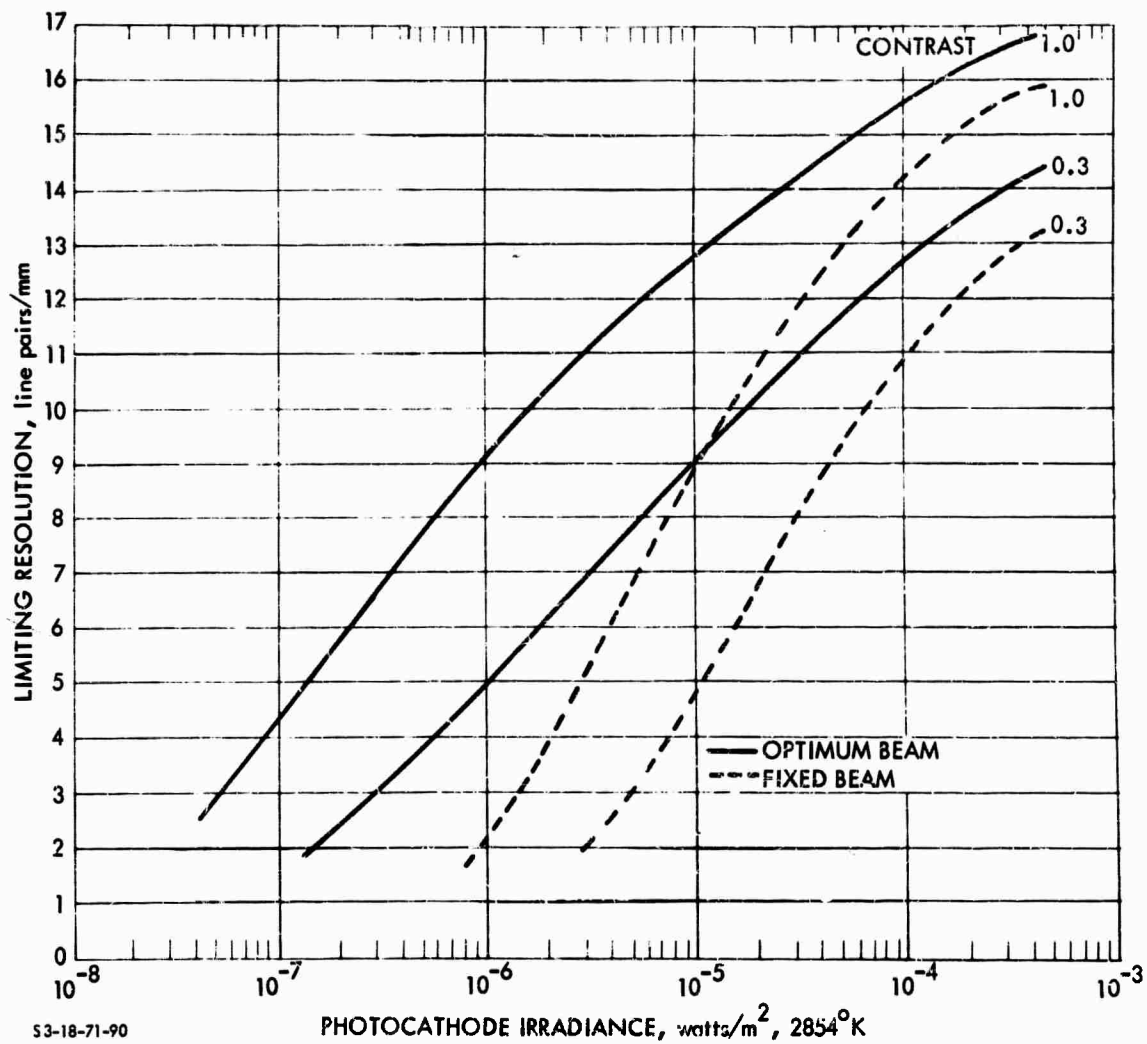


FIGURE V-E-10. Limiting Resolution Versus Photocathode Irradiance for the 3-inch, Thin-Film-Targeted Image Orthicon with Fixed and Optimum Beam Current

of the focus coil is approximately 5 to 5.5 in., depending on the wire size.

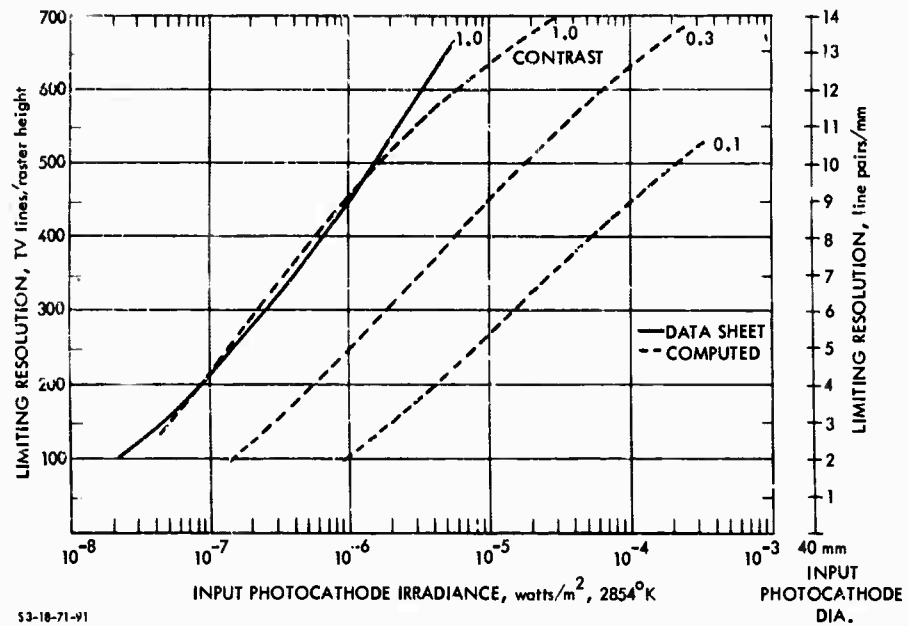


FIGURE V-E-11. Limiting Resolution Versus Input Photocathode Irradiance, Comparison of Computed Versus Data-Sheet Performance for the 3-inch, Thin-Film-Targeted Image Orthicon with Optimum Beam Current

i. Manufacturers' Literature. A sample of manufacturers' literature on image orthicons will be found in Chart V-E-1.

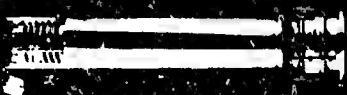
## 2. The Intensifier Image Orthicon

a. Principles of Operation. The lag of the IO is not generally acceptable for applications where the scene has any appreciable motion. Also, when the IO is set up with a moderately high fixed beam current, its sensitivity becomes too low. An additional image intensifier stage substantially solves these problems. The sensitivity of the intensifier image orthicon (I-IO) is not much greater than that of an IO operated with optimum beam current, but it does permit the operation of the I-IO without continual beam adjustment, and its lag is greatly reduced.

CHART V-E-1. SAMPLE OF MANUFACTURERS' LITERATURE  
ON IMAGE ORTHICONS

The units, definitions, and methods of measurement specified herein are not necessarily endorsed by the authors but are those used by the manufacturer quoted.

A



## GENERAL ELECTRIC

### SPECIAL PURPOSE IMAGE ORTHICONS

**7538**

**7409**

**7629**

**7967**

**Z-7806**

**7969**

**Z-7807**

General Electric offers this family of low light level image orthicons to meet a wide variety of requirements for military . . . scientific . . . and industrial applications . . . for operation under normal environments or severe shock and vibration conditions. Each type incorporates the high gain, thin film magnesium oxide target with a sensitivity ten to twenty times that of glass targets. The extreme thinness and anisotropic property of this semiconductor target virtually eliminates lateral leakage and increases the resolution 25 to 50 percent over that of the standard glass target. This

feature adapts the tube for service where the signal is stored for a very long period before being read out. This permits additional sensitivity using low frame rates or beam pulsing. Permanent stickiness and burn-in are virtually eliminated since operation depends on electron conduction, which is not a depletion process, rather than on ion conduction. As a result these tubes will provide very long life and reliable service. In addition, low gamma permits a very wide operating range.

**7538**

This type is designed for normal environmental operation and provides an effective low light level sensitivity of  $4 \times 10^{-7}$  foot candles photocathode illumination for resolution of 100 TV lines/target inch. The photocathode is S-10 with an overall spectral response from 3000 to 6950 angstroms.

**7409 RUGGEDIZED**

This type has all the features of the 7538 and is especially designed to operate under severe shock and vibration conditions in applications which preclude the use of standard tubes. Specific conditions of shock and vibration are listed on page 5.

**7629**

This type is designed for normal environmental operation in applications requiring an effective low light level sensitivity of  $3 \times 10^{-6}$  foot candles photocathode illumination (100 TV lines/target inch) or higher where extended integration is not a requirement. This type has an S-10 photocathode with overall spectral response from 3000 to 6950 angstroms.

**7967**

The most sensitive image orthicon available, this type is designed for normal environmental operation. It has an effective low light level sensitivity down to  $1.5 \times 10^{-7}$  foot candles photocathode illumination for a resolution of 100 TV lines/target inch. This image orthicon has an S-20 photocathode including red response and overall response from 3000 to 8000 angstroms.

**Z-7806 RUGGEDIZED**

This type has all the features of the 7967 and is especially designed to operate under severe shock and vibration conditions in application which preclude the use of standard tubes. Specific conditions of shock and vibration are listed on page 5.

**7969**

This type is designed for normal environmental conditions and provides an effective low light level sensitivity of  $4 \times 10^{-7}$  foot candles of photocathode illumination for resolution of 100 TV lines/target inch. The photocathode has an overall spectral response from 2200 angstroms (ultra-violet) to 6950 angstroms.

**Z-7807 RUGGEDIZED**

This type has all the features of the 7969 and is especially designed to operate under severe shock and vibration conditions in applications which preclude the use of standard tubes. Specific conditions of shock and vibration are listed on page 5.



7538  
7409  
7629  
7967  
Z-7806  
7969  
Z-7807

USER PROVEN AND SUGGESTED APPLICATIONS

**7538**  
This type has proved a dependable performer in applications where low light level capability is required . . . . . surveillance, satellite tracking, detection and electro-optical telescope systems for astronomical observations of 15 magnitude stars using its integration capability.

**7409**  
In severe ruggedization environments, this image orthicon has been successfully applied in tank fire control, drone guidance, and missile borne systems. This is a vastly improved image orthicon of the type which aided the submarine Skote to probe an historic path under the arctic icecap and surface exactly at the North Pole. The 7409 also adopts itself for ground vehicle systems operating over rough terrain.

**7629**  
This type is successful in X-ray intensifier applications to improve detectability of lower contrasts and detail than is possible with standard image orthicons using a gloss target. The high sensitivity has allowed lower radiation rates for longer continuous observations of patients. The 7629 is user-proven for low light level color and monochrome telecasting . . . . . as well as closed circuit training applications.

**7967**  
The most sensitive image orthicon available without an intensifier is being used both for underwater observation, missile detection and tracking as well as astronomical study of stars to the 20th magnitude. The 7967 can be applied readily in scintillation experiments with an image intensifier.

**7969**  
This type with an ultra-violet response photocathode lends itself for use in medical biological studies and spectrographic detectors. In addition, the 7969 has been used in special underwater observation experiments and for hydrogen flame detection.

ADDITIONAL GENERAL ELECTRIC IMAGE ORTHICONS AVAILABLE  
(DATA INFORMATION ON REQUEST)

SPECIAL PURPOSE • SCIENTIFIC • INDUSTRIAL • MILITARY				
TYPE	FEATURES	SPECTRAL RESPONSE	* RESOLUTION SENSITIVITY	APPLICATIONS-USER PROVEN†
Z-5395	magnesium oxide target infra-red sensitive (Ruggedized version is Z-7805)	3200-10,800 Å peak: infra-red S-1	500 @ 7.6 x 10 <sup>-5</sup> 200 @ 1.0 x 10 <sup>-5</sup>	*infra-red detection: passive and active daylight star tracking *aerial mapping *spectrographic detectors
Z-7809	similar to 7538 plus: fibre-optics faceplate			*medical television *fibre-optics systems *photographic printing *high speed information scanning
Z-7810	similar to 7967 plus: fibre-optics faceplate			*fibre-optics systems *radiation scintillator studies *photographic printing *high speed information scanning
Z-7814	same as 7967 plus: field mesh flatter fields improved corner resolution	same as 7967 except sensitivity limit is approximately 2.7 x 10 <sup>-7</sup> foot candles		electro-optical telescope systems extreme low light level surveillance underwater observation orthicon intensifier studies
COMMERCIAL BROADCAST • NETWORK • EDUCATIONAL				
7629a	high reliability very long life low light level sensitivity semiconductor target	3200-6950 Å S-10	*equivalent ASA rating 32,000-64,000	remote black/white as low as 1 ft-c scene illumination remote color as low as 5 ft-c scene illumination long life studio service
8092a	same as 7629 plus: field mesh flatter fields improved corner resolution		32,000-64,000	studio color 40 to 100 ft-c illumination remote color
5820a	glass target good gray scale stable performance		8000-16,000	studio black/white 100 ft-c scene illumination educational TV
7293	same as 5820 plus: field mesh flatter fields improved corner resolution		8000-16,000	studio black/white high quality monochrome educational TV
8093	same as 7293 plus: very high signal:noise ratio for video tape recording and color		5000-10,000	high quality video tape re- cording high quality color educational TV
Z-7866	same as 8092A plus: higher signal to noise ratio and extended contrast range designed specifically for color		32,000	studio and outdoor color works well nighttime under lights

\*Resolution sensitivity is defined as television lines per target inch @ specified photocathode illumination in foot-candles.  
†Equivalent ASA ratings based on exposure at knee of transfer characteristic curve and frame time of 1/30 sec.

effective low light  
of 100 TV lines/  
to 6950 angstroms.

to operate under  
if standard tubes.

ing an effective  
n (100 TV lines/  
type has an S-10

nal environmental  
et condles photo-  
icon has an S-20  
roms.

to operate under  
standard tubes.

ffective low light  
ution of 100 TV  
angstroms (ultra-

o operate under  
standard tubes.

A

7538

7409

7629

7967

# ESSENTIAL SPECIFICAT

## ELECTRICAL-ALL TYPES

Cathode-Unipotential			Focusing method-Magnetic
Heater voltage, AC or DC	6.3 ±10%	Volts	Deflecting method-Magnetic
Heater Current	0.6	Amperes	Direct interelectrode capacitance
Photocathode-Semi-transparent	Response		Anode to all other electrodes
7538 7409 7629	5-10		12 μpf
7967 Z-7906	5-20		
7969 Z-7807	U/V		
Rectangular image, 4 by 3 aspect ratio			
Useful size, maximum diagonal	1.8	Inches	
Orientation-Proper orientation is obtained when the vertical scan is essentially parallel to the plane passing through the center of the faceplate and pin No. 7 of the shoulder base.			

Operating  
tube, to  
Temperatu  
and any  
section

## MAXIMUM RATINGS-ABSOLUTE VALUES-ALL TYPES

Photocathode voltage	-600	Volts	Grid-No. 2 and dynode-No. 1 voltage	380	Volts	D
Photocathode illumination	50	Foot-Candlas	Grid-No. 3 voltage	400	Volts	D
Anode supply voltage (a)	1850	Volts	Grid-No. 4 voltage	300	Volts	D
Grid-No. 1 voltage			Grid-No. 5 voltage	150	Volts	D
Negative bias value	135	Volts	Grid-No. 6 voltage	-600	Volts	A
Positive bias value	0	Volts				V
Above voltage for highlight discharge	5	Volts				

## TYPICAL OPERATION-AVERAGE VALUES-ALL TYPES-FOR NORMAL PERFORMANCE

Photocathode voltage, image focus	-400 to -550	Volts	Grid-No. 2 and dynode-No. 1 voltage	300	Volts	D
Grid-No. 1 voltage for picture cutoff, beam	-45 to -125	Volts	Grid-No. 3 voltage (b), multiplier focus	225 to 330	Volts	D
Photocathode illumination			Grid-No. 4 voltage, beam focus	140 to 180	Volts	D
Scene illumination	P. 7		Grid-No. 5 voltage, decelerator	0 to 125	Volts	D
			Grid-No. 6 voltage, accelerator-			A
			75 to 85 percent of photocathode voltage,			D
			approximate	-300 to -465	Volts	S

## TYPICAL OPERATION-AVERAGE VALUES-ALL TYPES-FOR MAXIMUM SENSITIVITY

Photocathode voltage, image focus	-400 to -550	Volts	Grid-No. 2 and dynode-No. 1 voltage	370	Volts	D
Grid-No. 1 voltage for picture cutoff, beam	-45 to -135	Volts	Grid-No. 3 voltage (b), multiplier focus	225 to 380	Volts	D
Photocathode illumination			Grid-No. 4 voltage, beam focus	140 to 250	Volts	D
Scene illumination	P. 7		Grid-No. 5 voltage, decelerator	0 to 125	Volts	D
			Grid-No. 6 voltage, accelerator-			A
			75 to 85 percent of photocathode voltage,			D
			approximate	-300 to -465	Volts	S

## OPERATING NOTES-ALL TYPES

IMPORTANT! Some magnesium oxide targets may be subject to permanent damage if directly and intermittently exposed, while in operation, to extremely bright sources which result in high photoelectron densities occurring at the target. Such sources include the sun, photoflash lamps and exploding wire flashes. If damage does occur, it is in the form of black image spots burned into the target from the intense light.

## FOOT NOTES

- Ratio of dynode voltages is shown under Typical Operation.
- Adjust to give the most uniformly shaded picture near maximum signal.
- The target supply voltage should be adjustable from -3 to +5 volts with blanking voltage off. Maximum target voltage is +10 volts above target cutoff. Recommended target voltage is +2 volts above cutoff. Slight readjustment, usually only a small fraction of a volt, may be necessary to minimize microphonics.
- Direction of current should be such that a north-seeking pole is attracted to the image end of the focusing coil, with the indicator located outside of and at the image end of the focusing coil.
- Adjusted to produce flattest field with maximum response. Alignment is correct when the center of the picture merely goes through focus.

## PECIFICATIONS AND RATINGS

## THERMAL-ALL TYPES

Operating temperature of any part of bulb . . . . 70 °C Max.

Operating temperature of bulb at large end of  
tube, target section, minimum. . . . . 0 C.

Temperature difference between target section  
and any part of bulb hotter than target  
section . . . . . 7.5 C

## MECHANICAL-ALL TYPES

Over-all length	15.20	± 0.25	Inches
Greatest diameter of bulb	3.00	± 0.06	Inches
Deflection coil minimum inside diameter	2.3	8	Inches
Deflecting coil length	5		Inches
Focusing coil length	10		Inches
Alignment-coil length	15.16		Inch
Photocathode distance inside end of focusing coil	1.2		Inch
Weight, approximate	Nonruggedized	1.4	Ozs.
	Ruggedized	1.4	Lbs.
Operating position—Any, except with diaphragm base up and the tube axis at an angle of less than 20 degrees from vertical.			

380 Volts	Dynode-No. 2 to Dynode-No. 1 Voltage	350 Volts	Target voltage	
400 Volts	Dynode-No. 3 to Dynode-No. 2 Voltage	350 Volts	Above target cutoff, positive direction	10 Volts
300 Volts	Dynode-No. 4 to Dynode-No. 3 Voltage	6.0 Volts	Negative value	10 Volts
150 Volts	Dynode-No. 5 to Dynode-No. 4 Voltage	350 Volts	Peak heater-cathode voltage	
-600 Volts	Anode to Dynode-No. 5 Voltage	100 Volts	Heater negative with respect to cathode	125 Volts
	Voltage per multiplier stage	400 Volts	Heater positive with respect to cathode	10 Volts

**FOR NORMAL PERFORMANCE\***

..... 300 Volts	Dynode-No. 2 voltage .....	600 Volts	Target voltage .....	
us. 225 to 330 Volts	Dynode-No. 3 voltage .....	910 Volts	Target cutoff voltage (c) .....	-3 to +1 Volts
..... 140 to 180 Volts	Dynode-No. 4 voltage .....	1200 Volts	Target temperature range .....	15 to 55
..... 0 to 125 Volts	Dynode-No. 5 voltage .....	1490 Volts	Peak-to-peak blanking voltage .....	5 to 20 Volts
	Anode voltage .....	1550 Volts	Field strength at center of focusing coil (d) ..	.75 Gauss
oltage,	DC anode current, max. ....	30 Microamperes	Field strength of alignment coil, approximate (e) .....	0 to 3 Gauss
,-300 to -465 Volts	Signal output current, peak-to-peak - See light transfer characteristic curve, page 2.			

**FOR MAXIMUM SENSITIVITY PERFORMANCE AT EXTREME LOW LIGHT LEVEL CONDITIONS\*\***

370	Volts	Dynode-No. 2 voltage	770	Volts	Target voltage		
225 to 380	Volts	Dynode-No. 3 voltage	1080	Volts	Target cutoff voltage (c)	-3 to +3	Volts
140 to 250	Volts	Dynode-No. 4 voltage	1360	Volts	Target temperature range	15 to 55	C
0 to 125	Volts	Dynode-No. 5 voltage	1610	Volts	Peak-to-peak blanking voltage	5 to 20	Volts
		Anode voltage	1700	Volts	Field strength at center of focusing coil (d)	.75	Gausses
		DC anode current, max.	30	Microamperes	Field strength of alignment coil, approximate (e)	0 to 3	Gausses
-300 to -465	Volts	Signal output current, peak-to-peak - See light transfer characteristic curve, page 2.					

ly and intermittently  
densities occurring  
damage does occur,

The tubes will be protected in most cases by inserting a 20 to 80 megohm 1/4 watt resistor in series with the photocathode in the camera. This resistor in no way interferes with normal operation of these or other image orthicons which may be used in the modified camera.

In addition, if these or similar bright sources are to be continuously observed, appropriate exposure control of photocathode illumination can be applied by neutral density filters.

target voltage is +10 volts  
a small fraction of a volt,  
ing coil, with the indicator  
merely goes through focus

and does not rotate when beam focus (Grid-No. 4) is varied. For most commercial focus coils 75 gauss field results from focus coil current of 75 ma.

- Far Normal Performance

These tubes will perform in standard equipment. However, it is suggested that modification be made in accordance with the above stated values to improve effective sensitivity for most applications.

\*\* For Maximum Sensitivity Performance

For extreme low light level applications, maximum useful multiplier gain is desired. The values  $\gamma_{min}$  should be applied to obtain the best low light level sensitivity capability of the tube being considered.

The resolution sensitivity information contained in this data folder was derived with these higher multiplier voltages.

A

# SPECIFIC P

All curves on Page 2 on Page 7 ex-  
following conditions.

Camera Chain: General Electric TE-5  
Amplifier bandwidth

Resolution Chart: National Bureau of Sto

Contrast Ratio =  $\frac{T_c - T_b}{T_c} \times 100\%$ , where  $T_c$   
 $T_b$

(Note:  $T_c$  remains some of about 0.82 for  
light gray in the 7% chart.)

Window Chart: 100% contrast, 1% on

Light Source: 2870 Kelvin - tung

Light Level: Aperture and neutral d  
provide range from  $10^{-1}$   
scene brightness in fo  
illumination in foot co

Operating Temperature for image end: 25

Target Roster: Target diameter is 1.4  
roster dimensions are:

Aspect Ratio  
1 x 1 (square)  
4 x 3 (standard)  
Horizontal TV lines =  
Vertical TV lines (RE  
Resolution sensitivity  
Therefore, 700 TV line

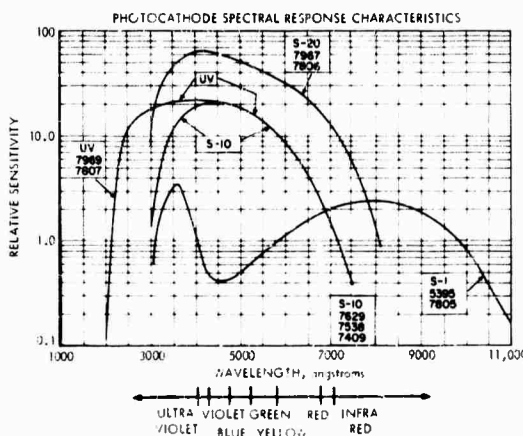
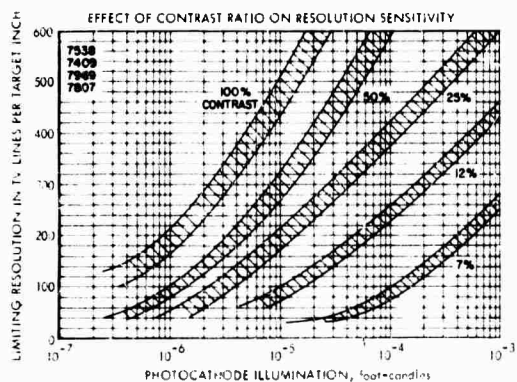
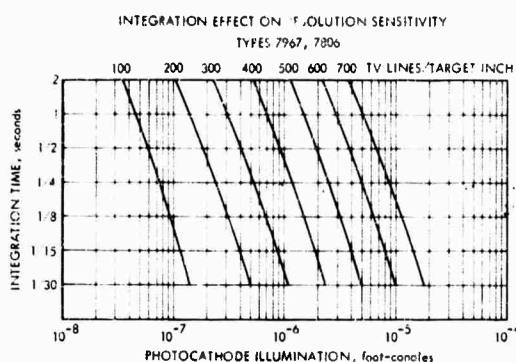
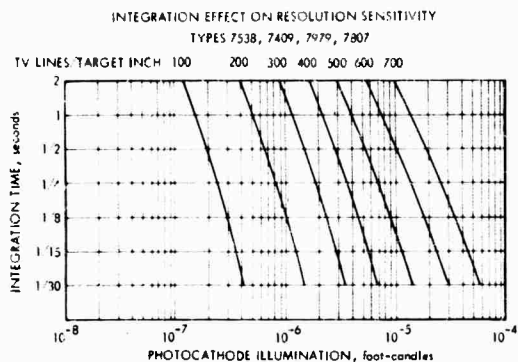
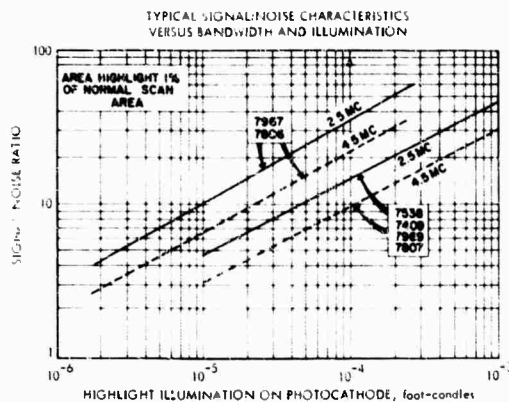
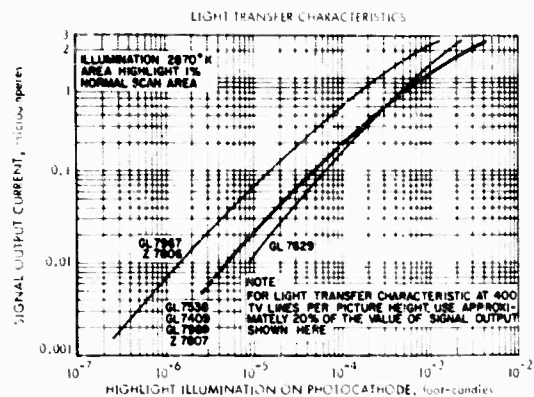
## ENVIR

Shock: Per specification MIL-E-  
A) 12 impact shocks of  
B) The shock shall be  
1.) Vertically perpe  
2.) Parallel to the  
C) The shock pulse wid

Vibration: Under the conditions spe  
of operating temperature  
photocathode illumination  
the frequency range from  
from 5 to 50 cycles per  
readable through any inte

Humidity: Under the conditions spe  
this test, the interelectr  
to all other end base pin  
ohms.

Acceleration: Constant acceleration v  
70G, s  
10 minutes.



## SPECIFIC PARAMETERS ON RECORDED DATA

All curves on Page 2 and Page 7 except Spectral Sensitivity Characteristics were recorded under the following conditions.

Camera Choin: General Electric TE-5 (modified)  
 Amplifier bandwidth - 20 mc (for high resolution measurements)  
 - 6 mc (for low-light measurements)

Resolution Chart: National Bureau of Standards Lens Test Chart 100% contrast transparency.

Contrast Ratio =  $\frac{T_c - T_b}{T_c} \times 100\%$ , where  $T_c$  = light transmission ratio of clear background of chart transparency, and  
 $T_b$  = light transmission ratio of resolution bars.

(Note:  $T_c$  remains some of about 0.82 for all contrast charts and  $T_b$  varies from very dense in the 100% chart to light gray in the 7% chart.)

Window Chart: 100% contrast, 1% area window for signal:noise and transfer characteristic data.

Light Source: 2870° Kelvin - tungsten

Light Level: Aperture and neutral density controlled (within specially constructed low light level box) to provide range from  $10^{-8}$  to  $10^{-2}$  foot candles illumination on photocathode. For corresponding scene brightness in foot lamberts when using Leitz f 1.5 lens (85 mm), multiply photocathode illumination in foot candles by 12.

Operating Temperature for image end: 25° to 30° centigrade.

Target Roster: Target diameter is 1.40 inches. For corners of scanning roster just touching target edge roster dimensions are:

Aspect Ratio	Horizontal	Vertical
1 x 1 (square)	0.99"	0.99"
4 x 3 (standard)	1.12"	0.84"
Horizontal TV lines = 1.12 x TV lines/target inch		
Vertical TV lines (RETMA) = 0.84 x TV lines/target inch		
Resolution sensitivity data is recorded in TV lines/target inch		
Therefore, 700 TV lines/target inch = 784 horizontal lines		
= 588 vertical lines (RETMA)		

## ENVIRONMENTAL SPECIFICATIONS

7409 Z-7806 Z-7807

Shock: Per specification MIL-E-5272C (ASG) Paragraph 4.15.5 with the following differences:

- 12 impact shocks of 30 G.
- The shock shall be applied in the following directions:
  - 1.) Vertically perpendicular to longitudinal axis, 3 shocks in each direction.
  - 2.) Parallel to the minor horizontal axis, 3 shocks in each direction.
- The shock pulse width is defined by the use of a 0.2 to 250-cycle-per-second filter.

Vibration: Under the conditions specified in MIL-E-5272C (ASG) Paragraph 4.7.12 Procedure XII except of operating temperature only. Center horizontal resolution of  $3 \times 10^{-5}$  maximum foot-candles, photocathode illumination will be at least 350 lines (RETMA) with 5 G applied acceleration in the frequency range from 50 to 500 cycles per second and a double amplitude of 0.036 inch from 5 to 50 cycles per second. Picture resolution of 350 TV lines (RETMA) is defined as readable through any interference that may occur.

Humidity: Under the conditions specified in MIL-E-5272C (ASG) Paragraph 4.4.1 Procedure I. Following this test, the interelectrode insulation of the end pins 5, 6, 7, 8, 9 and 10 each with respect to all other end base pins grounded and with 350 volts (minimum) applied is greater than 500 ohms.

Acceleration: Constant acceleration when applied perpendicular to the longitudinal axis of the tube for 70G, s 10 minutes.

**BLANK PAGE**

The added intensifier is assumed to have an S-25 photocathode having a radiant sensitivity of  $4 \times 10^{-3}$  amp/watt and a diameter of either 80 mm or 40 mm. The electron gain at the phosphor-photocathode interface is assumed to be 40.

b. Signal Transfer Characteristic. The signal transfer characteristic for various intensifier combinations is shown in Fig. V-E-3. The shift is a factor of 50 to the left for the 40/40-mm I-IO, which results from a photocathode sensitivity increase of 1.25 times the electron gain of 40. For the 80/40-mm I-IO, a further shift of a factor of four towards lower irradiance levels is obtained because of the four times larger area.

c. Amplitude Response. The sine-wave amplitude response of the intensifier and the square-wave response of the I-IO are shown in Fig. V-E-4. These curves are identical for the 80- and 40-mm input photocathodes when resolving power is specified in units of TV lines/raster height, but differ by a factor of two when resolving power is specified in units of line pairs/millimeter, as shown in the figure.

d. Video and Display Signal-to-Noise Ratios. The additional gain of the intensifier is sufficient to make all of the noises negligible except for the photoelectron noise and the beam noise. The video signal-to-noise ratio may then be written as

$$\text{SNR}_{V,0,1} = \frac{I_{S \text{ max}}}{(\bar{I}_e^2 + \bar{I}_B^2)^{\frac{1}{2}}} \quad (\text{V-E-8})$$

where

$$\begin{aligned} I_{S \text{ max}} &= \text{the output signal current} \\ &= G_P(G_T - 1) G_M T_M i_{S \text{ max}}/e_v e_h. \end{aligned} \quad (\text{V-E-9})$$

$$\begin{aligned} \bar{I}_e^2 &= \text{the mean square photoelectron noise} \\ &= G_P^2 (G_T - 1)^2 G_M^2 T_M^2 e \Delta f i_{s \max} / e_v e_h. \end{aligned} \quad (\text{V-E-10})$$

$$\begin{aligned} I_B^2 &= \text{mean square beam noise} \\ &= \frac{2 G_P (G_T - 1) G_M^2 T_M^2 e \Delta f i_{s \max}}{m e_v e_h} \text{ for optimum beam} \end{aligned} \quad (\text{V-E-11})$$

$$= \frac{2 G_M e \Delta f I_{SF \max}}{m} \text{ for fixed beam} \quad (\text{V-E-12})$$

The terms in the expressions above are identical to those used in Sections V-E-1-b and V-E-1-d, except that  $G_P$  is the electron gain at the intensifier-phosphor/IO-photocathode and  $I_{SF \max}$  is the maximum possible output signal current. The various signal and noise currents are plotted in Fig. V-E-12 and  $SNR_{V,0,1}$  is plotted in Fig. V-E-13. As can be seen by comparison with Fig. V-E-6, the beam noise is still a factor in the case of the I-IO, but its effect is much reduced by the added intensifier.

This display signal-to-noise ratio is calculated as before and plotted in Fig. V-E-14.

e. Limiting Bar-Pattern Resolution. The limiting bar-pattern resolution is determined from Fig. V-E-14 and is plotted in Fig. V-E-15 as a function of input photocathode current. The limiting resolution resolution in line pairs/millimeter versus photocathode irradiance is plotted in Figs. V-E-16 and V-E-17 for two input photocathode diameters and a radiant sensitivity of  $4 \times 10^{-3}$  amp/watt.

f. Computed versus Measured Results. The computed resolving power is compared to that measured on a single sample in Fig. V-E-18 and shows good correlation in the contrast range from 0.3 to 1.0, but, as expected, the measured resolving power exceeds that predicted at the lowest contrast ( $C = 0.1$ ).



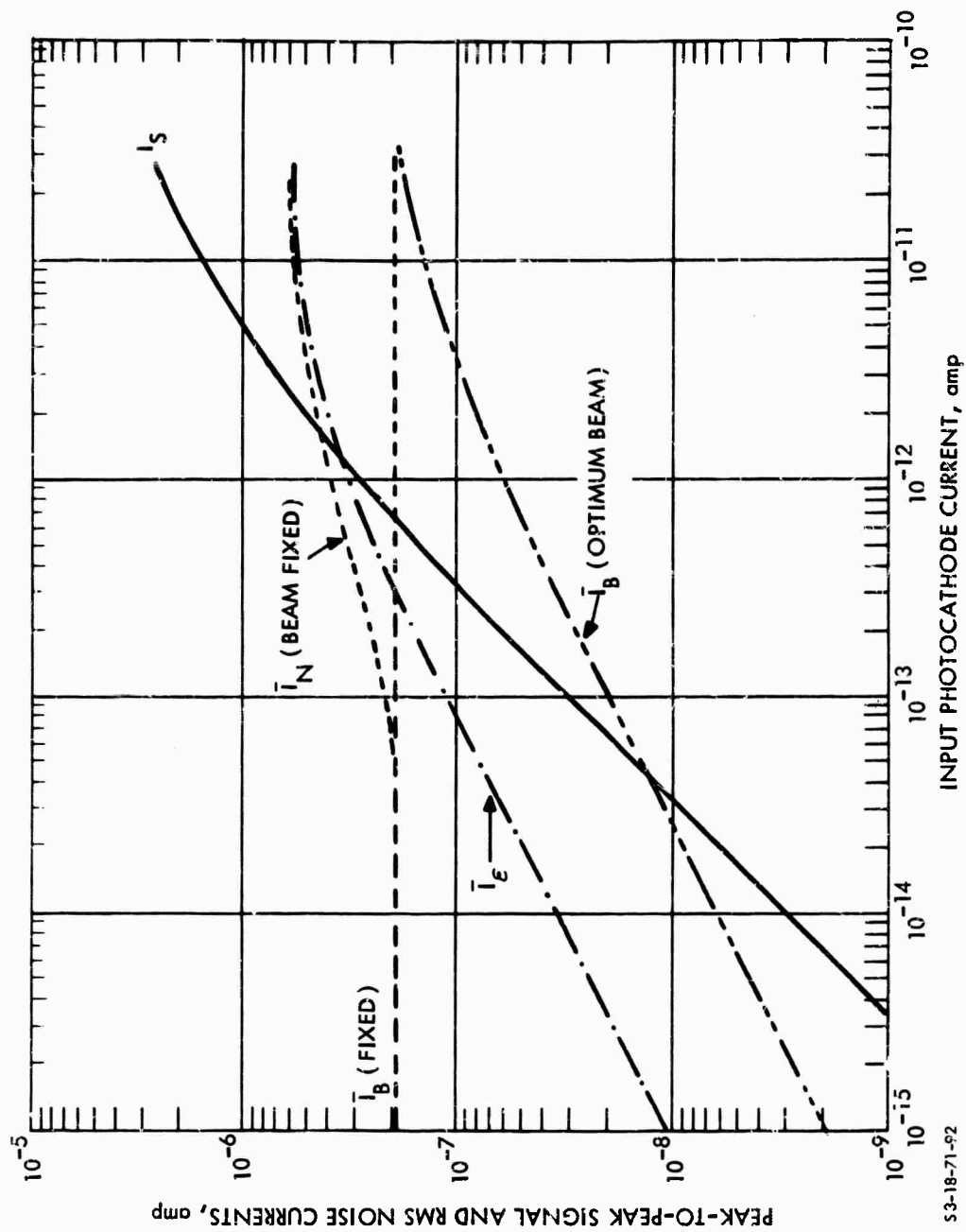


FIGURE V-E-12. Peak-to-Peak Signal and RMS Noise Output Current Versus Input Photocathode Current for the Intensifier Image Orthicon

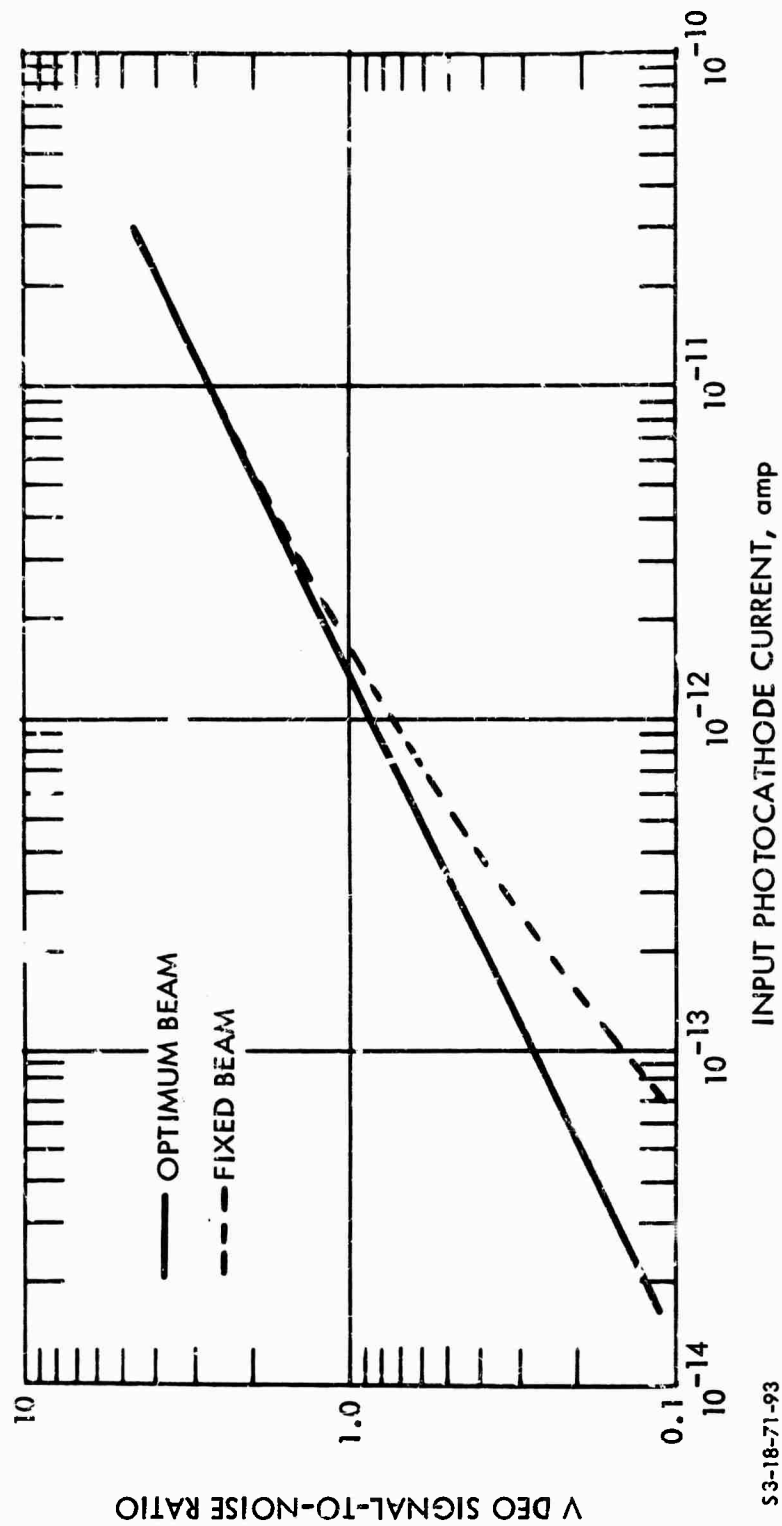


FIGURE V-E-13. Video Peak-to-Peak Signal-to-RMS-Noise Ratio for the Intensifier Image Orthicon Versus Input Photocathode Current for a Video Bandwidth of 10 MHz. (Note: Input Image is Assumed to be of Unit Contrast and of Low Spatial Frequency.)

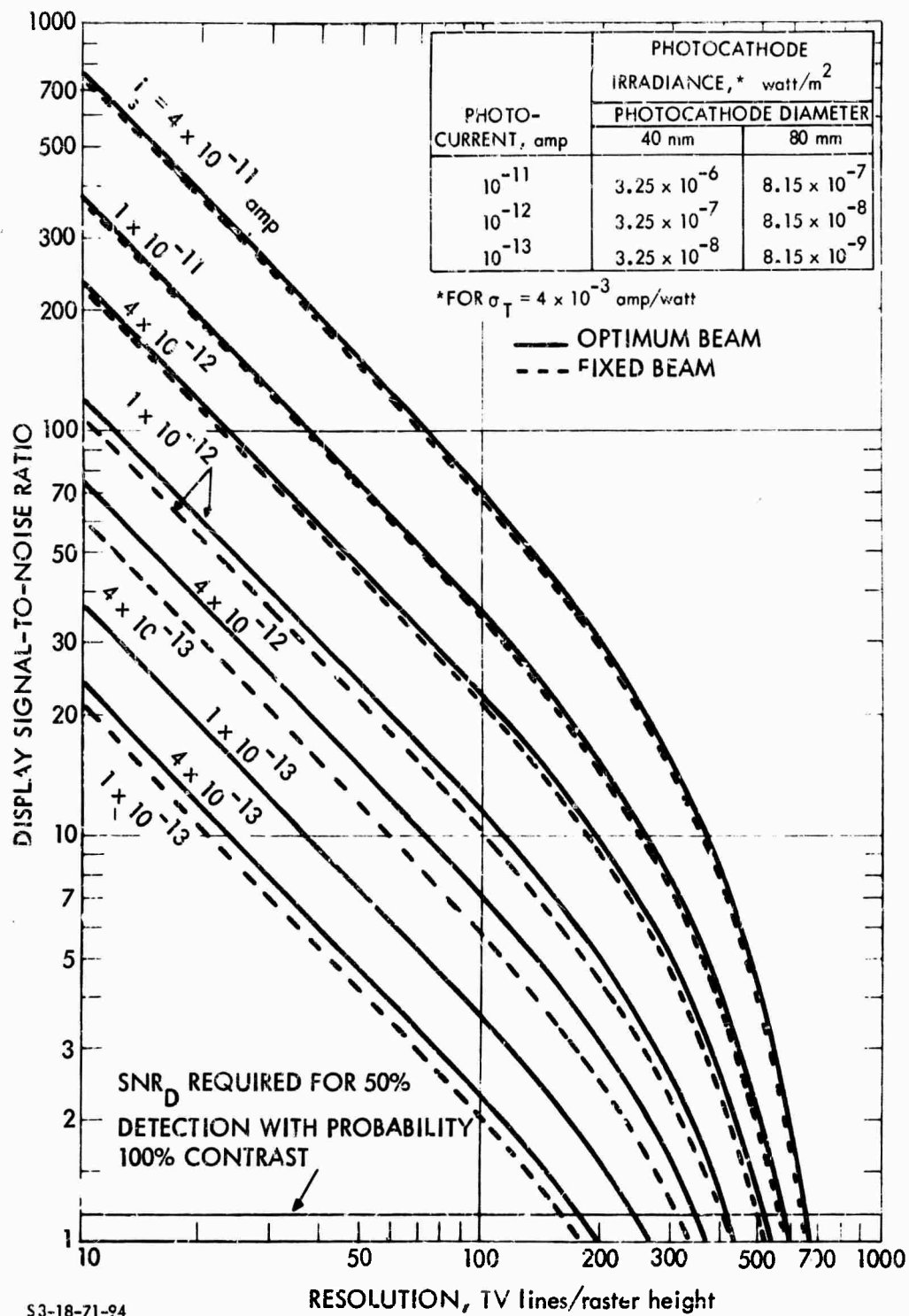
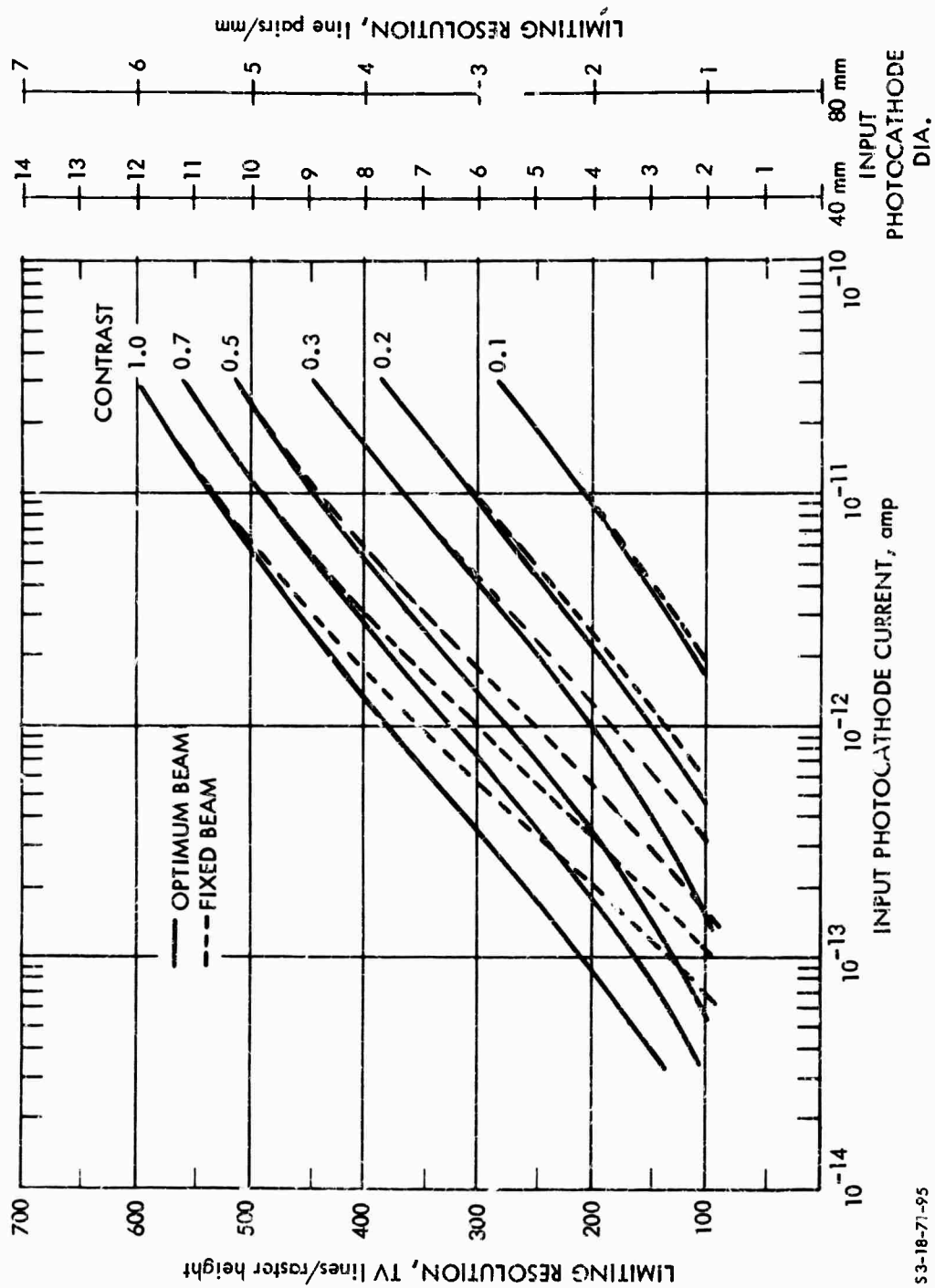


FIGURE V-E-14. Display Signal-to-Noise Ratio Versus Resolution for the Intensifier Image Orthicon for Various Input Photocathode Currents



S3-18-71-95

FIGURE V-E-15. Limiting Resolution Versus Input Photocathode Current for the Intensifier Image Orthicon for Various Input Image Contrasts with Fixed Beam Current and Optimum Beam Current

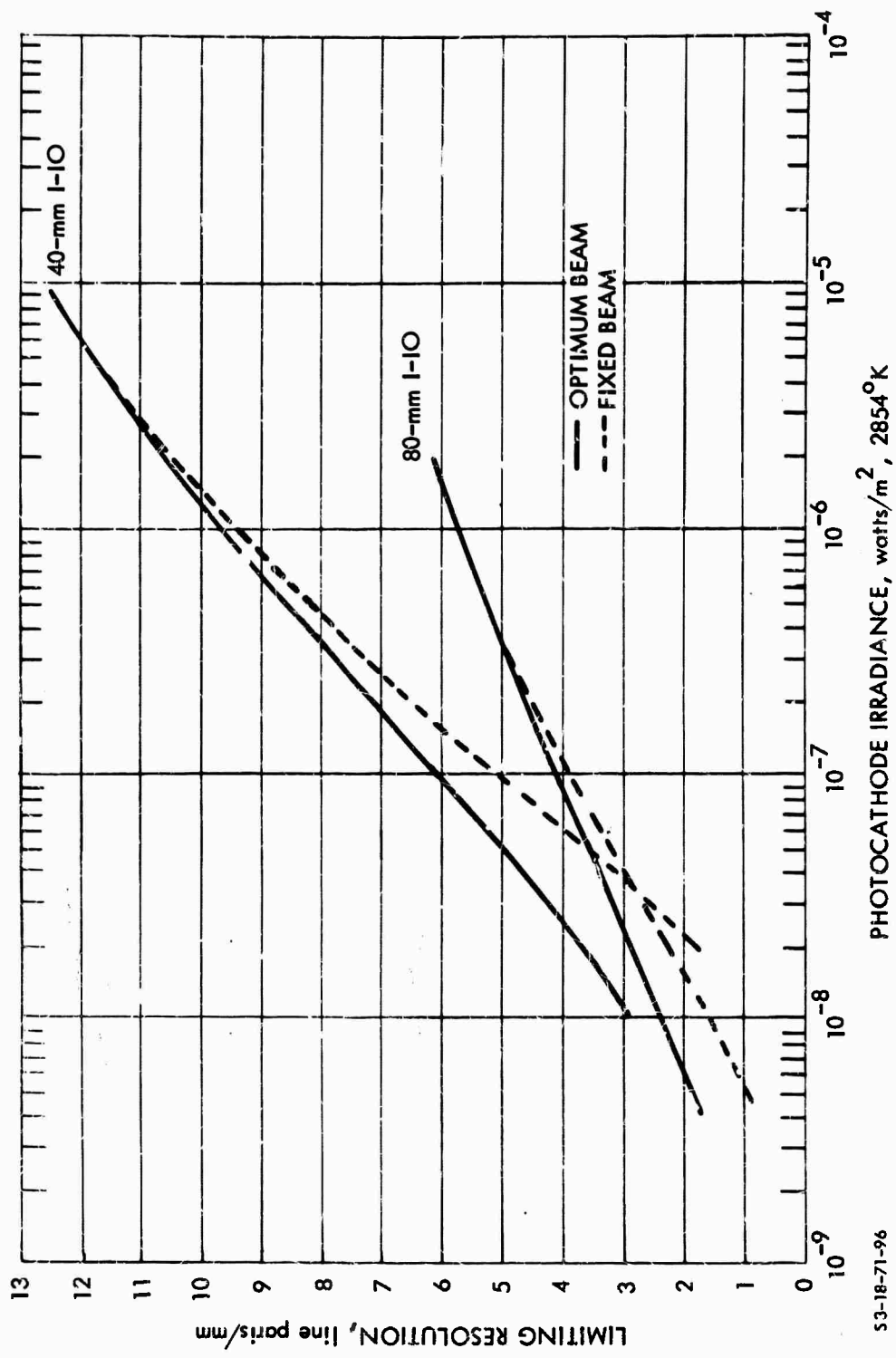


FIGURE V-E-16. Limiting Resolution Versus Photocathode Irradiance, Contrast 100%,  
for the Intensifier Image Orthicon with Optimum and Fixed Beam Current

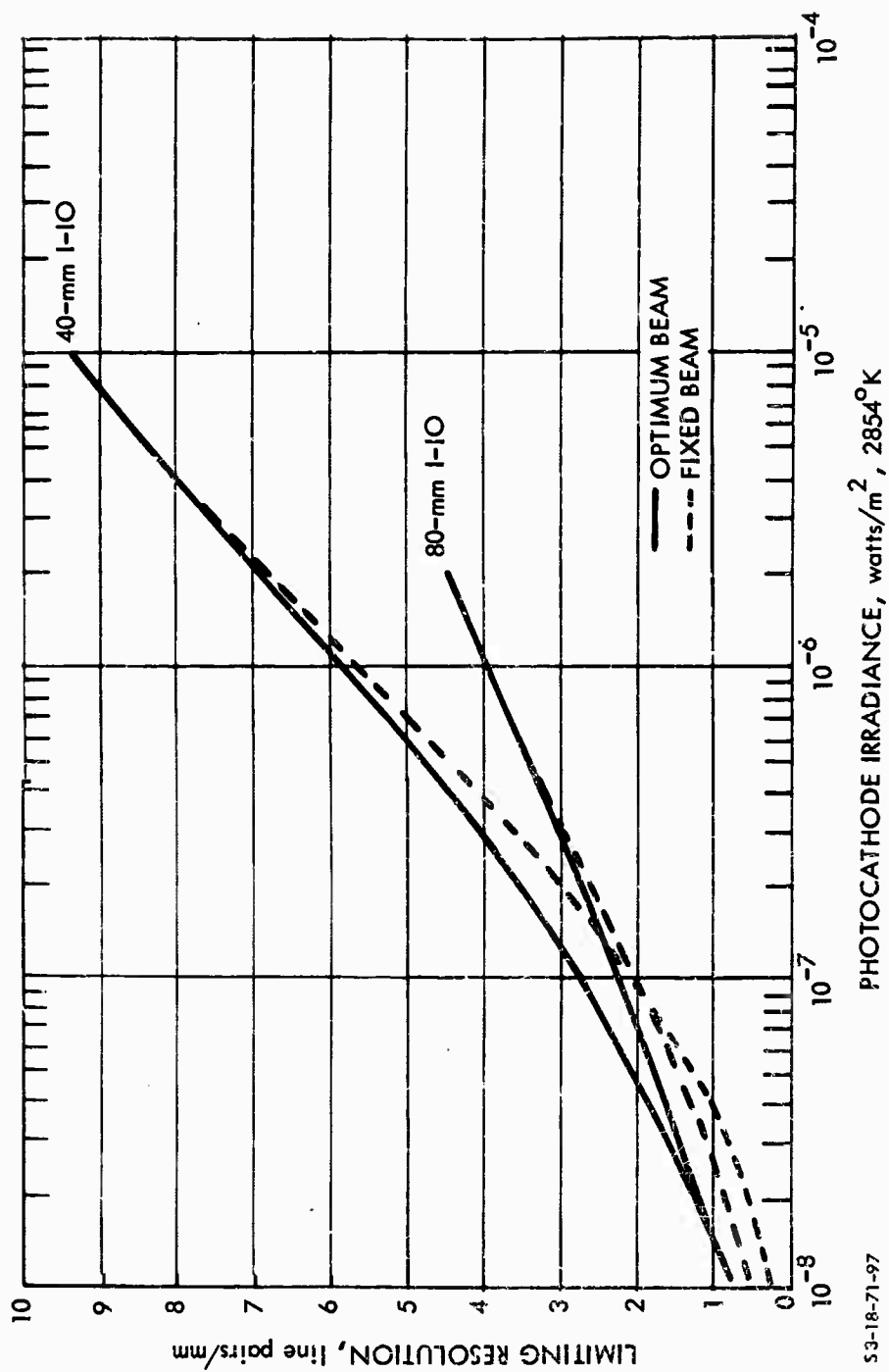
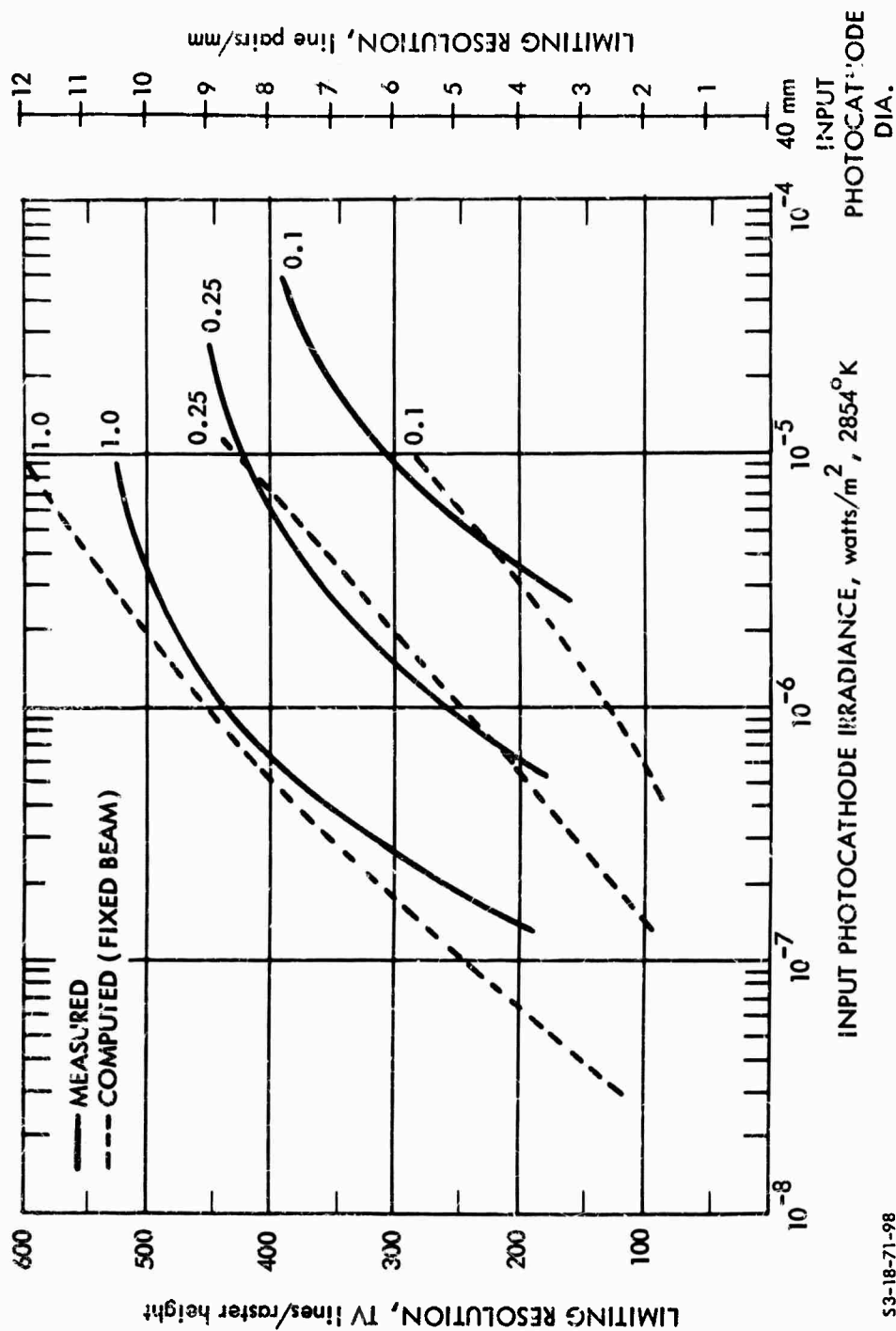


FIGURE V-E-17. Limiting Resolution Versus Photocathode Irradiance, Contrast 30%, for the Intensifier Image Orthicon with Optimum and Fixed Beam Current



53-18-71-98

FIGURE V-E-18. Limiting Resolution Versus Input Photocathode Irradiance. Comparison of Computed Versus Measured Resolving Power for the 40-mm Intensifier Image Orthicon

g. Lag Characteristic. Third-field lag characteristics are not currently available for the I-10, but a measurement of dynamic resolving power has been made, as shown in Fig. V-E-19. In this measurement, the bar pattern is moved across the field of view in the time period noted.

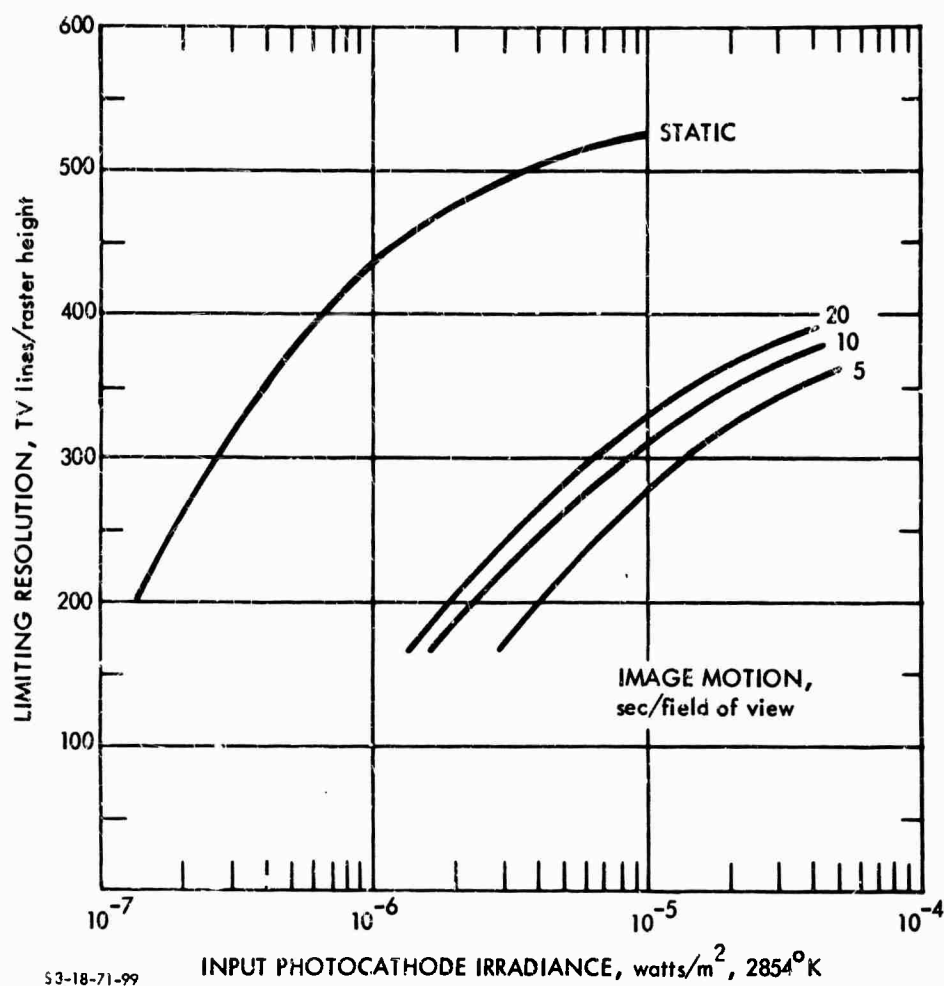


FIGURE V-E-19. Limiting Resolution Versus Input Photocathode Irradiance.  
Effect of Bar-Pattern Image Motion for the 40-mm Intensifier  
Image Orthicon



### 3. The Image Isocon

The essential features of the image isocon (II) were described in 1949, but early tubes had setup problems and incomplete beam separation problems that prevented the production of practical tubes. In the last few years, these problems have been solved to a satisfactory degree, and tubes of high quality are now available. The main merits of the II are an ability to provide very high signal-to-noise ratios and very high resolving powers with adequately illuminated scenes. Relative to the IO as described in Section V-E-1, the II is less sensitive, but it provides a wider dynamic range and a picture that is noise free in the blacks of the scene. With an additional stage of image intensification, the II becomes capable of low-light-level imaging with the particular merit of being relatively immune from damage by bright lights.

a. Principles of Operation. The II is shown schematically in Fig. V-E-20. The image section is essentially identical to that of the image orthicon, as is the electron gun. The principal difference is in the return-beam readout. In the II, the beam current  $i_b$ , approaching the target, deposits enough electrons to discharge the target. The portion of the beam that lands is numerically equal to  $(G_T - 1)i_s$ . Another portion of the electron beam,  $i_{scat}$ , is scattered by interaction with the target, and a third portion  $i_{refl}$  does not possess sufficient energy to reach the target and is specularly reflected. Thus, the total beam current can be written as

$$i_b = (G_T - 1)i_s + i_{scat} + i_{refl} \quad (V-E-13)$$

In the image orthicon, both the scattered and reflected beam components are returned to the electron multiplier with the result that

$$\begin{aligned} I_S &= G_M [i_b - (G_T - 1)i_s] \\ &= G_M [i_{scat} + i_{refl}] \end{aligned} \quad (V-E-14)$$

It is seen that the output current  $I_s$  is a maximum when the image signal  $i_s$  is zero, and thus maximum beam noise occurs in the picture blacks.

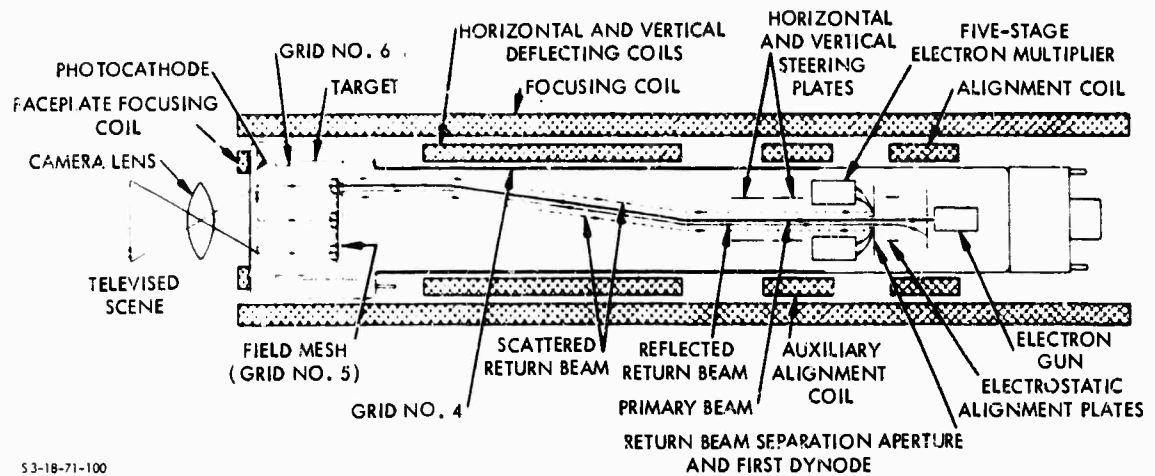
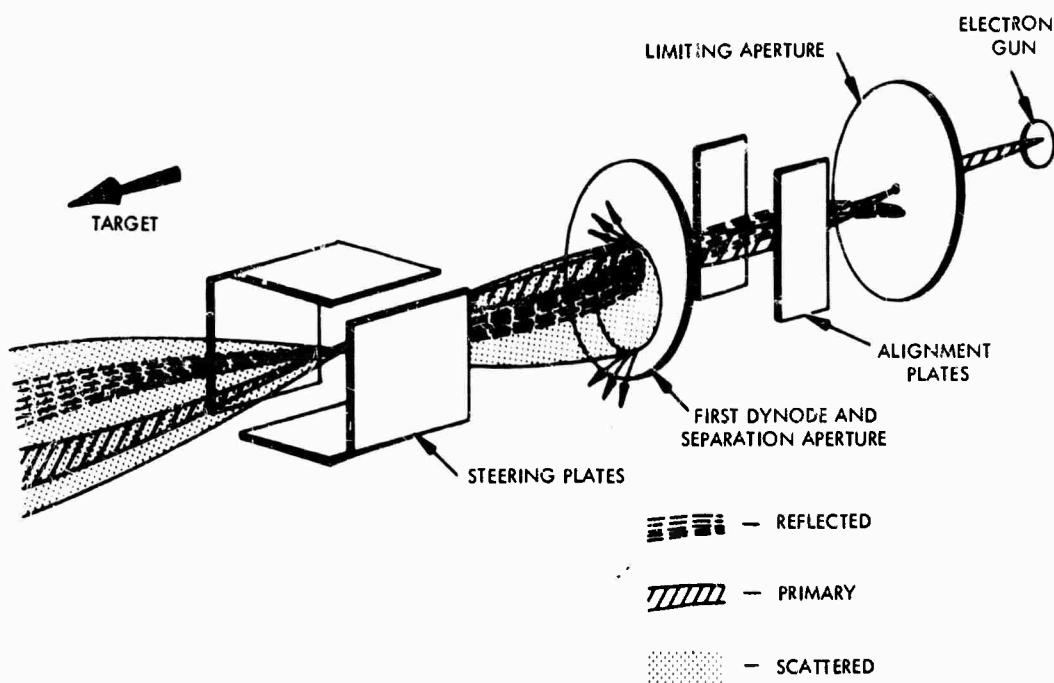


FIGURE V-E-20. Schematic Arrangement of the New Image Isocon. (The Arrangement of the RCA C21095 Image Isocon is Simpler than This.)

The isocon readout makes use of the fact that the scattered portion of the electron beam  $i_{scat}$  is proportional to the target current  $(G_T - 1)i_s$ . Thus,

$$i_{scat} = G (G_T - 1) i_s \quad (V-E-15)$$

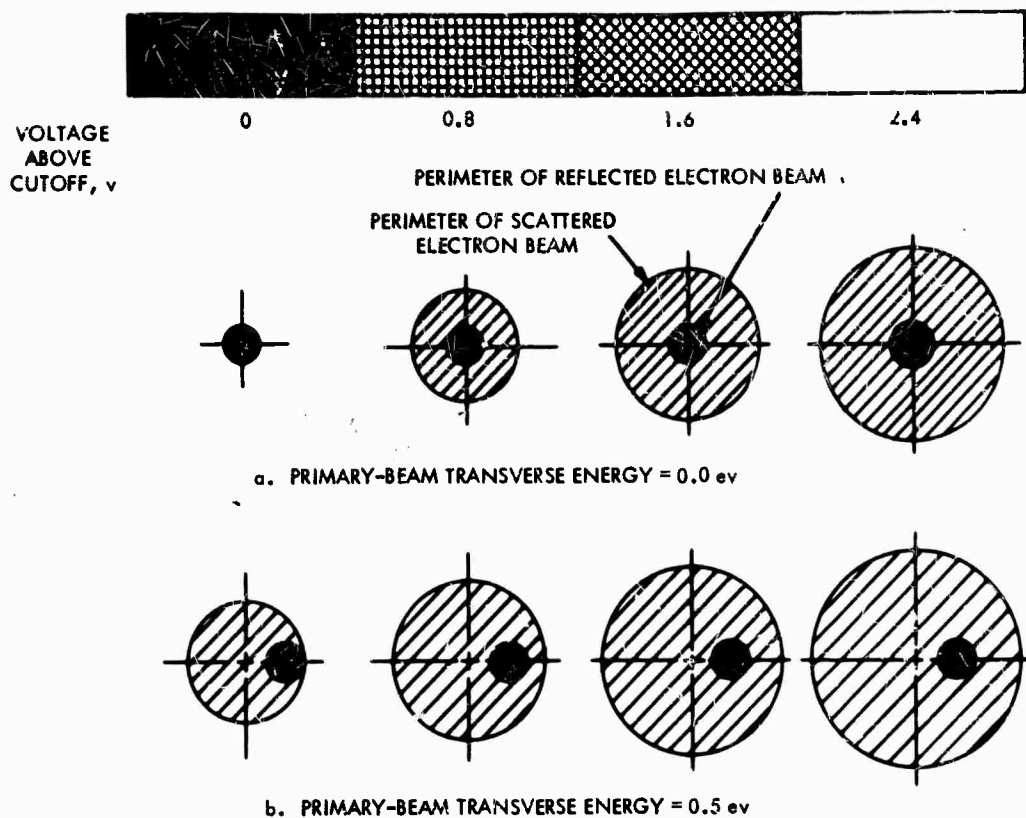
where  $G$  is a scatter gain that depends upon the particular target material employed. To make use of this proportionality, it is necessary to separate the scattered electrons from the reflected electron beam. The method of separation is as shown in Fig. V-E-21 and indicates the shape of the beam at the first dynode position. The primary beam is seen spiraling out from the gun through the limiting aperture, past the alignment plates, through the separation aperture of the first dynode, past the steering plates, and finally to the target.



53-18-71-101

FIGURE V-E-21. Image Isocon Beam Separation System

At the target, the scattered electron beam and the reflected electron beam that comprise the total return beam are formed. The energy spread of the scattered electron is always greater than that of either the primary-beam electrons or the reflected-beam electrons. Therefore, the scattered electron beam always includes both the primary and reflected beams. The scattered electrons receive maximum energy increments from high signal (white) areas of the target and minimum energy from low signal (dark) areas, and thus the maximum scattered-beam diameter is dependent upon the signal at the target, as shown in Fig. V-E-22a. Since the reflected beam is included in the scattered beam, its position in the scattered beam must be such that removal of the reflected beam will least disturb the collection of the desired portions of the scattered beam by the multiplier.



53-81-71-102

FIGURE V-E-22. Return-Beam Cross Section at an Antinode

If the outgoing (primary) beam is aligned with the magnetic focus field and approaches the target perpendicularly, the reflected beam leaves the target similarly aligned. The transverse energy of scattered electrons from low signal areas of the target will not be very different from that of the reflected beam, so that both will disappear into the separation aperture, and the result is a black, clipped picture.

In order to collect scattered electrons with a full range of energies (representing all light levels on the target), it is necessary to apply transverse energy to the primary beam, as shown in Fig. V-E-22b. This may be accomplished by placing a voltage across the

alignment plates and/or by increasing the current in the auxiliary alignment coils. Through this action, the primary and reflected beams are removed from the center of the scattered beam. The most recent simplified isocon gun design uses only noninteracting electrostatic plates to align and position the electron beam.

The target material in the usual II is an electronically conducting glass. Because of the superior noise characteristics of the isocon readout, the II is reported to be more sensitive than an IO equipped with a similar target. However, an IO with an MgO target will be more sensitive than an II with a glass target. For low-light-level use, the II will employ a wide-spaced target-to-mesh assembly to increase sensitivity and reduce lag.

b. Signal Transfer Characteristic. The output signal current  $I_S$  of the II is related to the photocathode irradiance  $H_T$  by the equation

$$I_S = G_M(G_T - 1) G K_S T_M i_s / e_v e_h \quad (\text{V-E-16})$$

where the terms are as described above, except that  $G$  is the scatter gain of the isocon readout and  $K_S$  is a signal reduction factor that has been variously attributed to field mesh transmittance or incomplete separation of reflected and scattered electrons. The scatter gain is reported to be about two, and a value of 0.6 will be used for  $K_S$ .

The signal transfer curve reported for the II is shown in Fig. V-E-23. For calculations,  $G_M$  is taken to be 535,  $T_M$  is 0.66,  $\alpha_T$  is  $3.2 \times 10^{-3}$  amp/watt, and  $A$  is  $7.68 \times 10^{-4} \text{ m}^2$ . The target gain is calculated from the signal transfer curve, Eq. V-E-16, and the relation  $i_s = \alpha_T A E_T$ .

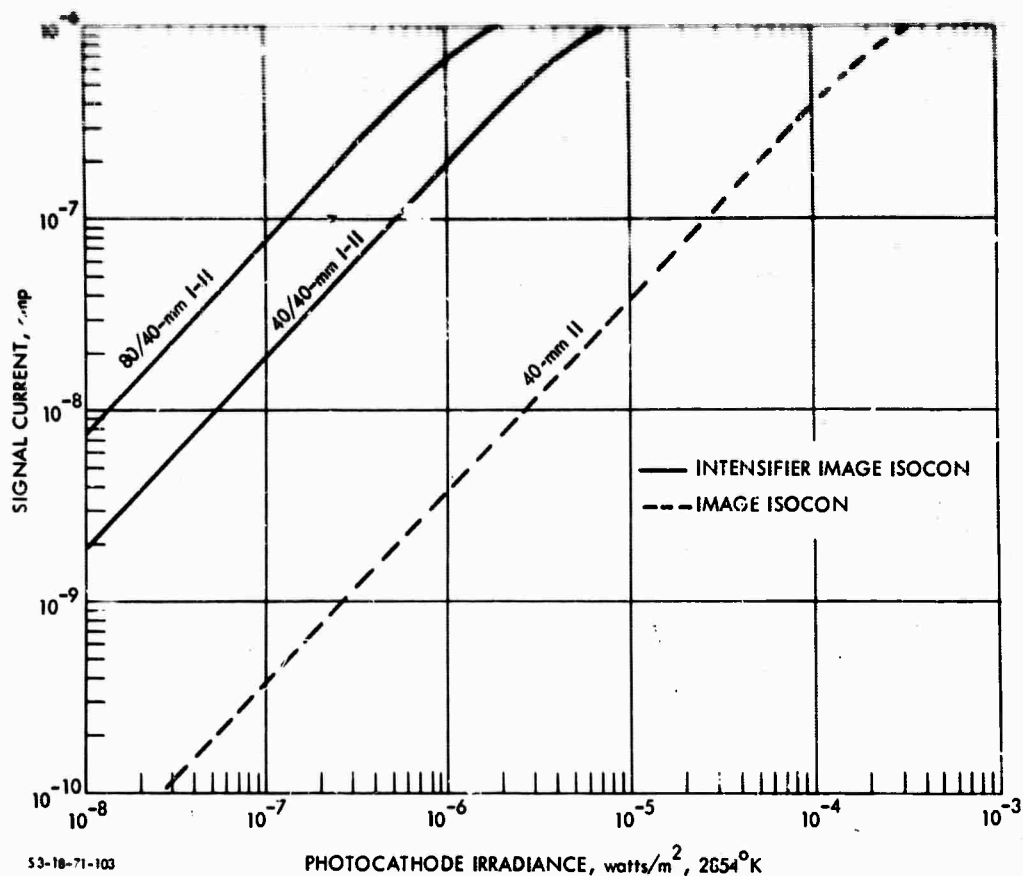


FIGURE V-E-23. Signal Current Versus Photocathode Irradiance Characteristic for the RCA C21095 Image Isocon and the Intensifier Image Isocon

c. Amplitude Response. The amplitude response of the II is a strong function of light level, as can be observed from the curves of Fig. V-E-24.\* This light-level dependency is the principal function limiting sensitivity at the lowest light levels. As will be shown, this sensitivity-degrading effect is considerably reduced by the added intensifier, which is needed to reduce lag in any case. No explanation

\* These curves were obtained from RCA data sheet for the Type C21095 image isocon, dated March 1968. RCA now claims improved response (Section V-E-4-i).

for the light-level dependence of amplitude response is offered at this time.

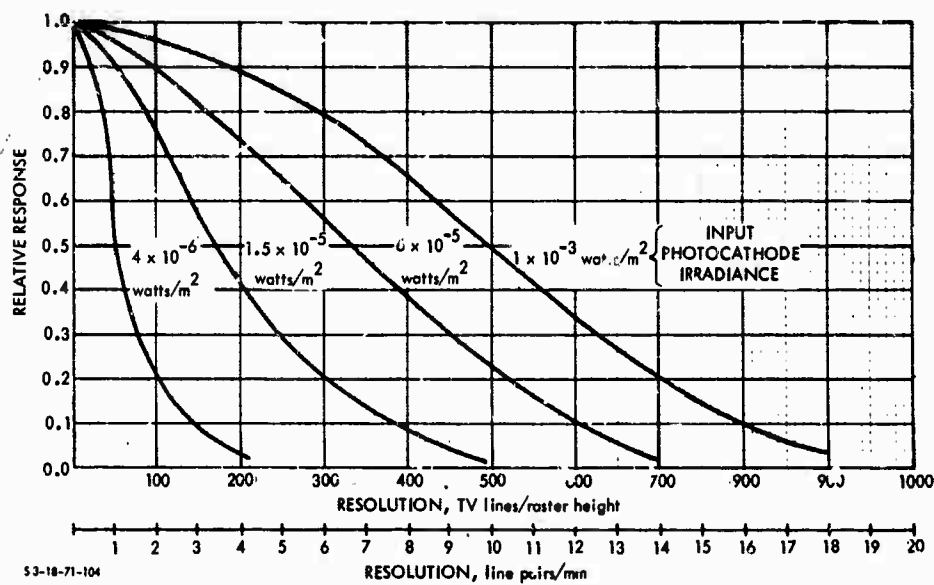


FIGURE V-E-24. Uncompensated Horizontal Square-Wave Response for the RCA C21095 Image Isocon at Various Input Photocathode Irradiance Levels. (See also Fig. V-E-36.)

d. Video and Display Signal-to-Noise Ratio. The video signal-to-noise ratio is written in the following form for the image isocor:

$$SNR_{V,0,1} = \frac{I_S}{\left(\bar{I}_e^2 + \bar{I}_T^2 + \bar{I}_{BD}^2 + \bar{I}_{BH}^2 + \bar{I}_{PA}^2\right)^{\frac{1}{2}}} \tag{V-E-17}$$

where

- $I_S$  is the output signal current, given by Eq. V-E-16
- $\bar{I}_e^2$  is the mean square photoelectron noise, given by

$$\bar{I}_e^2 = G_M^2 (G_T - 1)^2 G^2 \kappa_S^2 T_M e \Delta f i_{S \max} / e_v e_h \tag{V-E-18}$$

- $\bar{I}_T^2$  is the mean square target noise, given by

$$\bar{I}_T^2 = G_M^2 G_T^2 G^2 K_S^2 T_M e \Delta f i_{s \max} / e_v e_h \quad (V-E-19)$$

- $\bar{I}_{BD}^2$  is the mean square beam noise due to dark current, given by

$$\bar{I}_{BD}^2 = G_M^2 (G_T - 1) K_S e \Delta f T_M K_D i_{s \max} / e_v e_h \quad (V-E-20)$$

- $\bar{I}_{BH}^2$  is the mean square beam noise proportional to signal level, given by

$$\bar{I}_{BH}^2 = G_M^2 (G_T - 1) G K_S e \Delta f T_M i_{s \max} / e_v e_h \quad (V-E-21)$$

- $\bar{I}_{PA}^2$  is the mean square preamplifier noise.

In the above expressions, the photoelectron, target, and preamplifier noises are quite conventional, but the beam-current noise expressions assumed require some explanation.

The dark current represents that portion of the reflected electrons not separated from those scattered. In optimum operation, this is reported to be approximately 5 percent of the highlight signal current  $(G_T - 1) T_M i_{s \max} / e_v e_h$ . In a hands-off camera operation, a somewhat higher value will probably be necessary, and in these calculations it will be assumed to be 20 percent\* ( $K_D = 0.2$ ). A second component of beam noise will be that due to the signal itself, as represented by Eq. V-E-21. Both the beam dark current and beam signal noises are difficult to measure and are probably variable, depending on camera setup, but their impact on performance will not be great in any event.

---

\* Now claimed to be 5 percent at high light levels. Dark current noise is trivial in any event.



The various output signal and noise currents are plotted as functions of input photocathode current in Fig. V-E-25. At the lowest light levels the beam dark current dominates, while at the higher light levels photoelectron noise is largest, followed in turn by target noise and beam noise due to signal level. The preamplifier noise is negligible at all light levels. The video signal-to-noise ratio is plotted in Fig. V-E-26. It is seen that the II is capable of very high ratios at the higher light levels.

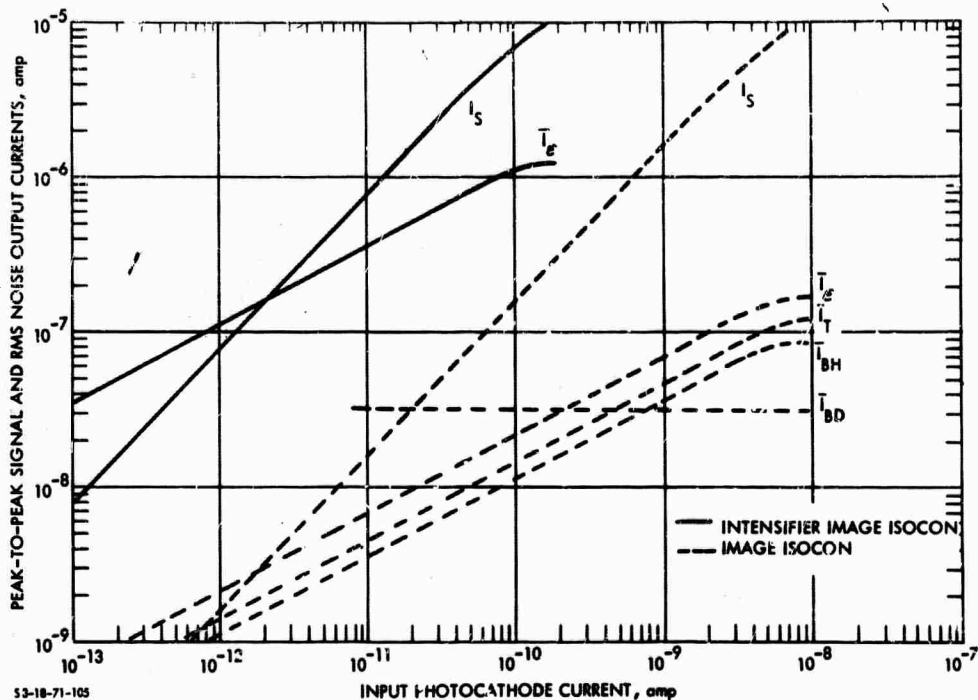


FIGURE V-E-25. Video Peak-to-Peak Output Signal-to-RMS-Noise Currents Versus Input Photocathode Current for the C21095 Image Isocon and the Intensifier Image Isocon

The display signal-to-noise ratio is calculated as previously explained and is plotted in Fig. V-E-27.

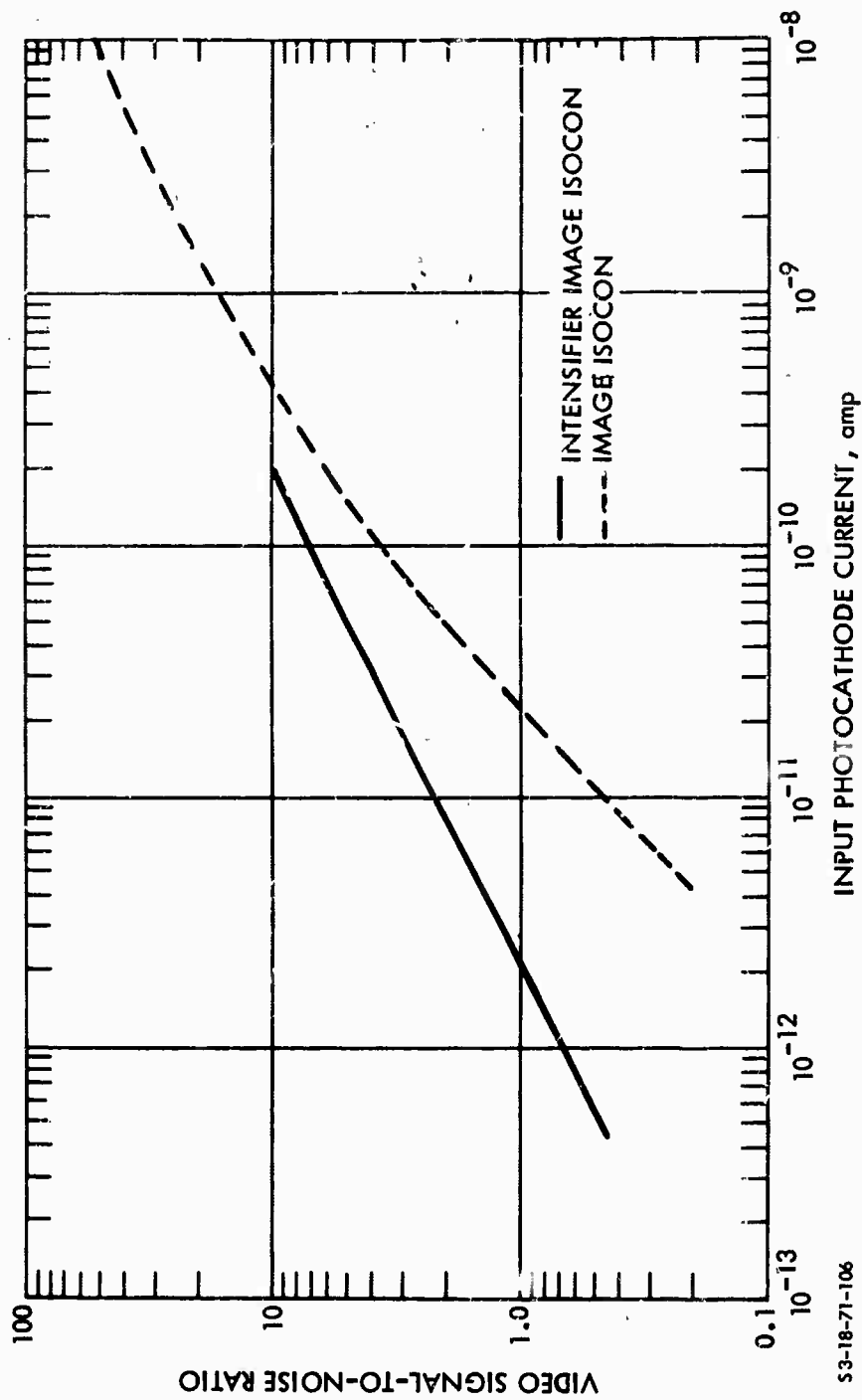


FIGURE V-E-26. Video Peak-to-Peak Signal-to-RMS Noise Ratio for the C21095 Image Isocon and the Intensifier Image Isocon for Images of Low Spatial Frequency and Unit Contrast

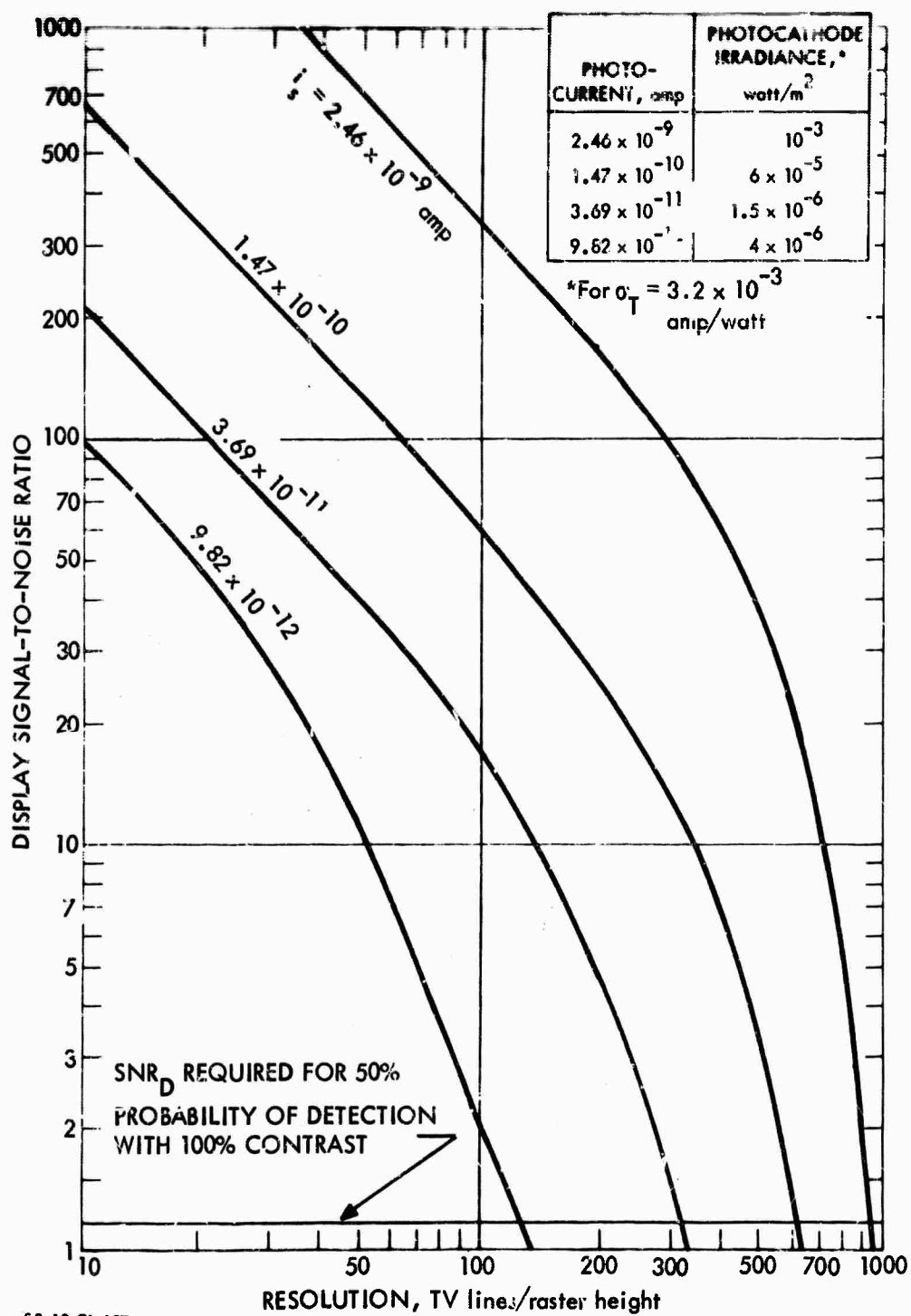


FIGURE V-E-27. Display Signal-to-Noise Ratio Versus Resolution for the C21095 Image Isocon for Various Input Photocathode Currents

e. Limiting Bar-Pattern Resolution. Limiting resolution versus input photocathode current is determined by setting  $SNR_D/C = 1.2$  and noting its intersection with the  $SNR_D$  curve plotted in Fig. V-E-27. The result is shown in Fig. V-E-28. The resolving power at the higher input photocathode currents is quite exceptional. Limiting resolution in line pairs/millimeter is plotted for image contrasts of 100 percent in Fig. V-E-29 and 30 percent in Fig. V-E-30.

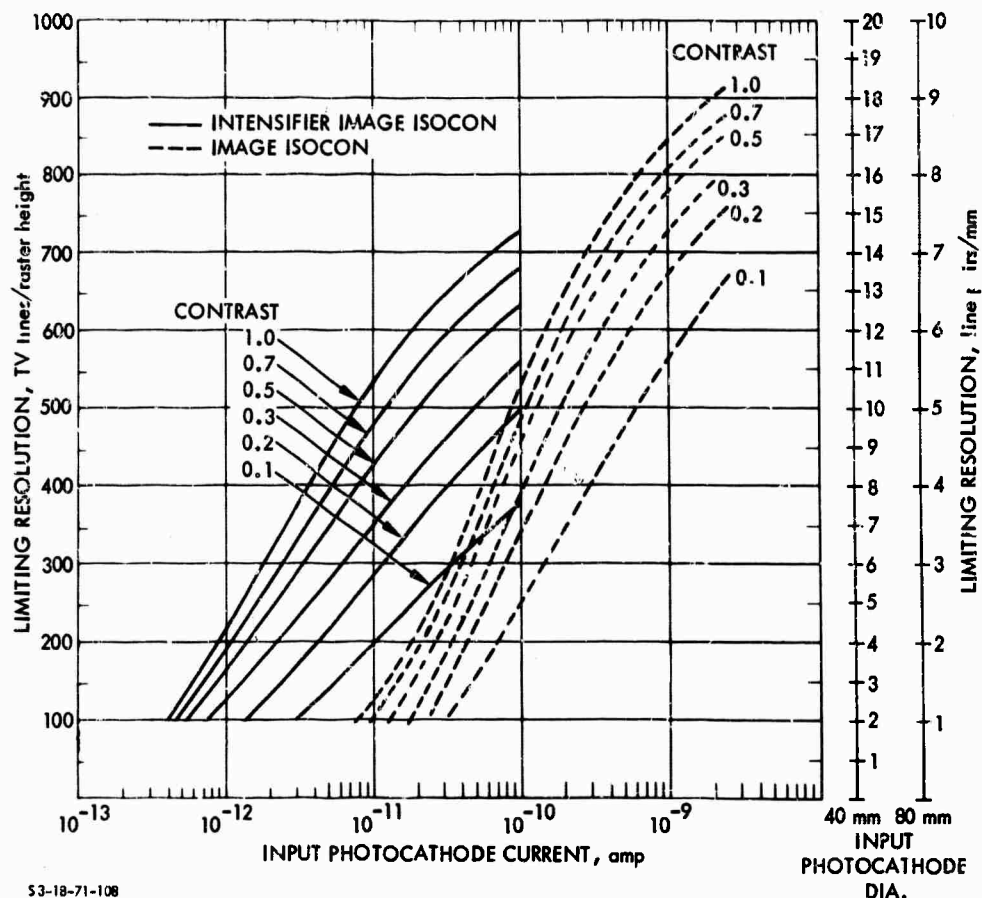


FIGURE V-E-28. Limiting Resolution Versus Input Photocathode Current for the C21095 Image Isocon and the Intensifier Image Isocon for Various Input Image Contrasts

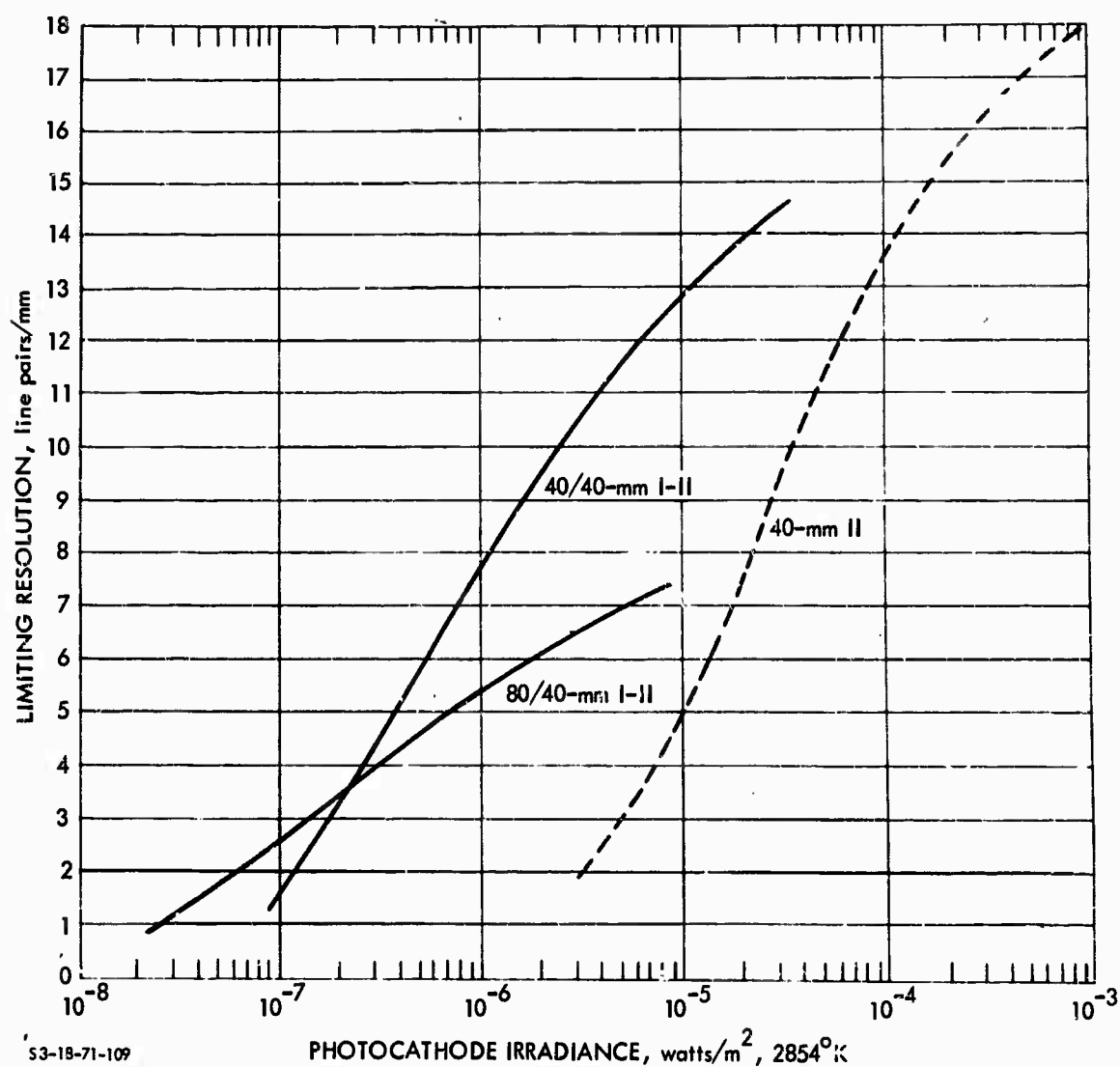


FIGURE V-E-29. Limiting Resolution Versus Photocathode Irradiance, Contrast 100%, for the Intensifier Image Isocon and the C21095 Image Isocon

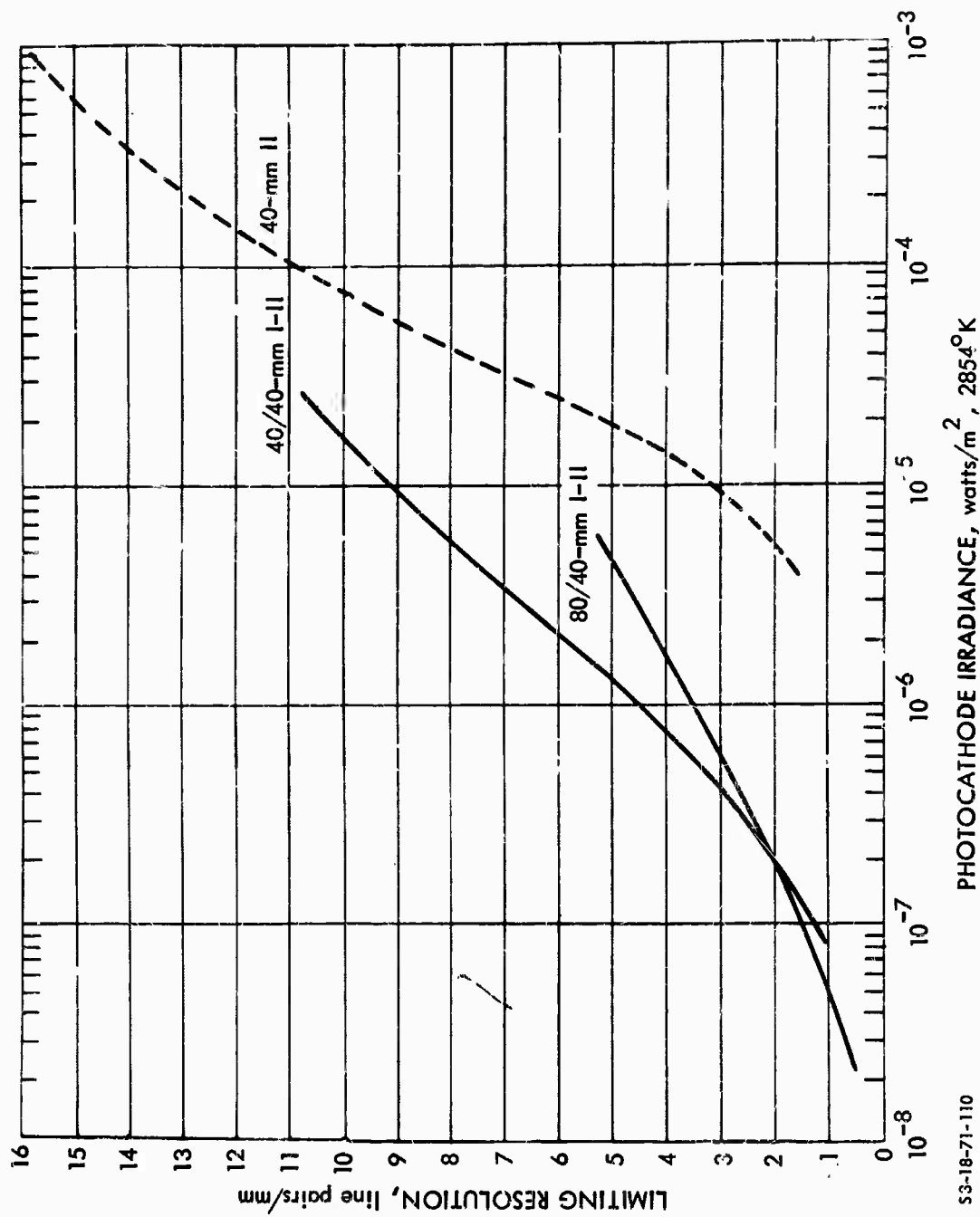


FIGURE V-E-30. Limiting Resolution Versus Photocathode irradiance, Contrast 30%, for the Intensifier image Isocon and the C21095 Image Isocon

f. Computed versus Measured Results. The computed performance is compared with the data-sheet performance in Fig. V-E-31.

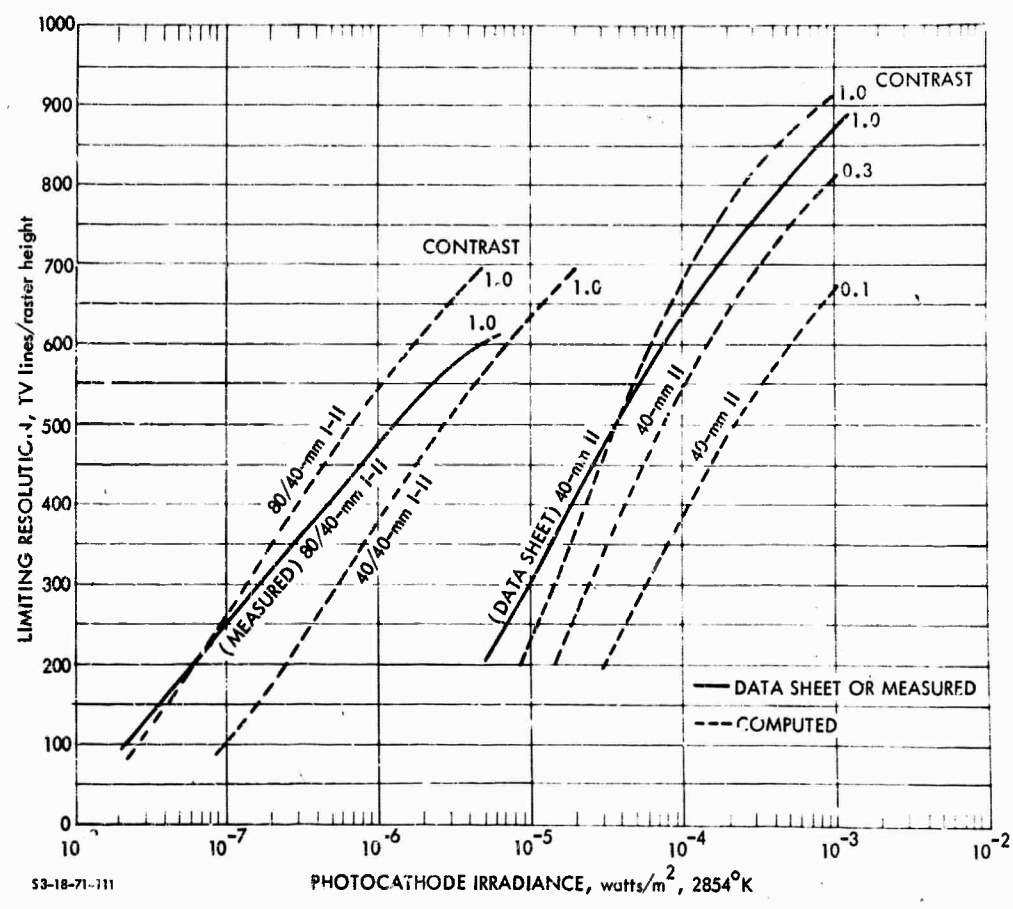


FIGURE V-E-31. Limiting Resolution Versus Photocathode Irradiance. Comparison of Computed Performance with Data-Sheet or Measured Performance for the Intensifier Image Isocon and the Image Isocon.

g. Lag Characteristics. Lag was the principal problem with the early II, but is much improved in the recent versions. This characteristic is plotted in the form of third-field residual signal versus photocathode irradiance in Fig. V-E-32. Dynamic resolution versus photocathode irradiance is plotted in Fig. V-E-33.

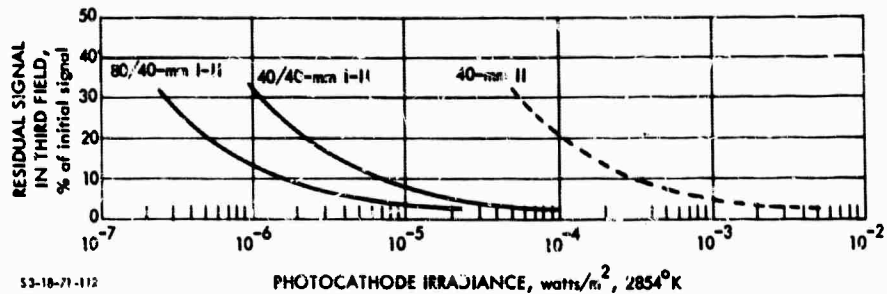


FIGURE V-E-32. Signal Lag Versus Photocathode Irradiance Characteristic for the Intensifier Image Isocon and the C21095 Image Isocon

h. Form Factor. The RCA C21095 image isocon is 17.25 in. in overall length and 3.06 in. in diameter. The diameter of the focus coil, which determines the maximum diameter in use, will be between 5 in. and 6 in., depending on the weight/power tradeoff.

i. Manufacturers' Literature. A sample of manufacturers' literature on image isocons will be found in Chart V-E-2.

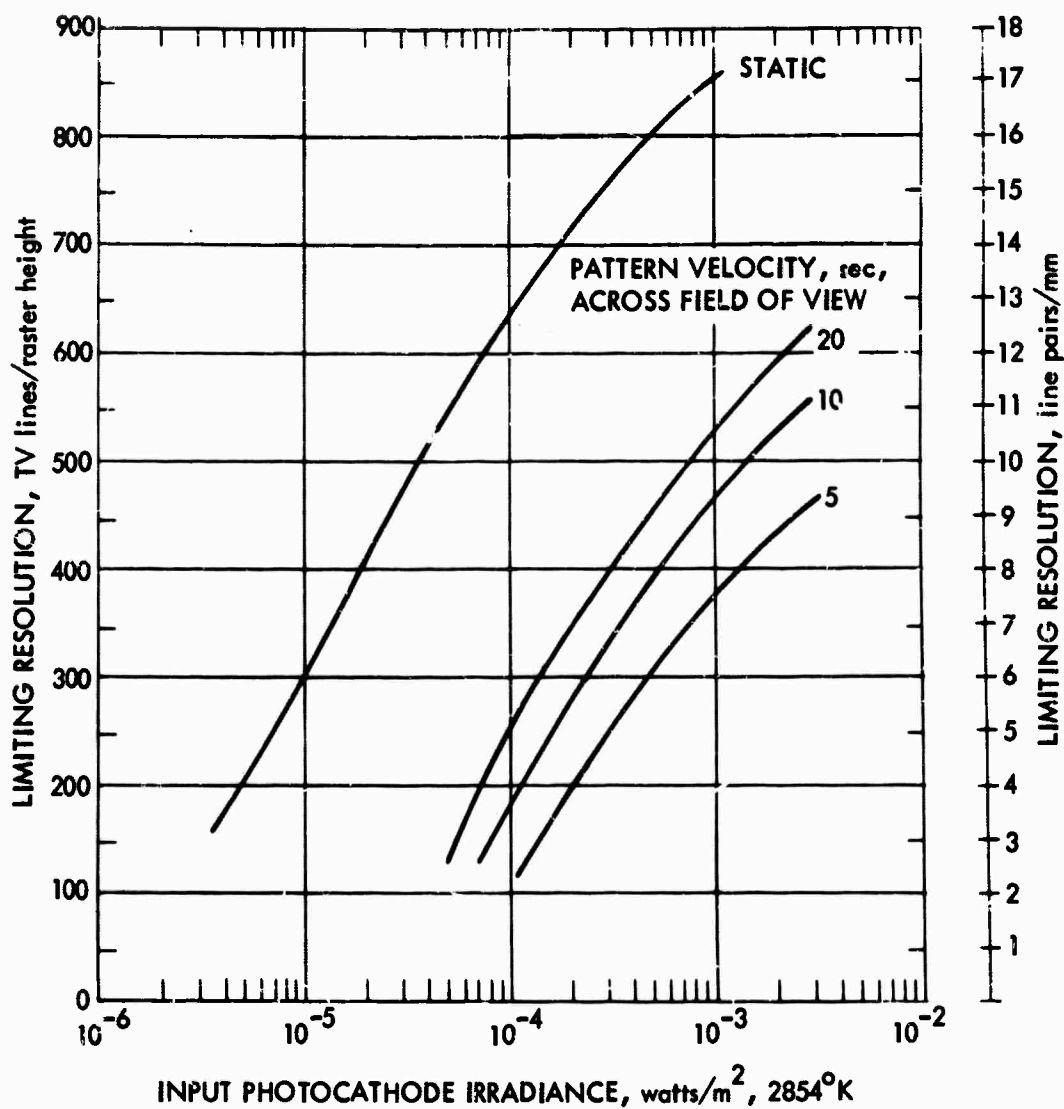
#### 4. The Intensifier Image Isocon

a. Principles of Operation. With a cascaded image intensifier, the II becomes suitable for use as a low-light-level sensor because of the resulting reduction in lag and improvement in the amplitude-response, photocathode-irradiance characteristic.

b. Signal Transfer Characteristic. As in the case of the IO, either 40-mm or 80/40-mm intensifiers can be used with the II. If an intensifier photocathode radiant sensitivity of  $4 \times 10^{-3}$  amp/watt is assumed, the shift in the signal-current curve to lower irradiance levels is a factor of 50 in the case of a 40/40-mm intensifier, as shown in Fig. V-E-23.

c. Amplitude Response. For the intensifier image isocon (I-II), as for the II, the amplitude response is light-level dependent (Section V-E-4-i). However, the characteristics occur at much lower light levels,





53-18-71-113

**FIGURE V-E-33. Limiting Resolution Versus Input Photocathode Irradiance for the C21095 Image Isocon as a Function of Bar-Pattern Velocity Across the Horizontal Field of View (Data-Sheet Specification)**

CHART V-E-2. SAMPLE OF MANUFACTURER'S LITERATURE  
ON IMAGE ISOCONS

The units, definitions, and methods of measurement specified herein are not necessarily endorsed by the authors but are those used by the manufacturer quoted.

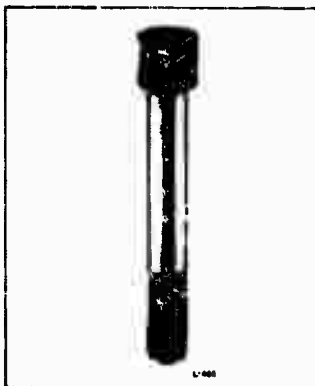


## Image Isocon

- Photographic-Quality Pictures
- Extremely Simple Set-Up Procedure
- No Background Shading
- Single Non-Critical Beam-Current Adjustment
- Very High Signal-to-Noise Ratio
- Exceptionally High and Uniform Resolution
- Bialkali Photocathode

RCA Developmental Type C21093A is an image isocon type of television camera tube designed for use in high-definition TV systems. Because of its inherently high resolution this tube is also recommended for use in high line number (1000 lines, or more) applications. The photographic-like quality of the pictures produced by the C21093A exceeds that of any type camera tube now available in live TV pickup systems.

The C21093A is intended for operation in the RCA AJ2172/V1 yoke assembly. It may also be operated in the AJ2147-series of yoke structures provided the alignment and auxiliary-alignment circuits in the yoke are de-energized.

Mechanically and operationally, the C21093A closely resembles a conventional 3"-diameter field-mesh type image orthicon having close target-to-mesh spacing, such as the RCA-8673. It differs operationally, however, in that it has much less noise (14 to 16 dB quieter in the blacks), has a greater dynamic range (at least one order of magnitude), has much higher resolution, and has virtually zero dark current. The set-up procedure used for the C21093A is somewhat simpler than is that customarily employed with the image orthicon.

The C21093A is similar to the image orthicon in that it employs an image section with a photoemissive light sensor and charge-integrating storage target. It also has a linear transfer characteristic (unity gamma) which extends to the "knee" region, extremely low lag, and high signal-output current provided by a five-stage electron-multiplier section. The design of the C21093A is such that no external adjustable magnetic-gun alignment circuits or shading-correction waveforms are required.

A television camera using a 3"-diameter, or larger, image orthicon can be readily adapted to use the C21093A and its associated scanning and focusing coil assembly, RCA type AJ2172/V1. The principal aspects of such adaptation include:

1. Proper dimensional allowance for the AJ2172/V1 assembly (18-1/2" length, 4-7/16" diameter), which completely contains the C21093A and any desired axial allowance for optical focusing purposes as well as allowance for connector/cable clearance.
2. Accommodation for the reversed polarity (compared with the image orthicon) of the video output signal.
3. Removal of the target blanking pulse circuitry normally used for the image orthicon. Electron gun blanking (at grid No.1) is used.
4. Provisions for the higher operating voltages required by the C21093A.
5. Provision for the specified focusing-coil current of 500 mA.
6. Use of conventional double-frame 35-mm optics to illuminate the 1.4" maximum usable photocathode diameter of the C21093A. The resulting field of view is reduced moderately compared with the "normal" field of view of the lens system.
7. Provision for required voltage for the electrostatic steering and misalignment electrodes. A low-current adjustable dc voltage-divider network similar to that used for cathode-ray oscilloscope centering circuits is satisfactory.
8. Possible modification of deflection-circuit impedance matching especially in the horizontal deflection system.

For further information or application assistance on this device, contact your RCA Sales Representative or write Camera Tube Marketing, RCA, Lancaster, PA 17604.

Developmental-type devices or materials are intended for engineering evaluation. The type designation and data are subject to change, unless otherwise arranged. No obligations are assumed for notice of change or future manufacture of these devices or materials.

Information furnished by RCA is believed to be accurate and reliable. However, no responsibility is assumed by RCA for its use, nor for any infringement of patents or other rights of third parties which may result from its use. No license is granted by implication or otherwise under any patent or patent rights of RCA.

Printed in U.S.A./ 4-70  
C21093A

## Camera Design Notes

1. Unless otherwise noted, the specified voltage values are referenced directly to the thermionic cathode which is grounded. No significant impedances should be introduced between the cathode and power-supply return points ("grounds"). The resistance of normal circuit conductors is deemed insignificant.

2. Designers familiar with conventional image orthicon circuitry are urged to note the following differences when designing circuits for use with the C21093A.

2.1 Gun (beam) blanking is used instead of target blanking.

2.2 The polarity (sense) of the isocon output video signal is the inverse of that of conventional image orthicons.

2.3 Although a separate connection is provided for the "persuader" multiplier focus electrode G<sub>3</sub>, its design is such that best operation is obtained when G<sub>3</sub> and G<sub>4</sub> are tied together. This eliminates a control.

2.4 The annular decelerator electrode, G<sub>5</sub>, featured in most image orthicons is not used, nor provided in the C21093A. The designator "G<sub>5</sub>" has been reassigned to the field mesh.

2.5 The insertion of shading signals is neither recommended nor necessary. This eliminates 2 or 4 controls.

2.6 The C21093A will NOT operate properly at any beam focus loop number other than that obtained by the application of the magnetic and electric focus fields shown under Typical Operation.

2.7 Automatic beam control is not needed.

3. The gain of the electron multiplier output section is readily varied by adjustment of its operating voltages. Depending on the range of control required, the voltage in one or several dynodes may be made adjustable. The following precautions should be observed.

3.1 Do not vary dynode-No.1 voltage for gain-control purposes.

3.2 Under most conditions, adjustment of only dynode-No.3 voltage is the preferred gain control mode.

3.3 Under no circumstances should operation be attempted where the voltage on a given dynode is outside the range established by the two adjacent dynodes, i.e.,  $E_{dyn-1} \leq E_{dyn} \leq E_{dyn+1}$ .

Operation outside of these limits will not damage the tube but will result in entirely unsatisfactory multiplier action. (This requirement is not unique to the C21093A—the principle applies generally to electron multiplier equipped camera tubes).

3.4 If several dynode voltages, including that of dynode No.5 are varied simultaneously, care should be taken to avoid allowing the voltage between dynode No.5 and anode to vary to the point where anode collection efficiency is reduced. A practical minimum voltage for  $E_5 - E_{dy5}$  is 35 volts.

4. "Raster zoom", at least 4:1, can be employed without damage to the tube. Resolution degradation can be expected to the same degree as the change in scan size.

5. Raster orientation (See Data) is extremely important. Vertical scan reversal is normally not recommended and should not be used without contacting your RCA field representative for factory recommendations concerning your system.

6. Scan-failure protection. Nothing elaborate is needed as long as grid-No.1 voltage does not fall to zero. In this context, note that a normal shutdown of equipment could cause damage unless the coupling time constants are such that the (negative) G<sub>1</sub> voltage will decay more slowly than the (positive) voltages on G<sub>2</sub> and/or G<sub>4</sub>.

## Data

## General:

## Direct Interelectrode Capacitance:

Anode to all other electrodes ..... 12 pF

## Target-to-Mesh:

Spacing ..... 0.001 in (0.0254 mm)

Capacitance ..... 200 pF

## Photocathode, Semitransparent:

Spectral Response ..... See Figure 2

Window Material ..... Corning No.7056, or equivalent

Photocathode Material ..... Bialkali (Cesium-Potassium-Antimony)

Useful size of Image ..... 1.4 in (36 mm) max. Diagonal

Note: The size of the optical image focused on the photocathode should be adjusted so that its maximum diagonal does not exceed the specified value. The corresponding electron image on the target should have a size such that the corners of the rectangle just touch the target ring.

Orientation of ..... Proper orientation is obtained when the vertical scan is essentially parallel to the plane passing through the center of the faceplate and the index pin 7 position of the shoulder base. The horizontal and vertical scan should start at the corner of the raster between pins 2 and 3 of the shoulder base.

Focusing Method ..... Magnetic

Deflection Method ..... Magnetic

Shoulder Base ..... Jumbo Annular Sevens 4-Pin (See Dimensional Outline)

End Base ..... Small-Shell Bidecal 20-Pin (JEDEC No.820-102)

Sockets ..... See footnote a

Associated Scanning and Focusing-Coil Assembly ..... RCA Type AJ2172/V1, or equivalent

Operating and Storage Position ..... Any

**Maximum and Minimum Ratings, Absolute-Maximum Values:<sup>b</sup>**

Voltages are with respect to thermionic cathode unless otherwise specified.

**Faceplate:**

Irradiance <sup>c</sup>	25 max. W/m <sup>2</sup> (watts/square meter)
Illuminance <sup>c</sup>	$\begin{cases} 50 \text{ max.} & \text{lm/ft}^2 \text{ (fc)} \\ 500 \text{ max.} & \text{lm/m}^2 \text{ (lux)} \end{cases}$

**Temperature:**

Any part of bulb <sup>d</sup>	80 max. °C
-------------------------------	------------

**Temperature Difference:**

Between target section and any part of bulb hotter than target section	5 max. °C
--	-----------

**Heater, for Unipotential Thermionic Cathode:**

Ac or dc current (pin No.1 and Pin No.20)	$\begin{cases} 0.63 \text{ max.} & \text{A} \\ 0.57 \text{ min.} & \text{A} \end{cases}$
---	--

**Peak Heater-Cathode Voltage:**

Heater negl. with respect to cathode	125 max. V
--------------------------------------	------------

Heater positive with respect to cathode	10 max. V
---	-----------

Photocathode Voltage ( $E_{pc}$ )	1000 max. V
-----------------------------------	-------------

Grid-No.6 Voltage ( $E_{g6}$ )	750 max. V
--------------------------------	------------

Target Voltage ( $E_t$ ):	
---------------------------	--

Positive value	10 max. V
----------------	-----------

Negative value	10 max. V
----------------	-----------

Grid-No.5 (Field-Mesh) Voltage <sup>e</sup> ( $E_{g5}$ )	$E_{g4} + 50 \text{ max. V}$
--	------------------------------

Grid-No.4 Voltage ( $E_{g4}$ )	600 max. V
--------------------------------	------------

Grid-No.3 Voltage ( $E_{g3}$ )	600 max. V
--------------------------------	------------

Grid-No.2 Voltage ( $E_{g2}$ )	450 max. V
--------------------------------	------------

Grid-No.1 Voltage ( $E_{g1}$ )	-150 to -40 max. V
--------------------------------	--------------------

**Steering-Plate Voltage:**

Plate $SX_1$ ( $E_{s1}$ x 1)	600 max. V
------------------------------	------------

Plate $SX_2$ ( $E_{s2}$ x 2)	600 max. V
------------------------------	------------

**Misalignment-Plate Voltages:**

Plate $SY_1$ ( $E_{sy1}$ )	600 max. V
----------------------------	------------

Plate $SY_2$ ( $E_{sy2}$ )	600 max. V
----------------------------	------------

Anode Voltage ( $E_b$ )	1800 max. V
-------------------------	-------------

Voltage Between Adjacent Dynodes <sup>f</sup>	600 max. V
---	------------

**Typical Operating Values:<sup>g</sup>**

Stability of power supply and divider network circuitry should be such that the operating values specified below are held within the indicated limits.

Heater Current	±5%
----------------	-----

Focus Coil Currents (The values of currents for which this regulation requirement applies are contained in the data sheet describing the magnetic component, e.g., AJ2172/V1)

Grid-No.4 Voltage (As adjusted)	±0.2%
---------------------------------	-------

Other dc Voltages (Fixed or as adjusted)	±1.0%
--	-------

Beam Blanking Pulse Voltage	$\begin{cases} +50\% \\ -0\% \end{cases}$
-----------------------------	---

Voltages are with respect to thermionic cathode unless otherwise specified. Nominal electrode currents for control circuit design are shown with the electrode voltages. The specified current values include leakage.

**Heater for Unipotential Cathode: (Between pins 1 and 20)**

Current	0.6 A
---------	-------

Voltage (Nominal, for current of 0.6A)	6.3 V
Photocathode Voltage (Image Focus) <sup>h</sup>	700 to 900 V
Current	100 $\mu$ A, or less

Grid-No.6 Voltage (Accelerator)—Approximately 83% of Cathode Voltage	-440 to -570 V
--	----------------

Current	100 $\mu$ A, or less
---------	----------------------

Target Voltage Above Cutoff <sup>k</sup>	2.5 V
--	-------

Current	100 $\mu$ A, or less
---------	----------------------

Grid-No.5 (Field-Mesh) Voltage <sup>g</sup>	$E_{g4} + 12 \text{ V}$
---	-------------------------

Current	100 $\mu$ A, or less
---------	----------------------

Grid-No.4 Voltage <sup>m</sup>	400 to 440 V
--------------------------------	--------------

Current	10 $\mu$ A
---------	------------

Grid-No.3 Voltage	Connect to grid No.4
-------------------	----------------------

Current	10 $\mu$ A
---------	------------

Grid-No.2 Voltage	400 V
-------------------	-------

Current	200 $\mu$ A
---------	-------------

Grid-No.1 Voltage for Picture Cutoff	-120 to -60 V
--------------------------------------	---------------

Current	10 $\mu$ A
---------	------------

**Steering Plate Voltage and Current:**

(Center voltage same value as grid No.4)

Between plate  $SX_1$  and plate  $SX_2$ —

Voltage	0 to +70 max. V
---------	-----------------

Current including leakage	10 $\mu$ A
---------------------------	------------

**Misalignment Plate Voltage and Current:**

(Center voltage same value as grid No.4)

Between plate  $SY_1$  and plate  $SY_2$ —

Voltage	0 to +70 max. V
---------	-----------------

Current including leakage	10 $\mu$ A
---------------------------	------------

Dynode-No.1 Voltage	375 V
---------------------	-------

Dynode-No.2 Voltage	700 V
---------------------	-------

Dynode-No.3 Voltage <sup>n</sup>	750 to 1050 V
----------------------------------	---------------

Dynode-No.4 Voltage	1350 V
---------------------	--------

Dynode-No.5 Voltage <sup>p</sup>	1650 V
----------------------------------	--------

Anode Voltage	1700 V
---------------	--------

Current	25 $\mu$ A
---------	------------

Target Temperature Range	35 to 50 °C
--------------------------	-------------

**Beam Blanking Voltage (Applied to grid No.1):**

(Peak to peak)	40 V
----------------	------

**Field Strength at Center of Focusing Coil**

(Approx.) <sup>q</sup>	70 G
------------------------	------

**Performance Characteristics Range Values:<sup>g</sup>**

With conditions shown under Typical Operating Values, picture highlights at knee of the light transfer characteristic, 525 line scanning, interlaced 2:1, frame time of 1/30 second, and 1.4" picture diagonal with 4:3 aspect ratio.

	Min.	Typical	Max.	
Cathode Radiant Sensitivity at 400 nanometers	—	0.08	—	A/W
Cathode Luminous Sensitivity	60	100	—	$\mu$ A/lm
Signal-Output Current (Peak to peak) <sup>r</sup>	4	7	—	$\mu$ A

## Performance Characteristics (Cont'd.)

	Min.	Typical	Max.	
Photocathode Illumination at 2854° K Required to Reach "Knee" of Light Transfer Characteristic	-	0.01	0.03	lm/ft <sup>2</sup>
Photocathode Irradiance at 400 nm Required to Reach "Knee" of Transfer Characteristic	-	10 <sup>-4</sup>	-	W/m <sup>2</sup>
Signal-to-Noise Ratio: <sup>a</sup>				
Signal to noise-in-signal for highlights	36	-	-	dB
Highlight signal to dark current noise	46	-	-	dB
Amplitude Response at 400 TV Lines per Picture Height (Per cent of large-area black to large-area white) <sup>b</sup>	70	80	-	%
Limiting Resolution:				
At center of picture	850	1000	-	TV Lines/Picture Height
At corner of picture	750	950	-	TV Lines/Picture Height
Lag—Per cent of Initial Signal Output Current 1/20 Second After Illumination is Removed	-	5	10	%
Uniformity: <sup>c</sup>				
Ratio of Shading (Background) Signal to Highlight Signal	-	2	5	%
Variation of Highlight Signal (Per cent of maximum highlight signal)	-	12	20	%

<sup>a</sup> Both the end base socket and shoulder base socket are supplied as part of the RCA assembly AJ2172/V1.

<sup>b</sup> The maximum ratings in the tabulated data are established in accordance with the following definition of the Absolute-Maximum Rating System for rating electron devices.

Absolute-Maximum ratings are limiting values of operating and environmental conditions applicable to any electron device of a specified type as defined by its published data, and should not be exceeded under the worst probable conditions.

The device manufacturer chooses these values to provide acceptable serviceability of the device, taking no responsibility for equipment variations, environment variations, and the effects of changes in operating conditions due to variations in device characteristics.

The equipment manufacturer should design so that initially and throughout life no Absolute-Maximum value for the intended service is exceeded with any device under the worst probable operating conditions with respect to supply voltage variation, equipment component variation, equipment control adjustment, load variation, signal variation, environmental conditions, and variations in device characteristics.

<sup>c</sup> Faceplate illuminance is limited to 50 lm/ft<sup>2</sup> continuously. An exposure of 10<sup>4</sup> lm/ft<sup>2</sup> for a maximum period of 5 seconds can be tolerated provided the duty cycle limits the average value to 50 lm/ft<sup>2</sup>.

<sup>d</sup> Operation outside of the Recommended Target Temperature Range shown under Typical Operating Values will not damage the C21083A provided the Maximum Temperature Rating of the tube are not exceeded. Optimum performance, however, is only obtained when the tube is operated within the Recommended Target Temperature Range.

<sup>e</sup> With respect to grid No.4, Grid-No.5 (field-mesh) voltage must never be less than that of grid No.4.

<sup>f</sup> Dynode-voltage values are shown under Typical Operating Values.

<sup>g</sup> With the C21083A within an RCA-AJ2172/V1 scanning and focusing-coil assembly.

<sup>h</sup> Adjust for best focus. Nominal value is -770 V. This value is dependent upon the location of the tube within the yoke assembly with respect to the end of the focusing field.

<sup>i</sup> Nominal value is -485 V. This voltage should be obtained by means of a voltage-divider network between photocathode and "ground". The resistance values should be chosen to set the grid-No.6 voltage at the recommended 63% value of photocathode voltage which provides best focus.

<sup>k</sup> Normal setting of target voltage is +2.5 volts from target cutoff. Target cutoff is normally within one volt of thermionic cathode potential. The target supply voltage should be adjustable from -3 to +5 volts.

<sup>m</sup> Adjust for best focus. The focusing current of the associated assembly, e.g., AJ2172/V1, should be adjusted to keep grid-No.4 voltage within its recommended voltage range. Grid-No.4 voltage must be kept within this range to insure 5 focus loops in the scanning section.

<sup>n</sup> Adjust for required signal current.

<sup>p</sup> The gain of the electron multiplier may be varied to obtain the output current from a given tube most suitable for the associated video amplifier. Gain can be controlled by adjusting the voltage on one or two of the latter dynode stages; dynode No.3 is the preferred stage. To increase the range of gain control, the voltages on dynode Nos. 3 and 5 may be simultaneously adjusted.

<sup>q</sup> Direction of current must be such that a north-seeking pole is attracted to the image end of the focusing coil.

<sup>r</sup> Dynode-No.3 voltage is 1100 volts.

<sup>s</sup> The values shown are measured under the following conditions using a Video Noise Meter, Model UPSF (North American Version), or equivalent. This meter is manufactured by Rohde and Schwarz, Munich, West Germany.

Noise Meter: Video pass band is shaped by means of self-contained 100 kHz high-pass and 4.2 MHz low-pass filters.

Signal to noise-in-signal for highlights is measured with lens uncapped viewing a uniform white field; highlight signal to dark current noise, with the lens capped.

<sup>t</sup> Measured using an RCA Test Pattern style P200 with the frequency response of the video amplifier system (essentially "flat") adjusted for uniform response to all scan-generated video frequencies. Substantially identical measurements will be obtained by using a "multi-burst" test pattern with an amplifier having flat ( $\pm 0.1$  dB) frequency response to at least 14 MHz.

<sup>u</sup> Variation of response over scanned area.

### Set-Up Procedure

The set-up procedure described below should be followed carefully to obtain optimum performance from the C21083A. Before the specified voltages shown under *Typical Operating Values* are applied to the tube, the scanning coil, tube filament, and focusing coil should be energized. Focusing coil current, using the RCA assembly AJ2172/V1 should be adjusted to 800 milliamperes. The following steps should then be followed sequentially.

**Step 1:** Light should be admitted to provide a nominal face-plate illumination of 0.01 to 0.1 lumen/ft<sup>2</sup> (footcandle). This is a very important step for all image orthicons and image isocons.

**Step 2:** The voltage values specified under *Typical Operating Values* may then be applied to the tube with the exception that the steering-plate and misalignment plate differential voltages are set to the voltage values supplied with the tube or to +25 volts.

**Step 3:** Grid-No.1 voltage is adjusted to provide a small amount of beam current so that video information appears on the monitor.

**Step 4:** To center the image on the target, adjust the deflection circuits so that the beam will "overscan" the target. Note that overscanning the target results in a smaller-than-normal picture on the monitor. After centering the image, return to normal scan size.

**Step 5:** Grid-No.1 voltage is readjusted to fully discharge the target.

**Step 6:** Optical elements, photocathode voltage (image-section focus), and grid-No.4 voltage (scanning-section focus) are adjusted to provide best focus. The proper setting for grid No.4, about 420 volts, is that value providing best resolution regardless of picture polarity.

**Step 7:** Increase positive  $E_{sx1}$ - $E_{sx2}$  to picture cut-off and back off to best picture.

**Step 8:** Reduce target voltage to cut-off and set  $E_{sx1}$ - $E_{sx2}$  to the minimum positive value that eliminates bright edges.

**Step 9:** Increase target voltage by approx. 2.5 volts and adjust  $E_{sy1}$ - $E_{sy2}$  for best uniformity. Readjust beam if necessary.

**Step 10:** Reduce target voltage to determine new cut-off value. Target voltage was changed by the adjustment of  $E_{sy1}$ - $E_{sy2}$ . Set target voltage to  $2.5 \pm 0.2$  volts above cut-off.

### Principles of Operation

Similar to the conventional image orthicon, the C21083A has three functional sections— an image section, a scanning section, and an electron-multiplier-type signal current amplifier section— as shown in Figure 1. Operation of both the image section and the multiplier section is identical to that of the conventional image orthicon. The behavior of the

scanning beam of the image isocon, however, differs from that encountered in the image orthicon.

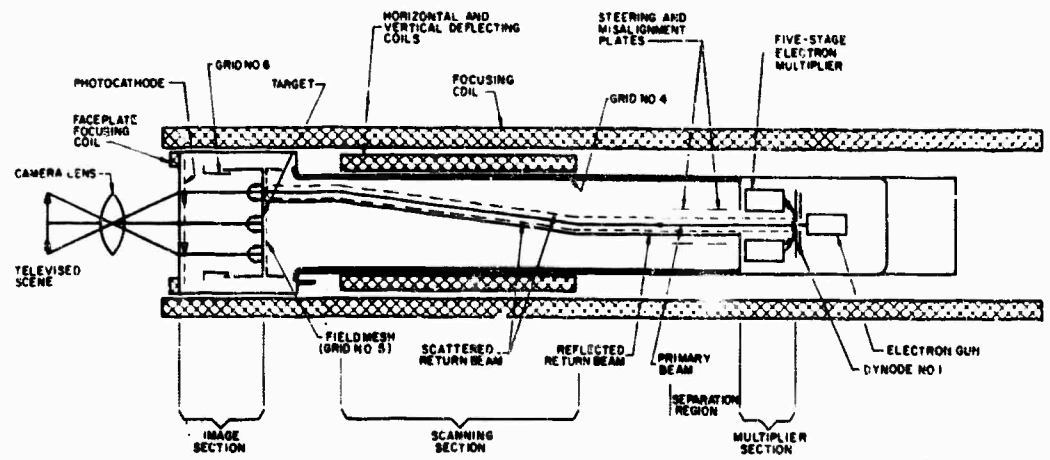
#### Scanning Operation

The charged target is scanned by a low-velocity electron beam produced by a conventional electron gun. The primary (outbound) beam receives the required amount of transverse energy and the proper trajectory to pass through the beam-separation structure by means of transverse fields established by the electrostatic alignment plates.

The beam emerging from the beam-separation structure is focused at the target by the magnetic field of the external focusing coils, the electrostatic field of the wall electrode (grid No.4), and the field mesh (grid No.5). Under the influence of these fields, each electron traverses a helical path; the paths converging at the target. The fields of the horizontal and vertical steering plates are used to deflect electrons of the primary and return beams to allow control over beam trajectory. Scanning is accomplished by transverse magnetic fields produced by the external scanning coils.

By proper adjustment of electrode voltages including those of the field mesh (grid No.5) and grid No.4, the beam, regardless of its lateral deflection, is caused to approach the target at a fixed angle with zero or nearly zero velocity. The beam deposits sufficient electrons to neutralize the positive charges accumulated during the preceding frame time. Beam electrons having insufficient energy to reach the target are specularly reflected and constitute part of the return beam. Beam electrons reaching the target at positively charged areas but not captured are scattered and also become part of the return beam.

The term scattered electrons applies exclusively to the non-specularly reflected electrons obtained when the beam interacts with the surface of the target and are thus distinguished from the remainder of the returning electrons which are termed reflected electrons. The number of scattered electrons obtained is at a maximum in the lighted portions (positively charged areas) and essentially zero in the dark portions of the target. (It is to be noted that although the total return beam is a minimum in the bright areas of the target where electrons are deposited, the number of scattered electrons is a maximum). The total return beam remains under the influence of the magnetic field of the focusing coil and the electrostatic field of grid No.4. The helices described by the scattered electron portion have greater diameters than those described by the reflected electrons. The return beam now comes under the influence of the field of the steering plates and is directed toward the beam-separation edge. The beam-separation edge passes the scattered electron portion of the return beam and captures the reflected electron portion. The scattered electrons accordingly strike the first dynode of the multiplier section. As a result, secondary emission occurs. The emitted secondaries, after multiplication, are collected by the anode as the signal output current.



32LM-3504

Figure 1 - Schematic Arrangement of Type C21083A

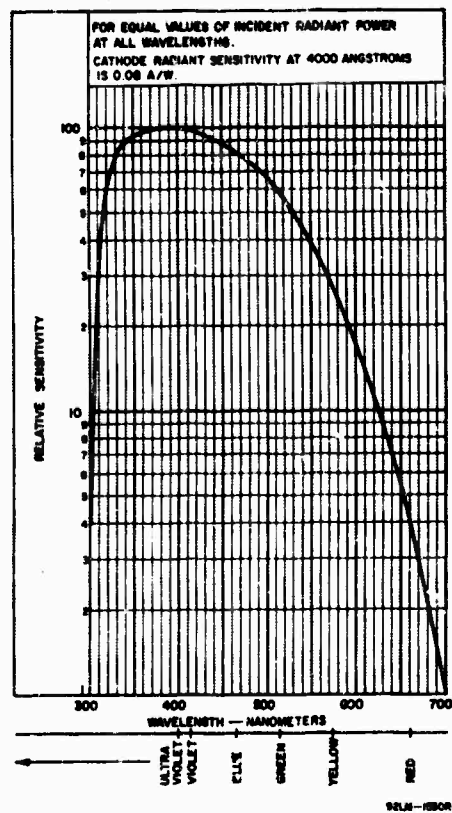
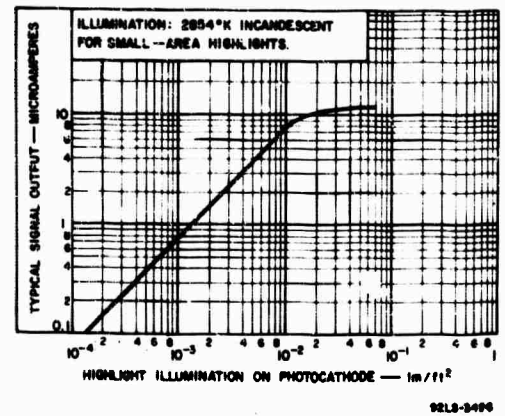


Figure 2 - Typical Spectral Sensitivity Characteristic



92LS-9499

Figure 3 - Basic Light Transfer Characteristic



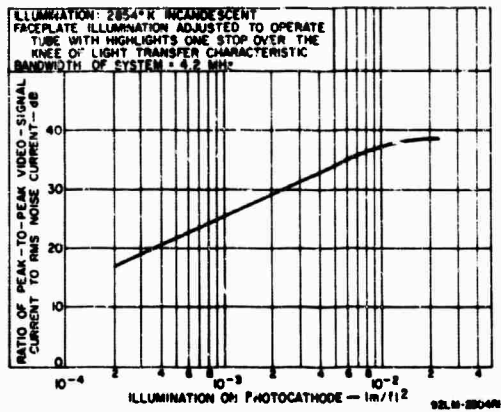


Figure 4 – Typical Signal to Noise-in-Signal Ratio as a Function of Photocathode Illumination

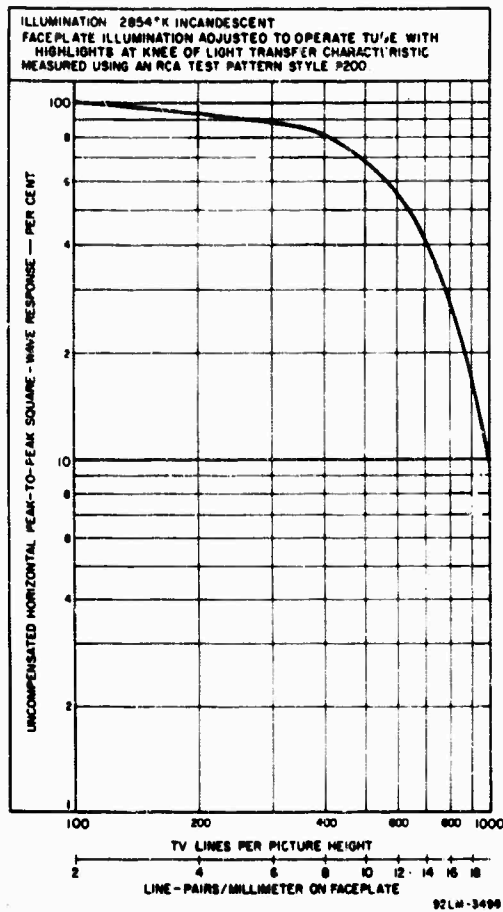
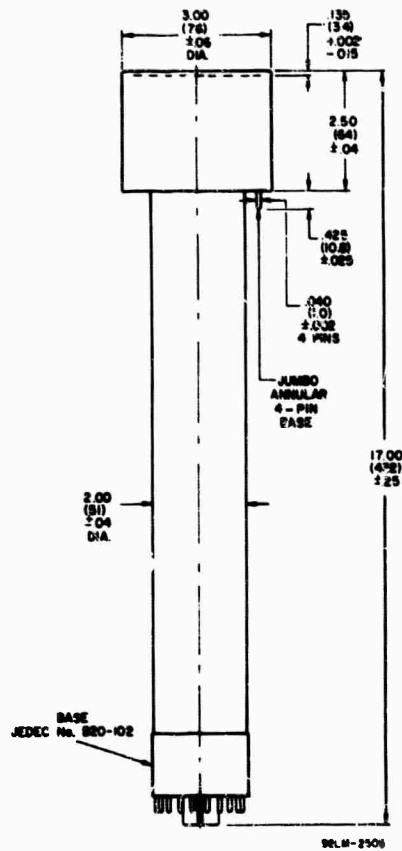
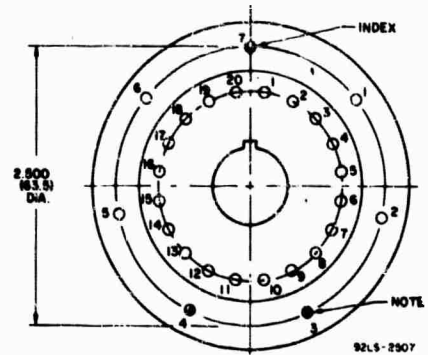


Figure 5 – Typical Amplitude Response Characteristic



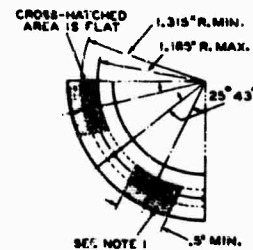
Dimensions are in inches unless otherwise stated. Dimensions in parentheses are in millimeters and are derived from the basic inch dimensions (1 in. = 25.4 mm)

Figure 6 - Dimensional Outline



Note: Pins 3, 4, and 7 of shoulder base are cut off.

Figure 7 - Enlarged Bottom View



Note 1: Dotted area is flat or extends toward bidirectional base end of tube by 0.080\"/>

Figure 8 - Detail of Bottom View of Jumbo Annular Base

#### Small-Shell Bidirectional 20-Pin Base (JEDEC No. B20-102)

- Pin 1: Heater
- Pin 2: Grid No.1
- Pin 3: Internal Connection—Do Not Use
- Pin 4: Steering Plate SX<sub>1</sub>
- Pin 5: Grid No.4
- Pin 6: Grid No.3
- Pin 7: Internal Connection—Do Not Use
- Pin 8: Misalignment Plate SY<sub>2</sub>
- Pin 9: Dynode No.2
- Pin 10: Dynode No.4
- Pin 11: Dynode No.5
- Pin 12: Anode
- Pin 13: Dynode No.3
- Pin 14: Steering Plate SX<sub>2</sub>
- Pin 15: Internal Connection—Do Not Use
- Pin 16: Dynode No.1
- Pin 17: Grid No.2
- Pin 18: Misalignment Plate SY<sub>1</sub>
- Pin 19: Cathode
- Pin 20: Heater

#### Jumbo Annular Receiver 4-Pin

- Pin 1: Grid No.0
- Pin 2: Photocathode
- Pin 3: Field Mesh (Grid No.5)
- Pin 4: Target

as is shown in Fig. V-E-34, wherein the sine-wave response of the intensifier and the square-wave responses of the II are plotted for various input photocathode irradiances.

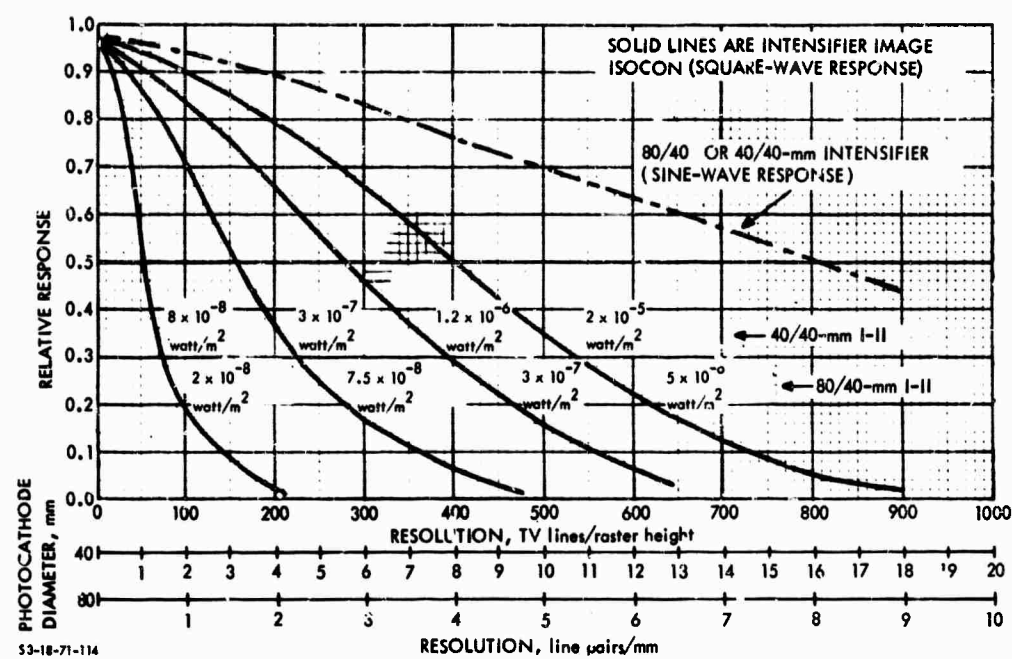


FIGURE V-E-34. Uncompensated Horizontal Square- or Sine-Wave Response for the Intensifier image Isocon for Various Photocathode Irradiance Levels

d. Video Signal-to-Noise Ratios. In view of the reduced beam noise of the II, the additional gain provided by the intensifier is sufficient to make the I-II photoelectron noise limited. Thus, the video signal-to-noise ratio becomes

$$\begin{aligned} \text{SNR}_{V,0,1} = I_S/\bar{I}_e &= \frac{G_P G_M (G_T - 1) T_M G K_S i_s e_v e_h}{\left[ G_P^2 G_M^2 (G_T - 1)^2 G^2 K_S^2 e \Delta f T_M i_s/e_v e_h \right]^{1/2}} \\ &= \left[ \frac{T_M i_s/e_v e_h}{e \Delta f} \right]^{1/2} \end{aligned} \tag{V-E-22}$$

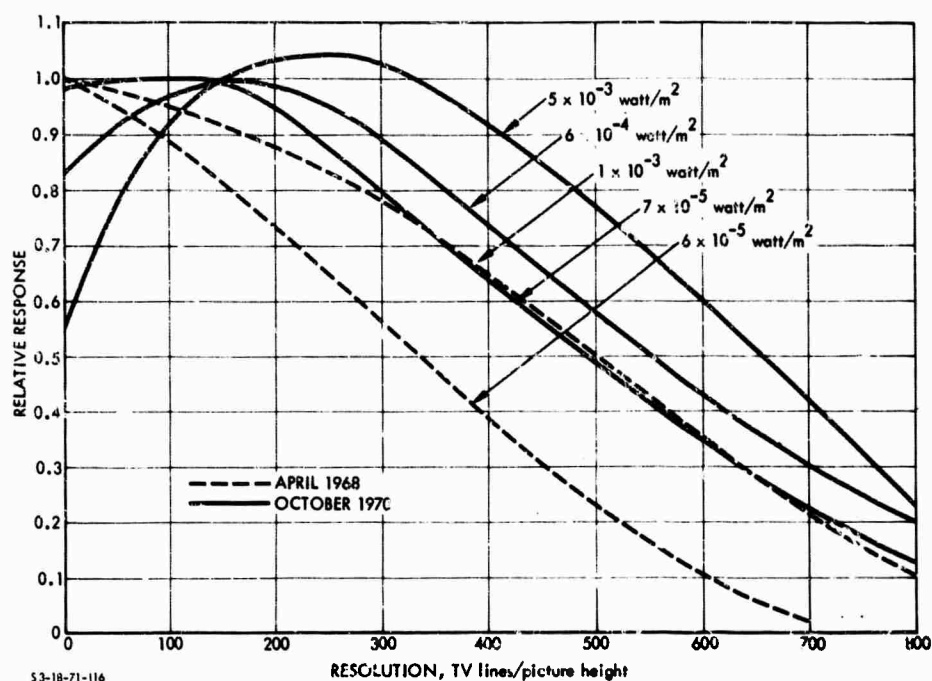


FIGURE V-E-36. Uncompensated Horizontal Square-Wave Response for the C21095 Image Isocon, as Reported by RCA

In more recent correspondence, RCA provided the MTF curves shown as the solid lines in Fig. V-E-36. The dashed curves, corresponding to roughly equivalent irradiance levels, were taken from Fig. V-E-24. As can be seen, the more recent curves show that the MTF of the image isocon is irradiance-level dependent, and the falloff is at a rate comparable to that previously given in the data sheet of April 1968. The absolute values are much higher, however. Thus, a reevaluation appears to be indicated. This would require more data regarding the specific tube on which the new MTF curves were measured.

The measured limiting resolution versus photocathode irradiance curves correlate closely with those calculated in this section. As far as is known, no exceptions have been taken to these results.

#### F. THE SILICON ELECTRON BOMBARDMENT INDUCED RESPONSE CAMERA TUBE AND ITS INTENSIFIED VERSION

The SEBIR camera tube is the most promising new tube now in development for low-light-level imaging applications. Barring unforeseen difficulty, this tube bids fair to replace all other tubes for this purpose. At this writing, a number of good, operable tubes have been constructed and tested. The principal remaining problems are to increase sensor amplitude response and to eliminate blemishes. The amplitude response is currently limited by the size of the SEBIR target, the spacing of diodes in the target structure, the target thickness, and the electron scanning beam. The blemishes, due to target imperfections, appear as bright, white spots. Because of these blemishes, current tube yields are low, resulting in high tube prices and low availability. The blemish problem is being rapidly resolved, however.

In format, the typical SEBIR tube is similar to the SEC camera tube discussed in Section V-D. The photocathode is usually an S-20 or an S-25 photoemitter followed by an electrostatically focused image section and the SEBIR target. This target, like the SEC target, amplifies and stores the image prior to readout by the scanning-electron-beam readout section. However, the gain of the SEBIR target is 10 to 20 times higher than the SEC target, so that the SEBIR is of quite high sensitivity even without an intensifier. A SEBIR camera is comparable in operational simplicity to the SEC camera and, in addition, it is much less subject to image burn-in, either temporary or permanent. With an intensifier, the SEBIR becomes photoelectron-noise limited since overall gain is then more than sufficient to make the preamplifier, and all other system-generated noises, negligible. We will remark here that neglecting the spatial filtering effect of the sensor's apertures on the photoelectron noise is more serious for the I-SEBIR than for the I-SEC, where the noise is a mixture of preamplifier and photoelectron noise. Hence, the performance of the I-SEBIR as predicted herein will tend to be pessimistic.

The SEBIR target consists of a matrix of silicon diode elements. The amplification of signal current is due to an electron bombardment

induced response (EBIR) effect which takes place within the target. The maximum resolving power (or amplitude response) of the matrix is partly limited by the density of the diodes. In current practice, this density is about 650 by 850 or 550,000 elements in a 3/8- by 1/2-in. area.

The silicon diode matrix target is also used as a photoconductor in the silicon vidicon. In this mode, the silicon matrix array converts scene photons to electrons and stores the image for subsequent readout but provides no gain. As used in the SEBIR tube, the silicon diode matrix target amplifies and stores the photoelectron signal generated by an entirely separate photoemitter. The silicon vidicon should not be confused with the SEBIR tube, for the latter tube is many factors of ten more sensitive.

# 1. The Silicon Electron Bombardment Induced Response Camera Tube

a. Principles of Operation. The SEBIR tube, shown schematically in Fig. V-F-1 is identical to the SEC tube shown in Fig. V-D-1, except that the SEC target is replaced by the SEBIR target and the suppressor mesh is deleted. The SEBIR tube is also identical in operation except for the detailed gain mechanism within the target.

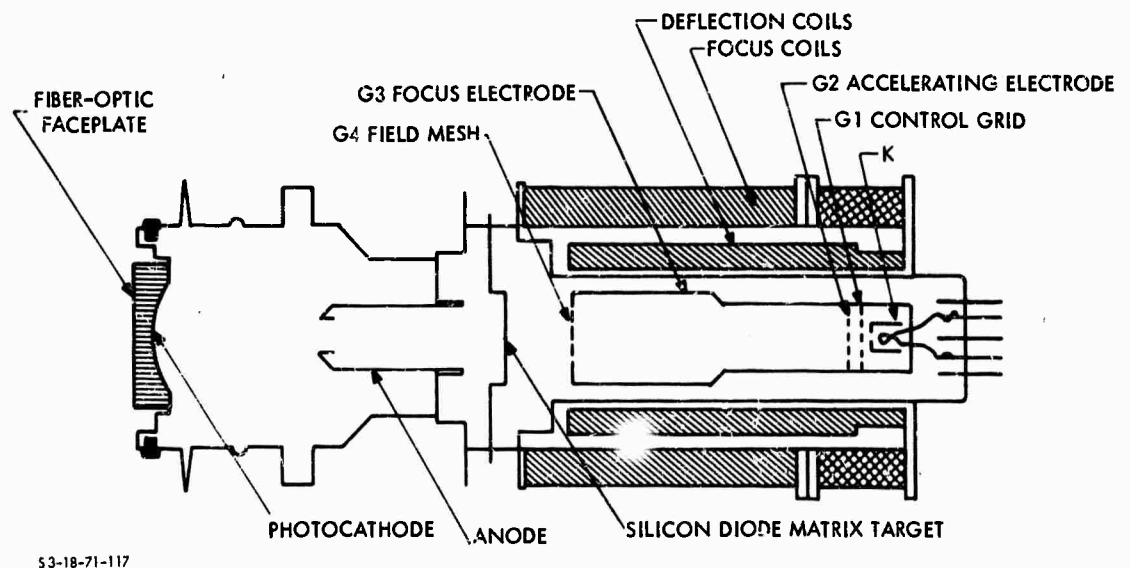


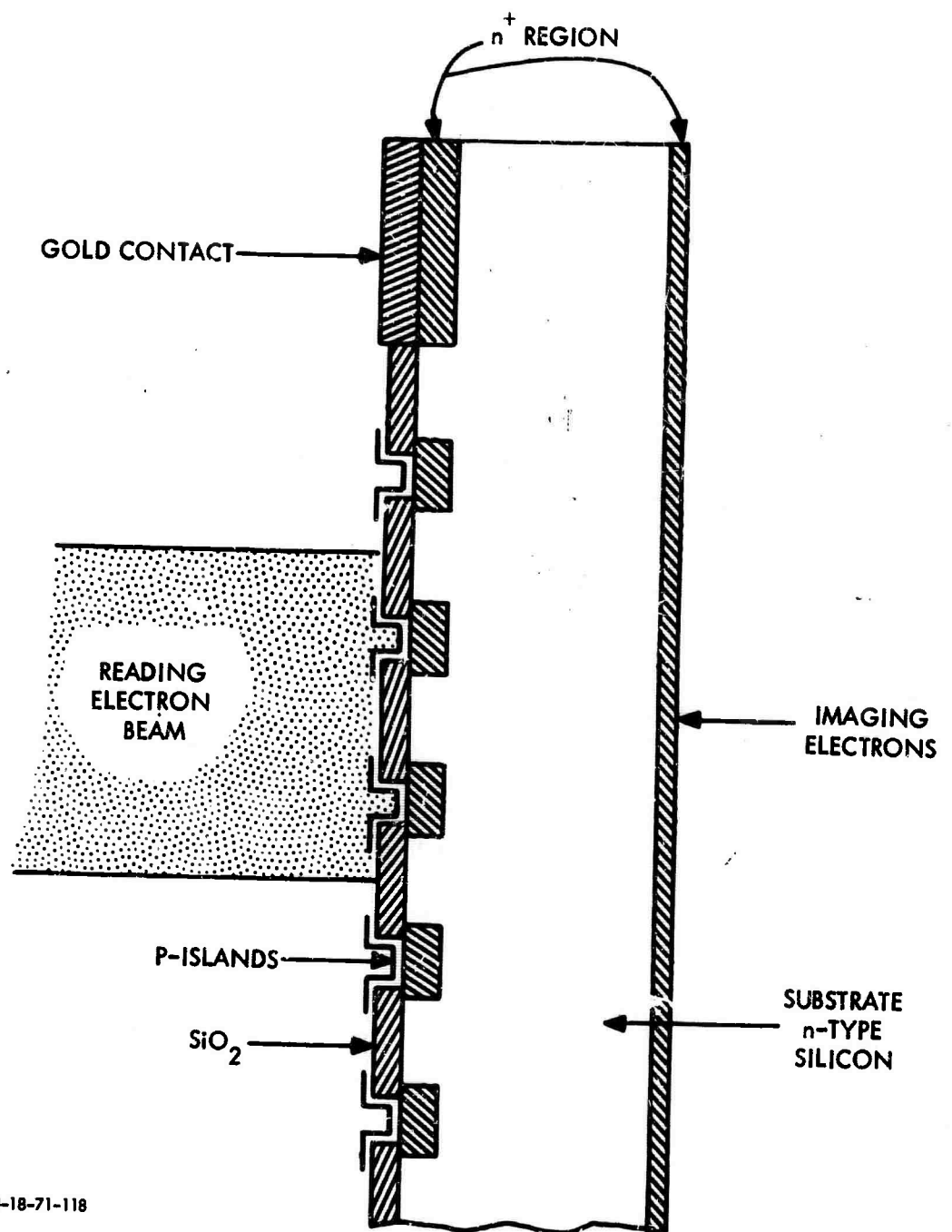
FIGURE V-F-1. Cross Section of a SEBIR Camera Tube

Target operation is described by reference to Fig. V-F-2.

Suppose the n-type silicon slice to be biased approximately 10 v. positive with respect to reading-electron-beam cathode. By scanning the back surface of the target with the electron beam, the p-type islands and the  $\text{SiO}_2$  surface are charged to the read-gun cathode potential, and the p-n junctions become reverse biased. In effect, a junction capacitor is formed at each diode. Because of the low leakage current, this bias is retained during the frame time period when no signal photoelectrons are incident. When a photoelectron image is incident on the target, holes are generated in the n-type silicon. These holes diffuse to the p-type islands and alter the charge on the diodes. The input photoelectrons are accelerated to the target with relatively high energy (about 10 kev). For each 3.4 ev of electron energy, one hole-electron pair is formed in the n-type silicon, on the average. Theoretically, 2930 hole-electron pairs are generated within the n-type silicon for each 10-kev photoelectron. This is equivalent to a signal amplification of the same amount. The actual gain is somewhat less and is controlled by the loss of holes due to recombination at the front surface and in the bulk of the target material. However, gains of 1500 to 2000 are readily obtainable.

As in the case of the SEC camera tube, the video signal is developed directly from the portion of the electron beam that lands on the target and that flows in the target lead resistor as the beam scans the target point by point.

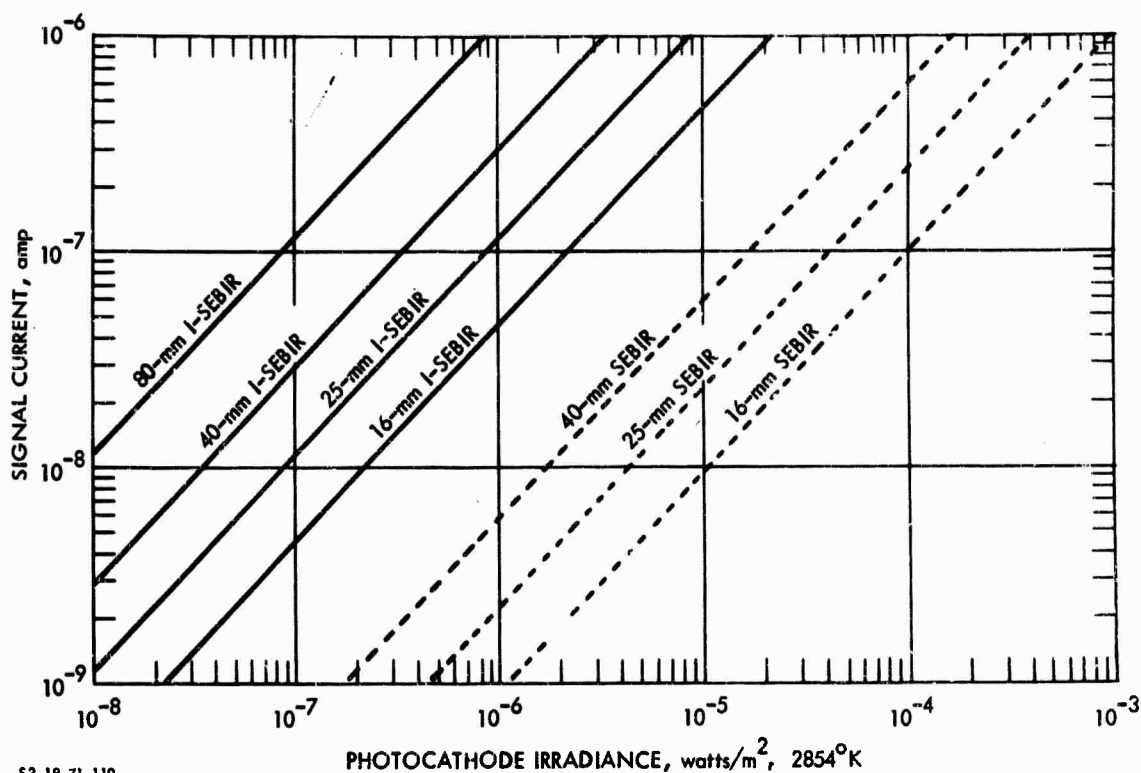
b. Signal Transfer Characteristic. The signal current versus photocathode irradiance curves for the current state-of-the-art SEBIR tube are shown in Fig. V-F-3 for three photocathode diameters, 16, 25, and 40 mm. The gamma of the signal transfer curve is essentially unity. No "knee" in the signal transfer curve is reported, although eventually the signal output current available will be beam-current limited. As a practical matter, some semblance of a knee will be introduced by means of an electronic target gain control whereby the potential between the photocathode and target is reduced as light level increases.



S3-18-71-118

FIGURE V-F-2. Schematic of SEBIR Target



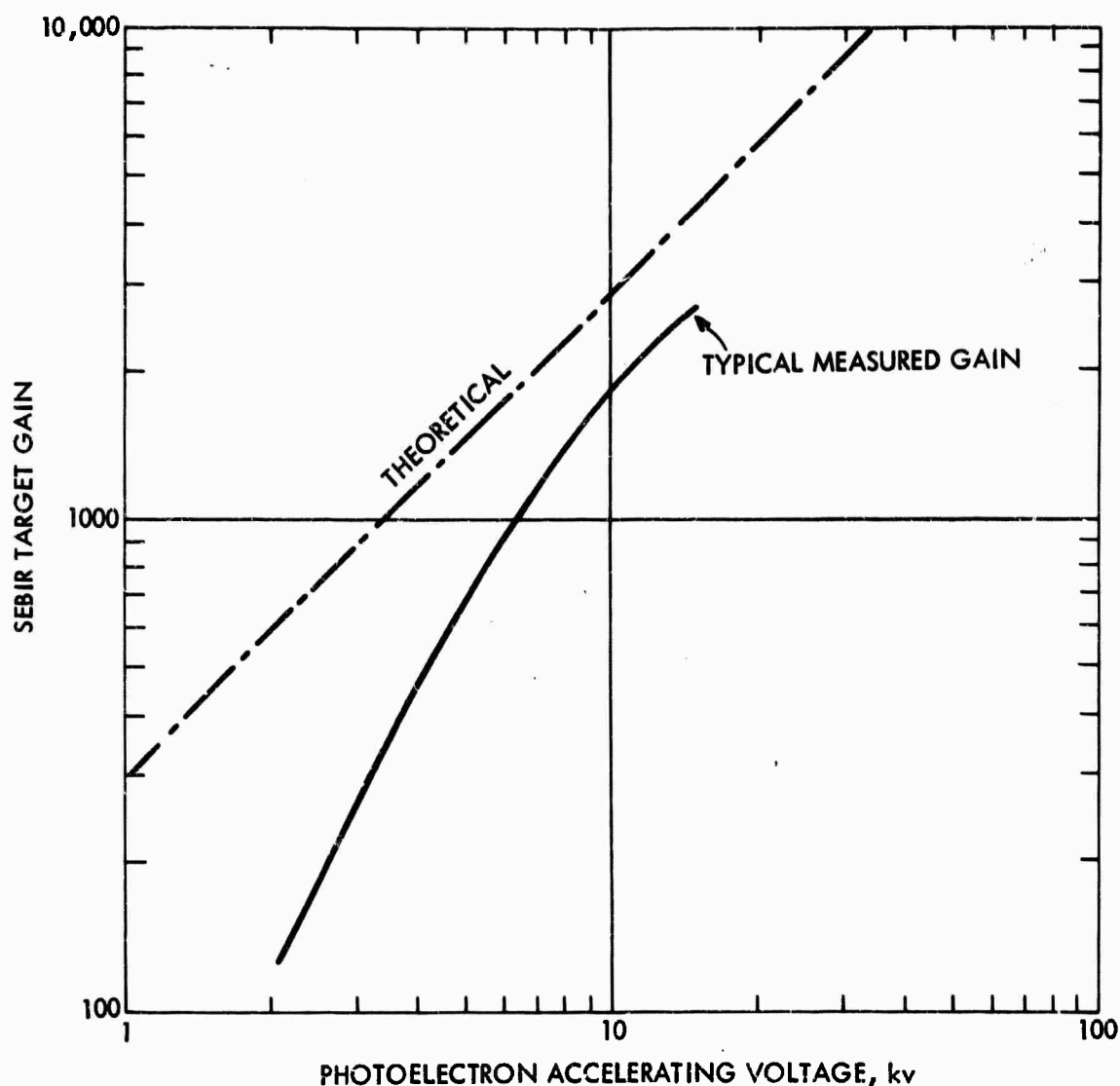


53-18-71-119

**FIGURE V-F-3. Signal Current Versus Photocathode Irradiance Characteristic for the SEBIR and I-SEBIR Cameras for Various Input Photocathode Diameters**

The gain of the SEBIR target is primarily a function of the photocathode voltage as shown in Fig. V-F-4. For the current tubes, an absolute maximum voltage of -15 kv is specified, typical operation being in the range of -12 to -3 kv. This places maximum gain in the area of 2500 to 3000, and minimum gain a factor of about 10 lower. Above -15 kv, excessive dark current and positive ion bombardment of the photocathode can be expected to be a problem; at voltages below -3 kv, some image defocusing and rotation will occur, although this may be tolerable in some instances.

For the signal transfer curves shown in Fig. V-F-3, a photocathode radiant sensitivity of  $3.2 \times 10^{-3}$  amp/watt and a SEBIR target gain of 1890 are assumed in calculations.



53-18-71-120

FIGURE V-F-4. SEBIR Target Gain Versus Photoelectron Accelerating Voltage

c. Amplitude Response. The square-wave amplitude response of current SEBIR camera tubes is shown in Fig. V-F-5 for tubes with a diode density of 1800/inch. The response is shown to be the same for 40-, 25-, and 16-mm tubes when the resolution is expressed in terms of TV lines/raster height. This similarity in response is based on the premise that all three tubes use the same target and that the target and the electron beam are the primary factors limiting response.

Actually, the photocathode with its fiber-optic faceplate will have some small effect on amplitude response, but its influence will probably be less than the normal variations encountered from tube to tube.

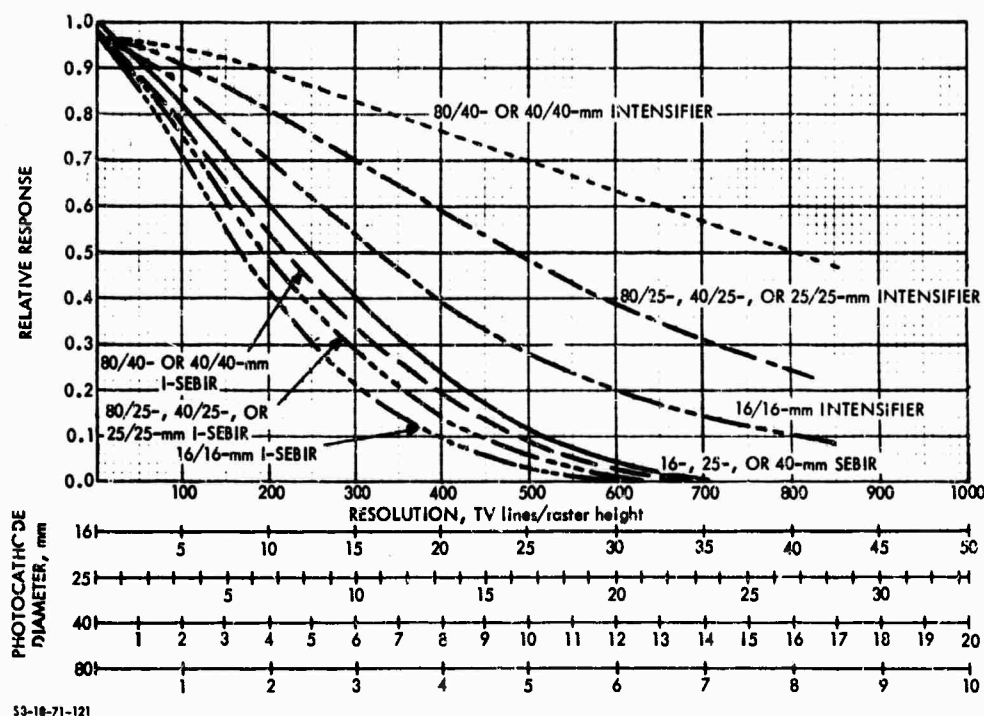


FIGURE V-F-5. Uncompensated Horizontal Square- or Sine-Wave Response for the SEBIR and I-SEBIR Cameras. (Note: Intensifier Responses are Sine Wave; I-SEBIR and SEBIR Responses are Square Wave.)

Resolving power in terms of line pairs/millimeter is also shown on the same curve. The scale selected must correspond to the diameter of the input photocathode of the tube under consideration. Thus, when a tube with a 25-mm input photocathode diameter is used, the 25-mm input photocathode diameter scale is used, and so on.

d. Video and Display Signal-to-Noise Ratio. The ratio of peak-to-peak video signal to rms noise for a SEBIR camera is calculated from Eq. V-D-3, and the terms are identical to those defined, except that  $G_T$  is now the SEBIR target gain. The video signal and rms noise currents for unity contrast and square-wave response are plotted as a function of photocathode current in Fig. V-F-6. As can be seen, the SEBIR camera is substantially photoelectron noise limited for input photocurrents above about  $10^{-11}$  amp. For this calculation, a video bandwidth of 7.5 MHz and a preamp noise of  $3 \times 10^{-9}$  amp was assumed. A 3-na preamplifier noise is consistent with the 20-pf interelectrode capacitance associated with the SEBIR target. The video signal-to-noise ratio for the same conditions assumed above is plotted in Fig. V-F-7, and  $SNR_D$  is plotted in Fig. V-F-8 for various photocathode currents.

e. Limiting Bar-Pattern Resolution. The limiting resolution versus photocathode current is determined from Fig. V-F-8, and the result is shown in Fig. V-F-9 in the form of limiting resolution versus photocathode current for various input image contrasts. These results are replotted in Fig. V-F-10 as limiting resolution in line pairs per millimeter referenced to the input photocathode versus photocathode irradiance. A 100 percent input contrast, a  $2854^{\circ}\text{K}$  tungsten source, and a photocathode of radiant sensitivity  $3.2 \times 10^{-3}$  amp/watt to such a source are assumed. In Fig. V-F-11, the performance at 30 percent contrast is plotted.

f. Computed versus Measured Performance. The currently quoted sensor resolving power versus that computed is shown for the SEBIR camera in Fig. V-F-12. At present, data is available only for an input photocathode diameter of 40 mm and an image contrast of 100 percent. These data show good correlation with that measured.

g. Lag Characteristic. The lag characteristic, measured as percentage of signal remaining in the third field versus irradiance level is shown in Fig. V-F-13. Data are not currently available to show the dynamic limiting resolution characteristics.

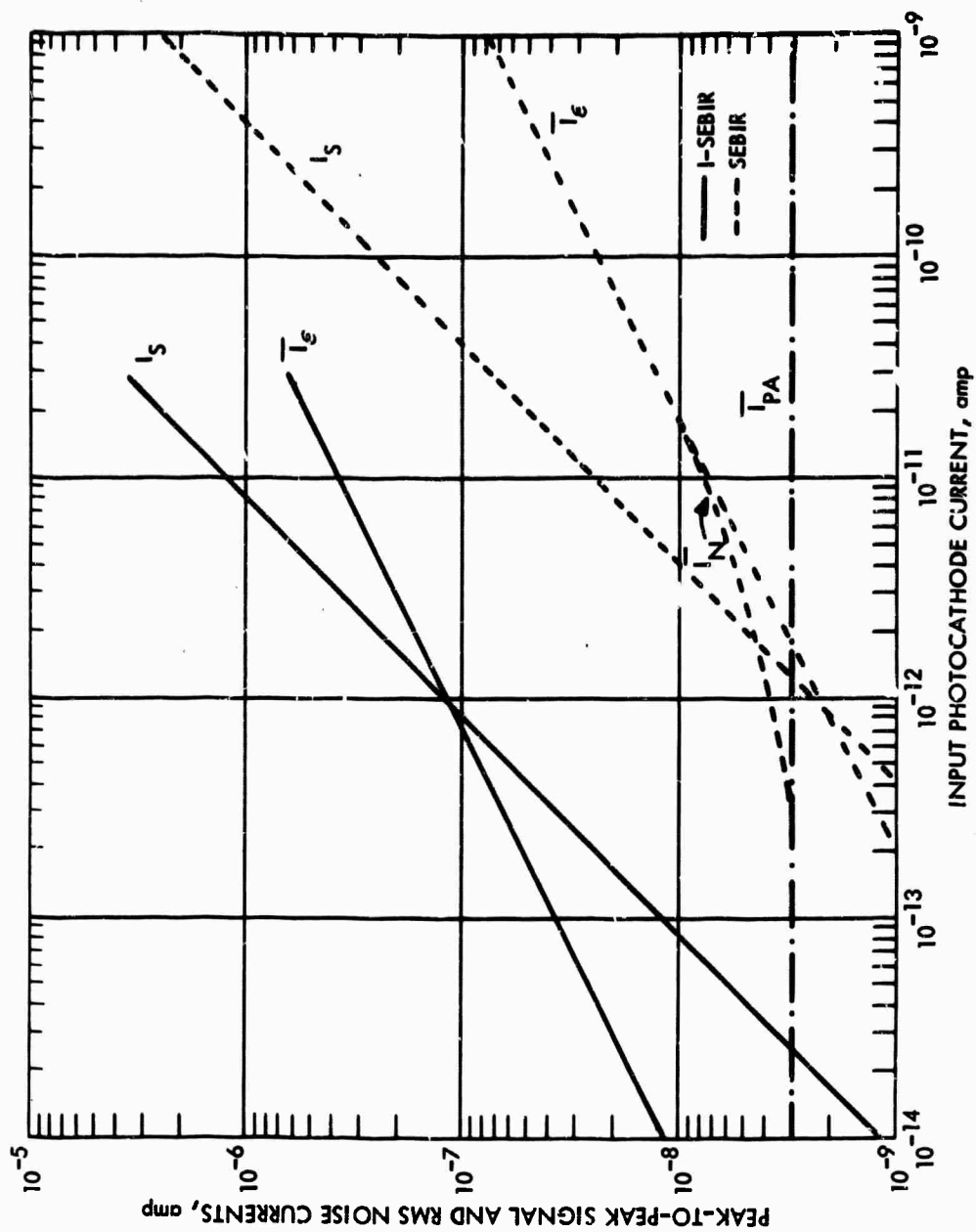
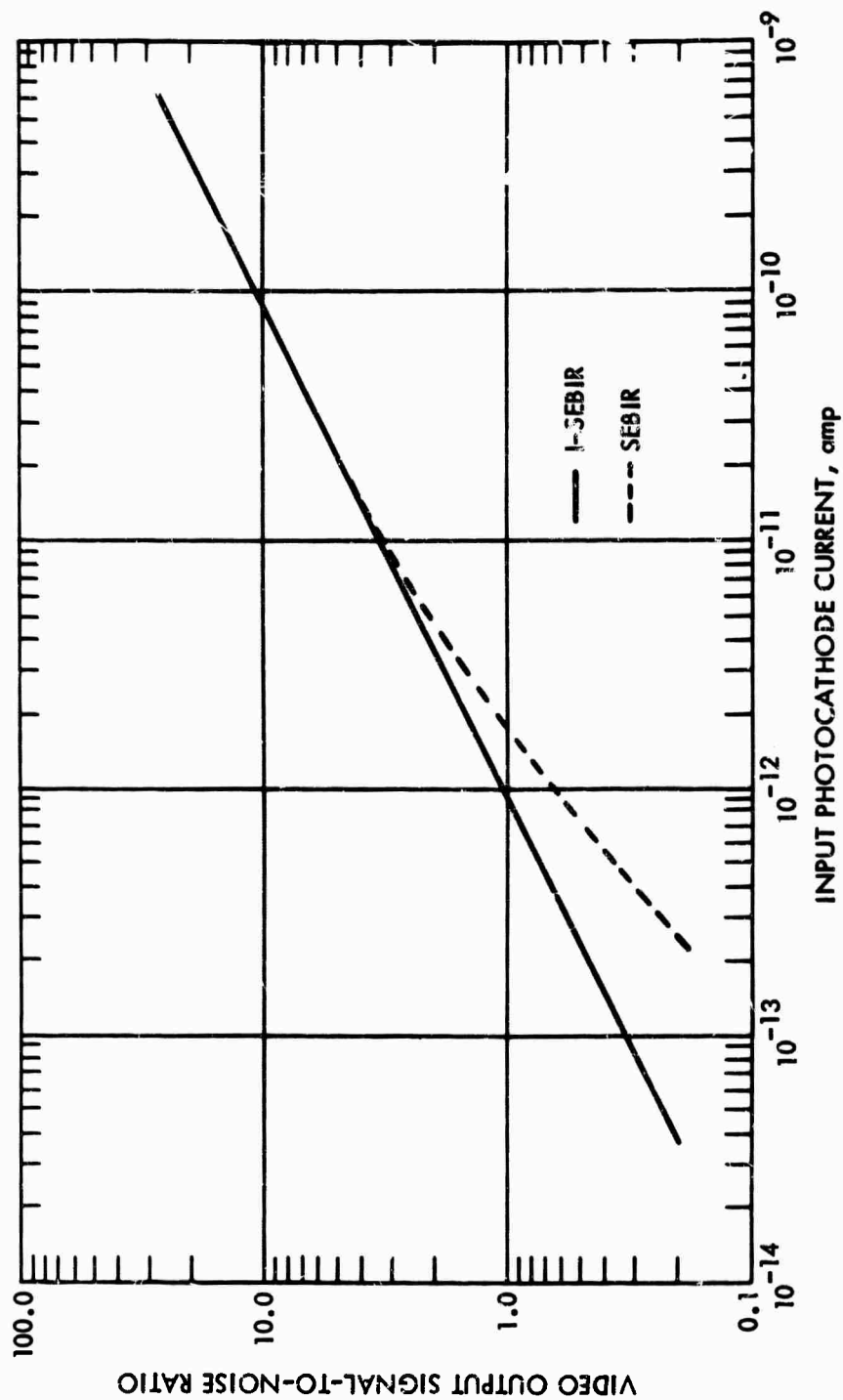


FIGURE V-F-6. Peak-to-Peak Signal and RMS Noise Output Currents for the SEBIR and I-SEBIR Cameras as a Function of Input Photocathode Current



S3-18-71-123

FIGURE V-F-7. Video Peak-to-Peak Signal to RMS Noise Output Current Ratios Versus Input Photocathode Current for the SEBIR and I-SEBIR Cameras for a Video Bandwidth of 7.5 MHz. (Note: The Input Image is Assumed to be of Unit Contrast and of Low Spatial Frequency.)

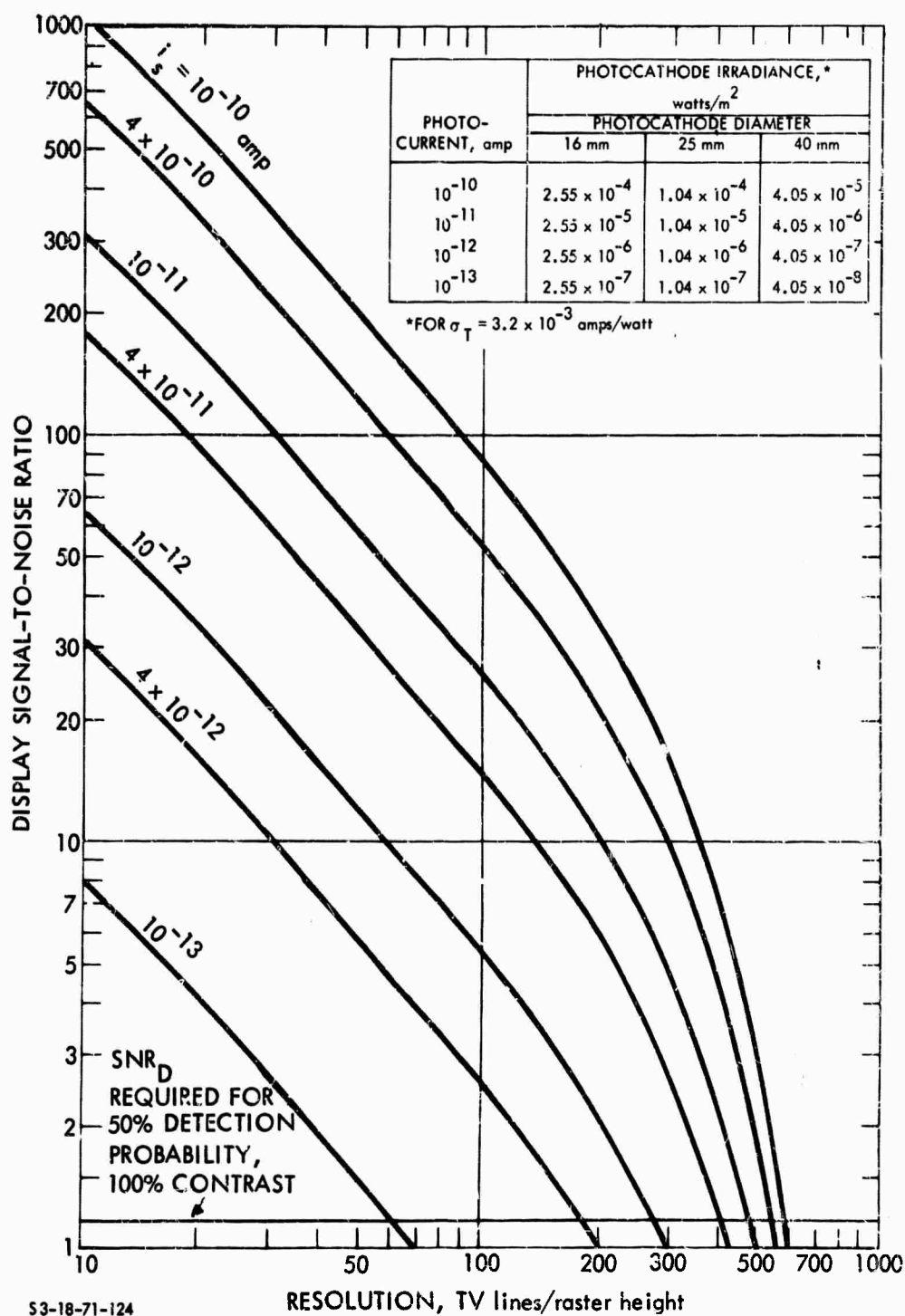


FIGURE V-F-8. Display Signal-to-Noise Ratio for SEIR Cameras for Various Input Photocathode Currents as a Function of Pattern Resolution.

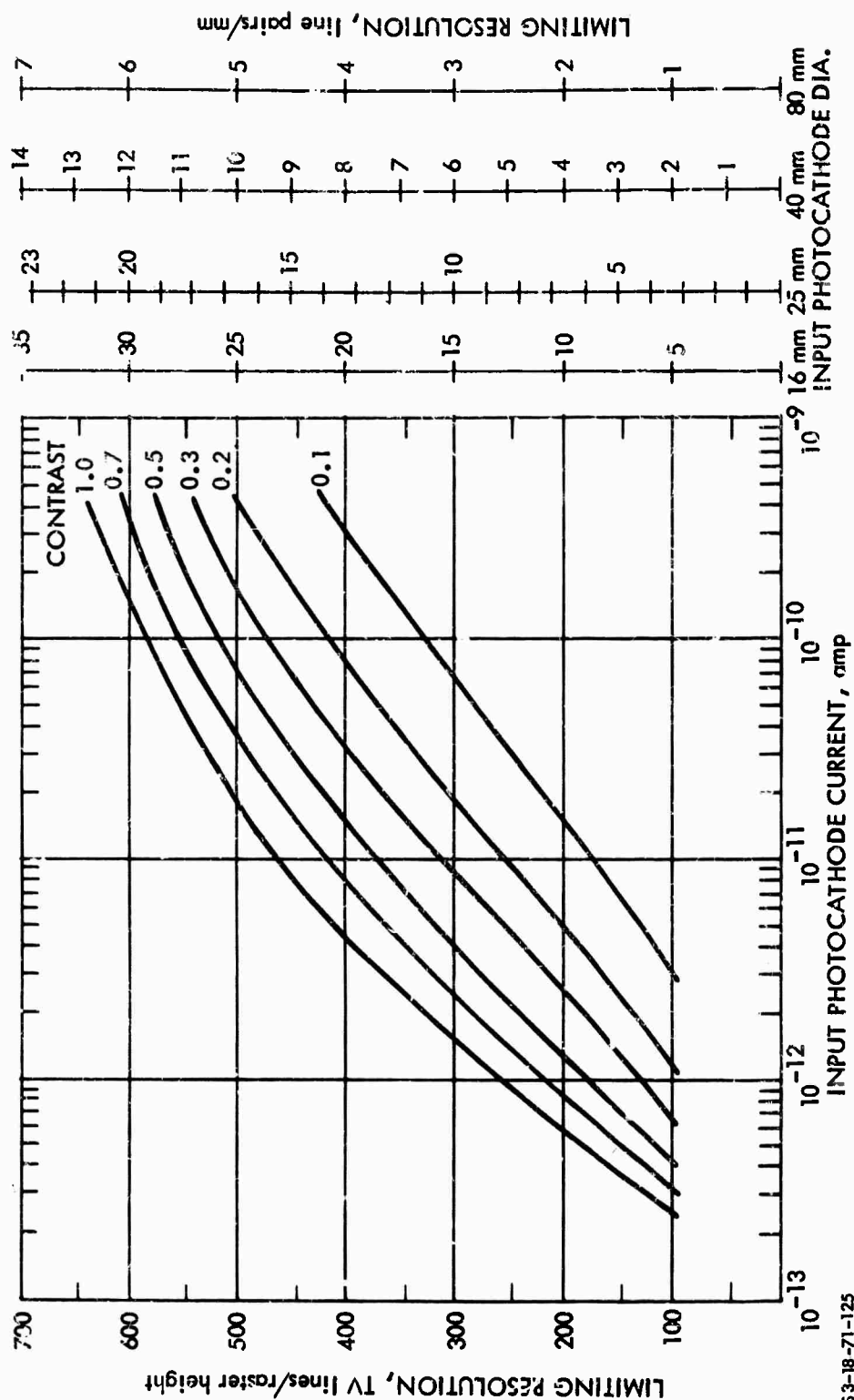


FIGURE V-F-9. Limiting Resolution Versus Input Photocathode Current for SEIR Cameras as a Function of Input Image Contrast



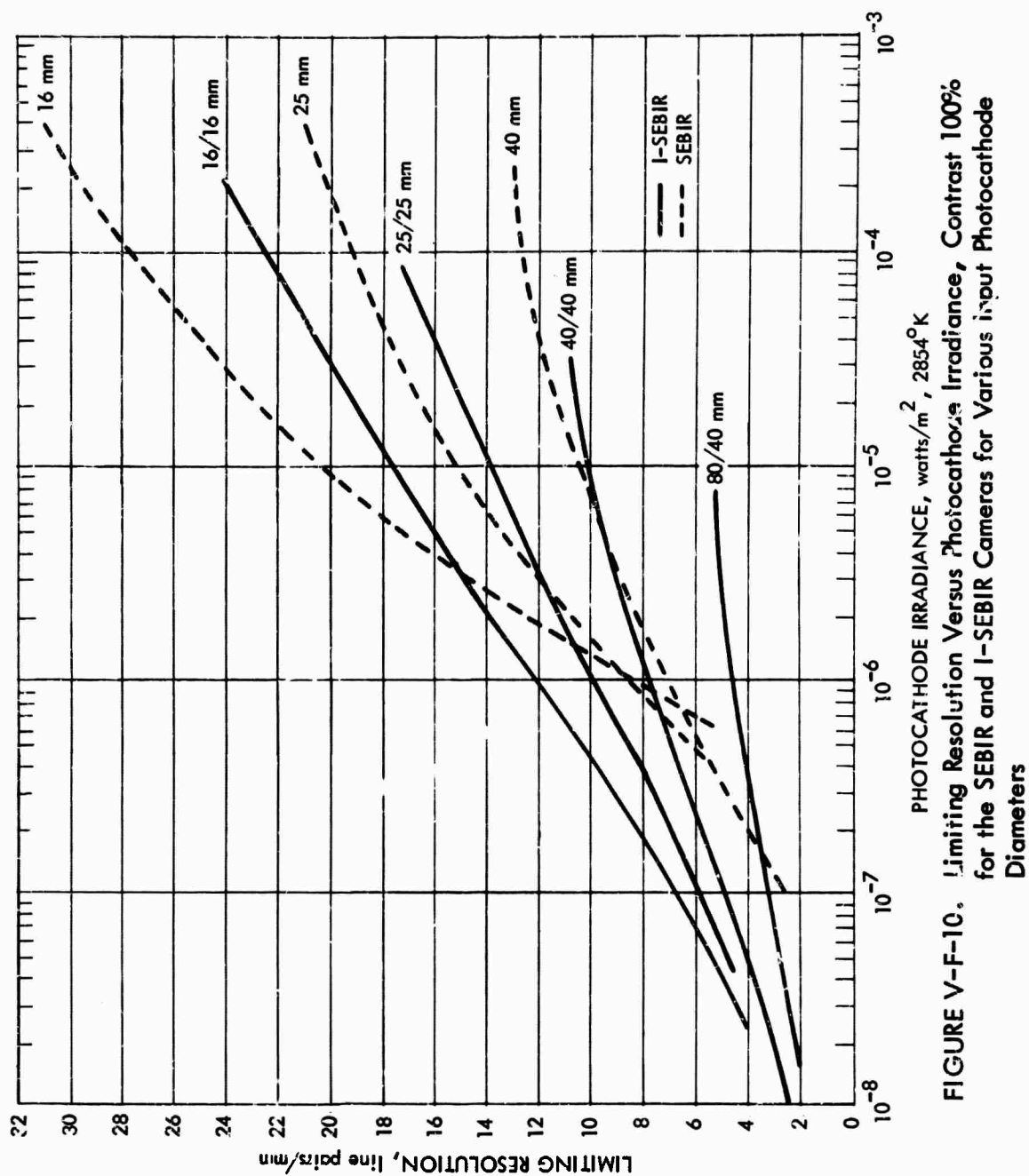


FIGURE V-F-10. Limiting Resolution Versus Photocathode Irradiance, Contrast 100% for the SEBIR and I-SEBIR Cameras for Various input Photocathode Diameters

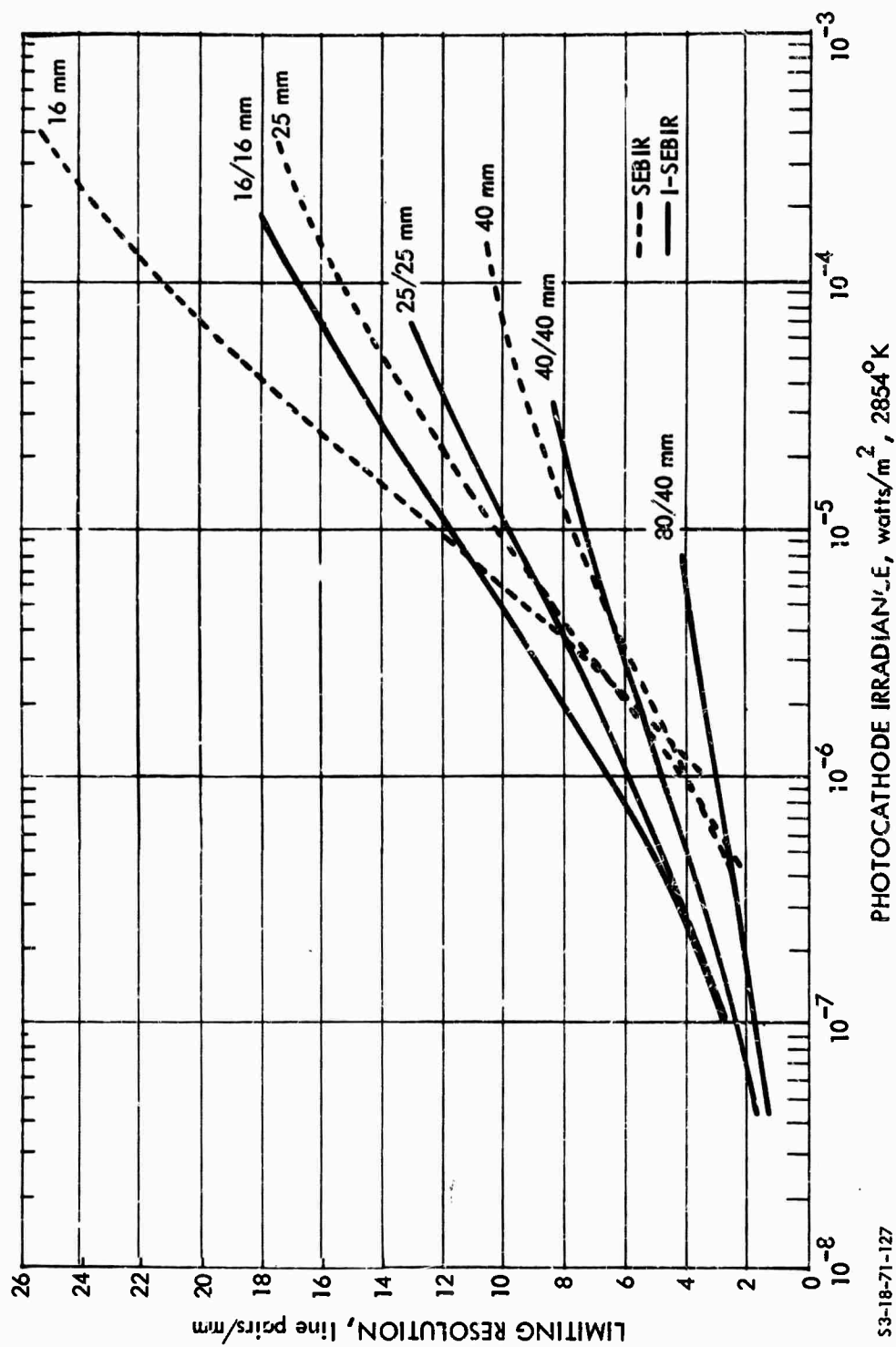
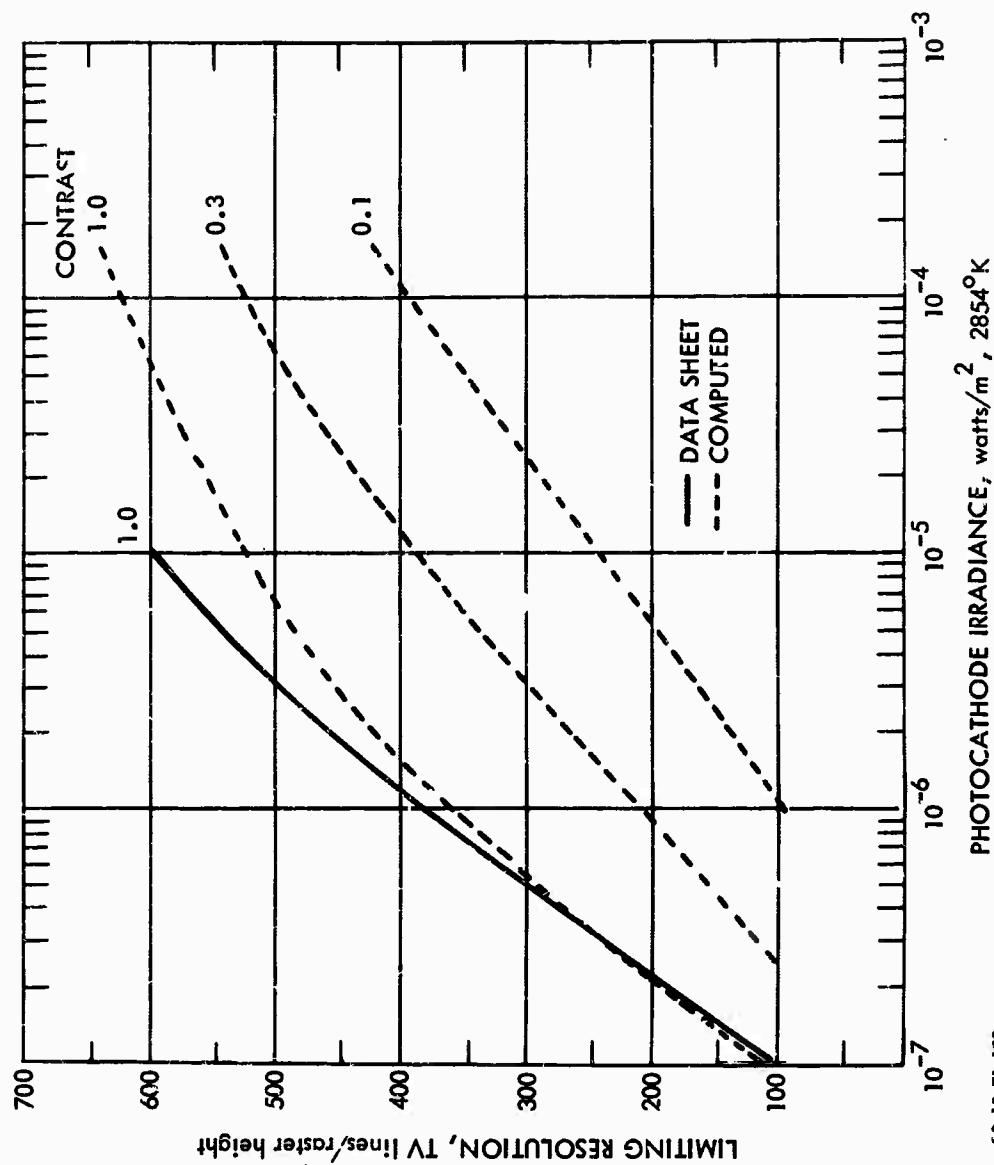


FIGURE V-F-11. Limiting Resolution Versus Photocathode Irradiance, Contrast 30%, for the SEBIR and I-SEBIR Cameras for Various Input Photocathode Diameters

S3-18-71-127



53-18-71-128

FIGURE V-F-12. Limiting Resolution Versus Photocathode Irradiance. Comparison of Computed Versus Data Sheet Performance for the RCA C2117B, 40-mm SEBIR Camera

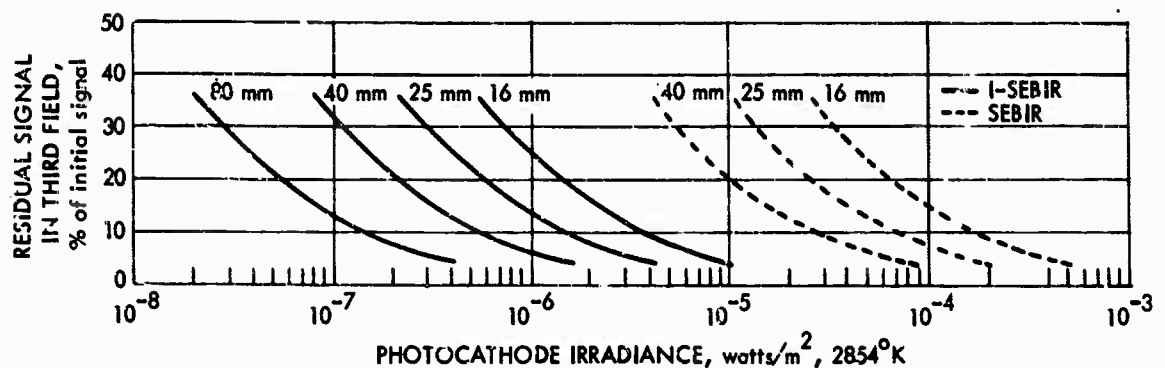


FIGURE V-F-13. Signal Lag Versus Photocathode Irradiance Characteristic for the SEBIR and I-SEBIR Cameras for Various Input Photocathode Diameters

h. Form Factor. The majority of the current SEBIR camera tubes are based on the use of a 5/8-in.-diameter target, which results in a read section of about 1-in. outside diameter and about 5 to 6 in. in length. The image sections are 2 in. to 3 in. in outside diameter and 3 to 4 in. in length, depending on the photocathode diameter used. Overall tube length is thus 8 to 10 in. in current designs.

## 2. The Intensifier SEBIR Camera

a. Principles of Operation. An additional intensifier fiber-optically coupled to the basic SEBIR tube provides more than sufficient gain, so that preamplifier noise becomes negligible at all light levels of interest. The lag characteristic is also improved to the point where it should not ordinarily be a problem. As usual, these benefits are somewhat offset by an overall reduction in aperture response and an increase in blemishes. The additional intensifier is assumed to have an S-25 photocathode of radiant sensitivity  $\sigma_T = 4 \times 10^{-3}$  amp/watt. The phosphor is assumed to be a modified P-20 surface which in conjunction with the SEBIR tube's photocathode, provides an electron gain of 40. The aperture response of the intensifier is assumed to be limited primarily by the output intensifier phosphor.

b. Signal Transfer Characteristic. The signal transfer characteristic for various I-SEBIR combinations is shown in Fig. V-F-3.

c. Amplitude Response. The overall sensor square-wave response is the product of the intensifier sine-wave responses and the SEBIR camera square-wave responses, as shown in Fig. V-F-5.

d. Video and Display Signal-to-Noise Ratio. As noted above, the gain provided by the intensifier is sufficient to ensure that the pre-amplifier noise is negligible at all light levels of interest. The I-SEBIR signal and noise currents are as shown in Fig. V-F-6. The video signal-to-noise ratio is calculated from the relation

$$\text{SNR}_{V,0,1} = \frac{i_s/e_v e_h}{[e \Delta f i_s/e_v e_h]^{1/2}} \quad (\text{V-F-1})$$

This function is plotted in Fig. V-F-7 as a function of the input photocathode current, and the display signal-to-noise ratio is plotted in Fig. V-F-14. The  $\text{SNR}_D$  is similar for the various tube combinations, except for the influence of the square-wave response as shown in the figure for  $i_s = 10^{-10}$  amp. The curves at other photocathode currents were drawn for the 25-mm photocathode case.

e. Limiting Bar-Pattern Resolution. Limiting resolution versus photocathode current is shown in Figs. V-F-15, -16, and -17. Limiting resolution in line pairs/millimeter versus photocathode irradiance is shown in Fig. V-F-10 for 100 percent image contrast and in Fig. V-F-11 for 30 percent image contrast.

f. Computed versus Measured Results. No measured results are now available.

g. Lag Characteristics. The estimated lag versus irradiance level characteristic is plotted in Fig. V-F-13 for various I-SEBIR combinations. The low lag at the  $10^{-6}$  to  $5 \times 10^{-7}$  watt/m<sup>2</sup> range is particularly notable.

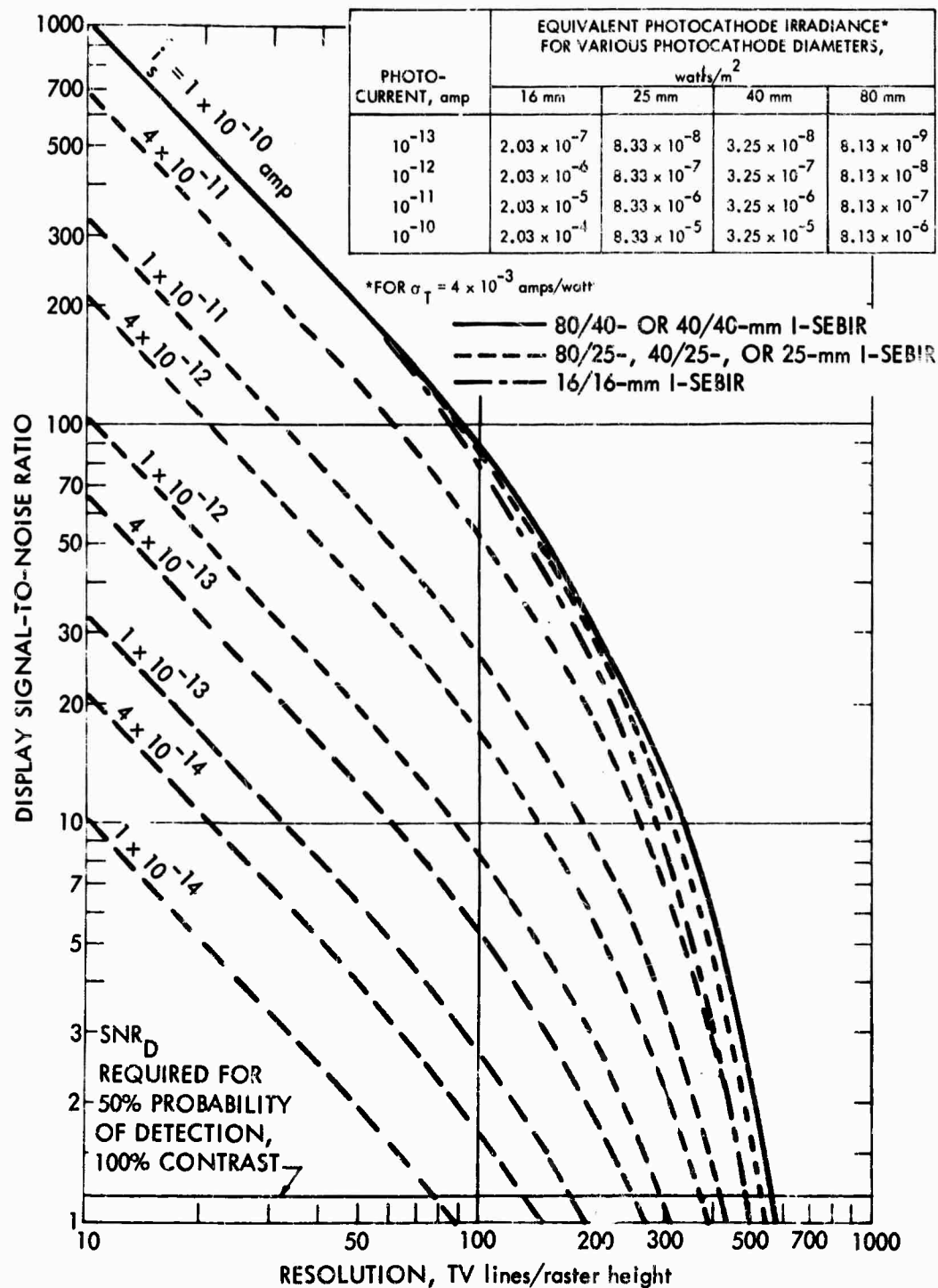
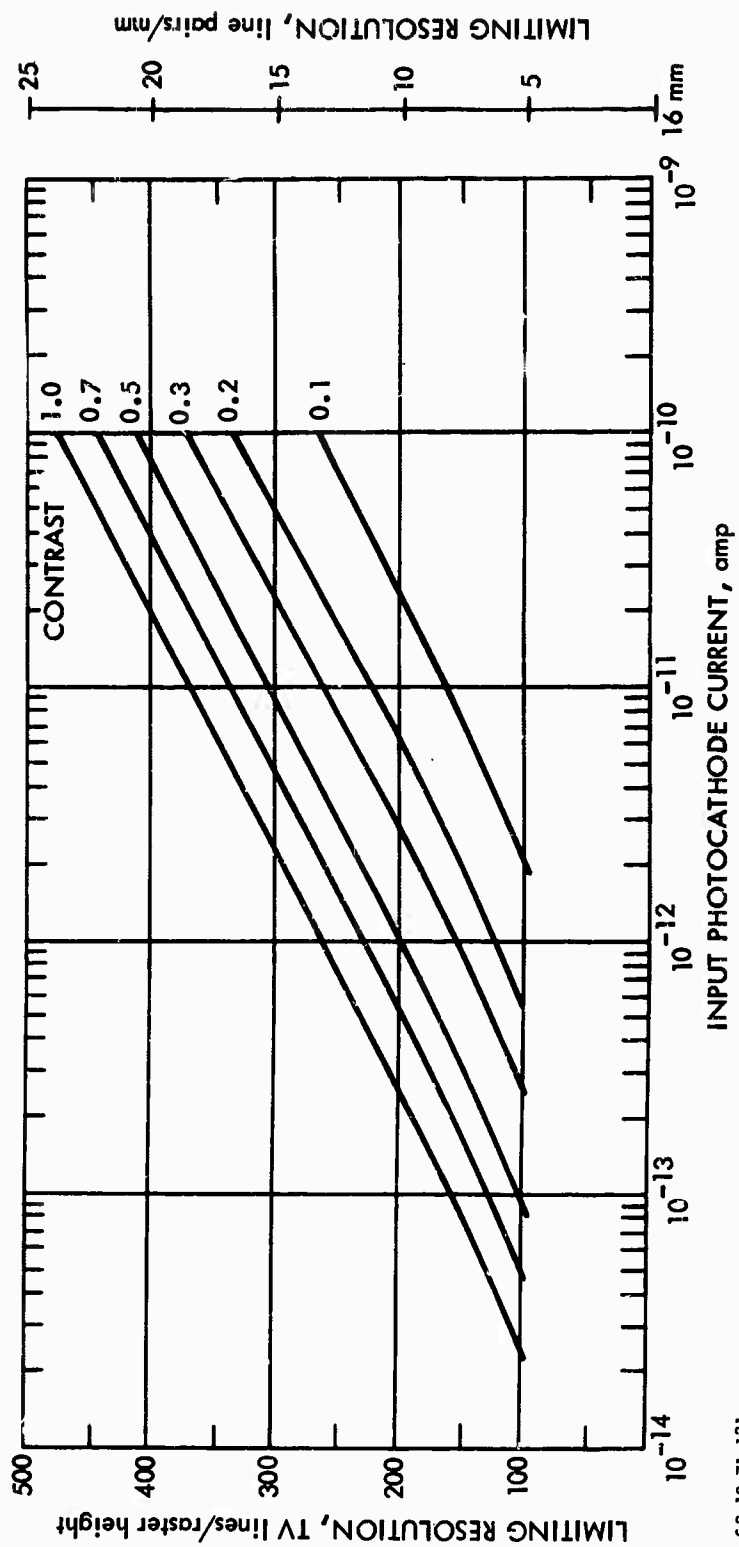
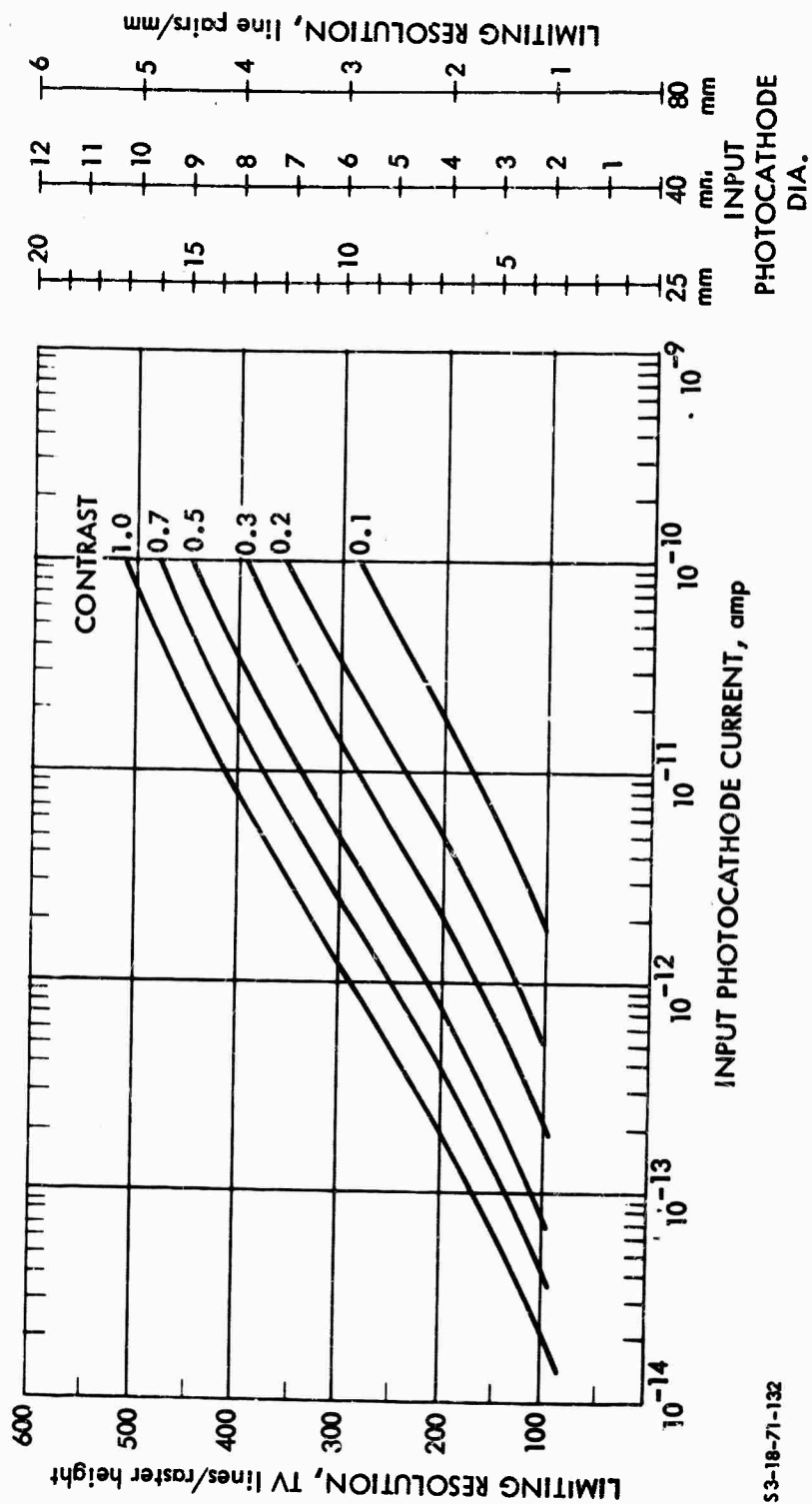


FIGURE V-F-14. Display Signal-to-Noise Ratio for the Intensifier-SEBIR Cameras for Various Input Photocathode Currents as a Function of Pattern Resolution, for 25-mm SEBIR, Except as Noted Above in the Legend



S3-10-71-131

FIGURE V-F-15. Limiting Resolution Versus Input Photocathode Current for the 16/16-mm I-SEBIR Camera for Various Input Image Contrasts



S3-18-71-132

FIGURE V-F-16. Limiting Resolution Versus Input Photocathode Current for the 80/25-, 40/25-, and 25/25-mm I-SEBIR Cameras for Various Input Image Contrasts



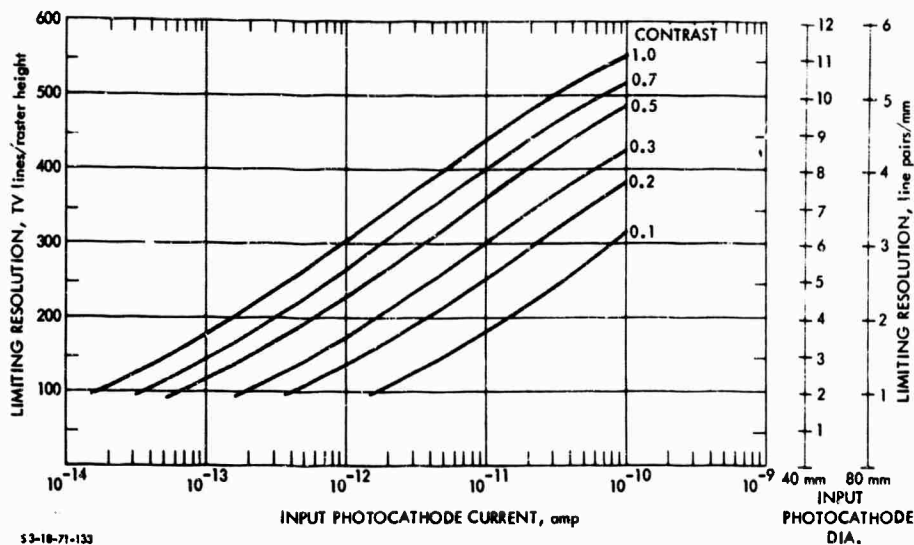


FIGURE V-F-17. Limiting Resolution Versus Input Photocathode Current for the 80/40- and 40/40-mm I-SEBIR Cameras for Various Input Image Contrasts

h. Form Factor. Intensifiers mainly add length from 2 in. to 6 in., depending on the input photocathode diameter. Diameter is not substantially increased, except in the 80-mm case, where the tube diameter is 5 in. to 6 in. Sensor package size will vary from 11 in. to 16 in. in overall length and 2 in. to 6 in. in diameter.

G. CORRELATION BETWEEN MTFA AND  $SNR_D$

In Part II, Snyder showed the correlation between MTFA and viewer error, while here in Part V, Rosell has derived the concept of  $SNR_D$ , the display signal-to-noise ratio. If these two concepts could be related, the missing link between the physical properties of electro-optical devices and operator performance would be established. This was the hope that was expressed by Snyder at the end of Part II. As will be shown, there is a one-to-one correspondence between MTFA and the area under the  $SNR_D$  curves, provided that sine-wave patterns are used as test inputs in calculating or measuring  $SNR_D$ .

The beginning point of Snyder's analysis is Eq. II-1, which states that the eye's threshold detection requirements for a sine-wave pattern of frequency  $k$  is

$$M_t(k) = 0.034 [dD/d(\log_{10} E)]^{-1} [0.033 + \sigma_D^2 k^2 S^2]^{\frac{1}{2}} \quad (V-G-1)$$

where  $[dD/d(\log_{10} E)]$  is a sensor gamma.  $\sigma_D^2$  is noise, and  $S$  is a threshold signal-to-noise ratio.  $M_t(k)$  should not be confused with the sensor's MTF. It has no relation to it.  $M_t(k)$  is the signal modulation needed by the eye to detect the pattern in the presence of noise. The constant term in the root bracket pertains to low spatial frequencies wherein the eye is limited by spatial image extent, its dc response, or other factors. To a first approximation, one can ignore it. Then, for sensor  $\gamma = 1$ ,

$$M_t(k) = 0.034 \sigma k S \quad (V-G-2)$$

To convert Eq. V-G-2 to Rosell's terminology, one lets  $\sigma$  equal the rms video noise,  $k$  be expressed in  $N_{TV}$  lines/picture height,  $S$  be  $SNR_{DT}$ , the display signal-to-noise ratio required for 50 percent probability of pattern detection, and the constant 0.034 be changed to  $\beta$  to reflect the change in nomenclature and units. Now,

$$M_t(N_{TV}) = \beta \cdot i_n \cdot N_{TV} \cdot SNR_{DT} \quad (V-G-3)$$

or

$$SNR_{DT} = \frac{1}{\beta} \frac{M_t(N_{TV})}{N_{TV}} \cdot \frac{1}{i_n} \quad (V-G-4)$$

If next one lets  $M_t(N_{TV})$  be equal to

$$M_t(N_{TV}) = \Delta i_{ST} \quad (V-G-5)$$

where  $\Delta i_{ST}$  is the threshold video signal, then

$$SNR_{DT} = \frac{1}{\beta} \cdot \frac{1}{N_{TV}} \cdot \frac{\Delta i_{ST}}{i_n} \quad (V-G-6)$$

but  $\Delta i_{ST}/i_n$  is the threshold video signal-to-noise ratio  $SNR_{V,0,T}$  required, so that

$$SNR_{DT} = \frac{(1/\beta) \cdot SNR_{VT}}{N_{TV}} \quad (V-G-7)$$

which is the relationship between threshold display signal-to-noise and threshold video signal-to-noise ratio as used by Rosell throughout his analysis.

Next, one turns to the concept of MTFA, which Snyder defines as

$$MTFA = \int_0^{k_0} \left[ T(k) - \frac{M_t(k)}{M_o} \right] dk \quad (V-G-8)$$

where  $T(k)$  is the sensor's MTF,  $M_o$  is an object modulation, and  $k_o$  is a specific spatial frequency to be defined. In our terminology  $T(k) = R_w(N)$ , the sine-wave response.

If one uses Eqs. V-G-5 and V-G-6 in Eq. V-G-8 and lets  $M_o = C \Delta i_s$ , the product of input image contrast and highlight signal current, Eq. V-G-8 becomes

$$MTFA = \int_0^{N_o} R_w(N_{TV}) - \left[ \frac{\beta SNR_{DT} \cdot N_{TV} \cdot i_n}{C i_s} \right] dN \quad (V-G-9)$$

where  $N_o$  is the frequency corresponding to  $k_o$  but now expressed in terms of TV lines per picture height. Note that  $C i_s/i_n$  is the broad-area video signal-to-noise ratio that the sensor can produce, i.e.,

$$\text{SNR}_{V,0,C} = C i_s / i_n \quad (\text{V-G-10})$$

and

$$\begin{aligned} \text{MTFA} &= \int_0^{N_0} \left[ R_W(N_{TV}) - \frac{\beta \text{SNR}_{DT} \cdot N_{TV}}{\text{SNR}_{V,0,C}} \right] dN \\ &= \int_0^{N_0} \left[ \frac{R_W(N_{TV}) \cdot \text{SNR}_{V,0,C} - \beta \text{SNR}_{DT} \cdot N_{TV}}{\text{SNR}_{V,0,C}} \right] dN \end{aligned} \quad (\text{V-G-11})$$

Now, using Eq. V-G-7

$$\text{MTFA} = \int_0^{N_0} \frac{[R_W(N_{TV}) \cdot \text{SNR}_{V,0,C} - \text{SNR}_{VT}]}{\text{SNR}_{V,0,C}} dN \quad (\text{V-G-12})$$

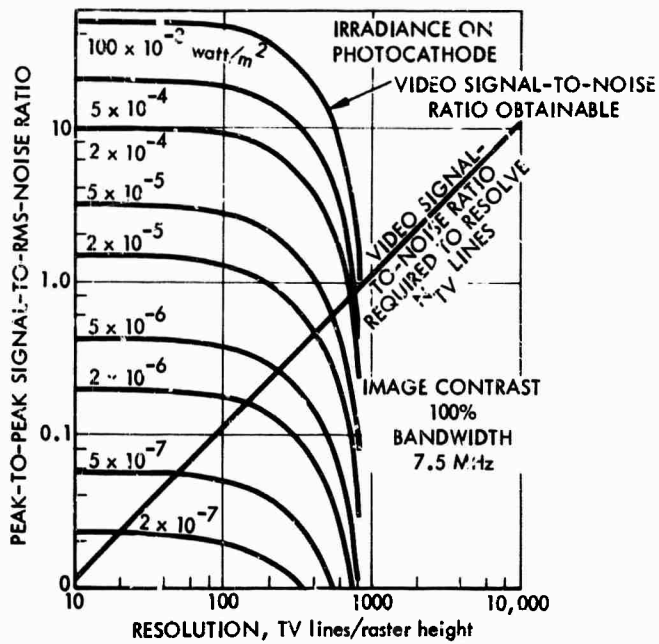
and then noting that the actual video signal-to-noise ratio at line number  $N_{TV}$  is equal to

$$\text{SNR}_{V,N,C} = R_W(N_{TV}) \cdot \text{SNR}_{V,0,C} \quad (\text{V-G-13})$$

one sees that Eq. V-G-12 becomes

$$\text{MTFA} = \int_0^{N_0} \left[ \frac{\text{SNR}_{V,N,C} - \text{SNR}_{VT}}{\text{SNR}_{V,0,C}} \right] dN \quad (\text{V-G-14})$$

and the interpretation of MTFA becomes quite clear--it is the integral of the difference between the video SNR that the sensor can provide less that required by the observer normalized to that which the sensor can provide at zero spatial frequency. The limits of integration are to the line number where  $\text{SNR}_{V,N,C}$  intersects  $\text{SNR}_{V,T}$ , as shown in Fig. V-G-1.



53-24-71-1

FIGURE V-G-1. Peak-to-Peak Video Signal-to-Noise Ratio Required Versus that Obtainable as a Function of Resolving Power for the I-SEC

In an alternate derivation, one reverts to Eq. V-G-11 and divides numerator and denominator by  $1/\beta N_{TV}$ . Then,

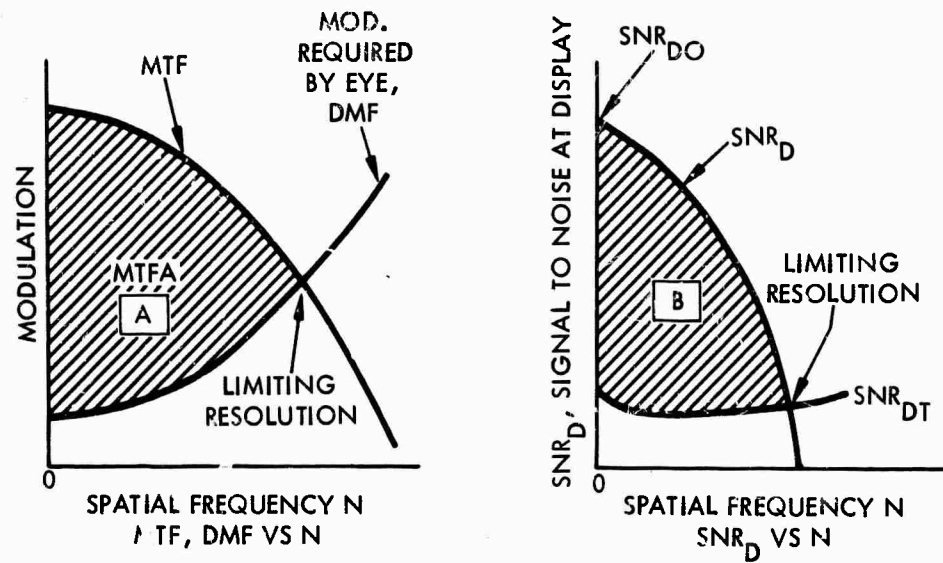
$$\begin{aligned}
 \text{MTFA} &= \int_0^{N_0} \left[ \frac{(\text{SNR}_{V,0,C} \cdot R_w(N_{TV})/\beta N_{TV}) - \text{SNR}_{DT}}{\text{SNR}_{V,0,C}/\beta N_{TV}} \right] dN \\
 &= \int_0^{N_0} \left[ \frac{\text{SNR}_D - \text{SNR}_{DT}}{\text{SNR}_{D0}} \right] dN \quad (\text{V-G-15})
 \end{aligned}$$

where  $\text{SNR}_D$  is the display SNR obtainable from the sensor,  $\text{SNR}_{DT}$  is that needed by the eye, and  $\text{SNR}_{D0}$  is that obtainable at zero spatial frequency.

The relationship between the two methods is shown by comparing areas A and B in Fig. V-G-2. The shaded areas are equal, i.e.,

$$\text{Area A} = \text{Area B}$$

$$\text{MTFA} = \text{Area A} = \text{Area B}$$



$$\boxed{A} = \boxed{B}$$

- |                   |   |
|-------------------|---|
| MTF               | - MODULATION TRANSFER FUNCTION                            |
| MTFA              | - MODULATION TRANSFER FUNCTION AREA                       |
| DMF               | - DEMAND MODULATION FUNCTION                              |
| N                 | - SPATIAL FREQUENCY, TV LINES/PICTURE HEIGHT              |
| $\text{SNR}_D$    | - DISPLAY SIGNAL-TO-NOISE RATIO                           |
| $\text{SNR}_{DT}$ | - DISPLAY SIGNAL-TO-NOISE RATIO, THRESHOLD                |
| $\text{SNR}_{DO}$ | - DISPLAY SIGNAL-TO-NOISE RATIO AT ZERO SPATIAL FREQUENCY |

S8-27-70-7

FIGURE V-G-2. Comparison of MTFA and  $\text{SNR}_D$

## PART V. REFERENCES

1. A. Rose, "The Sensitivity Performance of the Human Eye on an Absolute Scale," J. Opt. Soc. Am., Vol. 38, No. 2, pp. 196-208, February 1948.
2. H. de Vries, "The Quantum Character of Light and its Bearing upon the Threshold of Vision, Differential Sensitivity and Visual Acuity of the Eye," Physica, Vol. 10, p. 553, 1943.
3. J.W. Coltman and A.E. Anderson, "Noise Limitations to Resolving Power in Electronic Imaging," Proc. IRE, Vol. 48, p. 858, May 1960.
4. R. Legault, "Visual Detection Process for Electrooptical Images: Man--The Final Stage of an Electrooptical Imaging System," Chapter 4 in L.M. Biberman and S. Nudelman, eds., Photoelectronic Imaging Devices, Vol. I, Plenum Press, New York, 1971.
5. Y.W. Lee, Statistical Theory of Communication, John Wiley and Sons, New York, 1961.
6. M. Goodman, Introduction to Fourier Optics, McGraw-Hill, New York, 1968.
7. M. Schwartz, Information Transmission, Modulation, and Noise, McGraw-Hill, New York, 1959.
8. I. Limansky, "A New Resolution Chart for Imaging Systems," The Electronic Engineer, June 1958.
9. J.W. Coltman, "The Specification of Imaging Properties by Response to a Sine Wave Input," J. Opt. Soc. Am., Vol. 44, No. 6, p. 468, June 1954.
10. J.S. Parton and J.C. Moody, "Performance of Image Orthicon Type Intensifier Tubes," in National Aeronautics and Space Administration, Proc. Image Intensifier Symposium, Ft. Belvoir, Va., 24-26 October 1961, NASA SP 2.

11. O.H. Schade, Sr., "Optical and Photoelectric Analog of the Eye," J. Opt. Soc. Am., Vol. 46, No. 9, pp. 721-739, September 1956.
12. General Electric Company, Schenectady, N.Y., Present and Future Performance of Photoconductive Camera Tubes, Research Report 58-RL-1990, R.W. Damon, J.R. Eshback, and R.W. Redington, July 1958.



## VI. A COMPARISON OF TELEVISION CAMERA TUBES

by Lucien M. Biberman

### A. INTRODUCTION

New and different types of television camera tubes are becoming available at an ever-increasing rate. At the time the studies leading to this report were begun, and at the time this report was published, the principal efforts in camera tube design were improvements in quantum efficiency, time constants, electron optics, gain mechanisms, and noise characteristics. The subject for most intensive development was, and is, the electron charge storage medium--the target.

The low gain, high lag of the image orthicon electron charge storage target gave way to the SEC target at the expense of very low-light-level performance but at a considerable gain in performance at modest light levels for moving scenes.

The traditional blooming characteristic of the image orthicon target, considered highly undesirable by many, was absent in the SEC tubes, but that very absence made the SEC increasingly vulnerable to highly localized overloads such as that caused by a bright light in a dark scene. These overloads resulted in many SEC tube failures.

The increased definition available in new and improved targets was not matched by corresponding improvements in the electron optics used in most low-light-level devices.

During 1969 and 1970, the SEC target was modified to include a metallic mesh for heat dissipation. Calculation will show that point overloads in the low-density SEC layer could result in two catastrophic conditions. The first was accumulating charge beyond the potential at which the surface became a secondary emitter when bombarded by the reading beam, introducing a runaway potential increase until arc-over

(and thus tube failure) occurred. The second was associated temperature rises measured in tens of thousands of degrees per second at the point of overload, resulting in severe target burn (Section VI-B).

Methods were introduced to limit the target potential, and the mesh did reduce burn susceptibility, but it was apparent that the tube of the future would be based upon principles like that in the silicon diode array mosaic with its high-gain, low-lag, highly burn-resistant target. That tube of the future is, as of summer 1971, not quite here. We look forward to its arrival with its various limitations conquered.

This report, and especially the material in Part V, deals with the better tubes but deals with the SEC tubes at greater length. By far the greatest number and the best in performance of current low-light-level televisions systems use SEC camera tubes.

It must be recognized that the better low-light-level camera tubes available today are compromises. The SEC tubes, with their low-capacity, high-gain targets, achieve a moderately good aperture function and a moderately good sensitivity at low light levels. The SEC is a moderately good tube with moderate resolution at moderate light levels and under conditions of moderate image motion, but the physical limitations imposed by the low capacitance of the target and the broadness of the beam prevent the tube performance from increasing dramatically with increasing light levels.

The silicon-electron-bombardment induced-response (SEBIR) tubes are generally limited by beam width, diode spacing, and lateral charge diffusion in the target at higher light levels.

At low signal levels the remarkably high gain of an intensifier coupled to a silicon target tube yields the best resolution together with acceptable lag properties at low light levels, and fairly good resolution but increasing lag as the light levels decrease further.

At these very low levels there may be applications where only very low resolution is required. For such applications gain is the

principal parameter, and the modulation transfer function, which falls but very little at low spatial frequencies, is of little concern. A cheap, effective, but laggy camera for such very low-level, very low-resolution television could employ a standard vidicon with three intensifiers as preamplifiers.

At the extreme low light levels one can decrease lag through the use of an additional intensifier. This further reduces resolution but can result in tolerable levels of lag. The principal disadvantage is the need for very high voltages in order to apply about 20 kv per intensifier, i.e., about 80 kv for the preamplifier string!

As the light levels increase, little improvement occurs in the imagery of the multiple-intensifier vidicon camera. Though there is more than adequate signal, the cascading of the component MTFs is the primary limitation, resulting in very low image quality.

There is a trend in cheap cameras toward the use of channel-plate light amplifiers coupled to vidicons. Unfortunately, some designers believe that such cameras will yield better performance than the stack of three cascaded intensifiers and a vidicon. The use of a channel plate does make for much smaller size, and the overall lag of channel plate plus vidicon is similar to or slightly better than that of three cascaded intensifiers plus vidicon, but the cost is appreciably higher and the image quality is about the same.

No serious new designs for low-light-level image orthicon cameras have materialized in the past few years. The previous "Queen of the Studio" has been replaced by the Plumbicon<sup>®</sup> PbO vidicon in commercial broadcasting and by the SEC in airborne low-light-level television.

The offshoot of the image orthicon, the image isocon, has recently been simplified so that its improvements over the orthicon (Ref. 1) can be achieved with rather simple camera circuitry. Unfortunately, the timing of the isocon development was just too late for the commercial studio market and too late for the rush of camera designs for airborne low-light-level applications. Actually, at all but the lowest end of the light scale, the image isocon, with one additional

stage of intensification for adequate gain, is about the best of the present camera tubes. Its excellent electron optics make possible the best aperture function of any low-light-level tubes for light levels of, say, quarter moonlight or better. At lower light levels its performance decreases rather rapidly, but at these or higher levels the tube can produce excellent imagery.

Unfortunately, good tubes do not always make good cameras. Some remarkably good tubes have been employed in remarkably poor cameras. Perhaps a discussion of a particular design can illustrate how a bad camera design completely nullified every advantage that advanced tube design offered.

Let us examine the design of a variable-field-of-view (zoom) camera by two different approaches. The first method, the one most widely used, employs an image intensifier with a cathode 80 mm in diameter and a phosphor screen 40 mm in diameter coupled to a 40-mm camera tube.

The electron optics permit focusing the full 80 mm of cathode onto the full 40 mm of phosphor when the light levels are limited or when a wide angular field is desired. When the light level permits and when a narrower field of view is desired so as to present more detail on some smaller portion of the field, the electron optics are adjusted to image some fraction of the cathode on the full phosphor screen. This method of zoom is quite effective. It utilizes the full collecting aperture of the optical system. In principal, as the light level increases, and thus as the number of resolvable lines per millimeter at the cathode increases, the image can be zoomed to a smaller and smaller section of the cathode while maintaining a constant number of resolvable lines at the phosphor. The phosphor is fiber-optics-coupled to the camera tube. Thus, the total system can be adjusted to give a variable field of view by decreasing the linear photocathode dimensions used. Since the resolution at the photocathode is greater than at any other part of the electronics, the field of view can be chosen to equal or exceed the resolution capability of the camera tube input.

On the other hand, the camera tube target and beam are quite specifically limiting in the maximum resolution obtainable. Typically, a photocathode at low light levels can produce resolutions of about 100 line pairs per millimeter, while a typical low-light-level camera tube target and beam will produce less than 1000 television lines per picture height. Thus, an 80-mm intensifier is capable of displaying 8000 line pairs or 16,000 television lines, while the target of the television camera tube will limit at less than 1000 lines. Clearly, the interaction of beam and target is much more a limit than the intensifier cathode, and yet two camera designs--one for the A-6C TRIM and one for the AH-1G HUEY COBRA--were based upon underscanning the camera tube target rather than upon decreasing the area of photocathode used while using all of the camera tube target, as in the electronic zoom discussed earlier. Both cameras were designed (by the same vendor) to save space. The designs in fact wasted space because their performance was poor. Zooming to get higher "resolution" gave a larger displayed picture of the object to be viewed but gave no increase in resolution or in information. This process was like looking at a screened newsprint photograph through a microscope. All one sees is larger dots.

If progress is to be made, one must use care and judgment in design, not just data from new sensor catalogs. Most of the errors inherent in the design choice discussed above could have been corrected by the expensive design, production, and testing of a prototype or by calculations of the kind described in Part V of this report.

#### B. DAMAGE TO ELECTRON CHARGE STORAGE TARGETS\*

All television camera tubes can be permanently damaged if exposed to a sufficiently intense source of illumination for a long enough period of time. The problem is particularly severe for sensitive low-light-level television camera tubes. The very bright sources of illumination in the real world to which the tubes can be exposed represent

---

\* An abridgement of material reported at the Westinghouse Electronic Tube Division, Elmira, N.Y., principally by Martin Green and Peter R. Collings.

even more of an extreme stress for them than for the less sensitive conventional pickup tubes.

Recent experiments, to be discussed below, have explored the threshold of permanent burn for a variety of low-light-level television camera tubes. The results of these experiments lead to the following conclusions:

- Despite the choice of the most unfavorable operating conditions (i.e., the use of a fixed photocathode voltage supplied by a low impedance source), permanent burn did not occur until illuminations of  $10^4$  to  $10^{10}$  times higher than the normal operating ranges were reached.
- The cause of permanent burn in the silicon-electron-bombardment induced-response (SEBIR) tube appears to be X rays produced by the impact of the photoelectrons on the silicon target.
- S-20 photocathodes deposited on fiber-optic substrates can deliver, from small areas, current densities of  $0.1 \text{ amp/cm}^2$  for several minutes without damage.
- For illumination levels up to  $5 \times 10^3 \text{ watts/m}^2$ , the recently developed burn-resistant SEC camera tube shows a permanent white burn threshold similar to that of the image orthicon and the SEBIR tube. The mesh-supported SEC target is 10 to 30 times more burn resistant than its predecessor.

In most camera tube applications, the extreme conditions discussed here will not be encountered. However, there will be cases where the camera designer is faced with the possibility that his equipment will see very intense sources. It is hoped that in these circumstances the data presented here will be useful in the selection of sensors and in the design of appropriate protective circuitry.

#### 1. Target Burn in SEC Camera Tubes

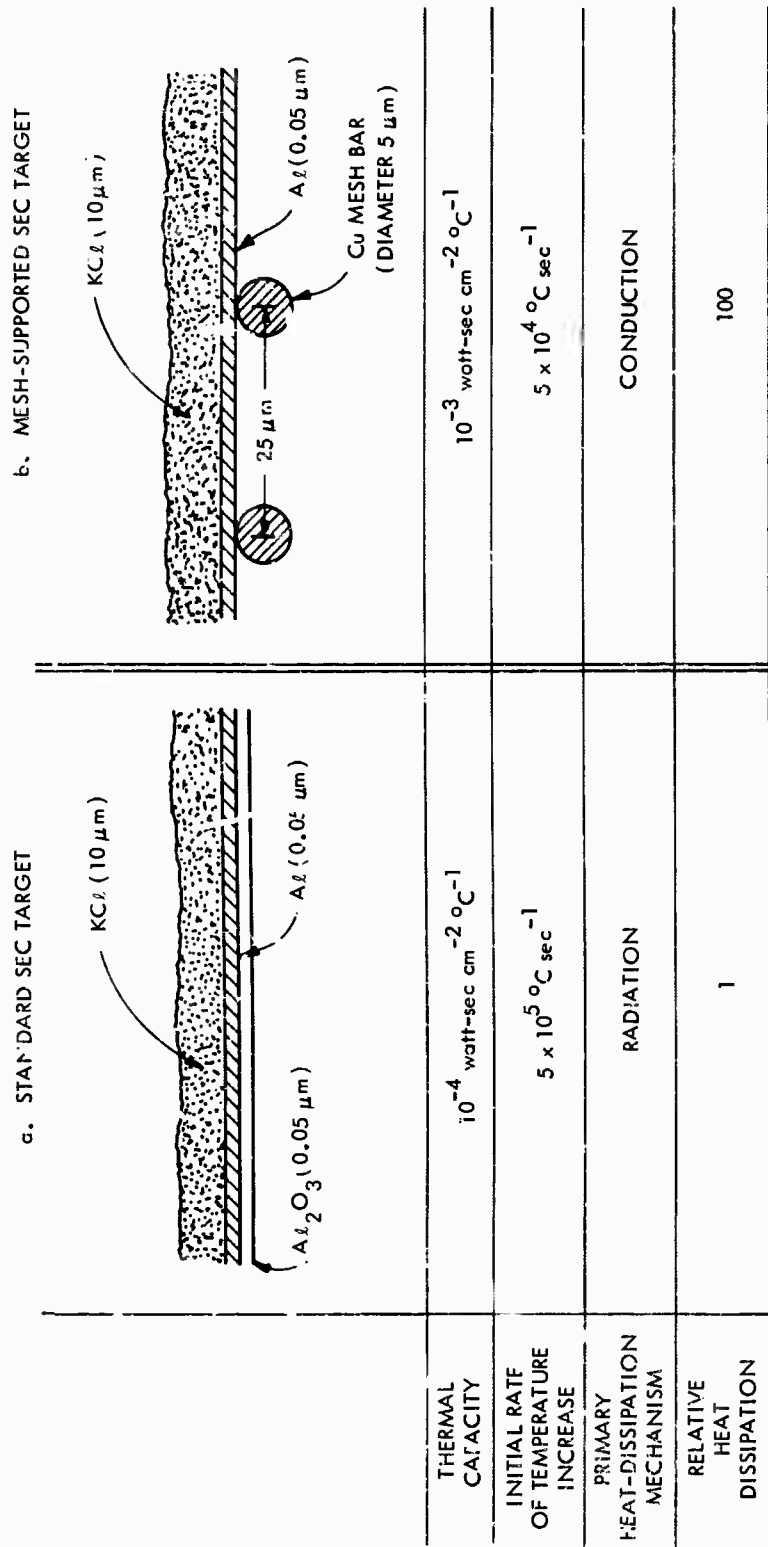
The SEC tube is one member of a general class of sensitive TV camera tubes in which electrons released from a photocathode are accelerated onto a storage target by an electrostatically or magnetically focused image section. Other tubes of this type are the image orthicon,

the isocon, and the SEBIR tube. When these devices are exposed to an intense source of illumination such as an explosion or the sun, very large current densities can be drawn from the photocathode. At these high illuminations photocathode currents of 100  $\mu\text{a}$  can be emitted from image areas a few tenths of a millimeter in diameter, corresponding to photocathode loadings of  $0.1 \text{ amp/cm}^2$ . The electron flux from the photocathode is accelerated by the voltage across the image section, producing an electron beam with a power capable of damaging or destroying the charge storage target. In the case of a photocathode loading of  $0.1 \text{ amp/cm}^2$ , the electron beam in an image section operated at 10 kv will have a power density of  $1000 \text{ watts/cm}^2$ .

The effect of such a power dissipation in the storage target will be to raise its temperature to the point where the input flow of energy is balanced by conduction or radiation of heat. This increase in temperature will occur in all tubes of the general type under discussion. In many cases, the temperature rise is itself sufficient to cause permanent damage to the target. In addition, however, the energetic electrons and the X rays that they produce in the target may also cause nonthermal damage to the target. Thus, either thermal or nonthermal damage or both may occur, depending on the exact nature of the storage target and the intensity of the source imaged onto the tube.

Let us now examine in a more quantitative manner the effects of an exposure to an intense source of illumination. We are concerned here primarily with the SEC camera tube and how it can be modified to offer improved resistance to burn, so this tube will be used as a basis for our discussion.

As can be seen in Fig. VI-1a, the standard SEC target consists of a supporting film of aluminum oxide ( $\text{Al}_2\text{O}_3$ ) approximately  $0.05 \mu\text{m}$  thick, covered with an aluminum (Al) signal plate of the same thickness. Deposited on the signal plate and facing the reading section of the tube is a low-density layer of potassium chloride (KCl) about  $10 \mu\text{m}$  thick.



5-25-71-1

FIGURE VI-1. Comparison of Standard and Mesh-Supported SEC Targets



When the standard SEC target is exposed to an electron flux from the photocathode produced by a source of illumination one or two orders of magnitude higher than the normal peak operating levels, a temporary loss of gain occurs. The result is a dark burn that is believed to be caused by nonthermal effects somewhat similar to the production of color centers in a solid KCl layer. This conjecture is supported by the observation that either exposure of the tube to normal light levels or a heat treatment can remove the burn.

Of a more serious nature and the subject of our present discussion is the permanent white burn produced as exposure levels are increased from four to six orders of magnitude above the normal peak faceplate illumination levels. Consider the specific example of an SEC camera tube exposed through an f/8 lens to the hot filament of a tungsten lamp. The corresponding faceplate irradiance will be approximately  $25,000 \text{ watts/m}^2$ . This is some 5 million times greater than the normal operating levels of the SEC camera tube.

If the power supply of the camera has a low enough impedance, and this is true for the discussions of theoretical and experimental data throughout this section, the current from the photocathode can be calculated from the known photoresponse of the tube unless there are any intrinsic emission limitations. Data discussed later show that for small sources linearity is maintained between faceplate illumination and photocathode current up to loadings of  $0.1 \text{ amp/cm}^2$ .

Thus, in our example a total faceplate irradiance\* of  $2.5 \text{ watts/cm}^2$  incident on a good S-20 photocathode will give a current density of  $10^{-2} \text{ amp/cm}^2$  unaffected by saturation. The image section of the SEC tube is operated at 7 kv, and about 5 kev of the energy of each photoelectron is dissipated in the target, the remaining 2 kev being carried away by the transmitted electrons or being lost by other means. The power density dissipated in the SEC target is therefore  $5000 \text{ v times } 10^{-2} \text{ amp/cm}^2$  or  $50 \text{ watts/cm}^2$  for a tube with a unity-magnification image section.

---

\* From a source such as an open fire or flame.

To evaluate the effect of this power dissipation, it is necessary to examine the thermal characteristics of the standard SEC target. As Fig. VI-1a shows, the thermal capacity per unit area is approximately  $10^{-4}$  watt-sec  $\text{cm}^{-2} \text{ }^{\circ}\text{C}^{-1}$ . A power density of 50 watts/ $\text{cm}^2$  applied to a structure with this thermal capacity will produce an initial rate of rise of temperature of  $500,000^{\circ}\text{C}$  per second. It is clear that most automatic protection systems could not act fast enough to save the tube from damage.

Further analysis shows that in a fraction of a second the temperature of the target reaches the melting point of KCl ( $776^{\circ}\text{C}$ ). Target material leaves the substrate by sublimation and by evaporation, producing a permanent white burn, since the reading beam of the camera tube can now land directly on the signal plate.

Two remedies are available. The first is increasing the thermal capacity of the target to slow down the initial rate of rise of temperature so that protection circuits can be activated. The second, and more important, is increasing the thermal conductivity of the target so that the final equilibrium temperature is reduced to a point where sublimation either does not occur or is a much slower process.

Both of these modifications are present in the second structure shown in Fig. VI-1b. This is the mesh-supported or burn-resistant SEC target, where a fine copper mesh replaces the aluminum-oxide layer used for support in the standard target. As Fig. VI-1b shows, the thermal capacity per unit area of the mesh-supported target is  $10^{-3}$  watt-sec  $\text{cm}^{-2} \text{ }^{\circ}\text{C}^{-1}$ , ten times larger than that of the standard target. Its thermal conductivity is 100 times larger than that of the standard target in which the  $0.05\text{-}\mu\text{m}$  aluminum signal plate is the only layer that contributes significantly to the transport of heat. The other two components of the standard target, the low-density potassium chloride layer and the aluminum oxide support layer, have very low thermal conductivities.

Thus, adding a high-thermal-conductivity mesh with bars  $5 \mu\text{m}$  in diameter has a large impact on the heat transport characteristics of

the target structure. This can be demonstrated by calculating the equilibrium temperatures of the two types of target for the 50-watt/cm<sup>2</sup> power density loading of our previous example. Considering a simplified model where the effects of sublimation and evaporation are neglected, we find that the standard target reaches equilibrium close to 2000°C, heat being dissipated by radiation. The mesh-supported target reaches equilibrium at a temperature below 500°C, and heat is dissipated by conduction.

Because of its increased thermal capacity, the mesh-supported target has an initial rate of rise of temperature of 50,000°C per second, 10 times lower than the standard target. The experimental results to be presented later show that the increased thermal capacity and conductivity raise by a factor of 10 to 30 the exposure required to produce a permanent white burn. In addition, even when the illumination levels are high enough to produce a white burn in the mesh target, no tearing or rupturing of the target, as is sometimes observed with the standard target, can occur. It is important to note that these improvements have been obtained without changing the electrical performance of the SEC camera tube.

Figure VI-2 shows a sample of target-burn test results obtained with a standard SEC tube and with an SEC tube with a mesh-supported target. The lens aperture was f/2. The pictures in Fig. VI-2 show the target-burn observed immediately after the end of each exposure. They were photographed from the monitor with the camera head pointed at a uniformly illuminated grey surface so that both light and dark burns would be recorded. The light sources seen by the camera were arranged in a vertical line. They were as follows:

Top: A 120-v, 100-watt frosted bulb covered with a neutral density filter to yield a source brightness of  $1 \times 10^2$  ft-L. The choice of the bulb-to-camera distance and the focal length of the camera lens gave a circular image at the camera tube with a diameter of 10 TV lines.

SOURCE BRIGHT- NESS, watts/m <sup>2</sup>	EXPOSURE TIME AT f/2 LENS APERTURE						
	1/25 sec	1/5 sec	1 sec	5 sec	30 sec	3 min	15 min
0.5 x 10 <sup>2</sup>							
2.5 x 10 <sup>4</sup>							
0.5 x 10 <sup>7</sup>							

STANDARD SEC TARGET

0.5 x 10 <sup>2</sup>							
2.5 x 10 <sup>4</sup>							
0.5 x 10 <sup>7</sup>							

BURN-RESISTANT SEC TARGET

FIGURE VI-2. SEC Target Burns Produced by Exposing SEC Camera Tube to Intense Sources of Light

Center: A 120-v, 100-watt unfiltered frosted bulb giving a source brightness of  $5 \times 10^4$  ft-L. Same image size as above.

Bottom: The bare filament of a 600-watt tungsten-halogen lamp, the type used on home movie cameras and commonly known as a Sun Gun. This source has a brightness of  $1 \times 10^7$  ft-L. It produced a rectangular image of approximately  $1 \times 4$  TV lines.

Figure VI-2 clearly demonstrates the superior resistance of the mesh-supported SEC target to the development of white burn. With the 50,000-ft-L source, the standard tube suffers a permanent white burn from exposures greater than 1/5 sec. The tube with the mesh-supported SEC target does not show a white burn after a 15-min exposure to the 50,000-ft-L source, and although white burns do occur with the  $10^7$ -ft-L source, they are smaller in area and less objectionable at all light levels. As noted earlier, the mesh support of the burn-resistant SEC target also completely eliminates the possibility of puncturing of the substrate, which can occur in the standard target.

A comparison of the dark burns produced in the two tubes shows that their appearance and intensity do not differ significantly. This similarity of behavior was anticipated in the earlier discussion. All but the most severe dark burns will fade away within periods ranging from minutes to hours if the tube is operated with uniform illumination.

Figure VI-2 illustrates test results for one particular aperture setting, f/2. To obtain data over a wide range of operating conditions, exposures were made with aperture settings from f/2 to f/22 and at a variety of photocathode voltages. In all cases, lower photocathode voltages resulted in reduced burn. This was to be expected, since the power dissipated in the target is directly related to the voltage applied to the image section.

The results for full photocathode voltage (7 kv) are summarized in Fig. VI-3, where the onset of permanent white burn for the two types

of SEC tube is plotted as a function of photocathode illumination and exposure time. Consider the data for the standard SEC tube, shown by the open circles and the dotted lines. The region bounded by the dotted lines marks the transition from an exposure that does not produce a permanent white burn (lower left portion of graph) to an exposure that does produce a permanent white burn (upper right portion of graph). A similar convention applies to the data in Fig. VI-3 for the burn-resistant SEC tube, represented by the filled circles and continuous lines, and also to the data in Figs. VI-5 and VI-6.

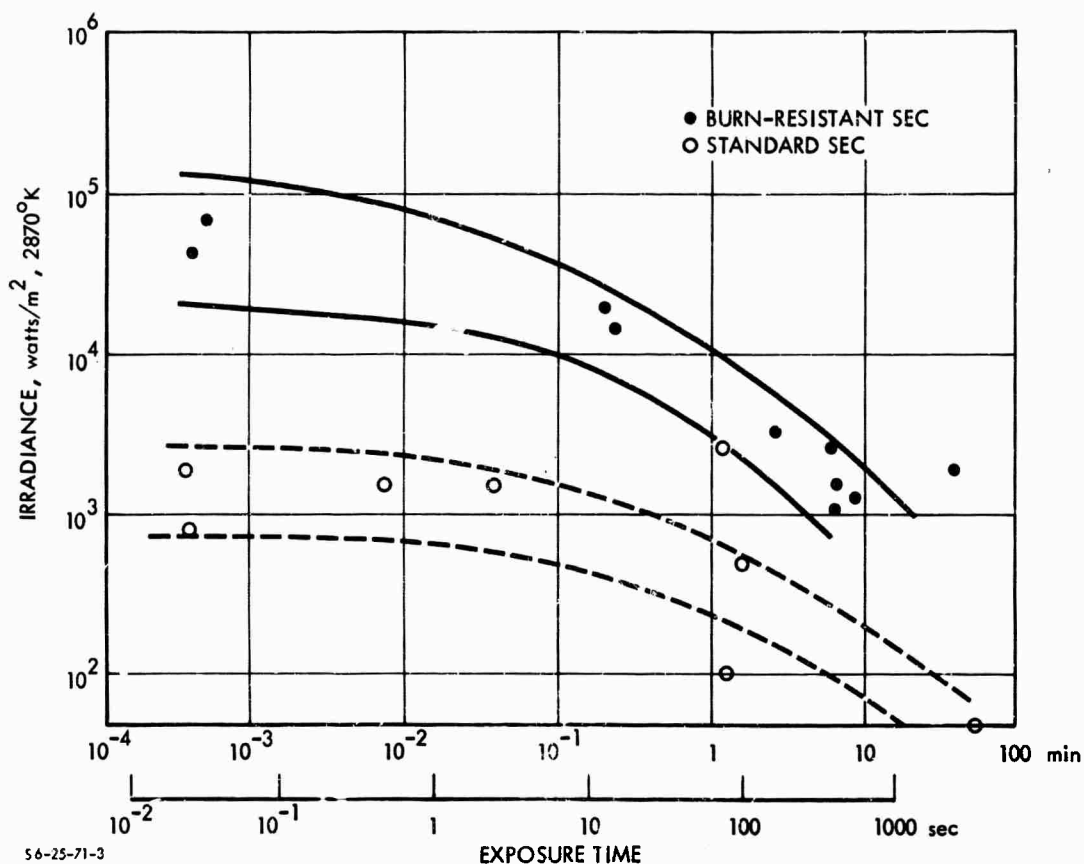


FIGURE VI-3. Onset of Permanent White Burn in Targets of Standard and Burn-Resistant SEC Camera Tubes at Full Photocathode Voltage (7 kv)

Both curves in Fig. VI-3 show a significant deviation from the 45-deg negative slope that would be observed if there were a reciprocal

relation between faceplate illumination and exposure time. In view of the burn mechanism discussed in the previous section, this is not surprising. The sublimation and evaporation processes by which potassium chloride is lost from the target are very temperature sensitive. A modest increase in faceplate irradiance produces a similar increase in target temperature. However, the sublimation and evaporation rates increase exponentially with temperature. Thus, the exposure time required to sublime or evaporate a given mass of potassium chloride (that is, to produce a white burn of given intensity) is reduced by a factor much greater than the corresponding increase in illumination. Examination of Fig. VI-3 shows that the observed burn behavior is in agreement with this analysis of the white burn process.

Of considerable interest during these experiments was the effect of the more intense light levels on the photocathodes of the tubes involved (ten tubes picked at random from a production run). All tubes tested employed S-20 photosurfaces deposited on fiber-optic substrates. Despite the severity of the exposures, amounting in some cases to almost a million footcandles for several minutes, no permanent photocathode damage was detectable at any point in the test program.

The response of the photocathodes of SEC and SEBIR tubes to intense irradiance was studied in a set of auxiliary experiments. The results are shown in Fig. VI-4. In these tests, currents up to 100  $\mu$ a were drawn for several minutes from a photocathode area of about  $6.25 \times 10^{-4}$   $\text{cm}^2$ , approximately the same image size as was used for the burn tests. As Fig. VI-4 shows, photocathode loadings as high as 0.1 amp/ $\text{cm}^2$  were obtained before any significant departure from proportionality between irradiation and photocurrent was observed.

## 2. Target Burn in Camera Tubes Other Than SEC

Experimental work with the SEC tubes stimulated an interest in the light levels at which permanent burns occur in other low-light-level camera tubes. Using the techniques and equipment developed for the SEC test program, similar experiments were carried out with image orthicons (IO) and silicon-electron-bombardment induced-response (SEBIR) camera tubes.

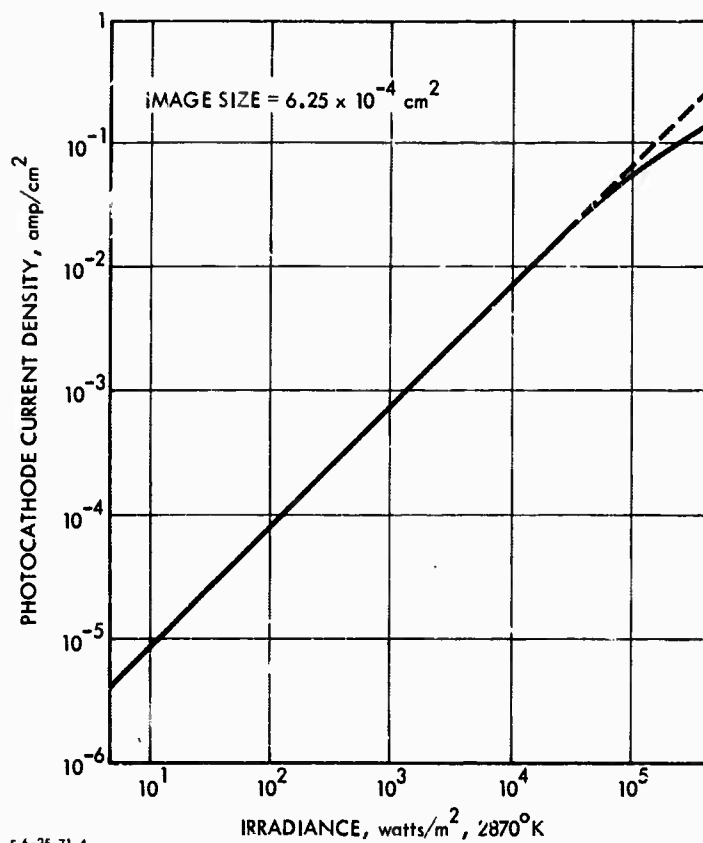


FIGURE VI-4. Proportionality of Response of SEC and SEBIR Tubes to Intense Irradiance

The results for an ionic-conduction, glass-target image orthicon and an aluminum-oxide, thin-film image orthicon are shown in Fig. VI-5. The same convention applies in this figure as in Fig. VI-3. Also shown for comparison are the corresponding curves for the standard and mesh-supported SEC camera tubes.

Damage to the thin-film image orthicon was manifested as a permanent white burn. In the glass-target tube the permanent damage showed up as an intense dark burn. The results in Fig. VI-5 demonstrate that both image orthicons suffered permanent damage at approximately the same exposure levels as the mesh-supported SEC tube. Following the reasoning given previously, the lack of reciprocity of both sets of image orthicon curves suggests that the damage is caused



primarily by a thermal mechanism. In the case of the thin-film image orthicon, puncturing of the target was observed.

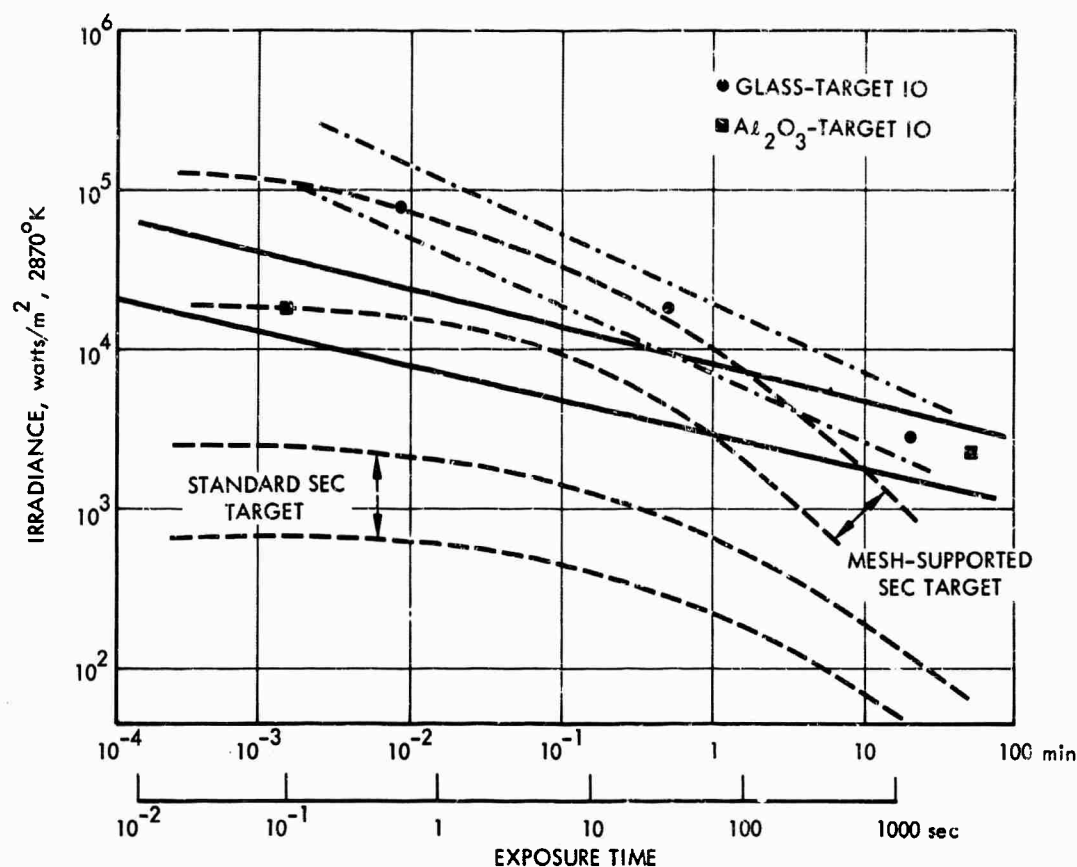
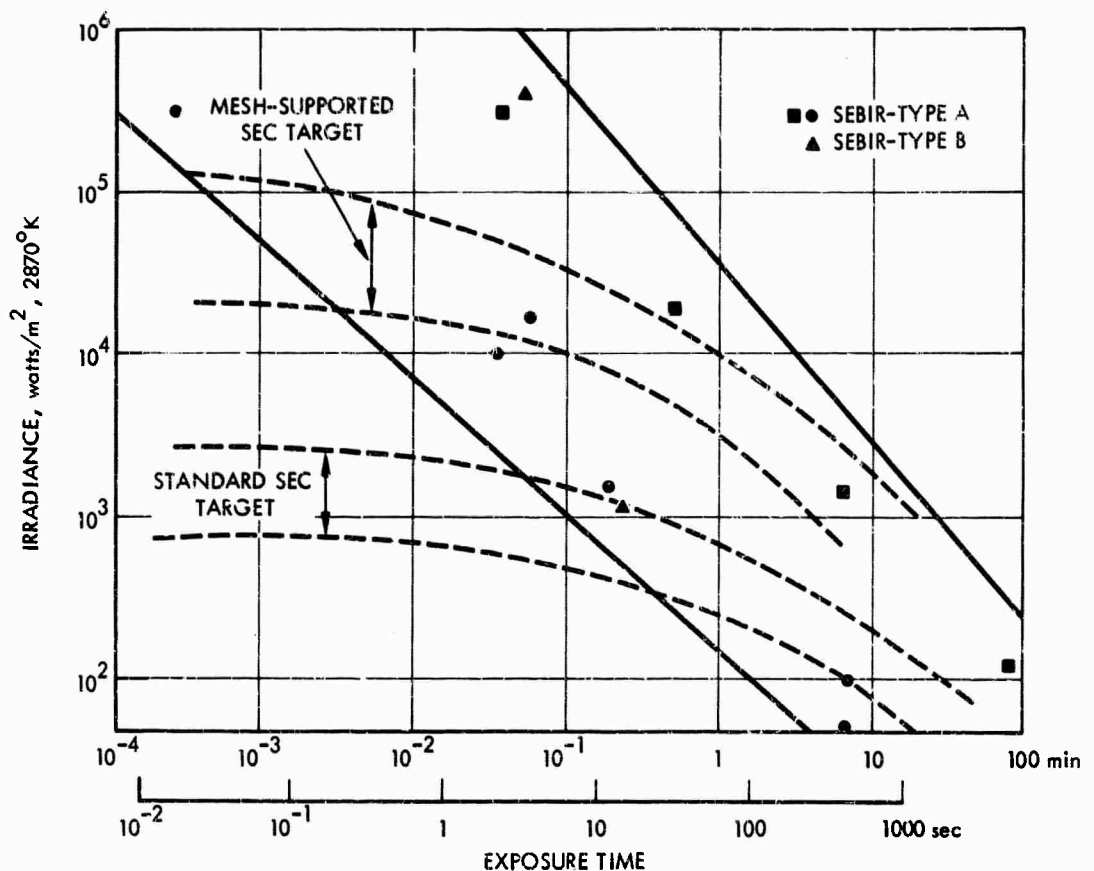


FIGURE VI-5. Onset of Permanent Damage to an Ionic Conduction, Glass-Target Image Orthicon and an Aluminum-Oxide, Thin-Film Image Orthicon. (Corresponding Curves for Standard and Burn-Resistant SEC Camera Tubes are also Shown.)

Figure VI-6 shows the results of burn tests made on three SEBIR camera tubes. In two tubes, labeled Type A on the figure, the diode array was covered by a resistive sea. In the third tube, labeled Type B, no resistive sea was used. In all three tubes, after sufficiently intense exposures, permanent white burns caused by an increased dark current in the burnt area were observed.

There is wide variation in behavior between the burn characteristics of the three tubes. As can be seen, this is not related in any

simple way to the presence or absence of the resistive sea. In the case of the most burn-resistant SEBIR tube (indicated in Fig. VI-6 by squares), the white burn characteristics are comparable to the mesh-supported SEC tube for exposures longer than 1 min but are superior for shorter periods.



56-25-71-6

FIGURE VI-6. Onset of Permanent White Target Burn in Three SEBIR Camera Tubes. (Corresponding Curves for Standard and Burn-Resistant SEC Camera Tubes are also Shown.)

The silicon-diode-array targets used in these tests were obtained from two distinct sources, and no correlation between source and burn characteristics were observed. Burn information on the SEBIR camera tubes of other manufacturers is not incompatible with the data presented here. Because of the wide spread in the data presented and in view of the fact that the SEBIR tube is a relatively recent development,

we believe that further experimentation is required before the burn characteristics of SEBIR tubes can be related to specific aspects of target fabrication and tube processing.

It is significant that the most burn-resistant SEBIR tube shows nearly perfect reciprocity between irradiance and exposure time. As was noted earlier, this strongly suggests a nonthermal cause for the damage. A silicon vidicon, a tube in which the diode array is directly activated by light, was used to test this hypothesis. From the SEBIR results it was known that, for the most burn-resistant tube, a photoelectron flux with a power density of  $200 \text{ watts/cm}^2$  incident on the target would produce a white burn in 1 min.

This power density is equal to that absorbed in the target of a silicon vidicon when the sun is imaged by an  $f/2$  lens. Thus, if the burn in the SEBIR tube is thermal in origin, the silicon vidicon should also show a white burn after a 1-min exposure to the sun at  $f/2$ . This experiment was carried out, and it was found that not only were no white burns produced after 1 min, but no white burns were produced after exposures as long as 20 min. This lends strong support to the conclusion that the damage mechanism in the SEBIR tube is not thermal in origin. After the 20-min exposures of the silicon vidicon, very faint dark burns were observed. This suggests that a different damage mechanism from the one producing white burns in a SEBIR tube is present.

It is known that X rays, produced when the scanning beam strikes the field mesh of a silicon-diode-array tube, cause an increase in dark current by increasing the fast state density at the silicon and silicon dioxide interface (Ref. 2).

Since the white burns produced in the SEBIR tubes by intense exposures are actually localized increases in dark current, it seems likely that an X-ray mechanism is also present here. The 10-keV photoelectrons penetrate the first micrometer of the silicon-diode-array target, producing X-rays with quantum energies ranging from a few electron volts up to 10 keV. Some of the X rays pass through the remaining 10 to 15  $\mu\text{m}$  of the silicon wafer to the gun side, where they

interact with the silicon and silicon-dioxide interface to increase the dark current permanently.

The silicon and silicon-dioxide interface cannot be directly affected by the photoelectrons because they are stopped in the first 1 to 2  $\mu\text{m}$  of the silicon wafer.

Extrapolating the results shown in Fig. VI-6 to normal operating irradiances ( $\sim 5 \times 10^{-4}$  watts/m<sup>2</sup>) suggests that the photoelectron impact process and the associated X-ray production will not be a serious limitation to the operating life of the SEBIR tube.

#### C. THE BLOOMING PROBLEM: LOW-LIGHT-LEVEL IMAGING IN THE PRESENCE OF HIGH-INTENSITY POINT SOURCES\*

Image devices designed to operate under low-light-level conditions are not, in general, capable of imaging points of high intensity within a low-light-level scene without severe spreading of the point-source image into adjacent areas of the scene. This effect is often called blooming. Low-light-level television systems in use today are often of little use in night surveillance of objects in close proximity to bright man-made illumination sources. These point sources--ground fires; flares; shipboard, aircraft, vehicle, or runway lights--often contribute a larger integrated flux level at the sensor than that contributed by the entire remainder of the scene, while providing little appreciable illumination to the objects under surveillance. The flux emitted by such sources is diffused or spread by the atmosphere and the optics. The resulting photocurrent is, in turn, further spread by the electron optics and is scattered and spread at target material of the camera tube. The result is a large signal spread over an area many times larger than the point source, obliterating detail over a significant portion of the picture.

---

\* Sections VI-C and VI-D are abridgements of material reported at the Naval Air Development Center, Johnsville, Pa., principally by Stephen B. Campana.

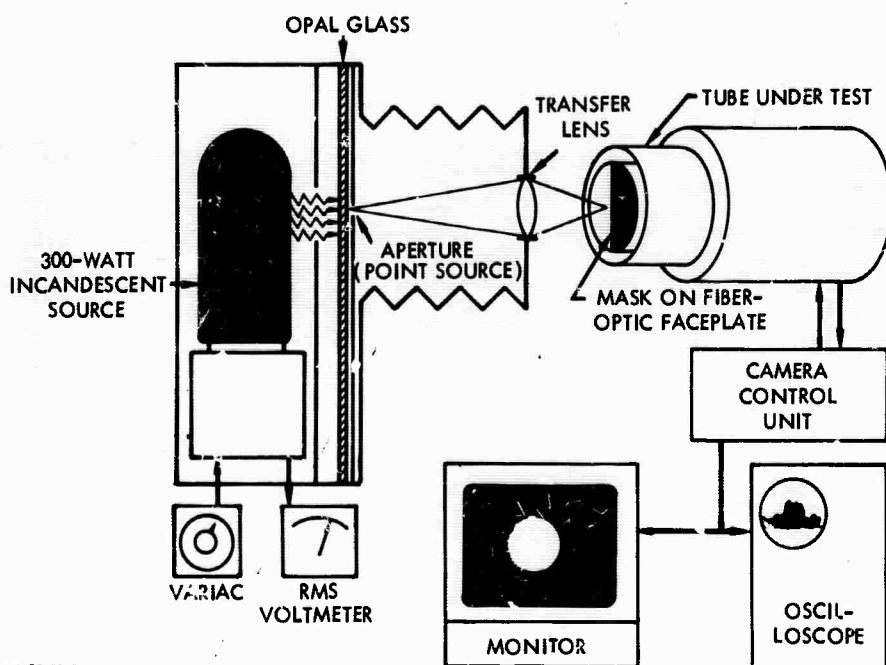
The following material describes the magnitude of the spreading that occurs in practical low-light-level sensors under realistic conditions of local overload. It emphasizes the seriousness of the problem faced by low-light-level technology.

### 1. Typical Flux Levels

The flux collected by a 3-in. f/0.87 lens from various general-service frosted lamps is often at levels as high as  $5 \times 10^{-8}$  to  $5 \times 10^{-7}$  watt in many otherwise low-light-level scenes. It will be shown that such flux levels are intolerable in existing low-light-level sensors.

### 2. Test Procedure

The equipment used to test the ability of camera tubes to contain the image of point sources is shown in Fig. VI-7. Apertures of varied diameter were positioned in front of an opal glass illuminated by a tungsten lamp. The image of the resultant point source was projected onto the faceplate of the sensor under evaluation.



56-25-71-7

FIGURE VI-7. Point-Source Test

Black electrical tape was used as a blocking mask over a portion of the fiber-optic faceplate. This provided a means of detecting any spreading that might have occurred in the projection lens. Flux spread by the lens could be blocked by the tape, while spreading behind the tape could be attributed to the camera tube. It was found in all instances that the lens spreading was negligible in comparison to the camera tube spreading.

The degree of spreading was measured on the oscilloscope and on the video display.

### 3. Test Results

a. Image Orthicon. Image spreading in the image orthicon is caused by several factors. Figure VI-8 is a photograph of the display of an image generated by a General Electric type Z7822 image orthicon. The flux level incident on the orthicon is  $10^{-6}$  watt. The central part of the image is a region of saturation of approximately 30 lines in diameter on a 500-active-line display. This region is surrounded by a black halo caused by redistribution of negative charges on the target area around the image. These redistributed charges neutralize positive charge induced by signal photocurrent, thus erasing the information adjacent to the point source. Further from the central core are rings of signal, apparently caused by the reflection of light transmitted to the inner structures of the image section. These spreading effects were unimpeded by the presence of the tape at the faceplate.

In Fig. VI-9, the diameter of these images is given for various levels of incident flux. The central saturated core did not increase beyond 35 lines, or 7 percent of the picture height. It appeared that further expansion of this core was inhibited by the neutralization effect of redistributed electrons. At flux levels above  $5 \times 10^{-8}$  watt the halo became the dominant effect. At these levels there were enough redistributed electrons to neutralize all but the highest signal levels. At flux levels above  $2.5 \times 10^{-7}$  watt the rings appeared. The signal level of the rings reached 100 na at  $1.5 \times 10^{-6}$  watt.

LIGHT OFF

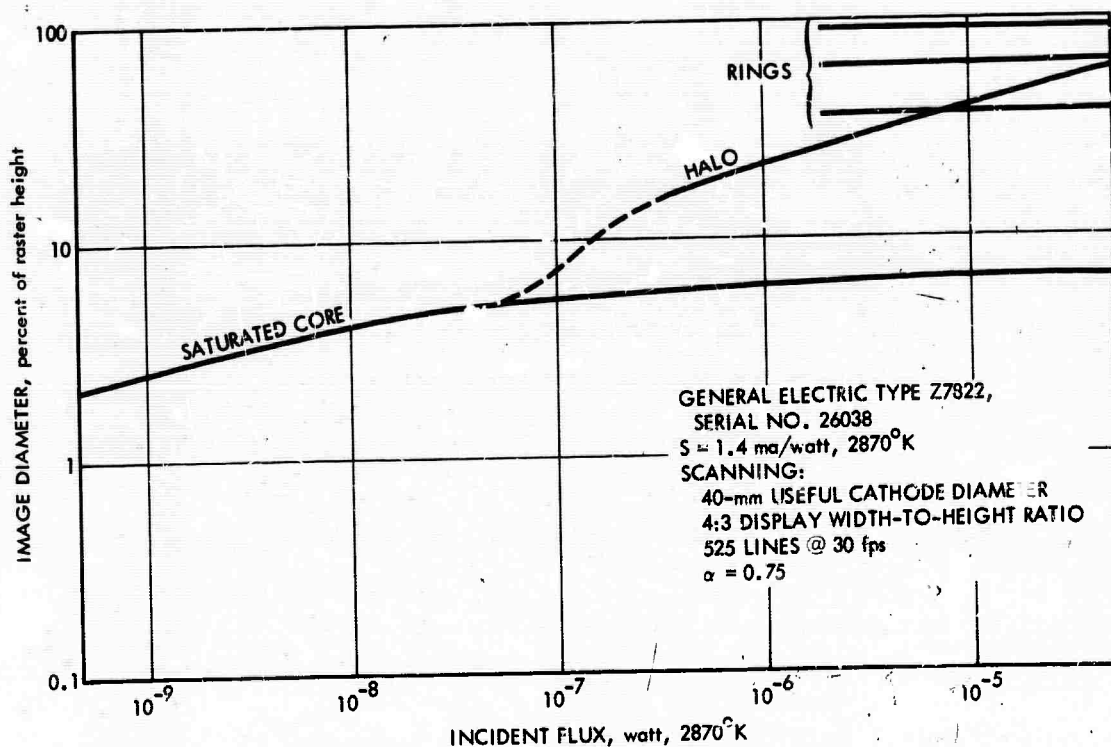
LIGHT ON



NOT REPRODUCIBLE

56-25-71-8

FIGURE VI-8. Image Spreading in 3-in. Orthicon. Flux Contributed by Point Source at Photocathode of General Electric Z7822 Orthicon is  $\sim 10^{-6}$  watt,  $2870^{\circ}\text{K}$



56-25-71-9

FIGURE VI-9. Image Spread in 3-in. Image Orthicon Versus Incident Flux

The performance of the image orthicon under these conditions is further degraded by an effect that does not appear in this data. To discharge the saturated core of the point-source image, the beam current had to be set to discharge 1  $\mu$ a of peak signal. Thus, in the presence of point sources the beam current cannot be reduced to optimize the signal-to-noise ratio of the low-light-level areas of the scene.

After being exposed to the various flux levels used in the evaluation, a negative afterimage of the saturated central area remained on the target. The persistence of this afterimage depended on the duration of the exposure, but it usually lasted several minutes. No permanent changes in the target quality were observed after testing was completed.

b. SEC Vidicon. A Westinghouse WX31189,\* 25-mm SEC vidicon was tested over the same range of incident flux. The line video of the image of the point source was bell-shaped, as indicated in Fig. VI-10. The top of the bell is clipped at a saturation level determined by the target voltage. The diameter of the distribution at various signal levels was measured and is plotted as a function of incident flux. The point-spread function above the 5-na level is extremely steep. Therefore, signal variation induced by scene details adjacent to the high-intensity point source would not be resolvable within the area bounded by the 5-na signal level diameter. Detail between the 1- and 5-na contours would be reduced in contrast to a degree dependent on the relative levels of the signal and stray flux.

It has been suggested (Ref. 3) that the increase in image area is due to the buildup of the "tail" of the point-spread function of the electrostatic image section lens, rather than to lateral leakage in the SEC target. Further investigation is required to determine the exact causes of image spreading in the SEC tube.

---

\* One of the very first SEC tubes that reached operational performance. Currently, the tube is considered obsolete, but it is interesting for the purposes of this analysis.



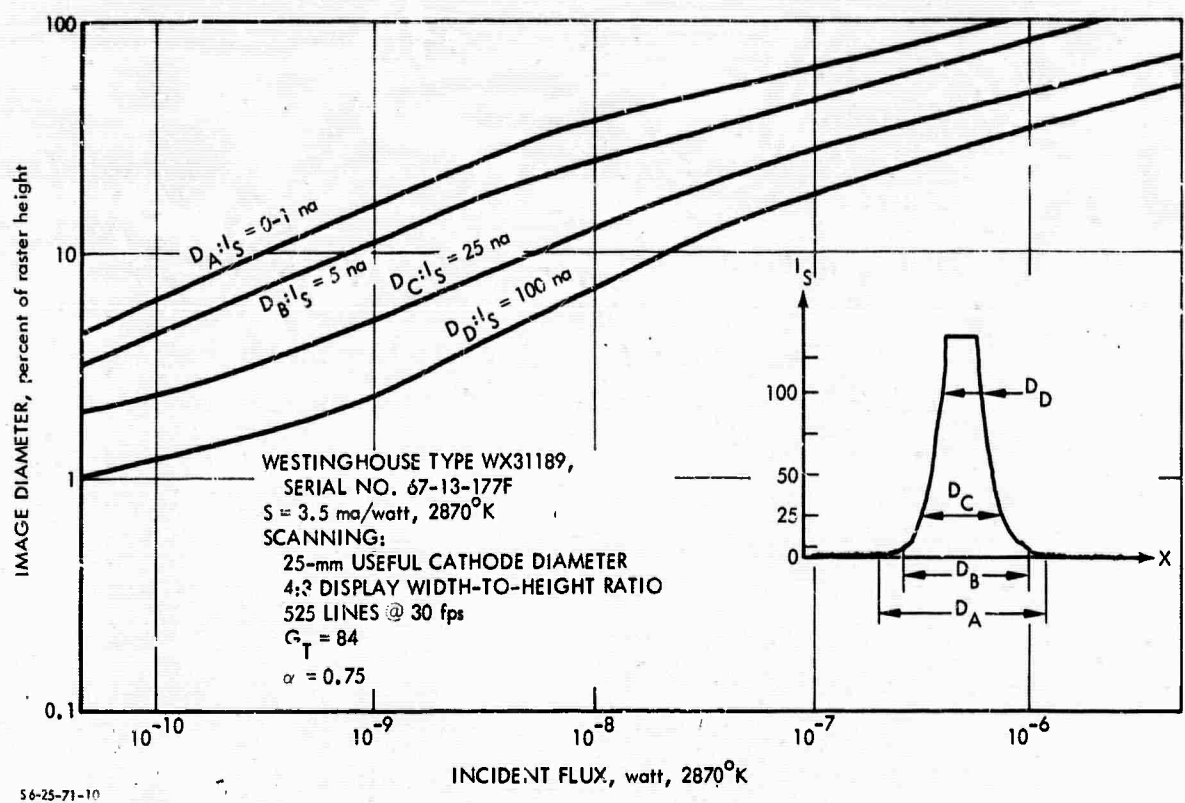


FIGURE VI-10. Image Spread in 25-mm SEC Vidicon Versus Incident Flux

The net effect of spreading in the SEC is that at  $5 \times 10^{-7}$  watt over 50 percent of the picture area is obscured by the point-source image.

Exposure to high flux levels resulted in a dark spot on the SEC target. This spot was visible only when the tube was illuminated, thus it appeared to be an area of decreased target gain. The intensity of the blemish seemed to fade with time. However, after 10 hours the current dip at the blemish was 10 na below a 150-na signal.

c. SEBIR Camera Tube [The RCA Silicon-Intensified-Target (SIT) Camera Tube]. The low-light-level performance characteristics of an RCA C21117B 40-mm SEBIR silicon-diode-array camera tube have shown that the tube has exceptional properties as a low-light-level sensor.

However, as with the other tubes, its performance is seriously degraded by its inability to contain point-source images. Figure VI-11 illustrates the progression of image spread at the silicon-diode-array target as the intensity of the point source is increased. It can be seen that the image spreads in a well-defined circle. Within the circle the signal current reaches the limit set by the beam, while the area outside the circle is dark except for the small signal induced by stray flux at the photocathode. In Fig. VI-12 the size of the point-source image is plotted as a function of the total incident flux contained in the image at the photocathode. At flux levels below  $5 \times 10^{-12}$  watt the diameter varies as the square root of the flux; thus, the area of the image increases in direct proportion to the intensity. It appears that this spreading occurs in the common substrate of the silicon diode target. As diodes in the vicinity of the point source become saturated, holes will diffuse laterally until they are swept across the reverse-biased junction of the nearest unsaturated diode. This abrupt circle of saturation is, therefore, caused by the switching of the diodes from a reverse-biased to an unbiased mode.

Beyond  $5 \times 10^{-11}$  watt the rate of spreading decreases and eventually approaches zero. This deviation from the half-power slope is due to bulk recombination in the substrate. While the holes are prevented from returning to the surface of the target by the  $n^+$  coating, they are still subject to the slower recombination rate in the bulk material. As flux increases, holes must travel longer distances in the substrate to reach back-biased diodes. At high flux levels a large proportion of the holes recombine, thus reducing spreading. In Fig. VI-13 an expression describing the balance of charge flow in the silicon target at equilibrium is developed. Values for the constants  $K$  and  $L_p$  have been calculated by using the empirical data. It should be noted that the derived value of  $L_p$  is higher than that usually associated with silicon. This may be due to the fact that little surface recombination is permitted by the  $n^+$  coating. Bulk recombination occurs much more slowly than surface recombination.



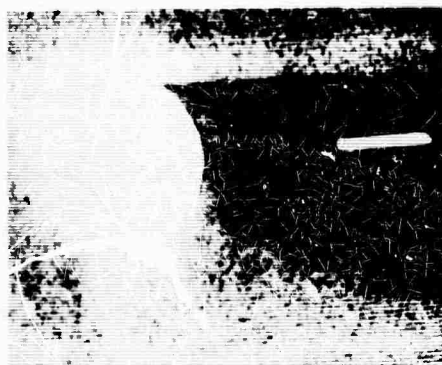
Spread Image Diameter: 4 TV lines  
Flux Level:  $5 \times 10^{-13}$  watt,  $2870^{\circ}\text{K}$



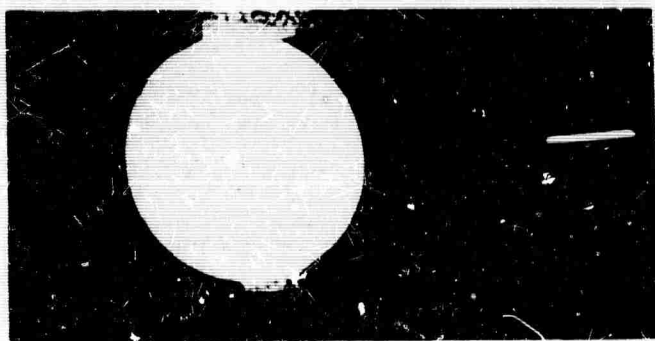
Spread Image Diameter: 13 TV lines  
Flux Level:  $1.5 \times 10^{-11}$  watt,  $2870^{\circ}\text{K}$



Spread Image Diameter: 31 TV lines  
Flux Level:  $1.5 \times 10^{-10}$  watt,  $2870^{\circ}\text{K}$



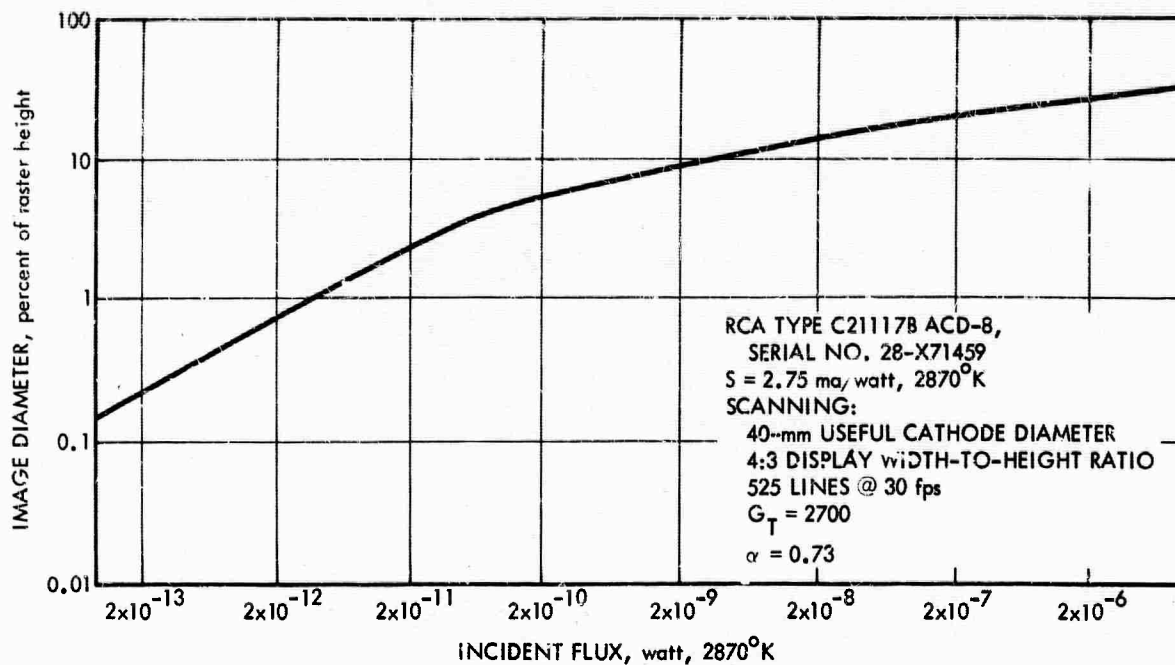
Spread Image Diameter: 62 TV lines  
Flux Level:  $3 \times 10^{-9}$  watt,  $2870^{\circ}\text{K}$



Spread Image Diameter: 95 TV lines  
Flux Level:  $3.5 \times 10^{-8}$  watt,  $2870^{\circ}\text{K}$

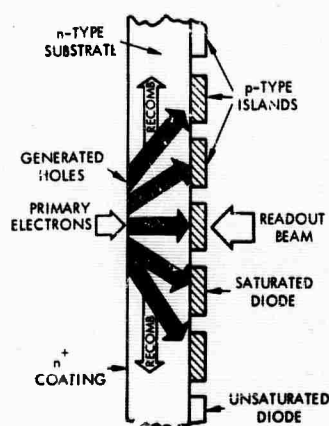
NOT REPRODUCIBLE

FIGURE VI-11. Image Spreading in 40-mm RCA SEBIR Camera Tube



56-25-71-12

FIGURE VI-12. Image Spread in 40-mm RCA SEBIR Camera Tube Versus Incident Flux



IN EQUILIBRIUM,  
 $Q_{IN} = Q_{BEAM} + Q_{RECOMBINATION}$   
 BUT  $Q_{RECOMBINATION} = Q_{IN} (1 - e^{-x/L_p})$   
 $\therefore Q_{IN} e^{-x/L_p} = Q_{BEAM}$  OR  
 $GSE A_T e^{-x/L_p} = I_{BEAM} \pi r^2 / A_T$   
 LET  $R = e^{-x/L_p}$ , THEN  $r = (GSE A_T / I_{BEAM} \pi)^{1/2}$   
 OR  
 $F = EA = (I_{BEAM} \pi r^2 / GS)^{1/2} \pi r^2 / L_p = K r^2 \pi / L_p$   
 FOR TEST DATA:  $K = 5 \times 10^{-4} \text{ watt/m}^2$   
 $L_p = 0.2 \text{ mm}$

DEFINITION OF TERMS			
A	ILLUMINATED AREA	$L_p$	DIFFUSION LENGTH OF HOLES
$A_T$	SCANNED TARGET AREA	r	RADIUS OF SPREAD
E	PHOTOCATHODE ILLUMINATION	S	PHOTOCATHODE SENSITIVITY
G	TARGET GAIN	t	INTEGRATION TIME
$I_B$	BEAM CURRENT	$\alpha$	SCAN EFFICIENCY

\*CONVERTED FROM  $K = 6 \times 10^{-6} \text{ lumen/in.}^2$  AND  $L_p = 0.009 \text{ in.}$ ,  
AS ORIGINALLY REPORTED.

FIGURE VI-13. Image Spreading in the Silicon Diode Array Target

The expression developed exactly fits the measured data. In Fig. VI-12 the spreading that might be expected in a target material with a shorter recombination time is shown. Recombination lengths shorter than one mil would reduce gain to unacceptable levels.

After the point-source testing of the SEBIR tube, some permanent target deterioration was observed. The deterioration, in the form of an increase in localized dark current, occurred after repeated exposure to the flux levels in the range of Fig. VI-12. The highest flux density used in all of the point-source testing was  $\sim 4.5$  watts/ $m^2$  at the photocathode. The dark current variation was less than 5 na and did not seriously impair the quality of the imagery.

d. Comparison of Results. In Fig. VI-14 the results presented previously are combined. Since each of the tubes tested had a different photocathode sensitivity, the spreading diameter is presented as a function of photocurrent rather than of flux. (A photocathode with a sensitivity of 2.0 ma/watt will generate  $10^{-10}$  amp for  $5 \times 10^{-8}$  watt at 2870°K.) It can be seen from these data that the problem in each of the tubes is of sufficient magnitude to merit concern.

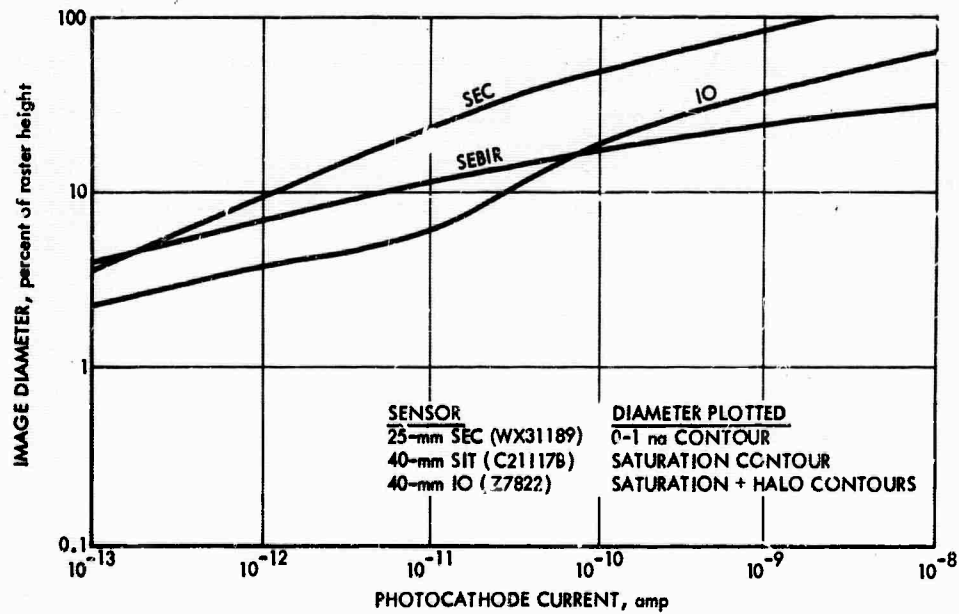


FIGURE VI-14. Point-Source Image Spread in LLL TV Camera Tubes

#### D. VARIOUS SPREAD EFFECTS IN SEBIR TUBES

The image spreading problem is further increased by the addition of a multielement, large-aperture lens. While image spreading occurs to some degree in every optical and electrooptical image transfer stage in every image device, there are three prime contributors of image spread in the SEBIR camera tube: (1) stray flux in the image section, (2) lateral target leakage, and (3) inversion.

##### 1. Stray Flux (Light Feed-Through) in the Image Section

The silicon-diode-array target material is, of course, photo-sensitive. Thus, in a SEBIR tube, precautions must be made to prevent radiation in the spectral range of silicon from reaching the target. Radiation from an inadequately shielded filament could, for example, raise the dark current of a SEBIR tube. Also, light passing through the semitransparent photocathode could conceivably reach the target and produce a spurious signal. Under average conditions, where the intrascene brightness range is not excessive, the true signal, produced by the SEBIR process, will completely mask this stray signal. However, when there is a small point of high intensity within an otherwise low-light-level scene, flux from the image point at the photocathode passes through the photocathode, and a substantial proportion may reach the target and drastically reduce contrast in areas surrounding the point. The fraction of this flux that reaches the target is reduced by the electron-optics elements of the image section. In particular, the aperture in the anode cone acts like a pinhole, imaging the flux pattern on the photocathode onto the target. Tubes whose electron optics designs utilize a very small anode cone aperture will, of course, transmit a very small proportion of stray flux to the target. Another effective means of preventing stray flux from producing a spurious signal is to add a buffering layer to the n-type substrate at the input side of the target.

The first SEBIR tubes built by RCA did not have the buffering layer. However, the triod electron lens used in the image section has a very small anode cone aperture, and there was little evidence of

stray flux in the early tubes. The buffering layer was added later to increase the gain control range. Until very recently, Westinghouse SEBIR tubes did not use a buffering layer. Their anode cone aperture was large enough (about 1/4 in. in diameter) to pass considerable stray flux to the target. Thus, the image of a point light source produced by these tubes was characterized by a halo of signal around a central saturated core (Ref. 4). A buffering layer has now been incorporated into the Westinghouse tubes, and some consideration is being made to decreasing the size of the anode cone aperture. Phillips tubes currently do not use a buffering layer.

## 2. Lateral Target Leakage

The most important component of image spread in silicon target tubes is lateral hole diffusion in the common substrate of the silicon target array. This mechanism has been completely described and modeled in Ref. 5. Carrier recombination serves to limit this effect. The recombination length exhibited by the Westinghouse tube reported in Ref. 4 was somewhat shorter than that of the RCA tube reported in Ref. 5. Phillips and Hughes claim to have tubes whose target structure provides a degree of diode isolation in the substrate, thereby inhibiting lateral spread and reducing the effective diffusion length. A program to reduce lateral silicon target spread has been initiated by the Army Night Vision Laboratories.

## 3. Inversion

The inversion process is characterized by an uncontrolled charge spreading under the silicon-dioxide layer on the readout side of the target. This effect is described in detail in Ref. 6. In brief, when a large voltage difference exists between adjacent diodes, an inversion layer forms under the oxide, thus shorting the originally isolated diodes. A large voltage difference occurs when a high signal is induced on a part of the target, while the remainder of the target is unaffected. The diodes in the signal area are discharged during the scanning cycle, thus reaching a voltage near the target bias potential. The unexposed diodes remain near gun potential. Thus, the maximum

potential between diode elements is the difference between the target bias and gun potential, the latter of which is usually at ground potential. Shorted diodes are a prime target for inversion. However, one cannot assume that because inversion has not occurred around blemishes it will never occur. Most defective diodes have sufficient resistivity to prevent the p-type island from reaching maximum target potential. However, a high-intensity point source completely saturates diodes in an area around it. At the boundary of this area, the maximum lateral voltage difference exists, and inversion could occur. When inversion does occur, an irregular area spreads outward from the point until discontinuities in the target structure halt its growth. When the target bias potential is gradually lowered, a point is reached where inversion cannot occur, and the spread image abruptly switches from a large irregular oval shape to a smaller regular circular area concentric with the point. For the Westinghouse SEBIR tube reported in Ref. 4, this switch occurred at about 12.5 volts, although the manufacturer recommended operation at 15 volts. To avoid the extreme spreading effects of inversion, tubes should be operated at a target potential below the breakover point. In some tubes, the lag experienced at the reduced target potential may be excessive. Therefore, lag, dark current, and image spreading should be specified at a fixed target potential. RCA targets utilize a "conductive sea" structure, and are therefore not susceptible to inversion. Among "resistive sea" type tubes, it is expected that a wide variation of inversion characteristics will be encountered.

#### 4. Summary

To summarize briefly, three prime contributors to image spreading in SEBIR tubes are (1) stray flux in the image section; (2) lateral charge leakage in the target substrate; and (3) inversion. Stray flux can be adequately controlled by depositing an opaque layer on the input side of the target. Inversion can be avoided by using "conductive sea" targets, or by carefully selecting "resistive sea" targets with regard to their inversion properties. Lateral charge leakage remains a problem to be solved by modification to the target structure.



These effects must be considered when tube specifications are written. Specifications that define the ratio of acceptable image growth for a given set of point source intensity conditions do not adequately reflect the physical characteristics of the SEBIR camera tube. The image diameter at no less than two signal levels should be specified for a given input image size and at an intensity several orders of magnitude above the saturation point.

The following image spreading specification has been used in a contract for a 25-mm SEBIR tube:

"The spreading of the image of a point source whose intensity is sufficient to saturate the target locally shall fall within the following constraints:

1. No spreading due to an inversion in the silicon dioxide layer shall occur at the rated target voltage.
2. The signal current produced by image spreading in the camera tube shall not exceed 5 na outside a diameter around the center of the image that is 25% of the picture height and 50 na outside a diameter that is 20% of the picture height, when a circular image less than .02" in diameter is incident on the tube faceplate with an intensity sufficient to provide 15 na of primary photocurrent.
3. Spreading measurements shall be done with the same tube operating voltages as used in making all other measurements."

The above specification may not be greeted eagerly by all tube manufacturers. Depending on his application, a buyer may wish to relax the specification in some respects. However, this specification takes into consideration all of the SEBIR characteristics, and leaves no room for surprises upon receipt of the tubes. A specification of this kind must be flexible and must be tightened to reflect improvements in silicon diode array technology as they are made.

## PART VI. REFERENCES

1. Lucien M. Biberman and Sol Nudelman, eds., Photoelectronic Imaging Devices, Vol. 2, Chapter 10, Plenum Press, New York, N.Y., 1971.
2. L.H. von Ohlsen, "Soft X Ray Effects Upon Silicon-Diode Arrays Aged in Camera Tubes," IEEE Journal of Solid-State Circuits, Vol. SC-5, No. 5, pp. 261-265, October 1970.
3. R.R. Beyer, M. Green, and G.W. Goetze, "Point Source Imaging with the SEC Target," Advances in Electronics and Electron Physics, Vol. 22A, p. 251, Academic Press, New York, N.Y., 1966.
4. Naval Air Development Center, Test and Evaluation of the Westinghouse WX31792 Electron Bombarded Silicon Camera Tube, Technical Memorandum ADC:AEYE:SBC, in preparation.
5. Stephen B. Campana, Naval Air Development Center, Low Light Level Imaging in the Presence of High Intensity Point Sources, personal communication, August 1970.
6. M.H. Crowell and E.F. Labuda, "The Silicon Diode Array Camera Tube," The Bell System Technical Journal, May-June 1969.

## VII. SOME BRIEF COMMENTS ON IMPORTANT TUBE PARAMETERS AND THEIR SPECIFICATION

by Lucien M. Biberman

In an effort to better relate specifications and performance, it is now necessary to admit that the military application of low-light-level television is different from the use of commercial studio television cameras in bright white light.

### A. SIGNAL-TO-NOISE DEPENDENCE ON SPECTRAL COMPOSITION

A meaningful specification of the performance of camera tubes must be based on S/N at the display versus spatial frequency (Fig. VII-1) when flooded by irradiance of a known spectral composition at a known power level. It makes no sense to calibrate a camera with visible light of some given spectral distribution and use it with some other kind of distribution, i.e., invisible (covert) irradiance.

### B. SIGNAL-TO-NOISE VERSUS LIMITING RESOLUTION

It has been shown that probability of detection is related to the signal-to-noise ratio as a function of spatial frequency at the display and is in general not determined by "limiting resolution."

### C. SPECTRAL RESPONSE

If broad-band spectral sensitivity is desired, and it is often useful for quality control or rough comparative calculations, one should specify the performance in terms of a known distribution source and bandwidth, i.e., a 2854°K source between 0.6 and 0.95 micron. Such a specification permits one to compare tubes in the region of interest. Thus, one might quote a response of 3 ma/watt of 2854°K radiation between 0.6 and 0.95 micron as a somewhat useful criterion

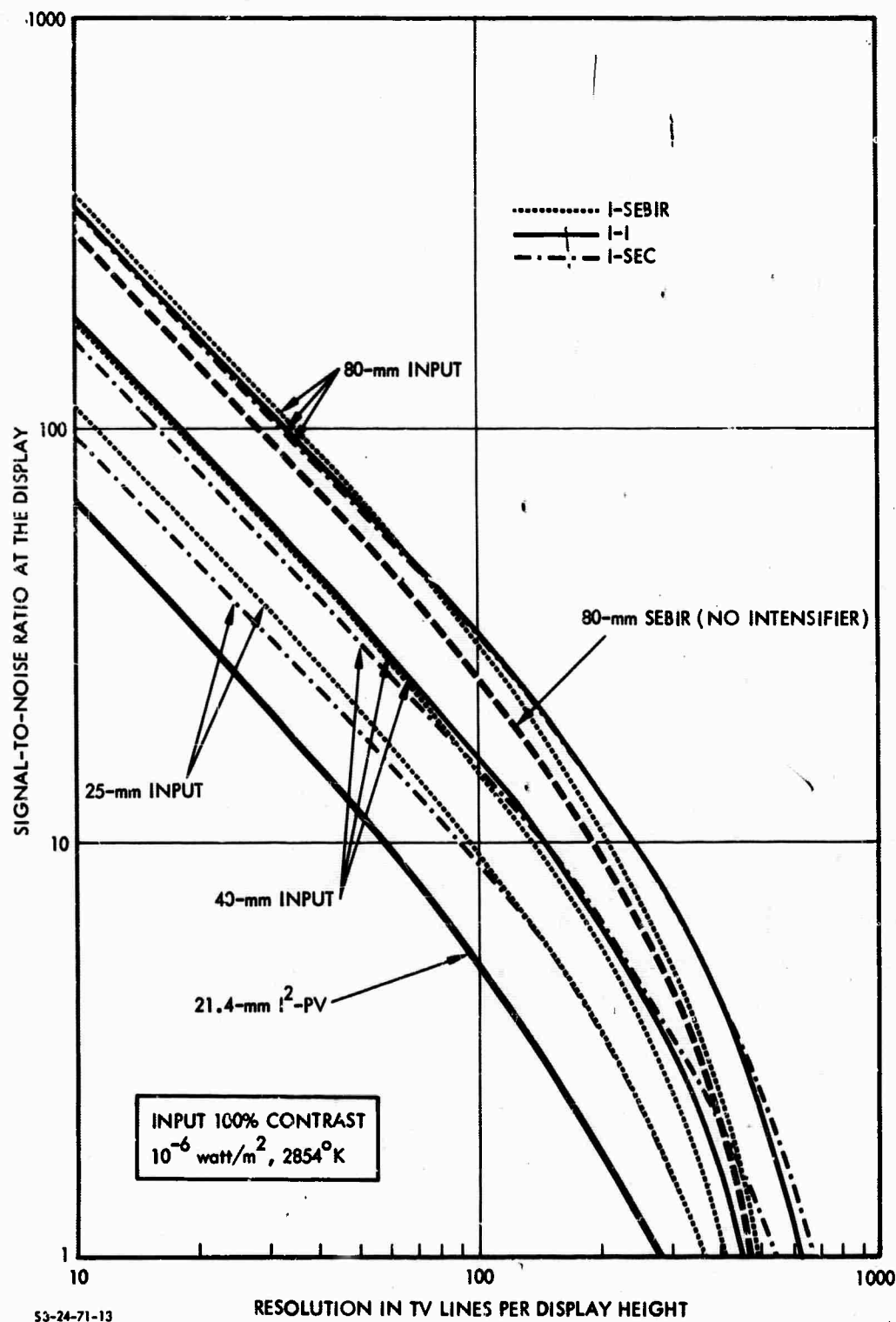


FIGURE VII-1. The Performance of Some Tube-Intensifier Combinations

for tubes to be used with that sort of irradiance.\* Under many conditions a source of  $2000^{\circ}\text{K}$  may be appropriate, while under other conditions a source or a source plus a filter to yield a distribution of  $4000^{\circ}\text{K}$  or even  $5000^{\circ}\text{K}$  may be appropriate.

The usual values of microamperes per lumen that are used in commercial broadcast television do not offer much help or guidance in evaluating tubes to operate under natural levels of light distribution from the night sky. They make even less sense when used with camera tubes that see by reflected laser radiation in the near infrared, where, by definition, there are no footcandles.

If the anticipated application for a device is under a moonless night sky, an appropriate test source would be a  $2000^{\circ}\text{K}$  source. On the other hand, if the night sky is moonlit, a more appropriate test source would be  $5000^{\circ}\text{K}$ . At any rate, the universal  $2854^{\circ}\text{K}$  test lamp is useful only for arbitrary quality control and does not lend insight into performance in actual applications.

#### D. SENSITIVITY AND RESOLUTION

Sensitivity and resolution must not be quoted as two independent parameters. Rather, one should specify  $\text{SNR}_D$  as a function of spatial frequency for a number of light levels. The actual data required are data of the form of Fig. VII-1. For more limited appraisals one can use an approximation to  $\text{SNR}_D$ , i.e.,  $I_S R_w(N)$ , where  $I_S$  includes the cathode response and tube gain factors while  $R_w(N)$  is the spatial frequency response of the tube. One may well compare tubes on the basis of this factor of merit as long as comparison is made at the same specific value of input illumination and the same specific value of resolution.

---

\* Spectral distributions for real and standard sources are given and discussed in Ref. 1.

## E. LAG EFFECTS

In some tubes, lag is an asset for some important application, while in others it is the chief demerit. Needs in this area are not clearly defined, and only interim methods are available for measurement and characterization.

An analytical description of capacitive lag has been available since 1957 (Ref. 2) and it has been used within the last year (Ref. 3) to predict in accurate quantitative detail the lag performance of a particular camera tube for a wide variety of conditions. Capacitive lag requires two parameters for its description--one electron gun parameter and one target parameter. Lag in the target or from the phosphors in an intensifier can also be described by two parameters since they are also in general hyperbolic decays. There is no big theoretical problem in handling lag--it is a people problem. As long as people insist on trying to describe a multiparameter phenomenon with one number there will be a problem in describing lag and camera tube systems in general.

Lag is troublesome in moving scenes. Lag causes image smear. It deteriorates aperture response,  $SNR_D$ , and image quality. It is a fuzz factor. Like most fuzzy things, it has as yet no good metric.

In a recent paper (Ref. 4) Otto Schade has summarized the most important factors governing the performance of high definition electro-optical systems. That most excellent paper applies quite broadly to such systems, even though its emphasis is on the ASOS surface vidicons. We have therefore included an abridged portion of that paper as part of these comments to indicate the use of the preceding equations and calculations in Part V.

In the following material Schade points out that the basics of high-definition systems at lower light levels lie in storage of sufficient signal in a suitable charge storage surface. He goes on to

relate the characteristics of the storage surface to readout time. This treatment, along with the Redington paper (Ref. 2), helps in understanding the lag problem.

**T**HE PRINCIPAL purpose in most applications of a high-definition imaging system is the detection and recognition of the fine structure of small objects over a large range of object contrasts.

A low-noise system having a moderately good frequency response can provide the same resolving power as a system having a considerably higher frequency response and higher noise level, particularly at low object contrasts.

High signal-to-noise ratios in small areas require, in principle, a high particle, or quantum, density, i.e., a large number of photons, electrons, or grains per unit area. It follows that high resolution can be obtained at very low levels of illumination only by long time exposures and accumulation of quanta in a suitable storage surface. Therefore, when the gain of a system is increased by the addition of multiplier or intensifier stages to compensate for reduced photon\* input (for low light-level operation), the resolving power of a theoretically perfect system decreases. However, because a practical system contains additional noise sources that may limit performance more than noise in the photon conversion process, the resolving power of a practical system may be increased at low light levels. The usefulness of signal-intensifier stages depends on the location and value of the noise sources in the system. It further depends on the frequency characteristic of the intensifier stage, which must be considerably better than that of the remaining system elements in order not to offset a decrease in overall noise by a decrease of high-frequency signals.

The calculated values of resolving-power functions can be used to predict the performance of an imaging system and evaluate proposed changes in system elements intended to improve the sensitivity or the general performance of the system.

The resolving power of the storage surface in television cameras is basically independent of area. However, the observable resolving power may be a function of area because it depends on the parameters of the camera, that is, the optics used for exposure, the electron optics required for signal readout, and the signal development process, which are generally functions of area ( $X, Y$ ) and time. The development of a signal, for example, requires a certain time for each square millimeter of the storage surface. Thus, the sequential signal development in a television camera requires a read-out time proportional to the number of square millimeters in a given storage surface.

The time required for reading out a unit surface area ( $1 \text{ mm}^2$ ) is a function of the unit capacitance, the charge potential, and the  $V/\epsilon$

---

\* Photon in this paper is used as a unit of radiation energy. It is not meant to imply a "noisy" flow of random quanta.

characteristics of the reading beam. To clarify the dependence of sensitivity, conversion efficiency, and resolution on the time-to-capacitance ratio  $t/C$ , and to avoid misinterpretation of the resolving-power functions computed subsequently for specific operating modes, a discussion of the signal read-out process is appropriate.

### 1. Characteristics of Charge Storage Surfaces

The storage surface of a television camera tube is charged and discharged by essentially constant currents. The charge  $q_{(1)}$  in a unit area of storage surface is given by

$$q_{(1)} = C_{(1)} V = i_{s(1)} t, \quad (15a)$$

and the electron density is given by

$$n_{(1)} = q_{(1)} / q_e, \quad (15b)$$

where

$q_{(1)}$  = charge/mm<sup>2</sup> (coulombs),

$C_{(1)}$  = capacitance/mm<sup>2</sup> (farads),

$V$  = potential (volts),

$i_{s(1)}$  = mean current density (per mm<sup>2</sup>) during time  $t$

$q_e = 1.6 \times 10^{-19}$  = charge of one electron.

The electron or charge density in the storage surface is built up by a current ( $i$ ) during a short exposure time  $t = t_e$ . This charge potential can be removed or read out by an identical current when the read-out time  $t_r$  equals  $t_e$ , or by smaller or larger currents when  $t_r$  is made correspondingly larger or smaller than  $t_e$ .

The maximum charge potential that can be read out by a low-velocity electron beam is generally limited to  $V_{\max} = 6$  volts, because of electron reflection and secondary emission at the storage surface. (This value may be somewhat higher for very porous surfaces and lower for smooth surfaces, and it decreases for high field gradients.) For high-definition signals, the value of the read-out current is limited to less than 200 nA because of the increasing spread of electron velocities with current density. Therefore, in high-definition storage surfaces, which must have a high unit capacitance and a large surface area, the minimum read-out time may be in the order of seconds.

The unit capacitance  $C_{(1)}$  required for a storage surface having the resolving power of high-resolution aerial film (470 cycles/mm for Kodak type 4404) can be determined from the noise equivalent particle density of this emulsion, which has the value  $\bar{n}_{s(1)f} = 1.0 \times 10^7$  electrons per mm<sup>2</sup> at maximum resolving power.<sup>1</sup> Because of the added beam-current noise in the television read-out, the equivalent electron density must be approximately 5 times this value, that is,  $\bar{n}_{s(1)f} \approx 5 \times 10^7$  electrons/mm<sup>2</sup>. This value represents the equivalent charge density of



Table I—Approximate Characteristics and Minimum Readout Times of Charge Storage Surfaces ( $V = V_{max}$ , 90% Discharge)

Type of Surface	Equiv. Thickness (microns)	$C_{eq}$ (pF)	$n_{eq}$ /volt	Charge Potential $V_{max}$	Readout Time* $t_r$ (Sec) ( $A=1\text{ cm}^2$ ) ( $A=25\text{ cm}^2$ )	
4404 Film	2	8	$5 \times 10^7$	4.25	0.0345	0.86
ASOS photo-conductor	1	160	$1 \times 10^8$	6	0.385	9.60
		80	$5 \times 10^8$	6	0.192	4.8
Porous photo-conductor (Vidicon)	4	10	$6.25 \times 10^7$	6	0.024	0.60
Plumbicon	14.3	3.7	$2.3 \times 10^7$	6	0.0089	Insuff. storage
S.E.C. (Westinghouse)	12	0.8	$5 \times 10^6$	6	0.0019	0.0475
Glass Target Image Orthicon	25	0.35	$2.2 \times 10^6$	4	0.00158	0.0395

\*  $t/C = 24$  for  $V_{max} = 6\text{ V}$   
 $t/C = 45$  for  $V_{max} = 4\text{ V}$

the 4404 emulsion obtained with a 1-volt potential, because this emulsion has a sufficient number of grains for 4.25 times this density, or an equivalent electrical potential of 4.25 volts. The equivalent unit capacitance of this film is  $C_{(1)} = 8 \times 10^{-12}$  farad.

The noise equivalent sampling area of the 4404 emulsion has a diameter of 2 microns. Because the equivalent potential spread of a point charge on an electrical storage surface is approximately equal to its thickness  $d$ , an electrical storage surface having a thickness of 2 microns has the same sampling area as the 4404 emulsion. (The beam senses the potential and not the charge itself.)

Table I compares the constants of various charge storage surfaces with these reference values.

The minimum read-out time ( $t_r$ ) computed for a 90% discharge (see following section) is given for a  $1\text{ cm}^2$  area (one-inch vidicons and similar television camera tubes) and for the  $25\text{-cm}^2$  area of developmental high-definition vidicons.

The last three surfaces listed in Table I have small capacitances and are thus particularly suited for live pickup in standard television systems because an adequate discharge can be obtained in 1/30 second. Their resolving power is lower, however, because of the greater thickness and lower electron density.

It can be seen that lag is a complex thing to define as a "one-number parameter." It is a function principally of the capacitance of the storage surface, the reflectance of that surface, the magnitude and geometry of the reading beam, and the level of the signal stored.

All tubes exhibit appreciable lag when operating at very low signal levels. For example, the Plumbicon<sup>®</sup> can provide useful low-light-level imagery if cascaded to two intensifier stages, but the signal level is so low that the lag makes the  $I^2$ -PV camera of little value. Three intensifiers or a channel plate can drive the Plumbicon hard enough to make lag come within reasonable bounds, but now the MTF of the intensifiers or the channel plate renders the image quality too low for any demanding applications.

Unfortunately, though the interrelation of resolving power, signal level, and lag are qualitatively and intuitively understood by some and perhaps definitively understood by a few, no good relationship is available to allow the interaction to be expressed as a simple factor of merit by which to broadly classify the quality of tubes.

To a large extent, the best tubes are all good, perhaps with different degrees of excellence in different specific parameters. The plot shown in Fig. VII-2 shows that the  $SNR_D$  curves cluster rather tightly for the better tubes at a given level of signal current. It can be seen in that figure that the rank order of the tubes changes with light level, and, at a given light level, with the amount of resolution desired.

These differences in  $SNR_D$  for the better tubes are not great, however, and it now becomes necessary to choose among the good tubes on the basis of other factors such as lag, burn resistance, and life.

One must consider, for example, the excellent spatial resolution of the isocon at the higher of the nighttime light levels, but one must not forget how quickly that spatial resolution decays at the lower levels. Where the levels are moderate, it will be hard to find a better tube than the 4.5-in. (40-mm cathode) isocon. The secondary electron redistribution effect (blooming) in the isocon is a built-in overload protection that simultaneously gives a form of edge sharpening to some imagery (at the expense of other properties) and ensures against target damage from localized bright images.

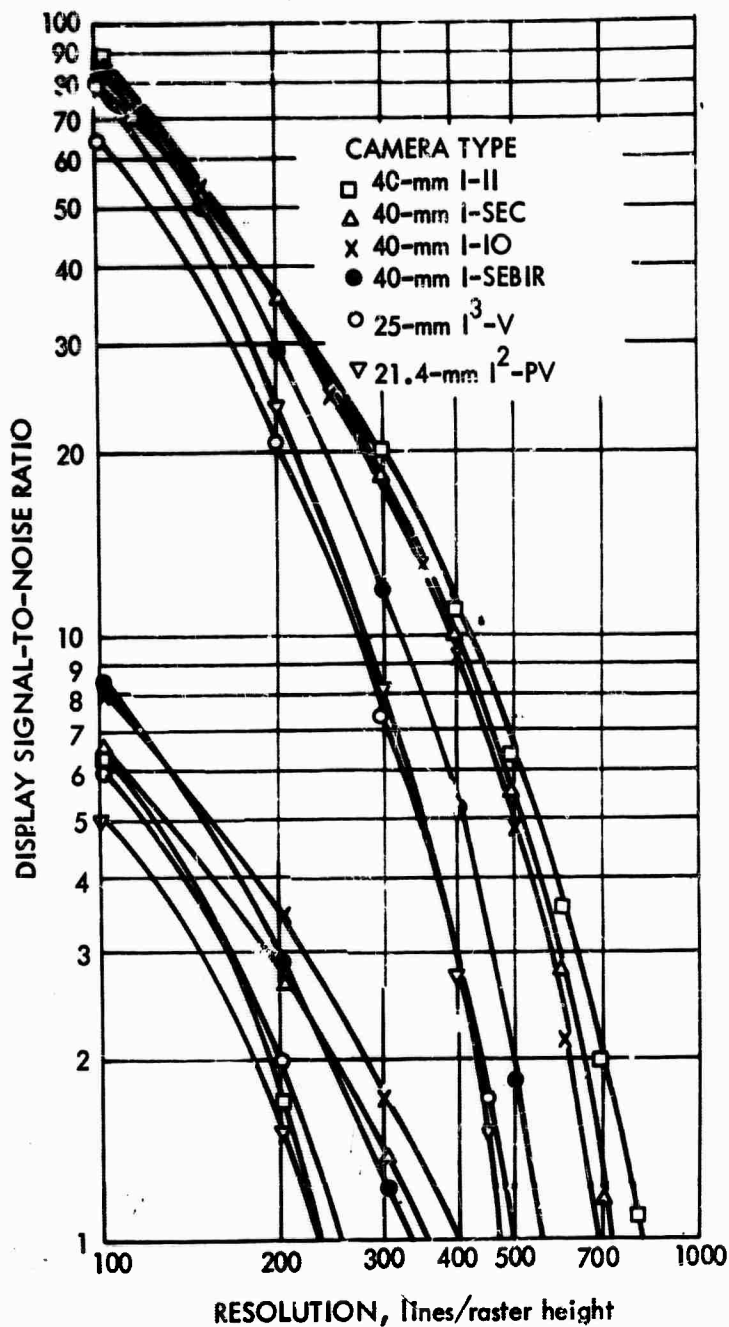


FIGURE VII-2. Comparison of  $SNR_D$  Versus Resolution for Various Low-Light-Level Cameras at Input Photocathode Currents of  $10^{-12}$  amp (Curves at Left) and  $10^{-10}$  amp (Curves at Right)

One must also temper one's enthusiasm for the performance of the silicon diode array devices with some caution about tube life. Various conflicting reports range from industrial guarantees of not over 500 hours to industrial reports of several thousands of hours of satisfactory operation. Part VI of this report shows that in some experiments the damage threshold of the better targets has reached a more or less common level.

One might well begin to recognize that the present need is not so much for better camera tubes as it is for a means to concentrate on a few tubes to get production volume on these better tubes up and prices down.

It may well be that excessive specifications for some noncritical parameters are making the yield on deliverable tubes too low and thus prices too high for most military applications. Specifications have a way of getting written for the obvious but not necessarily important factors, while the critical, less well understood parameters are ignored.

#### F. OTHER FACTORS

In addition to the performance of the sensor, one must treat with equal care most of the topics discussed previously plus all the additional factors of a display that can seriously degrade image quality or perception.

Thus, one must specify for the display adequate size, brightness, and dynamic range, and freedom from distortion, banding, line jitter, crawl, and twinning.

Haste for procurement at the expense of realistic definitive specifications has filled the refuse bins with expensive failures in the night vision area. As the old adage goes, "If you want it bad enough, that's just the way you'll get it."

## PART VII. REFERENCES

1. Lucien M. Biberman and Sol Nudelman, eds., Photoelectronic Imaging Devices, Vol. I, Chapters 2 and 3, Plenum Press, New York, 1971.
2. R.W. Redington, "The Transient Response of Photoconductive Camera Tubes Employing Low-Velocity Scanning," IRE Trans. on Electron Devices, Vol. 4, pp. 220-225, 1957.
3. R.L. Rodgers, 3rd, et al., "Silicon Intensifier Target Camera Tube," Proc. 1970 IEEE International Solid-State Circuits Conference, pp. 176-177, February 1970.
4. Otto H. Schade, Sr., "The Resolving-Power Functions and Quantum Processes of Television Cameras " RCA Review, Vol. 28, p. 460, September 1967.

**BLANK PAGE**

## APPENDIX

### DERIVATION OF DETECTION PROBABILITY CURVE

As the mean number of photoelectrons in the spatial and temporal sampling interval becomes large, the Poisson probability density distribution approaches a Gaussian or normal probability density distribution given by

$$f_X(x) = \exp \left[ -1/2 \left[ (x-m)/\sigma \right]^2 \right] / \sigma (2\pi)^{1/2} \quad (A-1)$$

where  $X$  is the random variable,  $x$  is the independent variable,  $m$  is the mean, and  $\sigma$  is the standard deviation. Consider two photoelectron population densities, the first representing the image with mean  $M_2$  and standard deviation  $\sigma_2$ , and the second being the background with mean  $M_1$  and standard deviation  $\sigma_2$ . We wish to determine how the difference  $m_2 - m_1$ , which represents the signal, is distributed statistically. To obtain the new distribution, we use the concept of moment-generating functions, which are defined by

$$M_X(\theta) = \int_{-\infty}^{\infty} \exp(\theta x) \cdot f_X(x) dx \quad (A-2)$$

and we generate moments through the formula

$$d [M_X(\theta)] / d \theta^k \big|_{\theta=0} = a_k \quad (A-3)$$

where  $\theta$  is a dummy variable and  $a_k$  is the moment of order  $k$ .

Also, note that

$$M_{(x_1 + x_2)}(\theta) = M_{x_1}(\theta) \cdot M_{x_2}(\theta), \quad (A-4)$$

and

$$M_{cg(x)}(\theta) = M_{g(x)}(c\theta). \quad (A-5)$$

For a normal distribution

$$M_x(\theta) = \exp [m\theta + (1/2)\sigma\theta^2] \quad (A-6)$$

In the mathematical detection model, we express the signal as being the difference between the true means  $m_2$  and  $m_1$  of the image and background signals, and this will be true on the average. However, in any given sampling interval, the difference may be some different number  $x_2 - x_1$ , where  $x_2$  and  $x_1$  are randomly distributed. Suppose we take a number of samples of  $x_1$  and  $x_2$  and take the average. Then,

$$\bar{x}_1 = \frac{1}{k} \sum_{i=1}^k x_{1i} \text{ and } \bar{x}_2 = \frac{1}{k} \sum_{i=1}^k x_{2i} \quad (A-7)$$

In the limit as  $k$ , the number of samples is increased indefinitely, and  $\bar{x}_1$  and  $\bar{x}_2$  become the true means  $m_1$  and  $m_2$ . However, for finite sample numbers,  $\bar{x}$  is a random number equal to the mean of a sample of size  $k$ .

Since  $x_i$  is normally distributed with mean  $m_x$  and variance  $\sigma_x^2$ , its moment-generating function is given by equations A-4, A-5, and A-7, as follows:

$$M_{\bar{x}}(\theta) = M_{\frac{1}{k} \sum x_i}(\theta) = M_{\sum \frac{1}{k} x_i}(\theta) = M_{x_i} \left[ \frac{\theta}{k} \right]^k \quad (A-8)$$



and by equation A-6:

$$M_{\bar{X}}(\theta) = \left[ \exp \left[ m_x \cdot \frac{\theta}{k} + (1/2) \left( \sigma_x^2 \frac{\theta^2}{k^2} \right) \right] \right]^k$$

$$= \exp \left( m_x \theta + \frac{1}{2} \frac{\sigma_x^2}{k} \theta^2 \right)$$
(A-9)

By comparison with Eq. A-6, we recognize Eq. A-9 as the moment-generating function of a normally distributed variable with mean  $m_x$  and variance  $\sigma_x^2/k$ . Having shown that  $\bar{X}_2$  and  $\bar{X}_1$  are normally distributed, we now inquire about the distribution of the difference  $\bar{X}_2 - \bar{X}_1$ . Again, we use the moment-generating functions:

$$M_{\bar{X}_2}(\theta) = \exp \left[ m_2 \theta + 1/2 \frac{\sigma_2^2}{k} \theta^2 \right]$$
(A-10)

$$M_{\bar{X}_1}(\theta) = \exp \left[ -m_1 \theta + 1/2 \frac{\sigma_1^2}{k} \theta^2 \right]$$

Thus,

$$M_{\bar{X}_2 - \bar{X}_1}(\theta) = \exp \left[ (m_2 - m_1) \theta + 1/2 \frac{(\sigma_2^2 + \sigma_1^2)}{k} \theta^2 \right]$$
(A-11)

Again, by comparison with Eq. A-6, we see that  $(\bar{X}_2 - \bar{X}_1)$  is normally distributed with mean equal to  $(m_2 - m_1)$  and standard deviation equal to  $[(\sigma_2^2 + \sigma_1^2)/k]^{1/2}$ . In viewing television scenes, the eye integrates a number of samples ( $k = 1$ ), while in viewing a noisy photograph, only one sample is involved.

If next we let  $\Delta n$  be the random variable  $\bar{X}_2 - \bar{X}_1$ , and  $\bar{\Delta n}$  be the mean  $m_2 - m_1$ ,  $\Delta n$  is recognized as the number of signal photoelectrons used. Let  $(\sigma_2^2 + \sigma_1^2) k = \bar{n}_{\max} + \bar{n}_{\min}$ . We now define a new random variable

$$Z = (x - m)/\sigma = (\Delta n - \bar{\Delta n})/(\bar{n}_{\max} + \bar{n}_{\min}) \quad (\text{A-12})$$

If  $x$  is a normally distributed random variable with mean  $m$  and standard deviation  $\sigma$ , then  $z = (x - m)/\sigma$  can be shown to be normally distributed with zero mean and unit standard deviation. Also, observe that the probability of detection  $P_d$  is equal to the cumulative probability that  $Z$  will fall in the range from  $-\infty$  to some value  $z_2$  is expressed by the integral

$$P_d(-\infty < Z < z_2) = \frac{1}{(2\pi)^{1/2}} \int_{-\infty}^{z_2} \exp(-z^2/2) dz \quad (\text{A-13})$$

When  $z_2 = 0$ ,  $P_d = 0.5$ , we have previously defined the threshold  $\text{SNR}_{D-T}$  as being that value at which  $P_d = 0.5$ . Thus, since

$$Z = \frac{\Delta n - \bar{\Delta n}}{\sigma} = 0,$$

when

$$\frac{\Delta n}{\sigma} = \frac{\bar{\Delta n}}{\sigma} = \text{SNR}_{DT}, \quad (\text{A-14})$$

$$\sigma = (\bar{n}_{\max} + \bar{n}_{\min})^{1/2}.$$

Therefore, we can interpret  $\Delta n/\sigma$  as being the actual display signal-to-noise ratio (and a random variable and  $\bar{\Delta n}/\sigma$  as being the threshold display signal-to-noise ratio), i.e.,

$$Z = \text{SNR}_D - \text{SNR}_{DT} \quad (\text{A-15})$$